

Acta Neurochirurgica
Supplements

Editor: H.-J. Steiger

Intracranial Pressure and Brain Monitoring XIV

Edited by
M.U. Schuhmann, M. Czosnyka

Acta Neurochirurgica
Supplement 114

Prof. Dr. Martin U. Schuhmann, M.D.
Eberhard-Karls-Universität, Universitätsklinikum, Klinik für Neurochirurgie, Hoppe-Seyler-Strasse 3,
72076 Tübingen, Germany
martin.schuhmann@med.uni-tuebingen.de

Dr. Marek Czosnyka
University of Cambridge, Addenbrooke's Hospital, Department of Neurosurgery, Hills Road,
CB2 2QQ Cambridge, United Kingdom
mc141@medschl.cam.ac.uk

This work is subject to copyright.

All rights are reserved, whether the whole or part of the material is concerned, specifically those of translation, reprinting, re-use of illustrations, broadcasting, reproduction by photocopying machines or similar means, and storage in data banks.

Product Liability: The publisher can give no guarantee for all the information contained in this book. This does also refer to information about drug dosage and application thereof. In every individual case the respective user must check its accuracy by consulting other pharmaceutical literature. The use of registered names, trademarks, etc. in this publication does not imply, even in the absence of a specific statement, that such names are exempt from the relevant protective laws and regulations and therefore free for general use.

©2012 Springer-Verlag/Wien
Printed in Germany
SpringerWienNewYork is part of Springer Science+Business Media
springer.at

Typesetting: SPI, Pondichery, India

Front cover: background cover image and logo by Martin U. Schuhmann

Printed on acid-free and chlorine-free bleached paper
SPIN: 80023938

Library of Congress Control Number: 2012901692

With 170 (partly coloured) Figures

ISSN 0065-1419
ISBN 978-3-7091-0955-7 e-ISBN 978-3-7091-0956-4
DOI 10.1007/978-3-7091-0956-4
SpringerWienNewYork

Preface

In 1972, the first ICP conference was organized in Germany at Hannover Medical School by Mario Brock. This first meeting of clinical research enthusiasts and basic scientists has initiated a most successful chain of 14 successive conferences, traveling between Europe, Asia, and North America. Intracranial pressure remains one of the most important parameters to cast light on the “black box” of a sick brain, acutely injured by trauma, hemorrhage, or stroke or less acutely affected by hydrocephalus or idiopathic intracranial hypertension. Monitoring of the intracranial pressure has become more sophisticated and is often today mostly computerized, which opens new avenues for online computation of derived parameters describing e.g. autoregulation. Other invasive and non-invasive brain monitoring modalities and several imaging techniques supplement ICP monitoring. The broader our knowledge about the ongoing brain pathophysiology, the more we are potentially able to counteract harm in time and to improve the outcome of our patients.

The 14th International Conference on Intracranial Pressure and Brain Monitoring (12–16 September 2010) returned 38 years after its foundation to Germany. About 280 clinicians and scientists from 40 different countries met and focused over 5 days on ICP and brain monitoring topics and experienced an intense time of knowledge exchange at the old University of Tübingen, located in the geographical heart of Europe. The conference was again what it has traditionally been: a platform where clinicians from neurosurgery, neurology and intensive care medicine met scientists from all possible areas of intercept with the brain, a span that ranged from electrical engineers to physicists, and from mathematicians to molecular biologists. We had the impression that we recreated the hallmark of the previous ICP conferences: a friendly, interested and focused atmosphere, where the “young and keen” met the “old and wise.”

This volume is an excerpt of the conference, where 231 abstracts were submitted. They were presented as 97 oral presentation and 134 posters according to the score and preference of the authors. The supplement volumes of *Acta Neurochirurgica* (papers published therein are listed in PubMed, of course, the book series itself does not carry an impact factor) are an ideal marketplace for publication of new ideas and approaches to the field. Thus many of the papers can be seen as an inspiration for future research. The editors and the International Advisory Board stress the fact, that those titles nevertheless are important milestones in ICP history, documenting the progress of the field in an unique fashion over almost 40 years. Therefore, we were happy to receive more than 80 contributions to continue this legacy and document the current topics and developments. Seventy-seven of the papers have passed review and revision and are now at your hands.

This collection of scientific papers does not only document the 14th International Conference on Intracranial Pressure and Brain Monitoring, but also stimulates readers to continue and expand their research. We are therefore confident that this publication will help to remember Tübingen 2010 and to prepare for the 2013 ICP conference in Singapore.

Tübingen, Germany
Cambridge, UK

Martin U. Schuhmann
Marek Czosnyka

Contents

Historical Perspective

Digitised ICP over Three Decades	1
David J. Price	

Methods of Brain Monitoring and Data Analysis

Latency Relationships Between Cerebral Blood Flow Velocity and Intracranial Pressure	5
Shadnaz Asgari, Paul M. Vespa, Marvin Bergsneider, and Xiao Hu	

The Linear Relationship Between Transcranial Doppler Pulsatility Indices and Intracranial Pressure Is Influenced by Traumatic Brain Injury and Vasospasm	11
Thomas C. Glenn, Arun K. Sherma, David L. McArthur, Xiao Hu, Christopher R. Hanuscin, Mehjabeen S. Furreedan, David A. Hovda, Paul M. Vespa, and Neil A. Martin	

Time Constant of the Cerebral Arterial Bed	17
Magdalena Kasprowicz, Jennifer Diedler, Matthias Reinhard, Emmanuel Carrera, Peter Smielewski, Karol P. Budohoski, Enrico Sorrentino, Christina Haubrich, Peter J. Kirkpatrick, John D. Pickard, and Marek Czosnyka	

Pulse Amplitude and Lempel–Ziv Complexity of the Cerebrospinal Fluid Pressure Signal	23
D. Santamarta, D. Abásolo, J. Fernández, and R. Hornero	

Association Between ICP Pulse Waveform Morphology and ICP B Waves	29
Magdalena Kasprowicz, Marvin Bergsneider, Marek Czosnyka, and Xiao Hu	

Computerized Data Analysis of Neuromonitoring Parameters Identifies Patients with Reduced Cerebral Compliance as Seen on CT	35
Rupert Faltermeier, Martin A. Proescholdt, and Alexander Brawanski	

Early Warning of EUSIG-Defined Hypotensive Events Using a Bayesian Artificial Neural Network	39
Rob Donald, Tim Howells, Ian Piper, I. Chambers, G. Citerio, P. Enblad, B. Gregson, K. Kiening, J. Mattern, P. Nilsson, A. Ragauskas, Juan Sahuquillo, R. Sinnott, and A. Stell	

Trigger Characteristics of EUSIG-Defined Hypotensive Events	45
Rob Donald, Tim Howells, Ian Piper, I. Chambers, G. Citerio, P. Enblad, B. Gregson, K. Kiening, J. Mattern, P. Nilsson, A. Ragauskas, Juan Sahuquillo, R. Sinnott, and A. Stell	
Go Green! Reusing Brain Monitoring Data Containing Missing Values: A Feasibility Study with Traumatic Brain Injury Patients	51
Mengling Feng, Liang Yu Loy, Feng Zhang, Zhuo Zhang, Kuralmani Vellaisamy, Pei Loon Chin, Cuntai Guan, Liang Shen, Nicolas K.K. King, Kah Keow Lee, and Beng Ti Ang	
Investigation of the Relationship Between Transcranial Impedance and Intracranial Pressure	61
Martin Shaw, I. Piper, P. Campbell, C. McKeown, J. Britton, K. Oommen, L. Stewart, I. Whittle, R. Gregson, and E. Clutton	
Bioinformatics Analysis of Mortality Associated with Elevated Intracranial Pressure in Children	67
Mark S. Wainwright and Remigiusz Lewandowski	
ICM+: A Versatile Software for Assessment of CSF Dynamics	75
Peter Smielewski, Zofia Czosnyka, Magdalena Kaspruwicz, John D. Pickard, and Marek Czosnyka	
Modified Brainstem Auditory Evoked Responses in Patients with Non-brainstem Compressive Cerebral Lesions	81
James L. Stone, John Fino, Prasad Vannemreddy, and Fady Charbel	
Analysis of Intracranial Pressure Time Series Using Wavelets (Haar Basis Functions)	87
Hans E. Heissler, Kathrin König, Joachim K. Krauss, and Eckhard Rickels	
Stationarity in Neuromonitoring Data	93
Hans E. Heissler, Kathrin König, Joachim K. Krauss, and Eckhard Rickels	
Methods of Invasive and Non-invasive ICP Assessment	
Is ICP Solid or Fluid? In Vitro Biomechanical Model Using a Fluid-Saturated Gel	97
M. Ros, P. Yameogo, P. Payoux, P. Swider, and Eric Schmidt	
Implantable ICP Monitor for Improved Hydrocephalus Management	101
Ellyce Stehlin, Simon Malpas, Peter Heppner, Patrick Hu, Matthew Lim, and David Budgett	
Intracranial Pressure Telemetry: First Experience of an Experimental In Vivo Study Using a New Device	105
Berk Orakcioglu, Christopher Beynon, Modar M. Kentar, Regina Eymann, Michael Kiefer, and Oliver W. Sakowitz	

Telemetric ICP Measurement with the First CE-Approved Device: Data from Animal Experiments and Initial Clinical Experiences.	111
Michael Kiefer, Sebastian Antes, Steffen Leonhardt, Melanie Schmitt, Berk Orakcioglu, Oliver W. Sakowitz, and Regina Eymann	
The New ICP Minimally Invasive Method Shows That the Monro–Kellie Doctrine Is Not Valid	117
Sérgio Mascarenhas, G.H.F. Vilela, C. Carlotti, L.E.G. Damiano, W. Seluque, B. Colli, K. Tanaka, C.C. Wang, and K.O. Nonaka	
Non-Invasively Estimated ICP Pulse Amplitude Strongly Correlates with Outcome After TBI	121
Karol P. Budohoski, Bernhard Schmidt, Peter Smielewski, Magdalena Kasprowicz, Ronny Plontke, John D. Pickard, Jurgen Klingelhöfer, and Marek Czosnyka	
Realization of a Comprehensive Non-invasive Detection of Intracranial Pressure Analyzer Based upon FVEP and TCD.	127
J.I. Zhong, Yang Li, Xu Minhui, and Zhang Yihua	
Electrophysiological Monitoring of Cochlear Function as a Non-invasive Method to Assess Intracranial Pressure Variations	131
Laurent Sakka, Aurélie Thalamy, Fabrice Giraudet, Thierry Hassoun, Paul Avan, and Jean Chazal	
The Role of Autoregulation	
Autoregulatory Model Comparison and Optimisation Methodology	135
Martin Shaw, Ian Piper, and Michael Daley	
Assessment of Cerebral Autoregulation from Respiratory Oscillations in Ventilated Patients After Traumatic Brain Injury	141
Philip M. Lewis, Peter Smielewski, Jeffrey V. Rosenfeld, John D. Pickard, and Marek Czosnyka	
Monitoring of the Association Between Cerebral Blood Flow Velocity and Intracranial Pressure	147
Philip M. Lewis, Peter Smielewski, Jeffrey V. Rosenfeld, John D. Pickard, and Marek Czosnyka	
How Does Moderate Hypocapnia Affect Cerebral Autoregulation in Response to Changes in Perfusion Pressure in TBI Patients?	153
Christina Haubrich, Luzius Steiner, D.J. Kim, Magdalena Kasprowicz, Piotr Smielewski, Rolf R. Diehl, John D. Pickard, and Marek Czosnyka	
Correlation of Clinical Outcome and Angiographic Vasospasm with the Dynamic Autoregulatory Response After Aneurysmal Subarachnoid Hemorrhage.	157
Martin Barth, Julius Moratin, Martin Dostal, Armin Kalenka, Johann Scharf, and Kirsten Schmieder	

The Role of Tissue Oxygenation and Near-Infrared Spectroscopy

Comparison of a New Brain Tissue Oxygenation Probe with the Established Standard	161
Stefan Wolf, P. Horn, C. Frenzel, L. Schürer, P. Vajkoczy, and J. Dengler	

Comparing Brain Tissue Oxygen Measurements and Derived Autoregulation Parameters from Different Probes (Licox vs. Raumedic)	165
M. Dengl, M. Jaeger, C. Renner, and J. Meixensberger	

Experimental Comparison of the Measurement Accuracy of the Licox® and Raumedic® Neurovent-PTO Brain Tissue Oxygen Monitors.	169
Matthias H. Morgalla, R. Haas, G. Grözinger, Christian Thiel, Karolin Thiel, Martin U. Schuhmann, and Martin Schenk	

Is $P_{br}O_2$ Pressure Reactivity Index (ORx) Dependent on the Type of Oxygen Probe? An In Vivo Study	173
G. Grözinger, Martin Schenk, Christian Thiel, Karolin Thiel, Matthias H. Morgalla, and Martin U. Schuhmann	

Continuous Quantitative Monitoring of Cerebral Oxygen Metabolism in Neonates by Ventilator-Gated Analysis of NIRS Recordings	177
Thomas Heldt, Faisal M. Kashif, Mustafa Suleymanci, Heather M. O'Leary, Adré J. du Plessis, and George C. Verghese	

Near Infrared Spectroscopy as Possible Non-invasive Monitor of Slow Vasogenic ICP Waves.	181
Ruwan Alwis Weerakkody, Marek Czosnyka, Christian Zweifel, Gianluca Castellani, Peter Smielewski, Ken Brady, John D. Pickard, and Zofia Czosnyka	

Drift of the Bowman Hemedex® Cerebral Blood Flow Monitor Between Calibration Cycles	187
Stefan Wolf, P. Vajkoczy, J. Dengler, L. Schürer, and P. Horn	

Hydrocephalus/IIH: Imaging and Diagnosis

Quantification of Pulsatile Cerebrospinal Fluid Flow within the Prepontine Cistern.	191
Robert Hamilton, Justin Dye, Andrew Frew, Kevin Baldwin, Xiao Hu, and Marvin Bergsneider	

Delta-ADC (Apparent Diffusion Coefficient) Analysis in Patients with Idiopathic Normal Pressure Hydrocephalus.	197
T. Osawa, M. Mase, T. Miyati, H. Kan, K. Demura, H. Kasai, M. Hara, Y. Shibamoto, and K. Yamada	

Evidence for Altered Spinal Canal Compliance and Cerebral Venous Drainage in Untreated Idiopathic Intracranial Hypertension.	201
Noam Alperin, Byron L. Lam, Rong-Wen Tain, Sudarshan Ranganathan, Michael Letzing, Maria Bloom, Benny Alexander, Potyra R. Aroucha, and Evelyn Sklar	

Automated Extraction of Decision Rules for Predicting Lumbar Drain Outcome by Analyzing Overnight Intracranial Pressure	207
Xiao Hu, Robert Hamilton, Kevin Baldwin, Paul M. Vespa, and Marvin Bergsneider	
Lack of Correlation of Overnight Monitoring Data and Lumbar Infusion Data in iNPH Patients	213
Andreas Speil, Jordana C. Sosa, Bernd E. Will, and Martin U. Schuhmann	
Shunt-Dependent Hydrocephalus Following Subarachnoid Hemorrhage Correlates with Increased S100B Levels in Cerebrospinal Fluid and Serum	217
S. Brandner, Y. Xu, C. Schmidt, Irene Emtmann, Michael Buchfelder, and Andrea Kleindienst	
Normal Hypocretin-1 (Orexin A) Levels in Cerebrospinal Fluid in Patients with Idiopathic Intracranial Hypertension	221
Maria Antonia Poca, Rosa Galard, Elena Serrano, Mari Angels Merino, Patricia Pozo-Rosich, Elisabeth Solana, Olga Mestres, Maria Dolores de la Calzada, and Juan Sahuquillo	
Frontal and Temporal Horn Ratio: A Valid and Reliable Index to Determine Ventricular Size in Paediatric Hydrocephalus Patients?	227
Sebastian Antes, Michael Kiefer, Melanie Schmitt, Miriam Lechtenfeld, Martina Geipel, and Regina Eymann	
Intraventricular Cooling During CSF Infusion Studies	231
Melanie Schmitt, Regina Eymann, Sebastian Antes, and Michael Kiefer	
An Uncommon Case of Idiopathic Intracranial Hypertension with Diagnostic Pitfalls	235
Manuel Mrfka, Karin Pistracher, Bernadette Schökler, Sonja Wissa, and Senta Kurschel-Lackner	
Management and Therapy of Hydrocephalus	
Micro-fabricated Shunt to Mimic Arachnoid Granulations for the Treatment of Communicating Hydrocephalus	239
Francis Kralick, Jonghyun Oh, Tim Medina, and Hongseok (Moses) Noh	
On the Method of a Randomised Comparison of Programmable Valves with and Without Gravitational Units: The SVASONA Study	243
Johannes Lemcke, Ullrich Meier, Cornelia Müller, Michael Fritsch, Michael Kiefer, Regina Eymann, Uwe Kehler, Niels Langer, Martin U. Schuhmann, Andreas Speil, Friedrich Weber, Victor Remenez, Veit Rohde, Hans-Christoph Ludwig, and Dirk Stengel	
Idiopathic Normal Pressure Hydrocephalus: Results of a Prospective Cohort of 236 Shunted Patients	247
Maria Antonia Poca, Elisabeth Solana, Francisco Ramón Martínez-Ricarte, Mónica Romero, Dario Gándara, and Juan Sahuquillo	
Idiopathic Normal Pressure Hydrocephalus (iNPH) and Co-Morbidity: An Outcome Analysis of 134 Patients	255
Johannes Lemcke and Ullrich Meier	

Intracranial Pressure Measurement in Infants Presenting with Progressive Macrocephaly and Enlarged Subarachnoid Spaces	261
M. Schulz, S.A. Ahmadi, B. Spors, and Ulrich-W. Thomale	
Treatment Options for Intracranial Arachnoid Cysts: A Retrospective Study of 69 Patients	267
Anders Vedel Holst, Patricia L. Danielsen, and Marianne Juhler	
Management and Therapy of Traumatic Brain Injury	
A Microdialysis Study of Oral Vigabatrin Administration in Head Injury Patients: Preliminary Evaluation of Multimodal Monitoring	271
Keri L.H. Carpenter, Ivan Timofeev, Jürgens Nortje, Marek Czosnyka, John D. Pickard, and Peter J. Hutchinson	
The Atrial Natriuretic Peptide Does Not Serve Osmoregulation but Predicts Outcome Following Brain Injury	277
Andrea Kleindienst, Georg Brabant, Nils G. Morgenthaler, Irene Emtmann, Nadine Scheufler, and Michael Buchfelder	
Bedside Study of Cerebral Critical Closing Pressure in Patients with Severe Traumatic Brain Injury: A Transcranial Doppler Study.	283
Corina Puppo, J. Camacho, B. Yelich, L. Moraes, A. Biestro, and H. Gomez	
Traumatic Brain Injury in the Elderly: A Significant Phenomenon.	289
B. Depreitere, G. Meyfroidt, G. Roosen, J. Ceuppens, and F. Guiza Grandas	
Fixed, Dilated Pupils Following Traumatic Brain Injury: Historical Perspectives, Causes and Ophthalmological Sequelae	295
Adel Helmy, Peter J. Kirkpatrick, Helen M. Seeley, Elizabeth Corteen, David K. Menon, and Peter J. Hutchinson	
Why Mortality Is Still High with Modern Care of 613 Evacuated Mass Lesions Presented as Severe Head Injuries 1999–2009	301
Leon Levi, Joseph Guilburd, Jean Soustiel, Gill Svir, Marius Constantinescu, and Menashe Zaaroor	
Late Decompressive Craniectomy as Rescue Treatment for Refractory High Intracranial Pressure in Children and Adults.	305
Catrien van der Meer, Erik van Lindert, and Ronald Petru	
CT Angiography as a Confirmatory Test in Brain Death	311
Stefan Welschehold, Stephan Boor, Katharina Reuland, Christian Beyer, Thomas Kerz, Andre Reuland, and Wibke Müller-Forell	
The Imaging Diagnosis and Prognosis Assessment of Patients with Midbrain Injury in the Acute Phase of Craniocerebral Injury	317
Ming-kun Yu and Wei Ye	

Management and Therapy of Subarachnoid and Intracranial Haemorrhage

The Effect of Intraventricular Thrombolysis in Combination with Low-Frequency Head Motion After Severe Subarachnoid Hemorrhage: Interim Analysis of Safety, Clot Clearance Rate and Delayed Cerebral Ischemia	323
Sven O. Eicker, Kerim Beseoglu, Nima Etminan, Jason Perrin, Arzu Taskin, Hans-Jakob Steiger, and Daniel Hänggi	
Early CT Perfusion Measurement After Aneurysmal Subarachnoid Hemorrhage: A Screening Method to Predict Outcome?	329
Marcel A. Kamp, Hi-Jae Heiroth, Kerim Beseoglu, Bernd Turowski, Hans-Jakob Steiger, and Daniel Hänggi	
Cerebrospinal Fluid Lactate Concentration After Withdrawal of Metabolic Suppressive Therapy in Subarachnoid Hemorrhage	333
Marco Stein, Julia Schomacher, Wolfram Scharbrodt, Matthias Preuss, and Matthias F. Oertel	
Effect of Increased ICP and Decreased CPP on DND and Outcome in ASAH	339
Krissanee Karnchanapandh	
Prior Statin Use Has No Effect on Survival After Intracerebral Hemorrhage in a Multiethnic Asian Patient Cohort	343
Nicolas K.K. King, Vincent Khwee-Soon Tay, John Carson Allen, and Beng-Ti Ang	
The Impact of Silver Nanoparticle-Coated and Antibiotic-Impregnated External Ventricular Drainage Catheters on the Risk of Infections: A Clinical Comparison of 95 Patients	347
Johannes Lemcke, Felix Depner, and Ullrich Meier	
Experimental Approaches to Acute Brain Disease	
Dependence of Cerebrospinal Fluid Pressure and Volume on the Changes in Serum Osmolarity in Cats	351
Ivana Jurjević, Jurica Maraković, Darko Chudy, Ivona Markelić, Marijan Klarica, Ana Froebe, and Darko Orešković	
The Effect of Body Position on Intraocular and CSF Pressures in the Lateral Ventricle, and in Cortical and Lumbar Subarachnoid Spaces in Cats	357
Tomislav Kuzman, Ivana Jurjević, Inga Mandac, Milan Radoš, Darko Orešković, Hrvoje Jednačak, and Marijan Klarica	
Pressure Reactivity Index Correlates with Metabolic Dysfunction in a Porcine Model of Intracerebral Hemorrhage	363
Edgar Santos, Berk Orakcioglu, Modar M. Kentar, Jennifer Diedler, Yoichi Uozumi, Michael Schöll, Andreas Unterberg, and Oliver W. Sakowitz	

Evidence of Spreading Depolarizations in a Porcine Cortical Intracerebral Hemorrhage Model	369
Berk Orakcioglu, Yoichi Uozumi, Modar M. Kentar, Edgar Santos, Andreas Unterberg, and Oliver W. Sakowitz	
Spontaneous Cortical Spreading Depression and Intracranial Pressure Following Acute Subdural Hematoma in a Rat	373
B. Alessandri, J. Stephan Tretzel, Axel Heimann, and Oliver Kempfski	
The Peptide AF-16 and the AF Protein Counteract Intracranial Hypertension	377
Hans-Arne Hansson, Mohamed Al-Olama, Eva Jennische, Kliment Gatzinsky, and Stefan Lange	
Influence of Isoflurane on Neuronal Death and Outcome in a Rat Model of Traumatic Brain Injury	383
Daniel Hertle, Christopher Beynon, K. Zweckberger, B. Vienenkötter, C.S. Jung, K. Kiening, Andreas Unterberg, and Oliver W. Sakowitz	
Correlation of the Intracranial Pressure to the Central Venous Pressure in the Late Phase of Acute Liver Failure in a Porcine Model	387
Kathrin Scheuermann, Christian Thiel, Karolin Thiel, Wilfried Klingert, Elmar Hawerkamp, Johannes Scheppach, Alfred Königsrainer, Matthias H. Morgalla, Pamela Leckie, Andrew Proven, Rajiv Jalan, Nathan Davies, Martin U. Schuhmann, and Martin Schenk	
Visualisation of Cortical pO₂ During an Epidural Mass Lesion in Rodents	393
Jan Warnat, Gregor Liebsch, Eva-Maria Stoerr, and Alexander Brawanski	
Development of an Experimental Model to Study the Pathophysiology of Cerebral Salt Wasting Following Subarachnoid Hemorrhage	399
Andrea Kleindienst, Sven M. Schlaffer, Nikhil Sharma, Lisa Linde, Michael Buchfelder, and Joseph G. Verbalis	
Author Index	405
Subject Index	409

Digitised ICP over Three Decades

David J. Price

Abstract I describe a personal journey of experience in applying computer technology to the intracranial pressure signal for the 30 years from 1968 to 1998. After experimenting with off-line applications, I used a desk-top computer to automate infusion tests for the measurement of outflow resistance. For 10 years from 1975, we programmed a minicomputer to control ICP automatically with mannitol infusion and integrate nursing data from a dedicated bedside terminal. In 1986, we were introduced to and subsequently used PC software, which was developed in Warsaw. I briefly review the trends in the applications of computers during that period as recorded in the first ten ICP conference books.

Keywords Intracranial pressure • Computing • Normal pressure hydrocephalus • Outflow resistance • Buffering capacity • Fourier transform • Closed loop controller

Introduction

I was first interested in applying computer technology to the intracranial pressure signal in 1968, but my initial attempts were rudimentary and off-line. Over the subsequent 30 years, I used more sophisticated hardware and software, which made it possible to gain more detailed information from that signal. In particular, this work contributed to more effective decision-making and treatment of intracranial hypertension in patients with head injury.

I retired from clinical practice at Pinderfields Hospital, Wakefield in 1998, and this is an opportunity to use an instrument referred to by Professor Mario Brock as a 'Retrospectroscope' to objectively review my failures and disappointments as well as some successes in those 30 years.

D.J. Price
Emeritus Consultant Neurosurgeon,
Pinderfields Hospital, Wakefield, West Yorkshire, WF1 4DG, UK
e-mail: david.price@doctors.org.uk

The Earliest Years

I attended my first computer training day in 1967, and in the following year had access to a mainframe computer for head injury research. I was at that time a resident at a trauma centre in Birmingham, UK and introduced ICP monitoring using a Millar catheter-tipped transducer, which had been developed for cardiologists. I had no access to a chart recorder and asked the nurses in the intensive care unit to record the ICP from a digital meter every 15 minutes each day, I used a Porta-punch to transfer those numbers to Hollerith cards and fed these into the mainframe computer for generation of a summary and a distribution histogram.

After a series of only two patients, I moved to Glasgow for 2 years of formal neurosurgical training. ICP monitoring of head injuries was well-established there and I found that there was a PDP8 minicomputer in the building. My hopes of using that computer for ICP monitoring were dashed when I realised that it was used every day for cerebral blood flow research and it was installed a long distance from the intensive care unit. In early 1972, I was appointed to a consultant post in Yorkshire.

The First ICP Conference

I attended the first ICP conference in Hannover in June 1972 with my senior neurosurgical colleague, Myles Gibson, and an anaesthetist, Professor Gordon McDowell. I particularly remember a charismatic, enthusiastic and amusing Professor Mario Brock and we are all so disappointed that he has not been able to attend this conference. In Hannover, I listened particularly carefully to the three pioneering papers concerning the application of computers. Dr. Pierre Janny from Chamalieres in France [4] described off-line analysis of the ICP on a mainframe and Dr Kullberg from Lund in Sweden had embarked on on-line monitoring using an 'electronic class interval counter' [5]. They both generated histogram summaries.

The most outstanding contribution was from Dr. Tony Marmarou. We mourn his death earlier this year. I met him at all the conferences I attended and remember him as kind, quietly spoken and humble, with a brilliant logical mind. At the time of that first conference, he had submitted his thesis on 'A theoretical model and experimental evaluation of the cerebral fluid system' [6]. He and his colleague, Kenneth Schulmann [7], had carefully collected physiological experimental data and formulated a series of equations taking into account the CSF formation rate, resistance to outflow and CSF space compliance. They incorporated these into a computer model and then induced CSF ventricular volume changes in cats, finding that there was an excellent correlation between the experimental results and the computer's predictions. The error for steady pressure changes was less than 3% and for sudden changes, less than 5%. This was the first of many excellent contributions by Tony Marmarou at ICP conferences.

Automated Infusion Tests

Following that conference, I was determined to purchase my own computer. I could only afford a microcomputer, but this would not have had sufficient power for continuous on-line analysis in the intensive care environment. I had, by then, developed an interest in normal pressure hydrocephalus. I purchased a Hewlett Packard HP85 desk-top computer for £4,000 with an analogue-to-digital converter and a parallel line interface, which operated in the Basic language with which I was familiar. I wrote the software to acquire the ICP signal, recognise steady-state levels with each infusion rate and increase that rate automatically each time under computer control. A linear regression of the ICP and flow rate produced the outflow resistance and the graph was displayed on the inbuilt screen and printer. After using this system for about a year, I reluctantly conceded that it was simpler to recognise and measure each steady-state level with the naked eye on a chart recording and change the infusion speed manually [9]!

Early On-line Monitoring

We became increasingly aware that the nursing staff had difficulties in estimating the mean ICP from a fluctuating tracing on a chart recorder. The medical staff were slightly more accurate [10]. The other problem was choosing the optimal paper speed. If it was too slow, the respiratory and cardiac components were lost, and at a higher speed, the rolls of paper generated took up too much storage space.

In 1975, I was given a £20,000 grant to purchase a DEC PDP11 minicomputer. I stipulated that it had to have a foreground and background operating system to allow two programs to run synchronously. It was too difficult for me to write all the software and the hospital kindly appointed a physicist of my choice, installed air conditioning and purchased a battery-backed continuous power supply. The computer room was adjacent to a newly designed seven-bed intensive ward where four coaxial cables connected each bed to banks of sockets close to the computer. The visual display, which showed a graph of half-minute ICP means, was installed at the nurses' station. As I lived 10 miles from the hospital, I linked my Apple computer at home to the minicomputer by telephone modem, enabling me to visualise a crude colour graphic display of quarter-hourly means.

The Significance of the Amplitude/Mean Relationship

My physicist colleague, John Mason, and I were impressed with the work of Cees Avesaat and his colleagues [1] in Rotterdam and we visited their computer system, which accurately measured the amplitude of the pulse wave by timing systole from the ECG signal. This was most ingenious, but the time-scale was in heart beats rather than real time. We had in our own system already digitised the ICP at 200 Hz in our foreground program written in Fortran by John Mason. Every 1.4 seconds, paired maximum and minimum values were written to one of the two 1.2-megabyte hard disks. I then used Basic in the background part of the operating system to retrieve 600 of these pairs to generate means and standard deviations of the ICP mean, amplitude and a ratio of amplitude and mean. We did not, however, recognise the significance of this amplitude until we read a paper by Tony Marmarou and his colleagues in 1975 [8] and subsequently Jerzy Szewczykowski and his colleagues from Warsaw in 1977 [13]. They all suggested that it may indicate the current position on the pressure volume curve, which we referred to as 'buffering capacity'.

Closed Loop Control of Intracranial Hypertension

In 1977, we had been very aware of our inadequacy in controlling intracranial hypertension using mannitol following head injury. The selection of the dose seemed rather 'hit and miss', and we therefore decided to delegate the signal acquisition, human decision-making process and the administration of the mannitol entirely to the computer system. I wrote

the necessary software in the background operating system to take account how high the mean ICP was above the chosen upper limit, of the current buffering capacity, the effectiveness of the mannitol as calculated from the response to the last dose and of the mannitol renal clearance. The selected dose was then given by a computer-controlled Ihmed pump at the bedside linked by an RS232 interface. When the administration was complete, the pump confirmed this to the computer. For the morning round at 8 am, a graph printout was generated. This showed quarter-hourly mean ICP and the volumes of mannitol required to maintain it below the selected limit for the morning ward round and for filing in the case records [11]. This system worked successfully for almost 10 years. During that time, it was necessary to have a one-in-two rota for the physicist and I for setting up the computer for each admission in addition to my one in three neurosurgical rota. In 1983, Iwata and his colleagues [3] gave a preliminary report of a closed loop mannitol controller for the management of head injuries, but there was no response learning or attention to the current buffering capacity embedded in the software.

Attempts to Replace the Bedside Intensive Care Charts

Our aim was to integrate all the data collected by hand at the bedside into the computer data-base. The first attempt was based on a large board with thumbwheel switches delegated to each parameter. It worked superbly, but was a disaster because we had failed to involve the nursing staff with the design. It was therefore necessary to return to the drawing board with the help of an electronics engineering Ph.D. student, who spent time planning it with the nursing staff. This much smaller keyboard was powered by a microprocessor with software written in machine code to conserve the then expensive memory chips. This proved successful.

Fourier Transform

After 10 years of almost continuous use of the minicomputer, we thought it advisable to take advantage of a hardware upgrade and we also decided to upgrade the operating system. This was a big mistake as our learning curve for the more advanced operating system was too steep and we were then unable to implement the closed loop controller or support the bedside data input keyboards. It was fortunate that at this difficult time in 1986, we heard of the work of Marek Czosnyka who had implemented a monitoring system based on a fast Fourier transform which was able to isolate cardiac,

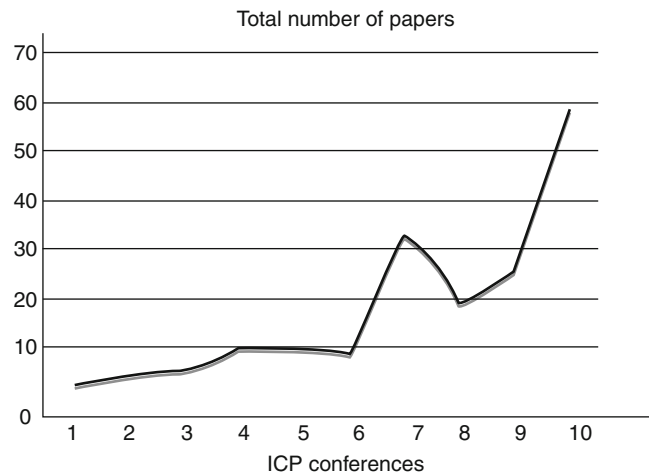


Fig. 1 During the period of the first ten ICP conferences, there was a steady increase in reliance on computer technology

respiratory and sub-respiratory slow-wave components from the signal. After visiting Marek in Warsaw, he came to Yorkshire to install his software at Pinderfields Hospital the following year. The earliest colour display was confined to the ICP and cerebral perfusion pressure [2] but there was the option of generating a graph of the ICP and the pulse amplitude for any selected period of time. Marek Czosnyka subsequently showed that the regression coefficient of the relationship between the amplitude and mean (RAP) is a sensitive index able to indicate when the brain buffering capacity is becoming exhausted and when the subsequent vascular response is compromised with imminent ischaemia [12, 14]. This additional parameter was added to the display when the software was upgraded to ICM. I continued to use this monitoring system up to retirement in 1998.

A Review of Trends in Emphasis as Recorded in the First Ten ICP Conferences

This is an opportunity to briefly review the trends in the utilisation of computer applications as recorded in the first ten ICP conference books in the period from 1972 to 2000.

Of 181 papers, all reporting the reliance on computer technology, 82% came from 5 countries. Eleven percent from Poland, 12% from Japan, 12% from Germany, 20% from the United States and 27% from the United Kingdom. As expected, there was a steady increase in reliance on computers over the years reflected in 3–58 papers published from the first to the tenth conferences respectively (Fig. 1). Seventy six percent of the papers concerned patient care, 32% were applied to animal experiments and the remaining 6% referred to use in modelling and equipment testing. There was an increased number of applications for animal experiments in

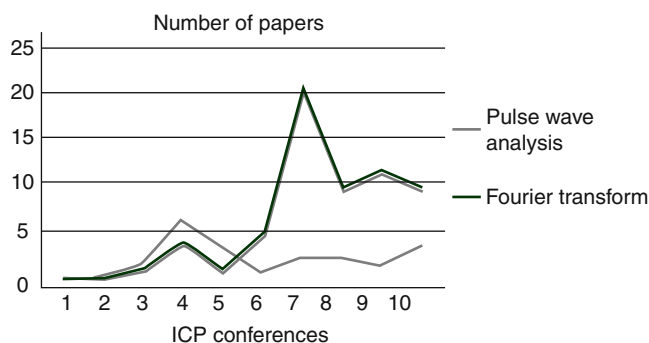


Fig. 2 Between 1972 and 1997, Fourier transform (darker line) replaced other methods of pulse wave analysis (thin line)

the 1980s and 1990s. Off-line computing was abandoned in the 1980s but emerged as more useful subsequently. Presentation at the bedside in the format of histograms was abandoned by the 1990s and there was a steady increase in the use of Fourier analysis as distinct from calculations of pulse amplitude from maximum and minimum values (Fig. 2). Minicomputers were used less frequently and the number of computerised infusion studies increased.

In the first 10 years of this century, there have been numerous advances and it will be interesting to know if there will be the same or more practical improvements in the application of computer technology to the ICP signal in the first 30 years of this century as compared with the last 30 years of the twentieth century.

Conflict of interest statement The author declares that he has no conflict of interest.

References

1. Avezaat CJJ, van Eijndhoven JHM, de Jong DA, Moolenaar WCJ (1976) A new method of monitoring intracranial volume/pressure relationship. In: Beks JWF, Bosch DA, Brock M (eds) *Intracranial pressure III*. Springer, Berlin/Heidelberg/New York, pp 308–313
2. Czosnyka M, Price DJ, Williamson M (1994) Monitoring of cerebrospinal dynamics using continuous analysis of intracranial pressure and cerebral perfusion pressure in head injury. *Acta Neurochir (Wien)* 126:113–119
3. Iwata K, Yuasa H, Sugiyama T, Yamazaki A (1983) Automatic ICP controller: a new device. In: Ishii S, Nagai H, Brock M (eds) *Intracranial pressure V*. Springer, Berlin/Heidelberg/New York/Tokyo, pp 157–162
4. Janny P, Jouan JP, Janny L, Gourgand M, Gueit UM (1972) A statistical approach to long-term monitoring of intracranial pressure. In: Brock M, Dietz H (eds) *Intracranial pressure*. Springer, Berlin/Heidelberg/New York, pp 59–64
5. Kullberg G (1972) A method for statistical analysis of intracranial pressure recordings. In: Brock M, Dietz H (eds) *Intracranial pressure*. Springer, Berlin/Heidelberg/New York, pp 65–69
6. Marmarou A (1973) A theoretical model and experimental evaluation of the cerebral fluid system. Thesis Drexel University, Philadelphia
7. Marmarou A, Shulman K (1972) Computer modelling of CSF pressure/volume and its relationship to hydrocephalus. In: Brock M, Dietz H (eds) *Intracranial pressure*. Springer, Berlin/Heidelberg/New York, pp 275–279
8. Marmarou A, Schulman K, La Morgese J (1975) Compartmental analysis of compliance and outflow resistance of the cerebrospinal fluid system. *J Neurosurg* 43:523–534
9. Price DJ (1988 or 1989) Attempts to predict the probability of clinical improvement following shunting of patients with presumed normal pressure hydrocephalus. In: Hoff JT, Betz AL (eds) *Intracranial pressure VII*. Springer, Berlin/Heidelberg/New York/London/Paris/Tokyo/Hong Kong, pp 390–393
10. Price DJ, Driscoll P (1986) The problems of averaging ICP by eye. In: Miller JD, Teasdale GM, Rowan JO, Galbraith SL, Mendelow AD (eds) *Intracranial pressure VI*. Springer, Berlin/Heidelberg/New York/Tokyo, pp 705–712
11. Price DJ, Dugdale RE, Mason J (1980) The control of ICP using three synchronous closed loops. In: Shulman K, Marmarou A, Miller JD, Becker DP, Hochwald GM, Brock M (eds) *Intracranial pressure IV*. Springer, Berlin/Heidelberg/New York, pp 395–399
12. Price DJ, Czosnyka M, Williamson M (1993) Attempts to continuously monitor autoregulation and compensatory reserve in severe head injuries. In: Avezaat CJJ, van Eijndhoven JHM, Maas AIR, Tans JThJ (eds) *Intracranial pressure VIII*. Springer, Berlin/Heidelberg/New York/London/Paris/Tokyo/Hong Kong/Barcelona/Budapest, pp 61–66
13. Szewczykowski J, Sliwka S, Kunicki A, Dytko P, Korsak-Sliwka J (1977) A fast method of estimating the elastance of the intracranial system. A practical application in neurosurgery. *J Neurosurg* 47:19–26
14. Williamson M, Price DJ, Czosnyka M (1993) Further attempts to anticipate post-traumatic intracranial hypertension by on-line analysis. In: Avezaat CJJ, van Eijndhoven JHM, Maas AIR, Tans JThJ (eds) *Intracranial pressure VIII*. Springer, Berlin/Heidelberg/New York/London/Paris/Tokyo/Hong Kong/Barcelona/Budapest, pp 67–70

Latency Relationships Between Cerebral Blood Flow Velocity and Intracranial Pressure

Shadnaz Asgari, Paul M. Vespa, Marvin Bergsneider, and Xiao Hu

Abstract Pulsatile intracranial pressure (ICP) is a key to the understanding of several neurological disorders in which compliance is altered, e.g., hydrocephalus. A recently proposed model suggests that ICP pulse is a standing wave and not a transmitted wave. The present work, aimed at obtaining a better understanding of the pulsatility in the cranium, tries to test the following hypotheses: first, ICP pulse onset latency would be lower than that of cerebral blood flow velocity (CBFV) pulses measured at a distal vessel; second, CBFV pulse at different intracranial arteries will have different pulse onset latencies, and hence they are not generated as a standing wave. The dataset used in the present study consists of ICP and CBFV signals collected from 60 patients with different diagnoses. The results reveal that the ICP pulse leads CBFV for 90% of the patients regardless of the diagnosis and mean ICP value. In addition, we show that CBFV pulse onset latency is roughly determined by the distance of the measurement point to the heart. We conclude that the ICP signal is not generated as a standing wave and that ICP pulse onset may be related to the arteries proximal to the heart.

Keywords Intracranial pressure • Cerebral blood flow velocity • Pulse onset latency • Pulsatility

S. Asgari

Department of Neurosurgery, Neural Systems and Dynamics Laboratory, The David Geffen School of Medicine, University of California, Los Angeles, CA 90095, USA

P.M. Vespa

Neurocritical Care Program, Department of Neurosurgery, The David Geffen School of Medicine, University of California, Los Angeles, CA 90095, USA

M. Bergsneider and X. Hu (✉)

Department of Neurosurgery, Neural Systems and Dynamics Laboratory, The David Geffen School of Medicine, University of California, Los Angeles, CA 90095, USA

Biomedical Engineering Graduate Program, Henry Samueli School of Engineering and Applied Science, University of California, Los Angeles, CA 90095, USA
e-mail: xhu@mednet.ucla.edu

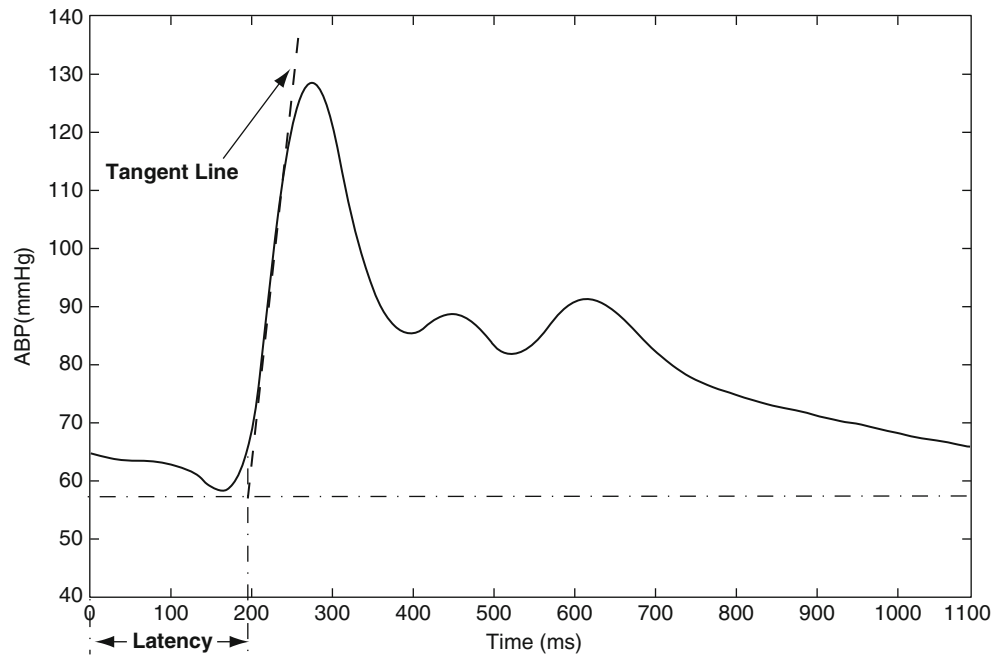
Introduction

For three decades, many clinical investigators have indicated that abnormalities of intracranial pulsations could play an important role in the pathophysiology of several neurological conditions (e.g., hydrocephalus) and have consequently employed the intracranial pressure (ICP) response to cardiac pulsations for characterization of compliance [5, 7, 10, 20]. In 1981, Foltz underlined the significance of intraventricular cerebral spinal fluid (CSF) pulsatility as the cause of hydrocephalus by showing that the power of intraventricular CSF pulsations is augmented by four times in chronic hydrocephalus [13, 14]. Since then, several interesting models of normal CSF pulsations have been proposed that relate CSF pulsatile flow to ICP, cerebral blood flow (CBF) or arterial blood pressure (ABP). While each model has its own specific set of assumptions, all of them suggest a major role of pulsatility in the cranium [4, 12, 14].

In 2000, Bateman reported decreased pulsatility at the cortical veins; measured for the first time in hydrocephalus patients, using magnetic resonance imaging (MRI) [3]. He suggested that reversible elevation in cortical vein pressure and reversal of the normal absorption pathway for CSF may be behind the pathophysiology of normal pressure hydrocephalus (NPH). Other studies have also employed the advanced magnetic resonance measurements of the transfer function between vascular pulsations and the pulsatile response of CSF to characterize intracranial mechanical factors [2, 8, 9, 18].

A recently proposed pulsatile CSF model postulates that the ICP pulse is a standing pulse and hence could even lead the carotid arterial pressure pulse if the mean ICP value is not high [11]. This theory has been shown to be valid to certain degree in animal data. To shed some light on the issue of timing of the ICP pulse, we test the following hypotheses in the present work, using a dataset of ICP and cerebral blood flow velocity (CBFV) signals collected from 60 patients with different neurological disorders: first, the ICP pulse onset latency would be lower than that of CBFV pulses measured at a distal vessel, regardless of mean ICP value; and second,

Fig. 1 Example of arterial blood pressure (ABP) pulse waveform recorded at the left radial artery and the estimated latency using an intersecting tangent line. $t=0$ corresponds to the onset of ventricular ejection (i.e., R-wave on the ECG)



the CBFV pulse at different intracranial arteries will have different pulse onset latencies (proportional to the distance of the measurement point to the heart). This study may help us to re-evaluate our current understanding of the way in which the ICP pulse is generated and processed. Consequently, it may affect the management of several neuropathological conditions not limited to hydrocephalus, e.g., traumatic brain injury (TBI) and arteriosclerosis.

Materials and Methods

Definition of Pulse Latency and Its Importance

To develop clinically viable tools that are capable of continuously assessing the cerebral vasculature, a focus of our laboratory has been to explore novel methods of extracting physiological information by analyzing continuously acquired signals of intracranial origin [16, 17]. Latency of the onset of a vascular pulse relative to an extracranial timing signal (i.e., time delay between the electrocardiogram (ECG) QRS peak and the initial inflection in the resulting blood pressure pulse) is one of the parameters that could be continuously extracted from an intracranial signal.

Moens–Korteweg equation (Pulse Wave Velocity = $PWV = \sqrt{\frac{Eh}{2\rho_b R}}$), establishes a deterministic relationship between

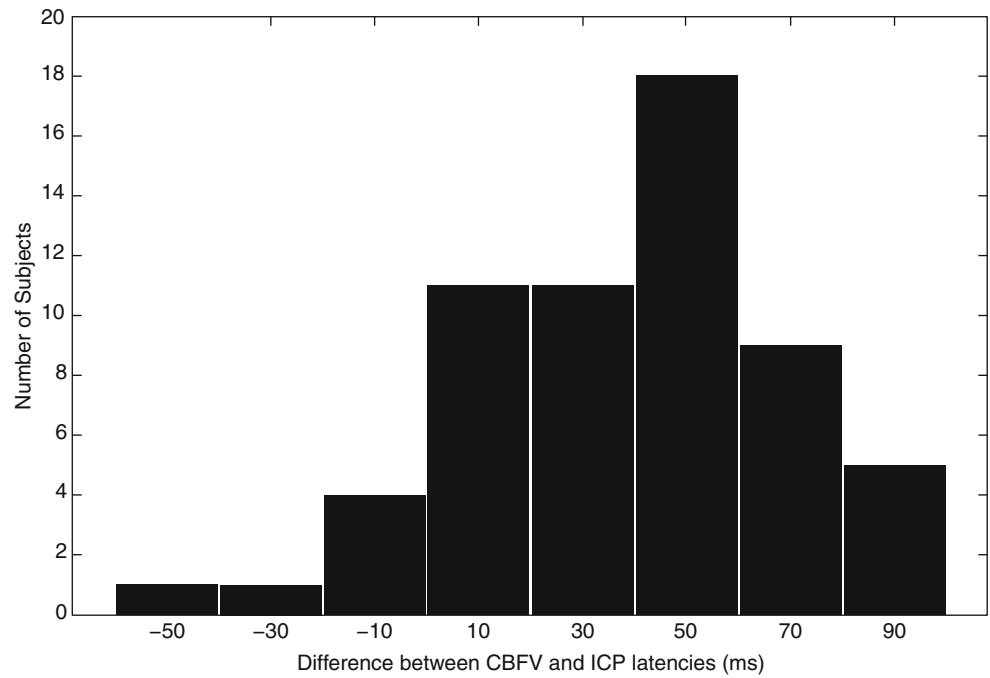
PWV (the velocity at which a blood pressure or a flow velocity pulse travels through the cerebral vasculature) and the basic properties of this vascular route, including Young's elastic modulus E , wall thickness h , internal radius R , and the

blood density ρ_b . As the changes in PWV would manifest with reciprocal changes in pulse waveform latency, the latency of a pulsatile intracranial signal could be considered to be a cerebrovascular index. Figure 1 shows an example of an ABP signal for one cardiac cycle and its extracted latency using the tangent intersect method [6].

Patient Data

The ECG, ICP, and CBFV data were collected from 60 inpatients including 20 female and 40 male, who were treated for various ICP-related conditions at UCLA Ronald Regan Medical Center; 21 cases of TBI, 21 cases of subarachnoid hemorrhage (SAH), 10 cases of hydrocephalus, 4 cases of intracerebral hemorrhage (ICH) and 4 cases of headaches. Patients' ages ranged from 18 to 89 years with the mean and standard deviation of 48 and 20 respectively. No explicit criteria were used to select the aforementioned patients other than the availability of ECG, ICP, and CBFV signals. ICP was monitored continuously using Codman intraparenchymal microsensors (Codman and Schurtleff, Raynaud, MA, USA) placed in the right frontal lobe. Simultaneous cardiovascular monitoring was performed using the bedside GE monitors and CBFV was measured using transcranial Doppler (TCD) machines (Multi-Dop X, Compumedics DWL, Singen, Germany). ICP, CBFV, and lead II of the ECG signals were archived using either a mobile cart at the bedside that was equipped with the PowerLab SP-16 data acquisition system (ADInstruments, Colorado Springs, CO, USA) with sampling frequency of 400 Hz or the BedMaster system

Fig. 2 Histogram of the latency difference between cerebral blood flow velocity (CBFV) and intracranial pressure (ICP) signals over 60 patients



that collects data (sampling frequency of 240 Hz) from the GE Unity network to which the bedside monitors were connected. The use of these archived waveform data in an anonymous fashion has been granted a waiver of consent by the UCLA IRB.

To verify the hypothesis that CBFV pulse at different intracranial arteries will have different pulse onset latencies (and hence they are not generated as a standing wave), the CBFV signal was measured for two healthy subjects (subject 1: a 24-year-old woman and subject 2: a 29-year-old man), at the following vessels: intracarotid artery (ICA), vertebral (VERT), posterior cerebral artery (PCA), middle cerebral artery (MCA), anterior cerebral artery (ACA).

Data Analysis

All the signals were time synchronized and re-sampled at 400 Hz. ECG QRS detection was performed using a previously published algorithm [1] on lead II of the ECG. Then, an ECG-aided pulse detection algorithm [17] was used to delineate each pulse of ICP and CBFV. In addition, each detected ICP and CBFV pulse was saved and visualized using the custom software developed in-house to screen obvious noise or artifacts, so that only clean beats were further processed. Latencies were measured from the onset of each clean pulse relative to ECG QRS as described in the previous subsection. Then all extracted latencies were corrected based on the subjects' heart rate using Weissler's regression equation [15, 22, 23].

Table 1 The mean and standard deviation of the heart rate corrected CBFV pulse latencies (in ms) measured at different intracranial arteries for two healthy subjects

Measured artery	Subject 1 (a 24-year-old woman)	Subject 2 (a 29-year-old man)
ICA	Not measured	140.3 ± 4.4
VERT	155.7 ± 4.6	152.2 ± 4.1
PCA	172.8 ± 6.6	Not measured
MCA	175.9 ± 5.6	169.2 ± 8.3
ACA	194.7 ± 9.4	167.4 ± 8.5

Results

The mean and standard deviation of the corrected ICP and CBFV latencies over all 60 patients were $120.85 \pm 29.6(ms)$ and $160.1 \pm 30.93(ms)$ respectively.

Figure 2 demonstrates the histogram of the corrected latency difference between CBFV and ICP (corrected CBFV latency – corrected ICP latency) over all 60 patients. The mean and standard deviation of this latency difference is $40 \pm 30(ms)$. As the histogram shows, only 6 out of 60 subjects had a negative latency difference. These subjects had a different diagnosis: two cases of TBI, two cases of ICH, one case of NPH, and one case of SAH. As a result, ICP pulse leads CBFV pulse measured at MCA for 90% of the patients in this study. A simple correlation analysis reveals that the amount of leading does not seem to be related to the mean ICP value ($\rho = -0.16, p = 0.22$).

Table 1 summarizes the results of the corrected CBFV pulse latencies measured at different intracranial arteries for

the two healthy subjects. We observe that the latency results for each of the two subjects are consistent with the distances of the measurement points to the heart ($Latency_{ICA} \leq Latency_{VERT} \leq Latency_{PCA} \leq Latency_{MCA} \leq Latency_{ACA}$). In other words, as the measurement point of CBFV at the ICA is closer to the heart than that of VERT, one would expect to have a shorter CBFV latency measured at ICA than at VERT. We also observe that the corrected CBFV latency measured at MCA for the two normal subjects is at least 12 ms longer than those of the patients (average of 160 ms). This observation is consistent with the fact that patients may have stiffer vessels and consequently a higher pulse wave velocity, which itself results in a shorter pulse latency.

As the mean of the corrected ICP latency for the patients was 120 ms; considering the latency difference between healthy subjects and the patients, we can conclude that the latency of ICP is close to the latency of the CBFV measured at the ICA; a point relatively closer to the heart than the MCA.

Discussion

While several clinical investigations have focused on studying the intracranial pulsations in hydrocephalus and the effect on treatment, there have only been a few studies that explain the underlying physiological causes [21]. In a recent study, Egnor et al. proposed that the ICP pulse is a standing wave and hence could even lead the carotid arterial pulse [11]. In addition, a negative correlation between mean ICP and the latency difference between the ICP and the carotid arterial pulse has been found in dogs when the mean ICP is not high.

Our results show that the ICP pulse leads CBFV measured at the MCA for 90% of the patients in the study and there is no significant correlation between the amount of leading and the value of mean ICP. Also, the results of a multi-vessel TCD study on two normal subjects revealed that CBFV pulse at different intracranial arteries have different pulse onset latencies that are proportional to the distance of the measurement point to the heart; hence, these pulsatile signals cannot be generated as standing waves.

The observation that the ICP pulse precedes the CBFV is counterintuitive, because, first, the location of the ICP measurement is further away from heart than that of the CBFV; and second, a flow pulse usually leads the pressure pulse [19]. We propose that the following factors could contribute to the observed leading phase of the ICP versus CBFV:

1. As the ICP pulse is the summation of all cerebral blood volume and CSF pulsations in the cranium, ICP pulse onset may be related to the arteries proximal to the heart.
2. The current definition of the onset of a pulse is not compatible for different pulses and needs to be modified accordingly.
3. Different analog filter settings on the amplifier of ICP and CBFV recording systems can affect the estimated latency of the pulses.

Conclusion

The latency relationship between the ICP and CBFV signals was described in studies in 60 patients with different neurological disorders. It was found that ICP pulse leads CBFV, but no significant correlation between mean ICP and the latency difference was observed. The leading phase of the ICP relative to the CBFV measured at the MCA could be explained by the fact that the ICP pulse is the summation of all cerebral blood volume and CSF pulsations in the cranium. As a result, ICP pulse onset may be related to the arteries proximal to the base of the skull rather than the MCA. An additional intracranial multi-vessel study on two normal subjects confirmed that the CBFV latency is roughly determined by the distance of the corresponding measurement site to the heart and thus intracranial pulsatile signal cannot be generated as a standing wave. Gaining a deeper insight into the mechanisms underlying the link between pulsations and hydrocephalus and other pathophysiological conditions involving the cerebral blood flow could be helpful in the design of therapies based on the regulations of intracranial dynamics.

Conflict of interest statement We declare that we have no conflict of interest.

References

1. Afonso VX, Tompkins WJ, Nguyen TQ, Luo S (1999) ECG beat detection using filter banks. *IEEE Trans Biomed Eng* 46:192–202
2. Alperin N, Vikingstad EM, Gomez-Anson B, Levin DN (1996) Hemodynamically independent analysis of cerebrospinal fluid and brain motion observed with dynamic phase contrast MRI. *Magn Reson Med* 35:741–754
3. Bateman GA (2003) The reversibility of reduced cortical vein compliance in normal-pressure hydrocephalus following shunt insertion. *Neuroradiology* 45:65–70
4. Bergsneider M, Alwan AA, Falkson L, Rubinstein EH (1998) The relationship of pulsatile cerebrospinal fluid flow to cerebral blood flow and intracranial pressure: a new theoretical model. *Acta Neurochir Suppl* 71:266–268
5. Cardoso ER, Rowan JO, Galbraith S (1983) Analysis of the cerebrospinal-fluid pulse-wave in intracranial-pressure. *J Neurosurg* 59:817–821
6. Chiu YC, Arand PW, Shroff SG, Feldman T, Carroll JD (1991) Determination of pulse wave velocities with computerized algorithms. *Am Heart J* 121:1460–1470

7. Chopp M, Portnoy HD (1980) Systems-analysis of intra-cranial pressure – comparison with volume-pressure test and csf-pulse amplitude analysis. *J Neurosurg* 53:516–527
8. Chu D, Levin DN, Alperin N (1998) Assessment of the biomechanical state of intracranial tissues by dynamic MRI of cerebrospinal fluid pulsations: a phantom study. *Magn Reson Imaging* 16:1043–1048
9. de Marco G, Idy-Peretti I, Didon-Poncelet A, Baledent O, Onen F, Feugeas MC (2004) Intracranial fluid dynamics in normal and hydrocephalic states: systems analysis with phase-contrast magnetic resonance imaging. *J Comput Assist Tomogr* 28:247–254
10. Dubin MJ, Magram G, Prasad AK (1998) Intracranial pressure waveform analysis: computation of pressure transmission and waveform shape indicators. *Neurol Res* 20:533–541
11. Egnor M, Wagshul M, McCormack E, McAllister P, Madsen J, Zou R, Zhen L, Peng J (2006) Pressure phase relationships between carotid arterial pressure and intracranial pressure: the ‘violin’ analogy of intracranial pulsations. 50th annual meeting of the Society for Research into Hydrocephalus and Spina Bifida Cambridge, UK.
12. Egnor M, Zheng L, Rosiello A, Gutman F, Davis R (2002) A model of pulsations in communicating hydrocephalus. *Pediatr Neurosurg* 36:281–303
13. Foltz EL, Aine C (1981) Diagnosis of hydrocephalus by CSF pulse-wave analysis: a clinical study. *Surg Neurol* 15:283–293
14. Greitz D (2004) Radiological assessment of hydrocephalus: new theories and implications for therapy. *Neurosurg Rev* 27:145–165, discussion 166–147
15. Hassan S, Turner P (1983) Systolic time intervals: a review of the method in the non-invasive investigation of cardiac function in health, disease and clinical pharmacology. *Postgrad Med J* 59:423–434
16. Hu X, Subudhi AW, Xu P, Asgari S, Roach RC, Bergsneider M (2009) Inferring cerebrovascular changes from latencies of systemic and intracranial pulses: a model-based latency subtraction algorithm. *J Cereb Blood Flow Metab* 29:688–697
17. Hu X, Xu P, Lee DJ, Vespa P, Baldwin K, Bergsneider M (2008) An algorithm for extracting intracranial pressure latency relative to electrocardiogram R wave. *Physiol Meas* 29:459–471
18. Miyati T, Mase M, Banno T, Kasuga T, Yamada K, Fujita H, Koshida K, Sanada S, Onoguchi M (2003) Frequency analyses of CSF flow on cine MRI in normal pressure hydrocephalus. *Eur Radiol* 13:1019–1024
19. Nichols WW, O'Rourke MF (2005) McDonald's blood flow in arteries: theoretical, experimental and clinical principles. Hodder Arnold, London
20. Piper IR, Chan KH, Whittle IR, Miller JD (1993) An experimental study of cerebrovascular resistance, pressure transmission, and craniospinal compliance. *Neurosurgery* 32:805–815, discussion 815–806
21. Wagshul ME, Kelly EJ, Yu HJ, Garlick B, Zimmerman T, Egnor MR (2009) Resonant and notch behavior in intracranial pressure dynamics. *J Neurosurg Pediatr* 3:354–364
22. Weissler AM, Harris WS, Schoenfeld CD (1968) Systolic time intervals in heart failure in man. *Circulation* 37:149–159
23. Weissler AM, Kamen AR, Bornstein RS, Schoenfeld CD, Cohen S (1965) The effect of deslanoside on the duration of the phases of ventricular systole in man. *Am J Cardiol* 15:153–161

The Linear Relationship Between Transcranial Doppler Pulsatility Indices and Intracranial Pressure Is Influenced by Traumatic Brain Injury and Vasospasm

Thomas C. Glenn, Arun K. Sherma, David L. McArthur, Xiao Hu, Christopher R. Hanuscin, Mehjabeen S. Furreedan, David A. Hovda, Paul M. Vespa, and Neil A. Martin

Abstract The pulsatility index (PI) and the intracranial pressure (ICP) may or may not be correlated; the evidence to date differs widely. A study of multiple measures of PI and the corresponding ICP in patients with severe traumatic brain injury (TBI) showed that some of the relationships were moderately strong when calculated as conventional Pearson correlation coefficients. However, that method makes no adjustment of any kind for statistical outliers in the data. With the TBI patients demonstrating a large fraction of skewed measurements, a set of robust correlations were calculated that demonstrated that the apparent relationships between PI and ICP were entirely attributable to the statistical outliers. We conclude that the fundamental relationship of PI to ICP is weakly positive at best.

Keywords Traumatic brain injury • Vasospasm • Craniectomy • Pulsatility index • Intracranial pressure • Transcranial Doppler

Introduction

Developing a noninvasive technique for measuring human intracranial pressure (ICP) has been a goal for many scientists and clinicians. One such technique that has garnered interest over three decades has been transcranial Doppler (TCD). TCD is a device that transmits and receives, from the red blood cells in the major cerebral arteries, ultrasound waves representing cerebral blood flow velocities. A wave form spectrum of the velocities during a cardiac cycle yields useful information such as peak systolic and peak diastolic

velocities and calculations such as the Gosling pulsatility index (PI) can be derived [4, 11]. It is the relationship between the PI and ICP that has generated the greatest interest in non-invasive ICP determination.

Several studies in a variety of patient types have determined that a moderate to strong positive correlation exists between PI and ICP [6, 7, 10, 12, 14]. One of the most recent studies conducted in a mixed population of intensive care (ICU) patients reported a significant coefficient of $r=0.94$ between PI and ICP. However, other recent studies in normal pressure hydrocephalus and pediatric trauma patients have indicated that the PI and ICP correlations were weak, with an $R^2=0.22$ and $r=0.4$ respectively [5, 9]. Thus, there is no current consensus in the literature on the utility of PI to correlate with ICP in patients in the ICU setting.

The purpose of this study was to investigate the relationship between the PIs of the major cerebral arteries and ICP in patients with severe traumatic brain injury (TBI). Additionally, potential confounding factors such as gender, vasospasm, and surgery were investigated.

Materials and Methods

Patient Enrollment

Eligible patients included severe (Glasgow Coma Scale [GCS] <9) TBI patients aged 14 and over who were admitted to the UCLA Medical Center. Surrogate consent was obtained from the patients' legal representatives and the research protocol was approved by the UCLA Medical Institutional Review Board.

Patient Management

Our management protocol has been previously published [1]. Ventriculostomy catheters are placed for all GCS <12 with suspected elevated ICP. ICP was kept below 20 mmHg

T.C. Glenn (✉), A.K. Sherma, D.L. McArthur, X. Hu, C.R. Hanuscin, M.S. Furreedan, D.A. Hovda, P.M. Vespa, and N.A. Martin
Department of Neurosurgery,
David Geffen School of Medicine
at the University of California-Los Angeles,
10833, Le Conte Avenue, Los Angeles,
CA 90095-7039, USA
e-mail: tglenn@mednet.ucla.edu

using a stepwise management strategy. The order to ICP treatment is:

1. Cerebrospinal fluid (CSF) drainage for ICP > 20 mmHg × 5 min up to 10 cm³/h
2. Moderate hyperventilation with PCO₂ 20–24 mmHg
3. Continuous 3% NaCl to keep Na > 140 mEq/dL
4. Continuous sedation with midazolam 2–10 mg/h to avoid agitation
5. Normothermia to temperature 36.5–37°C through the use of medication and intravascular and surface cooling devices

If ICP continues to be elevated > 20 mmHg, then a jugular venous oximetry (SJO₂) was performed to monitor for jugular venous desaturation and blood pressure was adjusted to keep the SJO₂ between 60 and 70%. Cerebral perfusion pressure is kept > 60 mmHg using norepinephrine, if needed. If ICP continues to be elevated, then barbiturate coma is used to induce burst suppression on EEG.

Measurement Techniques of Physiological Parameters

Transcranial Doppler Ultrasound

Vessels, including the middle cerebral artery (MCA), anterior cerebral artery (ACA), posterior cerebral artery (PCA), extracranial internal carotid artery (ICA), and vertebral artery (VA), were insonated bilaterally, along with the basilar artery (BA), using the general method described by Aaslid et al. [2, 3]. Recordings were performed using a 2-MHz pulsed probe and a commercially available TCD unit (Neuroguard Cerebrovascular Diagnostic System, Nicolet Biomedical, Inc., Madison, WI, USA or Multi-Dop X, Compumedics DWL, Singen, Germany). Mean flow velocity values represent an average over four cardiac cycles. Gosling's PI was calculated automatically for each recording using the formula of peak systolic velocity minus peak diastolic velocity divided by mean velocity. ICP values were measured via ventricular catheter (Medtronic, Minneapolis, MN, USA).

Cerebral Blood Flow Measurements

Cerebral blood flow measurements were performed using the intravenous ¹³³Xe clearance technique with a portable, commercially available apparatus (Cerebrograph Cortexplorer, Ceretronix, Randers, Denmark) as previously described [13]. CBF₁₅, an index of mean gray and white matter flow, was determined according to Obrist and Wilkinson [15]. Mean right and left CBF₁₅ values (uncorrected for arterial pCO₂) were obtained by averaging five or eight regional detectors placed over each hemisphere. Coordinated TCD and CBF studies were performed sequentially as simultaneous measurements were technically not feasible.

Cerebral Vasospasm

Vasospasm was defined as MCA velocities greater than 120 cm/s, a Lindegaard ratio (MCA/ICA) greater than 3, and a spasm index (MCA/CBF₁₅) of greater than 3.4 [16].

Statistical Analysis

Pearson correlations and robust correlations using the method called percentage bend correlation [17] were computed between PI obtained at each of 13 separate standard anatomical locations within the skull and the ICP measure. Useful here precisely because measures of PI are frequently highly skewed even if valid, the percentage bend correlation, part of the more general statistical family called M estimators, is not overly sensitive to changes in distributions and outliers. Logistic regression was also used in this study to examine the possible predictability of elevated ICP (> 20 mmHg) by PI. R version 2.11.1 (R Core Development Team, 2010) was used for all analyses.

Results

Patient Demographics

Ninety-nine patients (mean age 36.1 ± 16.9 years) with concurrent ICP (532 total measurements) and TCD measurements (4,582 total PI measurements) were studied. The mean number of concurrent studies was 5.4 per patient (range 1–11) with a mean number of PI measurements of 46.3 per patient (range 8–137). Twenty subjects were female and 79 were male.

Correlation Analyses

Statistically, PI was skewed by the presence of a total of 430 values (9.4% of the 4582 measured) exceeding a robust maximum (the upper whisker of the corresponding boxplot) up to fourfold. As the Pearson correlation makes no correction whatsoever for outliers, the Pearson and robust correlation calculations often yielded values that differed substantially from one another. Importantly, there were only three instances, each contributed by different participants, in which all of the available PI measures for a given recording session exceeded the corresponding upper whiskers (0.5% of 532 sessions). The results of both Pearson and robust correlation analyses for the entire dataset are shown in Table 1. All cerebral artery PIs correlated positively with ICP to varying degrees. Overall, the right middle cerebral artery (RMCA) PI had the strongest Pearson correlation with ICP, $r = 0.45$; however, when the robust correlation, which decreases the

Table 1 Correlations of pulsatility index (PI) with intracranial pressure (ICP) for all cases, by gender, and by vasospasm

PI	All cases		Gender		Females		Vasospasm		Yes	
			Males				No			
	Pearson r	Robust r	Pearson r	Robust r	Pearson r	Robust r	Pearson r	Robust r	Pearson r	Robust r
RMCA	0.452	0.127	0.372	0.171	0.619	0.008	0.482	0.139	0.343	0.330
RACA	0.275	0.133	0.288	0.173	0.310	0.049	0.287	0.144	0.183	0.203
RPCA	0.225	0.142	0.369	0.188	-0.136	-0.006	0.222	0.139	0.293	0.301
RICA	0.100	0.089	0.132	0.145	0.057	-0.054	0.097	0.079	0.103	0.176
RVERT	0.373	0.176	0.429	0.238	-0.150	-0.043	0.342	0.159	0.017	0.072
BAS	0.312	0.173	0.392	0.270	-0.225	-0.220	0.336	0.224	-0.223	-0.092
LMCA	0.334	0.115	0.298	0.175	0.481	-0.036	0.358	0.150	0.203	0.181
LACA	0.243	0.114	0.309	0.179	-0.008	-0.064	0.269	0.140	0.071	0.129
LPCA	0.373	0.160	0.459	0.238	-0.060	-0.121	0.398	0.158	0.15	0.254
LICA	0.162	0.100	0.206	0.161	0.112	-0.054	0.164	0.094	0.035	0.022
LVERT	0.239	0.119	0.314	0.196	-0.246	-0.241	0.215	0.078	0.045	-0.004

Note: Robust correlations computed as percentage bend correlations [17]

RMCA right middle cerebral artery, RACA right anterior cerebral artery, RPCA right posterior cerebral artery, RICA right internal carotid artery, RVERT right vertebral artery, LMCA left middle cerebral artery, LACA left anterior cerebral artery, LPCA left posterior cerebral artery, LICA left internal carotid artery, LVERT left vertebral artery

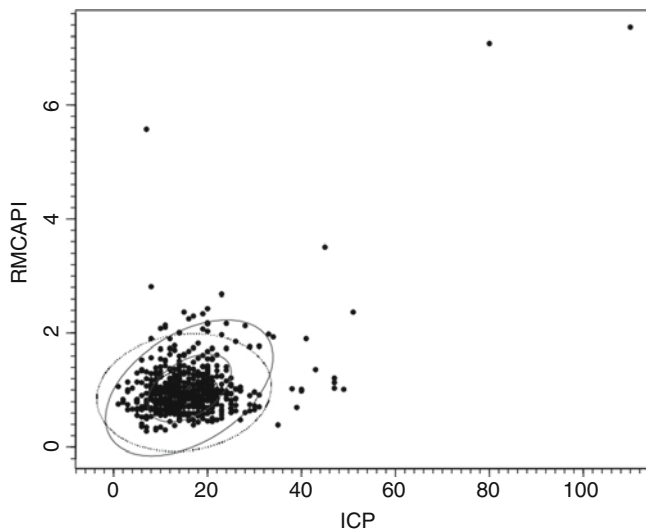


Fig. 1 Dotplot of intracranial pressure (ICP) and right middle cerebral artery (RMCA) pulsatility index (PI). Pearson $r=0.452$; 95% confidence ellipse shown by a solid line. Robust $r=0.127$; 95% confidence ellipse shown by the dotted line. The difference between these correlations is wholly due to how statistical outliers are treated

leverage caused by outliers, was used, then the coefficient was dramatically smaller, $r=0.13$ (Fig. 1).

Logistic Regression Analysis

As 20 mmHg is considered a clinical target for ICP control, a logistic regression analysis was performed to determine if PI could predict a threshold value of 20 mmHg. One hundred and nine values were greater than or equal to an ICP of 20 mmHg. No PI significantly predicted an ICP over 20 mmHg.

Correlates of Gender

When categorized by gender, the correlations between the PIs and ICP were different than for the entire dataset (Table 1). Although female patients showed a stronger Pearson correlation than male patients for the RMCA PI and ICP, by contrast, correlation of the other PIs with ICP were weaker and in some cases negative. Furthermore, the robust correlations showed that the correlations were weaker for female patients than male patients.

Consequences of Cerebral Vasospasm

For this study population, a stringent definition for cerebral vasospasm (see “[Materials and methods](#)”) was used which included both TCD and CBF measurements. Eighteen

patients showed at least one incidence of cerebral vasospasm. Vasospasm resulted in a significantly lower Pearson correlation, yet variably greater robust correlation between PI and ICP (Table 1).

Effects of Neurological Surgery

When patients were categorized into three groups, those being No Surgery ($n=43$ patients), Craniotomy ($n=34$ patients), or Craniectomy ($n=22$ patients), both the No Surgery and Craniectomy groups showed significant weak Pearson correlations between PI and ICP, while the Craniotomy did not (Table 2). When a robust analysis was performed the Craniectomy group showed the strongest positive correlations while the other two groups showed very weak correlations.

Discussion

The overall findings of this study indicate that positive yet weak correlations exist between TCD PI values and ICP. With a more stringent statistical tool that diminishes the leverage caused by outliers, the correlations become even weaker. Additionally, as the Guidelines for the Management of Severe Traumatic Brain Injury [1] recommend a target ICP goal of 20 mmHg, we determined that PI was not a good predictor of treatment threshold ICP values. When other factors such as gender, vasospasm, and type of neurological surgery were considered, unique differences in the strength of the correlations between PI and ICP were observed. Thus, TBI patients did not respond similarly.

An important question to consider is why so much variability exists between published results for the relationship between PI and ICP. Earlier studies by Chan et al. [8] found that cerebral perfusion pressure correlated better with PI than ICP. Another reason, emphasized in this study, is the type of statistical analysis employed. As stated above, Pearson correlations can be strongly influenced by outlying values, while robust correlations are designed to reduce or eliminate that influence. Pearson and robust correlations thus did not always lead to the same conclusions, as was seen in the comparison between presence and absence of vasospasm. Therefore, reliance on only one statistical test may overstate the strength of the results. As these analyses point out, the number and extent of outliers play a large role in determining the difference. For example, while a very high ICP might be associated with a very high PI (and serve to leverage the Pearson correlation) the frequency of pairs of values in this range is very low (and such pairs are downweighted by the robust correlation).

Table 2 Correlation analyses of PI with ICP by surgery group

PI	Operation					
	None		Craniotomy		Craniectomy	
	Pearson <i>r</i>	Robust <i>r</i>	Pearson <i>r</i>	Robust <i>r</i>	Pearson <i>r</i>	Robust <i>r</i>
RMCA	0.554	0.026	0.035	0.025	0.508	0.323
RACA	0.268	0.078	0.017	−0.033	0.403	0.313
RPCA	−0.005	0.048	0.032	−0.013	0.488	0.377
RICA	0.133	0.024	−0.023	0.017	0.131	0.200
RVERT	0.275	0.009	−0.025	0.050	0.571	0.438
BAS	0.315	0.369	−0.002	0.015	0.514	0.354
LMCA	0.437	0.034	−0.065	−0.074	0.410	0.396
LACA	0.12	0.065	−0.056	−0.080	0.476	0.345
LPCA	0.136	0.045	0.003	−0.017	0.601	0.396
LICA	0.13	0.129	0.016	0.015	0.269	0.308
LVERT	0.11	0.011	0.011	−0.053	0.596	0.334

Note: Robust correlations are computed as percentage bend correlations [17]

There were several limitations to the study design. First, not all patients were studied identically, i.e., each patient did not have the same number of studies. Not all arteries could be insonated on every study day. For example, if the cervical spine had not been cleared and a neck brace was present, then the posterior arteries (basilar and vertebrals) could not be studied.

Conclusion

Regardless of the statistical technique used, the correlations between PI and ICP can be best described as moderate to nil. Thus, the clinical usefulness of TCD as a predictor of ICP is also weak. More sophisticated analyses of TCD and ICP waveforms may yield more clinically useful results.

Acknowledgements This work was supported by the University of California Neurotrauma Initiative and NIH/NINDS 1P01NS058489-01.

Conflict of interest statement We declare that we have no conflict of interest.

References

- Brain Trauma Foundation, American Association of Neurological Surgeons, Congress of Neurological Surgeons, Joint Section on Neurotrauma and Critical Care, AANS/CNS. (2007) Guidelines for the management of severe traumatic brain injury, ed 3. *J Neurotrauma* 24 (Suppl 1):S1–S106
- Aaslid R, Markwalder TM, Nornes H (1982) Noninvasive transcranial Doppler ultrasound recording of flow velocity in basal cerebral arteries. *J Neurosurg* 57:769–774
- Aaslid R, Huber P, Nornes H (1984) Evaluation of cerebrovascular spasm with transcranial Doppler ultrasound. *J Neurosurg* 60: 37–41
- Beasley MG, Blau JN, Gosling RG (1979) Changes in internal carotid artery flow velocities with cerebral vasodilation and constriction. *Stroke* 10:331–335
- Behrens A, Lenfeldt N, Ambarki K, Malm J, Eklund A, Koskinen LO (2010) Transcranial Doppler pulsatility index: not an accurate method to assess intracranial pressure. *Neurosurgery* 66:1050–1057
- Bellner J, Romner B, Reinstrup P, Kristiansson KA, Ryding E, Brandt L (2004) Transcranial Doppler sonography pulsatility index (PI) reflects intracranial pressure (ICP). *Surg Neurol* 62:45–51, discussion 51
- Boishardy N, Granry JC, Jacob JP, Houi N, Fournier D, Delhumeau A (1994) Value of transcranial Doppler ultrasonography in the management of severe head injuries. *Ann Fr Anesth Reanim* 13: 172–176
- Chan KH, Miller JD, Dearden NM, Andrews PJ, Midgley S (1992) The effect of changes in cerebral perfusion pressure upon middle cerebral artery blood flow velocity and jugular bulb venous oxygen saturation after severe brain injury. *J Neurosurg* 77:55–61
- Figaji AA, Zwane E, Fieggen AG, Siesjo P, Peter JC (2009) Transcranial Doppler pulsatility index is not a reliable indicator of intracranial pressure in children with severe traumatic brain injury. *Surg Neurol* 72:389–394
- Goh D, Minns RA, Pye SD, Steers AJ (1991) Cerebral blood flow velocity changes after ventricular taps and ventriculoperitoneal shunting. *Childs Nerv Syst* 7:452–457
- Gosling RG, King DH (1974) Arterial assessment by Doppler-shift ultrasound. *Proc R Soc Med* 67:447–449
- Homburg AM, Jakobsen M, Enevoldsen E (1993) Transcranial Doppler recordings in raised intracranial pressure. *Acta Neurol Scand* 87:488–493
- Martin NA, Alsina G, Kordestani R, Lee JH (1996) The Simonsen cerebrograph cortexplorer. *Neurosurgery* 39:1059–1061
- Moreno JA, Mesalles E, Gener J, Tomasa A, Ley A, Roca J, Fernandez-Llamazares J (2000) Evaluating the outcome of severe head injury with transcranial Doppler ultrasonography. *Neurosurg Focus* 8:e8
- Obrist WD, Wilkinson WE (1990) Regional cerebral blood flow measurement in humans by xenon-133 clearance. *Cerebrovasc Brain Metab Rev* 2:283–327
- Oertel M, Boscardin WJ, Obrist WD, Glenn TC, McArthur DL, Gravori T, Lee JH, Martin NA (2005) Posttraumatic vasospasm: the epidemiology, severity, and time course of an underestimated phenomenon: a prospective study performed in 299 patients. *J Neurosurg* 103:812–824
- Wilcox RR (2005) Introduction to robust estimation and hypothesis testing. Elsevier, New York

Time Constant of the Cerebral Arterial Bed

Magdalena Kasprowicz, Jennifer Diedler, Matthias Reinhard, Emmanuel Carrera, Peter Smielewski, Karol P. Budohoski, Enrico Sorrentino, Christina Haubrich, Peter J. Kirkpatrick, John D. Pickard, and Marek Czosnyka

Abstract We have defined a novel cerebral hemodynamic index, a time constant of the cerebral arterial bed (τ), the product of arterial compliance (C_a) and cerebrovascular resistance (CVR). C_a and CVR were calculated based on the relationship between pulsatile arterial blood pressure (ABP) and transcranial Doppler cerebral blood flow velocity. This new parameter theoretically estimates how fast the cerebral arterial bed is filled by blood volume after a sudden change in ABP during one cardiac cycle. We have explored this concept in 11 volunteers and in 25 patients with severe stenosis of the internal carotid artery (ICA). An additional group of 15 subjects with non-vascular dementia was studied to assess potential age dependency of τ . The τ was shorter ($p = 0.011$) in ICA stenosis, both unilateral ($\tau = 0.18 \pm 0.04$ s) and bilateral ($\tau = 0.16 \pm 0.03$ s), than in controls ($\tau = 0.22 \pm 0.0$ s). The τ correlated with the degree of stenosis ($R = -0.62, p = 0.001$). In controls, τ was independent of age. Further study during

cerebrovascular reactivity tests is needed to establish the usefulness of τ for quantitative estimation of haemodynamics in cerebrovascular disease.

Keywords Cerebrovascular haemodynamics • Internal carotid artery occlusive disease • Transcranial Doppler

Introduction

Transcranial Doppler ultrasound (TCD) offers the non-invasive and relatively simple investigation of cerebral haemodynamics at the level of the basal cerebral arteries. Several TCD-based haemodynamics indices have been introduced before [1, 8, 9, 12, 14]; however, their ability to quantify cerebrovascular haemodynamics is limited and the lack of their ambiguous interpretation generates considerable controversy in the literature. In this study we proposed a novel ultrasound-based index termed ‘time constant of the cerebral arterial bed’ (τ). This parameter theoretically estimates how fast arterial blood volume stabilizes during a step-change in arterial blood pressure (ABP). It is a product of arterial compliance (C_a) and resistance (CVR) of the cerebral vasculature. An important advantage of τ is its clear physical interpretation and independence of the cross-sectional area of the insonated vessel. We hypothesized that chronic states, such as a stenosis of the carotid artery, might affect the time constant. To test this hypothesis we compared τ in healthy volunteers and patients with ICA stenosis, both unilateral and bilateral.

Materials and Methods

In total, 51 subjects have been studied. Twenty-five patients (20 male and 5 female, median age: 62 years, range 47–77) with occlusive disease of one or both internal carotid arteries demonstrated by angiography. Measurement of stenosis was performed using the North American angiographic protocol.

M. Kasprowicz
Academic Neurosurgical Unit, Addenbrooke’s Hospital,
Box 167, Cambridge CB2 2QQ, UK and
Institute of Biomedical Engineering and Instrumentation,
Wroclaw University of Technology, Wroclaw, Poland

J. Diedler
Academic Neurosurgical Unit, Addenbrooke’s Hospital,
Box 167, Cambridge CB2 2QQ, UK and
Department of Neurology, University of Heidelberg,
Heidelberg, Germany

M. Reinhard
Department of Neurology, University of Freiburg,
Freiburg, Germany

E. Carrera, P. Smielewski, K.P. Budohoski, E. Sorrentino,
P.J. Kirkpatrick, J.D. Pickard, and M. Czosnyka (✉)
Academic Neurosurgical Unit, Addenbrooke’s Hospital,
Box 167, Cambridge CB2 2QQ, UK
e-mail: mc141@medschl.cam.ac.uk

C. Haubrich
Academic Neurosurgical Unit, Addenbrooke’s Hospital,
Box 167, Cambridge CB2 2QQ, UK

Department of Neurology, University Hospital Aachen,
Aachen, Germany

Sixteen patients had unilateral ICA stenosis (median stenosis 84.5%, range 50–100% on one side). Nine patients had bilateral disease (median stenosis 95%, range 50–100% on both sides). Among the 16 unilateral cases 15 had symptoms consistent with the side of stenosis and 1 presented with no symptoms. Of nine patients with bilateral carotid disease three patients had bilateral symptoms, four had unilateral symptoms, and two were asymptomatic. Eleven normal volunteers (8 male, 3 female, median age 21 years, range: 20–41) were included in the study as a control group. To assess the possible dependence between age and τ , data from young volunteers were compared with those of 15 subjects (2 female and 13 male, median age: 68, range 44–73) with no evidence of extracranial vascular diseases (4 patients were diagnosed from NPH and 11 patients suffered from dementia). These subjects were age-matched to carotid disease patients. All patients and volunteers underwent simultaneous recording of middle cerebral artery (MCA) blood flow velocity (CBFV) and arterial blood pressure (ABP). MCA CBFV was recorded bilaterally using transcranial Doppler ultrasound (TCD) with two 2-MHz probes attached with a headband (Neuroguard, 2 MHz, Medasonics, Fremont, CA, USA). ABP was measured non-invasively (Finapres, Ohmeda 2300; BOC Group Inc., Englewood, CO, USA) via a miniature cuff placed around the middle finger of the left hand at the level of the heart. Measured signals were digitized and stored by ICM+ software (Cambridge University, UK, <http://www.neurosurgery.cam.ac.uk/icmpls>). Patients with carotid artery disease were examined in the Cerebrovascular Clinic, Addenbrooke's Hospital, Cambridge, UK (PJK). Material was analyzed anonymously, as a part of a standard clinical audit and no individual consent was required at the time of recording. Recordings in volunteers (healthy, young) and in patients with non-vascular dementia were approved by the local ethics committee and individual consents were obtained.

Data Analysis

The concept of τ originates from a measure known in physics and electronics as a time constant in an electrical RC (resistor–capacitor) circuit and it is the time response of the circuit when a change in voltage or signal is applied. We simplified the complex system of cerebral blood flow circulation into a basic circuit consisting of a single resistor and capacitor representing CVR and C_a respectively. Hence, cerebrovascular τ can be evaluated, by analogy with an electrical RC circuit, as a product of compliance of the cerebral arterial bed (C_a) and cerebrovascular resistance (CVR):

$$\tau = C_a \times \text{CVR} [\text{s}] \quad (1)$$

In our study the compliance of the cerebral arterial bed (C_a) and cerebrovascular resistance (CVR) was estimated based on a mathematical model [4] of the relationship between pulsatile ABP and TCD flow velocity (CBFV) signals.

$$C_a = \frac{\text{Amp}_{C_a \text{BV} \times S_a}}{\text{Amp}_{\text{ABP}}} \left[\frac{\text{cm}^2 \times \frac{\text{cm}}{\text{s}} \times \text{s}}{\text{mmHg}} \right] \quad (2)$$

$$\text{CVR} = \frac{\text{meanABP}}{\text{meanCBFV} \times S_a} \left[\frac{\text{mmHg}}{\frac{\text{cm}}{\text{s}} \times \text{cm}^2} \right] \quad (3)$$

Estimation of arterial cerebral blood flow ($\text{CBF}_a = \text{mean CBFV} \times S_a$) and cerebral arterial blood volume ($C_a \text{BV}$), needed for calculation of C_a and CVR from CBFV, requires knowledge of the cross-sectional area of the insonated vessel (S_a) [11] (see Eqs. 2 and 3). In most studies the assumption of an unchanging vessel caliber is made [2, 5, 6, 10, 13]. However, a consequence of the unknown diameter of arterial vessels is that $C_a \text{BV}$ and CBF_a cannot be calibrated. A multiplication of C_a by CVR enables the unknown parameter (S_a) to be eliminated from calculation, and then τ can be calibrated in seconds. The methodology of CaBV , C_a , and CVR calculation was described in detail in our previous studies [5, 10]. An example of the waveforms of CBFV_a , ABP and $C_a \text{BV}$ is presented in Fig. 1.

Statistical Analysis

One-way ANOVA with post-hoc comparison (Fisher LSD test) was used to compare mean τ across three groups of subjects:

1. Patients with ICA unilateral stenosis (separately on the ipsi- and contralateral sides to the occluded artery)
2. Patients with ICA bilateral stenosis (the side with a higher percentage of stenosis was taken into consideration)
3. Healthy volunteers

The t test for dependent samples was utilized to analyze differences in means of parameters between the ipsilateral and contralateral sides, in the case of unilateral ICA stenosis, and the left vs. the right side in volunteers. The relationships between the cerebrovascular reactivity indexes and the degree of stenosis or τ as well as the age dependency of τ were assessed based on Pearson's correlation coefficient. The level of significance was set at 0.05.

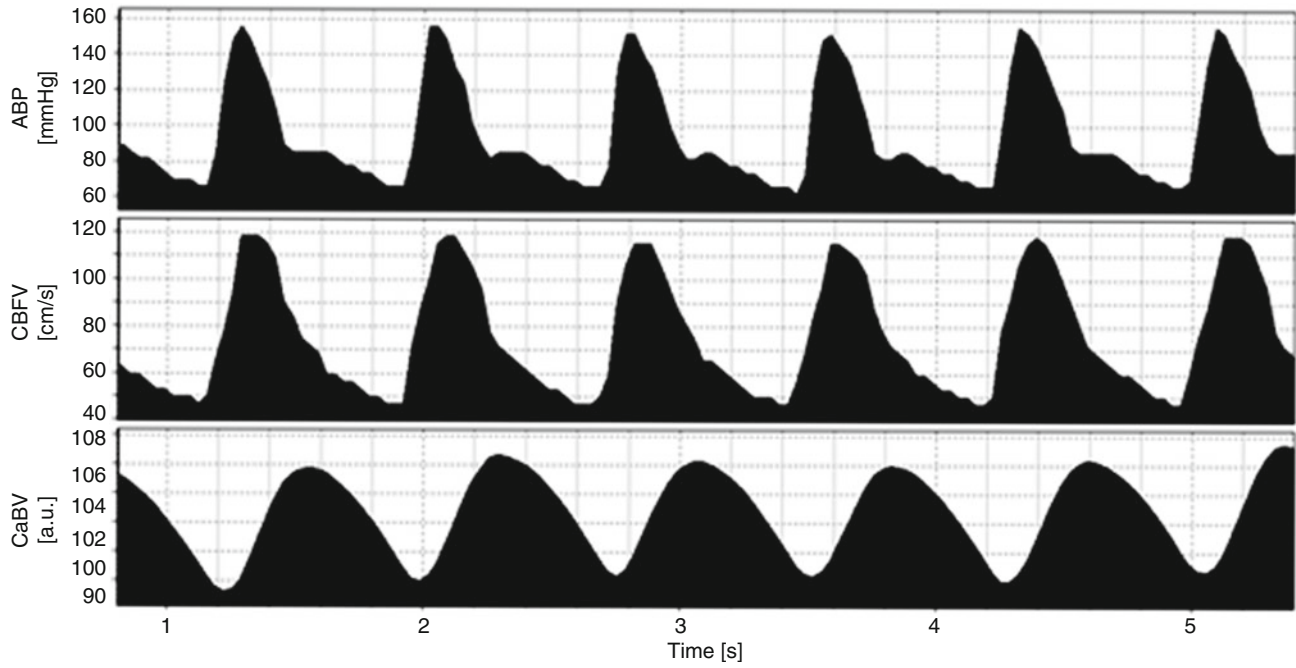


Fig. 1 Example of waveforms: arterial blood pressure $ABP(t)$, cerebral arterial blood flow velocity $CBFV_a(t)$, and cerebral arterial blood volume $CaBV(t)$, indicating that all signals have a clear pulsatile component (fundamental frequency equal to a heart rate), which is used for

calculation of compartmental compliance C_a . Note that $CaBV$ has been expressed in arbitrary units: percentage of the deviation from the mean value, which is caused by an unknown cross-sectional area of the middle cerebral artery (MCA) (S_a)

Table 1 Comparison of the parameters analyzed at different levels of $EtCO_2$ for three groups: healthy volunteers, unilateral internal carotid artery (ICA) stenosis and bilateral ICA stenosis

	Volunteers	Unilateral stenosis		Bilateral stenosis	p
		Contra	Ipsi		
ABP [mmHg]	90.1 ± 14.9	90.6 ± 14.7		83.4 ± 14.1	n.s.
Amp_{ABP} [mmHg]	10.9 ± 2.1	21.1 ± 5.0		21.1 ± 6.6	$= 0.0001$
CBFV [cm/s]	65.8 ± 12.8	61.4 ± 16.1	51.8 ± 16.9	54.5 ± 23.4	n.s.
τ [s]	0.22 ± 0.06	0.21 ± 0.04	0.18 ± 0.04	0.16 ± 0.03	$= 0.011$

Values are means \pm SD. The p value refers to analysis of variance

Results

The longest τ was presented by normal subjects (Table 1) and was significantly shortened in patients with both unilateral stenosis on the ipsilateral side and patients with bilateral stenosis (Fig. 2). Patients with more severe stenosis presented significantly shorter τ ($R = -0.62$, $p = 0.001$). In the case of unilateral stenosis τ was significantly shorter on the ipsilateral side than on the contralateral side ($p = 0.001$). There was no difference in τ between the left and right sides in volunteers.

There was no significant difference in τ between 11 young volunteers and the group of 15 patients with non-vascular dementia (0.22 ± 0.06 s vs. 0.25 ± 0.02 s, $p = 0.46$). There was also no significant correlation between age and τ when these two groups were analyzed jointly.

Discussion

We introduced a new method for continuous (changes in the time constant can be monitored on heartbeat to heartbeat basis), non-invasive monitoring of the time constant of the cerebral arterial bed (τ). We found that in patients with ICA stenosis τ was significantly shorter on the ipsilateral side and on the more stenotic side in the case of bilateral disease in comparison with normal subjects. No such difference was found for the contralateral side. Additionally, we found that τ correlated with the degree of stenosis: patients with more severe stenosis (as a percentage) demonstrated shorter τ . Comparison with the age-matched patients in the control group did not show any evidence of dependency between τ and age. Although all these findings suggest the suitability of

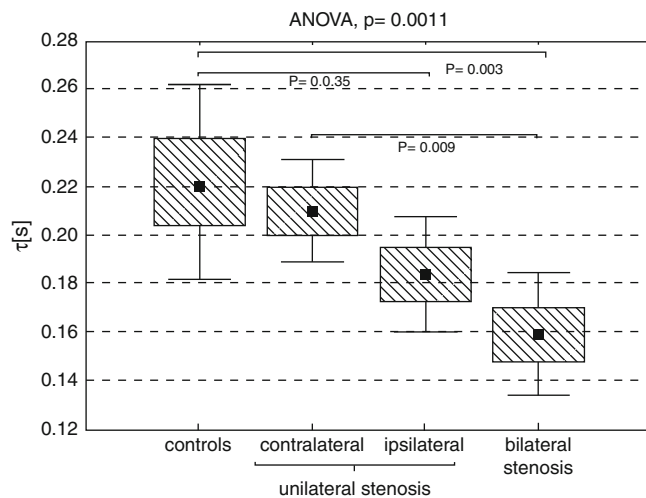


Fig. 2 Mean \pm SE (box) \pm 95% confidence interval (whiskers) of the time constant of the cerebral arterial bed (τ) obtained for: controls, patients with unilateral ICA stenosis (contralateral and ipsilateral sides) and patients with bilateral stenosis. In addition to the p value resulting from ANOVA analysis, the significant post-hoc differences are marked to determine which specific pairs are differentially expressed

τ as an index of hemodynamic dysfunction in cerebrovascular disease, further study is needed to establish its usefulness and validity, e.g. during cerebrovascular reactivity tests such as $p\text{CO}_2$ or acetazolamide challenge. More research is required to determine whether the time constant of the cerebral arterial bed might be useful to identify ICA patients at high risk of subsequent stroke and who would therefore benefit from invasive therapies such as angioplasty or stenting.

Limitation of the Study

There were some limitations to the study. First, some simplifying assumptions have been made in the pulsatile volume modeling, and in particular that the volume outflow of the venous flow remains constant during a cardiac cycle. In reality the cerebral blood outflow is pulsatile; however, the magnitude of these venous pulsations is much lower than arterial ones [3, 17].

Second, ABP measured non-invasively by Finapres devices provides only an estimation of cerebral ABP. It has been demonstrated that non-invasive measurement of mean arterial pressure (meanABP) from a finger differs from meanABP recorded at the aortic level [15, 16]. To minimize this potential error, we use in our study the first harmonic of peak to peak values to calculate C_a [7]. CVR is linearly dependent on meanABP. However, this systematic error in the calculations may only act to change the statistical significance of τ . Careful use and further improvement of the non-invasive ABP measurement technique can minimize this limitation.

Another point here is that we measure true changes in blood flow velocity downstream from the stenosis, but have no way of saying how much the arterial pressure and its waveform is altered by stenosis. And this issue is entirely independent of the actual ABP measurement technique. Further, the number of patients investigated in our retrospective study was small. However, our intention was not to revisit the hemodynamic consequences of stenotic disease, but to justify interpretation of a new hemodynamic index. The sample was sufficient to demonstrate significant correlation between τ and a state of altered haemodynamics in carotid artery stenosis and thus validate the concept behind this new methodology. A prospective larger study is needed to establish potential usefulness of τ in clinical practice.

Finally, the model and τ performance should be validated with other monitoring or imaging techniques, and with MRI in particular.

Conclusion

The time constant (τ) of the cerebral arterial bed determined as a product of vascular resistance and compliance theoretically reflects how fast the cerebral vasculature copes with arterial blood load during the cardiac cycle. The τ can be estimated non-invasively using ABP and TCD waveforms. It seems to correlate with the hemodynamic derangement in carotid artery stenosis, showing the potential to become *the* diagnostic modality in cerebrovascular investigations.

Acknowledgements The project was supported by the Foundation for Polish Science (MK); National Institute of Health Research, Biomedical Research Centre, Cambridge University Hospital Foundation Trust – Neurosciences Theme plus Senior Investigator Award (JDP) and Clifford and Mary Corbridge Trust (KPB).

Conflict of interest statement ICM+ (www.neurosurg.cam.ac.uk/icmplplus) is licensed by University of Cambridge, UK. PS and MC have an interest in a part of the licensing fee.

References

1. Aaslid R (1992) Cerebral hemodynamics. In: Newell DW, Aaslid R (eds) Transcranial Doppler. Raven Press Ltd, New York, pp 49–55
2. Aaslid R, Newell DW, Stooss R, Sorteberg W, Lindegaard KF (1991) Assessment of cerebral autoregulation dynamics from simultaneous arterial and venous transcranial Doppler recordings in humans. *Stroke* 22:1148–1154
3. Alperin N, Sivaramakrishnan A, Lichtor T (2005) Magnetic resonance imaging-based measurements of cerebrospinal fluid and blood flow as indicators of intracranial compliance in patients with Chiari malformation. *J Neurosurg* 103:46–52
4. Avezaat CJ, van Eijndhoven JH (1986) The role of the pulsatile pressure variations in intracranial pressure monitoring. *Neurosurg Rev* 9:113–120

5. Carrera E, Kim DJ, Castellani G, Zweifel C, Smielewski P, Pickard JD, Czosnyka M (2011) Effect of hyper- and hypocapnia on cerebral arterial compliance in normal subjects. *J Neuroimaging* 21:121–125
6. Czosnyka M, Richards H, Pickard JD, Harris N, Iyer V (1994) Frequency-dependent properties of cerebral blood transport – an experimental study in anaesthetized rabbits. *Ultrasound Med Biol* 20:391–399
7. Czosnyka M, Richards HK, Czosnyka Z, Piechnik S, Pickard JD, Chir M (1999) Vascular components of cerebrospinal fluid compensation. *J Neurosurg* 90:752–759
8. Evans DH, Levene MI, Shortland DB, Archer LN (1988) Resistance index, blood flow velocity, and resistance-area product in the cerebral arteries of very low birth weight infants during the first week of life. *Ultrasound Med Biol* 14:103–110
9. Gosling RG, King DH (1974) Arterial assessment by Doppler-shift ultrasound. *Proc R Soc Med* 67:447–449
10. Kim DJ, Kaspruwicz M, Carrera E, Castellani G, Zweifel C, Lavinio A, Smielewski P, Sutcliffe MP, Pickard JD, Czosnyka M (2009) The monitoring of relative changes in compartmental compliances of brain. *Physiol Meas* 30:647–659
11. Kontos HA (1989) Validity of cerebral arterial blood flow calculations from velocity measurements. *Stroke* 20:1–3
12. Michel E, Hillebrand S, vonTwickel J, Zernikow B, Jorch G (1997) Frequency dependence of cerebrovascular impedance in preterm neonates: a different view on critical closing pressure. *J Cereb Blood Flow Metab* 17:1127–1131
13. Panerai RB, Coughtry H, Rennie JM, Evans DH (1993) A model of the instantaneous pressure–velocity relationships of the neonatal cerebral circulation. *Physiol Meas* 14:411–418
14. Panerai RB, Kelsall AW, Rennie JM, Evans DH (1996) Analysis of cerebral blood flow autoregulation in neonates. *IEEE Trans Biomed Eng* 43:779–788
15. Panerai RB, Sammons EL, Smith SM, Rathbone WE, Bentley S, Potter JF, Samani NJ (2007) Transient drifts between Finapres and continuous intra-aortic measurements of blood pressure. *Blood Press Monit* 12:369–376
16. Philippe EG, Hebert JL, Coirault C, Zamani K, Lecarpentier Y, Chemla D (1998) A comparison between systolic aortic root pressure and finger blood pressure. *Chest* 113:1466–1474
17. Stolz E, Kaps M, Kern A, Babacan SS, Dorndorf W (1999) Transcranial color-coded duplex sonography of intracranial veins and sinuses in adults. Reference data from 130 volunteers. *Stroke* 30:1070–1075

Pulse Amplitude and Lempel–Ziv Complexity of the Cerebrospinal Fluid Pressure Signal

D. Santamarta, D. Abásolo, J. Fernández, and R. Hornero

Abstract *Background:* The complexity of the intracranial pressure (ICP) signal decreases with intracranial hypertension in children with acute brain injury as well as during infusion studies in adults with hydrocephalus. In this study we have analysed the pressure signal obtained in the lumbar subarachnoid space during infusion testing. The pulse amplitude rises when the ICP is increased by additional external volume. Our objective was to determine the relative influence of the pressure range and pulse amplitude on the loss of complexity observed during infusion-related intracranial hypertension.

Materials and Methods: The Lempel–Ziv (LZ) complexity of the cerebrospinal fluid pressure (CSFP) signal was analysed in 52 infusion studies performed in patients with normal pressure hydrocephalus (median age 71 years, IQR: 60–78). Four sequences during the baseline, infusion, steady plateau and recovery periods of each infusion study were selected. The mean values of the CSFP (mCSFP), pulse amplitude and LZ complexity in every sequence were measured. Correlations between LZ complexity and CSFP parameters were explored.

Results: Significant inverse correlations were found among LZ complexity, pulse amplitude and mCSFP during all periods of infusion testing, except at baseline. Partial correlation analysis controlling the effect of mCSFP emphasised the relationship between pulse amplitude and LZ

complexity. When pulse amplitude is held constant the partial correlation between LZ complexity and mCSFP is not significant.

Conclusions: The pulse amplitude of the CSFP signal seems to be a major determinant of the waveform complexity.

Keywords Intracranial pressure • Cerebrospinal fluid • Pulse pressure waveform • Hydrocephalus • Lempel–Ziv complexity • Non-linear analysis

Introduction

The metric of complexity proposed by Lempel and Ziv to evaluate the randomness of finite sequences has been widely used in biomedical signal analysis [1]. This complexity measure is related to the number of distinct substrings (i.e., patterns) and the rate of their occurrence along a given sequence of symbols [12]. During intracranial hypertension the Lempel–Ziv (LZ) complexity of the intracranial pressure (ICP) signal decreases in children with traumatic brain injury [10], as well as in infusion studies performed in adult patients with hydrocephalus [13].

A rise in pulse amplitude occurs when CSF pressure (CSFP) is increased by additional external volume [3]. We hypothesised that the loss of complexity in the CSFP signal during the infusion period mainly depends on changes in pulse amplitude. The goal of this study was to determine the relative influence of mean CSFP and pulse amplitude on the loss of complexity observed during the infusion period.

Materials and Methods

We analysed retrospectively 52 infusion studies performed in the Department of Neurosurgery, University Hospital of León, Spain. All patients presented clinical symptoms of hydrocephalus and ventriculomegaly. The ventricular size was

D. Santamarta (✉) and J. Fernández
Department of Neurosurgery,
University Hospital of León,
Altos de Nava, s/n, 24080 León, Spain
e-mail: genarotumbado@gmail.com

D. Abásolo
Division of Mechanical, Medical and Aerospace Engineering,
FEPS, Centre for Biomedical Engineering,
University of Surrey,
Guildford, Surrey, UK

R. Hornero
Department of Signal Theory and Communications,
ETSIT, University of Valladolid,
Valladolid, Spain

measured with the Evans ratio. Measurement of the CSF outflow resistance (R_{OUT}) through a constant-rate lumbar infusion study is part of the usual clinical routine in the management of patients with chronically developed hydrocephalus. Complexity analysis of the CSFP signal was made off line. The local ethics committee approved the study. Informed consent was obtained from either the patient or a close relative.

Lumbar Infusion Test and Derived Parameters

The infusion studies were performed using a variant of the original method described by Katzman and Hussey [11]. The procedure has been previously described in detail [13] and will only be summarised here. With the patient in the lateral recumbent position, two lumbar needles (19 Gauge) were inserted into the lower lumbar region. The rostral cannula was connected via a three-way stopcock equipped with a short extension line to a pressure microtransducer (Codman MicroSensor™ ICP transducer, Codman & Shurtleff, Raynham, MA, USA). Through the caudal needle, Ringer solution was infused at a constant rate of 1.5 mL/min. The infusion was switched off when a steady plateau pressure level was achieved.

For every infusion study, we carefully selected four artefact-free time windows during the baseline (W_0), early infusion (W_1), steady-state plateau (W_2) and the recovery (W_3) segments of the infusion studies. Mean values of CSFP, pulse amplitude and LZ complexity of the four sequences were determined in each infusion study. Amplitude was defined as the peak-to-peak value of the pulse wave. R_{OUT} was calculated as the plateau pressure minus the opening pressure, divided by the infusion rate.

Data Acquisition and Complexity Analysis

The pressure signal from the analogue output of the monitor was amplified and digitised (PowerLab 2/25 Data recording system ML825, ADI Instruments, Milford, MA, USA). The analogue-to-digital converter was fitted into a computer for real-time display, storage and processing of the digital signals (PowerLab software; ADI Instruments). Pressure data were sampled at a frequency of 100 Hz.

The LZ complexity analysis was applied to a binary sequence generated from the original signal using the median of a 5-s moving window as the threshold. Previous studies have shown that 0–1 conversion is adequate to estimate the LZ complexity in biomedical signals [14, 15]. There was 4 s of overlap between consecutive windows. To compute LZ complexity, the sequence has to be scanned from left to right and a complexity counter is increased by one unit every time a new subsequence of consecutive characters is encountered. The detailed algorithm to estimate LZ complexity can be

Table 1 Baseline characteristics of the patients and cerebrospinal fluid (CSF) parameters during the infusion studies

Characteristic	Value
<i>Sex (No.)</i>	
Male	23
Female	29
<i>Age: median (IQR)</i>	
Years	71 (60–78)
<i>Etiology (No.)</i>	
Idiopathic normal pressure hydrocephalus	23
Secondary normal pressure hydrocephalus	25
Shunt dysfunction	4
<i>Ventricular size: median (IQR)</i>	
Evans index	0.37 (0.30–0.40)
<i>CSF pressure parameters: median (IQR)</i>	
Opening pressure (mmHg)	8.21 (6.34–11.25)
Plateau pressure (mmHg)	26.22 (21.14–32.04)
CSF outflow resistance (mmHg ml ⁻¹ min)	12 (8.75–15.20)

No. number, IQR interquartile range

found elsewhere [1, 14, 15]. In order to obtain a complexity measure that is independent of the sequence length, the complexity value should be normalised. The normalised LZ complexity reflects the rate of new patterns arising in the sequence. A larger value of LZ complexity means that the chance of new pattern generation is greater, so the sequence is more complex. The complexity value of a given sequence was normalised with regard to the baseline LZ complexity (LZ_0) in order to quantify the dynamics of LZ complexity throughout the infusion study ($\otimes LZ_n = LZ_n / LZ_0$).

Statistical Analysis

Data were analysed using SPSS, version 17.0 (SPSS Inc., Chicago, IL, USA). Quantitative variables were expressed as median and interquartile range (IQR). Association between quantitative variables was assessed by the Spearman rank correlation test. Partial correlation analyses between two variables were performed to control the effect of a third variable. The chosen level of significance was $p < 0.05$.

Results

Baseline characteristics of patients and the results of the measurements of the CSF parameters to obtain R_{OUT} are given in Table 1. LZ complexity values are higher at baseline. During the infusion the complexity of the CSFP signal usually diminishes, yielding the lowest value during the

Table 2 Parameters derived from the cerebrospinal fluid pressure (CSFP) signal in the different periods of the infusion study

	Baseline (W_0)	Infusion (W_1)	Plateau (W_2)	Recovery (W_3)
Sequence length (s)	180 (145–200)	300 (300–360)	490 (455–600)	180 (180–240)
mCSFP (mmHg)	8.2 (6.3–11.2)	17.3 (15.1–20)	26.2 (21.1–32)	16.8 (13.7–19.8)
AMP (mmHg)	2.6 (1.6–3.4)	5.5 (3.5–8.6)	9.7 (5.5–13.8)	5.7 (3.9–7.6)
LZ complexity	0.27 (0.24–0.31)	0.21 (0.18–0.25)	0.18 (0.16–0.24)	0.20 (0.18–0.27)
⊗LZ	NA	0.77 (0.64–0.95)	0.68 (0.57–0.91)	0.75 (0.63–0.98)

Data are presented as median (interquartile range)

s seconds, mCSFP meanCSFP, AMP pulse amplitude, LZ Lempel–Ziv, ⊗LZ normalised LZ complexity value, NA not applicable

steady-state plateau (LZ2). ⊗LZ2 values lower than 1 in 44 patients (85%) reflect this behaviour.

Table 2 summarises LZ complexity values along with pulse amplitude and mean CSFP in the four segments of the infusion tests. As expected, the amplitude of the wave increases during the infusion. All parameters tend to recover towards the baseline level once the infusion has been interrupted.

The results of the correlation analysis between LZ complexity, pulse amplitude and mean CSFP revealed significant inverse correlations during all periods of the infusion testing, except baseline (Fig. 1). The correlation coefficients were always higher between LZ complexity and pulse amplitude (W_1 : $\rho = -0.82$, $p < 0.01$; W_2 : $\rho = -0.83$, $p < 0.01$; W_3 : $\rho = -0.76$, $p < 0.01$) than between LZ complexity and mean CSF pressure (W_1 : $\rho = -0.54$, $p < 0.01$; W_2 : $\rho = -0.63$, $p < 0.01$; W_3 : $\rho = -0.41$, $p < 0.01$).

Partial correlations were performed given the known dependence between mean CSFP and amplitude during infusion studies. A first-order partial correlation holding constant the effect of mean CSFP confirms the correlation between LZ complexity and pulse amplitude during the infusion (W_1 : $\rho = -0.40$, $p < 0.01$; W_2 : $\rho = -0.32$, $p < 0.05$) and during the recovery period (W_3 : $\rho = -0.38$, $p < 0.01$). However, the partial correlation coefficient controlling the effect of the amplitude rejects a correlation between LZ complexity and mean CSFP (W_1 : $\rho = -0.18$; $p = 0.20$; W_2 : $\rho = -0.23$; $p = 0.09$; W_3 : $\rho = -0.03$; $p = 0.82$).

Finally, the magnitude of the complexity change (i.e. ⊗LZ values) appeared to correlate inversely with R_{OUT} (⊗LZ1: $\rho = -0.42$, $p < 0.01$; ⊗LZ2: $\rho = -0.47$, $p < 0.01$; ⊗LZ3: $\rho = -0.55$, $p < 0.01$). These results mean that a high loss of complexity of the CSFP signal (i.e. decomplexification phenomenon) is associated with higher values of R_{OUT} . No correlations were found between age or ventricular size and ⊗LZ values.

Discussion

Most physiological systems behave non-linearly. They display irregular variations without being random. A major feature of non-linear phenomena is the sensitivity of the

generating system to variations in the initial conditions. Non-linear dynamics studies this system's feature as being one cause of complex behaviour. Physiological variability in ICP dynamics has been recognised since the early period of ICP monitoring [4, 8]. Thorough analysis of the CSF pulse wave through visual inspection of printed recordings was enough to recognise the spontaneous variations in all components of the wave, as well as the changes in the wave configuration under specific conditions [4, 7, 9]. At that time, it was thought that the wave morphology could have potentially important clinical implications. This assumption, however, was pushed aside until recently, when renewed interest in the pulsatile component of ICP dynamics has brought the waveform into the field of discussion once again [2, 5, 6].

Complex systems analysis provides tools to address this physiological variability. There are a number of approaches to characterising complexity. Lempel and Ziv proposed a useful complexity measure that can characterise the degree of predictability in a time series and that does not require long data segments to compute [12]. The signal must be transformed into a finite symbol sequence, which in the context of biomedical signal analysis is usually a binary sequence. LZ complexity analysis is applied to a binary sequence generated from the original signal using a simple threshold. This metric operates like a sliding window algorithm scrutinising the signal. It deals with the wave morphology and it focuses on the pulsatile component of the pressure signal. The Lempel–Ziv algorithm gives the number of distinct patterns contained in the given finite sequence. After normalisation, the relative LZ complexity measure reflects the rate of new pattern occurrences in the investigated sequence. Values of LZ complexity close to 0 correspond to periodic signals, while a value close to 1 corresponds to random noise.

Hornero et al. have shown in paediatric patients with traumatic brain injury that the LZ complexity of the ICP signal recorded intracranially decreases during periods of acute intracranial hypertension [10]. The loss of complexity has also been detected during infusion studies performed in adult patients with hydrocephalus when the CSFP signal is within the range of intracranial hypertension [13].

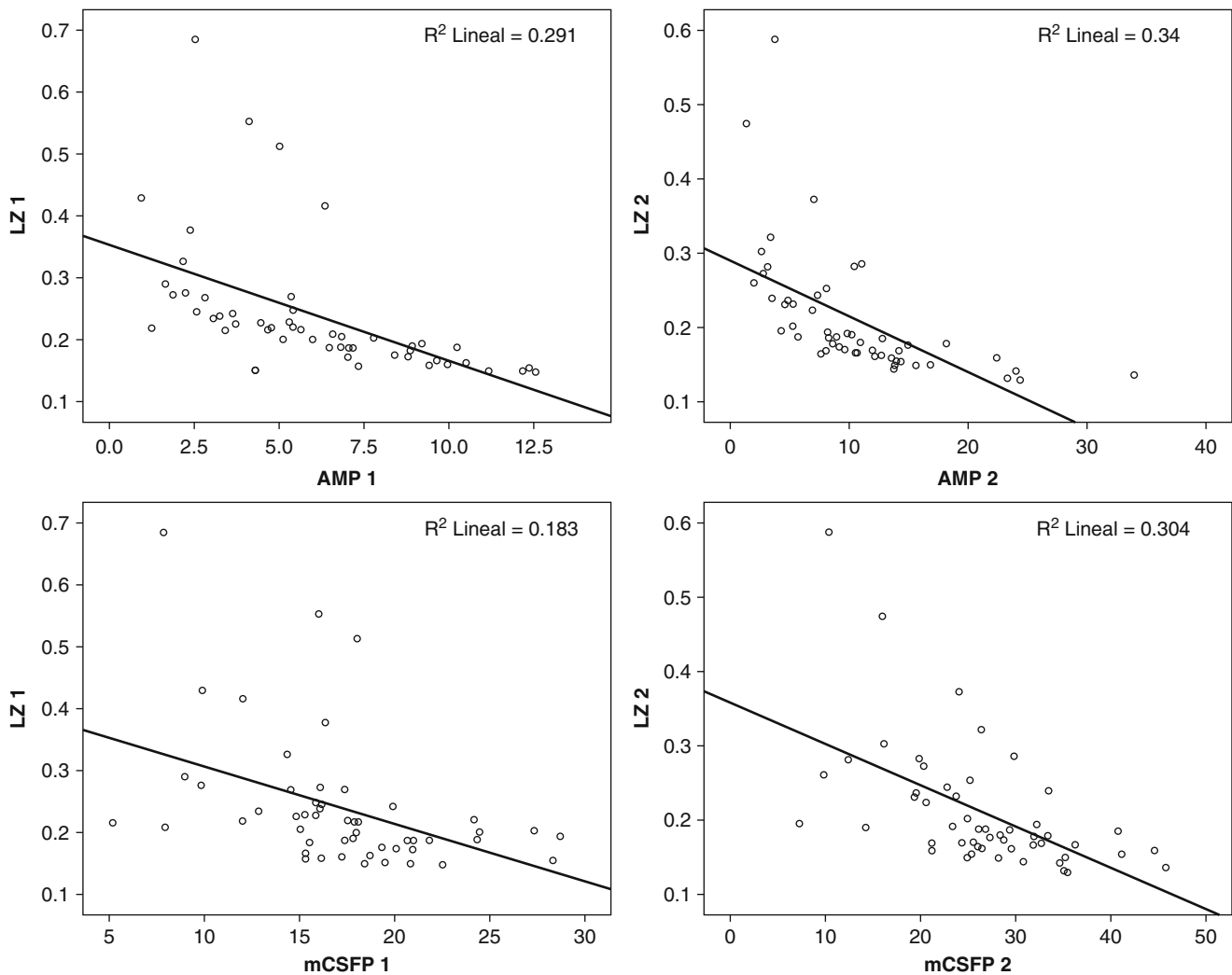


Fig. 1 Graphs showing a higher correlation between LZ complexity and pulse amplitude (*upper row*) than between LZ complexity and mean CSFP (*down row*) during the infusion period (*left column*) and during the plateau (*right column*). LZ1 LZ complexity during infusion,

AMP1 pulse amplitude during the infusion, mCSFP1 mean CSFP during infusion, LZ2 LZ complexity during the plateau, AMP2 pulse amplitude during the plateau, mCSFP2 mean CSFP during the plateau

Conclusion

The main observation from this study is that the loss of complexity in the CSFP signal observed during infusion-related intracranial hypertension seems to correlate more with the pulse amplitude than with the level of pressure. The correlation coefficients between LZ complexity and pulse amplitude were higher than between LZ complexity and mean CSF pressure throughout all the infusion segments. A partial correlation analysis was performed given the strong correlation between pulse amplitude and the pressure level during infusion testing. The partial correlation coefficient between LZ complexity and pulse amplitude diminishes, but it still remains significant when the effect of mCSFP is controlled. This means that the relationship between the two variables is modulated by the variable submitted to control (namely,

mean CSFP). The partial correlation coefficient between LZ complexity and mCSFP does not reach statistical significance when controlling the effect of amplitude. This means that the simple inverse correlation between the two variables is substantially modified if the effect of the amplitude is held constant. Therefore, we assume that pulse amplitude is a major determinant of CSFP signal complexity. Whether ICP complexity analysis holds relevant clinical information or not has yet to be investigated.

Acknowledgements This study was supported in part by Consejería de Sanidad, Junta de Castilla y León, project code GRS 493/B/10 given to David Santamarta.

Conflict of interest statement The authors declare that they have no conflict of interest.

References

1. Aboy M, Hornero R, Abásolo D, Álvarez D (2006) Interpretation of the Lempel–Ziv complexity measure in the context of biomedical signal analysis. *IEEE Trans Biomed Eng* 53:2282–2288
2. Anile C, De Bonis P, Albanese A, Di Chirico A, Mangiola A, Petrella G, Santini P (2010) Selection of patients with idiopathic normal-pressure hydrocephalus for shunt placement: a single-institution experience. *J Neurosurg* 113:64–73
3. Avezaat CJ, van Eijndhoven JH, Wyper DJ (1979) Cerebrospinal fluid pulse pressure in intracranial volume–pressure relationships. *J Neurol Neurosurg Psychiatry* 42:687–700
4. Cardoso ER, Rowan JO, Galbraith S (1983) Analysis of the cerebrospinal fluid pulse wave in intracranial pressure. *J Neurosurg* 59:817–821
5. Carrera E, Kim D-J, Castellani G, Zweifel C, Czosnyka Z, Kasparowicz M, Smielewski P, Pickard JD, Czosnyka M (2010) What shapes pulse amplitude of intracranial pressure? *J Neurotrauma* 27:317–324
6. Eide PK, Sorteberg W (2010) Diagnostic intracranial pressure monitoring and surgical management in idiopathic normal pressure hydrocephalus: a 6-year review of 214 patients. *Neurosurgery* 66:80–91
7. Foltz EL, Aine C (1981) Diagnosis of hydrocephalus by CSF pulse-wave analysis: a clinical study. *Surg Neurol* 15:283–293
8. Gega A, Utsumi S, Lida Y, Lida N, Tsuneda S (1980) Analysis of the wave pattern of CSF pulse wave. In: Shulman K, Marmarou A, Miller JD, Becker DP, Hochwald GM, Brock M (eds) *Intracranial pressure IV*. Springer, Berlin/Heidelberg/New York, pp 188–190
9. Hirai O, Handa H, Ishikawa M, Kim S-H (1984) Epidural pulse waveform as an indicator of intracranial pressure dynamics. *Surg Neurol* 21:67–74
10. Hornero R, Aboy M, Abasolo D (2007) Analysis of intracranial pressure during intracranial hypertension using Lempel–Ziv complexity: further evidence. *Med Biol Eng Comput* 45:617–620
11. Katzman R, Hussey F (1970) A simple constant-infusion manometric test for measurement of CSF absorption. I. Rationale and method. *Neurology* 20:534–544
12. Lempel A, Ziv J (1976) On the complexity of finite sequences. *IEEE Trans Inf Theory* 22:75–81
13. Santamarta D, Hornero R, Abásolo D, Martínez-Madrigal M, Fernández J, García-Cosamalón J (2010) Complexity analysis of the cerebrospinal fluid pulse waveform during infusion studies. *Childs Nerv Syst* 26:1683–1689
14. Zhang XS, Zhu YS, Thakor NV, Wang ZZ (1999) Detecting ventricular tachycardia and fibrillation by complexity measure. *IEEE Trans Biomed Eng* 46:548–555
15. Zhang XS, Roy RJ, Jensen EW (2001) EEG complexity as a measure of depth of anesthesia for patients. *IEEE Trans Biomed Eng* 48:1424–1433

Association Between ICP Pulse Waveform Morphology and ICP B Waves

Magdalena Kasprowicz, Marvin Bergsneider, Marek Czosnyka, and Xiao Hu

Abstract The study aimed to investigate changes in the shape of ICP pulses associated with different patterns of the ICP slow waves (0.5–2.0 cycles/min) during ICP overnight monitoring in hydrocephalus. Four patterns of ICP slow waves were characterized in 44 overnight ICP recordings (no waves – NW, slow symmetrical waves – SW, slow asymmetrical waves – AS, slow waves with plateau phase – PW). The morphological clustering and analysis of ICP pulse (MOCAIP) algorithm was utilized to calculate a set of metrics describing ICP pulse morphology based on the location of three sub-peaks in an ICP pulse: systolic peak (P_1), tidal peak (P_2) and diastolic peak (P_3). Step-wise discriminant analysis was applied to select the most characteristic morphological features to distinguish between different ICP slow waves. Based on relative changes in variability of amplitudes of P_2 and P_3 we were able to distinguish between the combined groups NW+SW and AS+PW ($p < 0.000001$). The AS pattern can be differentiated from PW based on respective changes in the mean curvature of P_2 and P_3 ($p < 0.000001$); however, none of the MOCAIP feature separates between NW and SW. The investigation of ICP pulse morphology associated with different ICP B waves may provide additional information for analysing recordings of overnight ICP.

Keywords Intracranial pressure • Waveform analysis • Hydrocephalus

Introduction

Previously, we have studied the feasibility of distinguishing ICP B waves (0.5–2.0 cycles/min) of any shape and strength from flat ICP recordings based on ICP pulse morphology and mean value of ICP [9]. The present study was designed to investigate whether ICP B waves of different shapes are associated with different ICP pulse waveform morphology. Mean values of ICP were excluded from this study in order to solely investigate changes in ICP pulse shape. We hypothesised that ICP waveform morphology reflects cerebrovascular changes [10]. Given that ICP B waves are thought to arise from vasomotor instability and ICP, waveform morphology associated with B waves should be unique. The study aimed to investigate whether or not the shape of the ICP pulse waveforms changes in association with the ICP B wave occurrence and to identify the discriminating power of metrics describing ICP pulse waveform morphology to differentiate between different patterns of ICP B wave activities in overnight monitoring of hydrocephalus.

Materials and Methods

A total number of 276 episodes of four clearly distinctive ICP slow wave activities (Fig. 1a–d) were selected from retrospectively analysed pre-shunt operation, overnight intracranial pressure (ICP) recordings performed in 44 patients (18 female and 26 male; mean age: 68 ± 17 years, range 32–94 years) hospitalised at the UCLA Adult Hydrocephalus Centre. The preliminary diagnosis (based on brain scans and clinical picture) for all patients was hydrocephalus. One hundred and thirty-one selections of flat ICP patterns containing no episodes of slow waves (NW), 74 selections of symmetrical slow waves (SW), 45 selections of asymmetrical slow

M. Kasprowicz

Neural Systems and Dynamics Laboratory, Department of Neurosurgery, The David Geffen School of Medicine, University of California, NPI 18-265, 10833, Le Conte Avenue, Los Angeles, CA 90095, USA

Institute of Biomedical Engineering and Instrumentation, Wrocław University of Technology, Wrocław, Poland and Academic Neurosurgical Unit, Addenbrooke's Hospital, Cambridge, UK

M. Bergsneider and X. Hu (✉)

Neural Systems and Dynamics Laboratory, Department of Neurosurgery, The David Geffen School of Medicine, University of California, NPI 18-265, 10833, Le Conte Avenue, Los Angeles, CA 90095, USA

Biomedical Engineering Graduate Program, Henry Samueli School of Engineering and Applied Science, University of California, Los Angeles, CA, USA
e-mail: xhu@mednet.ucla.edu

M. Czosnyka

Academic Neurosurgical Unit, Addenbrooke's Hospital, Cambridge, UK

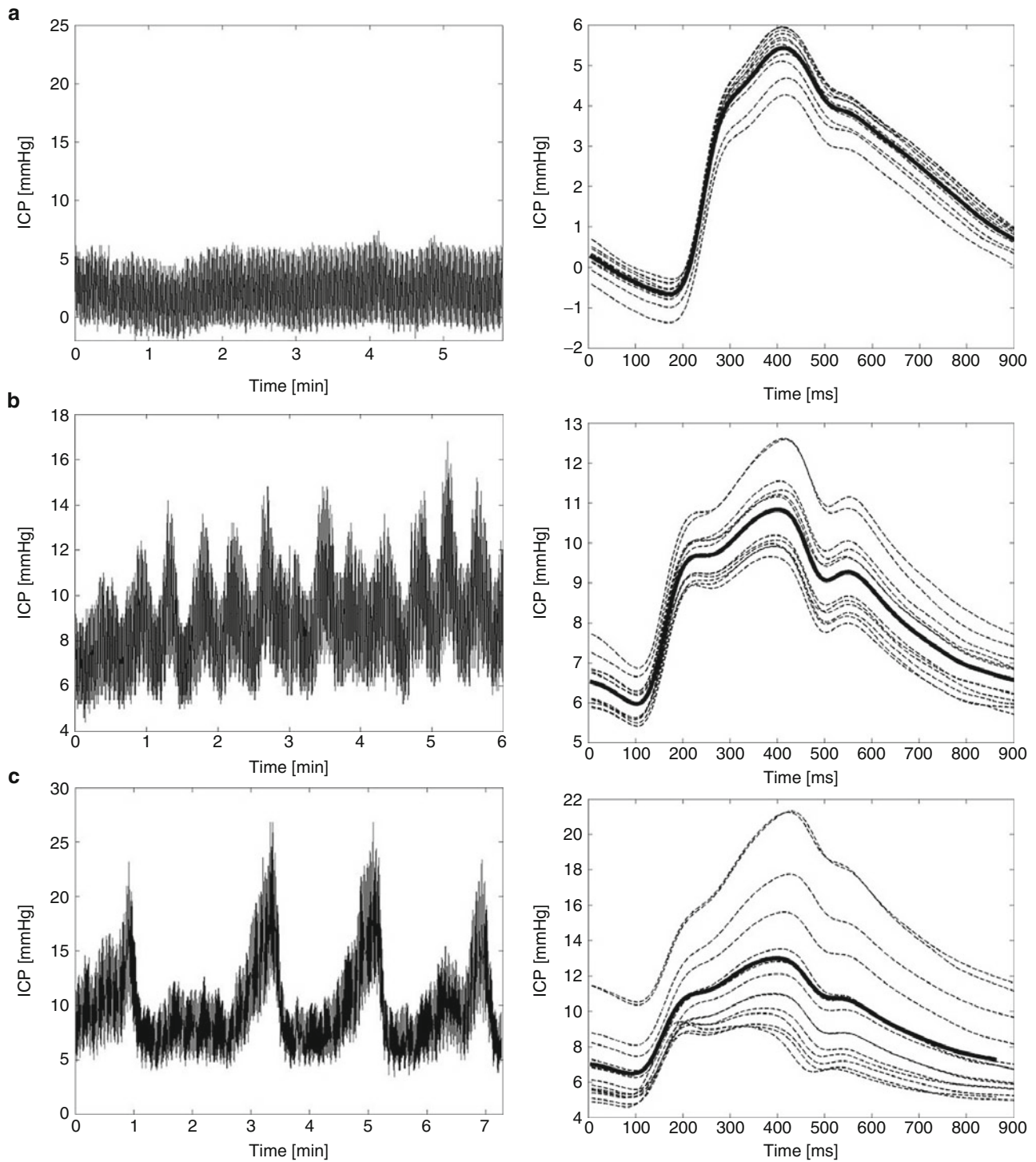


Fig. 1 Four patterns of intracranial pressure (ICP) oscillations and corresponding dominant ICP pulses: (a) NW – no episodes of ICP B waves, (b) SW – symmetrical ICP B waves, (c) AS – asymmetrical ICP

B waves, (d) PW – slow ICP B with plateau phase. Each dominant pulse was extracted from 30 s of data

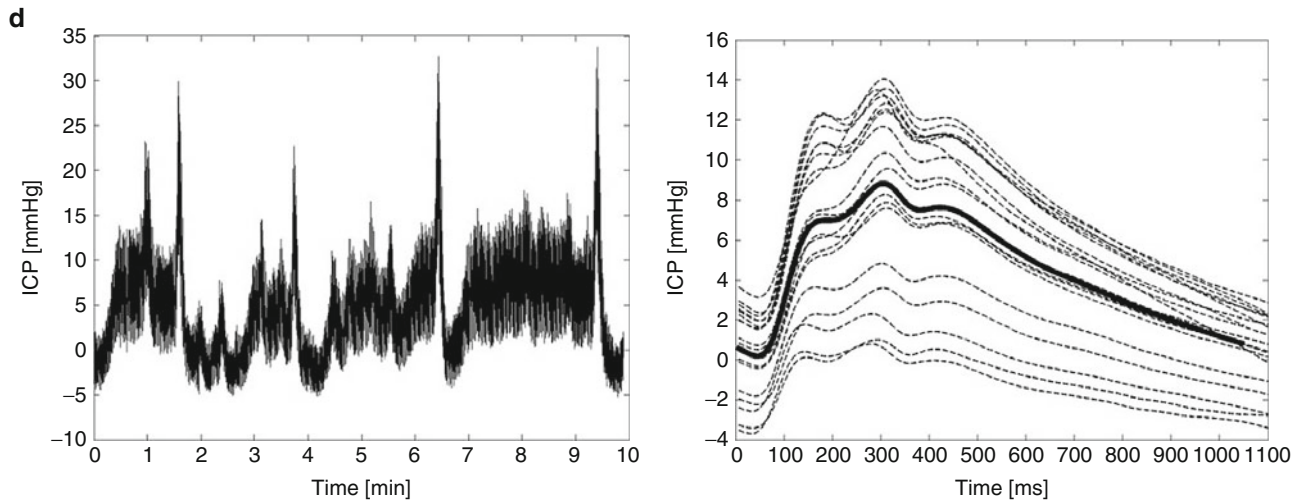


Fig. 1 (continued)

waves (AS) and 26 selections of slow waves with plateau phase (PW) were included into this study. Mean duration of selection was $9 \text{ min } 58 \text{ s} \pm 4 \text{ min } 15 \text{ s}$. An ICP intraparenchymal microsensor (Codman and Schurtleff, Raynaud, MA, USA) was inserted into the right frontal lobe. Simultaneous recordings of ICP and ECG signals were performed using either a PowerLab™ SP-16 acquisition system (ADInstruments, Colorado Springs, CO, USA) connected to the analogue outputs of the Codman ICP Express Box and the GE bedside monitor or the BedMaster™ system, which acquire data from bedside monitors. A different sampling rate was used by the acquisition systems: PowerLab™ – 400 Hz and BedMaster™ – 240 Hz. An insertion of the ICP sensor and data acquisition were approved by the local IRB committee and informed consent was obtained from each patient or from their family member.

The morphological clustering and analysis of ICP pulse (MOCAIP) algorithm was utilized to measure the set of ICP pulse metrics based on the location of sub-peaks in an ICP pulse: systolic peak (P_1), tidal peak (P_2) and diastolic peak (P_3). Details of this algorithm were precisely described in another publication [8]. The set of 10 ICP pulse metrics was calculated to describe the morphology of ICP pulsation: amplitudes of pulse peaks (dP_1 , dP_2 , dP_3), latency (L_T) between the peak of the QRS complex of ECG and the corresponding onset of the ICP pulse, latencies between the onset of ICP pulse and the location of three peaks (L_1 , L_2 , L_3) and curvatures of the three sub-waves of ICP pulse wave ($Curv_1$, $Curv_2$, $Curv_3$). The average of the MOCAIP features quantitatively estimates the ICP pulse wave shape, although it ignores the changes during slow wave occurrence (Fig. 1). Therefore, besides mean values of 10 MOCAIP metrics, we also calculated their standard deviations (S.D.). Hence, a total number of metrics analysed increased to 20 (Table 1).

Statistical Methods

With regard to statistical analysis, the forward step-wise discriminant analysis (DA) [12] was used to investigate which features are the most significantly altered by ICP B wave occurrence. At each step of analysis 20 MOCAIP metrics were reviewed and evaluated to determine which one will contribute most to the discrimination between four patterns of ICP B wave activity (NW, SW, AS and PW). The step-wise procedure was controlled by F to enter value (set at 4.0) and minimum tolerance value ($1 - R^2$ set at 0.01). We repeated the analysis 44 times; in every run the samples from one patient were excluded and the selections from the remaining 43 patients were used to build the discriminant model. Only the metrics that were selected most often (more than 22 times) were included in the final analysis. The significance of the discriminant functions obtained was tested based on a multivariate F value (Wilks' lambda statistics). Standardised beta coefficients were utilised for estimation of the unique power of discrimination of the variables. To identify between which of the groups the respective function discriminates we looked at the means of canonical variables.

Results

Mean values and standard deviations of ICP pulse metrics along with the number indicating how many times a particular metric was chosen by DA were summarised in Table 2. Nine out of 20 ICP pulse metrics were selected more than 22 times. Eight of them (highlighted in grey in Table 2) were accepted (based on the p value for the F statistic < 0.05) into the final model (Wilks' lambda: 0.31, $F = 16.2$, $p < 0.0001$).

Table 1 Intracranial pressure (ICP) pulse wave metrics

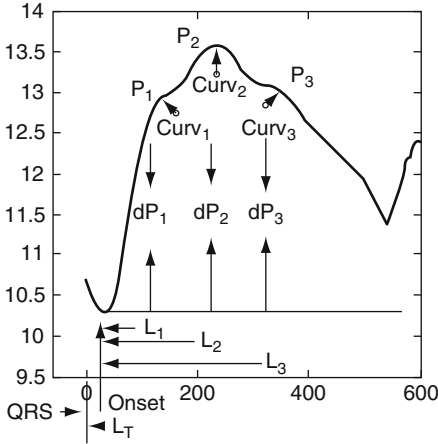
	MOCAIP Metric Group	Mean	S.D.
	Pulse wave amplitudes	dP_1, dP_2, dP_3	$SDdP_1, SDdP_2, SDdP_3$
	Pulse waves latencies	L_T, L_1, L_2, L_3	$SDL_T, SDL_1, SDL_2, SDL_3$
	Pulse curvatures	$Curv_1, Curv_2, Curv_3$	$SDCurv_1, SDCurv_2, SDCurv_3$

Table 2 Mean (\pm SD) and standard deviation (\pm SD) of the ICP pulse metrics for four patterns of ICP fluctuations

		No DA select	NW \pm SD (N=131)	SW \pm SD (N=74)	AS \pm SD (N=45)	PW \pm SD (N=26)
dP_1 (mmHg)	Mean	0	4.08 ± 1.56	4.66 ± 1.84	5.93 ± 2.29	5.98 ± 2.55
	SD	10	0.25 ± 0.14	0.41 ± 0.23	0.89 ± 0.57	1.00 ± 0.80
dP_2 (mmHg)	Mean	0	5.16 ± 2.08	6.40 ± 2.46	8.42 ± 3.75	9.03 ± 3.56
	SD	44	0.46 ± 0.22	0.92 ± 0.48	2.13 ± 1.21	2.02 ± 1.11
dP_3 (mmHg)	Mean	39	3.71 ± 1.77	4.77 ± 1.87	6.17 ± 2.64	6.85 ± 3.08
	SD	0	0.46 ± 0.23	0.84 ± 0.44	1.73 ± 0.93	1.66 ± 0.95
L_T	Mean	0	108.6 ± 32.5	109.1 ± 30.0	105.1 ± 35.2	102.7 ± 30.4
	SD	0	2.6 ± 1.5	3.8 ± 6.5	3.8 ± 2.0	3.4 ± 1.7
L_1	Mean	0	100.6 ± 13.4	101.2 ± 11.8	103.4 ± 9.9	107.0 ± 13.9
	SD	31	4.6 ± 2.7	5.4 ± 3.4	6.9 ± 3.8	6.7 ± 3.1
L_2	Mean	1	233.6 ± 27.7	236.9 ± 35.3	249.8 ± 21.6	241.6 ± 25.8
	SD	1	6.6 ± 4.3	6.7 ± 3.5	10.2 ± 6.0	5.7 ± 2.1
L_3	Mean	35	370.9 ± 30.4	363.7 ± 43.5	380.4 ± 28.8	356.6 ± 31.2
	SD	43	6.1 ± 3.0	6.5 ± 3.3	10.0 ± 3.8	8.1 ± 4.1
$Curv_1^{-3}$ (1/mmHg)	Mean	1	4.5 ± 6.8	4.0 ± 5.8	4.1 ± 6.7	2.7 ± 7.0
	SD	41	1.3 ± 1.2	2.2 ± 3.0	2.4 ± 2.7	1.1 ± 1.1
$Curv_2^{-3}$ (1/mmHg)	Mean	26	5.8 ± 5.0	8.9 ± 6.6	8.2 ± 5.6	10.0 ± 6.9
	SD	23	0.8 ± 0.7	1.7 ± 1.6	3.2 ± 2.9	2.0 ± 1.5
$Curv_3^{-3}$ (1/mmHg)	Mean	25	3.5 ± 3.4	3.5 ± 3.3	4.3 ± 3.3	2.1 ± 2.3
	SD	0	0.6 ± 0.4	0.8 ± 0.6	1.4 ± 1.1	0.9 ± 1.2

Eight metrics (*highlighted in grey*) were accepted (based on the p value for the F statistic <0.05) into the final discriminant model

Three discriminant functions (the maximal possible number) were statistically significant. The first function (Function 1, $p < 0.000001$) differentiates between two groups: combined PW and AS vs combined SW and NW. It explains 83.6% of discriminating power while the second and the third ones

account for 16.4% of total power. The standardized coefficients for the two variables $SDdP_2$ and $SDdP_3$, demonstrated the greatest values; therefore, their contributions to discrimination between PW+AS vs SW+NW are the most significant (Eq. 1).

$$2.3SDdP_2 - 1.3SDdP_3 - 0.4SDCurv_1 + 0.3SDL_1 + 0.3SDL_3 + 0.2Curv_2 - 0.2SDCurv_2 - 0.1Curv_3 \quad (1)$$

The Function 2 ($p < 0.000001$) discriminates between PW and AS groups mostly based on inverse changes in mean $Curv_2$ and $Curv_3$ (Eq. 2).

$$1.2Curv_2 - 1.1Curv_3 - 0.6SDCurv_2 - 0.4SDL_3 + 0.2SDL_1 + 0.2SDCurv_1 + 0.2SDdP_3 + 0.0SDdP_2 \quad (2)$$

The Function 3 ($p < 0.002$) separates between PW and SW and the variables $SDdP_2$ and $SDdP_3$ have the biggest impact on this discrimination (Eq. 3)

$$2.1SDdP_2 - 2.0SDdP_3 - 0.7SDCurv_2 - 0.7SDCurv_1 + 0.3Curv_3 + 0.2SDL_1 - 0.1Curv_2 + 0.1SDL_3 \quad (3)$$

To visualise how the two functions discriminate between groups the individual scores for the two functions (Function 1 vs Function 2) were plotted on Fig. 2.

The variation of amplitudes of peaks P_2 and P_3 contributes to the distinction between NW+SW vs AS+PW (Fig. 3). Mean values of $SDdP_2$ and $SDdP_3$ evolve from NW to PW when different ICP patterns were compared (Fig. 3a). The discriminating power, however, was attributed to the relative changes between $SDdP_2$ and $SDdP_3$: profound variations in dP_2 prevailed over the changes in dP_3 during AS and PW, but the range of variation in amplitudes of these two peaks was similar during SW and NW (Fig. 3a). The highest discriminating power to distinguish between PW and AS was ascribed to the mean curvatures of the two peaks P_2 and P_3 . A more rounded sub-wave of P_2 along with a less sharp sub-wave of P_3 seems to be typical for PW (Fig. 3b). We could not find any significant combination of MOCAIP features to distinguish between SW and NW.

Discussion

Based solely upon ICP pulse morphological features (mean ICP values were not taken into account in this study), we were able to demonstrate that different subtypes of ICP B waves are indeed associated with different shaped ICP pulsations and a different range of alterations of MOCAIP metrics. Our finding suggests then that AS and PW might be physiologically distinct from SW and NW. Moreover, AS and PW may also be physiologically different.

The changes in ICP pulse morphological features reflect acute changes in intracranial conditions and changes in the

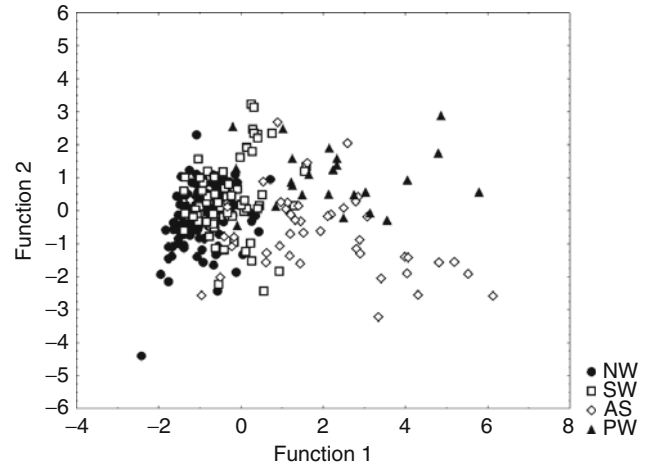


Fig. 2 Scatter plot of the canonical scores from the discriminant analysis of (•) no ICP B waves, (□) symmetrical ICP B waves, (◇) asymmetrical ICP B waves, (▲) slow ICP B with plateau phase PW

cerebral haemodynamics [1, 2]. The origin of the three peaks in ICP pulse waveform has not yet been established. The P_2 component is thought to be dependent upon intracranial compliance [6] whereas pulsations of major arteries and choroid plexus may contribute to the P_1 component [2, 13]. Miller noted that venous hypertension from jugular venous or sagittal sinus occlusion causes an increase in the terminal portion of the ICP pulse wave, which suggests the venous pressure dependency of P_3 [2, 13]. Recent study in TBI patients showed that the amplitude of ICP was mostly affected by changes in the pulsatility of the cerebral blood volume (CBV), whereas in patients with NPH, who underwent an infusion study, amplitude was more dependent upon mean ICP, which was increased during the test in a controllable manner [3]. In the case of ICP B waves, both factors (mean ICP and increased pulsatility of CBV) play a significant role. As the ICP slow waves are most probably vasogenic in origin, they may be dependent on cerebral blood volume pulsatility [4, 7]. Moreover, the compliance in NPH patients is usually reduced owing to underlying pathological conditions, which may amplify an increase in mean ICP during ICP B waves and provoke proportional changes in ICP pulse amplitude [11, 15].

In our study the distinguishing power was mostly related to variation in the amplitudes of two peaks: P_2 and P_3 , which may reflect more reduced intracranial compliance and increased venous pressure because of an elevation in ICP during AS and PW ICP B waves compared with during NW and SW. It was suggested by recent studies [5] that an increased amplitude of ICP pulsation may have predictive value for selecting shunt responders. It was also discussed in an early work [14], where a five-category classification of B wave was proposed, that only the asymmetrical B wave has a predictive value with regard to outcome after shunting. Therefore,

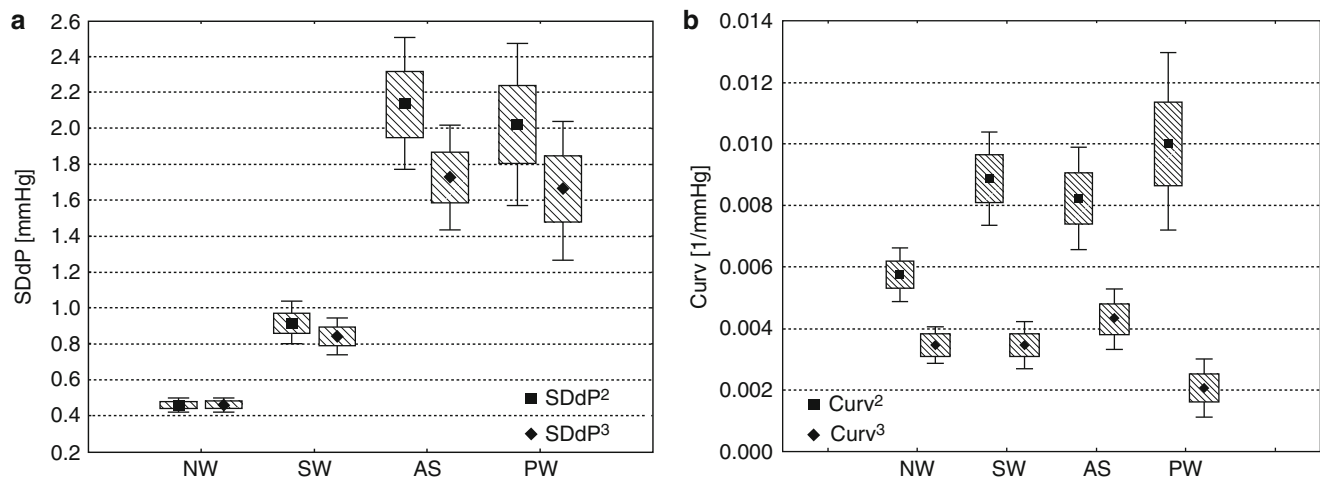


Fig. 3 Mean \pm SE (box) \pm 95% confidence interval (whiskers) of (a) SDdP₂ and SDdP₃ and (b) Curv₂ and Curv₃ for four patterns of ICP oscillation: NW – no episodes of ICP B waves, SW – symmetrical ICP B waves, AS – asymmetrical ICP B waves, PW – slow ICP B with the plateau phase

we think that joint analysis of both ICP pulse wave amplitudes and ICP B waves (AS and PW in particular) performed in hydrocephalic patients undergoing overnight monitoring might be ideal for overnight ICP analysis. Further study is needed to establish the usefulness of such a joint approach.

Conclusion

Subtypes of ICP slow wave are associated with different configurations of morphological features describing ICP pulse waves, which may suggest that they are physiologically distinct.

Acknowledgement The present work is partially supported by NINDS R21 awards NS055998, NS055045 and NS059797 and R01 awards NS054881 and NS066008. MK is supported by the Foundation for Polish Science.

Conflict of interest statement We declare that we have no conflict of interest.

References

1. Avezaat CJ, van Eijndhoven JH, Wyper DJ (1979) Cerebrospinal fluid pulse pressure and intracranial volume-pressure relationships. *J Neurol Neurosurg Psychiatry* 42:687–700
2. Cardoso ER, Rowan JO, Galbraith S (1983) Analysis of the cerebrospinal fluid pulse wave in intracranial pressure. *J Neurosurg* 59:817–821
3. Carrera E, Kim DJ, Castellani G, Zweifel C, Czosnyka Z, Kasprówicz M, Smielewski P, Pickard J, Czosnyka M (2009) What shapes pulse amplitude of intracranial pressure? *J Neurotrauma* 27:317–324
4. Droste DW, Krauss JK, Berger W, Schuler E, Brown MM (1994) Rhythmic oscillations with a wavelength of 0.5–2 min in transcranial Doppler recordings. *Acta Neurol Scand* 90:99–104
5. Eide PK, Brean A (2006) Intracranial pulse pressure amplitude levels determined during preoperative assessment of subjects with possible idiopathic normal pressure hydrocephalus. *Acta Neurochir (Wien)* 148:1151–1156; discussion 1156
6. Germon K (1988) Interpretation of ICP pulse waves to determine intracerebral compliance. *J Neurosci Nurs* 20:344–351
7. Haubrich C, Czosnyka Z, Lavinio A, Smielewski P, Diehl RR, Pickard JD, Czosnyka M (2007) Is there a direct link between cerebrovascular activity and cerebrospinal fluid pressure-volume compensation? *Stroke* 38:2677–2680
8. Hu X, Xu P, Scalzo F, Vespa P, Bergsneider M (2009) Morphological clustering and analysis of continuous intracranial pressure. *IEEE Trans Biomed Eng* 56:696–705
9. Kasprówicz M, Asgari S, Bergsneider M, Czosnyka M, Hamilton R, Hu X (2010) Pattern recognition of overnight intracranial pressure slow waves using morphological features of intracranial pressure pulse. *J Neurosci Methods* 190:310–318
10. Kirkness CJ, Mitchell PH, Burr RL, March KS, Newell DW (2000) Intracranial pressure waveform analysis: clinical and research implications. *J Neurosci Nurs* 32:271–277
11. Marmarou A, Shulman K, LaMorgese J (1975) Compartmental analysis of compliance and outflow resistance of the cerebrospinal fluid system. *J Neurosurg* 43:523–534
12. McNitt-Gray MF, Huang HK, Sayre JW (1995) Feature selection in the pattern classification problem of digital chest radiograph segmentation. *IEEE Trans Med Imaging* 14:537–547
13. Miller JD, Peeler DF, Pattisapu J, Parent AD (1987) Supratentorial pressures. Part I: differential intracranial pressures. *Neurol Res* 9:193–197
14. Raftopoulos C, Deleval J, Chaskis C, Leonard A, Cantraine F, Desmyttere F, Clarysse S, Brotschi J (1994) Cognitive recovery in idiopathic normal pressure hydrocephalus: a prospective study. *Neurosurgery* 35:397–404; discussion 404–395
15. Szewczykowski J, Sliwka S, Kunicki A, Dytko P, Korsak-Sliwka J (1977) A fast method of estimating the elastance of the intracranial system. *J Neurosurg* 47:19–26

Computerized Data Analysis of Neuromonitoring Parameters Identifies Patients with Reduced Cerebral Compliance as Seen on CT

Rupert Faltermeier, Martin A. Proescholdt, and Alexander Brawanski

Abstract *Objective:* Computer-assisted analysis of neuromonitoring parameters may provide important decision-making support to the neurointensivist. A recently developed mathematical model for the simulation of cerebral autoregulation and brain swelling showed that in the case of an intact autoregulation but diminished cerebral compliance, a negative correlation between arterial blood pressure (ABP) and intracranial pressure (ICP) occurs. The goal of our study was to verify these simulation results in an appropriate patient cohort.

Methods: Simultaneously measured data (ABP, ICP) of 6 patients (1 female; 5 male) with severe head trauma ($n=5$) and stroke ($n=1$) were used to calculate time resolved multi-taper cross coherence. Further, we calculated the Hilbert phases of both signals, defining a negative correlation in case of a mean Hilbert phase difference greater than 130° . To validate the results, CT scans performed during the critical phases identified were analyzed.

Results: In five out of six datasets we found long lasting events of negative correlation between ABP and ICP. In all patients, corresponding CT scans demonstrated changes in the intracranial compartment characterized by diminished cerebral compliance.

Conclusions: Our data indicate that complex multidimensional data analysis of neuromonitoring parameters can identify complication-specific data patterns with a high degree of accuracy.

Keywords Intracranial compliance • Brain edema • ICP • Coherence analysis • Hilbert phase • Mathematical model

Introduction

Neurocritical care treatment focuses on the management of patients with severe neurological diseases. To ensure optimal treatment, an increasing amount of neurophysiological data is provided to the neurointensivist by multimodal neuromonitoring systems [1]. The main goal of multimodal neuromonitoring is to detect and treat critical patient conditions before permanent injury has occurred [5, 13]. However, the large amount of data generated by the monitoring systems is frequently difficult to interpret at the bedside; consequently, the monitoring data will not be acted upon quickly enough to be of benefit to the patient [15]. Computer-assisted analysis of neuromonitoring parameters may allow the integrative interpretation of the data and provide the neurointensivist with important decision-making support [6]. Recently, a mathematical model consisting of arteries, capillaries, veins, superior sagittal sinus, brain tissue, cerebrospinal fluid (CSF) and an additional, artificial compartment to simulate brain swelling was developed [8]. The intention of the model was to perform simulations of cerebral perfusion and oxygen supply under different conditions such as impaired autoregulation or brain swelling leading to reduced intracranial compliance. First simulations showed that in the case of an intact autoregulation but diminished cerebral compliance, generated by brain swelling, a long-lasting negative correlation between arterial blood pressure (ABP) and intracranial pressure (ICP) occurs (Fig. 1). The goal of our study was twofold. First, we wanted to verify the simulation results produced by the mathematical model of cerebral perfusion and oxygen supply. Second, we wanted to validate the results and the physiological assumptions of the model through clinical data such as imaging results in particular.

Materials and Methods

For the subsequent evaluation we used simultaneously and continuously measured ABP and ICP (Sample rate 0.2 Hz)

R. Faltermeier (✉), M.A. Proescholdt, A. Brawanski
Department of Neurosurgery, University Regensburg Medical Center,
Franz Josef Strauß Allee 11, 93053 Regensburg, Germany
e-mail: rupert.faltermeier@klinik.uni-regensburg.de

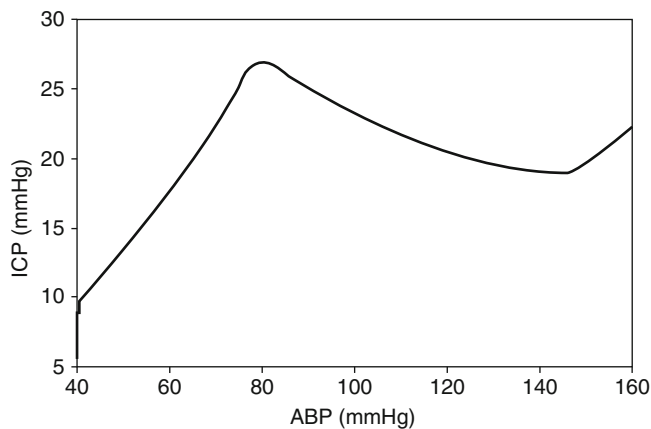


Fig. 1 Predicted correlation between arterial blood pressure (ABP) and intracranial pressure (ICP) for intact autoregulation but diminished compliance. In this case a negative correlation is predicted

in 6 patients (5 male; 1 female) treated in our neurosurgical ICU with a mean age of 37.3 years (maximum: 52 years; minimum: 21 years). The mean of all time segments with continuous data registration was 46.6 h (maximum: 123.1 h; minimum: 3.8 h). The patients were treated for severe traumatic brain injury ($n=5$) or stroke ($n=1$).

The first step of data analysis was to detect time periods of significant correlation between both parameters within the observation period. Therefore, we used a windowing technique combined with multitaper coherence analysis [7, 9]. We calculated the number of significant coherent frequencies in every subsequent window (2,048 data points) for frequencies lower than 0.002 Hz. The restriction to the low frequency band is essential to rule out fast variations that are not reflected by the mathematical model used. From this density of significant coherent frequencies we deduced information

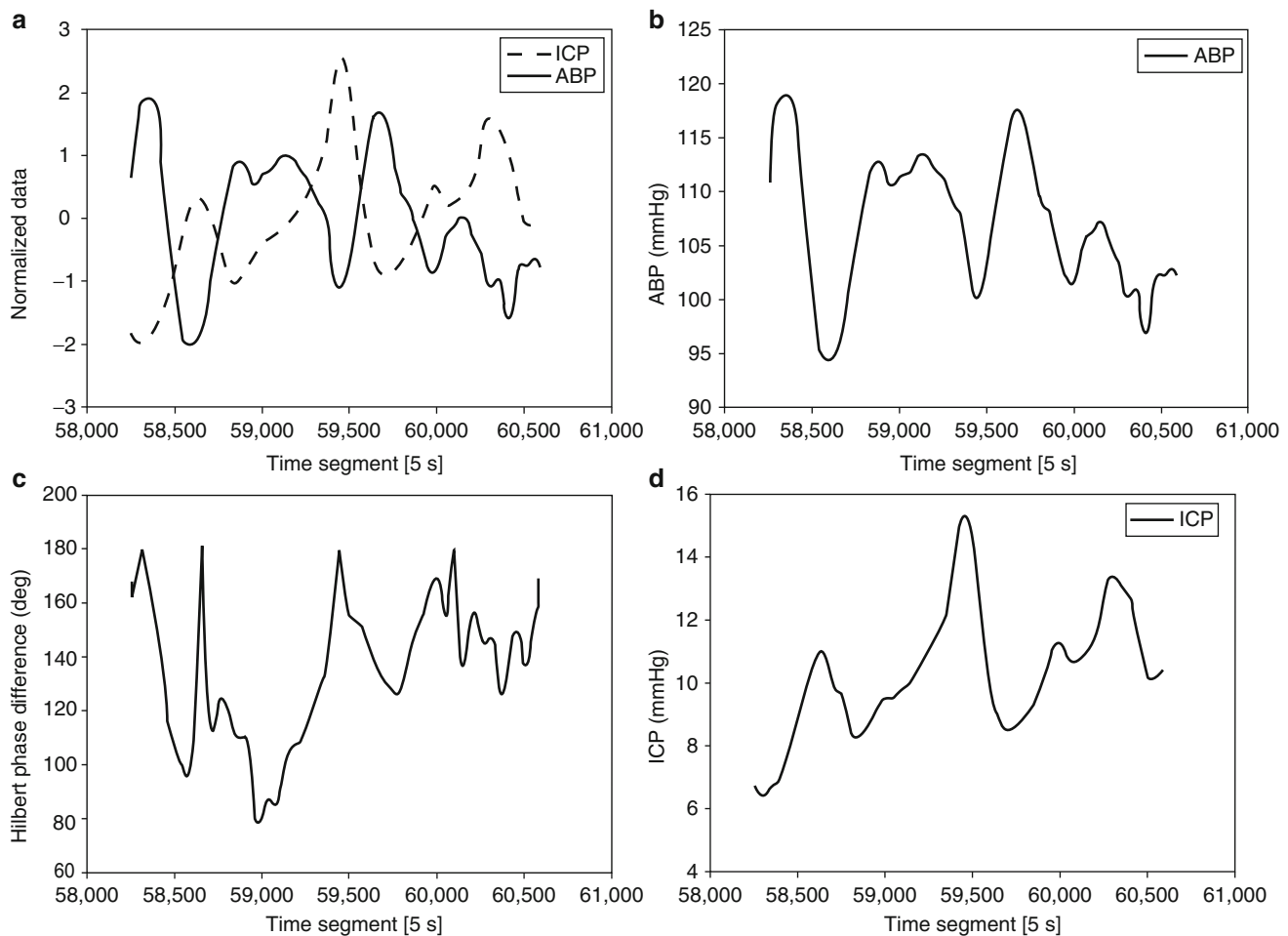


Fig. 2 The phasing of the data was determined by calculating the difference in the appropriate Hilbert phases. For a mean phase difference greater than 130 negative correlation was assumed. (a) Data normalized

to mean value zero and standard deviation one; (c) Difference in Hilbert phases; (b) Low-pass-filtered ABP; (d) Low pass filtered ICP

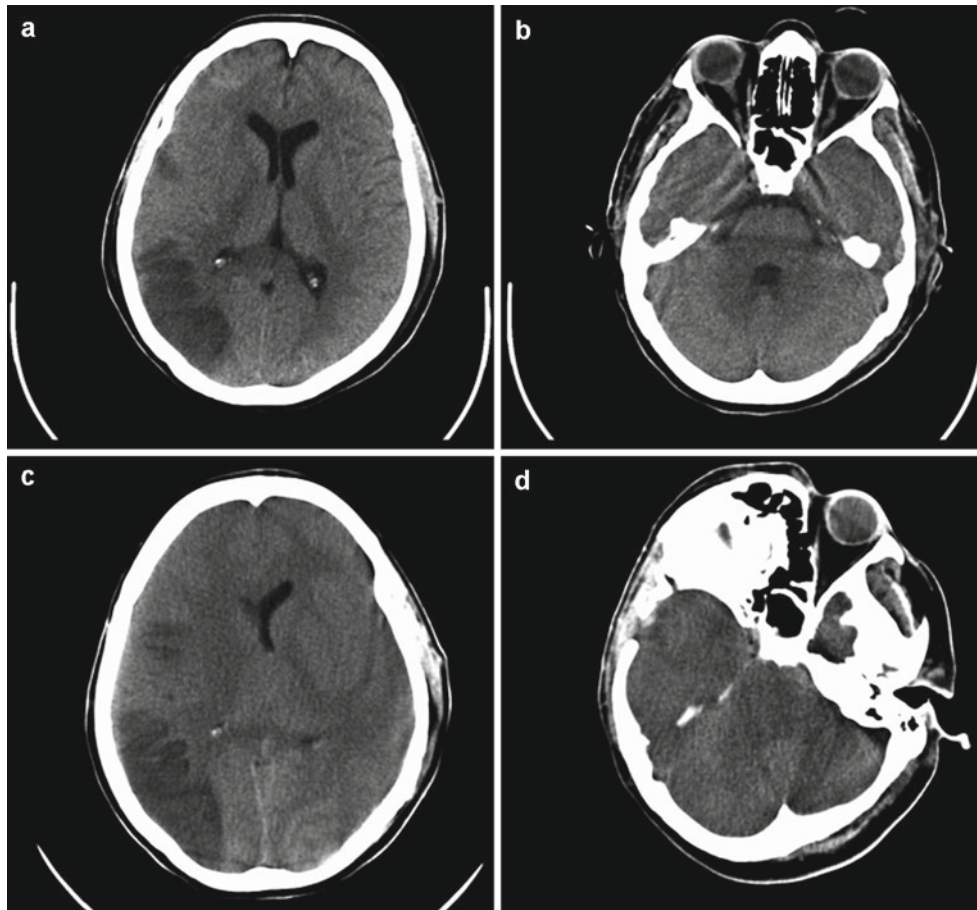


Fig. 3 Serial CT of a patient following severe head trauma (GCS 6). Initial scans show partial stroke of the right ACM (a), basal cisterns and fourth ventricle appear inconspicuous (b). Follow-up scans performed

at a period with highly negative correlation between ABP and ICP show reduced subarachnoid space, compressed lateral ventricles (c) and basal cisterns (d) indicating diminished intracranial compliance

about time segments of significant coherence. A detailed description of the method used can be found in Brawanski et al. [4]. The last step of data analysis was to single out the time segments of negative correlation between ABP and ICP. For this, we have low-pass-filtered the original data to reflect the long-term variations as detected by the multitaper method. Subsequently, the filtered signals were used to calculate the Hilbert phases of both signals and the associated phase difference. We defined the correlation to be negative (Fig. 2c) if the mean Hilbert phase difference was greater than 130°

intracranial compliance as predicted by the mathematical model was 3.3 h (maximum: 5.3 h; minimum: 2.9 h). In all patients, CT obtained at the phases of reduced intracranial compliance as identified by the multimodal neuromonitoring data analysis demonstrated changes in the intracranial compartment characterized by significant edema formation or enlargement of contusional lesions, leading to diminished cerebral compliance (Fig. 3). Most notably, the mean ICP recorded during the time periods detected was not significantly elevated (mean \pm STD: 14.1 ± 6.0 mmHg).

Results

The analysis revealed in five out of six datasets time segments in the observation period with events of negative correlation between ABP and ICP (Fig. 2a). The mean duration of the phases with this negative correlation indicating reduced

Discussion

In the initial phase after injury, the brain is particularly vulnerable to secondary insults such as cytotoxic or vasogenic brain edema, ischemia, and seizures. Consequently, the general treatment guidelines focus on the avoidance of secondary

injury by the neurointensivist [12]. The dynamic nature of the brain can lead to rapid deterioration that is not revealed by clinical examination until secondary damage is irreversible [13]. Imaging studies such as CT or MRI provide a snapshot at one point in time, providing only very limited information about the dynamic condition of the brain. Thus, a number of monitoring techniques have been developed such as intracranial pressure monitoring, cerebral perfusion pressure measurement, jugular venous oxygen saturation, detection of brain tissue oxygenation as well as transcranial Doppler ultrasound and continuous electroencephalography [2, 3, 10, 15]. The goal of monitoring multiple parameters in a combined fashion is to overcome some of the disadvantages of each technique and to achieve a higher degree of accuracy in detecting secondary brain insults [5]. However, interpretation of the data provided by multimodal neuromonitoring can be overwhelming. Efficient use of such information requires methods to integrate the different sets of information, and analyze the interrelationships between them [12]. The contribution of our study is twofold. First, we were able to show that intercorrelations between ABP and ICP predicted by a mathematical model simulating reduced intracranial compliance can in fact be detected in patients. Second, corresponding imaging studies confirmed the prediction of the model by displaying increased brain swelling, leading to diminished cerebral compliance. This is particularly important as the ICP values, frequently used as the primary parameter of intracranial dynamics, were not significantly increased during the time segments of low cerebral compliance, which is in accordance with the Monro–Kellie hypothesis stating that an increase in one intracranial compartment (brain, blood) will result in the decrease of another (CSF) [11]. The pressure may stay normal despite diminished intracranial compliance [14]. If the point of decompensation is reached, a rapid increase in ICP will occur, as predicted by the established pressure volume curve.

Conclusion

Our data indicate that complex multidimensional data analysis of neuromonitoring parameters can identify those patients

at risk because of reduced intracranial compliance, potentially leading to more efficient clinical management.

Conflict of interest statement We declare that we have no conflict of interest.

References

1. Barazangi N, Hemphill JC 3rd (2008) Advanced cerebral monitoring in neurocritical care. *Neurol India* 56(4):405–414
2. Bhatia A, Gupta AK (2007) Neuromonitoring in the intensive care unit. I. Intracranial pressure and cerebral blood flow monitoring. *Intensive Care Med* 33(7):1263–1271
3. Bhatia A, Gupta AK (2007) Neuromonitoring in the intensive care unit. II. Cerebral oxygenation monitoring and microdialysis. *Intensive Care Med* 33(8):1322–1328
4. Brawanski A, Faltermeier R, Rothoerl RD, Woertgen C (2002) Comparison of near-infrared spectroscopy and tissue $p(O_2)$ time series in patients after severe head injury and aneurysmal subarachnoid hemorrhage. *J Cereb Blood Flow Metab* 22(5):605–611
5. De Georgia MA, Deogaonkar A (2005) Multimodal monitoring in the neurological intensive care unit. *Neurologist* 11(1):45–54
6. Gather U, Imhoff M, Fried R (2002) Graphical models for multivariate time series from intensive care monitoring. *Stat Med* 21(18):2685–2701
7. Ghil M, Allen RM, Dettinger MD, Ide K, Kondrashov D, Mann ME, Robertson A, Saunders A, Tian Y, Varadi F, Yiou P (2002) Advanced spectral methods for climatic time series. *Rev Geophys* 40(1):3.1–3.41
8. Jung A, Faltermeier R, Rothoerl R, Brawanski A (2005) A mathematical model of cerebral circulation and oxygen supply. *J Math Biol* 51(5):491–507
9. Mann ME, Park J (1993) Spatial correlations of interdecadal variation in global surface temperatures. *J Geophys Res* 20:1055–1058
10. Mazzeo AT, Bullock R (2007) Monitoring brain tissue oxymetry: will it change management of critically ill neurologic patients? *J Neurol Sci* 261(1–2):1–9
11. Mokri B (2001) The Monro–Kellie hypothesis: applications in CSF volume depletion. *Neurology* 56(12):1746–1748
12. Vespa PM (2005) Multimodality monitoring and telemonitoring in neurocritical care: from microdialysis to robotic telepresence. *Curr Opin Crit Care* 11(2):133–138
13. Wartenberg KE, Schmidt JM, Mayer SA (2007) Multimodality monitoring in neurocritical care. *Crit Care Clin* 23(3):507–538
14. Wolfla CE, Luerssen TG, Bowman RM, Putty TK (1996) Brain tissue pressure gradients created by expanding frontal epidural mass lesion. *J Neurosurg* 84(4):642–647
15. Wright WL (2007) Multimodal monitoring in the ICU: when could it be useful? *J Neurol Sci* 261(1–2):10–15

Early Warning of EUSIG-Defined Hypotensive Events Using a Bayesian Artificial Neural Network

Rob Donald, Tim Howells, Ian Piper, I. Chambers, G. Citerio, P. Enblad, B. Gregson, K. Kiening, J. Mattern, P. Nilsson, A. Ragauskas, Juan Sahuquillo, R. Sinnott, and A. Stell

Abstract Background: Hypotension is recognized as a potentially damaging secondary insult after traumatic brain injury. Systems to give clinical teams some early warning of likely hypotensive instability could be added to the range of existing techniques used in the management of this group of patients. By using the Edinburgh University Secondary Insult Grades (EUSIG) definitions for hypotension (systolic arterial pressure <90 mmHg OR mean arterial pressure

<70 mmHg) we collected a group of ~2,000 events by analyzing the Brain-IT database. We then constructed a Bayesian Artificial Neural Network (an advanced statistical modeling technique) that is able to provide some early warning when trained on this previously collected demographic and physiological data.

Materials and Methods: Using EUSIG defined event data from the Brain-IT database, we identified a Bayesian artificial neural network (BANN) topology and constructed a series of datasets using a group of clinically guided input variables. This allowed us to train a BANN, which was then tested on an unseen set of patients from the Brain-IT database. The initial tests used a particularly harsh assessment criterion whereby a true positive prediction was only allowed if the BANN predicted an upcoming event to the exact minute. We have now developed the system to the point where it is about to be used in a two-stage Phase II clinical trial and we are also researching a more realistic assessment technique.

Key Results: We have constructed a BANN that is able to provide early warning to the clinicians based on a model that uses information from the physiological inputs; systolic and mean arterial pressure and heart rate; and demographic variables age and gender. We use 15-min SubWindows starting at 15 and 30 min before an event and process mean, slope and standard deviations. Based on 10 simulation runs, our current sensitivity is 36.25% (SE 1.31) with a specificity of 90.82% (SE 0.85). Initial results from a Phase I clinical study shows a model sensitivity of 40.95% (SE 6%) and specificity of 86.46% (SE 3%) Although this figure is low it is considered clinically useful for this dangerous condition, provided the false positive rate can be kept sufficiently low as to be practical in an intensive care environment.

Conclusion: We have shown that using advanced statistical modeling techniques can provide clinical teams with useful information that will assist clinical care.

Keywords Traumatic Brain Injury • Prediction • Hypotension • Bayesian Artificial Neural Network

R. Donald (✉)

School of Mathematics and Statistics, University of Glasgow,
Glasgow, Scotland, UK
e-mail: r.donald.1@research.gla.ac.uk, rob@statsresearch.co.uk

T. Howells, P. Enblad, and P. Nilsson
Department of Neurosurgery, Uppsala University Hospital,
Uppsala, Sweden

I. Piper
Department of Clinical Physics, Institute of Neurological Sciences,
Southern General Hospital, 1345 Govan Road, Glasgow,
Scotland G514TF, UK

I. Chambers
Department of Medical Physics, James Cook University Hospital,
Middlesbrough, UK

G. Citerio
Neuroranimazione, Hospital San Gerardo, Monza, Italy

B. Gregson
Department of Regional Medical Physics, Newcastle General Hospital,
Newcastle, UK

K. Kiening and J. Mattern
Department of Neurosurgery, Ruprecht-Karls-Universitat Hospital,
Heidelberg, Germany

A. Ragauskas
Head of Telematics (Biomedical) Sc. Lab.,
Kaunas University of Technology, Kaunas, Lithuania

J. Sahuquillo
Department of Neurosurgery, Vall d'Hebron University Hospital,
Barcelona, Spain

R. Sinnott
Department of Information Systems, University of Melbourne,
Melbourne, Australia

A. Stell
National eScience Centre, University of Glasgow, Glasgow, UK

Introduction

Patients being treated in an intensive care unit (ICU) for traumatic brain injury (TBI) are at risk of secondary insults [8]. Hypotension, critically low blood pressure, is one type of secondary insult and has been shown to be related to poor outcome [3, 7].

As part of a current European Union (EU) funded research project AvertIT [1], we have been researching the use of a statistical technique called a Bayesian artificial neural network (BANN) to assess whether this technique can be used to give clinicians early warning of this condition.

This report details our approach to using the BANN technique and provides some early indications of the results of using this technique in a Phase I clinical trial in six neurointensive care facilities throughout Europe: Uppsala, Sweden; Glasgow, Scotland; Vilnius, Lithuania; Heidelberg, Germany; Monza, Italy; and Barcelona, Spain.

Materials and Methods

This section of the report provides details on the data source used for initial investigations; the data preparation required; and the use of this prepared material to train the BANN.

Data Source

The data for our research comes from the BrainIT consortium [2]. The database comes from a multi-center study across 22 hospitals in Europe and it contains three classes of information: demographic data; physiological data; and episodic data.

The BrainIT database contains 199 patients although only 119 patients met our criteria of both BPs and BPm available with a sufficiently low number of short data gaps. The average age of the 119 patients was 39.04 years (range=15–83, median=34.05), with 85% being male. Nineteen patients had no events but these patients are included in the training data to reflect the small but present chance of this subgroup. Further details of the BrainIT database are available in Piper et al. [10].

Data Preparation

After statistical classification using definitions from clinical practice, we decided to use the published work on secondary insults by Jones and colleagues at Edinburgh University [7]. We use the definition for hypotension which is $BP \leq 90$ mmHg or $BPm \leq 70$ mmHg for a hold-down of 5 min. Using the EUSIG definition we built a list of 2,081 events from 100 patients with project-specific software [4].

Our next task was to produce a series of datasets that could be used to decide the topology of the BANN and then

calculate the various coefficients that form the heart of the BANN software, which runs in the clinical environment. We chose to use an approach called SubWindows in which each relevant physiological signal is divided into sections of time, and each SubWindow is summarized by multiple statistical calculations. Each statistical calculation within a SubWindow becomes a single input into the BANN. With reference to Fig. 1, we can see that for BPm, the slope of SubWindow 1 forms an input into the BANN.

An input definition syntax was developed and a software application was produced that scanned the BrainIT database on a minute by minute basis for each patient to build up a series of vectors (rows of data). Each vector of data contains a timestamp, a group of demographic and physiological signals as specified by the input definition file, and finally a flag that indicates whether or not a hypotensive event started or not at the appropriate prediction window.

BANN Topology and Training

This process used software based on a core of routines from Radford Neal at the University of Toronto [9] to perform the Bayesian calculations. We were guided by the clinical experience of the AvertIT neurosurgical teams in selecting likely inputs and time ranges. We carried out 33 runs over a 2-month period from September to October 2008. The top five runs showed a sensitivity of >40% and these are summarized in Table 1. Full details can be found in Howells and Donald [6]. We chose to further investigate the 30_15 BasicWithSlope model as its constituent measurements of Age, Sex, BPs, BPm, and heart rate were available in all centers.

A single BANN run is constructed by randomly assigning half of the patients (~50) to the training group and the other half to the test group. The positive vectors for each group are balanced by a proportion of negative vectors to form the training and test sets for the training run. It is important to ensure that vectors from a patient in the training group are not included in the test group.

We then constructed a series of BANN training runs. After each run an assessment was made on model performance as described in the section Test Set Model Assessment. The performance of the top five models is shown in the Results section in Table 1.

BANN Test Runs

A training run produces a series of coefficients for the BANN and the performance of this set of model parameters is tested by running the calculations over a set of unseen inputs provided from the test set. This produces a prediction list with

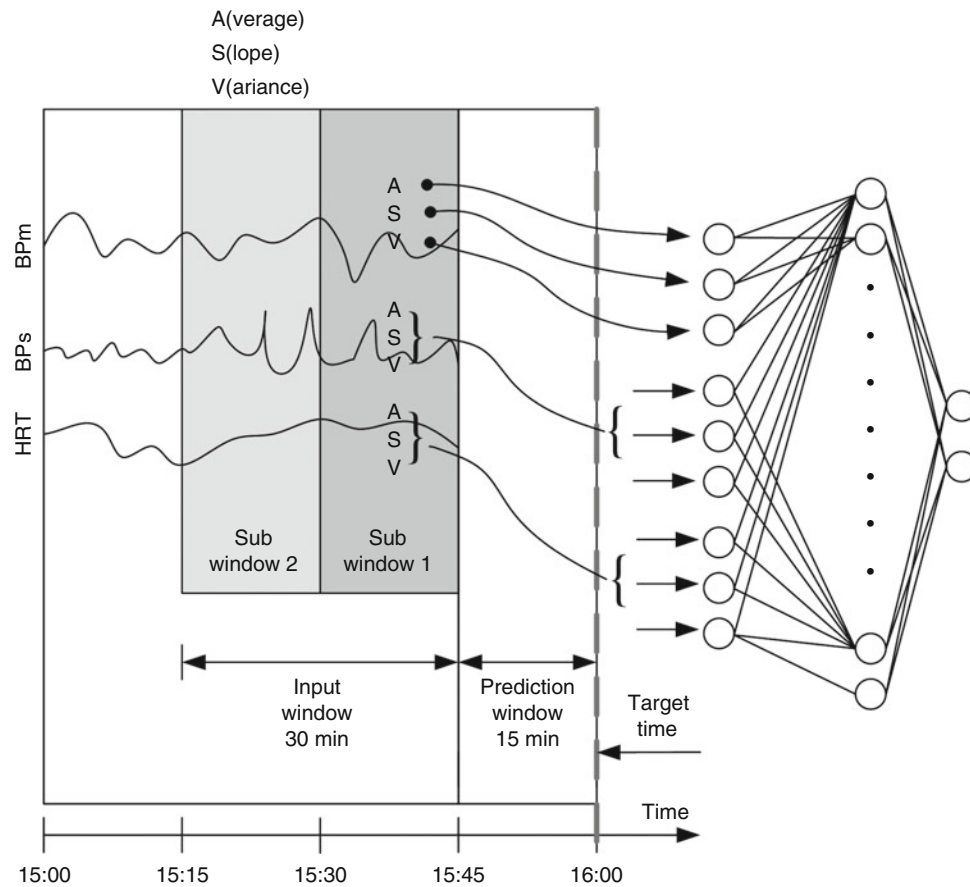


Fig. 1 SubWindow technique used to provide inputs for the Bayesian artificial neural network (BANN)

Table 1 Top five performing models

Date	Group	Name	Duration (H:M:S)	Sensitivity (%)	Specificity (%)
2008-10-09	30_15	BasicWithETCO2	01:14:11	43.9	85.1
2008-10-16	30_15	BasicSlopeVar550Nets	15:16:45	43.3	88.3
2008-10-09	30_15	BasicWithSlope	05:27:44	42.1	85.0
2008-10-07	25_10	Basic	03:01:08	41.4	91.1
2008-10-13	30_15	BasicWithSlope16HL	02:43:39	41.2	85.4

the probability of a hypotensive event occurring in the given prediction window. We then use the standard ROC procedure [5] for assessing a classifier.

Clinical Tests

Our testing has moved beyond the research phase and we are currently (October 2010) about to conclude a Phase I clinical study designed to quantify measures of the sensitivity and specificity of the system when operating under clinical conditions. The Phase I study software has been installed on a dedicated server in each one of the six participating neurointensive care units. A research nurse from the project works

with ward staff to admit a patient to the study and once relative assent has been obtained, the system transfers the minute by minute physiological data on an hourly basis to a central data store at the national eScience center at the University of Glasgow (NeSC) [11].

Test Set Model Assessment

The initial assessment method used for feature selection was particularly harsh. During this early phase of the research we took the more mathematical view that if the model had been trained on data at 15 min ahead of an event, we would only score a correct prediction if the model predicted this event to

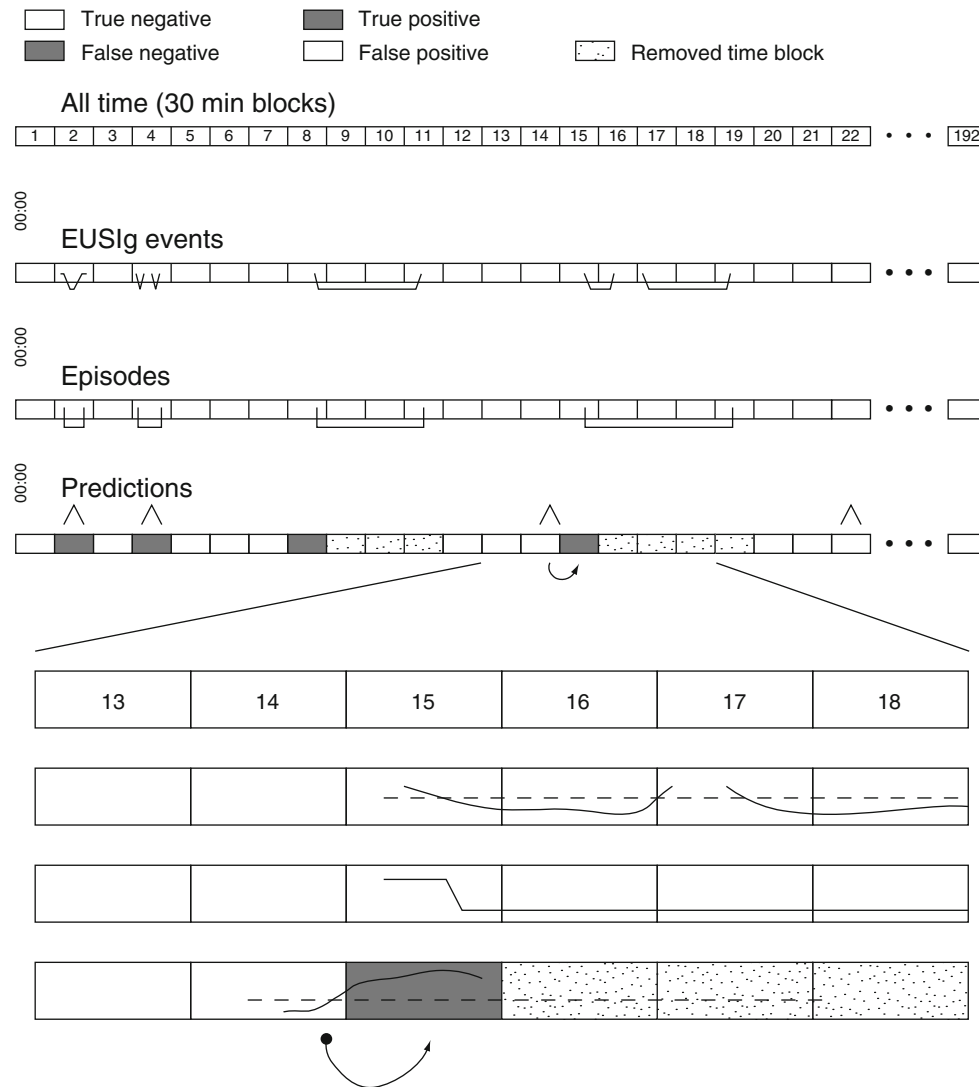


Fig. 2 Model assessment methodology

the minute. We applied this method to all 33 BANN training runs as described in the section BANN Topology and Training.

We felt that a more realistic approach was required because we have noticed that frequently groups of false positive events occur just before the 15-min actual event time. This means that we were getting *more* than 15 min warning, a better performance, but our assessment criterion was penalizing the model. We have therefore recently been using a technique that we feel provides a more clinically practical assessment of model performance.

Phase I Model Assessment

We present a proposal for a scoring system that we believe makes better clinical sense and gives a more realistic assessment of model performance. This section describes how the

events are grouped into blocks of time to allow the calculation of values for true positives, true negatives, false positives and false negatives.

With reference to Fig. 2, consider a system where the overall time in the ICU is split into 30-min blocks. For this example we have 4 days in the ICU, which equates to 192 possible blocks. We have, from the HypoPredict system, the times and durations of the actual hypotensive events that occurred given the EUSIG definitions. These can be assigned to the appropriate block as seen in the “EUSIG Events” line.

We then perform a further grouping of these events into “Episodes” of hypotension as it has been observed that the events sometimes occur in groups one after the other. The important characteristic of an early warning system from a clinician’s point of view is a system that gives a warning of the start of an episode. We will consider an inter-event time of 15 min or less to define the existence of a group. This allows us to fill in the line “Episodes.” In this line it can be seen that the two events in block 4 have become a single episode. The events

that started in blocks 15 and 17 have also been combined into a single episode running from block 15 to block 19.

The gated output from the model is used where “gated” means that the model probabilities are not considered during a hypotensive event or for a recovery period after the end of an event. This recovery period is required so that the model is using non-hypotensive data in its calculations. The recovery period is model-specific; the current model being tested has a 30-min recovery time. Using these definitions, we obtain the “Predictions” line in Fig. 2. We now consider each type of prediction block in turn using a prediction threshold of 0.3. The value of 0.3 was chosen from an ROC analysis carried out during the model selection procedure.

True Positive

A single true positive is generated if the model produces an output above 0.3 for 3 consecutive minutes and an event occurs within 30 min (the block size) of the start of the warning. Note that it is possible for a warning to start just at the end of one block and the episode occurs, for example, 20 min into the following block. This situation is handled by the protocol described in the section Episode Prediction in the Following Block.

True Negative

A true negative means that the model output was below the 0.3 threshold for the entire 30-min block and indeed there were no episodes during that time.

False Positive

A single false positive is generated if the model output stays above 0.3 for 3 consecutive minutes and no episode starts within 30 min (i.e. a block size time) of the start of the warning. Again, this has the potential to spill over into the next block and if this occurs it is handled by the rules described in the section Episode Prediction in the Following Block.

False Negative

A false negative is generated when an episode occurs and there is no warning output from the model.

Episode Prediction in the Following Block

When the model produces a warning output – in the examples above this has been defined as a probability greater than 0.3 – the actual event may occur in the following block. This is shown in the expanded view in Fig. 2. The scoring rule is

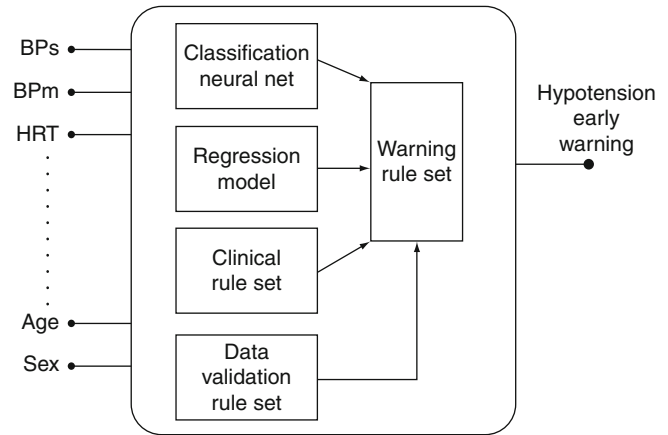


Fig. 3 HypoPredict engine components

defined such that the following block (block 15 in this case) is given the true positive score rather than the block where the prediction first occurred.

The rule to determine a false positive score is defined in the opposite manner. In the case of a false positive prediction that occurs just at the end of one block, if no event occurs within 30 min of the start of the prediction, which requires checking in the following block, then the block where the false prediction occurred is marked as false positive (see Fig. 2).

False Positive Suppression

We recognized from an early stage that the BANN classifier would only form one part of an eventual HypoPredict Engine, which could possibly be used within a clinical environment. This is shown diagrammatically in Fig. 3.

As a consequence of the initial indications from the Phase I clinical trial, we have recently begun to investigate using suppression techniques based on the statistical properties of the distribution curve produced by the BANN for each minute’s prediction along with, crucially, clinical experience used when assessing the raw blood pressure and heart rate traces. These clinical heuristics have given us a promising tool in our efforts to reduce the false positive rate of the system.

Results

Model Selection

The model selection is shown in Tables 1.

Phase I Trial Early Indications

Early indications from the Phase I clinical study, based on 20 patients collected from the 6 participating neurointensive care units, indicate that we are achieving a sensitivity of 43.85% (SE 7%) with a specificity of 83.21% (SE 3%). By applying our first pass suppression techniques these values change to a sensitivity of 40.95% (SE 6%) with a specificity of 86.46% (SE 3%). The average warning time is 21 min (SE 0.74).

Discussion

We have shown that it is possible to construct a system that provides useful early warning of the dangerous traumatic brain injury secondary insult condition of hypotension. This system is based on an advanced statistical modeling technique called a Bayesian Artificial Neural Network (BANN) and we have described the not inconsiderable data preparation required to use this technique. We feel that the topic of model assessment has been addressed in a manner that includes the requirements from clinical teams to produce systems that not only provide accurate warning of an event of interest, but which also recognize the need to maintain a low number of false positives. Finally, we have shown that this research has translated from an experimental result to a system that works under real clinical conditions.

Conclusion

Areas of future research include assessing the influence of different probability cutoff thresholds on calculated false positive rate. Although higher sensitivities are desirable and the addition of other more complex signals such as EEG may improve accuracy, the lead emphasis clinically is on a technology that has more ubiquitous application in ITUs with only basic physiological monitoring, and of course that it be clinically practical by generating as few false warnings as possible. A technology that could detect even 1 in 3 (33%

sensitivity) hypotensive events could be clinically significant, but only if the clinicians alter their management of hypotension accordingly. To show this would ultimately require a further clinical trial.

Conflict of interest statement The authors declare that they have no conflict of interest.

References

1. AvertIT (2008) Avert-it project (FP7-217049-AVERT-IT). URL: <http://www.avert-it.org/> Accessed on: 2010.09.01
2. BrainITTeam (2007) BrainIT. URL: <http://www.brainit.org/> Accessed on: 2007.12.22
3. Chesnut RM, Marshall LF, Klauber MR, Blunt BA, Baldwin N, Eisenberg HM, Jane JA, Marmarou A, Foulkes MA (1993) The role of secondary brain injury in determining outcome from severe head injury. *J Trauma* 34(2):216–222
4. Donald R (2008) Event definition analysis, preliminary results. Technical report, Avert-IT Project URL: <http://www.avert-it.org>. Accessed on: 2010.09.01
5. Fawcett T (2004) ROC graphs: notes and practical considerations for researchers. URL: http://home.comcast.net/~tom.fawcett/public_html/papers/ROC101.pdf. Accessed on: 2009.03.04
6. Howells T, Donald R (2008) Hypopredict provisional build (t2.3). Technical report, Avert-IT Project. URL: <http://venus.nesc.gla.ac.uk/wordpress>. Accessed on: 2009.01.08
7. Jones P, Andrews P, Midgley S, Anderson S, Piper I, Tocher J, Housley A, Corrie J, Slattery J, Dearden M, Miller D (1994) Measuring the burden of secondary insults in head-injured patients during intensive care. *J Neurosurg Anesthesiol* 6:4–14
8. Miller JD, Becker DB (1982) Secondary insults to the injured brain. *J R Coll Surg Edinb* 27:292–298
9. Neal RM (1996) Bayesian learning for neural networks. Lecture notes in statistics, vol 118. Springer, New York
10. Piper I, Chambers I, Citerio G, Enblad P, Gregson B, Howells T, Kiening K, Mattern J, Nilsson P, Ragauskas A, Sahuquillo J, Donald R, Sinnott R, Stell A (2010). The brain monitoring with information technology (BrainIT) collaborative network: EC feasibility study results and future direction. *Acta Neurochir* 1–13. ISSN 0001–6268. URL: <http://dx.doi.org/10.1007/s00701-010-0719-1>; 10.1007/s00701-010-0719-1
11. Stell A, Sinnott R, Jiang J, Donald R, Chambers I, Citerio G, Enblad P, Gregson B, Howells T, Kiening K, Nilsson P, Ragauskas A, Sahuquillo J, Piper I (2009) Federating distributed clinical data for the prediction of adverse hypotensive events. *Philos Transact A Math Phys Eng Sci* 367(1898):2679–2690. doi:10.1098/rsta.2009.0042, URL: <http://rsta.royalsocietypublishing.org/content/367/1898/2679>. Abstract

Trigger Characteristics of EUSIG-Defined Hypotensive Events

Rob Donald, Tim Howells, Ian Piper, I. Chambers, G. Citerio, P. Enblad, B. Gregson, K. Kiening, J. Mattern, P. Nilsson, A. Ragauskas, Juan Sahuquillo, R. Sinnott, and A. Stell

R. Donald (✉)
School of Mathematics and Statistics,
University of Glasgow, Glasgow, Scotland, UK
e-mail: r.donald.1@research.gla.ac.uk, rob@statsresearch.co.uk

T. Howells, P. Enblad, and P. Nilsson
Department of Neurosurgery,
Uppsala University Hospital,
Uppsala, Sweden

I. Piper
Department of Clinical Physics, Institute of Neurological Sciences,
Southern General Hospital, 1345 Govan Road,
Glasgow, Scotland G514TF, UK

I. Chambers
Department of Medical Physics,
James Cook University Hospital,
Middlesbrough, UK

G. Citerio
Neuroranimazione,
Hospital San Gerardo,
Monza, Italy

B. Gregson
Department of Regional Medical Physics,
Newcastle General Hospital,
Newcastle, UK

K. Kiening and J. Mattern
Department of Neurosurgery,
Ruprecht-Karls-Universitat Hospital,
Heidelberg, Germany

A. Ragauskas
Head of Telematics (Biomedical) Sc. Lab.,
Kaunas University of Technology, Kaunas, Lithuania

J. Sahuquillo
Department of Neurosurgery,
Vall d'Hebron University Hospital,
Barcelona, Spain

R. Sinnott
Department of Information Systems,
University of Melbourne,
Melbourne, Australia

A. Stell
National eScience Centre,
University of Glasgow, Glasgow, Scotland, UK

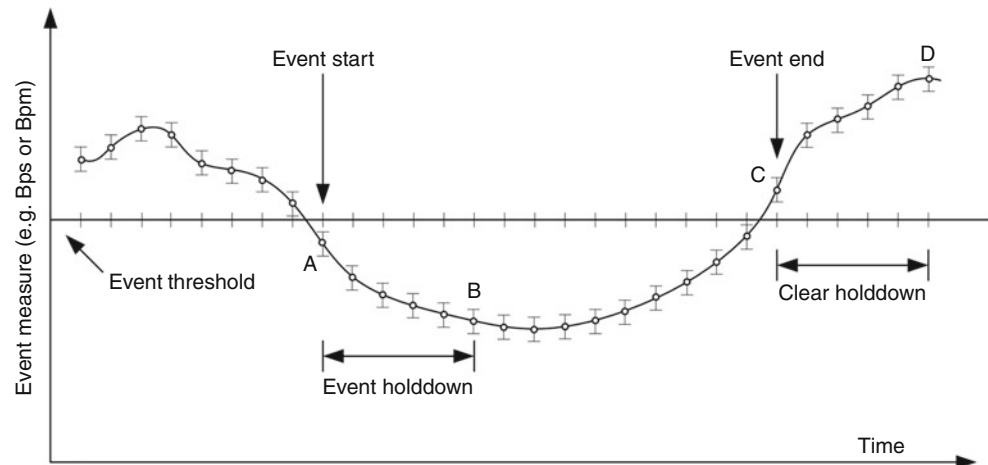
Abstract *Background:* Hypotension is a recognized secondary insult after traumatic brain injury (TBI). There are many definitions of hypotension, an often cited example being the Brain Trauma Foundation's current (2007) "Guidelines for the Management of Severe Traumatic Brain Injury," which defines hypotension as systolic pressure <90 mmHg. However, this same document declares "The importance of mean arterial pressure, as opposed to systolic pressure should also be stressed," Our work shows that when using the Edinburgh University Secondary Insult Grades (EUSIG) definitions, which require monitoring of both systolic and mean arterial pressures, that most hypotensive events are in fact triggered by a breach of the mean arterial level of 70 mmHg. We suggest that close monitoring of mean arterial pressure would enable clinical teams to avoid more potentially damaging hypotensive events.

Materials and Methods: An analysis of 100 patients from the Brain-IT database was performed. Using the EUSIG definitions, 2,081 events can be obtained by analyzing the systolic and mean blood pressures on a minute by minute basis. A software program was written to identify and classify the trigger pattern for each event. A categorical analysis of these triggering patterns has been carried out.

Key Results: Our analysis shows that most events are triggered by a drop in mean arterial pressure. In fact a large number of events (91%) occur where the mean arterial pressure is below the threshold limits whereas the systolic pressure does not cross the 90 mmHg limit at all.

Conclusion: We suggest that more emphasis should be placed on closely monitoring mean arterial pressure as well as systolic pressure when trying to guard against hypotensive problems in traumatically brain injured patients. In future work we will study the underlying physiological mechanisms and attempt to further classify concomitant conditions that may be contributing to the onset of a hypotensive event.

Keywords Traumatic Brain Injury • Hypotension • Systolic Arterial Blood Pressure • Mean Arterial Blood Pressure • Secondary Insults

Fig. 1 Event definition

Introduction

It has been known since the 1980s that secondary insults are a major factor in the treatment of traumatically brain injured patients [9]. Although there are several classes of secondary insults, several authors have shown that significant periods of arterial hypotension consistently relate to clinical outcome [5, 7, 8, 12, 13]. As part of a current European Union (EU) funded research project Avert-IT [1] an investigation has been undertaken into the characteristics of the physiological signals surrounding a hypotensive incident. This report details the methods used to investigate these characteristics and the results of these analyses.

Current guidelines from the Brain Trauma Foundation [4] recommend using systolic arterial pressure ≤ 90 mmHg as a threshold but make no mention of a holddown period. Recent work by Bijker and colleagues [2] continues to highlight the difficulty in obtaining a consensus on a hypotensive definition, with this group identifying more than 45 definitions used in various publications.

Materials and Methods

This section of the report provides details of the data used in the analysis; defines the threshold characteristics of a hypotensive event; defines a series of trigger and clearance profiles; and a description of the two software methods used to obtain the results.

Data Source

We based our investigations on the BrainIT database, which is a rich resource of data collected by the BrainIT organization [3] during an EU-funded project from 2002 to 2005. This database was the result of a multicenter study across 22

hospitals in Europe and it contains anonymized demographic information, treatment data, and minute by minute physiological signals of 199 patients who were admitted with severe brain injury defined as $GCS \leq 8$.

The BrainIT database contains 199 patients; however, only 119 patients met the criteria of having both BPs and BPm available. Of these 119 patients a further 19 were removed because they did not have any EUSIG-defined hypotensive events. The average age of the eligible 100 patients was 39.04 years (range=15–83, median=34.5), with 85% being male. Full details of the data available in the BrainIT database can be found in Piper et al. [10].

Event Parameters

A conceptual description of an event is provided in Fig. 1.

If we consider a trace of either BPs or BPm that is being scanned, the sequence of events that occurs is: A – trace falls below the “Event Threshold”; B – trace remains below the event threshold for the defined “Event Holddown” period. The event is now “Active” starting from point “A”; C – trace rises above the event threshold; D – trace remains above the event threshold for the “Clear Hold-down” period. At this point the event is declared complete, the event is defined from point “A” to “C.” One problem when attempting to construct experiments on classifying hypotensive events is obtaining an agreed definition for such an event. The six centers participating in the AvertIT project all provided a different definition of what their clinical teams used to monitor a patient for a hypotensive condition. These definitions are provided in Table 1.

Event Profiles

Using the EUSIG event definition described in the Results section, there are 11 possible event profiles that can occur. These are defined by the type of event trigger (BPs or BPm)

Table 1 Hypotensive definition by center

Location						
Parameter	Uppsala	Glasgow	Kaunas	Heidelberg	Monza	Barcelona
Measure and threshold	BPs < 100	BPm < 70	BPs/BPd = 90/50 and BPm < 70	CPP < 50	BPs < 90	BPs < 90
Event holddown	2	5	5	5	5	5
Clear holddown	BPs > 100; 5 m*	BPm > 70; 5 m*	BPm > 70; 5 m	CPP > 60; 5 m	BPs > 90; 10 m	BPs > 90; 15 m

Note the * values were estimated as the center did not define this parameter

Table 2 Event profile definitions

Trigger	Clear	Profile name
BPs (Type 1)	BPs	T-BPs-C-BPs-BPm-Enclosed --- (1)
	BPs	T-BPs-C-BPs-BPs-Only --- (2)
	BPm	T-BPs-C-BPm --- (3)
	Both	T-BPs-C-Both --- (4)
BPm (Type 2)	BPm	T-BPm-C-BPm-BPs-Enclosed --- (5)
	BPm	T-BPm-C-BPm-Only --- (6)
	BPs	T-BPm-C-BPs --- (7)
	Both	T-BPm-C-Both --- (8)
Both BPs, BPm (Type 3)	BPs	T-Both-C-BPs-BPm-Enclosed --- (9)
	BPm	T-Both-C-BPm-BPs-Enclosed --- (10)
	Both	T-Both-C-Both --- (11)

and the event clear mechanism (BPs and BPm). In Table 2, T=trigger, C=Clear, and --- (x)=Event Profile (Fig. 2).

Data Analysis

The method used to initially investigate this problem was to develop a Java-based application called “Data Set Generator” (DSG) to scan the BrainIT database for hypotensive events; this is outlined in the section Java-Based Software. After deciding that investigations should focus on the use of the Edinburgh University Secondary Insult Grades (EUSIG) definitions, the DSG was programmed to classify each event as coming from one of the 11 profiles described in the section Event Profiles. As the results emerged it was decided to verify the findings by using an alternative technique based on SQL and PERL scripts, this is described in the section SQL and PERL Scripts.

Java-Based Software

The DSG program is a Java-based application that we have coded for the AvertIT project.

It reads a configuration file that details the parameters to be used, as defined by one of the six neurosurgery centers. The DSG program produces a series of output files that are

then further processed using the “R” statistical package [11] to produce the statistical plots and results that are included in this report. More detailed notes on the structure and operation of the DSG program are provided in a project report [6], which can be obtained from the lead author.

The initial results (see the Results section) showed that most events were associated with the BPm signal crossing the threshold. Accordingly, the DSG program was modified to look for trigger patterns, as described in the section Event Profiles.

SQL and PERL Scripts

Because the results showed such a striking dominance of BPm triggered events, it was decided to obtain confirmation of these trigger patterns using a different software approach. To this end, a simple SQL script was coded to select the timestamp, BPs and BPm values from the entire database that fell below the EUSIG definition. This produced two files, one for BPs and one for BPm, and these two files were further processed by a single PERL script, which counted the number of event starts/stops for each patient.

Results

An initial investigation using the definitions from Table 1 showed that the highest number of events occurred when using the definition from Glasgow, which is based on mean arterial pressure (BPm). The second highest number of events was produced using the Uppsala definition. Although the Uppsala definition is based on systolic arterial pressure, the threshold value and holddown used of 100 mmHg for 2 min are stricter than the more usual values of 90 mmHg with a hold-down of 5 min. The next highest number of events was produced using the Heidelberg definition, which uses cerebral perfusion pressure (CPP), which of course uses BPm in its calculation.

Given these results it was decided to investigate a scheme that uses both BPm and BPs, and therefore the work by Jones and colleagues at Edinburgh University in the mid 1990s was used as a starting point for another sweep through the BrainIT database [7]. This previous work had produced the “Edinburgh University Secondary Insult Grades” (EUSIG) and provides

Fig. 2 BPm triggers event profiles

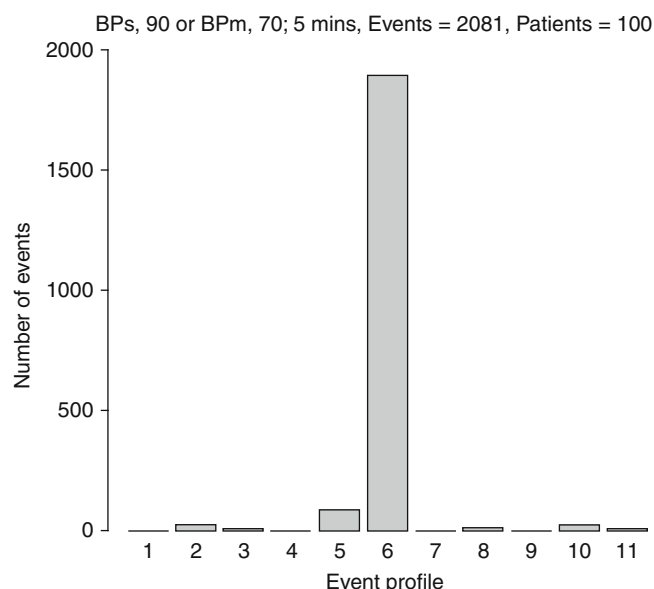
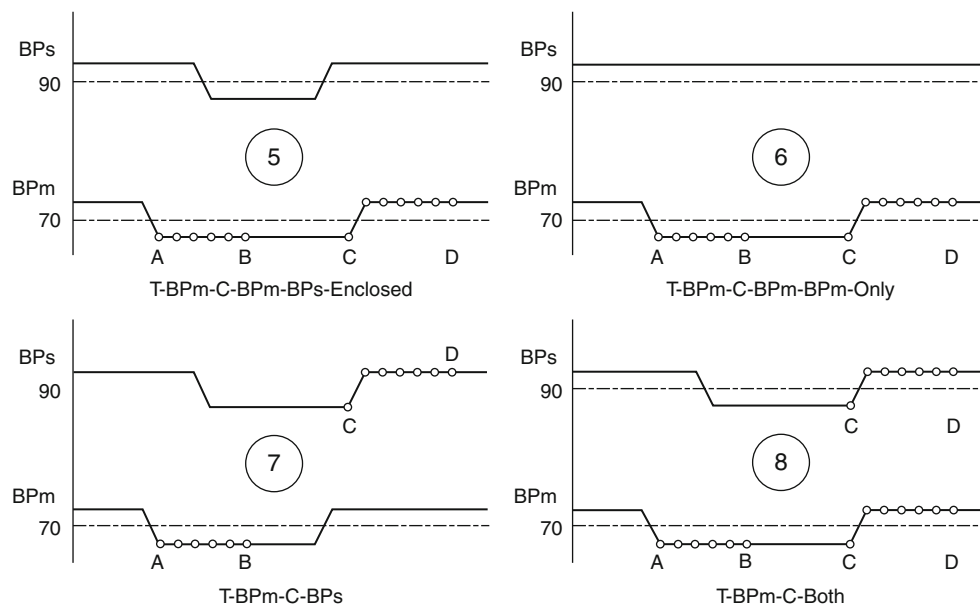


Fig. 3 Events classified by event profile type (Table 2)

threshold values for 14 secondary insult categories. Our research uses the definition for hypotension, which is $BPs \leq 90$ mmHg or $BPm \leq 70$ mmHg for a holddown of 5 min. Using the EUSIG definition we were able to identify 2,081 events from 100 patients.

During the analysis using the EUSIG events it was noticed that the majority of the events were triggered by a breach of the BPm threshold and it was often the case that the BPs trace was considerably above the 90-mmHg threshold. As described in the sections Event Profiles and Data Analysis, the DSG program was modified to classify the trigger and clearance characteristics of the events (Fig. 3).

The vast majority of events turn out to be Type 6, which are purely BPm-driven. This result was so striking that we

decided to confirm our finding using a different software technique based on SQL and PERL scripts as described in the section SQL and PERL scripts. The results of this exercise confirmed the pattern first shown with the Java-based DSG software. For BPm triggers there were 147 patients with 3,905 events. For BPs triggers there were 41 patients with 99 events. The higher numbers of events generated using this method are due to the simplistic nature of the script, which does not use a holddown mechanism. The key result is that the pattern of the majority of events being triggered by BPm is confirmed.

Discussion

Our research contributes to the debate regarding which physiological measure should be used when guarding against hypotensive conditions in TBI patients. We have shown that when using a measure based on mean arterial pressure that the prevalence of hypotension may be more widespread than previously considered. Future work should be carried out to determine if the hypotensive events identified as being driven purely by BPm can be associated with a poorer outcome for this group of patients.

Conclusion

To quote from the Brain Trauma Foundation guidelines 2007, page S-8 [4], “The importance of mean arterial pressure, as opposed to systolic pressure, should also be stressed, not only because of its role in calculating CPP, but because the lack of a consistent relationship between

systolic and mean pressures makes calculations based on systolic pressures unreliable. It may be valuable to maintain mean arterial pressures considerably above those represented by systolic pressures of 90 mmHg throughout the patient's course, but currently there are no data to support this." We believe that our work provides a start to this body of evidence.

Conflict of interest statement The authors declare that they have no conflict of interest.

References

1. AvertIT (2008) Avert-it project (FP7-217049-AVERT-IT). URL: <http://www.avert-it.org/> Accessed on: 2010.09.01
2. Bijker JB, van Klei WA, Vergouwe Y, Eleveld DJ, van Wolfswinkel L, Moons KGM, Kalkman CJ (2009) Intraoperative hypotension and 1-year mortality after noncardiac surgery. *Anesthesiology* 111(6):1217–1226. doi:10.1097/ALN.0b013e3181c14930
3. BrainIT Team (2007) BrainIT. URL: <http://www.brainit.org/> Accessed on: 2007.12.22
4. Brain Trauma Foundation (2007) Guidelines for the management of severe traumatic brain injury, 3rd edn. *J Neurotrauma* 1:1–117, URL: https://www.braintrauma.org/pdf/protected/Guidelines_Management_2007w_bookmarks.pdf Accessed on: 2008.09.28
5. Chesnut RM, Marshall LF, Klauber MR, Blunt BA, Baldwin N, Eisenberg HM, Jane JA, Marmarou A, Foulkes MA (1993) The role of secondary brain injury in determining outcome from severe head injury. *J Trauma* 34(2):216–222
6. Donald R (2008) Event definition analysis, preliminary results. Tech rep, Avert-IT Project URL: <http://www.avert-it.org> Accessed on: 2010.09.01
7. Jones P, Andrews P, Midgley S, Piper I, Tocher J, Housley A, Corrie J, Slattery J, Dearden M, Miller D (1994) Measuring the burden of secondary insults in head-injured patients during intensive care. *J Neurosurg Anesthesiol* 6:4–14
8. Marmarou A, Anderson R, Ward J et al (1991) Impact of ICP instability and hypotension on outcome in patients with severe head trauma. *J Neurosurg* 75:S59–S66, URL: <http://jnsonline.org/jns/issues/v75n5s/pdf/n0750059.pdf> Accessed on: 2007.12.31
9. Miller J, Becker D (1982) Secondary insults to the injured brain. *J R Coll Surg Edinb* 27:292–298
10. Piper I, Chambers I, Citerio G, Enblad P, Gregson B, Howells T, Kiening K, Mattern J, Nilsson P, Ragauskas A, Sahuquillo J, Donald R, Sinnott R, Stell A (2010) The brain monitoring with information technology (BrainIT) collaborative network: EC feasibility study results and future direction. *Acta Neurochir* 152(11):1–13. URL: <http://dx.doi.org/10.1007/s00701-010-0719-1>, doi:10.1007/s00701-010-0719-1 Accessed on: 2010.05.29
11. R Development Core Team (2008) R: A language and environment for statistical computing. R foundation for statistical computing, Vienna. URL: <http://www.R-project.org>, ISBN 3-900051-07-0 Accessed on: 2008.04.17
12. Signorini DF, Andrews PJD, Jones PA, Wardlaw JM, Miller JD (1999) Adding insult to injury: the prognostic value of early secondary insults for survival after traumatic brain injury. *J Neurol Neurosurg Psychiatry* 66:26–31, URL: <http://jnnp.bmj.com/cgi/reprint/66/1/26> Accessed on: 2008.01.09
13. Signorini DF, Andrews PJD, Jones PA, Wardlaw JM, Miller JD (1999) Predicting survival using simple clinical variables: a case study in traumatic brain injury. *J Neurol Neurosurg Psychiatry* 66:20–25, URL: <http://jnnp.bmj.com/cgi/reprint/66/1/20> Accessed on: 2008.01.09

Go Green! Reusing Brain Monitoring Data Containing Missing Values: A Feasibility Study with Traumatic Brain Injury Patients

Mengling Feng, Liang Yu Loy, Feng Zhang, Zhuo Zhang, Kuralmani Vellaisamy, Pei Loon Chin, Cuntai Guan, Liang Shen, Nicolas K.K. King, Kah Keow Lee, and Beng Ti Ang

Abstract Background: Despite the wealth of information carried, periodic brain monitoring data are often incomplete with a significant amount of missing values. Incomplete monitoring data are usually discarded to ensure purity of data. However, this approach leads to the loss of statistical power, potentially biased study and a great waste of resources. Thus, we propose to reuse incomplete brain monitoring data by imputing the missing values – a green solution! To support our proposal, we have conducted a feasibility study to investigate the reusability of incomplete brain monitoring data based on the estimated imputation error.

Materials and Methods: Seventy-seven patients, who underwent invasive monitoring of *ICP*, *MAP*, *PbtO₂* and brain temperature (*BTemp*) for more than 24 consecutive hours and were connected to a bedside computerized system, were selected for the study. In the feasibility study, the imputation error is experimentally assessed with simulated missing values and 17 state-of-the-art predictive methods. A framework is developed for neuroclinicians and neurosurgeons to determine the best re-usage strategy and predictive methods based on our feasibility study.

Results/Conclusion: The monitoring data of *MAP* and *BTemp* are more reliable for reuse than *ICP* and *PbtO₂*; and, for *ICP* and *PbtO₂* data, a more cautious re-usage strategy should be employed. We also observe that, for the scenarios tested, the lazy learning method, K-STAR, and the tree-based method, M5P, are consistently 2 of the best among the 17 predictive methods investigated in this study.

Keywords Traumatic brain injury • Brain monitoring • Intracranial pressure • Missing values/data • Data re-usage • Feasibility study

Introduction

Background

Traumatic brain injury (TBI) [5] constitutes a large portion of the workload of neuro-critical care, and it is a major cause of death and disabilities worldwide [20]. The major challenge in TBI patient treatment is that: primary traumatic brain damage is often compounded by secondary pathophysiological insults that occur after trauma, during the patient's stay in the intensive care unit [10]. Many studies [13, 22] have demonstrated that secondary insults have significant effects on the mortality and recovery rates of TBI patients. Secondary insults can potentially be reduced or prevented with the help of continuous patient monitoring and timely interventions [7]. Continuous brain monitoring of TBI patients has become a gold standard in most neuro-intensive care units (NICUs) [1, 14]. Contemporary brain monitoring involves multiple global and local modalities, such as intracranial pressure (*ICP*), mean arterial pressure (*MAP*), brain tissue oxygenation (*PbtO₂*) and brain temperature (*BTemp*) [19, 23, 24]. The periodic brain monitoring signals, which possess substantial physiological and pathological information, are extremely valuable for statistical analysis and knowledge discovery in clinical research [12]. However, despite the wealth of information carried, the monitoring data are often incomplete with a significant

M. Feng (✉), L.Y. Loy, F. Zhang, Z. Zhang, K. Vellaisamy, P.L. Chin, and C. Guan
Institute for Infocomm Research, A*STAR,
1 Fusionopolis Way, #21-01, Connexis (South),
Singapore, Singapore
e-mail: mfeng@i2r.a-star.edu.sg; lyloy@i2r.a-star.edu.sg;
fzhang@i2r.a-star.edu.sg; zzhang@i2r.a-star.edu.sg;
vkmani@i2r.a-star.edu.sg; plchin@i2r.a-star.edu.sg;
ctguan@i2r.a-star.edu.sg

L. Shen
Unit of Biostatistics, Yong Loo Lin School of Medicine,
National University of Singapore, Block 1E Kent
Ridge Road, Singapore, Singapore
e-mail: medsl@nuhs.edu.sg

N.K.K. King, K.K. Lee, and B.T. Ang
Department of Neurosurgery, National Neuroscience Institute,
11 Jalan Tan Tock Seng, Singapore, Singapore
e-mail: nicolas_kon@nni.eom.sg; kah_keow_lee@nni.eom.sg;
beng_ti_ang@nni.eom.sg

amount of missing values [17, 18]. Given the complicated and constrained environment of the NICUs, missing values in the monitoring data can be caused by multiple factors [15], e.g., movement of patients, faults with monitoring probes, connection problems, errors in recording systems or human errors.

Problem

Missing values in brain monitoring data can jeopardize the validity and credibility of corresponding statistical studies and can also lead to false knowledge discovery when left untouched. Therefore, as suggested by Fan et al., Ian et al. and Scalzo et al. [9, 16], the most common approach to addressing missing values is to exclude and discard incomplete monitoring data. This approach is often referred to as the “Complete Case” approach in the literature [11]. The “Complete Case” approach, to certain extent, does ensure the purity of the data and guarantee the validity of the study. However, the Complete Case approach suffers from three main shortcomings:

1. The approach inevitably sacrifices useful information and reduces the effective sample size, and it consequently causes a loss of statistical power.
2. Under the Complete Case approach, fewer training cases are taken into consideration, which may lead to biased analysis.
3. The approach causes waste. “Data is the currency for progress in neuroscience” [4]. Simply discarding incomplete brain monitoring data leads to great waste of time, resources, and human effort.

Therefore, in this paper, we propose to reuse incomplete brain monitoring data by imputing the missing values – a green solution!

Contributions

To support our proposal, we conducted a feasibility study to investigate whether incomplete brain monitoring data can be reused with missing value imputations. We conducted the feasibility study based on the monitoring data of TBI patients. The reusability of incomplete monitoring data is assessed based on the estimated imputation error, which is experimentally measured with simulated missing values. In addition, we further demonstrate that the estimated imputation error can be used as a guideline to facilitate neuroclinicians and neurosurgeons decisions regarding the re-usage strategy for incomplete brain monitoring data.

Materials and Methods

Patients and Monitoring

This analytical study was conducted based on the monitoring data of TBI patients, who were admitted to the neuro-critical care unit of a tertiary hospital between January 2002 and December 2007. Seventy-seven patients, who underwent invasive monitoring of *ICP*, *MAP*, *PbtO₂* and brain temperature (*BTemp*) for more than 12 consecutive hours, were selected for the study. After informed consent was obtained, intraparenchymal probes were inserted based on the pre-operative CT findings. *ICP* was continuously monitored using a fiber-optic intraparenchymal gauge (Codman and Shurtleff, Taynham, MA, USA), and Licox polarographic Clark-type microcatheters (Integra Neuroscience, Plainsboro, NJ, USA) were inserted into peri-lesional brain tissues to measure the brain temperature and *PbtO₂*. *MAP* was measured through an arterial line from the radial artery using a standard pressure monitoring kit (Biosensors International Pte. Ltd., Netherlands). The continuously monitored physiological readings were sampled and recorded every 10 s. *PRx* was calculated as a moving correlation between the last 30 consecutive samples of *ICP* and *MAP* readings. All patients underwent multi-modality monitoring with continuous recording of clinical data on a Hewlett-Packard Carevue System.

Patients were managed based on a protocol incorporating the guidelines for the management of severe TBI [3]. *ICP* of patients was optimized based on an incremental regimen to maintain *ICP* <20 mmHg and *CPP* >60 mmHg. First-tier *ICP* control treatment included elevation of the bed to 30°, sedation with propofol (2–10 mg/kg/h), and adequate analgesia (intravenous morphine 1–5 mg/h). Boluses of 20% mannitol (2 mg/kg up to a plasma osmolarity of 320 mosmol/L) were administered, if there was a sudden increase in *ICP*. Second-tier measures then included paralysis, cooling of the core body temperature to 36°C and institution of a barbiturate coma, which is achieved with intravenous thiopentone 250-mg boluses of over 10–20 min (up to a total dose of 500–1,000 mg) with a maintenance dose of 125–500 mg/h titrated to *ICP* control or to maintain burst suppression on EEG. Surgical decompression was also used, when *ICP* could not be controlled with second-tier measures.

Reusability of Incomplete Brain Monitoring Data: A Feasibility Study

Input of the feasibility study includes the continuous monitoring data of *ICP*, *MAP*, *PbtO₂* and brain temperature (*BTemp*). Total sample size is 77 patients. Detailed characteristics of the input data are summarized in Table 1.

Table 1 Summary of input data characteristics

Measurement	Characteristics			
Size of samples	77			
Sample length (h)	Minimum (13)	Average (115.5)	Maximum (493)	
Gender	Male (58)	Female (19)		
Age of admission	10–30 (15)	31–50 (24)	51–70 (30)	71–90 (8)
Ethnic	Chinese (59)	Indian (10)	Malay (7)	Others (1)

As the input data are “real” brain monitoring data collected from the NICU, as illustrated in graph form in Fig. 1, it contains a considerable amount of missing values, also referred as “gaps” in data. It is impossible for us to assess the imputation error on “real” missing values. This is because, for “real” missing values, we have no idea of their actual values. Thus, we have no baseline – “ground truth” – to compare with and to calculate the imputation error. As a result, we propose to estimate the imputation error by removing known data points to simulate the existence of missing values. In this proposed approach, a set of complete data is required as the “ground truth” data.

Segmentation is the first process of the feasibility study, whose purpose is to segment out a block of complete data that can be used as the “ground truth” data. We define the “ground truth” data as the longest continuous block of data that contains no missing values (“gaps”) in all four of the modalities concerned. In Fig. 1, the block of “ground truth” data is highlighted from the input data with a dotted square.

Simulated missing values are then introduced by randomly removing data points from the “ground truth” data. In this paper, we focus our investigation only on the univariate of missing values. This implies that simulated missing values are introduced to one modality at a time. Moreover, we also assume that the missing values are “missing completely at random” [2]. This means simulated missing values are randomly introduced, assuming that each data point is equally likely to be missing with no bias nor influence from prior knowledge. Note that the univariate and “missing completely at random” assumptions may not completely describe all realistic scenarios. However, as this paper is the pioneer work in studying the feasibility of reusing incomplete brain monitoring data, these assumptions are made to narrow down the scope of our study.

The imputation error is tested under various scenarios, where different amounts, ranging from 1% to 25%, of missing values are introduced. The data introduced with simulated missing values are then regarded as the testing data for the feasibility study.

Imputation of missing values then follows. This process takes the testing data with simulated missing values as input and employs predictive methods to impute the missing values. To obtain a balanced and generalized assessment, 17 state-of-the-art predictive methods are employed in our study. Among the selected algorithms, six of them

are *regression methods*, which includes Gaussian process, isotonic regression, piecewise regression, simple linear regression, enhanced linear regression, and least median squared linear regression. One *kernel-based method*, support vector machine (SVM) regression, and one *multi-perceptron neural network learning method* are also included. *Lazy learning methods*, K-nearest neighbor (KNN), K-STAR, and locally weighted learning model (LWL), are also selected due to their simplicity. Representative *rule-based and tree-based methods*, including conjunctive rule-based learner, M5Rules, M5P, decision table, RepTree and decision stump, are also employed in our study. Details of the predictive methods employed are referred to in Hall et al. [8]; all the methods are implemented with WEKA 3.6 [8] and are employed with default settings.

The *imputation error assessment* phrase then compares the imputed missing values with their actual values in the “ground truth” data. The imputation error is evaluated for each predictive method. Conventional performance metrics, including mean square error (MSE) and relative absolute error (RAE), are used. The imputation performance of the predictive methods is also evaluated based on the coefficient of determination, R^2 . R^2 is calculated as:

$$R^2 = 1 - \frac{\sum_i (y_i - \hat{y}_i)^2}{\sum_i (y_i - \bar{y}_i)^2}$$

where y_i refers to the actual value, \hat{y}_i refers to the imputed value and \bar{y}_i refers to the sample mean of the testing data. R^2 basically compares the square error of the predictive method with that of simply replacing the missing values with the sample mean. R^2 is positive if the predictive method outperforms the sample mean imputation method, and the larger the R^2 the more superior the predictive method is. R^2 is negative if otherwise. In addition, a newly defined metric, $\sigma_{\%}$, is employed in our study. $\sigma_{\%}$ is defined as the percentage of imputed missing values that fall within σ away from their actual values. σ here refers to the standard deviation of the testing data.

Moreover, given that all parameters are the same, different sets of randomly simulated missing values may result in different imputation error. Therefore, to obtain a stable estimation, the imputation error is estimated based on the average performance over ten repeated simulation trials.

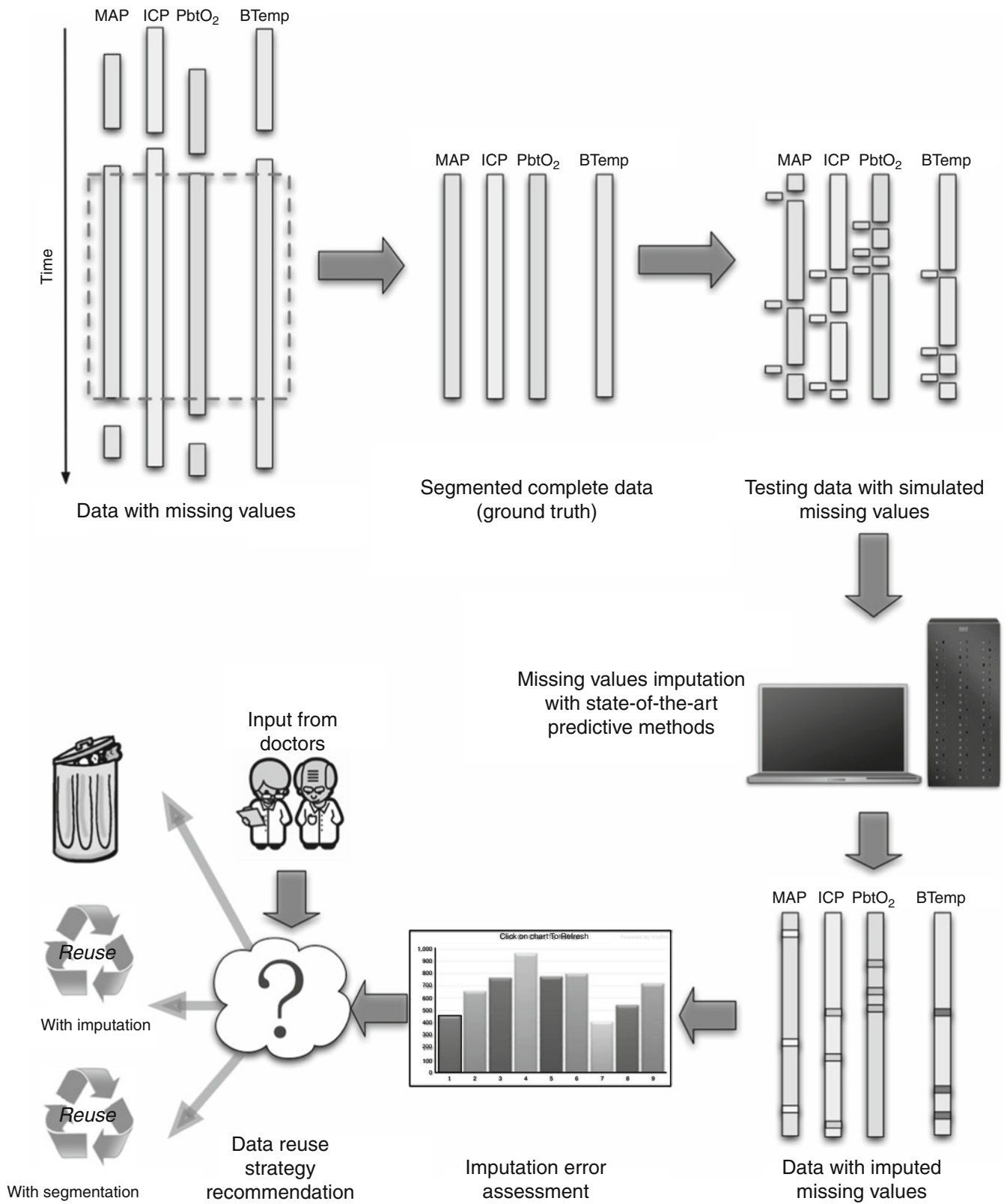


Fig. 1 Graph of the major processes in the proposed feasibility study

The average performance across all 17 predictive methods then provides us with a general estimation of the imputation error. Based on the estimation, we can then investigate under various scenarios how feasible it is to reuse incomplete brain monitoring data. The complete flow of the proposed feasibility study is graphically demonstrated in Fig. 1.

Re-usage Strategy Recommendation

The results of our feasibility study can be further used to recommend re-usage strategies for incomplete brain monitoring data. Suppose, as shown in Fig. 1, a set of re-usage criteria, e.g., thresholds for relative absolute error, is defined by neurosurgeons or neuroclinicians. We suggest the re-usage strategy as follows.

1. If the estimated imputation error satisfies the expert-defined criteria, the incomplete brain monitoring data then should be reused with missing value imputation. Moreover, the best imputation method/methods can be suggested based on the imputation performance evaluation of predictive methods from our feasibility study.
2. If the estimated imputation error does not satisfy the criteria, but comes close, then just the complete segment of the incomplete monitoring data can be reused. This approach is formally known as the “available case” approach [11].
3. If both of the above situations fail, then the incomplete monitoring data – the “complete case” approach may have to be discarded [11].

Results and Discussion

Figure 2 summarizes in graph form the average relative absolute error and R^2 over the monitoring data of *MAP*, *ICP*, *PbtO₂* and *BTemp*. The imputation error is investigated under testing scenarios when simulated missing values from 1% to 25% are introduced. Figure 3 then compares the detailed imputation performance of each individual predictive method when 25% simulated missing values are introduced. The performance comparison metrics include mean square error (MSE), relative absolute error (RAE), coefficient of determination, R^2 and the proposed metric, $\sigma_{\%}$.

General Observation

It can be observed from Fig. 2 that, as the amount of introduced missing values increases, the average RAE remains relatively stable. For example, as the introduced missing

values increase from 1% to 25%, the average RAE of *MAP* and *ICP* increases only slightly from 3.79% to 3.83% and from 10.3% to 10.5% respectively. This observed stability of RAE over various amounts of introduced missing values can be explained by the “missing completely at random” assumption of our feasibility study. In our study, simulated missing values are introduced assuming each data point has an equal chance of being missed. As a result, introduced missing values tend to be sparsely distributed all over the data. This sparseness further leads to the phenomenon that, regardless of the amount of missing values, the temporal information immediately before and after the introduced missing value is usually well preserved. This allows missing values to be imputed almost equally well over various amounts of missing values.

On the other hand, the average R^2 values are also observed to increase gradually as the amount of introduced missing values increases. As mentioned, R^2 is an imputation performance metric that compares the mean square error of predictive methods and the sample mean imputation approach. The sample mean imputation approach may still be able to achieve reasonable performance with a small amount, e.g. 1%, of missing values. However, as the amount of missing values increases, the performance of the sample mean approach will inevitably degrade dramatically, which directly results in an increase in R^2 value.

Reusability of Incomplete Data

Different scientific studies have different levels of tolerance for error. For example, preliminary and exploratory studies have much higher tolerance for error compared with verification studies. Therefore, the reusability of incomplete brain monitoring data has to be discussed in the context of error tolerance allowed the underlying study. Given the error tolerance level, the reusability of incomplete brain monitoring data can be easily determined based on the imputation error estimation results of our feasibility study.

As an example, let us suppose the error tolerance of the underlying study is 10%. For *MAP* and *PbtO₂*, as demonstrated in Fig. 2, the overall average RAE over various amounts of missing values is 3.6% and 0.19% respectively. Even when 25% of missing values are introduced, as shown in Fig. 3, the average RAE of *MAP* still stays at 3.66% (standard deviation 1.45%) and, for *BTemp*, the average RAE is at 0.19% (standard deviation 0.11%). Based on these observations, we conclude that: given 10% as the error tolerance and assuming data are missing completely at random, the monitoring data of *MAP* and *BTemp* can be confidently reused with imputation when up to 25% of data are missing. On the other hand, for *ICP* and *PbtO₂*, the average RAE is slightly below 10%, which does satisfy the error tolerance

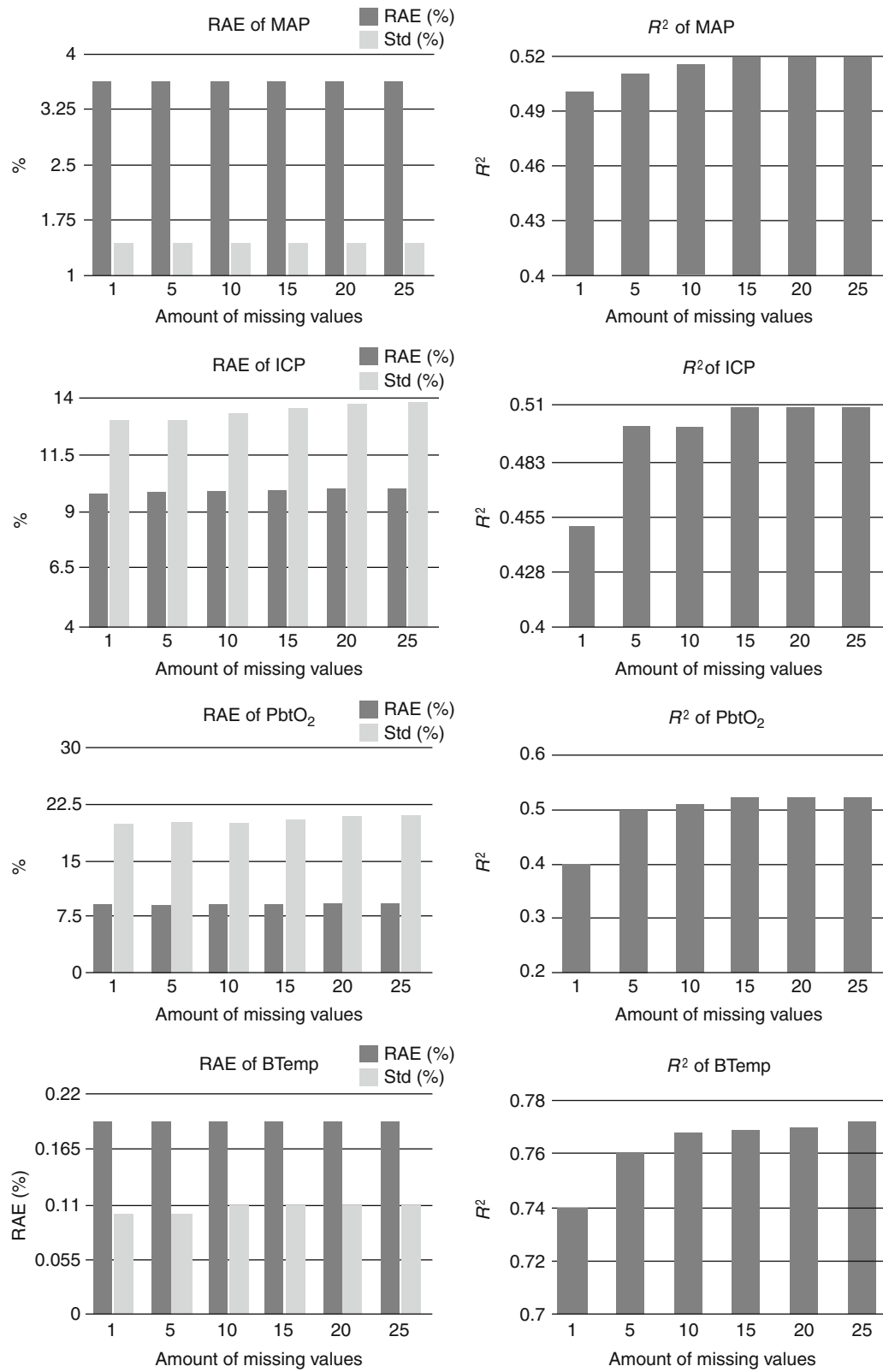


Fig. 2 Average relative absolute error (RAE) with its standard deviation and R^2 values of four brain monitoring modalities, MAP, ICP, PbtO₂, and BTemp

a

Method	Model name	MAP				ICP			
		MSE	RAE (%)	R^2	$\sigma\%$ (%)	MSE	RAE (%)	R^2	$\sigma\%$ (%)
Regression	Gaussian processes	27.73	3.29	0.63	92.66	7.16	9.27	0.62	92.11
	Isotonic regression	43.98	4.38	0.42	86.36	11.30	11.92	0.43	87.05
	Linear regression (enhanced)	42.63	4.35	0.45	87.31	10.72	12.14	0.42	86.61
	Linear regression (simple)	53.60	5.02	0.32	83.27	13.95	12.77	0.30	83.47
	Linear regression (LMS)	82.23	4.57	0.01	85.59	16.57	11.78	0.09	84.95
	Pace regression	41.30	4.28	0.46	87.69	10.62	12.07	0.44	87.09
Kernel	SVM regression	44.98	4.10	0.42	87.78	11.54	10.90	0.38	87.56
Neural network	Multi-perceptron NN	37.06	3.99	0.51	88.74	9.84	12.09	0.49	88.15
Lazy learning	KNN	20.50	2.35	0.69	94.89	5.03	5.96	0.70	94.53
	K-STAR	15.06	2.07	0.78	96.43	3.87	5.42	0.78	96.37
	LWL	43.70	4.34	0.44	87.50	11.40	11.91	0.44	88.33
Rule-based	Constructive rule	49.43	4.69	0.38	85.43	13.37	12.94	0.37	85.99
	M5 Rules	20.45	2.51	0.72	95.03	5.16	6.93	0.71	94.64
Tree-based	M5P	18.08	2.35	0.75	95.67	4.65	6.50	0.74	95.33
	Decision stump	51.45	4.84	0.35	84.55	14.10	13.46	0.34	85.30
	Decision table	24.32	2.72	0.67	94.15	6.13	7.32	0.67	94.06
	Rep Tree	19.46	2.38	0.72	95.10	5.22	6.46	0.70	94.76
Average		37.41	3.66	0.51	89.89	9.45	9.99	0.51	89.78

b

Method	Model name	PbtO ₂				BTemp			
		MSE	RAE (%)	R^2	$\sigma\%$ (%)	MSE	RAE (%)	R^2	$\sigma\%$ (%)
Regression	Gaussian processes	13.05	8.17	0.61	93.72	0.01	0.17	0.84	96.63
	Isotonic regression	20.01	12.83	0.40	88.45	0.02	0.21	0.75	94.06
	Linear regression (enhanced)	20.20	11.13	0.39	88.66	0.02	0.22	0.73	93.46
	Linear regression (simple)	23.58	16.78	0.29	85.54	0.02	0.26	0.67	91.64
	Linear regression (LMS)	29.42	13.46	0.17	86.79	0.04	0.25	0.46	89.94
	Pace regression	19.67	11.04	0.40	88.83	0.02	0.22	0.73	93.46
Kernel	SVM regression	22.44	9.79	0.35	89.12	0.02	0.21	0.71	92.75
Neural network	Multi-perceptron NN	15.32	9.96	0.44	89.92	0.01	0.18	0.80	95.45
Lazy learning	KNN	5.37	2.82	0.81	96.97	0.00	0.06	0.90	97.64
	K-STAR	5.21	3.52	0.83	97.38	0.00	0.08	0.93	98.73
	LWL	18.55	11.64	0.43	89.41	0.03	0.31	0.68	92.61
Rule-based	Constructive rule	21.27	12.97	0.36	87.64	0.04	0.36	0.62	90.28
	M5 Rules	8.75	5.18	0.72	95.75	0.00	0.09	0.91	98.39
Tree-based	M5P	7.32	4.64	0.77	96.41	0.00	0.09	0.92	98.70
	Decision stump	22.10	13.52	0.33	86.90	0.04	0.36	0.61	89.91
	Decision table	9.32	5.06	0.72	95.63	0.01	0.13	0.87	97.48
	Rep Tree	8.29	4.16	0.74	96.25	0.00	0.08	0.91	98.33
Average		15.87	9.22	0.52	91.37	0.02	0.19	0.77	94.67

Fig. 3 Detailed imputation performance of predictive methods when 25% of simulated missing values are introduced: (a) MAP and ICP data, (b) PbtO₂, and BTemp data

requirement. However, we also observe from Fig. 2 that the standard deviations of RAEs of *ICP* and *PbtO₂* are significantly high at around 14% and 20%. This implies that the actual imputation error is likely to fall way beyond the average 10%. Therefore, we recommend that the most reliable re-usage strategy for *ICP* and *PbtO₂* monitoring data is the “available case” approach, where only the complete segment of the monitoring data is reused. Nevertheless, after looking into individual predictive methods, we discover that the best performing predictive methods, such as K-STAR and M5P,

actually produce significantly lower error compared with the rest. As shown in Fig. 3, when 25% of missing values are introduced, the RAE of *ICP* is only around 6% and that of *PbtO₂* is even below 5%. Therefore, alternatively, one may still consider reusing the *ICP* and *PbtO₂* data by imputing the missing values with the best predictive methods.

Based on the results of our feasibility study, we summarize that, owing to their relatively stable nature, the monitoring data of *MAP* and *BTemp* are more reliable for reuse compared with *ICP* and *PbtO₂*, and, for *ICP* and *PbtO₂* data,

a more cautious re-usage strategy should be employed. This further implies that a more careful monitoring process should be employed for *ICP* and *PbtO₂*, as missing values in them cannot be accurately imputed.

Recommendation of the Predictive Method

In our study, we have also compared the imputation performance of different predictive methods. The comparison results for 25% of simulated missing values are showcased in Fig. 3. The top three predictive methods are also highlighted. Based on our imputation error study, we discover that the lazy learning method, K-STAR, and the tree-based method, M5P, are the best performing predictive methods of all the scenarios tested. Both K-STAR and M5P consistently perform as one of the top three predictive methods. Moreover, both K-STAR and M5P outperform the rest considerably. As shown in Table (b) of Fig. 3, the RAE of K-STAR and M5P is at 3.52% and 4.64%, which is only half of the overall average RAE across all predictive methods. Moreover, according to the R^2 values, K-STAR and M5P always outperform the sample mean imputation approach by at least five times.

Conclusion

We proposed to reuse incomplete brain monitoring data with imputation of missing values. To support our proposal, we have conducted a feasibility study to investigate the reusability of incomplete brain monitoring data. The reusability of incomplete monitoring data was assessed based on the estimated imputation error, which was experimentally measured with 17 state-of-the-art predictive methods and simulated missing values. Taking the monitoring data of TBI patients as input, the feasibility study consists of four major processes:

1. Segmentation of “ground truth” data
2. Simulation of missing values
3. Imputation of missing values
4. Imputation error assessment

In addition, we have also demonstrated how the results of our feasibility study can be used to facilitate the task of the neuroclinicians and neurosurgeons to select the most suitable predictive methods and re-usage strategy.

Based on the results of our feasibility study, we summarize that: the monitoring data of *MAP* and *BTemp* are more reliable for reuse compared with *ICP* and *PbtO₂*; and, for *ICP* and *PbtO₂* data, more cautious re-usage strategy should be employed. We further suggest that a more careful monitoring process should be employed for *ICP* and *PbtO₂*, as

their missing values cannot be accurately imputed. We also observed that, for the scenarios tested, the lazy learning method, K-STAR, and the tree-based method, M5P, are constantly two of the best among 17 predictive methods investigated in this study.

As a pioneer study, we have focused only on the univariate case of missing values and scenarios, where data are missing completely at random. In future, we plan to further our study based on the framework proposed in this paper to investigate more complicated scenarios, where both univariate and multivariate of missing values are possible, and where data not only may be missed completely at random, but may also be missed randomly in clusters.

Acknowledgement This work was supported by A*STAR, Singapore, under SERC grant 092-148-0067.

Conflict of interest statement We declare that we have no conflict of interest.

References

1. Abad N, Druzgalski C (2009) Medical and engineering support and needs in neurological intensive care units. In: Proceedings of PAHCE'09, Mexico City, pp 157–159
2. Acock A (2005) Working with missing values. *J Marriage Fam* 67(4):1012–1028
3. Bullock M, Povlishock J (2007) Guidelines for the management of severe traumatic brain injury. *J Neurotrauma* 24(S1):1–106
4. Cheung K, Lim E, Samwald M, Chen H, Marengo L, Holford M, Morse T, Mutalik P, Shepherd G, Miller P (2009) Approaches to neuroscience data integration. *Brief Bioinform* 10(4):345–353
5. Dutton R, McCunn M (2003) Traumatic brain injury. *Curr Opin Crit Care* 9(6):503–509
6. Fan J, Kirkness C, Vicini P, Burr R, Mitchell P (2010) An approach to determining intracranial pressure variability capable of predicting decreased intracranial adaptive capacity in patients with traumatic brain injury. *Biol Res Nurs* 11(4):317–324
7. Ghajar J (2000) Traumatic brain injury. *Lancet* 356(9233):923–929
8. Hall M, Frank E, Holmes G, Pfahringer B, Reutemann P, Witten I (2009) The WEKA data mining software: an update. *ACM SIGKDD Explorations Newsl* 11(1):10–18
9. Ian P, Iain C, Giuseppe C (2010) The brain monitoring with information technology (BrainIT) collaborative network: EC feasibility study results and future direction. *Acta Neurochir* 152:1859–1871
10. Jones P, Andrews P, Midgley S, Anderson S, Piper I, Tocher J, Housley A, Corrie J, Slattery J, Dearden N (1994) Measuring the burden of secondary insults in head-injured patients during intensive care. *J Neurosurg Anesthesiol* 6(1):4–14
11. Little R (1992) Regression with missing X's: a review. *J Am Stat Assoc* 87(420):1227–1237
12. Low D, Kuralmani V, Ng S, Lee K, Ng I, Ang B (2009) Prediction of outcome utilizing both physiological and biochemical parameters in severe head injury. *J Neurotrauma* 26(8):1177–1182
13. Robertson C, Valadka A, Hannay H, Contant C, Gopinath S, Cormio M, Uzura M, Grossman R (1999) Prevention of secondary ischemic insults after severe head injury. *Crit Care Med* 27(10):2086–2095

14. Ross N, Eynon CA (2005) Intracranial pressure monitoring. *Curr Anaesth Crit Care* 16(4):255–261
15. Rubin D (1976) Inference and missing data. *Biometrika* 63(3): 581–592
16. Scalzo F, Xu P, Bergsneider M, Hu X (2008) Random subwindows for robust peak recognition in intracranial pressure signals. *Adv Vis Comput* 5358(1):370–380
17. Schafer J, Graham J (2002) Missing data: our view of the state of the art. *Psychol Methods* 7(2):147–177
18. Schafer J, Olsen M (1998) Multiple imputation for multivariate missing-data problems: a data analyst’s perspective. *Multivar Behav Res* 33(4):545–571
19. Swiercz M, Mariak Z, Krejza J, Lewko J, Szydlak P (2000) Intracranial pressure processing with artificial neural networks: prediction of ICP trends. *Acta Neurochir* 142(4):531–542
20. Signorini D, Andrews P, Jones P, Wardlaw J, Miller J (1999) Predicting survival using simple clinical variables: a case study in traumatic brain injury. *Br Med J* 66(1):20–25
21. Vik A, Nag T, Fredriksli O, Skandsen T, Moen K, Schirmer-Mikalsen K, Manley G (2008) Relationship of “dose” of intracranial hypertension to outcome in severe traumatic brain injury. *J Neurosurg Pediatr* 109(4):678–684
22. Wald S, Shackford S (1993) The effect of secondary insults on mortality and long-term disability after severe head injury in a rural region without a trauma system. *J Trauma* 34(3):377–382
23. Wright W (2007) Multimodal monitoring in the ICU: when could it be useful? *J Neurol Sci* 261(1–2):10–15
24. Xiao H, Peng X, Asgari S, Vespa P, Bergsneider M (2010) Forecasting ICP elevation based on prescient changes of intracranial pressure waveform morphology. *IEEE Trans Biomed Eng* 57(5):1070–1078

Investigation of the Relationship Between Transcranial Impedance and Intracranial Pressure

Martin Shaw, I. Piper, P. Campbell, C. McKeown, J. Britton, K. Oommen, L. Stewart, I. Whittle, R. Gregson, and E. Clutton

Abstract Studies on piglets have shown that cranial bioimpedance (Z) measurements correlate well with invasively measured intracranial pressure (ICP). We have tested the feasibility of collecting transcranial impedance from a clinical device for measuring whole-body water content (ImpediMed SFB7). In the clinical study, 50 normal healthy volunteers had transcranial impedance measured using nine different head montages (forehead to mastoid (left/right), temporal to mastoid (left/right), forehead to temporal (left/right), forehead to occipital (left/right) and temporal to temporal). Impedance was measured 20 times over a frequency range per montage and ANOVA used to test for effects of electrode position upon recorded value. For the experimental study, five sedated and ventilated Marino sheep were instrumented for intraventricular ICP and transcranial impedance measurement. Measures of ICP were recorded while ICP was increased from baseline to greater than 50 mmHg in five steps using an intraventricular infusion of mock CSF. There is a significant effect of electrode position and gender upon transcranial impedance ($p < 0.001$). The temporal-mastoid electrode position had significantly lower impedance values in keeping with

its shorter path length. ICP correlated with craniospinal compliance measurements and Impedance vs Freq by ICP step shows a clear ICP dependence ($p = 0.007$) across the sheep.

Keywords Impedance • Total body water measurement • CBF autoregulation • Intracranial pressure • Head trauma

Introduction

The non-surgical management of patients with traumatic brain injury (TBI) focuses upon the prevention of secondary insults such as drops in arterial blood pressure (ABP) or intracranial hypertension. The latter (raised ICP) is of particular concern as increases in ICP will decrease cerebral perfusion pressure ($CPP = ABP - ICP$) and can lead to decreases in cerebral blood flow (CBF). Cerebral autoregulation is a physiological mechanism that maintains CBF constant in the face of changing CPP and can become impaired following brain injury [3].

A number of indirect methods for determining autoregulatory status have been developed. For example, Czosnyka et al. have studied the correlation between inherent fluctuations in BP and ICP deriving an index called the PRx, which has been shown to relate to the clinical outcome of patients and indirectly to the degree of autoregulatory impairment [2, 7].

These (data-driven) approaches rely on invasive measures of physiological time series (such as ICP) and do not provide clinically useful information about the underlying mechanism for autoregulatory impairment, which would prove useful in the appropriate targeting of medical management. An alternative to this approach is to base autoregulatory status assessment upon a mathematical model.

A relevant example of a purely mathematical model would be the simple two compartment model developed by Ursino and Lodi [8]. It can be thought of as a combination of three processes affecting arterial-arteriolar compliance for a given percentage change in CBF. The first process is the autoregulatory gain, the next is the static sigmoidal autoregulatory response function and the last component is a low pass

M. Shaw (✉)
Department of Clinical Physics, Sothorn General Hospital,
Glasgow, UK
e-mail: martin.shaw@nhs.net

Department of Clinical Physics, Institute of Neurological Sciences,
Sothorn General Hospital, 1345 Govan Road, Glasgow,
G514TF, UK

I. Piper, C. McKeown, J. Britton, and K. Oommen
Department of Clinical Physics, Sothorn General Hospital,
Glasgow, UK

P. Campbell and L. Stewart
Department of Neuroanaesthesia, Southern General Hospital,
Glasgow, UK

I. Whittle
Department of Neurosurgery, Western General Hospital,
Edinburgh, UK

R. Gregson and E. Clutton
Department of Veterinary Anaesthesia, Royal Edinburgh
Veterinary School, Edinburgh, UK

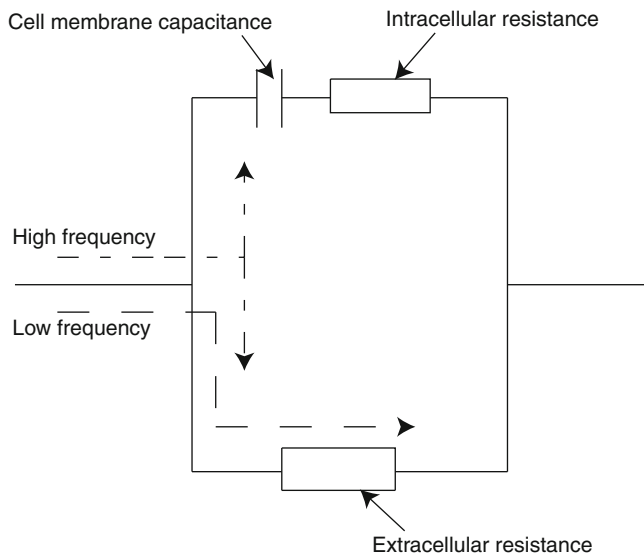


Fig. 1 Cellular equivalence circuit

transfer function. The maximum autoregulatory gain is defined to be the slope of the static autoregulatory curve at its centre point.

However, one limitation in the Ursino and Lodi model is that it needs a measure of arterial compliance, which is difficult to measure in a clinical setting.

Towards this end, a direct non-invasive method of measurement is required and transcranial impedance measurement is a possible candidate. Impedance measurements are now routinely carried out clinically as a gauge of intra- and extra-cellular water content across the whole body, which in turn can be linked to general well being. So when this technique is applied to the cranial space the tissue impedance will depend upon intracellular swelling and the size of the extracellular space and so too does intracranial compliance. As there is a well-defined exponential relationship between intracranial pressure and intracranial compliance there should also be a definable relationship between raised ICP and transcranial impedance.

Total Body Water Measurement

Total body water (TBW) or whole body impedance (WBI) measurement is a measure of the ratio of intracellular to extracellular water content. Consider the circuit diagram (Fig. 1): the extracellular component is modelled by the bottom leg of the circuit and the intracellular component by the upper leg of the circuit. When an electrical signal of variable frequency is passed over the circuit the signal passes from only going through the extracellular resistor at low frequency to travelling over both legs simultaneously at high frequency. If the resistance and reactance is measured and then plotted

on a complex plane each of the vectors to those points will be an impedance reading.

Using Cole–Cole analysis [1] on these impedance measurements a circular fit to the data is then made and the resistance at infinite frequency, R_∞ , and zero frequency, R_0 , can be estimated from the crossing points. The characteristic impedance, Z_C , can also be estimated from the turning point for the fit. From these values a TBW value is then calculated, normally from either R_∞ or Z_C .

There are a number of mature technologies in clinical use that apply the above technique, including the Maltron Bioscan 916S [6] and the Impedimed SBF7 [4]. All subsequent studies were carried out with the ImpediMed SBF7. This device has an operational variable frequency range of 3 kHz to 1 MHz and applies the Cole–Cole technique to calculate TBW values. This device has been assessed against a normative database with claimed accuracy close to 5% compared with direct measurement methods.

The feasibility of using this type of commercial technology for assessing transcranial impedance has been shown experimentally in a neonatal piglet model of brain tissue hypoxia, showing that transcranial impedance correlates well with both direct cerebral tissue impedance and raised ICP [5].

The Main Aims of the Research

This research addresses three questions. First, can a normal data range for the impedance when used “transcranially” be established in healthy normals? Second, what influence does electrode position have upon impedance in healthy normals? Finally, can evidence be provided that transcranial impedance is related to intracranial events?

Materials and Methods

Experimental Protocol for the Normative Study

Fifty normal adult volunteers were recruited (Table 1), with a gender split of 19 men and 31 woman and an age range of 21–64 with a mean of 39. The following electrodes were placed on the head of each of the volunteers for both the right and left sides at the following sites: forehead, temporal, occipital and mastoid. The skin at each electrode site was abrasively cleaned (using a gel abrasive) in order to provide good electrode contact. All the electrodes were placed before any measurements were taken, and no electrodes were removed until after all measurements were recorded. The volunteers’ details (height, weight, sex and age) were inputted into the impedance device. Subjects then lay on their back on

Table 1 Volunteer demographics

Number of volunteers	50
Gender	Male = 19, female = 31
Age	21–64 (mean = 39)
Height	150–188 cm (mean = 170)
Weight	49–140 kg (mean = 77)
BMI	19–51 (mean = 26)
Head circumference	54–62 cm (mean = 57)

a bed and closed their eyes. Measurements were then taken from each pair of electrode sites forehead to mastoid (FM), forehead to temporal (FT), forehead to occipital (FO), temporal to mastoid (TM) and finally temporal to temporal (TT). Each measurement consisted of 20 signal sweeps from 3 kHz to 1 MHz in 256 steps over 40 s using the device.

Experimental Protocol for the Animal Study

Anaesthesia

Five healthy adult female blackface sheep were used for the experiments. They weighed between 46 and 60 kg and were fasted overnight. Anaesthesia was induced by intravenous etomidate (0.5 mg/kg) and midazolam (0.5 mg/kg) and the animal was intubated (Size 10.5 ETT). Ventilation was commenced with a tidal volume of 50 cc/kg/breathe with 100% O₂ and isoflurane (1 MAC). Bilateral auricular artery cannulae were inserted for ABP monitoring, together with a saphenous intravenous cannula. Paralysis was with atracurium (0.5 mg/kg). ECG, level of muscle paralysis and Endtidal CO₂, inhalational agent concentrations were all monitored continuously. Buprenorphine (20 g/kg) was given IV prior to surgery. During the experiment the animal received 10 mL/kg/h of lactated Ringers solution.

Neurosurgical Preparation

Once general anaesthesia has been induced and all monitoring lines inserted and stabilised the head was positioned prone, in a semi-sitting position, with the cranium supported in a dedicated head rest. Two 21G needles were inserted into the lateral side of each scalp and connected to the impedance monitor for measurement of intracranial impedance.

A midline incision was then made starting between the horns and going posteriorly 5–6 cm. A self-retaining retractor was positioned and the periosteum elevated to display the junction of the metopic suture and the coronal suture. An 11-mm burr hole was then drilled on either side of the midline (centre approx 6 mm lateral to midline) with one being centred 1 cm behind the metopic suture and the other 15 mm behind it. The dura was then diathermied and opened with an 11 blade.

A dedicated ventricular catheter (Codman) was then passed into the lateral ventricle on either side. Accuracy of ventricular cannulation was confirmed by obtaining a good quality ICP waveform. All monitoring lines were secured to the scalp using 2.0 Silk. The burr holes were then covered with chopped Surgicel (Johnson and Johnson) and filled with cold setting methylmethacrylate cement to make them watertight.

ICP and Arterial Pressure Manipulation and Recording

The arterial blood pressure was elevated using an infusion of phenylephrine (10 mg) and adrenaline (200 g) mixed in 500 mL normal saline. The ICP was elevated with an infusion of mock CSF into the opposite ventricular line to the ICP monitor. All monitoring was carried out via a Spiegelberg Compliance-Monitor CMP 27.1 for the ABP and ICP lines. From these monitors continuous waveform recording to the computer hard drive was carried out. The experimental protocol was carried out in two distinct sections pre- and post-autoregulatory impairment. With the same main actions being carried out in each run, first, readings of all monitored parameters (blood gases, ICP, ABP and Z) are taken and a baseline measurement of static autoregulation status via a BP challenge was recorded. Next, a stepped increase in ICP of 10 mmHg was performed and all parameters measured again; this sequence was then repeated from baseline to the highest achievable ICP level of approximately 50 mmHg. After that, normal cerebral autoregulation was disrupted through a period of prolonged systemic arterial hypertension and the main sequence of actions carried out again at an ICP of between 10 and 50 mmHg.

Removal and Examination of the Brain

At the end of the experiment the animal was sacrificed with a lethal dose of pentobarbital. A craniectomy was then performed and the brain removed and placed in 10% formalin. After 48 h fixation it was cut coronally, and the parenchyma was assessed for intracerebral contusion or haemorrhage and the ventricles for evidence of any intraventricular haemorrhage.

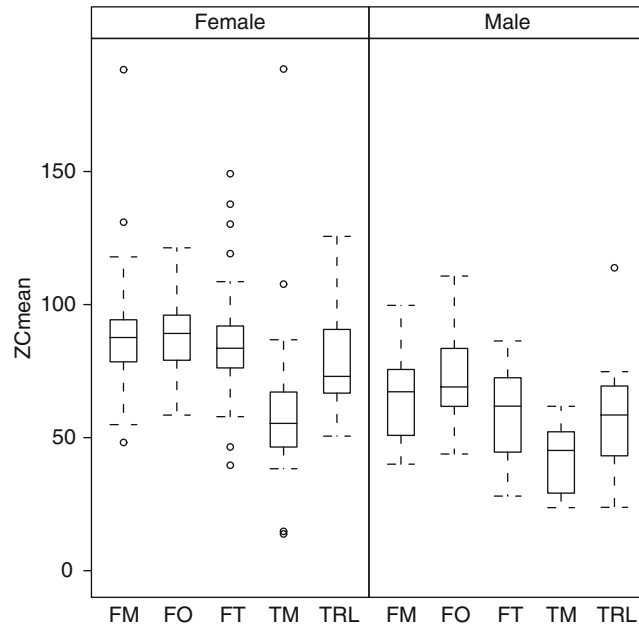
Results

The Normative Study

For this study the mean of the characteristic impedance value was taken across each of the 20 readings per electrode position per volunteer. Analysis of variance was applied to the data with electrode placement, gender and measurement side (left/right) as factors in the analysis. Results showed that there was no side bias in the data, but there were highly

Table 2 Normative ranges (mean \pm sd) for the characteristic impedance per electrode position

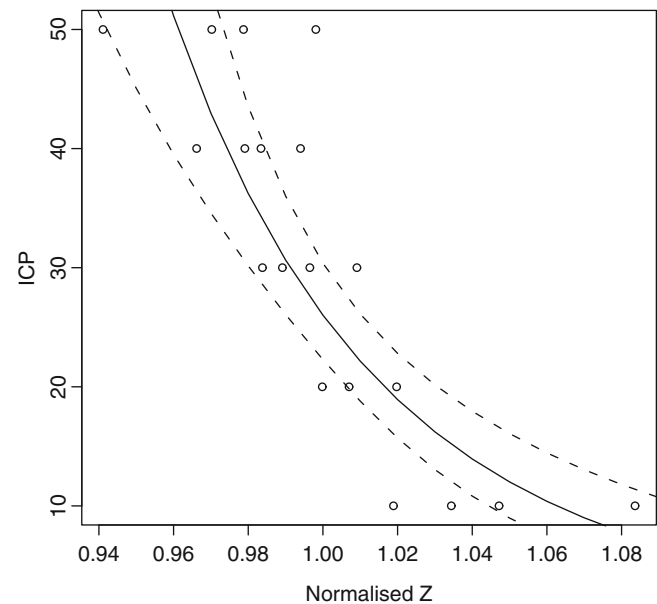
Electrode position	Male range	Female range
Forehead to mastoid	65.8 \pm 15.0	98.8 \pm 47.2
Forehead to occipital	72.7 \pm 15.6	88.2 \pm 12.9
Forehead to temporal	60.3 \pm 16.3	89.0 \pm 35.9
Temporal to temporal	58.2 \pm 24.2	78.0 \pm 17.9

**Fig. 2** Box plot of the characteristic impedance per electrode position split by gender. *FM* forehead to mastoid, *FO* forehead to occipital, *FT* forehead to temporal, *TM* temporal to mastoid, *TT* temporal to temporal

significant ($p < 0.001$) influences by both gender and electrode placement location. Further investigation with a Tukey highest significant difference test then showed that the temporal to mastoid reading had a significantly lower mean than the rest of the electrode placements. The gender split was then shown to have the female impedance readings higher than their male counterpart on all electrode positions. The main normative data range is shown in Table 2 and illustrated in Fig. 2.

The Experimental Study

For the animal study the data were analysed using a repeated measures ANOVA, which looks at both within-subject and between-subject interactions in the model and accounts for any multiple sampling error that could occur. This analysis looked at the variance difference in the mean impedance value per animal per ICP step level, between 10 and 50 mmHg

**Fig. 3** Regression plot through the mean normalised impedance per animal against ICP with confidence intervals

in steps of 10 mmHg. This showed that there was a statistically significant difference ($p < 0.007$) in impedance values per level. There was however a large inter-animal variance in the data that is present at all ICP levels.

The absolute relationship between ICP and impedance has been modelled. To minimise the variance in the data a normalisation technique was applied to the impedance data by dividing each value by the mean of a subset of the data at the beginning of the set, this adjusts the output range of the independent experimental samples into similar ranges, which can then be directly compared. The mean value of this now normalised range was then taken per ICP level, giving an overall summary for that ICP value. This was then plotted and the simple exponential model, $ICP = \exp(a/Z + b)$, fitted to these data (Fig. 3). This model gave an R^2 correlation of 0.7.

Discussion

From the normative study analysis it has been shown that there is a distinct placement effect for the temporal to mastoid electrode position measurement. Why this is so different to the other electrode positions is mostly likely due to the general path being much shorter than the other position pairs and possibly an extracranial path predominates. Thus, in general, any electrode set chosen for this type of measurement needs to have a long enough path length to cover a large enough part of the cranial space to ensure an intracranial path. This placement effect is also highlighted again in the animal study where the large inter-animal variance in the

temporal to temporal electrode set is likely to be caused by placement differences. With the better understood landmarks of the human head this variance seen on the sheep should be reduced in any further clinical studies.

Also, from the normative study it was shown that there was no side bias either left or right, thus enabling grouping of data and so it doubles our dataset per volunteer and also opens up the possibility of testing for midline shift in future studies. A further study in patients comparing transcranial impedance directly with invasive ICP (as a surrogate of compliance) is warranted.

Conclusions

A normative range for transcranial impedance has been established, with a gender bias of higher impedance for female subjects. Practical electrode positions of any type that include a large enough volume of the cranial space have been identified as most likely being the forehead to occipital or the temporal to temporal positions. The dependence of impedance measurement on ICP has been established. However, further work is needed to identify which physical and physiological factors need be measured to provide a more stable absolute measure of transcranial impedance.

Conflict of interest statement We declare that we have no conflict of interest.

References

1. Cole KS, Cole RH (1941) Dispersion and absorption in dielectrics. I. Alternating current characteristics. *J Chem Phys* 9:341
2. Czosnyka M, Smielewski P, Piechnik S, Steiner LA, Pickard JD (2001) Cerebral autoregulation following head injury. *J Neurosurg* 95:756–763
3. Hlatky R, Furuya Y, Valadka AB, Gonzalez J, Chacko A, Mizutani Y, Contant CF, Robertson CS (2002) Dynamic autoregulatory response after severe head injury. *J Neurosurg* 97:1054–1061
4. Impedimed. ImpediMed : SFB7 for Body Composition, <http://www.impedimed.com/products/sfb7-for-body-composition/>. Accessed 9 Sep. 2010
5. Lingwood BE, Dunster KR, Colditz PB, Ward LC (2002) Noninvasive measurement of cerebral bioimpedance for detection of cerebral edema in the neonatal piglet. *Brain Res* 945:97–105
6. Maltron. Maltronint.com - BioScan 916 - Body Fat Analyser, <http://www.maltronint.com/popup%5fpages/bioscan916.htm>. Accessed 9 Sep. 2010
7. Steiner LA, Coles JP, Johnston AJ, Chatfield DA, Smielewski P, Fryer TD, Aigbirhio FI, Clark JC, Pickard JD, Menon DK, Czosnyka M (2003) Assessment of cerebrovascular autoregulation in head-injured patients: a validation study. *Stroke* 34:2404–2409
8. Ursino M, Lodi CA (1997) A simple mathematical model of the interaction between intracranial pressure and cerebral hemodynamics. *J Appl Physiol* 82:1256–1269

Bioinformatics Analysis of Mortality Associated with Elevated Intracranial Pressure in Children

Mark S. Wainwright and Remigiusz Lewandowski

Abstract *Introduction:* Multivariate data analyses have the potential to enrich the use of the complex plethora of data gathered in the care of critically ill patients. We sought to apply hierarchical cluster analysis to investigate factors affecting outcome in children with acute brain injury requiring ICP monitoring.

Methods: We performed a retrospective analysis on patients admitted to the pediatric intensive care unit with ICP monitoring for management of acute brain injury between 2003 and 2008. We performed cluster analysis comparing survivors and non-survivors. We compared the area under the curve (time and duration above a determined value) between groups.

Results: We identified 32 patients among whom 8 died during hospitalization. Cluster analysis identified an association among CPP, PaCO₂, and end-tidal CO₂, and among ICP, central venous pressure, and lactate, in addition to other unexpected associations. Values (mean ± SD) for ICP in survivors (13.7 ± 7.9 mmHg) were lower than (42.7 ± 36.2) in non-survivors. Mean (59.4 vs 41.3), and minimum (47.3 vs 28.1) CPP were higher in survivors. The AUC for ICP was greater in the subjects who died and cluster analyses supported the importance of ICP and CPP related to outcome.

Conclusions: The dose of abnormal ICP may contribute to outcome in insults that involve increased ICP. These results are proof of principle of the potential application of hierarchical clustering to the clinical practice of pediatric neurocritical care.

Keywords Cluster analysis • Pediatric • Intracranial pressure • Outcome • Cerebral perfusion pressure

Introduction

Thresholds for intracranial pressure (ICP) and cerebral perfusion pressure (CPP) are used in the clinical management of patients with severe traumatic brain injury (TBI). There are relatively limited pediatric data [4]. Thresholds for the treatment of ICP (above 20 mmHg) and maintaining CPP (above 40 mmHg) in children have been recommended [1, 2]. More recent studies have addressed the question of the age dependence of these measures in children with head injury, suggesting three different CPP thresholds for children between the ages of 2 and 16 years [5].

Numerous other physiological and laboratory variables are monitored in critically ill patients who require ICP monitoring. There is a mismatch between the plethora of these data and the analytical tools required to identify and analyze multivariate relationships. Management decisions, exemplified by the approach to ICP and CPP, are often based on changes from a threshold value. To overcome these limitations of univariate analyses of complex systems, recent work in adult neurotrauma has used hierarchical clustering methods to demonstrate both the capacity to integrate large volumes of data, and the potential of these analytical methods to identify clinically significant changes in the patient's status [6, 7]. This approach has not been reported for pediatric brain injuries.

Here, we used hierarchical clustering methods to analyze a large dataset of heterogeneous data classes (laboratory, physiology, device settings, socioeconomic status), collected as part of the routine care of children who

M.S. Wainwright (✉)

Division of Critical Care, Department of Pediatrics,
Children's Memorial Hospital, Northwestern University
Feinberg School of Medicine, Chicago, IL, USA

Division of Neurology, Department of Pediatrics,
Children's Memorial Hospital, Northwestern University
Feinberg School of Medicine, Chicago, IL, USA

Department of Pediatrics, Center for Interdisciplinary Research
in Pediatric Critical Illness and Injury, Children's Memorial Hospital,
Northwestern University Feinberg School of Medicine,
Chicago, IL, USA

Division of Neurology No. 51, Children's Memorial Hospital,
2300 Children's Plaza, Chicago, IL 60614, USA
e-mail: m-wainwright@northwestern.edu

R. Lewandowski

Department of Pediatrics, Center for Interdisciplinary Research
in Pediatric Critical Illness and Injury, Children's Memorial Hospital,
Northwestern University Feinberg School of Medicine,
Chicago, IL, USA

Table 1 Patient demographics and outcome

Outcome	N (%)	M:F	Condition (n)	Age (years) (mean \pm SD)
Survived	15 (47)	6:9	ALF (2); TBI (6); ICH (2); Stroke (3); DKA (1)	11 \pm 7
Poor outcome (G-tube and/or Trach)	9 (28)	5:4	TBI (5); ICH (1); ALF (1); Stroke (1); ADEM (1)	9 \pm 1
Died	8 (25)	5:3	TBI (1); ICH (4); ALF (2); Metabolic (1)	8 \pm 5

Summary of patient characteristics and outcomes

G-tube gastrostomy, *Trach* tracheostomy, *ALF* acute liver failure, *TBI* traumatic brain injury, *ICH* intracerebral hemorrhage, *DKA* diabetic ketoacidosis, *ADEM* acute disseminated encephalomyelitis

underwent ICP monitoring for treatment of acute brain injuries. We sought to provide proof of concept that the use of this approach in pediatric neurocritical care could generate new insights into complex interactions of physiological and biochemical parameters that affect outcome after acute brain injuries in children.

Materials and Methods

Data Collection

Data were collected as part of a larger study using bioinformatics in the Pediatric Intensive Care Unit (PICU) approved by the local Institutional Review Board. All data were collected retrospectively and were de-identified before importing into the Xenobase relational database. Laboratory, device settings, and physiological data were imported from values recorded in the electronic medical record (CareVue, Philips Medical Systems). Patients admitted to the PICU at Children's Memorial Hospital between 2003 and 2008 who underwent ICP monitoring were included in this study. Patients with ventriculoperitoneal shunts who underwent ICP monitoring in the course of evaluation for shunt revision were excluded. We identified those patients who survived and those who died during the hospitalization. We used the medical informatics tool Xenobase (XB Transmed Systems) to collect and analyze all data [8].

Descriptive Statistics and Calculation of Area Under the Curve

We first performed descriptive statistics to determine the ranges and distribution of all variables. We separated subjects into survivors and non-survivors and calculated the mean value for each variable in the two groups. The use of mean values or thresholds in the management of pediatric neurotrauma is based on limited data [5]. Using the

value of the survivor group as the threshold, we then calculated the percentage time [3] and total area under the curve (AUC) above the threshold for both survivors and non-survivors.

Hierarchical Clustering

From a total of 33,106 laboratory, device setting, socioeconomic, and physiological variables, we selected those variables present in 65% of the cases, resulting in 208 variables across a total of 32 cases. We did not identify specific variables a priori, and used this approach to increase the opportunity to discover unexpected associations among the data. We separated the subjects into two groups (survived to discharge or died during hospital stay) and used average linkage hierarchical clustering to cluster the laboratory and physiological variables. These data were then arranged into a two-dimensional grid in which correlated variables clustered near to one another. This enabled the examination of differences in the clustering of groups of variables between the two outcome groups.

Comparison of Intergroup Differences

We used Student's *t* test to measure intergroup differences. Significance was defined as $p < 0.05$ for all tests.

Results

We identified 32 children requiring ICP monitoring. The characteristics of these patients are summarized in Table 1. Mortality (25%) was high, and 9 of the 25 survivors (38%) required a gastrostomy (G) tube or tracheostomy. TBI was the most frequent indication for ICP monitoring, occurring in 12 cases (38%).

First, we performed hierarchical cluster analysis on the entire dataset (Fig. 1). We restricted the variables analyzed to

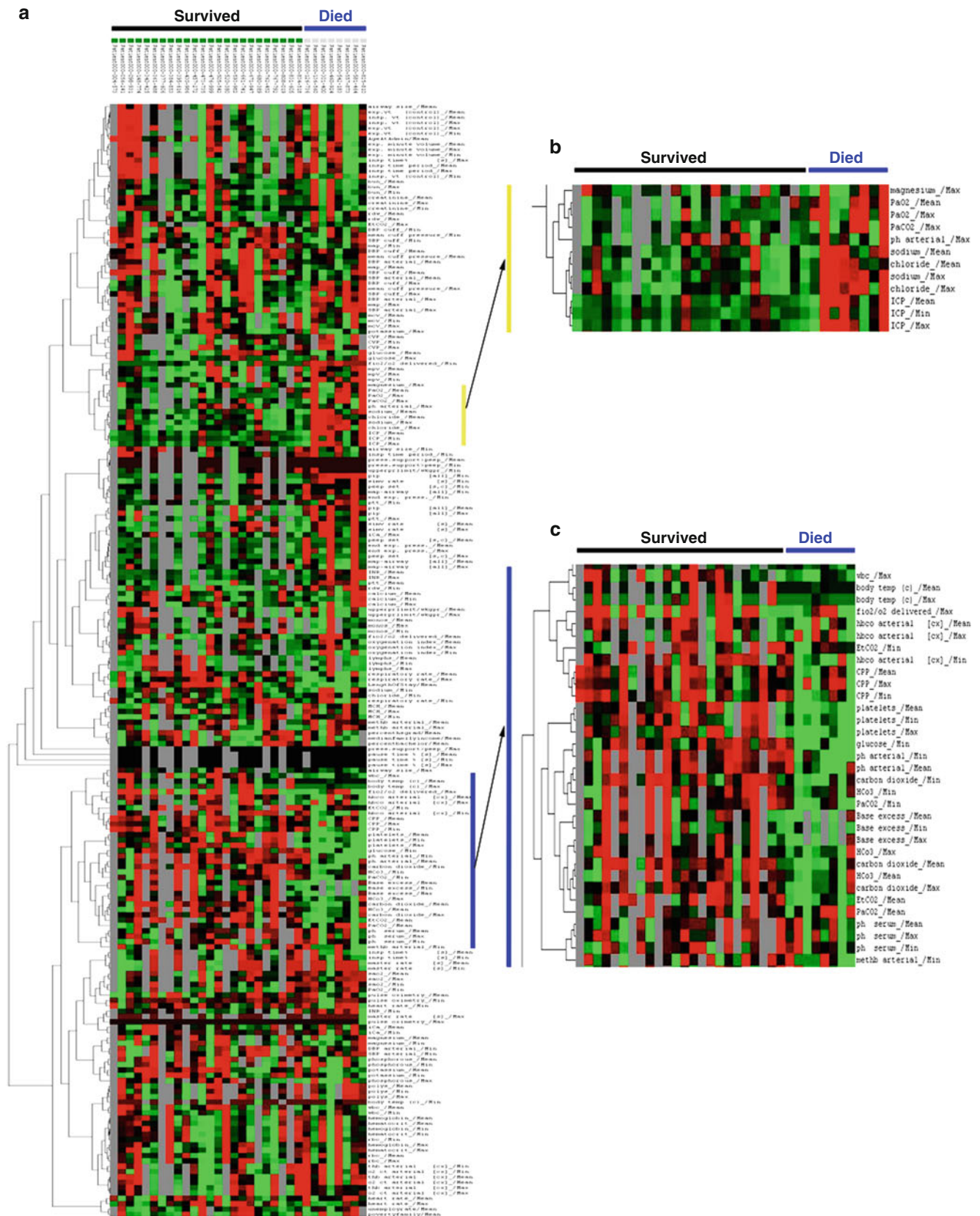


Fig. 1 Heat map and dendrograms for complete data set including all variables and all time points. Variables were restricted to those present in at least 65% of subjects. Each column represents a subject grouped by survivors and subjects who died. (a) Each row represents a variable and clustering has been performed only on the y-axis. The data are

mean-centered such that red and green represent relatively high (red) and low (green) extents, and black the mean value. (b) Values for ICP cluster with sodium (likely hyperosmolar therapy), pH, PaCO₂, and PaO₂, and differ between the two groups. (c) Clustering of CPP with measures of ventilation, acid-base status

those present in at least 65% of cases, but otherwise made no a priori selection of specific variables, which ranged from ventilator settings to demographic, laboratory, and physiological data (Fig. 1a). Despite the lack of selection for specific variables associated with outcome, this analysis identified plausible differences between the two groups. For example, ICP, PaO₂, PaCO₂, sodium, magnesium, and pH (Fig. 1b) were clustered together and differed between the groups. Other clusters for CPP, end tidal CO₂, and for platelets, glucose, and measures of acidosis (Fig. 1c) were also present.

We compared the mean values (data expressed as mean \pm SD) for ICP and cerebral perfusion pressure among all survivors (combining good and poor outcome). In the group of patients who survived, both values (ICP, 14.7 ± 9.2 ; CPP, 57.6 ± 13.9) were significantly different ($p < 0.05$ according to Student's *t* test) compared with non-survivors (ICP, 38.7 ± 26.0 ; CPP, 44.9 ± 18.2). These findings and the initial cluster analysis suggested that despite the variations in frequency of data collection the variables affecting mortality were consistent with other published data on factors affecting outcome following pediatric severe TBI.

There are limited data on the optimal values or goal thresholds for ICP and CPP in pediatric neurocritical care [3–5]. It is also clear that a threshold-based approach to management in neurocritical care is inadequate [7]. In the next sets of analyses, we sought to address these issues. First, we restricted the time window of analysis to the first 7 days after placement of the ICP monitor, reasoning that this is often the most critical time for management. Using the variables identified in the cluster analyses (Fig. 1a, b), which differed between the groups, we calculated the mean value for each of these variables in the survivors. We used this value to generate AUC (total AUC, and percentage time above this threshold) for both groups (Table 2). Again, values for mean CPP and ICP were significantly different between survivors and those who died. In addition, the maximum ICP (mean \pm SD) in those who died (56.0 ± 40.1) was significantly increased compared with survivors (18.9 ± 8.8). Similarly, the minimum CPP in survivors (47.3 ± 14.4) was significantly higher than that measured in the group of patients who died (28.1 ± 21.1). Using AUC (duration and degree of deviation above the mean value in survivors) to compare groups, we found a significant increase in the subjects who died with regard to ICP, and sodium, but no difference with regard to CPP. We then calculated the percentage of time during this 7-day window that the value of any variable was increased compared with the mean of the survivor group. Here we found significant intergroup differences for end-tidal CO₂, PaCO₂, and platelet counts, but not for ICP or CPP. These data suggest that the 'dose' of abnormal ICP or CPP is more significant than the duration of deviation from a defined normal value.

We added results for the calculated AUC data to the total variable set and repeated hierarchical cluster analyses, restricting the time window to 7 days after the start of monitoring. In this next step, we divided the subjects into three groups, including non-survivors, poor outcome (gastrostomy and/or tracheostomy) or good outcome (Fig. 2). The differences persisted between survival and non-survival in variables clustered with CPP (Fig. 2b) and ICP (Fig. 2c).

Discussion

The main finding of this study is the demonstration of proof of principle for the application and utility of hierarchical clustering for unsupervised analyses of multivariate data in pediatric neurocritical care. Here, we show that multivariate analysis of large volumes of heterogeneous data identifies both associations that are plausible, as well as others that are unexpected and potentially fruitful for further studies.

The potential for nonsensical associations is high with the approach. However, we found a striking consistency in the extent to which variables we expect to cluster together do so. For example (Fig. 2), systolic and diastolic blood pressure cluster together, and are close to measures (BUN, creatinine) of renal function. Similarly, ICP (Fig. 2c), was closely linked to sodium, reflecting the use of hypertonic saline in the management of these patients. Our results are therefore consistent with those of previous reports in adult neurotrauma, indicating that this approach identifies meaningful groupings [6, 7].

Previous studies using hierarchical clustering of multivariate data in neurocritical care have been performed only in adults and used a more restricted ($n = 45$) set of variables [6, 7] although at a much higher frequency of recording than our data. Our larger study seeks to apply bioinformatics analyses to all critically ill children using combinations of laboratory, physiological, socioeconomic data combined with treatments, and device settings. Accordingly, we made no a priori assumptions about the inclusion of specific variables. It is striking, therefore, that the patterns that emerge separating survivors from those who died still identify CPP and ICP as key factors associated with outcome, consistent with other pediatric data [3–5].

The future of this approach in pediatric critical care or neurocritical care lies in the potential to exploit the data-rich environment of the PICU to develop better methods of displaying and analyzing complex data, to use these tools to enable earlier recognition of changes in patient states, and to suggest new approaches to treatment. This approach anticipates that unexpected patterns will emerge from these

Table 2 Physiology and laboratory variables for survivors and non-survivors during the first 7 days of ICP monitoring

Variable	Survivors		<i>p</i>	Non-survivors		<i>p</i>	Survivors		<i>p</i>
	Mean ± SD	Non-survivors		Total AUC ± SD	Non-survivors		Percentage duration ± SD	Non-survivors	
ICP mmHg	13.6 ± 7.9	42.7 ± 36.2	0.001	21.8 ± 44.2	120.6 ± 198.5	0.026	37.8 ± 47.6	66.5 ± 46.2	ns
CPP mmHg	59.4 ± 3.5	41.3 ± 23.8	0.013	40.4 ± 56.4	9.1 ± 20.8	ns	54.1 ± 48.9	27.2 ± 33.8	ns
Temp °C	37.0 ± 0.4	37.0 ± 0.0	ns	0.6 ± 2.1	0.0 ± 0.0	ns	6.9 ± 8.0	2.7 ± 6.0	ns
SBP mmHg	118.6 ± 16.4	111.8 ± 10.6	ns	64.9 ± 62.0	27.1 ± 45.0	ns	57.7 ± 43.1	38.5 ± 23.0	ns
DBP mmHg	72.2 ± 12.2	71.7 ± 10.2	ns	55.5 ± 58.9	24.3 ± 29.0	ns	59.8 ± 42.4	46.8 ± 22.0	ns
Heart Rate	105.5 ± 14.8	108.8 ± 15.2	ns	52.8 ± 60.7	15.2 ± 14.8	ns	49.1 ± 36.2	62.5 ± 31.4	ns
Oxygenation index	2.7 ± 1.0	3.7 ± 3.0	ns	11.9 ± 15.5	5.3 ± 13.6	ns	51.6 ± 46.0	62.4 ± 38.3	ns
PaCO₂ mmHg	39.0 ± 3.0	37.1 ± 8.0	ns	15.9 ± 21.2	4.2 ± 5.4	ns	56.8 ± 42.2	20.8 ± 24.3	0.031
Albumin g/dL	2.9 ± 0.9	2.8 ± 0.3	ns	2.2 ± 3.0	0.3 ± 0.4	ns	56.3 ± 50.3	38.2 ± 41.0	ns
EtCO₂ mmHg	38.0 ± 6.3	29.1 ± 4.6	0.002	18.8 ± 29.1	0.2 ± 0.3	ns	64.7 ± 41.1	2.0 ± 2.8	0.000
Hemoglobin g/dL	10.8 ± 1.4	10.9 ± 1.7	ns	4.4 ± 5.8	0.8 ± 1.0	ns	55.8 ± 44.2	52.2 ± 44.7	ns
Platelets thou/μL	339.5 ± 162.7	140.1 ± 71.7	0.003	544.4 ± 685.6	0.5 ± 1.4	0.034	45.1 ± 44.5	1.3 ± 3.8	0.010
Sodium mEq/L	138.5 ± 3.5	145.1 ± 7.7	0.003	8.6 ± 13.0	27.3 ± 34.1	0.030	50.5 ± 42.2	71.0 ± 29.3	ns
Glucose mg/dL	122.3 ± 14.4	115.2 ± 20.4	ns	51.6 ± 61.2	19.2 ± 31.0	ns	44.1 ± 38.5	27.6 ± 30.6	ns
Lactate mEq/L	1.5 ± 1.8	6.5 ± 9.8	ns	4.8 ± 9.1	5.8 ± 8.0	ns	27.5 ± 46.6	50.0 ± 54.8	ns
pH arterial	7.4 ± 0.0	7.4 ± 0.1	ns	0.1 ± 0.1	0.1 ± 0.1	ns	73.1 ± 36.8	54.5 ± 40.6	ns
Magnesium mg/dL	2.1 ± 0.2	2.0 ± 0.2	ns	0.5 ± 0.7	0.3 ± 0.5	ns	53.9 ± 42.2	35.2 ± 36.3	ns

For each variable, results were compared between groups for; (a) the mean value for both survivors and non-survivors; (b) the area under the curve (Total AUC) derived from the product of time and degree of deviation from the mean value in the survivor group; and; (c) the percentage of time (percentage duration) value was above the mean value in the survivor group. Variables with significant differences (according to Student's *t* test) are highlighted in bold

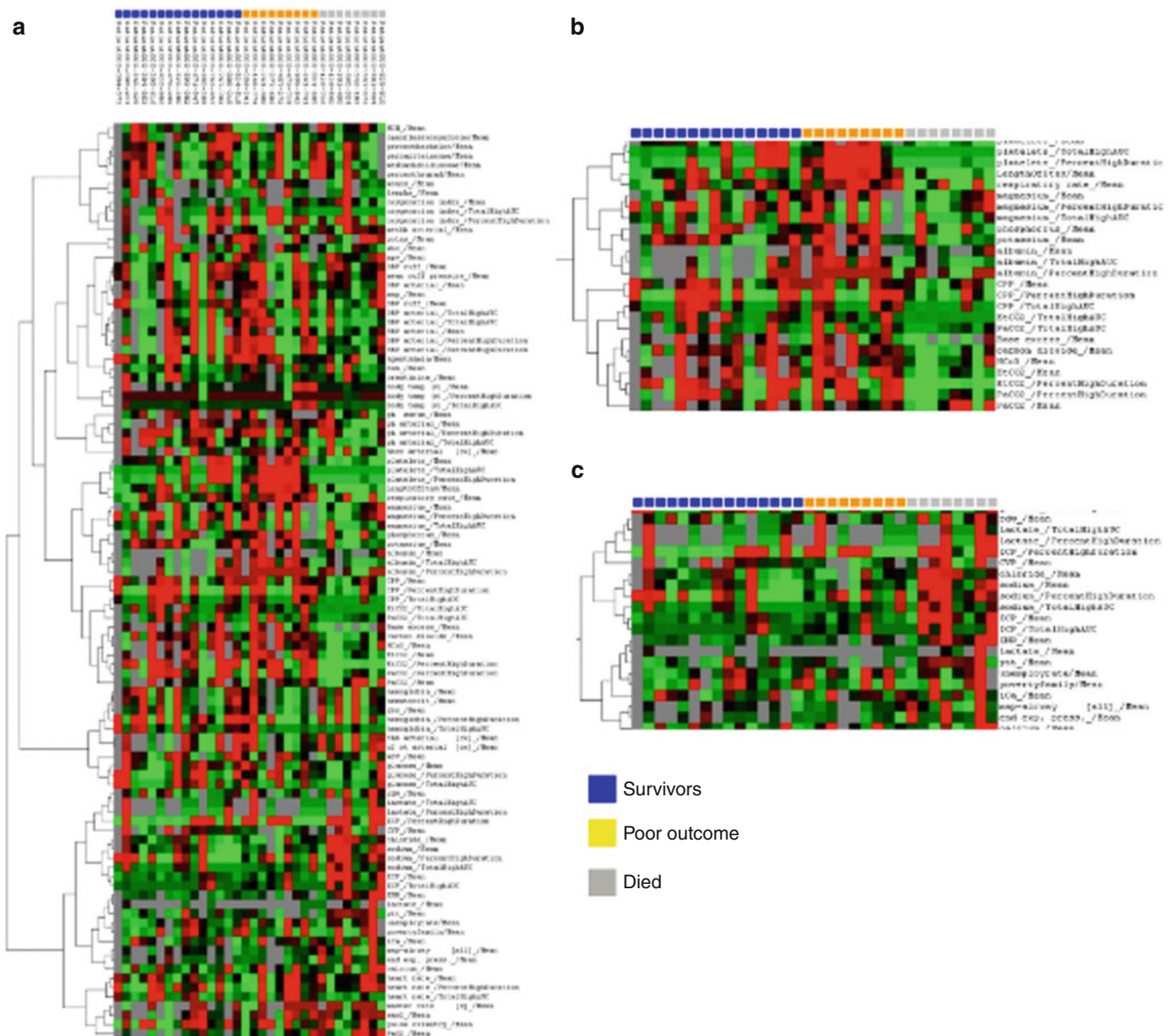


Fig. 2 Heat map and dendrograms for the first 7 days of ICP monitoring including area under the curve values from exploratory analyses. (a) Variables are clustered on the y-axis (laboratory and physiology data).

datasets. Indeed, we found (Fig. 2a) clusters of magnesium with glucose and hemoglobin, albumin with temperature and heart rate, socioeconomic status (household income) with oxygenation index, which will merit observation and may not otherwise have been anticipated.

The cluster analyses identified differences between survivors for variables linked both to ICP and CPP (Figs. 1 and 2). These clusters also included the AUC or percentage duration of abnormal values. As a novel step in this approach we used the mean value in the survivors to define the normal values. Our data suggest that the ‘dose’ (AUC) of abnormal ICP deviating from the normal (13.7 mmHg) is linked to

Outcomes are color-coded. Magnified view of variables clustered with CPP (b) and with ICP (c). Note the greater extent of clustering (red) in the subjects who died (grey boxes)

outcome. Although our study is not restricted to TBI, the minimum values in survivors in this study (47 mmHg) is consistent with that reported in other studies of pediatric TBI [5].

There are a number of limitations to this study. While ICP and CPP are age-dependent [4, 5] we did not stratify by age because of the small numbers. We used a crude outcome measure (death) to separate groups. While ICP was monitored for treatment of acute brain injury, this study combines a heterogeneous group of insults. The physiological data were obtained from the electronic medical record and therefore at a lower frequency (maximum every 30 min), which is optimal for this approach.

Conclusion

This study provides proof of principle of the application of hierarchical clustering to the analysis of data collected in the routine care of critically ill children. We show that this approach exploits all the data available in the PICU, generates results that are consistent with established norms, and others, that are hypothesis generating. These results support the long-term goal of applying complex data analyses in real time to support the management and improve the outcomes of critically ill children.

Conflict of interest statement Dr. Wainwright serves as a scientific consultant to TransMed Systems.

References

1. Adelson P, Bratton S, Carney N, Chesnut R, du Coudray H, Goldstein B, Kochanek P, Miller H, Partington M, Selden N, Warden C, Wright D (2003) Guidelines for the acute medical management of severe traumatic brain injury in infants, children, and adolescents. Chapter 8. Cerebral perfusion pressure. *Pediatr Crit Care Med* 4:S31–S33
2. Adelson P, Bratton S, Carney N, Chesnut R, du Coudray H, Goldstein B, Kochanek P, Miller H, Partington M, Selden N, Warden C, Wright D (2003) Guidelines for the acute medical management of severe traumatic brain injury in infants, children, and adolescents. Chapter 6. Threshold for treatment of intracranial hypertension. *Pediatr Crit Care Med* 4:S25–S27
3. Adelson P, Ragheb J, Muizelaar J, Kanev P, Brockmeyer D, Beers S, Brown S, Cassidy L, Chang Y, Levin H (2005) Phase II clinical trial of moderate hypothermia after severe traumatic brain injury in children. *Neurosurgery* 56:740–754
4. Chambers I, Jones P, Lo T, Forsyth R, Fulton B, Andrews P, Mendelow A, Minns R (2006) Critical thresholds of intracranial pressure and cerebral perfusion pressure related to age in paediatric head injury. *J Neurol Neurosurg Psychiatry* 77:234–240
5. Chambers I, Stobart L, Jones P, Kirkham F, Marsh M, Mendelow A, Minns R, Struthers S, Tasker R (2005) Age-related differences in intracranial pressure and cerebral perfusion pressure in the first 6 hours of monitoring after children's head injury: association with outcome. *Childs Nerv Syst* 21:195–199
6. Cohen M, Grossman A, Morabito D, Knudson M, Butte A, Manley G (2010) Identification of complex metabolic states in critically injured patients using bioinformatic cluster analysis. *Crit Care* 14:R10
7. Sorani M, Hemphill J, Morabito D, Rosenthal G, Manley G (2007) New approaches to physiological informatics in neurocritical care. *Neurocrit Care* 6:1–8
8. Webb C, Pass H (2004) Translational research: from accurate diagnosis to appropriate treatment. *J Transl Med* 2:35

ICM+: A Versatile Software for Assessment of CSF Dynamics

Peter Smielewski, Zofia Czosnyka, Magdalena Kasprowicz, John D. Pickard, and Marek Czosnyka

Abstract ICM+ software was introduced into the Cerebrospinal Fluid (CSF) Dynamics Laboratory, Addenbrooke's Hospital, Cambridge, UK, in 2003. Since then 1,447 constant rate infusion tests and 123 overnight ICP monitoring sessions (using intraparenchymal bolt) were performed. Various configurations were used: ICP only (identification of CSF dynamics model and overnight ICP monitoring with analysis of compensatory reserve and B waves); ICP and arterial pressure (ABP; analysis of the pressure reactivity index); ICP, ABP and transcranial Doppler blood flow velocity (for assessment of cerebral autoregulation); ICP, ABP and near-infrared spectroscopy (for analysis of the fluctuation of cerebral blood volume); ICP, sagittal sinus pressure and jugular vein pressure (in patients with idiopathic intracranial hypertension to assess the hydrodynamic consequences of cerebral venous sinus stenosis). To assess vascular factors of hydrocephalus a combination of CSF infusion study with PET-CBF studies was performed. The software contains a database of the shunts tested in the Cambridge Shunt Evaluation Laboratory, aiding shunt assessment in vivo in the case of possible underdrainage or overdrainage. The software also enables the digital recording of data, ready for post-hoc manual or batch analysis, the creation of virtual signals (such as critical closing pressure, cerebral compliance etc.) and analysis

of their dependency on primary modalities. A collected database of cases and signals forms a powerful reference tool in the investigation and understanding of the complex pathophysiology of hydrocephalus.

Keywords Hydrocephalus • Infusion test • Intracranial pressure • Software

Introduction

Computerised infusion study was introduced into clinical practice in mid-1980s at two neurosurgical centres: the Children's Health Centre, Warsaw, Poland [2] and Rigshospitalet, Copenhagen, Denmark [1]. The first version of the software was written in Basic for the ZX Spectrum computer and later in C language for the IBM PC. From the very beginning it was obvious that the CSF pressure (ICP) signal can be supplementally analysed to retrieve additional information describing CSF dynamics in patients suffering from hydrocephalus. In 2003 a new version of the software called ICM+ was designed, aiming to encapsulate the methodology used in clinical neuroscience for brain monitoring in various clinical scenarios. One of the procedures supported by ICM+ was infusion study including analysis of a dynamic model of CSF circulation and dedicated analysis of ICP waveform. This paper reviews the clinical applications of ICM+ to refine the management of patients suffering from hydrocephalus and other CSF disorders.

Materials and Methods

Needles and Transducers

The computerised infusion test is a modification of the traditional constant rate infusion test as described by Katzman and Hussey [6]. The method requires fluid infusion to be

P. Smielewski (✉), Z. Czosnyka, J.D. Pickard, and M. Czosnyka
Academic Neurosurgical Unit, Department of Clinical Neurosciences,
University of Cambridge, Box 167,
Addenbrooke's Hospital,
Cambridge, CB2 0QQ, UK
e-mail: ps10011@medschl.cam.ac.uk

M. Kasprowicz
Academic Neurosurgical Unit, Department of Clinical Neurosciences,
University of Cambridge, Box 167,
Addenbrooke's Hospital, Cambridge CB2 0QQ, UK

Institute of Biomedical Engineering and Instrumentation, Wrocław
University of Technology,
Wrocław, Poland

made into any accessible CSF compartment proximal to any hypothetical blockage in the CSF pathway. It may be performed in one of three ways

1. One wide lumbar (gauge 19) needle for pressure recording and infusion through a three-way connector.
2. Two lumbar needles (one for pressure recording and one for infusion).
3. One lumbar needle for infusion only, with simultaneous pressure recording via an intraparenchymal ICP sensor.

The alternative approach is intraventricular infusion into a subcutaneously positioned reservoir, connected to an intraventricular catheter or shunt-antechamber. In such cases two hypodermic needles (gauge 25) are used: one for the pressure measurement and the second for the infusion. Due care should be taken during skin preparation and the filling of manometer lines and transducers to minimise the risk of infection.

Hardware

A laptop computer, an analogue-to-digital converter (Data Translation 9600 Series), a pressure amplifier and an infusion pump are placed on a mobile trolley supporting the insulation power supply (Fig. 1).

Software

The baseline ICP is first recorded, the pulse amplitude of ICP was calculated via spectral analysis and the heart rate estimated. The right atrial pressure (RAP) index (a moving correlation coefficient between the changes in the pulse amplitude and mean ICP) is useful for assessment of the compensatory reserve. Then, infusion starts (at a rate of 1.5 or 1 mL/min), the pressure increases and after some time reaches a plateau. The pulse amplitude increases in accordance with the pressure rise. The RAP usually increases to values close to +1, indicating a loss of compensatory reserve during external CSF volume addition. Heart rate, calculated from the ICP waveform, is continuously displayed on the computer screen, providing a means of additional signal quality control (Fig. 2).

During the infusion test supplementary data, such as the power of respiratory waves and the slow waves of ICP, may be analysed and displayed as continuously updated time trends. The ratio of pulse amplitude to respiratory amplitude may also be helpful.

After the infusion, the model of CSF circulation is analysed, resulting in estimation of the full set of parameters



Fig. 1 Infusion test trolley containing a laptop computer running ICM+ software (*upper shelf*), a pressure monitor (Spiegelberg brain pressure monitor) and an analogue-to-digital converter (*middle shelf*), and a syringe infusion pump (*bottom shelf*)

describing CSF dynamics. Model fitting, analysis of the pressure–volume curve, analysis of the pulse waveform and the amplitude–pressure line are visualised to aid in quality assessment (Fig. 3).

Parameters like baseline pressure, amplitude, resistance to CSF outflow, elasticity, reference pressure, CSF formation rate are calculated.

For patients with a shunt in vivo, ICM+ includes a database of the nominal hydrodynamic performance parameters of the 24 most common shunts tested at the Cambridge Shunt Laboratory [5], which helps to detect causes of shunt malfunction.

Results

Over the last 7 years (2003–2010), 1,447 clinical infusion studies and 123 overnight ICP monitoring have been performed at Addenbrooke's Hospital, Cambridge, UK, in over 800 patients suffering from hydrocephalus of various

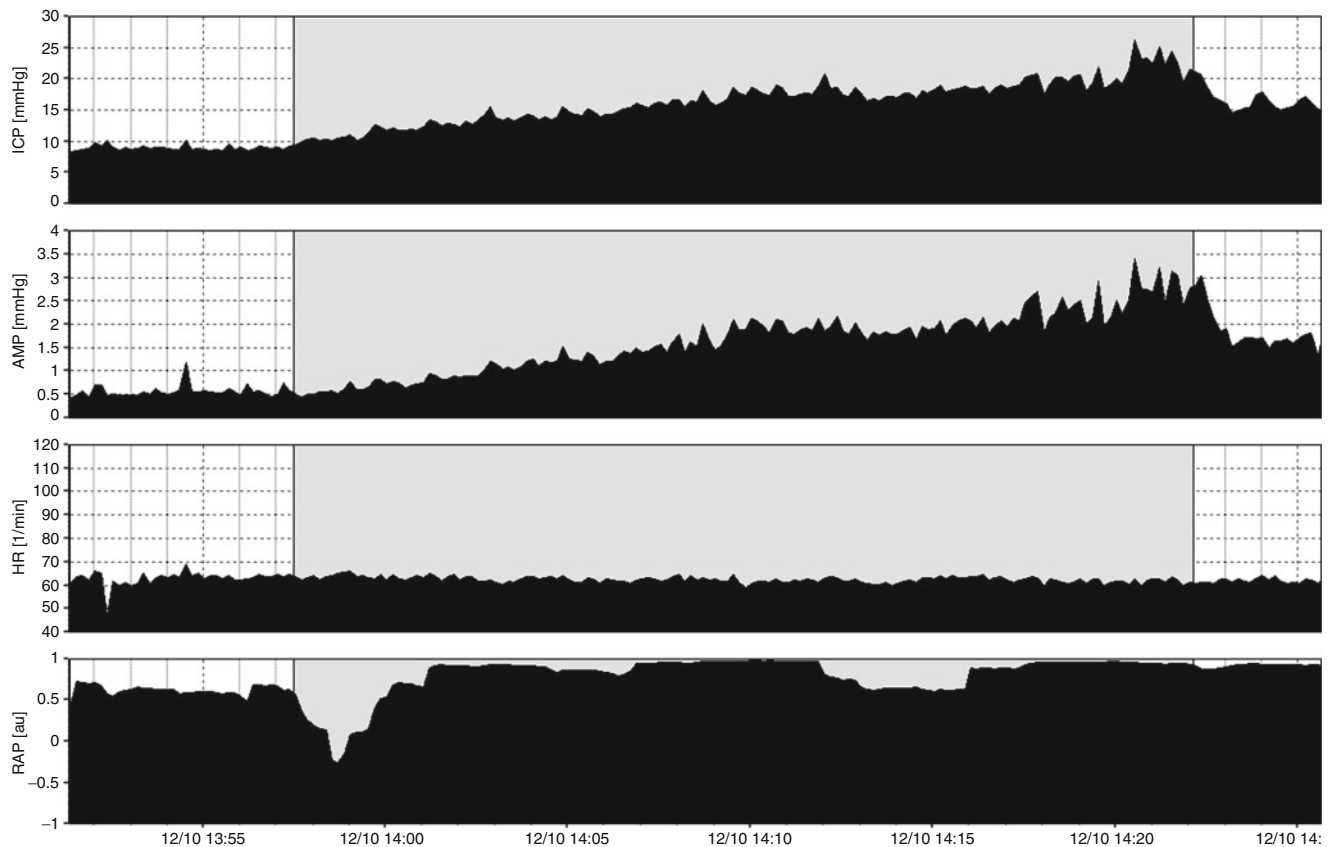


Fig. 2 Parameters displayed during infusion study: an example of recording in a patient with symptoms of normal pressure hydrocephalus (NPH). Normal baseline pressure (9 mmHg), normal baseline pulse amplitude, good compensatory reserve (right atrial pressure [RAP] index at baseline below 0.6). During the infusion at a rate of 1.5 mL/min (grey area) pressure increased to 20 mm (resistance to cerebrospinal fluid [CSF] outflow

was estimated at 7.7 mmHg/mL/min), the pulse amplitude increased in proportion with mean ICP. The elastance coefficient was low ($E=0.11/\text{mL}$). The RAP coefficient increased to +1 (indicating a decrease in compensatory reserve during infusion) and slow vasogenic waves appeared in intracranial pressure (ICP) and pulse amplitude (AMP) recordings during infusion. The overall picture of CSF compensation was normal

aetiologies (idiopathic NPH 45%, post-subarachnoid haemorrhage NPH 10%, other communicating hydrocephalus 23%, non-communicating hydrocephalus 22%). Mean age of the patients was 65 (range 23–94) and the male to female ratio was around 2:1. All of the patients had been referred to the CSF clinic by their treating neurosurgeon, geriatrician or neurologist, based on the presence of ventricular dilatation on a brain scan (CT or MRI), and symptoms of Hakim's triad and other relevant clinical presentations like headaches etc. This group of patients was investigated with a constant rate infusion study (via the lumbar approach 20%, a pre-implanted Ommaya reservoir, 41%, shunt pre-chamber, 36% or open EVD, 3%), in addition to the standard clinical and imaging assessment. In some, overnight ICP monitoring was performed in addition to or as an alternative to the infusion test. Forty-five percent of the infusion tests were performed in patients with shunts in situ to evaluate shunt performance where new or recurrent symptoms suggested altered shunt function.

An internal audit showed that the infection rate associated with infusion tests in the years 2007–2009 was less than 1%.

Synopsis of the Use of ICM+ in Pivotal Clinical Studies

Profiles of disturbance of CSF infusion study have been delineated: typical NPH, atrophy without disturbance in CSF compensation, acute hydrocephalus and normal CSF dynamics [3].

Infusion study into a shunt prechamber provides the opportunity to distinguish between a correctly functioning shunt and a blocked (positive predictive power >90%) or overdraining shunt [9].

For the assessment of cerebral autoregulation, measurement of ICP, Finapres arterial pressure and transcranial Doppler blood flow velocity allows detection of disturbed autoregulation, manifested as a positive mean velocity index

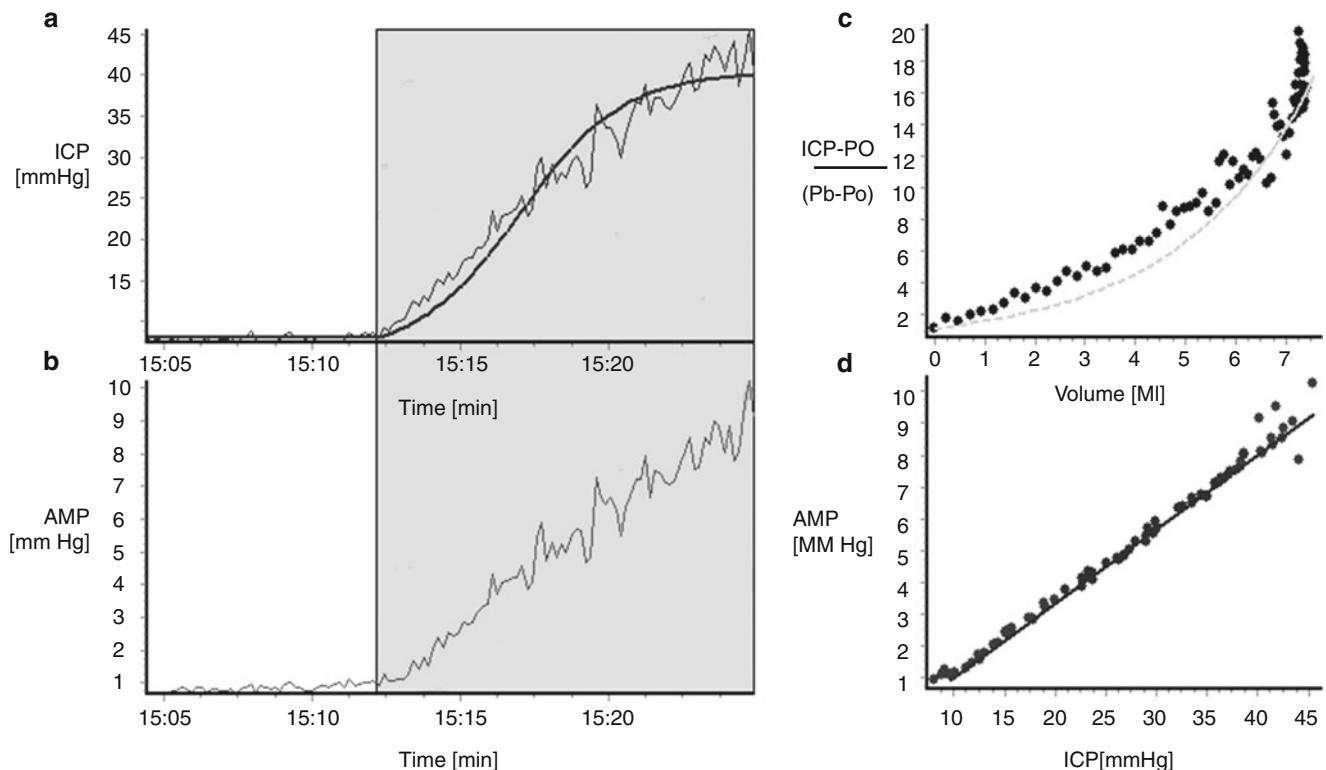


Fig. 3 Methods of identification of the model of CSF circulation during constant rate infusion study. (a) Recording of real CSF pressure (ICP) versus time increasing during the infusion with an interpolated modelling curve. Infusion at a constant rate of 1.5 mL/min for the period is indicated by the grey shaded area. (b) Recording of AMP during infusion. It is customary for AMP to be presented alongside the mean ICP. A rise in AMP is usually well correlated with a rise in ICP.

(c) Pressure–volume curve. On the x-axis the effective volume increase (i.e. infusion and production minus reabsorption of CSF) is plotted. On the y-axis: the increase in pressure measured as a gradient of current pressure minus the reference pressure P_o , relative to the baseline pressure P_b . (d) Linear relationship between pulse amplitude and mean ICP. Intercept of the line with x-axis (ICP) theoretically indicates the reference pressure P_o .

(Mx) [4]. It is often associated with normal resistance to CSF outflow, suggesting underlying cerebrovascular disease in patients who develop symptoms, but have normal conditions for CSF circulation [4].

The origin of slow waves in ICP occurring during the test can be investigated using near infrared spectroscopy (NIRS). Recording of ICP, Finapres ABP and NIRS variables, de-oxygenated and oxygenated haemoglobin, tissue oxygenation index and total haemoglobin index, show similar patterns to slow ICP waves [11].

Coupling between ICP and sagittal sinus pressure has been demonstrated in patients suffering from idiopathic intracranial hypertension [10].

A series of infusion tests with simultaneous PET-CBF imaging have been performed. ICP, Finapres ABP and TCD blood flow velocity recordings have been performed during a prolonged infusion test along with two PET-CBF imaging studies, at baseline and during the plateau of ICP. In patients suffering from NPH blood flow has been found to be significantly decreased in the area adjacent to the surface of the ventricles [8].

Finally, the software has also been used for overnight ICP monitoring, aiding detection of B waves and characterisation of compensatory reserve using the RAP index [7].

Conclusion

Various configurations are available within ICM+ to facilitate brain monitoring and aid management of patients suffering from hydrocephalus and other CSF disorders.

Acknowledgement The project was supported by the National Institute of Health Research, Biomedical Research Centre, Cambridge University Hospital Foundation Trust – Neurosciences Theme plus Senior Investigator Award (JDP) and the Foundation for Polish Science (MK).

Conflict of interest statement ICM+ is a software (<http://www.neurosurg.cam.ac.uk/icmplplus>) licensed by the University of Cambridge, Cambridge Enterprise Ltd. PS and MC have a financial interest in a part of the licensing fee.

References

1. Borgesen SE, Albeck MJ, Gjerris F, Czosnyka M, Laniewski P (1992) Computerized infusion test compared to steady pressure constant infusion test in measurement of resistance to CSF outflow. *Acta Neurochir (Wien)* 119:12–16
2. Czosnyka M, Batorski L, Laniewski P, Maksymowicz W, Koszewski W, Zaworski W (1990) A computer system for the identification of the cerebrospinal compensatory model. *Acta Neurochir (Wien)* 105:112–116
3. Czosnyka M, Whitehouse H, Smielewski P, Simac S, Pickard JD (1996) Testing of cerebrospinal compensatory reserve in shunted and non-shunted patients: a guide to interpretation based on an observational study. *J Neurol Neurosurg Psychiatry* 60:549–558
4. Czosnyka ZH, Czosnyka M, Pickard JD (2002) Shunt testing in-vivo: a method based on the data from the UK shunt evaluation laboratory. *Acta Neurochir Suppl* 81:27–30
5. Czosnyka ZH, Czosnyka M, Whitfield PC, Donovan T, Pickard JD (2002) Cerebral autoregulation among patients with symptoms of hydrocephalus. *Neurosurgery* 50:526–532; discussion 532–523
6. Katzman R, Hussey F (1970) A simple constant-infusion manometric test for measurement of CSF absorption. I. Rationale and method. *Neurology* 20:534–544
7. Kim DJ, Czosnyka Z, Keong N, Radolovich DK, Smielewski P, Sutcliffe MP, Pickard JD, Czosnyka M (2009) Index of cerebrospinal compensatory reserve in hydrocephalus. *Neurosurgery* 64:494–501; discussion 501–502
8. Momjian S, Owler BK, Czosnyka Z, Czosnyka M, Pena A, Pickard JD (2004) Pattern of white matter regional cerebral blood flow and autoregulation in normal pressure hydrocephalus. *Brain* 127:965–972
9. Petrella G, Czosnyka M, Smielewski P, Allin D, Guazzo EP, Pickard JD, Czosnyka ZH (2009) In vivo assessment of hydrocephalus shunt. *Acta Neurol Scand* 120:317–323
10. Pickard JD, Czosnyka Z, Czosnyka M, Owler B, Higgins JN (2008) Coupling of sagittal sinus pressure and cerebrospinal fluid pressure in idiopathic intracranial hypertension – a preliminary report. *Acta Neurochir Suppl* 102:283–285
11. Weerakkody RA, Czosnyka M, Zweifel C, Castellani G, Smielewski P, Keong N, Haubrich C, Pickard J, Czosnyka Z (2010) Slow vasogenic fluctuations of intracranial pressure and cerebral near infrared spectroscopy-an observational study. *Acta Neurochir (Wien)* 152:1763–1769

Modified Brainstem Auditory Evoked Responses in Patients with Non-brainstem Compressive Cerebral Lesions

James L. Stone, John Fino, Prasad Vannemreddy, and Fady Charbel

Abstract The brainstem auditory evoked response (BAER) is sensitive to pontomesencephalic integrity, transtentorial brain herniation, and at times increased intracranial pressure (ICP). The authors report their experience utilizing a recently described rapid rate, binaural, click and 1,000-Hz tone-burst modification of the BAER (MBAER) in 22 symptomatic non-trauma patients with non-brainstem compressive space-taking cerebral lesions. The majority presented with mild to moderate clinical signs suggestive of increased ICP, and focal neurological deficits. The cerebral lesions, mostly tumors (17), averaged 4–5 cm in diameter, with radiological signs of mass effect such as flattening of the sulci, midline shift, and narrowing of the basal cisterns. A number of significant changes in Wave V and V_n latency and less so amplitude were found in patients compared with age-matched normal volunteers, as well as those again studied after surgical decompression. Similar MBAER changes had been noted in normal volunteers placed in a dependent head position. Possible mechanisms to explain these findings are discussed. The methodology shows promise and if combined with automated peak recognition could make Neuro ICU monitoring practical.

Keywords Brainstem auditory evoked response • BAER • Brainstem auditory evoked potential • BAEP • Cerebral mass lesions • Intensive care monitoring • Sensory evoked response

Introduction

The brainstem auditory evoked response (BAER) is a well-accepted neurophysiological tool that is refractory to sedation, muscle paralysis, and general anesthesia [1, 6]. A moderately loud click stimulus is required to produce all five vertex positive waves (I to V), but less intense click stimuli, pure tone stimuli, and rapid stimulation rates still yield the prominent midbrain generated Waves V and V_n [4, 9]. Although frequently used to advantage in the operating room [6] the BAER has not found widespread monitoring usage in the Neuro ICU (NICU).

Animal studies as well as clinical reports of patients with intracranial lesions or hydrocephalus demonstrated BAER Wave V changes and correlations, at times reversible between Wave V and increased ICP, transtentorial brain herniation (TBH), and reduced midbrain perfusion [1, 3]. Based upon our BAER experience with a model of an expanding intracranial mass in the primate [8], and the use of a modified BAER (MBAER) in normal volunteers subjected to a dependent head position [9], we present MBAER findings in 22 symptomatic patients with large, non-brainstem compressive cerebral lesions. Approval was obtained from the University of Illinois and Advocate IL Masonic Hospitals, Chicago, in accordance with Federal and State guidelines. Our sponsor is Bio-logic System Corp., Mundelein, IL, USA (Natus-Biologic, San Carlos, CA, USA).

Materials and Methods

A review of BAER and modified MBAER methodology was recently published and is briefly summarized here [9]. A two-channel auditory evoked potential unit was used to stimulate, record, display, and visually analyze the responses in normals and patients. Routine surface EEG electrodes were placed at the nasion (ground), Fz (frontal hairline – active), and C2 neck (reference). Sound stimulus modalities – a click and 1,000 Hz tone-burst – were delivered by insert earphones as used for intraoperative BAER monitoring.

J.L. Stone (✉), J. Fino, P. Vannemreddy, and F. Charbel
Department of Neurological Surgery,
University of Illinois and Advocate Illinois Masonic Hospitals,
912 S. Wood St., 4th Floor,
Chicago, IL 60612, USA
e-mail: jlstone4@aol.com, jlstone4@gmail.com

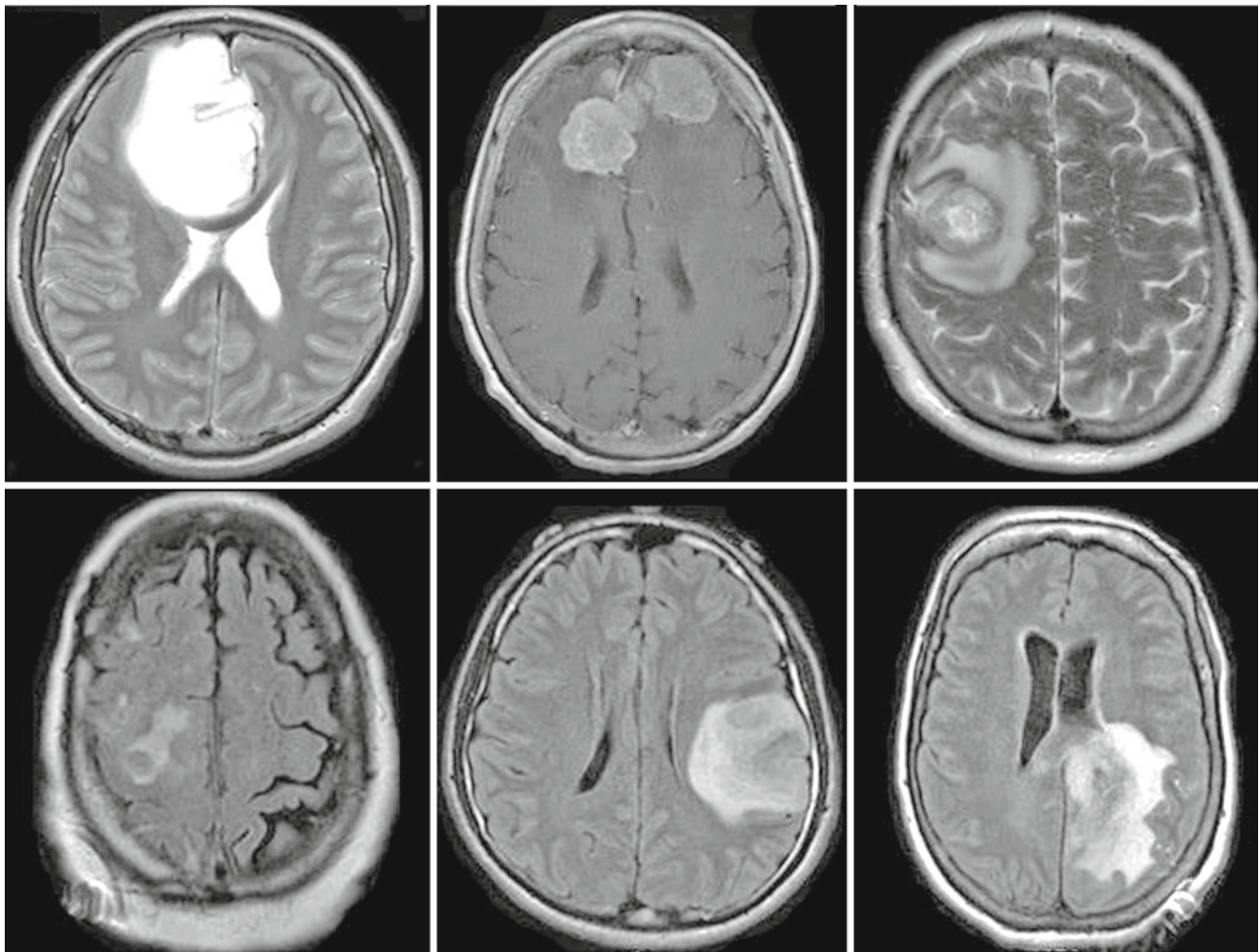


Fig. 1 Representative patient preoperative MRI scans

Both stimuli were presented binaurally at rapid rates of 59/s for the click and 44.4/s for the 1,000-Hz stimulus. The two stimuli were delivered at four diminishing sound intensities: 85, 75, 65, and 55 dB peSPL for the click and 95, 85, 75, and 65 dB peSPL for the 1,000-Hz tone-burst (eight trials). Two replications of 4,000 stimuli were required for each trial. Wave V and V_n absolute latencies and amplitudes were recorded.

Normative data were obtained from 27 healthy volunteers (11 female, 16 male), age range 27–71 years (mean 49 years). All had a normal screening audiogram, followed by the click and 1,000-Hz MBAER while positioned on a recliner with head elevation of 30°. The study took about 45 min to complete. Likewise, all patients underwent the MBAER test battery in bed with a 30° head elevation.

Patients were selected from the neurosurgical services between 2009 and 2010. Twenty-two non-trauma patients (8 female, 14 male) aged 26–64 years (mean 49.0 years) with magnetic resonance imaging (MRI) evidence of supratentorial mass effect without brainstem or eighth nerve

involvement were studied with MBAER. Headache and associated symptoms suggestive of mild to moderately increased ICP were present in 19 patients and focal cerebral signs were present in 19. Only three patients were drowsy and not consistently following commands at the time of initial MBAER testing. None of the patients exhibited pupillary or clinical brainstem signs. The patients had no history of hearing or temporal bone abnormality, previous neurological condition or skull fracture. The patients had large (3–7 cm³ including edema, mean 4.7 cm³) cerebral lesions (Fig. 1) consisting of cerebral tumors (17), abscess/inflammatory lesions (3), or spontaneous hemorrhages (2). All tumor patients had been treated with dexamethasone before the time of the initial MBAER testing. The predominant location of the above lesion(s) was frontal (9), parietal/occipital (6), basal ganglia/thalamus (5), and temporal (2). Midline shift (range 2.5–10 mm, mean 4.8 mm) and/or basal cistern compromise was present in 13. All were tested within 3 days of admission and brain imaging studies. No patients were studied pre-operatively while intubated and

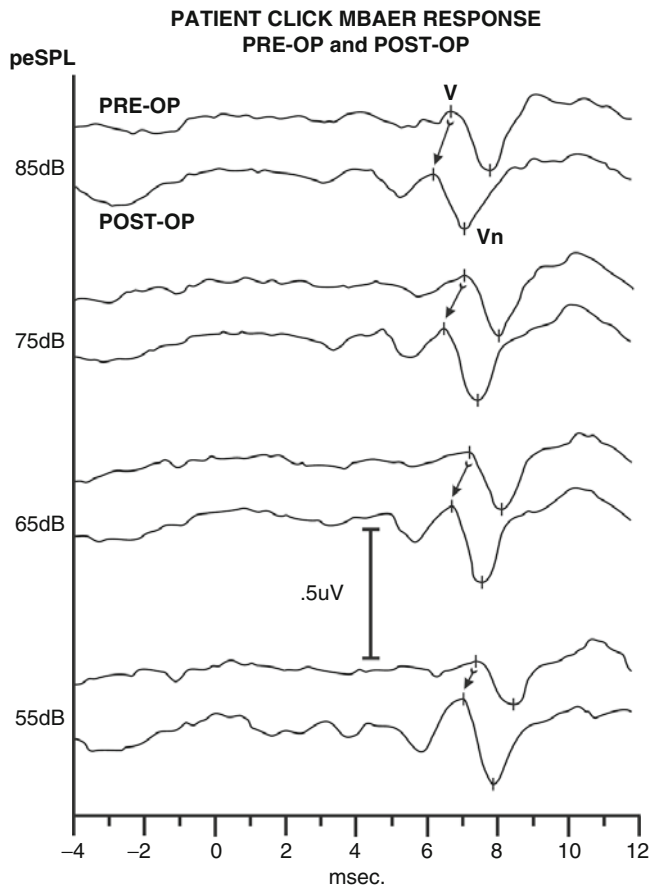


Fig. 2 Pre-operative and 8 days post-operative click study. Fz to C2 neck linkage. Wave V and V_n latency improvement noted. Twenty-six-year-old man with a left parieto-temporal low-grade glioma measuring 5 cm in diameter (see Fig 1, lower row, center)

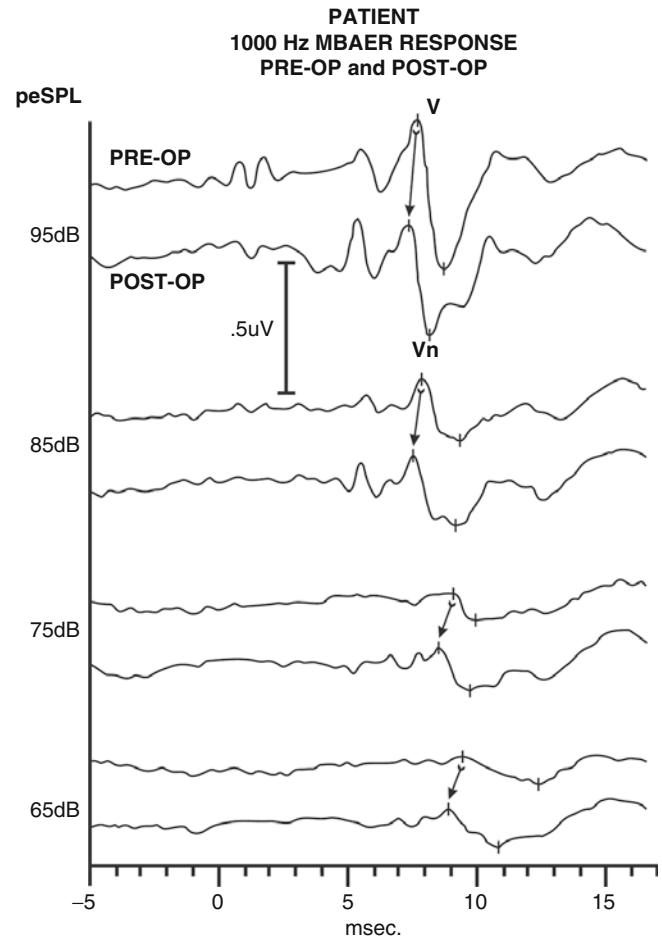


Fig. 3 Pre-operative and 8 days post-operative 1,000-Hz MBAER

Table 1 Absolute latencies/standard deviations

Peak	Normals (27)		Patients (22)	
	V	V_n	V	V_n
<i>Stimulus intensity(dB peSPL)</i>	<i>Click MBAER</i>			
85	6.56/.57	7.56/.54	6.87/.60	7.93/.59
75	7.05/.64	8.04/.72	7.47/.67	8.49/.62
65	7.69/.59	8.66/.76	7.99/.66	9.02/.71
55	8.13/.46	9.18/.63	8.69/.99	9.66/1.01
<i>Stimulus</i>	<i>1,000-Hz MBAER</i>			
95	7.61/.35	8.71/.44	7.66/.53	8.98/.57
85	7.93/.34	9.13/.38	8.26/.91	9.55/1.02
75	8.33/.49	9.60/.61	9.10/1.18	10.22/1.35
65	9.00/.56	10.39/.92	10.25/1.33	11.52/1.51

11 patients were again studied about 1 week after extubation following general anesthesia for decompressive craniotomy.

Representative waveforms are illustrated in Figs. 2 and 3. The means and standard deviations (SD) of Wave V and V_n

absolute latency measures of the normal volunteers and patients are illustrated in Table 1. Non-paired t tests were performed on patients versus normative data, paired t tests on each patient pre- and post-operatively, and non-paired t tests on post-operative patients versus normative data.

Table 2 Significant statistical results for latency

Peak	Click MBAER						1,000-Hz MBAER											
	55 dB		65 dB		75 dB		85 dB		65 dB		75 dB		85 dB		95 dB			
	V	V _n	V	V _n	V	V _n	V	V _n	V	V _n	V	V _n	V	V _n	V	V _n	V	V _n
<i>Patient groups vs normal controls</i>																		
All patients (22)	–	–	0.047	0.049	0.015	0.012	0.041	0.016	0.013	0.043	0.004*	0.028	–	0.042	–	–	0.035	–
Midline shift/basal cistern obliteration (13)	–	–	.012	0.020	0.014	0.002*	–	0.018	0.021	0.016	0.009*	0.010*	0.031	0.018	0.004*	0.004*	–	–
Frontals (9)	–	–	–	–	–	0.022	–	0.028	0.004*	0.002*	0.022	0.032	–	–	–	–	0.015	–
<i>Patient groups: pre-operative vs post-operative</i>																		
All patients (11)	–	–	0.019	0.027	0.044	0.015	0.009*	0.049	–	–	–	–	–	–	–	–	–	–
Midline shift/basal cistern obliteration (9)	–	–	0.026	–	–	0.026	0.017	–	–	–	–	–	–	–	–	–	–	–
Frontals (6)	–	–	0.036	–	0.009*	0.011	–	0.013	0.028	0.014	–	–	–	–	–	–	–	–

p values <0.05, *t* test, **p*≤0.01

Results

Statistical significance was a p value <0.05 . There was no significant age difference between the patients (mean 49.0 years) and normal volunteers (mean 49 years; $p=0.496$). Patient data compared with normals revealed Wave V_n or V absolute latency prolongations for click and 1,000-Hz MBAER at nearly all stimulus intensity levels. In the 11 patients studied both pre- and post-operatively, Wave V and V_n absolute latency improved (shortened) post-operatively, but only for the click stimulus.

The patients were further analyzed with regard to midline shift and/or basal cistern narrowing/obliteration (MS/BCO; 13 patients, 9 operated, mean age 47 years) and frontal involvement (Frontal; 9 patients, 6 operated, mean age 48 years; Table 2). The MS/BCO sub-group compared with normals showed marked Wave V and V_n prolonged latency for both click and 1,000-Hz stimuli at nearly all intensity levels. The Frontal location subgroup similarly showed Wave V and V_n prolonged latency for the 1,000 Hz and less so for the click stimulus. Pre- vs post-operative MS/BCO and Frontal groupings also disclosed significant latency improvements. Regarding post-operative patient groupings versus normals, no significant latency differences were noted. Significant amplitude changes were present in this study, but were much less common than latency changes.

Discussion

The analysis of Wave V and V_n click and 1,000-Hz MBAER latencies for patients vs age-matched normals, pre- vs post-operative patients, MS/BCO and frontal subgroups disclosed many significant findings. Overall, these changes resemble those found in normal volunteers required to hold a 10–15° downward tilted head position [9]. Fewer significant amplitude findings were found, as amplitudes are often more variable between individuals and testing sessions [1].

It is unclear why patients without apparent radiological or clinical midbrain involvement show latency prolongation or suppression of the midbrain-generated MBAER Wave V – V_n complex. We suggest that these changes might be secondary to a transtentorial compliance or pressure gradient, despite presumably only mild or moderately elevated ICP. Perhaps the MS/BCO and frontal lesions, due to their proximity to both the anterior transfacial and tentorial openings, create a localized pressure effect upon the upper brainstem or diencephalon. Subtle upper brainstem axial distortion or torque could create mechanical stresses on nuclei and axonal pathways at the tentorial incisura [2]. In this regard a major strength of the BAER is its ability to detect lesions of the brainstem in a number of neurological conditions [1, 4]. The BAER also captures critical, yet frequently reversible changes during intraoperative monitoring for posterior fossa, brainstem, and posterior circulation surgery

[6, 7]. Alternatively, these findings could reflect ICP changes transmitted to the cochlea by way of the cochlear aqueduct, which interfaces CSF and perilymph [5, 10].

Conclusion

The MBAER has been found to capture a number of significant reversible Wave V and V_n latency abnormalities in symptomatic patients with large but non-brainstem compressive supratentorial lesions. Similar changes had been noted in a recent study of the MBAER in normals required to hold a downward head tilt. Physiological reasons for these changes likely involve both central and peripheral mechanisms, such as a transtentorial compliance or pressure gradient, diminished midbrain and inferior colliculus perfusion, diencephalic or deep hemispheric involvement, or CSF to perilymph pressure transfer through the cochlear aqueduct. Further investigation appears warranted and could promote development of a practical and powerful monitoring device in the NICU.

Conflict of interest statement We declare that we have no conflict of interest, and guarantee that this paper has not been published in another journal nor will it be submitted for publication in another journal.

References

1. Chiappa KH (1997) Brain stem auditory evoked potentials: methodology. In: Chiappa KH (ed) *Evoked potentials in clinical medicine*, 3rd edn. Lippincott Raven, Philadelphia, pp 157–197
2. Fisher CM (1995) Brain herniation: a revision of classical concepts. *Can J Neurol* 22:83–91
3. Ghaly RF, Stone JL, Subramanian KS, Roccaforte P, Hughes JR (1988) Modified auditory brainstem responses. *Studies in patients with intracranial lesions*. *Clin Electroencephalogr* 19:95–107
4. Hall JW (2007) *New handbook of auditory evoked responses*. Allyn and Bacon, Boston, pp 212–280
5. Manwaring KH, Manwaring P, Manwaring J, Brenner J, Wickern D, Manwaring M (2005) Noninvasive brain compliance testing in patients with hydrocephalus: a provocative test to guide management. *J Neurosurg Pediatr* 103:A104
6. Moller AR (2006) *Intraoperative neurophysiological monitoring*, 2nd edn. Humana, Totowa, pp 85–124
7. Neuloh G, Schramm J (2008) Evoked potential monitoring during surgery for intracranial aneurysms. In: Nuwer MR (ed) *Intraoperative monitoring of neural function. Handbook of clinical neurophysiology*, vol 8. Elsevier, Amsterdam, pp 801–814
8. Stone JL, Ghaly RF, Subramanian KS, Roccaforte P, Kane J (1990) Transtentorial brain herniation in the monkey; analysis of brainstem auditory and somatosensory evoked potentials. *Neurosurgery* 26:26–31
9. Stone JL, Calderon-Arnulphi M, Watson KS, Patel K, Mander NS, Suss N, Fino J, Hughes JR (2009) Brainstem auditory evoked potentials – a review and modified studies in healthy subjects. *J Clin Neurophysiol* 26:167–175
10. Voss SE, Horton NJ, Tabucchi TH, Folowosele FO, Shera CA (2006) Posture-induced changes in distortion-product otoacoustic emissions and the potential for noninvasive monitoring of changes in intracranial pressure. *Neurocrit Care* 4:251–257

Analysis of Intracranial Pressure Time Series Using Wavelets (Haar Basis Functions)

Hans E. Heissler, Kathrin König, Joachim K. Krauss, and Eckhard Rickels

Abstract Purpose: Transforming intracranial pressure (ICP) into frequency domain commenced in the early 1980s, arriving at the conclusion that cerebrospinal dynamics were mapped by ICP spectral composition. Classical analysis tools were not suitable for handling intrinsic signal non-stationarity. To overcome inherent obstacles we introduce a novel approach based upon wavelets.

Methods: During routine diagnostic volume pressure testing epidural ICP was acquired in 118 patients with suspected cerebrospinal fluid circulatory disorders. Pressure was digitised and conditioned to separate low frequent signal components (<heart rate). ICP fluctuations were computed by subtraction of original and low frequent ICP constituents. Subsequently, multiresolution analysis was performed on fluctuations by discrete Haar wavelet transform and coefficients displayed in dyadic fashion (scalogram).

Results: Decomposition of ICP fluctuations led to typical patterns in the scalogram. Episodes of pathological wave activity and artificial ICP changes were topographically detectable in the time frequency plane.

Conclusions: The wavelet approach is a simple yet powerful signal processing method to estimate both static and dynamic properties of ICP in various clinical scenarios. It therefore outclasses classical spectral transforms that are limited to analysing real-world data. Haar wavelets are fast and robust. Their disadvantages seem not to counterbalance the advantages in this biomedical application.

Keywords Haar wavelets • Non-stationarity • Spectral analysis • Intracranial pressure • Infusion test

Introduction

The analysis of biomedical signals is based on operations in both the time and frequency domain. The latter is often carried out by classical Fourier transform, which has some limitations especially when dealing with real-world data. One application is the decomposition of intracranial pressure signal whose frequency content is expected to contain additional features indicating change in cerebrospinal integrity.

The Fourier transform is most effective under supervised conditions, i.e. when patients were part of controlled short-term studies. Under non-supervised conditions, however, artefacts from various sources most often corrupt signals. As an example, this situation occurs when patients with suspected cerebrospinal fluid circulatory disorders are selected for long-term intracranial pressure measurement over at least 24 h. All sorts of artefacts can be found to be traced back to intentional and spontaneous postural changes (static changes), all kinds of movements (dynamic changes), and all endogenous processes resulted in volumetric changes transferred to the cerebral circulation (e.g. extra-systoles). These artefacts ‘caused’ by a patient will most often lead to a signal characteristic known as non-stationarity. The crux with that is that presumptions of classical Fourier approaches do not comply with non-stationarity, in general, and therefore frequency domain results will suffer from this incompatibility/shortcoming. An effective alternative to Fourier approaches is the wavelet methodology, which provides a limited spectral resolution counterbalanced by an excellent temporal resolution. With wavelets the spectral contents can be attributed to a time point that cannot be accomplished by application of a Fourier transform.

A Glance at Wavelets

The last two decades have seen a rise in the application of wavelet methodology. The following lines give only a very rough description of what wavelets are about: the word wavelet means ‘small wave’ indicating their unique characteristics, as are scaling and translation in time:

H.E. Heissler (✉) and J.K. Krauss
Klinik für Neurochirurgie 7249, Medizinische Hochschule Hannover,
30623 Hannover, Germany
e-mail: heissler.hans.e@mh-hannover.de

K. König and E. Rickels
Klinik für Unfallchirurgie, Orthopädie und Neurotraumatologie,
AKH, Celle, Germany

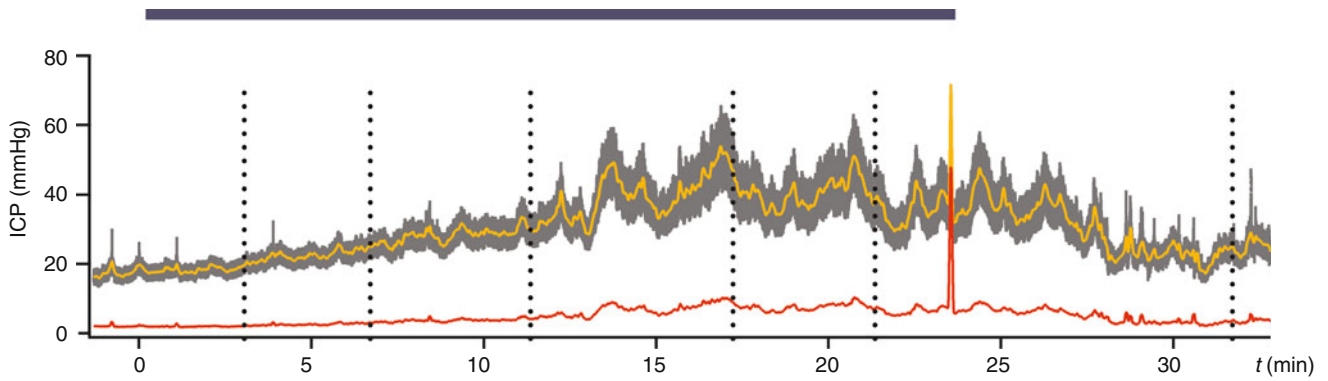


Fig. 1 Plot of a typical intrathecal infusion study (1.5 mL/min) in a patient with suspected cerebrospinal fluid circulation disorder. Intracranial pressure (ICP, grey) was measured by an epidural pressure sensor. Mean ICP (yellow) and pulse pressure amplitude (red) were computed by

windowed averaging (box car moving average) and determination of the envelope of the difference in the original and mean ICP data respectively. The black bar outlines the infusion interval. Spike artifact indicates end of infusion. Labels A–F denote distinct episodes of ICP

$$F(a, t) = \frac{1}{\sqrt{|a|}} \int_{-\infty}^{\infty} x(\tau) \phi\left(\frac{\tau - t}{a}\right) d\tau$$

where F : wavelet coefficient, ϕ : wavelet function, a : scaling, t : translation.

A practical interpretation of this formula shows that a wavelet (basis function) can be scaled and shifted representing frequency and time respectively. The wavelet is valid for combinations of scale and time thus enabling the analysis of mainly non-stationary time series, especially of jagged time series.

The term ‘multiresolution analysis’ is closely related to wavelet methodology implying the decomposition of a discrete signal at various scale levels ranging from very low frequency resolution to the finest, resulting in wavelet spectrogram. Multiresolution analysis is the heart of wavelet analysis [12].

Scalogram

As the wavelets transform decomposes a signal with regard to frequency and time, the results of transforms (wavelet coefficients) can be mapped as a plane representing the values of the wavelet coefficients as a function of time and frequency. Coefficients will be coded as colour values and the resulting image is called a scalogram.

Haar Wavelets

The simplest wavelet is the Haar wavelet, according to the definition proposed by Alfréd Haar in 1909. Haar wavelets consist

of a rapid fluctuation between non-zero values ($\pm 2^{-1/2}$) with zero mean. For illustration, the Haar wavelet is a biphasic rectangular pulse with amplitudes of $\pm 2^{-1/2}$.

Materials and Methods

Haar wavelets were computed by discrete wavelet transform on intracranial pulse pressure data from routine diagnostic infusion test studies (constant rate infusion test) in patients with suspected cerebrospinal fluid circulatory disorders.

Intracranial Pressure Measurement

Long-term measurements of epidural ICP and infusion studies were part of routine diagnostics in 118 patients with suspected cerebrospinal fluid circulation disorders determining cerebrospinal parameters such as compliance/elastance and resistance to outflow of cerebrospinal fluid. Intracranial pressure was measured by means of commercial intracranial pressure (ICP) transducers of various manufacturers, mainly Neurodur sensors (Raumedic AG, Helmbrechts, Germany). Because of high effective cut-off frequencies of this sensor system the dynamic error is small concerning the frequency content of ICP (≤ 20 Hz).

Signal Acquisition

The analogue ICP signal was digitised with respect to premises of the fast wavelet algorithm, i.e. to meet the 2^n rule that

is widely used in digital signal processing. Signals were sampled at $f_s = 40$ Hz (100 Hz) and stored [6]. Resampling was carried out off-line to achieve 64 Hz (128 Hz) sampling frequencies.

To estimate devolutions of intracranial pulse pressure and intracranial mean pressure relationships, pulse pressure waveforms were separated by the following algorithm: smoothing of the ICP (*boxcar moving average*), subtraction of the moving average from original ICP, and computation of the envelope of resulting pulse-pressure half-waves (Fig. 1).

Discrete Wavelet Transforms

Wavelet transform, i.e. the computation of wavelet coefficients, was performed by a recursive lifting scheme on 2^n data points, resulting in an $n \times 2^{n-1}$ wavelet coefficient matrix communicating the time frequency plane (wavelet spectrogram). The resolution in time yields $2/f_s$. Spectral frequency resolution is best at $f_s/2^n$. Frequency resolution declines as a power of 2 as the level decreases.

Wavelet transforms were computed using LabVIEW 8.6 (National Instruments, Austin, TX, USA) graphical software. An in-house Haar wavelet software package was programmed to compute both the Haar wavelet transform and its inverse based on multiresolution analysis [3]. The package offers the exclusion of scale level ranges and coefficient magnitudes for feature extraction or reconstruction of signals with a reduced set of wavelet coefficients (e.g. denoising). Resulting wavelet spectrograms (scalograms) could be plotted with either original or squared coefficients for entropy considerations. Calculations of some statistical parameters complete the software package. For details refer to Heissler et al. [4].

Results

In all 118 patients wavelet spectrograms were computed showing spectra of ICP with high temporal resolution. To plot the Haar wavelet spectrogram of intracranial pulse pressure devolutions during supervised pressure elevation data were transferred into a pseudo three-dimensional layout.

When the original signal changed rapidly as it did during systolic cycles wavelet coefficient magnitudes prevailed in regions of highest frequencies (scales). During diastolic ICP coefficients were more centred in the scalogram indicating slower signal changes. The frequency resolution of wavelet transforms was worse in comparison to Fourier transforms,

i.e. there was an inverse proportion between temporal and spectral resolutions whereas Fourier transforms was featured by an even spectral resolution (Fig. 2).

Discussion

In the last 30 years spectral analyses of ICP have been carried out preferably by applying classical Fourier transforms. These analyses were aimed at spectral features indicating some change in cerebrospinal system integrity. Spectral analysis of ICP seems closely related to pulse pressure waveform analysis because spectral changes are likely to imply alterations in intracranial volume reserve [1, 2, 5, 11]. Also, changes in cerebral circulation parameters mirror a spectral change of intracranial pulse pressure as shown in carbon dioxide challenging tests [10].

The application of the Fourier transform is based on the rationale of stationarity, which is a theoretical measure describing the fact that signals being analysed should not alter in statistical parameters. If signals do not conform to stationarity the estimation of spectral composition will suffer from leakage, i.e. spectral amplitudes will spread out into neighbouring spectral lines. Practically, this phenomenon was often encountered but seldom reported and much effort was put into the selection of episodes to meet Fourier series premises.

Ultimately, the intriguing question to answer is, why is wavelet analysis effective? Wavelet transforms have proven to be very efficient and effective in analysing a very wide class of real-world signals. The properties that give effectiveness are:

1. The unconditional basis of wavelets showed that wavelets are very close to being optimal for a wide class of signals for compression, denoising and detection.
2. The wavelet expansion allows a more accurate description in time and separation of signal characteristics. Fourier coefficients represent an everlasting component and, therefore, short-term events (e.g. artefacts) must be described by a phase characteristic that allows cancellation or reinforcement over large time periods. A wavelet coefficient represents a component that is itself local and easier to interpret. The wavelet transform may allow separation of components of a signal that overlap in both time and frequency.
3. Wavelets are flexible and conformable. Because there is not just one wavelet, they can be designed to fit individual applications.
4. Wavelets and the computation of the discrete wavelet transform is well suited to computers, as there are only operations that are basic to a central processing unit [7, 12].

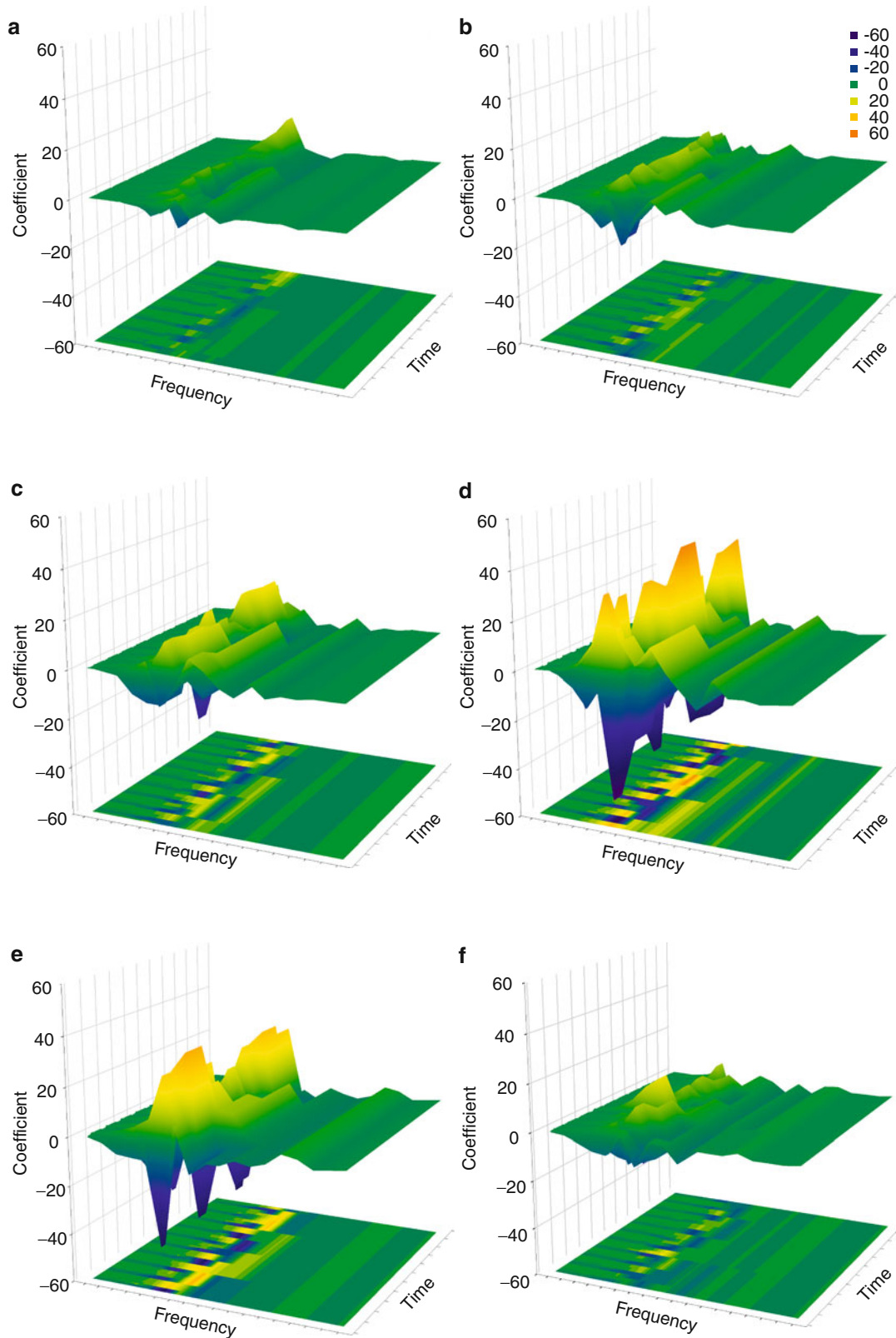


Fig. 2 Pseudo 3D wavelet spectrograms depicting the time frequency localization property of the discrete wavelet transform for intracranial pulse pressure episodes labelled (a–f) (refer to Fig. 1). Episodes (a–d) show the development of wavelet coefficients during increasing ICP, resulting in enhancement and spreading of the blue coded coefficient corresponding to a change in both the amplitude and frequency content.

Diastoles (yellow) are enhanced, but do not markedly leak indicating some change in amplitude but not in spectral composition. During ICP relaxation involution of coefficients takes place (compare b and f). The contours of the wavelet coefficients are given in arbitrary units; episodes are set to 10.24 s of duration (1,024 samples, sample frequency 100 Hz)

Conclusion

The wavelet transform is not intended to replace the classical Fourier transform, which is most effective when studying stationary signals and when local (time) information is not needed. Wavelet time frequency localisation properties can add to the analysis of the morphology of ICP waveforms and thus gain new cognitions and insights into ICP dynamics [8, 9].

Conflict of interest statement We declare that we have no conflict of interest.

References

1. Branch C, Chopp M, Portnoy HD (1981) Fast Fourier transform of individual cerebrospinal fluid pulse waves. *Biomed Sci Instrum* 17:45
2. Brawanski A, Gaab MR, Heissler HE (1983) Computer-analysis of ICP-modulations: clinical significance and prediction of ICP-dynamics. In: Ishii S, Nagai H, Brock M (eds) *Intracranial pressure* V. Springer, Berlin/Heidelberg, pp 186–190
3. Burrus CS, Gopinath RA, Guo H (1998) *Introduction to wavelets and wavelet transforms: a primer*. Prentice Hall, Upper Saddle River
4. Heissler HE, König K, Rickels E (2007) LabVIEW-Implementierung der Detailanalyse des Hirndrucks mit HAAR-wavelets. In: Jamal R, Jaschinski H (eds) *Virtuelle Instrumente in der Praxis*. Hüthig, Heidelberg, pp 22–25
5. Holm S, Eide PK (2008) The frequency domain versus time domain methods for processing of intracranial pressure (ICP) signals. *Med Eng Phys* 30:164–170
6. Holm S, Eide PK (2009) Impact of sampling rate for time domain analysis of continuous intracranial pressure (ICP) signals. *Med Eng Phys* 31:601–606
7. Kaplan I (2003) Wavelets and signal processing. http://www.bearcave.com/misl/misl_tech/wavelets/index.html. Accessed 2 Oct 2010
8. Krauss JK, Droste DW (1994) Predictability of intracranial pressure oscillations in patients with suspected normal pressure hydrocephalus by transcranial Doppler ultrasound. *Neurol Res* 16:398–402
9. Massel SR (2001) Wavelet analysis for processing of ocean surface wave records. *Ocean Eng* 28:957–987
10. Portnoy HD, Chopp M (1981) Cerebrospinal fluid pulse wave form analysis during hypercapnia and hypoxia. *Neurosurgery* 9:14–27
11. Portnoy HD, Branch C, Chopp M (1985) The CSF pulse wave in hydrocephalus. *Childs Nerv Syst* 1:248–254
12. Walker JS (1999) *A primer on wavelets and their scientific applications*. Chapman&Hall/CRC, Boca Raton

Stationarity in Neuromonitoring Data

Hans E. Heissler, Kathrin König, Joachim K. Krauss, and Eckhard Rickels

Abstract Purpose: Signals reflecting the metabolic and circulatory status of an injured central nervous system are normally corrupted systematically. The patient is part of a therapeutic control-loop and the signals acquired are rather determined by the quality of control (stationarity of signals) than by the underlying pathological process.

Methods: To verify the control-loop hypothesis, neuromonitoring data from 12 randomly selected severely head injured patients (initial GCS ≤ 8 , 7 men, 5 women) were analysed for circulatory (blood pressure, intracranial pressure [ICP], cerebral perfusion pressure [CPP]) and metabolic (arterial blood gases, jugular bulb oxygenation [SjvO₂], brain tissue oxygen partial pressure [ptiO₂]) variables ($n=10$). A total of 120 time series of generally not equidistant sample intervals were assessed for stationarity by Wallis & Moore's runs test.

Results: Non-stationarity could only be proven in 23 time series, i.e. the control-loop hypothesis was violated. Trends were mainly found in CPP ($n=5$) and ICP ($n=4$). The remaining cases spread out on all but one (temperature) signal. Nine patients showed at least one time series with a trend. One patient had clear trends in five out of ten variables that focused on SjvO₂, ptiO₂, ICP and CPP.

Conclusions: Absence of stationarity in about 20% of time series is credited to an effective therapeutic control-loop. For analytical purposes, however, the benefit seems to be overestimated. Consequently, neuromonitoring should be considered the analysis of short-term disturbances that are intentionally compensated for by a short response time. Information content is thus reduced even if the number of sensor devices increases.

Keywords Severe head injury • Neuromonitoring • Therapeutic control loop • Stationarity • Entropy

Introduction

Multimodal neuromonitoring is a concept of measuring signals in a critically ill patient to gain data about the patient's current status. Since the degree of miniaturisation and integration of sensors has been evolved to reasonable calibres, a multitude of physiological parameters (circulatory, metabolic, etc.) that produce streams of data have been feasible.

Our fundamental idea was to establish an early warning system based upon artificial neural networks (ANN) to predict intracranial pressure (ICP) elevations, hypothesising that an increase in ICP is a multivariate phenomenon, i.e. elevations could be traced back to some changes in the signals involved in monitoring. Real-world neuromonitoring implies that data are conditioned, i.e. signals (time series from biosignals) are kept within reasonable physiological limits and devolutions depict controlled variables from a therapeutic control-loop rather than a freely running signal (Fig. 1). Thus, we may have produced less promising results, because ANN training seems inadequate [1].

The term stationarity defines a statistical parameter denoting a signal that has both a constant average value and variance/standard deviation over time. Referring to real-world biomedical signals this definition describes an exception from the rule for biosignals that are intrinsically time-variant.

Many analytical procedures, however, imply stationarity as a necessary prerequisite.

To go beyond the limitations of the definition of stationarity, a more practical approach that accepts reasonably varying statistical parameters was applied: wide-sense stationarity [6]. In this context, stationarity and randomness are synonyms not least for the omnipresent control loop. Time series describe unresolvable superpositions of both pathophysiological and pharmacological dynamics. Therefore, randomness in time series is to be expected in the vicinity of a working control loop.

H.E. Heissler (✉) and J.K. Krauss
Klinik für Neurochirurgie 7249,
Medizinische Hochschule Hannover,
30623 Hannover, Germany
e-mail: heissler.hans.e@mh-hannover.de

K. König and E. Rickels
Klinik für Unfallchirurgie,
Orthopädie und Neurotraumatologie, AKH,
Celle, Germany

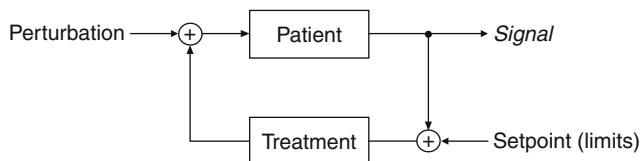


Fig. 1 Schematic diagram of the therapeutic control loop

Materials and Methods

Hypothesising that such limited time series data are of random nature, we screened neuromonitoring data from 12 arbitrarily selected severely head injured patients (initial GCS ≤ 8 , 7 men, 5 women) from a neurosurgical intensive care unit. Patients' circulatory (blood pressure, ICP, cerebral perfusion pressure) and metabolic variables (arterial blood gases, jugular bulb oxygenation, brain tissue oxygen partial pressure) were measured.

A total of 120 time series of mostly not equidistant sample intervals (≤ 4 /min) were assessed for stationarity by Wallis & Moore's runs test. By defining thresholds, time-series were conditioned. Thresholds were set being half the sum of the upper and lower alarm limit values. By means of thresholds all time series were thus dichotomised into data exceeding thresholds and data that did not. This coding resulted in sequences of binary data, whose patterns (runs) were tested for absence of trends, i.e. randomness of data, according to Wallis & Moore.

Results

Non-stationarity was found in 23 time series, i.e. the control loop hypothesis was violated. Trends were mainly found in CPP ($n=5$) and ICP ($n=4$). The remaining cases spread out in all but one signal (temperature). Nine patients showed at least one time series with trend. One patient had clear trends in five out of ten variables emphasising arterial and venous saturation, brain tissue oxygen partial pressure, ICP and cerebral perfusion pressure.

Discussion

It is undisputed that the measuring of biosignals and the analysis of time series is the source of knowledge necessary for reasoning and decision-making for the treatment of severely head injured patients. Naturally, a discussion arose as to whether concepts of multisensory/multimodal neuromonitoring are really beneficial to patients in comparison to conventional monitoring [4, 7, 9]. The argument was directed towards maintaining what is called the therapeutic

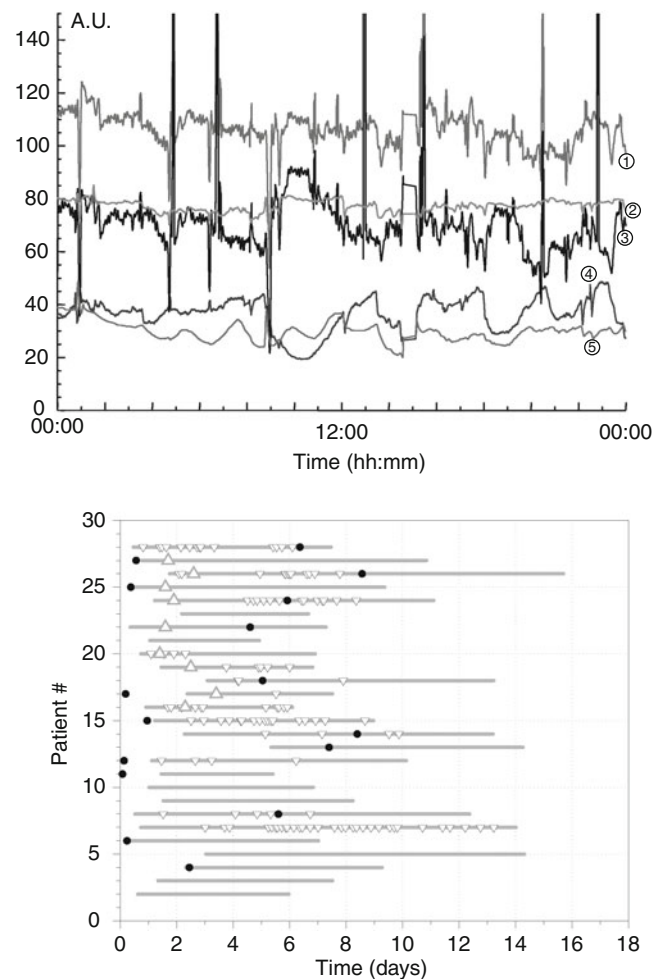


Fig. 2 Alternative monitoring concepts: continuous mode, intrinsically artificial, high data density (*upper*). Supervised real-world monitoring data recorded from one patient with a severe head injury patient treated with modified cerebral perfusion pressure-guided therapy. ① arterial blood pressure; ② cerebral perfusion pressure; ③ jugular bulb oxygenation; ④ intracranial pressure; ⑤ tissue oxygen partial pressure. Event mode, threshold/pattern based (*lower*): records of timestamps of therapeutic events and concomitant parameters during technical neuromonitoring (data acquisition) after trauma in various patients. Grey bars: monitoring interval; small triangles: ICP crises; points: decompressive craniectomy; large triangles: maximum of extracellular brain tissue glycerol

control loop, in particular, the organisation of that loop, the understanding of priorities, meaning, and adequate responses to alarms were considered (Fig. 2). Patient outcomes were also a consideration of this discussion [3, 5].

The results presented here contribute to this discussion from the aspect of signal analysis: it seems there is little to expect, except the fact that time series are more or less within the limits and stationarity was proven in about 80% of the time series analysed. This finding signifies a working and effective control loop, which is a compliment to the treating personnel. Findings also give cause for concern that current neuromonitoring concepts such as the continuous acquisition of signals provide little information about the signals being monitored.

Entropy

When signal entropy measures (approximate entropy, LEMPEL-ZIV-complexity) give high readings the signal is normally rated as being of random nature. Hornero et al. [2] and Santamarta et al. [8] gave impressive examples of this relationship stressing the point that increasing ICP is associated with a decrease in entropy. Intracranial hypertension is associated with “decomplexification” of ICP [8]. In our data, however, there is randomness under controlled physiological states owing to the treatments algorithm. A potential reason for these converging results may be differences in the data densities analysed: our working group concentrated on mean values assuming a maximum sample rate less than or equal to 4/min, in contrast to Hornero et al. [2] and Santamarta et al. [8], sampling at 125 and 100 Hz respectively. Investigations into these differences are still pending. Also, so-called decomplexification could presumably be found by inspection of the intracranial pulse pressure waveform as waveforms are mainly determined by venous and arterial influences in low and high elastance regions of the cerebrospinal volume pressure characteristic respectively. Venous modulations of ICP waveforms are more complex than their arterial counterparts. Another feature of these entropy measures is that they are all running in inverse proportion to ICP. Under practical considerations entropy measures of ICP do not contribute to reasoning for treatment.

Conclusion

Retrospective monitoring concepts are unlikely to add successfully to neuromonitoring and thus to the treatment of critically ill patients even if the number of monitored

biosignals increases. This deadlock can be broken if efforts are made in the opposite direction, i.e. when predictive ideas are realised. The impact of a working therapeutic control loop on prediction is largely unknown, as are the underlying processes in the supervision and treatment of patients suffering from traumatic brain injury.

Conflict of interest statement We declare that we have no conflict of interest.

References

1. Heissler HE, König K, Rickels E, Zumkeller M (2001) Nichtstationäre Eigenschaften posttraumatischer Neuromonitoring-Daten. In: Jamal R, Jaschinski H (eds) *Virtuelle Instrumente in der Praxis*. Hüthig, Heidelberg, pp 286–290
2. Hornero R, Aboy M, Abasolo D, McNamara J, Goldstein B (2005) Interpretation of approximate entropy: analysis of intracranial pressure approximate entropy during acute intracranial hypertension. *IEEE Trans Biomed Eng* 52:1671–1680
3. Mazzeo AT, Bullock R (2007) Monitoring brain tissue oxymetry: will it change management of critically ill neurologic patients? *J Neurol Sci* 261:1–9
4. McIntosh N (2002) Intensive care monitoring: past, present and future. *Clin Med* 2:349–355
5. Narotam PK, Morrison JF, Nathoo N (2009) Brain tissue oxygen monitoring in traumatic brain injury and major trauma: outcome analysis of a brain tissue oxygen-directed therapy. *J Neurosurg* 111:672–682
6. Priestly MB (1991) *Non-linear and stationary time series analysis*. Elsevier, Amsterdam
7. Sahuquillo J (2008) Does multimodality monitoring make a difference in neurocritical care? *Eur J Anaesthesiol Suppl* 42:83–86
8. Santamarta D, Hornero R, Abasolo D, Martínez-Madrugal M, Fernández J, García-Cosamalón J (2010) Complexity analysis of the cerebrospinal fluid pulse waveform during infusion studies. *Childs Nerv Syst* 26:1–7
9. Zygun D (2008) Can we demonstrate the efficacy of monitoring? *Eur J Anaesthesiol Suppl* 42:94–97

Is ICP Solid or Fluid? In Vitro Biomechanical Model Using a Fluid-Saturated Gel

M. Ros, P. Yameogo, P. Payoux, P. Swider, and Eric Schmidt

Abstract Intracranial pressure is mainly considered to be hydrostatic pressure, but observations demonstrated that ICP is heterogeneous within brain suggesting the presence of a solid pressure. Brain tissue is a biphasic material composed of solid and fluid phases. We hypothesized that in a saturated porous model, fluid and solid phases yielded two pressures. Our brain model was 0.5% agar gel. A *quasi* static compression was applied using a tensile machine. Pressures were gauged within the gel using two different microsensors. One sensor (A) has an open sensitive area measuring the total pressure, whereas the other sensor (B) has a pressure-sensitive area design that gauges mainly the fluid pressure. There was very good agreement between the pressure applied to the gel and the pressure inside the gel measured with sensor A. However, sensor B systematically underestimated the pressure in the gel. We assume that sensor A gauged the total pressure, which is the sum of the pore fluid pressure and mechanical stress, whereas sensor B probably measured only the fluid pressure. The difference between the two sensors reflects the solid part of the total pressure. ICP has to be considered to be the sum of fluid pressure and solid stress.

Keywords Intracranial pressure • Biomechanics • Fluid pressure • Solid pressure • Gel • Model

Introduction

Since Quincke, ICP has been defined as the hydrostatic pressure within the cerebrospinal fluid (CSF) in the ventricles. The hydrostatic approach of ICP is assumed to be the reference, and one considers that the CSF pressure within the ventricle is the gold standard technique, as defined by Miller [4]. Within the last two decades another way of measuring ICP has been developed by inserting a miniaturized pressure transducer within the brain parenchyma. This technique allows the pressure inside the brain tissue to be measured without ventricular access. The intraparenchymal measurement of ICP presumes that the pressure is evenly distributed in the parenchyma as in a porous medium according to the Hakim's concept of "the brain as a sponge" [3]. According to Pascal's law, ICP is deemed to be evenly distributed. The intraparenchymal measurement of ICP is frequently used in clinical practice as a reliable, easy to insert system, especially when the ventricles are too narrow to be catheterized. There are different types of commercialized ICP pressure transducers, mainly based on Wheatstone bridge strain gauge circuits to convert mechanical stress into an electrical output signal.

However, the hypothesis that intraparenchymal pressure is hydrostatic pressure faces three caveats: the model applied, the fluid porosity and the presence of pressure gradients.

Hakim proposed the concept of "the brain as a sponge" filled with water [3]. According to modern *continuum* mechanics, brain tissue is nowadays considered to be a biphasic material composed of a solid and a fluid phase intimately intermingled like the visco-elastic [2, 5, 10] fluid-saturated model [6, 8]. This model is in accordance with the notion that ICP is not the same everywhere within the cranial cavity in both experimental and clinical observations [9, 11–13].

So what do we measure with an intraparenchymal ICP probe? A fluid pressure or a solid stress?

M. Ros
Department of Neurosurgery,
CHU, Toulouse,
France

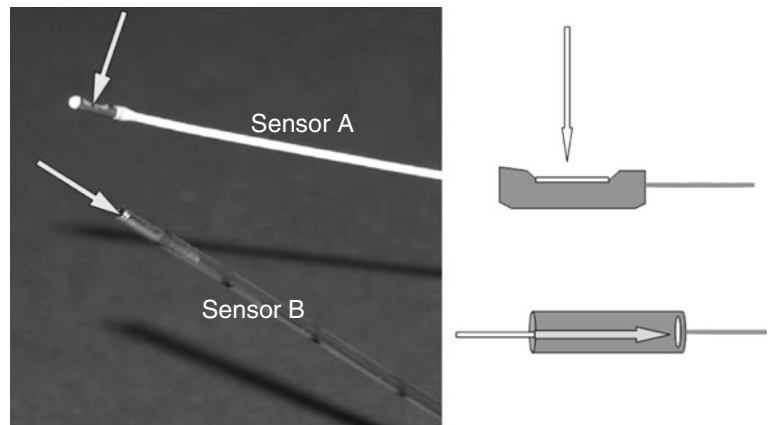
P. Yameogo
Department of Nanotechnology,
LAAS CNRS & CAPTOMED,
Toulouse, France

P. Payoux
Biophysics Laboratory,
Université Paul Sabatier,
Toulouse, France

P. Swider
IMFT UMR 5502, Université de Toulouse,
Toulouse, France

E. Schmidt (✉)
Department of Neurosurgery,
Hopital Purpan, Place Dr Baylac, TSA 40031,
31059, Toulouse, France
e-mail: schmidt.e@chu-toulouse.fr

Fig. 1 Sensors A and B: actual picture and schematic drawing. The sensitive cells are indicated with an *arrow*



We hypothesized that in an experimental saturated viscoporo-elastic model mimicking the brain's mechanical properties, fluid and solid phases yielded two stress fields that could be distinguished as fluid pressure and solid pressure.

Materials and Methods

In order to differentiate the two pressures in an in vitro simplified brain model, we chose two different types of sensors used in clinical practice.

The first microsensor termed A (CODMAN®) is a Wheatstone bridge strain gauge and has an open sensitive area (Fig. 1, top). The design of this sensor allows the measurement of total pressure including both solid and fluid components. The second microsensor, termed B (CAMINO®), is based on a fiber optic technique and the pressure-sensitive area is within a steel micro cylinder (Fig. 1, bottom). We assume that the structural characteristic of the sensor B is more sensitive to hydrostatic pressure. Indeed, the steel micro-cylinder acts as a shield that protects the sensitive cell from direct solid stress.

To define how the two sensors react in a gel model, we performed two experimental settings comparing the sensors in water and in gel, mimicking the brain's properties.

The first experimental setting was designed to compare the pure hydrostatic response of the sensors. The two sensors were connected to their monitors, zeroed and then inserted at the same level through two separate holes in the wall of a PVC tube. Analog output from the pressure monitor was connected to an analog-digital converter and stored in a computer running appropriate software (PCD-30A®). Then the tube was slowly filled with water at room temperature until the pressure reached 40 cm H₂O, i.e. 29.4 mmHg.

For the gel model, we chose the 0.5% agar-agar as an appropriate viscoporo-elastic material [7]. Agar-agar was boiled with water until dissolved, then poured into a silicon lubricated PVC tube and let cool until set in ambient air. The two sensors were connected to their monitors, zeroed and

then inserted into the agar at the same level through two separate holes in the wall of the tube. Analog output was connected to a converter and stored. A *quasi* static compression was applied onto the agar using a tensile machine (instron®). Data acquired were:

1. Displacement of the crosshead
2. Strength applied on the surface of the agar
3. Pressures gauged by the two different sensors within the gel

The experiment was stopped when the strength applied by the crosshead into the agar reached 9 N, which corresponds to a pressure of roughly 20 mmHg, considered to be a physiological limit.

We performed 13 consecutive experiments. In order to compare the pressure into the agar as gauged by the sensors with the pressure applied by the crosshead onto the agar. We used Bland-Altman analysis to compare sensor A with sensor B.

Results

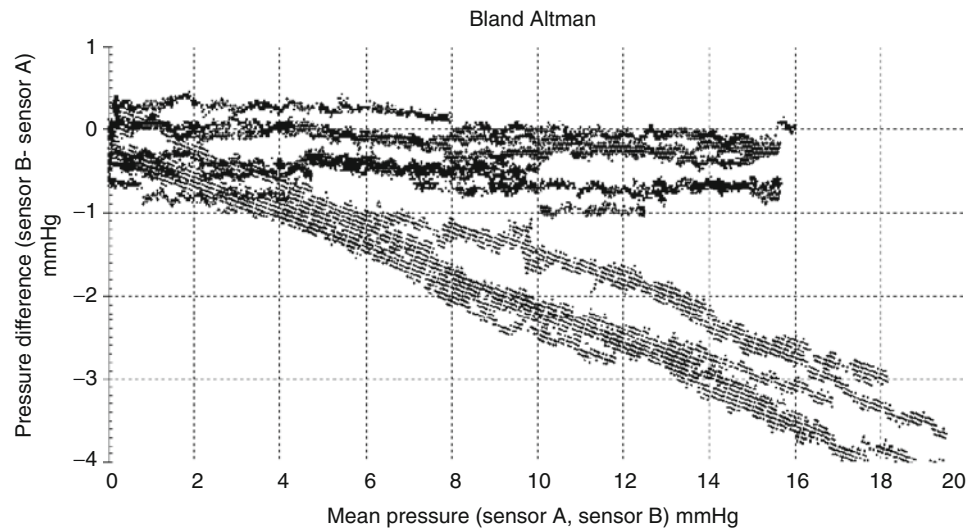
In the water, there is no significant difference between the pressures gauged by the two sensors.

In the gel, there was a very good agreement between the pressure applied on the agar and the pressure inside the gel as measured with sensor A, whereas sensor B systematically underestimated the values of the pressure within the gel. The underestimation of the pressure with sensor B increases in a proportional way as the pressure rises. This pattern is depicted using Bland-Altman analysis: the more the pressure increases, the greater the difference between the two sensors (Fig. 2).

Discussion

Both sensors measured the same hydrostatic pressure in water; however, in a saturated porous media the two sensors measured different pressures. We assume that sensor A gauged the

Fig. 2 Bland–Altman plot:
x-axis = mean values of the two
 sensors, *y-axis* = difference
 between the two sensors



total pressure, that is, the sum of the pore fluid pressure and mechanical stress in the solid substrate of the gel. Sensor B behaved differently as it probably measured only part of the total pressure. Owing to the design of the pressure-sensitive cell protected by a steel sheath, it could be reasonably assumed that sensor B measures preferentially the fluid pressure. Therefore, the discrepancy between the two transducers could be due to the consequences of the biphasic property of the gel. Then, the pressure difference between the two sensors could represent the solid part of the pressure in the gel.

Whether living brain is a fluid or solid material has been addressed for at least four decades. But the question of whether ICP measured in the parenchyma is mainly a fluid or solid stress has never been addressed. Our in vitro model in a fluid-saturated gel cast light on the probable mixed component of ICP. ICP is mainly driven by a fluid component, but there is also a solid part that has to be taken into account. ICP is biphasic fluid and solid.

The fluid part of ICP is the prominent component, as brain is a soft tissue bathed in water. In that respect, in a closed skull, ICP measured intraparenchymally represents the fluid pressure in accordance with the definition of ICP.

However, the presence of a solid part of ICP is strongly suggested in our model. This solid part seems to be not virtual and could be gaugeable. We assume that the difference between sensor A and B represents the solid stress. The presence of a solid part in ICP refers to the presence of gradients. If ICP was only fluid, like water in a can, the pressure should be evenly distributed according to Pascal's law without a pressure gradient under a load. This is the commonly accepted approach to ICP. If ICP was only solid, like concrete in a can, there should be no pressure within this solid media, but only stress inside, and stress gradients under load. Then the known presence of pressure gradients within the brain heralds the existence of a partial but actual structural component of ICP. Our results are in accordance with this hypothesis. Pressure gradients are present in physiology: the

pressure gradient from the arterial side to the venous side of the blood flow; the pressure gradient caused by systolic expansion of the cerebral mantle in the aqueduct of Sylvius, foramina of Magendie, the CSF drainage gradient towards sagittal sinus pressure, the gradient of interstitial fluid from the brain into the ventricles and subarachnoid space. Pressure gradients are also present in pathology in patients with brain tumors, mass lesions, head trauma etc. [9, 11–13].

In Fig. 2, the Bland–Altman analysis seems to display two clusters of data with the same tendency but two different slopes. This is probably an artifact related either to the temperature or friction of the gel on the surface of the tube. We chose to let the agar stiffen in the ambient air; thus, we did not precisely control the stiffening temperature. This might have influenced the total amount of water in the gel and consequently altered its physical properties. However, it does not invalidate our results.

To our knowledge, this is the first study that compares sensors not in water but in gel. Previous studies have shown no differences between the sensors in water [1]. Our simple bench test is very far from physiological conditions, but biomechanically closer to living tissue than water.

Conclusion

To better understand ICP, we reproduced increased pressure in a biphasic material mimicking brain tissue. Pressure measurement was dependent upon the sensor design and confirmed the significant role of fluid–structure interactions. ICP has to be considered to be the sum of fluid pressure and solid stress.

Acknowledgement The authors wish to acknowledge the Academic Neurosurgical Unit at Addenbrooke's Hospital, University of Cambridge Clinical School, and especially Dr. Alonso Pena as an author of the concept of the experiment.

Conflict of interest statement We declare that we have no conflict of interest.

References

1. Czosnyka M, Czosnyka Z, Pickard JD (1996) Laboratory testing of 3 ICP microtransducers. *Neurosurgery* 38:219–225
2. Gefen A, Margulies SS (2004) Are in vivo and in situ brain tissues mechanically similar? *J Biomech* 37:1339–1352
3. Hakim S, Venegas JG, Burton JD (1976) The physics of the cranial cavity, hydrocephalus and normal pressure hydrocephalus: mechanical interpretation and mathematical model. *Surg Neurol* 5: 187–210
4. Miller JD (1989) Measuring ICP in patients \pm its value now and in future? In: Hoff JT, Betz AL (eds) *Intracranial pressure*, vol 7. Springer, Berlin/Heidelberg/New York/Tokyo, pp 5–15
5. Miller K, Chinzei K, Orssengo G, Bednarsz P (2000) Mechanical properties of brain tissue in-vivo: experiment and computer simulation. *J Biomech* 33:1369–1376
6. Momjian S, Bichsel D (2008) Nonlinear poroplastic model of ventricular dilatation in hydrocephalus. *J Neurosurg* 109:100–107
7. Normand V, Lootens DL, Amici E, Plucknett KP, Aymard P (2000) New insight into agarose gel mechanical properties. *Biomacromolecules* 1:730–738
8. Peña A, Bolton MD, Whitehouse H, Pickard JD (1999) Effects of brain ventricular shape on periventricular biomechanics: a finite element analysis. *Neurosurgery* 45:107–118
9. Piek J, Plewe P, Bock WJ (1988) Intrahemispheric gradients of brain tissue pressure in patients with brain tumours. *Acta Neurochir* 93:129–132
10. Roth S, Raul JS, Ludes B, Willinger R (2007) Finite element analysis of impact and shaking inflicted to a child. *Int J Legal Med* 121:223–228
11. Sahuquillo J, Poca MA, Arribas M, Garnacho A, Rubio E (1999) Interhemispheric supratentorial intracranial pressure gradients in head injured patients: are they clinically important? *J Neurosurg* 1:16–26
12. Symon L, Pasztor E, Branston NM, Dorsch NWC (1974) Effect of supratentorial space occupying lesions on regional intracranial pressure and local cerebral blood flow: experimental study in baboons. *J Neurol Neurosurg Psychiatry* 37:617–626
13. Wolfla CE, Luerssen TG, Bowman RM (1996) Brain tissue pressure gradients created by expanding frontal mass lesion. *J Neurosurg* 84:642–647

Implantable ICP Monitor for Improved Hydrocephalus Management

Ellyce Stehlin, Simon Malpas, Peter Heppner, Patrick Hu, Matthew Lim, and David Budgett

Abstract *Background:* Hydrocephalus patients are commonly treated by insertion of ventriculoperitoneal shunts, but these have high complication rates. Monitoring of shunt and patient condition can be achieved through measuring intracranial pressure (ICP). Significant zero drift has limited previous developments towards a long-term implantable ICP monitor. We present a new implantable solid-state pressure sensor system appropriate for chronic (lifetime) monitoring of ICP.

Materials and Methods: Initial designs of the proposed ICP system were realised and the pressure sensor catheter underwent bench-top tests to analyse its characteristics. A drift rig was constructed for the long-term analysis of the sensor's zero drift. The pressure sensor catheter was used to continuously monitor blood pressure in rats.

Results: Three potential design solutions were realised: a standalone sensor, the sensor unit in line with a shunt system, and the sensor unit fully integrated into the shunt valve housing. Initial stability results across 46 days show a maximum drift of less than 2 mmHg and a minimum drift of less than 0.2 mmHg.

Conclusion: Initial experience with the new implantable solid-state pressure sensor system confirms its suitability for chronic pressure monitoring. The device is promising for providing vital information on shunt and patient condition.

Keywords Intracranial pressure • Telemetry • Sensor • Wireless

Introduction

Standard treatment of hydrocephalus is by implantation of a ventricular shunt to drain excess cerebrospinal fluid (CSF) from the brain's ventricle to a remote location in the body. These shunts have greatly improved the prognosis of a hydrocephalic patient; however, a number of shunt-related complications can subsequently be introduced. These complications can often lead to a shunted hydrocephalus patient requiring multiple shunt revision surgeries throughout their lifetime [1, 2]. Intracranial pressure (ICP) provides a strong indication of brain health and is a key component in the monitoring of conditions affecting the central nervous system. ICP values provide an indication of cerebral blood volume and flow, and are used to determine key health indicators such as cerebral perfusion pressure [3, 4]. A fully implantable telemetric (ICP) monitor would allow for constant, freely obtainable information on the condition of a hydrocephalus patient. Currently, shunt and patient condition is determined through expensive yet often inconclusive imaging techniques combined with placement of an acute, percutaneous ICP sensor [4–6]. A fully implantable, wireless ICP monitor would allow for similar information on patients to be obtained without further invasive surgeries or even hospital admission. Clinicians would also have the opportunity to perform less invasive infusion studies to determine shunt dynamics and to monitor patients in whom the requirement of a shunt is uncertain or to determine whether a patient's headaches are linked to changes in ICP. An implantable monitor would also be of value in the follow-up of patients in whom hydrocephalus is treated by endoscopic third ventriculostomy (ETV), and in whom the success of the surgery can be variable or short-lived [7]. The importance and value of a chronic ICP monitor was realised with the first implantable telemetric ICP sensor in 1967 [8]. However, this system and the numerous development attempts since have been limited by a range of flaws including unit

E. Stehlin and D. Budgett (✉)
Auckland Bioengineering Institute, University of Auckland,
Auckland, New Zealand
e-mail: d.budgett@auckland.ac.nz

S. Malpas and M. Lim
Telemetry Research,
Auckland, New Zealand

P. Heppner
Department of Paediatric Neurosurgery,
Starship Children's Hospital, Auckland, New Zealand

P. Hu
Department of Electrical and Computer Engineering,
University of Auckland, Auckland, New Zealand

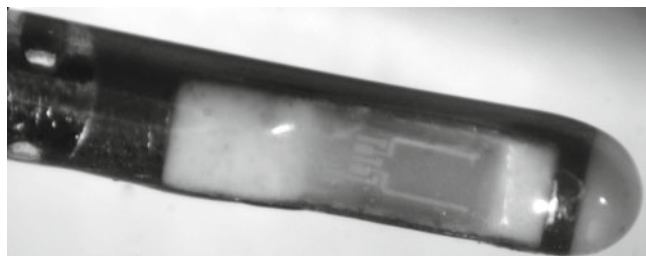


Fig. 1 Magnified view of the strain-gauge-based sensor tip

size, sensor drift, sensor accuracy, biocompatibility and robustness [9–11]. The most significant obstacle that continues to hold back a modern pressure sensor solution is zero drift, with sensor recalibration not possible post-implantation [12]. Initial development and testing with a new implantable pressure sensor system have been carried out to determine its suitability for chronic ICP monitoring.

Materials and Methods

The implantable pressure sensor system consists of a resistive strain-gauge-based sensor element embedded in a 2-French (0.7 mm in diameter) catheter, developed in conjunction with Millar Instruments. The strain-gauge is configured in a Wheatstone bridge with a resulting linear output response of $5 \mu\text{V/V/mmHg}$ (Fig. 1).

The associated telemetry and amplifier electronics required to operate the device were determined. The design of a potential encapsulated unit for suitable subcutaneous implantation embedded or above the skull has been realised with three potential configurations based on the ICP monitor's interaction with or without a hydrocephalus shunt.

A drift rig was constructed to analyse the sensor's stability over time. The rig was designed to simulate the intracranial cavity by holding a constant 20-mmHg head of pressure and a maintained temperature of 36.5°C . The head of pressure was achieved using a hydrostatic column of water and the sensors were continuously bathed in the water to maintain hydration. The pressure sensor drift rig is capable of monitoring up to eight pressure sensors simultaneously. An elongated elbow bend of Perspex tubing contained the pressure sensors in its horizontal section, with the vertical tube determining the head of pressure applied to the sensors. The level of the hydrostatic column was monitored and evaporation limited by a layer of oil on the surface. Touhy-borst adapters were used to hold the sensing catheters in place and prevent leakage out of the Perspex tubing. The rig was immersed in a large temperature controlled water bath with a modified aquarium heater and an additional external temperature control to maintain the temperature of the bath at $36.5^\circ\text{C} \pm 0.5^\circ\text{C}$. Four temperature sensors were used in the

system: one to provide feedback to the heater control, one in each the water bath and the Perspex tubing, and a final sensor recording the room temperature. An external bench-top pressure sensor was also used to monitor atmospheric pressure such that the recordings from the sensor test are absolute.

The sensor has also been used in animal experiments monitoring haemodynamics. Continuous operation of the pressure sensor was achieved in the rat model for several months, with measurements of arterial pressure transmitted to an external receiver and continuous wireless power supplied.

Results

ICP Monitor Design

The telemetry and amplifier circuits were determined to require a volume of 2 cm^3 , in a layout suitable for implantation under the skin. This volume is dependent on a battery-free operation where power is only supplied by inductive transfer when an external coil is in range of the device. Three potential configurations incorporating the sensing catheter and encapsulated electronics unit for the implantable ICP monitor were identified (Fig. 2).

Configuration (a) shows the ICP electronics in line with the hydrocephalus shunt similar to a shunt accessory. Configuration (b) shows the monitor as a standalone unit, completely independent of any shunt system. A dual catheter allows for the sensing catheter and drainage catheter to be combined. The final configuration, (c), has the electronics required for the ICP signal fully integrated into the shunt valve housing with a dual catheter.

ICP Sensor Characteristics

Initial results from the drift rig have been acquired for three 2 French pressure sensors. The resulting absolute drift in the sensors after 46 days ranges from 0.236 to 1.829 mmHg (Fig. 3).

The sensor's frequency response has a negative 3 dB value of 500 Hz, corresponding to no loss of signal up to 100 Hz.

Animal Testing with the Potential ICP Sensor

The resistive element pressure sensing catheter has been used to monitor blood pressure in the rat model. The sensor was inserted into the rat artery connected to a telemetry and amplifier circuit unit, which was also implanted, secured in the abdomen of the animal. This fully implanted device has been tested for between

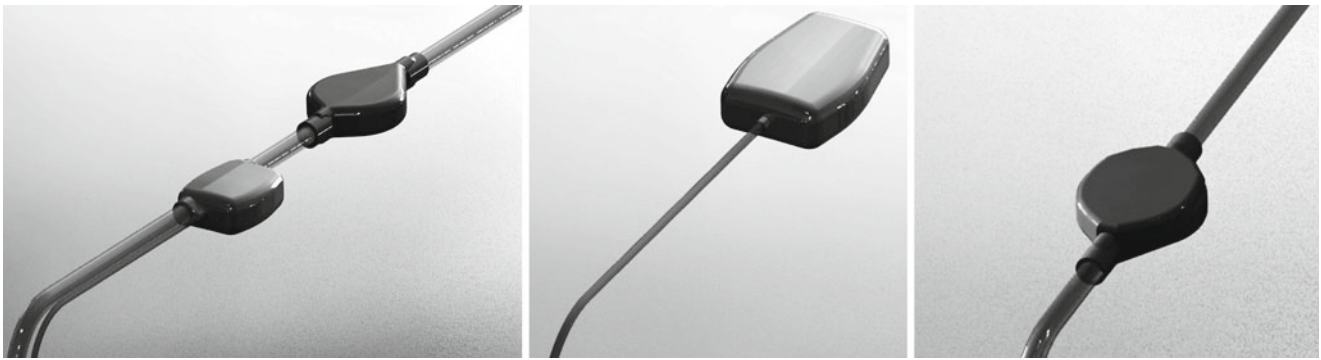


Fig. 2 Three potential configuration options for the intracranial pressure (ICP) monitor

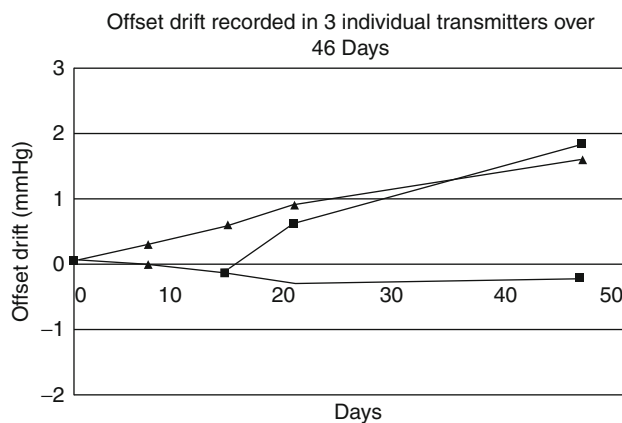


Fig. 3 Drift recorded from three different pressure sensing catheters over 46 days

1 and 6 months with continuous power supplied by inductive power transfer and transmission of data achieved through 2.4-GHz telemetry. The blood pressure signal is of a higher range and frequency compared with ICP, putting different demands on the sensor and less emphasis on zero drift.

Discussion

The implantable pressure sensor system's small size gives it great potential for ICP monitoring. The 2-French pressure sensing catheter tip is important to minimise damage to the brain parenchyma during the initial implantation procedure and throughout the lifetime of the implant. The volume required for the associated electronics is also of a minimal size – important for the large paediatric hydrocephalus population. Incorporation of a rechargeable battery for elongated periods of recording independent of an external power supply remains a potential option for the adult hydrocephalus population where a larger implant may be tolerated.

The standalone unit design has the advantage that the system is completely independent from any shunt. As a result, the integrity of the ICP monitor would not be compromised by any

failing shunt requiring a revision. In a shunted hydrocephalic patient the standalone unit could be positioned away from the shunt implant so if a revision was required, the ICP sensing implant could remain, without the risk of an introduced infection. The unit could also be used in non-shunted patients such as hydrocephalus patients who undergo ETV and require follow-up to confirm the procedure's effectiveness and longevity. As a standalone unit, however, the insertion of an implant requiring a burr hole into the skull would have to be justified. With the ICP sensing unit in line with the shunt, but separate from the valve, the system would be a single implant. Limited localised shunt complications would have the potential to be revised without disturbing the ICP monitor itself. Integrating the ICP monitor into the shunt valve housing would minimise the total volume of the implant. This configuration would also provide the opportunity to utilise the energy provided to the pressure sensor to manipulate the function of the shunt. As a single unit, however, any shunt complication requiring revision would result in the removal of the sensor system.

Preliminary results from the long-term drift rig show a maximum drift of less than 2 mmHg in 1 month. This level of drift is associated with an implantable monitor suitable for post-operative monitoring for up to 1 year. The target drift for the sensor is 2 mmHg per year, suitable for chronic monitoring. It is anticipated that the rate of change in drift will decrease after 1 month; however, quantification of this drift is ongoing and expanding to include more sensors for a more comprehensive analysis. The dynamic response of the sensor is more than adequate for ICP monitoring with a frequency response of 20 Hz required for the accurate representation of the low-range, low-frequency ICP waveform. The frequency response of the resistive pressure sensor will ensure that no loss of signal occurs in patients experiencing spikes in their ICP waveforms, or sudden posture-related changes due to decreasing brain compliance or persistent intracranial hypertension.

Implantation of the sensors in the rat model has confirmed its biocompatibility and ability to perform long-term in-vivo. The larger blood pressure signal made it less vulnerable to drift characteristics of the sensor and circuit unit and demonstrate the ability of the telemetry and inductive power system used.

Conclusion

Initial experience with a new implantable pressure sensor system is promising for use for ICP monitoring. This is supported by preliminary in vitro results on sensor characteristics and in vivo results demonstrating the sensor's stability in the implanted environment. Analysis of the sensor's drift is ongoing and ICP-specific animal testing planned.

Conflict of interest statement David Budgett, Patrick Hu, and Simon Malpas have a financial interest in Telemetry Research. We declare that no other authors have a conflict of interest.

References

1. Drake JM, Kestle JRW, Tuli S (2000) CSF shunts 50 years on – past, present and future. *Childs Nerv Syst* 16(10):800–804
2. Kestle J et al (2000) Long-term follow-up data from the Shunt Design Trial. *Pediatr Neurosurg* 33(5):230–236
3. Nulsen F et al (1980) Chronic intracranial pressure monitoring by telemetry: clinical experience. *Ann Biomed Eng* 8(4):505–513
4. Czosnyka M, Pickard JD (2004) Monitoring and interpretation of intracranial pressure. *J Neurol Neurosurg Psychiatry* 75(6):813–821
5. Fouyas IP et al (1996) Use of intracranial pressure monitoring in the management of childhood hydrocephalus and shunt-related problems. *Neurosurgery* 38(4):726–732
6. Lehman LB (1990) Intracranial pressure monitoring and treatment: a contemporary view. *Ann Emerg Med* 19(3):295–303
7. Sood S, Ham SD, Canady AI (2001) Current treatment of hydrocephalus. *Neurosurg Q* 11(1):36–44
8. Atkinson JR, Shurtleff DB, Foltz EL (1967) Radio telemetry for the measurement of intracranial pressure. *J Neurosurg Pediatr* 27(5):428–432
9. Kroin JS et al (2000) Long-term testing of an intracranial pressure monitoring device. *J Neurosurg* 93(5):852–858
10. Czosnyka MPD, Czosnyka ZMS, Pickard JD (1996) Laboratory testing of three intracranial pressure microtransducers: technical report. *Neurosurgery* 38(1):219–224
11. Miyake H et al (1997) A new ventriculoperitoneal shunt with a telemetric intracranial pressure sensor: clinical experience in 94 patients with hydrocephalus. *Neurosurgery* 40(5):931–935
12. Citerio G et al (2004) Bench test assessment of the new Raumedic Neurovent-P ICP sensor: a technical report by the BrainIT group. *Acta Neurochir* 146(11):1221–1226

Intracranial Pressure Telemetry: First Experience of an Experimental In Vivo Study Using a New Device

Berk Orakcioglu, Christopher Beynon, Modar M. Kentar, Regina Eymann, Michael Kiefer, and Oliver W. Sakowitz

Abstract Objective: To test two new telemetric intracranial pressure (ICP) probes (NEUROVENT®-P-tel, NEUROVENT®-S-tel) in a porcine model. We aimed to intraoperatively correlate the telemetric probes to parenchymal ICP probes and study their reliability in the first hours after implantation. The experimental set-up, new telemetric technology and first data will be presented.

Methods: We implanted a right parietal (parenchymal) and left parietal (subdural) telemetric ICP probe in 13 Göttingen mini-pigs under general anaesthesia. Through the left parietal burr hole a parenchymal ICP probe (Neurovent® ICP) was introduced. Intraoperatively, the head position was changed to provoke ICP changes every 10 min. The telemetric probes were left in situ and finally the parenchymal ICP probe was removed. We correlated mean differences between each telemetric probe and the conventional ICP measurement and Bland-Altman plots were generated for statistical analysis.

Results: We present first data containing intraoperative measurements of 26 telemetric probes after implantation. Intraoperatively, mean differences of 2.48 ± 1.52 mmHg SD (NEUROVENT®-P-tel) and 2.64 ± 1.79 mmHg (NEUROVENT®-S-tel) were observed. The Bland-Altman plot demonstrates good correlation of the telemetric probes compared with parenchymal ICP probes.

Conclusion: We present a new telemetric technology that was experimentally compared with a parenchymal ICP probe. We provide data that the new telemetric probes will

comparably measure ICP vs an external ICP probe. This stand-alone ICP tool may allow permanent measurement of ICP in hydrocephalus patients. Further continuation of our study will demonstrate whether this system guarantees acceptable long-term reliability.

Keywords Experimental model • ICP • Telemetry

Introduction

Since the introduction of telemetric ICP measurement in 1967 many efforts have been undertaken to introduce a reliable, drift-free and biocompatible telemetric device to meet modern neurosurgical needs [1–6]. Only the Cosman Sensor from Radionics, the Rotterdam TeleTransducer and the Aachen ICP TeleSensor, developed by Richard and Block, had limited clinical utility [1, 2, 6]. However, despite technical refinement of existing telemetric systems no sensor ever attained continuous and broad clinical acceptance. Concerns regarding the safety of these devices and the accuracy of the measurements obtained have outweighed the possible benefits so far.

Before the introduction of the new telemetric ICP probes NEUROVENT®-P-tel (parenchymal) and NEUROVENT®-S-tel (subdural) in humans we sought to investigate their accuracy and reliability in an experimental swine model on a long-term basis comparing them with parenchymal ICP measurements. The experimental model and our first experience with the new telemetric device are presented.

Methods

Study Protocol

Animal protocols for our study were approved by the institutional animal care and use committee (Protocol No.: 35–9185.81/G-89/08).

B. Orakcioglu (✉), C. Beynon, M.M. Kentar, and O.W. Sakowitz
Department of Neurosurgery,
University Hospital Heidelberg,
Im Neuenheimer Feld 400, D-69120
Heidelberg, Germany
e-mail: berk.orakcioglu@med.uni-heidelberg.de

R. Eymann and M. Kiefer
Department of Neurosurgery,
University Hospital of Saarland,
Homburg, Germany

Thirteen female barrier breed minipigs (Ellegaard, Denmark) with an average mean weight of 22.98 ± 4.25 (SD) kg were anaesthetised with ketamine (10 mg/kg), midazolam (5 mg/kg) and azaperone (40 mg/kg) administered by intramuscular injection, orally intubated and mechanically ventilated ($\text{FiO}_2 = 30\%$). Anaesthesia was maintained by use of 1.5% isoflurane inhalation. Rectal and brain temperature (T_r/T_{br}) were continuously monitored. Rectal temperature was maintained between 35.5°C and 37°C using an infrared heater. A venous line was placed into the right ear vein and capillary oxygen saturation (SO_2) was monitored from the left ear. Before the operative procedures blood was drawn for laboratory analysis including C-reactive protein and a full blood count. Twenty minutes before skin incision intramuscular antibiotics were applied (benzylpenicillin 30–50 mg/kg i.m.) as perioperative prophylaxis.

Operative Procedure

The skin was disinfected and draped in a sterile fashion. After a semicircular opening of the skin the flap was retracted to the right side. Two burr holes (diameter: 1 cm) were placed over the right and left coronal sutures 1.5 cm paramedially, the dura was coagulated and opened. Pial vessels at the catheter entry points were coagulated thoroughly to avoid parenchymal haemorrhage due to the insertion technique. The parenchymal telemetric catheter was introduced on the right side in a vertical manner. The subdural telemetric catheter was placed on the left side aiming occipitally with the catheter tip. Next to the subdural probe the parenchymal ICP probe was vertically inserted 1.5 cm intracerebrally (below the cortical surface) and secured transcutaneously for continuous monitoring of intracranial pressure (ICP). The fascia was tightly expanded over the probes to secure the telemetric probe position. Afterwards subcutaneous and intracutaneous resorbable sutures were used for skin closure. At the end of the measurements the ICP probe (Neurovent®-P) was removed. The wound was then sealed with silver oxide spray. After termination of anaesthesia the animals were extubated. For 3 days analgesics (carprofen 1.5 mg/kg) were administered intramuscularly when needed.

Technology

The implants as planned for use in humans have a ceramic cover resembling the passive telemetric unit, containing an antenna that receives energy from the extracorporeal reader via induction. After having reached the minimum amount of energy needed to work, the implant starts to measure the ICP

and transfers the acquired data via a radiofrequency identification (RFID) interface to the reader unit (TDT1 readP). The ICP is acquired five times a second with a silicon-based absolute pressure sensor chip. Within the chip a wheatstone bridge built with piezoresistive strain gauges changes output voltage as a result of deforming the silicon membrane. This analogue voltage difference represents the absolute pressure and gets digitalised by the ASIC on the telemetric board. Corresponding to the digital pressure value (D1), a digital temperature coefficient (D2) is generated. D1 and D2 are always coupled to seven chip-specific calibration parameters saved on the ASIC. These parameters ensure the accuracy of the measured value. The value package is then transmitted to the RFID interface on the telemetric board from where it is sent to the reader unit. The reader combines all values from the implant with its own values for atmospheric pressure. Finally the reader forwards the data to the Datalogger (MPR1, Fig. 1) where the ICP value is calculated from absolute in vivo pressure and surrounding atmospheric pressure. It also allows limited pulse wave analysis. In humans the telemetric corpus will be placed between the galea and the cranial bone, where it can be fitted into a drilled fossa. According to the manufacturer's description the measuring range of the telemetric probes is between -20 and $+400$ mmHg. They are factory-precanceled in a measuring fluid to a value of 0 mmHg. Resolution of ICP values is documented as 1.0 mmHg and signals are detected with 5 Hz. Previously performed in vitro measurements demonstrated a 29 days drift of ± 2 mmHg.

Monitoring

Heart rate, SO_2 and rectal temperature were continuously recorded. The reader for telemetric ICP assessment (RAUMEDIC® Reader TDT1 readP) was attached sequentially over each telesensor in order to transcutaneously measure the ICP. The ICP of the telemetric and parenchymal probes were recorded by the data logger. Continuous monitoring data were digitally sampled five times a second (5 Hz). The telemetric units and the ICP probes were factory-precanceled. In 10-min steps we performed changes in positioning in order to provoke ICP changes: At first NEUROVENT®-Stel was tested vs the parenchymal probe with the head at 0° , 30° head up and 30° head down (Fig. 2). This procedure was repeated for the NEUROVENT®-P-tel. The duration of monitoring was approximately 90 min after equilibration of ICP.

All data presented are expressed as mean values with standard deviations (\pm SDs). All data were normally distributed. All plots were generated using Sigmaplot 10.0 (SYSTAT Software Inc. San Jose, CA, USA). Bland–Altman plots were used to statistically compare Neurovent®-P with each telemetric probe.



Fig. 1 Telemetric unit showing the data logger (MPR 1, upper left) to display and store acquired data and the reader unit, which is placed under the cap. It is connected to the data logger. In between a subdural telemetric ICP probe (NEUROVENT[®]-S-tel) is displayed

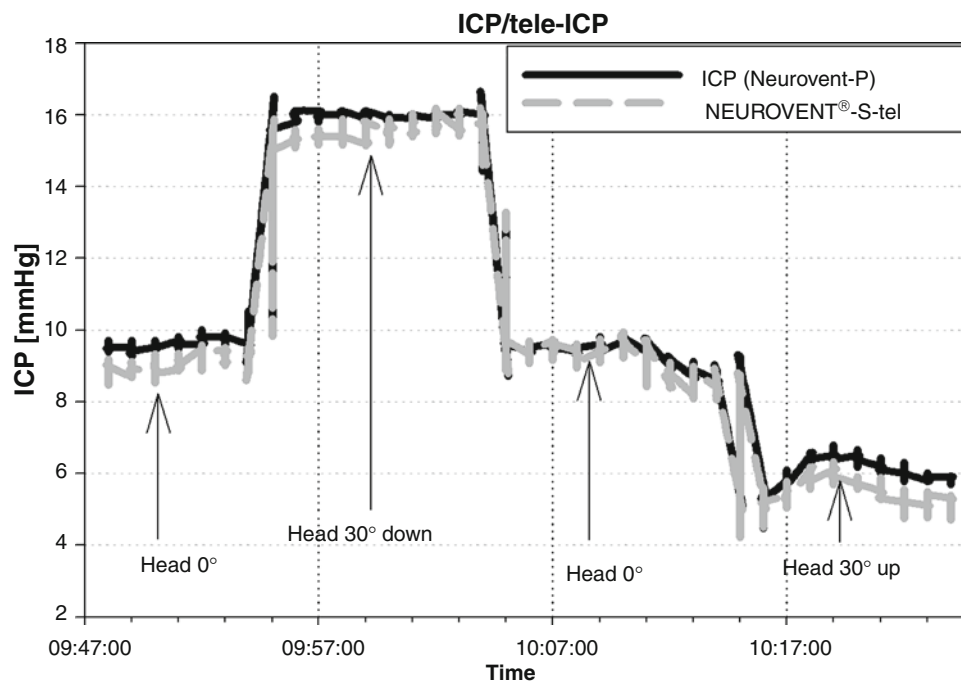


Fig. 2 Individual ICP recording with a conventional ICP probe vs the (NEUROVENT[®]-S-tel). Synchronous transmission of telemetric and parenchymal ICP values during intraoperative measurements is displayed

Results

A total of 26 telemetric ICP probes were inserted into 13 animals. Within 3 s after the reader was manually placed over the telemetric probe the current value was displayed with a rate of 5/s. In all animals ICP waveform analysis confirmed the intracranial placement of all inserted probes.

Trend parameters of ICP values were calculated as grand averages of individual means. Measurements revealed a mean difference between NEUROVENT®-S-tel and the parenchymal reference probe of 2.64 ± 1.79 mmHg (SD) over a total monitoring period of 40 min per probe. NEUROVENT®-P-tel differed with a mean of 2.48 ± 1.52 (SD) mmHg against the parenchymal probe. These results are summarised in a Bland–Altman plot (Fig. 3a). With the head tilted up 30° negative ICP values could be recorded with a mean decrease in ICP compared with baseline measurements of 4.8 ± 2.01 (SD) mmHg. Correspondingly, ICP increased by 5.36 ± 1.89 (SD) mmHg once the head was moved down by 30°. Figure 3b illustrates the Bland–Altman analysis using a subdural telemetric probe.

Laboratory results of blood samples drawn preoperatively were within normal range values. No soft tissue infection was diagnosed. All animals recovered well after the operations. No apparent neurological deficits occurred after insertion of the catheters.

Discussion

We compared two new telemetric ICP probes (NEUROVENT®-P-tel/NEUROVENT®-S-tel) with a parenchymal ICP probe (Neurovent®-P) in an experimental set-up. Our data suggest that both new devices are suitable for reliable short-term ICP measurements with good accuracy in comparison to conventional ICP measurement.

The exclusion of a ventriculo-peritoneal shunt insufficiency remains a neurosurgical challenge. Patients presenting with recurrent headaches or children with nausea and vomiting often achieve maximum diagnostic attention. Routinely shunt course x-rays, exclusion of papilloedema, cranial computed tomography (CCT) and or magnetic resonance imaging (MRI), ultrasound, chamber punctures with direct measurement of ICP and eventually surgical shunt revisions are pursued, if shunt malfunction is suspected. In many instances unnecessary shunt revisions significantly increase the subsequent risk of infection and malfunctions. Besides the medical aspect of exposing the patient to needless radiation or risks, economic factors also have to be considered in medical practice. In this context the benefits of a

telemetric ICP monitor have recently been discussed. The hypothesis underlying this study is that the reliable and easy telemetric self-assessment of each individual's ICP will prospectively reduce the rate of diagnostic and even therapeutic procedures significantly.

For a time period of four decades different groups have studied the reliability of telemetric ICP sampling in experimental and clinical settings [1–8]. Up to 30 prototypes of various telemetric ICP tools have been designed, but only four of them were used clinically in larger numbers. Owing to conceptual difficulties of the former telemetric systems such as placement into the epidural space or connection of the probes to the CSF pathways, and insufficiency of the covering materials used, long-term utility has not been proved so far. Epidural measurements inaccurately displayed the ICP beginning after 2 months, probably owing to calcifications of the dura that hampered the transmission of pulsations. Additionally, massive zero point drifts occurred in older models. The CSF-coupled telemetric probes were prone to inaccuracy once the proximal catheter was occluded and did not meet the standards for a reliable emergency ICP measurement.

As our results demonstrate, the telemetric probes were easy to handle and accurate in measuring ICP in comparison to the conventional ICP probe (Figs. 3a, 3b). Increases and decreases in the head position were instantly recorded without delay and signal quality was excellent (Fig. 2). All recordings were performed after skin closure. Despite the skin thickness of approximately 1.5 cm no signal interruptions occurred.

The telemetric probes are placed either intraparenchymally or subdurally. This may be interpreted as a physiological limitation in gaining the ideal ICP, but the potentially increased rate of infections has not yet justified the intraventricular placement in humans. However, the fact that these telemetric probes are “stand-alone” systems without connection to the CSF pathway should allow interpretation of ICP even in acute shunt insufficiencies once the system is implanted in VP-shunted patients.

Conclusion

We provide evidence that the new telemetric technology (NEUROVENT®-P-tel/NEUROVENT®-S-tel) will sufficiently measure ICP for short term use neither technical nor handling concerns exist for the routine clinical application of these new telemetric probes. Further continuation of our study will demonstrate whether this system guarantees acceptable long-term reliability and if drift phenomena occur.

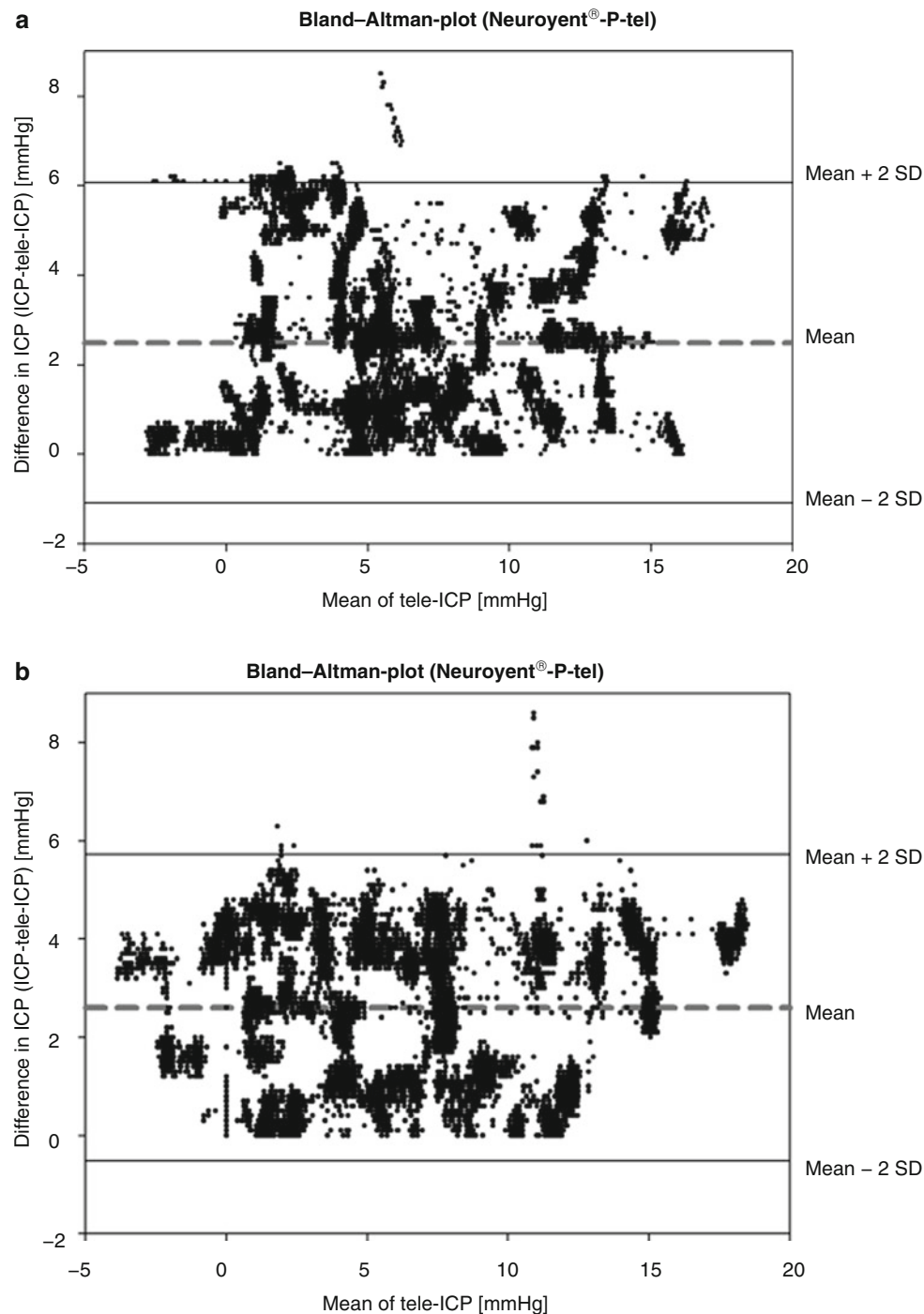


Fig. 3 (a) ICP Bland–Altman plot displaying the mean of telemetric ICP values measured by NEUROVENT®-P-tel (x-coordinate) vs the corresponding difference of both probes (y-coordinate). It presents an overall mean difference of $2.48 \text{ mmHg} \pm 1.52 \text{ (SD) mmHg}$. However, this may allow the conclusion that NEUROVENT®-P-tel will measure ICP comparable to the conventional ICP-probe. (b) ICP Bland–Altman

plot displaying the mean of telemetric ICP values measured by NEUROVENT®-S tel (x-coordinate) vs the corresponding difference of both probes (y-coordinate). It presents an overall mean difference of $2.64 \text{ mmHg} \pm 1.79 \text{ (SD) mmHg}$. However, this may allow the conclusion that NEUROVENT®-S-tel will measure ICP comparable to the conventional ICP probe

Funding Raumedic Germany funded this study. The sponsor neither played a role in the trial design, data collection and analysis, nor preparation of this manuscript.

Conflict of interest statement Michael Kiefer serves as a consultant for Raumedic AG, Helmbrechts, Germany.

References

1. Cosman ER, Zervas NT, Chapman PH, Cosman BJ, Arnold MA (1979) A telemetric pressure sensor for ventricular shunt systems. *Surg Neurol* 11:287–294
2. De Jong DA, Berfelo MW, de Lange SA, Maas AI (1979) Epidural pressure monitoring with the so-called Rotterdam transducer. Further in vivo results. *Acta Neurochir (Wien)* 45:301–309
3. Heppner F, Lanner G, Rodler H (1976) Telemetry of intracranial pressure. *Acta Neurochir (Wien)* 33:37–43
4. Zervas NT, Cosman ER, Cosman BJ (1977) A pressure-balanced radio-telemetry system for the measurement of intracranial pressure. A preliminary design report. *J Neurosurg* 47:899–911
5. Rylander HG, Taylor HL, Wissinger JP, Story JL (1976) Chronic measurement of epidural pressure with an induction-powered oscillator transducer. *J Neurosurg* 44:465–478
6. Richard KE, Block FR, Weiser RR (1999) First clinical results with a telemetric shunt-integrated ICP-sensor. *Neurol Res* 21:117–120
7. Miyake H, Ohta T, Kajimoto Y, Matsukawa M (1997) A new ventriculoperitoneal shunt with a telemetric intracranial pressure sensor: clinical experience in 94 patients with hydrocephalus. *Neurosurgery* 40:931–935
8. Osaka K, Ohta T (1980) Limits of various methods for evaluation of shunt function and development of new intracranial pressure meter incorporated in the shunt system (author's transl). *No Shinkei Geka* 8:811–817

Telemetric ICP Measurement with the First CE-Approved Device: Data from Animal Experiments and Initial Clinical Experiences

Michael Kiefer, Sebastian Antes, Steffen Leonhardt, Melanie Schmitt, Berk Orakcioglu, Oliver W. Sakowitz, and Regina Eymann

Abstract The objective was to evaluate the qualification of the new telemetric intracranial pressure (ICP) measurement (t-ICP) device Raumedic® NEUROVENT P-Tel and S-Tel. The proof of concept was examined in a pilot animal study measuring intraperitoneal pressure with a telemetric and a conventional ICP measurement probe at five rates for 1 h each. Moderate external pressure load allowed measuring values between 0 and 40 mmHg. To estimate long-term performance 18 t-ICP devices were implanted subdurally or intraparenchymally into minipigs. Reference measurements were performed regularly using conventional ICP probes. From the short-term as well as from the long-term perspective t-ICP proved to have excellent dynamic ICP signal components perception (e.g. pulse amplitude). Some zero drift of static ICP was found, ranging between 5 and 8 mmHg. While all telemetric, intraparenchymal probes kept their functionality throughout the follow-up, 33% of the subdurals failed for reasons detailed in another paper. Raumedic's NEUROVENT® P-Tel/S-Tel proved to provide reliable data over periods of up to 18 months. Minor zero drift can be well tolerated as the dynamic ICP signal is measured with excellent stability. Clinicians should focus more on such ICP dynamic signal

information than on static ICP when using the device over longer follow-up periods.

Keywords Experimental model • ICP • Telemetry • Hydrocephalus • Intracranial pressure • Non-invasive ICP measurement

Introduction

For more than four decades attempts have been made to establish a reliable method for telemetric measurement of intracranial pressure (ICP) [1–6]. Yet, as telemetric ICP monitoring requires the use of absolute pressure sensors – one within the implant, one outside to measure the surrounding pressure as a reference – the technical challenge is enormous. Offset-drift on the order of parts per thousand per year in the antidromic direction can result in clinically relevant misleading ICP values within a short time. Only the Cosman-Sensor (Integra Radionics, Burlington, MA, USA) [1, 7], the epidural “Rotterdam Transducer” [2], and the “Aachen-ICP-TeleSensor” (Telemeasurements, Aachen, Germany) [6] reached limited clinical impact.

Major obstacles to generalized acceptance were the inadequacy of some devices in measuring negative pressures, difficult handling, but most of all the lack of reliability. Hence, the risk involved in trusting in telemetrically measured unreliable values outweighed any potential benefits.

Recently new telemetric ICP sensors (NEUROVENT® P-Tel, NEUROVENT® S-Tel for intraparenchymal and subdural measurement, Raumedic AG, Helmbrechts, Germany) have been introduced, demonstrating obviously favourable in vitro performance with minimal drift over years.

We studied the in vivo reliability in one short- and one long-term animal experiment before the now CE-approved devices were implanted in humans. The experiences from these studies and from the first insertion in a patient are reported.

M. Kiefer (✉), S. Antes, M. Schmitt, and R. Eymann
Department of Neurosurgery,
Saarland University, Medical School,
66421 Homburg-Saar, Germany
e-mail: michael.kiefer@uks.eu

S. Leonhardt
Helmholtz-Institut, RWTH Aachen,
Aachen, Germany

B. Orakcioglu and O.W. Sakowitz
Department of Neurosurgery,
University Hospital,
Heidelberg, Germany

Materials and Methods

Animal Experiment 1

Design

To study the short-term performance of early prototypes of this new telemetric pressure sensor, we measured the intraperitoneal pressure in five adult, female Wistar rats (weight: 320–350 g) in parallel telemetrically and with conventional, intraparenchymal ICP sensor probes (NEUROVENT-P (diameter: 5F), Raumedic AG, Helmbrechts, Germany). Intraperitoneal pressure was varied by a custom mechanical apparatus, which allowed to apply a large-scale, uniform moderate compression of the rats' abdominal region. After catheter insertion the resting pressure of the two devices was measured minimally for 5 min. Thereafter, intraperitoneal pressure was varied with different frequencies to estimate the devices' dynamic response for at least 60 min. Both pressure signals were monitored and stored with a specifically redesigned Raumedic-Datalogger® (Raumedic Reader TDT1 readP, Raumedic AG, Helmbrechts), allowing parallel signal processing of both signals.

Anesthesia and Operative Procedure

Rats were anesthetized using 0.01% (RS)-(±)-2-(2-Chlorophenyl)-2-(methyl-amino)-cyclohexan-1-on (Ketavet®) (2 mL/kg) and 2% 2-(2,6-Dimethylphenylamino)-5,6-dihydro-4*H*-thiazin (Rompun®) (0.2 mL/kg), intraperitoneally providing sufficient narcosis for about 90 min without the need for artificial ventilation. The electronic part of the telemetric devices was inserted subcutaneously on the flank. Via a median micro-laparotomy the subcutaneously tunneled telemetric catheter and a conventional NEUROVENT-P catheter were inserted intraperitoneally. The peritoneum was firmly closed, applying purse-string sutures. Meticulous subcutaneous stitches and, for superficial closure, 2-Octyl-Cyanoacrylat skin adhesive (Dermabond®, ETHICON Products, Norderstedt, Germany) were used.

Animal Experiment 2

Design

To study the long-term performance of the final pre-release versions of the NEUROVENT® P-Tel, NEUROVENT® S-Tel telemetry sensors for at least 1 year, the devices were implanted in nine adult, male Ellegaard (Denmark) minipigs. In each animal one subdural and one parenchymal probe were inserted. As reference a conventional Neurovent-P catheter was also implanted. The correct positioning of the

probes was verified by X-ray in different plains, which furthermore served to revise for hydrostatic pressure differences. For data acquisition and storage the Raumedic Reader TDT1 readP was used. In each animal reevaluation occurred regularly after 3 ± 1 and 6 ± 1 months respectively inserting a new reference probe (Neurovent-P) via a new borehole. Again X-ray assessed the probes' positioning. After implantation (initially and during each control) resting pressure was measured in parallel to the reference for each telemetric probe for at least 10 min. Thereafter, changed positioning (head-up, head-down) provoked ICP alterations. Incline (between $+20^\circ$ and -20°) was measured and recorded electronically by a new designed apparatus whose precision has been verified previously. The same maneuvers were performed separately for each telemetric probe while the reference ICP was measured in parallel. One group (five animals) were euthanized after 9 and 12 months to study the histomorphological alterations of all the surrounding tissues while four minipigs are still alive to evaluate the devices' in vivo performance for at least 2 years.

Anesthesia and Operative Procedure

Anesthesia was induced with Ketavet® (10%/1 mg/10 kg i.m.) and 2,6-Diisopropylphenol (Propofol®; dosage depending on individual reactions). Given adequate preconditioning, each animal was intubated, artificially ventilated (30% O₂, nitrous oxide at 2.5 vol.%) and anesthesia sustained with i.v. *N*-(1-Phenethyl-4-piperidyl)propionanilide (Fentanyl®; 45–90 µg/kg/h) and vaporized (RS)-Difluormethoxy-1-chlor-2,2,2-trifluorethan (Isofluoran®) at 1.5–2.5 vol.%. Complete monitoring encompassed continuous control of rectal temperature, capillary oxygen saturation (S (O₂)), and ECG to maintain physiological values. For hydration left-ear vein i.v. line was used to administer Ringer-Lactate and 0.9% NaCl solutions. For perioperative antibiotic prophylaxis we used amoxicillin i.v. (weight adapted) 30 min before the skin incision, which was continued for a further 3 days. (RS)-2-(6-Chlor-9*H*-carbazol-2-yl)propan-acid (Carprofen®) served as post-interventional pain killer.

After skin disinfection with propan-2-ol, 1.0 g povidone-iodine (Braunoderm®) and sterile draping a semicircular skin incision on the fronto-parietal region was made. High-speed drills 5 mm in diameter were used for borehole trephination. The telemetric devices were inserted into the coronal suture level about 1.5 cm paramedian bilaterally, while the borehole for the reference probe was located more frontally. The opening of the tabula interna was minimized, allowing just catheters' scraping through to avoid cerebrospinal fluid (CSF) loss and preventing pathways for infections. We aimed to place all catheter tips at the same hydrostatic pressure level in neutral prone positioned animals. If necessary, according to X-ray control, the positions were corrected. Typically, the catheter

tip ended 1.5 cm below the tabula interna. For the regular invasive controls only a minimal skin incision frontally to the telemetric devices was made to insert the reference sensor.

After finalizing the whole measurement protocol during the initial and all control examinations the reference probe was removed and the dural leak sealed with wax or alpha-gelatin haemostatic sponges. Multilayered subcutaneous stitches and for superficial skin closure Dermabond® were used for wound closure. In addition to its better tolerance the importance of Dermabond® is its bactericide effect, which was demonstrated recently [8].

As implants' biotolerance was another scope of this study, animals were arbitrarily assigned to a short (3–12 months) or long-term (>12 months) follow-up. In the short-term follow-up group, one, two and one animal were finalized after 3, 6 and 12 months respectively, after undergoing one to three control ICP measurements. To reduce the overall burden of long-term survivors, follow-up examinations were restricted to 3 per year with arbitrary assignment whether the 3, 6 or 9 months' follow-up was omitted.

All animal experiments were approved by independent animal welfare committees and monitored by the institutional animal welfare delegate. Veterinarians supervised all procedures and performed anesthesia and monitoring-related activities in the minipigs.

Technology

The telemetric implant has a ceramic housing measuring 3 cm in diameter and 4 mm in height, which contains all electronics and the antenna for data and energy transfer (Fig. 1). Technology based on piezoresistive strain gauge silicon-based absolute-pressure sensors with a built-in Wheatstone bridge. ICP changes result in minimal deforming of this chip and the according output voltage changes. In parallel, the tip sensor measures local temperature. Both signals become digitized by the ASIC within the ceramic housing. During the manufacturers' individual calibration of each device 7 chip-specific parameters are generated and permanently saved on the ASIC to ensure maximal reliability. Without external energy input the implant remains inactive. The Raumedic Reader TDT1 readP identifies using RFID (radio-frequency identification) technology each individual implant and its specific calibration data. The externally applied antenna of the reader initially supplies the energy required to initiate the implants' measurement, which is received by the antenna too. This process of energy transfer and data transmission allows sampling at 5 Hz and a resolution of 1 mmHg. The working range encompasses –20 to +400 mmHg. Once the data package of absolute ICP and brain temperature has been transferred, the Datalogger®

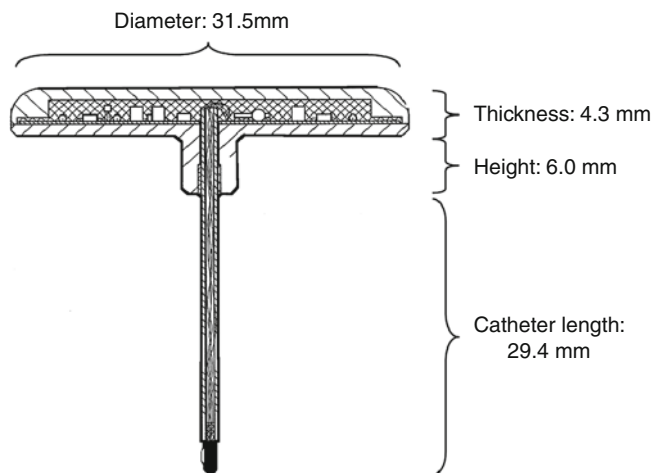


Fig. 1 Schematic drawing of the telemetric NEUROVENT® P-Tel device. The ASIC for data processing and exchange and the antenna for energy and data transfer are located in a ceramic housing. A piezoresistive strain gauge with silicon-based absolute-pressure sensors and built-in Wheatstone bridge measures the ICP on the tip of the 5F (diameter) catheter

computes the relative ICP by parallel measurement of the surrounding (atmospheric) pressure with a built-in second absolute, temperature-corrected pressure sensor. This computed relative ICP is displayed on the Datalogger's screen and stored on a built-in SSDS. A built-in power supply and the low weight of the Raumedic Datalogger Reader TDT1 readP allows ambulatory on-demand ICP measurement by patients by themselves after briefing.

Data Management and Statistics

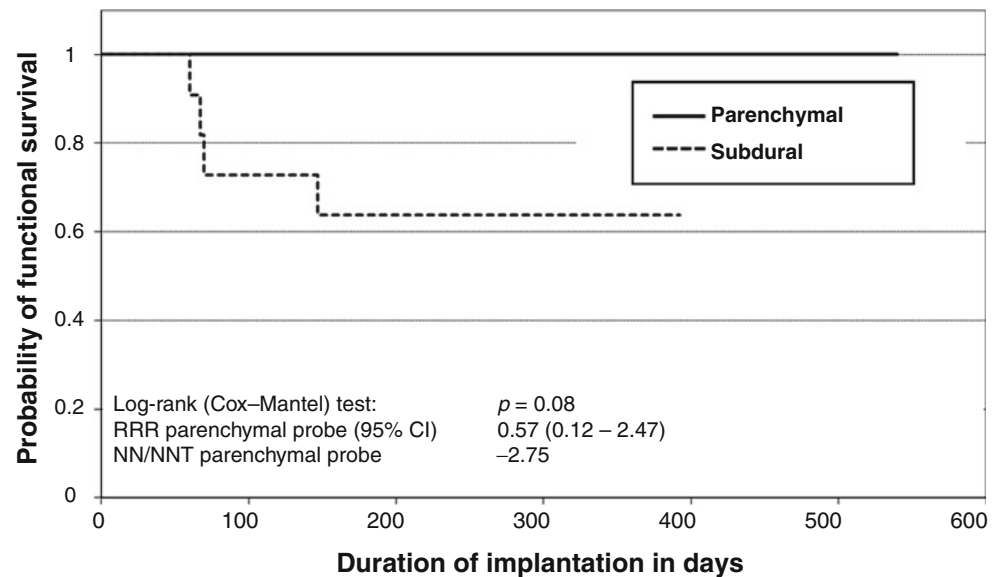
The software packages: Microsoft-Excel 2003 (Redmond, USA), PASW Statistics 18 (SPSS Inc, an IBM Company, Chicago, USA), Raumedic-Datalog® (RECO-Medizintechnik, Pirna, Germany), and WinSTAT® for Excel Version 2009.1 (R. Fitch Software, Bad Krozingen, Germany) were used for data management, analysis, and computation. Significance was assumed at $p < 0.05$.

Results

Animal Experiment 1

Intraperitoneal pressures between 0 and 40 mmHg could be measured with both the telemetric and the conventional probe. Telemetrically and conventionally measured pressure correlated in an excellent manner ($p < 0.000$), the maximal difference between the two was 1.8 ± 0.8 mmHg on average

Fig. 2 Kaplan–Meier “survival” analysis of telemetric probes: while all inserted intraparenchymal probes kept functionality for a maximum of 540 days, 33% of the subdural probes failed before the study endpoint



in one animal. In the others the mean difference was even smaller. Overall, during 310 min monitoring in five animals the mean pressure difference between control and telemetric probe measured was 1.1 ± 0.7 mmHg. The dynamic characteristics of the pressure signal as measured with both devices were nearly identical. Despite the 5-Hz sampling rate of the telemetric probe, the pulse amplitude could be measured precisely, with an overall pressure difference of 0.4 ± 0.3 mmHg on average and pulse amplitudes ranging between 1 and 6 mmHg and artificially induced (by short-term manual pressure) short-term ICP variations up to 15 mmHg during 1 s ($p < 0.000$).

Animal Experiment 2

Overall 12 subdural and 8 intraparenchymal telemetric devices were implanted in 9 minipigs (7 had both subdural and intraparenchymal probes; 2 had bilaterally subdural probes). During the observational period a total of 25 control measurements, 750 monitored minutes in total, were performed telemetrically and conventionally. Between 3 and 6 (group 1), 7 and 12 (group 2) and 18 (group 3) months after implantation 8, 11 and 6 controls were performed. While all implanted parenchymal probes are still functioning or reached the regular endpoint, 4 of the 12 implanted subdural probes failed (Fig. 2). Detailed descriptive statistics of the ICP differences measured between the reference and the telemetric probe are provided in Table 1. Excluding outliers at the level of one standard deviation (SD) or more provides more realistic data. Under these conditions pressure differences measured between the telemetric and the reference probe were 5.5 ± 4.0 mmHg (group 1), 4.5 ± 4.7 mmHg (group 2), and

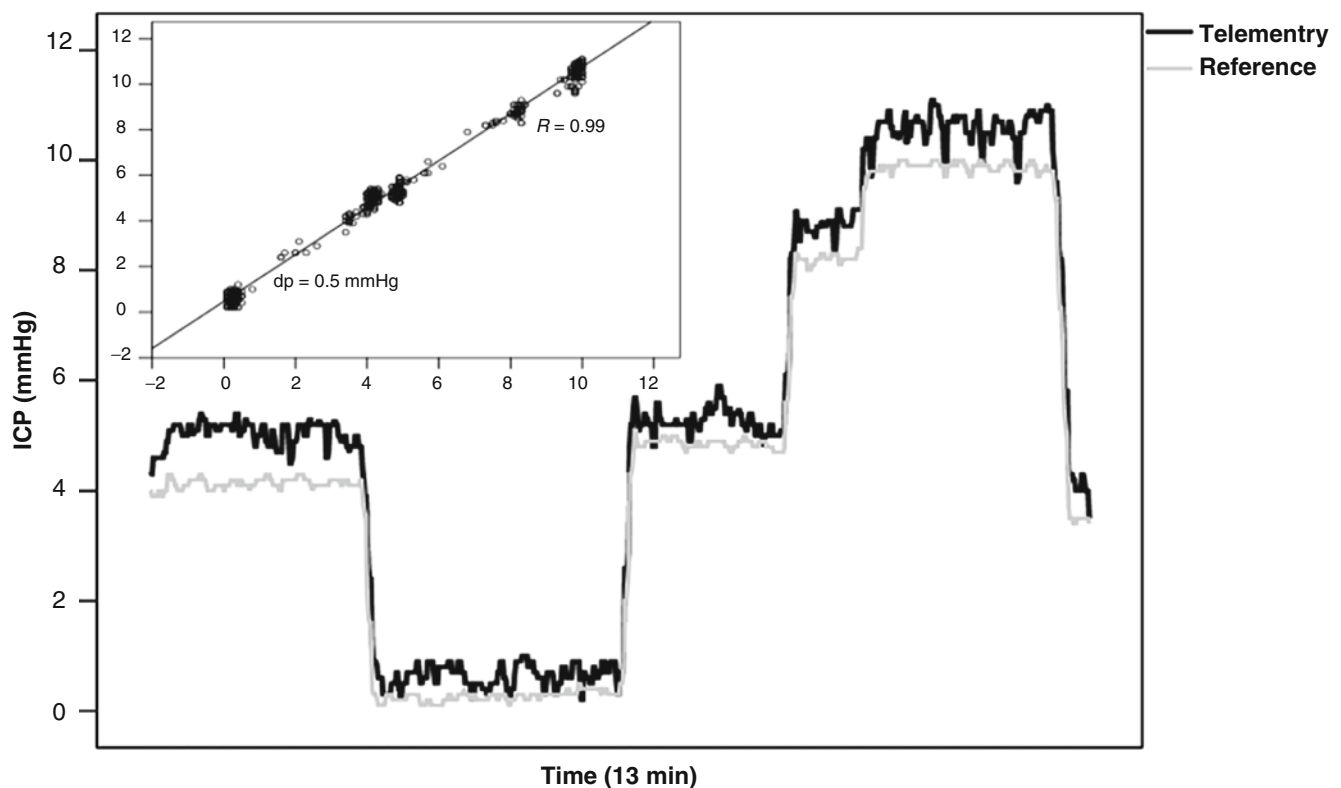
8.3 ± 3.7 mmHg (group 3). Neither ANOVA ($p = 0.853$) nor the Kruskal–Wallis test ($p = 0.717$) revealed a difference between the groups. As the groups stand for different follow-up periods when controls were performed, this result must be interpreted as a sign of measurement stability without increasing zero drift with time (Fig. 3). The most impressive finding was the reliability of the signals’ dynamic content measurement. Even probes with significant zero shift (outliers) provided comparable ICP signal dynamics, including pulse amplitude and ICP alterations due to positioning. The mean coefficients of determination (R^2), were calculated for groups 1 (first control (3–6 months after insertion)), 2 (second control (12 months after insertion)), and 3 (third control (18 months after insertion)) to be 0.899 ± 0.119 , 0.826 ± 0.225 , and 0.917 ± 0.113 respectively, indicating excellent signals’ dynamic ICP components perception during the whole follow-up period (ANOVA: $p = 0.520$; Kruskal–Wallis: $p = 0.342$; Fig. 3). Hence, even if the static ICP value is somewhat affected by zero drift, the excellent stability of the dynamic ICP signal content provides sufficient and reliable data over time to recognize alterations in cranio-spinal CSF dynamics.

Initial Clinical Experiences

As the NEUROVENT P-Tel has been CE-approved recently for clinical usage over a maximal period of 29 days, we were able to use such a device to clarify recurrent headache in an adolescent girl shunted for hydrocephalus. A multitude of clinical interventions (e.g. conventional ICP measurement, infusion tests, probatory shunt revision) have failed before, but meticulous clinical examinations could not find any explanation for her headache other than intermittent shunt failure. The telemetric

Table 1 Descriptive statistics of the second animal experiment

Months	Pressure differences (telemetric vs control) in mmHg			Correlation coefficient (telemetric vs control)		
	3–6	7–12	18	3–6	7–12	18
<i>n</i>	8	11	6	8	11	6
Mean	13	14	10	0.899	0.826	0.917
Mean (1/2 SD outliers excluded)	5.5	4.5	8.3	0.938	0.921	0.955
Number of outliers at 1/2 SD	0/1	4/0	1/0	0/1	1/1	1/0
Standard deviation	22	16	5	0.119	0.225	0.113
Standard error of mean	7.8	4.8	2.2	0.042	0.068	0.046
Variance	487	260	30	0.014	0.050	0.012
Variance coefficient	1.66	1.08	0.54	0.133	0.273	0.124
Minimum to maximum	0.9–67	0.2–43	4.6–19.1	0.62–0.99	0.24–0.99	0.72–0.99
25th percentile	2.9	2.3	5.6	0.864	0.867	0.800
Median	4.9	7.5	8.4	0.982	0.908	0.981
75th percentile	11.5	34.2	15.4	0.982	0.952	0.994

**Fig. 3** Example of 12-month control of telemetrically (intraparenchymal) and conventionally measured ICP during 13 min. Effects of positioning (neutral, head-up, neutral, two steps head-down) clearly provoke corresponding ICP changes. The average pressure difference between

control and telemetric probe was 0.5 mmHg. The perfect correlation of control and telemetric ICP measurement is also represented by the according scatter plot of both measured values (control on the y-axis, telemetric on the x-axis) in the smaller graphic

device was inserted left frontally and the patient was instructed how to measure ICP telemetrically at home when she suffers headache, but she was also advised to measure regularly three times per day if she had no complaints. Thus, an overall data record of about 4 h (2.5 h without complaints; 1.5 h with headache) could be gathered over 28 days. Neither the dynamic nor

the static ICP differed between episodes with and without complaints, proving that headaches were independent of ICP. All the data measured were reliable and the device proved its qualification for ambulatory ICP measurement by patients themselves. According to the specification the device was explanted on day 29. No side effects occurred throughout the whole treatment.

We found this methodology the most useful measure to exclude intermittent shunt failure.

Discussion

During the past four decades at least 30 prototypes for telemetric ICP measurement have been proposed [1–6, 9, 10], but only minority have reached limited clinical impact. In some of them, their failure can be well understood from a retrospective perspective. Foreign body reactions with calcifications must damp any transdural signal transfer in long-term epidural implants for telemetric ICP measurement. The integration of such devices into shunts and accordingly the CSF-coupled measurement was at risk of dangerous ICP underestimation at proximal catheter obstruction. The difficulty is that ICP pulsatility can be visible, yet because soft silicone tubes are compressible and some pulsation can be transferred to the decoupled water column, mimicking reliable ICP measurements. Accordingly, reliable telemetric ICP measurement needs intradural, tip-sensor-based data acquisition as realized with the Raumedic NEUROVENT® P-Tel and S-Tel probes. As our interim data analysis demonstrates, intraparenchymal probes in particular provide reliable data for up to 18 months. The median offset drift (range: 5–8 mmHg) remained quite stable during the follow-up of a maximum of 18 months. However, much more importantly: even devices with distinct zero shift of the static pressure signal maintained reliable dynamic signal acquisition. Even ICP pulse amplitude was correctly measured. This is of utmost importance for long-term monitoring of shunted patients. Knowing the dynamic signal characteristics resulting from physiological ICP variations (heartbeat, breathing) and positioning with a well-functioning shunt, Shunt failures must result in alterations in dynamic signal characteristics, as consequence of altered CSF-hydrodynamics.

The fundamental idea of developing subdural telemetric probes was to avoid any brain tissue violation as occurs with intraparenchymal probes. In our examination >30% of the subdural probes failed or provided unreliable data 6–10 months after implantation. Potential explanations have been detailed previously [11]. Hence, as not all subdural probes failed and have been examined, final statements on its qualification are pending. Probably, the comparatively small cranium of minipigs effectuates higher tensile stress on subdural probes, which does not occur in humans as they have a lower radius of curvature and larger skulls. Yet, in the clinical setting, we actually prefer intraparenchymal probes as a result of our findings. Almost negligible histomorphological alterations around 12 months in intraparenchymal probes implanted into minipigs support such a policy until all subdural probes have been examined.

Conclusion

The new Raumedic NEUROVENT® P-Tel and S-Tel telemetric ICP measurement device has been proven to provide reliable data for up to 1.5 years. Even if some zero shift occurs over time the dynamic signal content remains unaffected and of outstanding reliability.

Financial Disclosure This study has been performed with support of the German Ministry for Research and Education, which was granted to a consortium of the Saarland University (M. Kiefer, S. Antes, M. Schmitt, R. Eymann), the RWTH Aachen (Steffen Leonhardt), and Raumedic® AG (Helmbrechts, Germany) (BMBF-Grant ID-No.: 16SV3745). These authors have received no further financial benefits from this research work. B. Orakcioglu received some financial support from Raumedic AG for performing the study. No aspects of these studies (design, data acquisition and analysis or content of this manuscript) were influenced by any of the sponsors or the industrial partner of the consortium.

Conflict of interest statement We declare that we have no conflict of interest.

References

1. Cosman ER, Zervas NT, Chapman PH, Cosman BJ, Arnold MA (1979) A telemetric pressure sensor for ventricular shunt systems. *Surg Neurol* 11:287–294
2. de Jong DA, Berfelo MW, de Lange SA, Maas AI (1979) Epidural pressure monitoring with the so-called Rotterdam transducer. Further in vivo results. *Acta Neurochir (Wien)* 45:301–309
3. Heppner F, Lanner G, Rodler H (1976) Telemetry of intracranial pressure. *Acta Neurochir (Wien)* 33:37–43
4. Zervas NT, Cosman ER, Cosman BJ (1977) A pressure-balanced radio-telemetry system for the measurement of intracranial pressure. A preliminary design report. *J Neurosurg* 47:899–911
5. Rylander HG, Taylor HL, Wissinger JP, Story JL (1976) Chronic measurement of epidural pressure with an induction-powered oscillator transducer. *J Neurosurg* 44:465–478
6. Richard KE, Block FR, Weiser RR (1999) First clinical results with a telemetric shunt-integrated ICP-sensor. *Neurol Res* 21:117–120
7. Wilson MH, Milledge JMD (2008) Direct measurement of intracranial pressure at high altitude and correlation of ventricular size with acute mountain sickness: Brian Cummins' results from the 1985 Kishtwar expedition. *Neurosurgery* 63:970–975
8. Eymann R, Kiefer M (2010) Glue instead of stitches: a minor change of the operative technique with a serious impact on the shunt infection rate. *Acta Neurochir Suppl* 106:87–89
9. Miyake H, Ohta T, Kajimoto Y, Matsukawa M (1997) A new ventriculoperitoneal shunt with a telemetric intracranial pressure sensor: clinical experience in 94 patients with hydrocephalus. *Neurosurgery* 40:931–935
10. Osaka K, Ohta T (1980) Limits of various methods for evaluation of shunt function and development of new intracranial pressure meter incorporated in the shunt system. *No Shinkei Geka* 8:811–817
11. Schmitt M, Eymann R, Antes S, Kiefer M (2011) Subdural or intraparenchymal placement of long-term telemetric ICP measurement devices. *Acta Neurochir Suppl: Hydrocephalus*, 113. Aygok, Gunes A, Rekeate, Harold L. (Eds.); 2012, XII, ISBN 978-3-7091-0922-9

The New ICP Minimally Invasive Method Shows That the Monro–Kellie Doctrine Is Not Valid

Sérgio Mascarenhas, G.H.F. Vilela, C. Carlotti, L.E.G. Damiano, W. Seluque, B. Colli, K. Tanaka, C.C. Wang, and K.O. Nonaka

Abstract The Monro–Kellie doctrine states that the interior of the cranium is formed of three main components: blood, fluid and cerebral parenchyma. An increase in the volume of one or more components may increase the intracranial pressure (ICP). This doctrine also affirms that the skull cannot be expanded after the closure of the fontanelles. Monro and Kellie’s theory has been perfected during the last two centuries. This study leads to a new contribution that proves that even adults’ consolidated skulls present volumetric changes as a consequence of ICP variations.

Keywords Intracranial pressure • ICP • Monro–Kellie • Medical instrumentation • Minimally invasive system • Monitor

Introduction

Alexander Monro, a professor of anatomy at the Edinburgh College of Medicine, has applied some of the principles of physics to intracranial content. Studying patients and corpses he concluded, in 1783 [1], that:

1. The brain was inside a bony structure (skull) that could not be expanded
2. The substance forming the brain was almost incompressible

S. Mascarenhas (✉) and G.H.F. Vilela
Department of Biophysics, Physics Institute, University of São Paulo,
Av. Trabalhador são-carlense, 400 – Pq. Arnold Schmidt,
CEP: 13566-590 São Carlos, São Paulo, Brazil
e-mail: sergiomascarenhas28@gmail.com

C. Carlotti, B. Colli, and K. Tanaka
Surgery of Department, Medical School – University of São Paulo,
Ribeirão Preto, Brazil

L.E.G. Damiano, C.C. Wang, and K.O. Nonaka
Department of Physiology, Federal University of São Carlos,
São Carlos, Brazil

W. Seluque
Department of Biomedical Engineering, Clinical Hospital – University
of São Paulo, Ribeirão Preto, Brazil

3. Consequently, the blood volume inside the skull cavity was constant or almost constant, and a steady output of venous blood from the cranial cavity originated from a steady input of arterial blood.

Monro’s hypothesis were supported by the experiences of his pupil George Kellie de Leith, a Scottish doctor who had carried out several studies on corpses and observed facts that made it possible to complete and correct some points of the theory proposed by his professor.

Kellie, with his observations, also postulated the following statements [2]:

1. The brain was enclosed and completely occupied a bone box that could not be expanded in adults
2. The brain presented low compressibility
3. It was unlikely that any fluid could be removed or that any excess could be introduced inside the cranial cavity without equivalent simultaneous changes in ICP

Occasional citations in the literature nominated this doctrine as the “Monro–Abercrombie doctrine” [3]. John Abercrombie was a pathologist working in the Edinburgh College of Medicine who made the same observations as Kellie carrying out total bleeding tests in animals [4] and supporting Monro’s and Kellie’s conclusions. This was fundamental to the hypothesis being accepted [5].

The discrediting by the scientific community was not surprising, as Galeno’s idea, in the second century, that the cerebral ventricles were full of a “vital spirit,” had survived for many centuries. François Magendie, a French physiologist, deserves the credit regarding the proof that fluid was present in the cerebral ventricles; he proved that these ventricles communicated with the subarachnoid space and the fourth ventricle through a ventricle that today bears his name [6].

The recognition of the cerebrospinal fluid (or liquor cerebrospinalis) as a vital component added another dimension to the cranial content equation, causing a profound effect on the understanding of intracranial pressure.

Cushing offered a precise formula for the Monro–Kellie doctrine and postulated that when the cranial box is intact, the sum of brain volumes of fluid and intracranial blood is constant. Consequently, an increase in one component must

be compensated for by reduction of one of the other two [7]. Initially, the emphasis was directed to the intracranial pressure increase owing to its clinical implications. Intracranial hypotension, less severe and less common, was not initially taken into consideration.

In the original form, the hypothesis put forward by Monro and completed by Kellie had imperfections that were later corrected by other authors. What finally came to be known as the Monro–Kellie doctrine, or hypothesis, affirmed that the sum of the brain volumes of fluid and intracranial blood was constant. An increment in one of them must cause a reduction in one or in the other two intracranial components so that abnormalities do not occur. This hypothesis also implies that the cranial volume after closure of the fontanels is constant, that is, there is no cranial deformation in adults due to an increase or diminution of the intracranial components.

We have proved that it is possible to determine cranial deformations caused by internal pressure variations, and this implies that the Monro–Kellie doctrine is not strictly valid.

Materials and Methods

“In Vitro” Experiments

In order to simulate the ICP changes, sensors of deformation (strain gauges) were applied to the parietal region of human skulls. The sensor was glued with ethyl-cyanoacrylate and connected to a monitoring system especially developed for the purpose.

To achieve this, the skull was filled with a rubber balloon connected to a bulb device to pump air and a manometer to determine the corresponding internal pressure (Fig. 1).

During the procedure the balloon was inflated in order to reach up to 100 mmHg internal pressure. The air valve was then opened and the system was continually monitored until the pressure returned to 0 mmHg.

The experiment was repeated five times. The data were stored in a computer and used in subsequent analyses.

“In Vivo” Experiments

Five 3-month-old male Wistar rats weighing between 270 and 300 g received our sensor in the right parietal bone. The animals were fixed by the legs on wooden supports with the ventral region tightly bound to the wooden surface.

The posterior region of the animals was elevated to 30°, 45°, and 90° for 30 s and the animal returned to the horizontal position (0°) for 5 min so that one maneuver did not

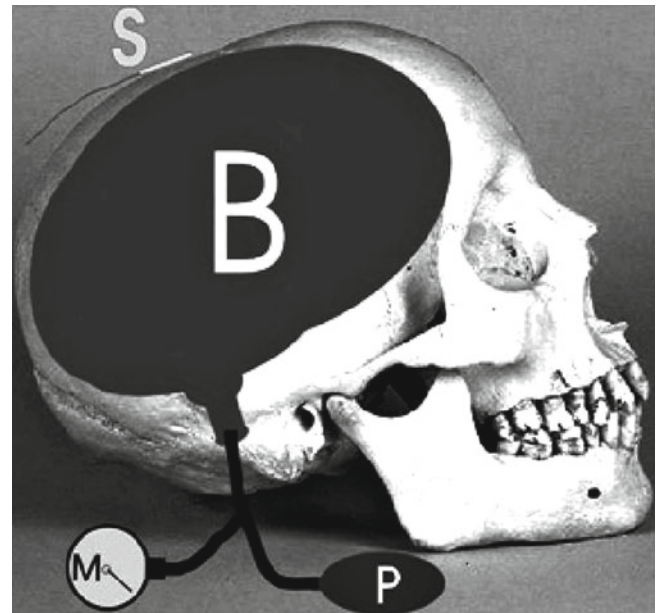


Fig. 1 System to measure bone deformation. *S* sensor; *B* balloon gas; *M* manometer, *P* pump air supply

interfere with the following. The tests were repeated three times in each animal. The same protocol was repeated elevating the anterior region of the animals.

Results

“In Vitro” Tests

Analyzing Fig. 2, one can observe that the sensor was able to capture the bone deformation provoked by an increase and decrease in the internal pressure. The chart contains the points that represent the average of the readings and the respective standard deviations.

The black squares represent the increased balloon pressure and the consequent cranial expansion. The sensor has shown sensitivity and reproducibility of results in all measurements as we can observe by the small standard deviation represented by the error bars.

The interpolated line through the points shows that the readings obtained are directly proportional to internal pressure. The gray points indicate the readings due to pressure reduction. The experiments have shown that the bone promptly responded to the internal pressure reduction, with no retardation or different values, to return to the initial readings; this has proved the non-existence of bone hysteresis, a fundamental rheological aspect that allows the quantitative validity of the method.

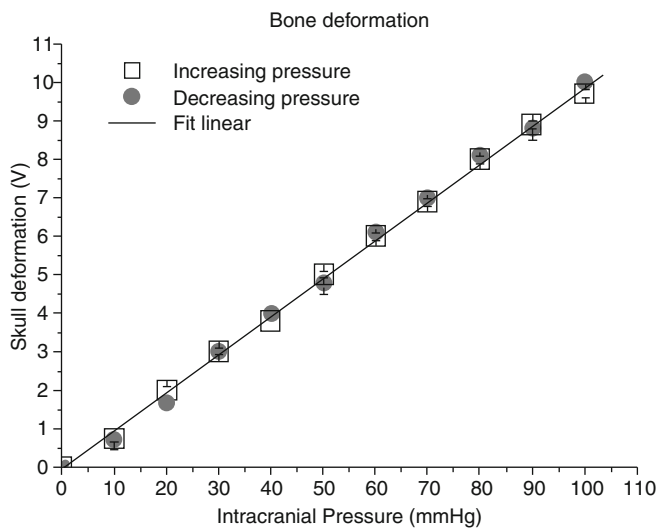


Fig. 2 Experiments in the skull. Hysteresis bone test. The *squares* represent the increase in internal pressure and the *circles* represent the decrease

“In Vivo” Tests

The ICP variation caused by postural maneuvers is also well known when this important physiological parameter is studied [7–11]. In hospitals, it is a common procedure to raise to 30° the head-rest of patients with intracranial hypertension [12]. When we raised the heads of patients or test animals, facilitation of the passage of the cerebrospinal fluid to the column occurred, reducing the volume of the fluid inside the skull and consequently reducing the ICP. Facilitation of the venous blood return also occurs, reducing the blood volume inside the skull and consequently reducing ICP.

The elevation of the posterior region of the animals produces exactly the opposite effect, as fluid migration into the skull occurs causing an ICP increase. This maneuver also contributes to the ICP variation as it diminishes the return of venous blood adding to the ICP increase.

Figure 3 shows the experimental results after elevation of the animal’s posterior region in angles shown on the ordinate axis. Each symbol represents one animal and each point represents the average of three repetitions; the error bar on each point represents the standard deviation for each determination.

The 30° elevation of the animals’ posterior region caused an ICP increase owing to fluid accumulation inside the skull and increased impedance to venous blood flow return. The same effect was observed with higher intensity when the animals were subjected to 45° and 90° inclinations.

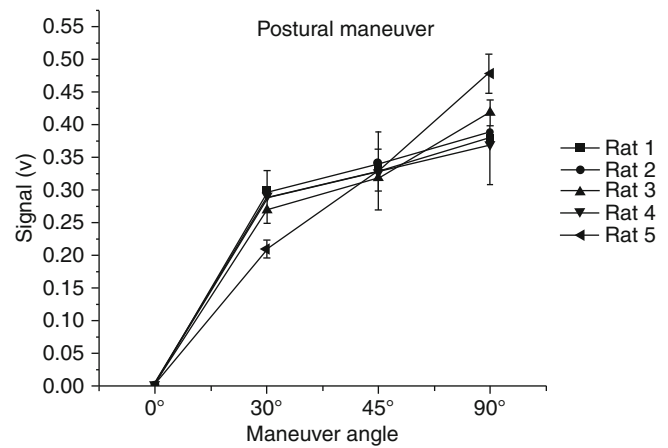


Fig. 3 Variation in the intracranial pressure through postural maneuvers. Elevation of the posterior region to increase intracranial pressure

Conclusion

1. Our proposed method shows that the hypothesis of an inextensible skull after the closure of the fontanels is not true.
2. The minimally invasive system to monitor the ICP detects the small changes (micrometers) in the skull volume.
3. Changes in the intracranial pressure lead to skull volume variations, we show this through in vitro and in vivo experimentations.
4. The relation between cranial deformation and internal pressure variation is linear, a fact that allows the minimally invasive method to monitor the ICP.

Conflict of interest statement We declare that we have no conflict of interest.

References

1. Monroe A (1783) Observations on structure and functions of the nervous system. Creech and Johnson, Edinburgh
2. Kellie G (1824) An account of the appearances observed in the dissection of two of the three individuals presumed to have perished in the storm of the 3rd, and whose bodies were discovered in the vicinity of Leith on the morning of the 4th November 1821 with some reflections on the pathology of the brain. Trans Med Chir Soc Edinb 1:84–169
3. Lundberg N (1983) The saga of the Monroe–Kellie doctrine in intracranial pressure V. In: Ishii S, Nagai H, Brock M (eds) Proceedings of the fifth international symposium on intracranial pressure. Springer, Tokyo, pp 68–76
4. Abercrombie J (1828) Pathological and practical researches on disease of the brain and spinal cord. Waugh and Innes, Edinburgh
5. Burrows G (1848) On disorders of the cerebral circulation and on the connection between affections of the brain and diseases of the heart. Lea & Blanchard, Philadelphia

6. Magendie F (1842) *Recherches anatomiques et physiologiques sur le liquide céphalo-rachidien ou cérébro-spinal*. Mequignon-Marvis, Paris
7. Fishman RA, Dillon WP (1993) Dural enhancement and cerebral displacement secondary to intracranial hypotension. *Neurology* 43:609–611
8. Barami K, Sood S, Ham SD, Canady AI (2000) Postural changes in intracranial pressure in chronically shunted patients. *Pediatr Neurosurg* 33:64–69
9. Mahfoud F, Beck J, Raabe A (2010) Intracranial pressure pulse amplitude during changes in head elevation: a new parameter for determining optimum cerebral perfusion pressure? *Acta Neurochir (Wien)* 152(3):443–450
10. Alperin N, Hushek SG, Lee SH, Sivaramakrishnan A, Lichtor T (2005) MRI study of cerebral blood flow and CSF flow dynamics in an upright posture: the effect of posture on the intracranial compliance and pressure. *Acta Neurochir Suppl* 95:177–181
11. Voermans NC (2009) Postural headache in marfan syndrome associated with spinal cysts and liquor hypotension. *Neuropediatrics* 40(4):201–204
12. Ng I, Lim J, Wong HB (2004) Effects of head posture on cerebral haemodynamics: its influence on intracranial pressure, cerebral perfusion pressure, and cerebral oxygenation. *Neurosurgery* 54:593–598

Non-Invasively Estimated ICP Pulse Amplitude Strongly Correlates with Outcome After TBI

Karol P. Budohoski, Bernhard Schmidt, Peter Smielewski, Magdalena Kaspruwicz, Ronny Plontke, John D. Pickard, Jurgen Klingelhöfer, and Marek Czosnyka

Abstract Introduction: An existing monitoring database of brain signal recordings in patients with head injury has been re-evaluated with regard to the accuracy of estimation of non-invasive ICP (nICP) and its components, with a particular interest in the implications for outcome after head injury.

Methods: Middle cerebral artery blood flow velocity (FV), ICP and arterial blood pressure (ABP) were recorded. Non-invasive ICP (nICP) was calculated using a mathematical model. Other signals analysed included components of ICP (n" indicates non-invasive): ICP pulse amplitude (Amp, nAmp), amplitude of the respiratory component (Resp, nResp), amplitude of slow vasogenic waves of ICP (Slow, nSlow) and index of compensatory reserve (RAP, nRAP). Mean values of analysed signals were compared against each other and between patients who died and survived.

Results: The correlation between ICP and nICP was moderately strong, $R=0.51$ (95% prediction interval [PI] 17 mm Hg). The components of nICP and ICP were also moderately correlated with each other: the strongest correlation was observed for Resp vs. nResp ($r=0.66$), while weaker for Amp vs. nAmp ($r=0.41$). Non-invasive pulse amplitude of ICP

showed the strongest association with outcome, with the difference between those who survived and those who died reaching a significance level of $p<0.000001$.

Discussion: When compared between patients who died and who survived mean nAmp showed the greatest difference, suggesting its potential to predict mortality after TBI.

Keywords Intracranial pressure • Non-invasive ICP • Pulse amplitude of intracranial pressure • Slow waves of intracranial pressure • Traumatic brain injury • Outcome

Introduction

Monitoring of intracranial pressure (ICP) is fundamental to the management of patients after traumatic brain injury (TBI). It has been shown that additional information may be extracted from the ICP wave, such as pulse waveform, the respiratory waves and the vasogenic slow waves, which may have implications for patient management and outcome [2, 3, 9]. Furthermore, various autoregulatory indices rely on the presence and identification of these components of the ICP signal [5].

There are, however, clinical scenarios in which invasive monitoring of ICP is either impossible or undesirable owing to its invasive character and the potential for complications. Various methods have been proposed for non-invasive assessment of ICP. These methods include monitoring of the tympanic membrane displacement [11, 14], the optic nerve sheath [6], pressure in the retinal veins [7] and various characteristics of the flow velocity (FV) signal assessed using transcranial Doppler (TCD) [10, 15]. Although these methods have been shown to estimate the ICP level reliably they are not capable of generating a continuous ICP signal and therefore have limited value in the monitoring of cerebral autoregulation. However, there are methods, predominantly utilising flow velocity characteristics that generate the ICP signal in a continuous manner [12, 13, 16].

This study aimed to assess the accuracy of non-invasive estimation of ICP and its three main components: the

K.P. Budohoski (✉), P. Smielewski, J.D. Pickard, and M. Czosnyka
Department of Clinical Neurosciences,
Division of Neurosurgery, Addenbrooke's Hospital,
Box 167, Level 4, Block A, Hills Road,
Cambridge, CB2 0QQ, UK
e-mail: kpb26@cam.ac.uk

B. Schmidt, R. Plontke, and J. Klingelhöfer
Department of Neurology,
University Hospital Chemnitz,
Chemnitz, Germany

M. Kaspruwicz
Department of Clinical Neurosciences,
Division of Neurosurgery, Addenbrooke's Hospital,
Box 167, Level 4, Block A, Hills Road,
Cambridge, CB2 0QQ, UK

Institute of Biomedical Engineering and Instrumentation,
Wrocław University of Technology,
Wrocław, Poland

Table 1 Baseline characteristics

No. of patients	No. of sessions	Age \pm SD (years)	Mean GCS \pm SD	GOS					Mean \pm SD	Monitoring time (range)
				1	2	3	4	5		
231	752	33 \pm 16	6 \pm 3	72	44	54	5	56	3 \pm 2	74.8 \pm 21.3 min (10–120 min)

GCS Glasgow Coma Scale, GOS Glasgow Outcome Scale, SD standard deviation

amplitude of ICP pulse (Amp), the amplitude of the respiratory component (Resp) and the amplitude of ICP slow waves (Slow), as well as the feasibility of estimating the pressure–volume compensatory reserve index (RAP). We have placed special emphasis on the possibility of predicting mortality using non-invasive estimates of ICP.

Materials and Methods

Multimodality brain monitoring including ICP, ABP and TCD is part of the standard clinical protocol used to care for patients after traumatic brain injury at our institution. The data were evaluated anonymously as a part of clinical audit. The study was approved by the Neurocritical Care User's Group.

The existing database of TCD recordings of patients who were admitted after TBI was evaluated. A total of 292 patients with a mean age of 33 \pm 16 years who had simultaneous ABP, ICP and TCD recordings available were identified (Table 1). ABP was monitored invasively from the radial artery using a pressure monitoring kit (Baxter Healthcare Corp. CardioVascular Group, Irvine, CA, USA). ICP was monitored via an intraparenchymal probe (Codman ICP MicroSensor, Codman & Shurtleff Inc., Raynham, MA, USA). FV was monitored bilaterally from the middle cerebral artery (MCA) using transcranial Doppler ultrasound (DWL Compumedics Ltd., Germany). The mean recording time was 74.8 \pm 21.3 min.

Non-invasive ICP estimation was carried out using a plugin for ICM+ software (Cambridge Enterprise, Cambridge, UK, <http://www.neurosurg.cam.ac.uk/icmplplus/>). This methodology utilises parameters derived from FV and ABP that act as coefficients of a transformation of ABP to FV. These coefficients are used to develop a dynamic transform function between ABP and ICP [12]. The output data comprise a pulse waveform of ICP (nICP).

The ICP waveform can be separated into components depending on the different frequencies of oscillations: the pulse waveform (50–180 cycles/min), the respiratory component (8–20 cycles/min), slow waves (Lundberg B waves) of ICP (0.3–3 cycles/min) [2, 3, 9]. The following invasive and non-invasive parameters were analysed ('n' indicates

that a parameter was calculated from the non-invasive estimation of ICP): ICP and nICP; Amp and nAmp; Resp and nResp; Slow and nSlow. Furthermore, the pressure volume compensatory reserve index (RAP and nRAP) was evaluated. RAP is calculated as a Pearson's moving correlation coefficient between mean Amp and mean ICP. The calculation is performed using a moving window of 300 s with an update period of 10 s. RAP represents the dynamic relationship between changes in ICP and changes in volume of the intracranial space, i.e., the pressure–volume curve [1, 2, 8].

For correlation between invasive and non-invasive parameters Spearman's correlation was used. For comparison between groups of patients who survived and those who died the two tailed *t*-test was used.

Results

Glasgow Outcome Scale (GOS) score was obtained from 231 patients. Estimation of nICP was possible from all 752 recordings. Figure 1 depicts examples of nICP estimations obtained using the methodology adopted.

Non-invasive estimation of ICP, nICP showed an overall moderately good correlation with the simultaneously obtained invasive measurements of ICP ($r=0.51$, $p<0.001$). The 95% prediction interval (PI) for prediction of ICP using non-invasive estimation was 17 mmHg. The components of nICP and ICP correlated moderately with each other. The highest correlation was seen for Resp vs. nResp ($r=0.66$, $p<0.001$), with a 95% PI of 0.9 mmHg, a weaker correlation was seen for Amp vs. nAmp ($r=0.44$, $p<0.001$), with a 95% PI for prediction of 2.5 mmHg, while the weakest for Slow vs. nSlow ($r=0.16$, $p<0.001$), with a 95% PI for prediction of 3.5 mmHg. nRAP showed weak correlation with RAP ($r=0.25$, $p<0.001$; Fig. 2).

When comparing groups of patients who died and those who survived a statistically significant difference between the mean values of the parameters analysed was observed for the following: ICP and nICP, Amp and nAmp, RAP and nSlow (Table 2). The biggest difference was shown for nAmp. Mean value of nAmp for patients who survived was 1.54 \pm 0.7 mmHg while for those who died it was 2.29 \pm 1.5 mmHg ($p<0.000001$).

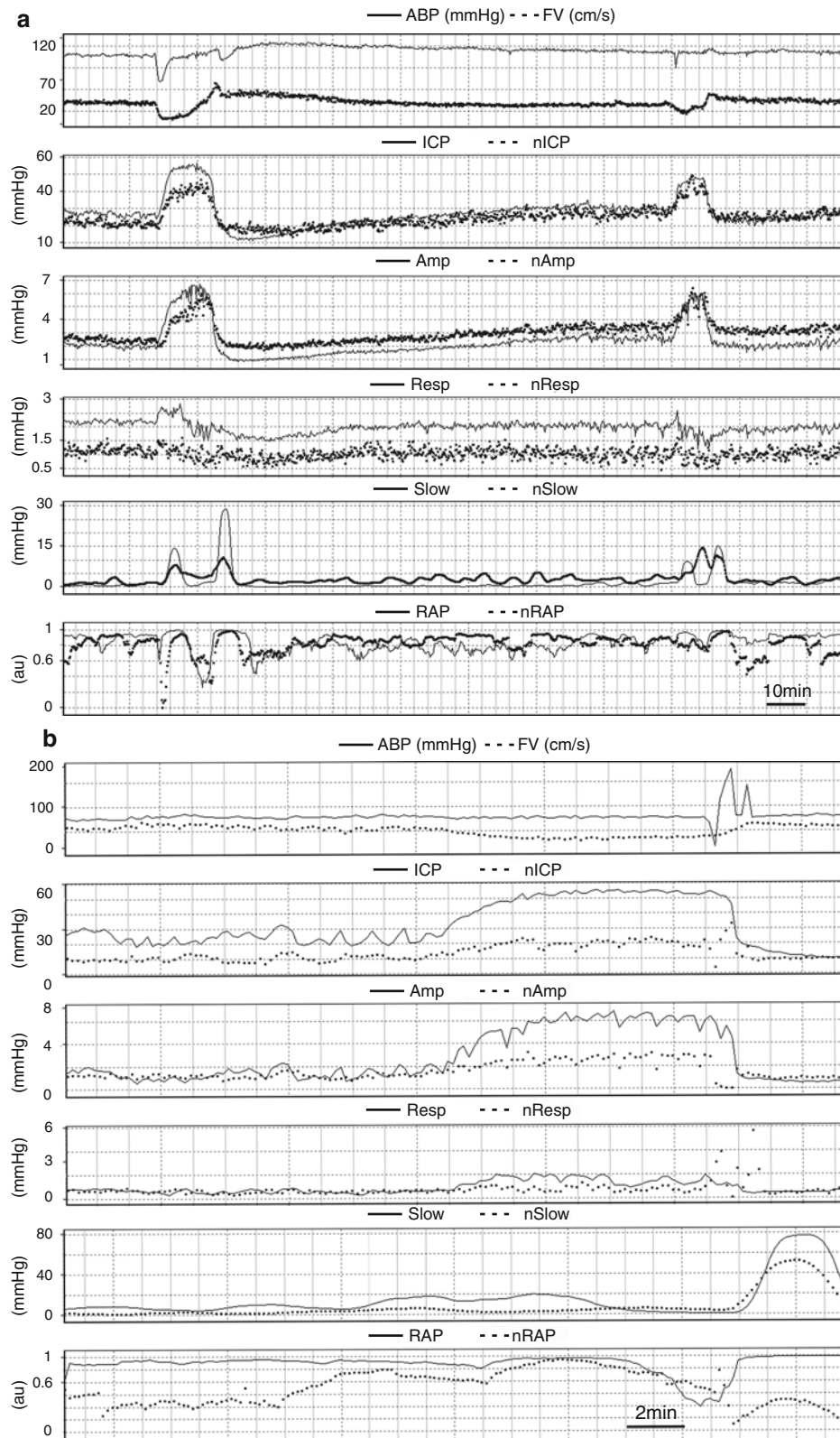


Fig. 1 Example of recordings of ABP, FV and ICP with the relevant vascular components (Amp, Resp, Slow) and the compensatory reserve index RAP (black lines) along with the non-invasive estimations (dashed lines). ABP and FV (top panels **a** and **b**) signals are used to calculate the nICP wave. Non-invasive estimation of vascular components is performed from nICP. (**a**) Good correlation of the estimated parameters with the invasively measured parameters; (**b**) poor correlation

of the invasive and non-invasive signals. *ABP* arterial blood pressure, *FV* flow velocity, *ICP* intracranial pressure, *nICP* non-invasive ICP, *Amp* pulse amplitude of ICP, *nAmp* pulse amplitude of nICP, *Resp* amplitude of the respiratory component, *nResp* amplitude of the respiratory component of nICP, *Slow* amplitude of slow waves, *nSlow* amplitude of slow waves of nICP, *RAP* pressure-volume index, *nRAP* pressure-volume index from nICP

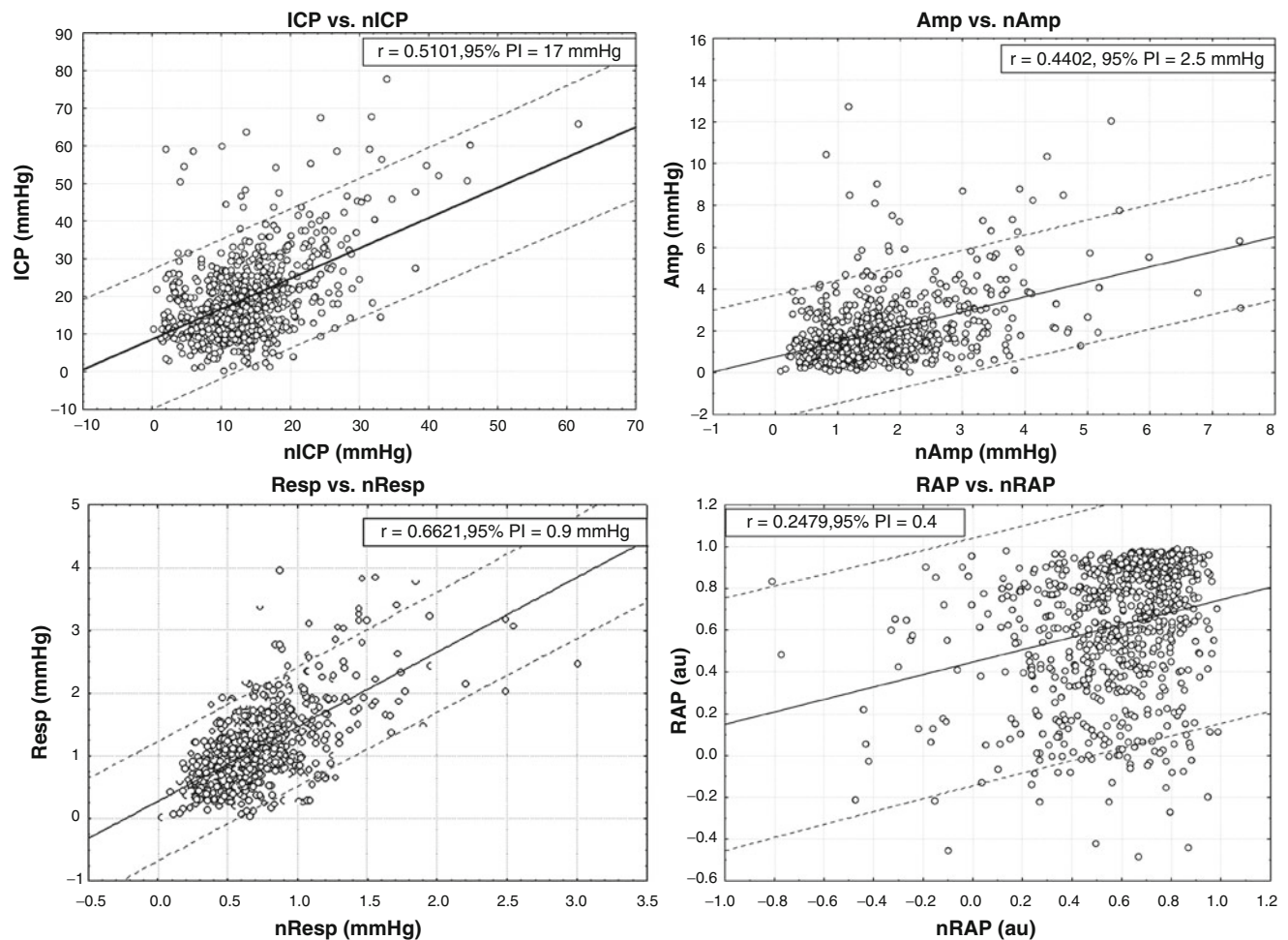


Fig. 2 Scatter plots demonstrating the correlation between nICP and ICP and the vascular components of both nICP and nICP and its components as well as the pressure–volume compensatory reserve index

RAP and nRAP estimated from the invasive ICP waveform and the nICP waveform. 95% PI 95% prediction interval

Table 2 Summary of differences in the parameters analysed between patients who died and patients who survived

Parameter	Survived (mean \pm SD)	Died (mean \pm SD)	<i>p</i>
<i>N</i>	159	72	
ICP (mmHg)	17.4 \pm 8.0	22.9 \pm 14	<0.0001*
nICP (mmHg)	12.5 \pm 5.1	15.3 \pm 8.1	<0.01*
Amp (mmHg)	1.76 \pm 1.16	2.73 \pm 2.4	<0.00001*
nAmp (mmHg)	1.54 \pm 0.7	2.29 \pm 1.5	<0.000001*
Resp (mmHg)	1.10 \pm 0.6	1.21 \pm 0.7	=0.23
nResp (mmHg)	0.68 \pm 0.27	0.75 \pm 0.42	=0.14
Slow (mmHg)	1.35 \pm 1.57	1.41 \pm 2.32	=0.83
nSlow (mmHg)	2.09 \pm 1.74	2.80 \pm 2.37	=0.022*
RAP (au)	0.63 \pm 0.25	0.53 \pm 0.28	<0.01*
nRAP (au)	0.56 \pm 0.20	0.59 \pm 0.17	=0.23

ICP intracranial pressure, nICP non-invasive ICP, Amp pulse amplitude of ICP, nAmp pulse amplitude of nICP, Resp amplitude of the respiratory component, nResp amplitude of the respiratory component of nICP, Slow amplitude of slow waves, nSlow amplitude of slow waves of nICP, RAP pressure–volume index, nRAP pressure–volume index from nICP, SD standard deviation

*Statistically significant difference

Discussion

The results obtained confirm that it is possible to estimate ICP and its components non-invasively with moderate accuracy. However, the 95%PI for prediction of ICP of 17 mmHg is not sufficient to justify routine use of nICP in clinical practice in specialised treatment centres. Analysis of the pulse waveform of ICP gives additional information in the management of patients with head injury, such as the implementation of monitoring of indices of autoregulation including RAP and PRx [2, 4]. The feasibility to estimate the major components of the ICP waveform, despite sub-optimal accuracy (95%PI for the prediction of Amp was 2.5 mmHg), is a step toward non-invasive monitoring of autoregulation.

The ICP and ICP pulse amplitude have been previously shown to be related to outcome in patients with head injury [2, 3]. The study confirms these findings and extended them to nICP and nAmp. Interestingly, it was observed that the difference in nAmp between patients who died and those who survived had a higher level of significance than that for ICP, nICP and Amp. We did not perform multivariate analysis and it is impossible to state whether nAmp was an independent factor from nICP, which is a limitation of the study. Using invasive measurements it has been demonstrated in multivariate analysis that it is in fact mean ICP and not Amp that is an independent predictor of outcome after TBI [5].

Conclusions

The results obtained demonstrate that it is possible to determine ICP non-invasively with moderate accuracy. Furthermore, it was possible to extract respiratory and pulse wave components of the intracranial pressure from the estimated nICP. Values of nICP and nAmp were significantly different when comparing groups of patients who died and those who survived. This suggests that nICP and nAmp have the potential be used to stratify the outcome in patients after traumatic brain injury.

Conflict of interest KPB was sponsored by the Graduate Travel and Research Fund of St. Catharine's College, University of Cambridge, UK and the Clifford and Mary Corbridge Trust. ICM+ software is licensed by the University of Cambridge, Cambridge Enterprise Ltd. PS and MC have a financial interest in a part of its licensing fee. Non-invasive ICP Plugin is protected by patent DE 19600983. BS and MC have a financial interest in part of its licensing fee.

References

1. Avezaat CJ, van Eijndhoven JH, Wyper DJ (1979) Cerebrospinal fluid pulse pressure and intracranial volume-pressure relationships. *J Neurol Neurosurg Psychiatry* 42:687–700
2. Balestreri M, Czosnyka M, Steiner LA, Schmidt E, Smielewski P, Matta B, Pickard JD (2004) Intracranial hypertension: What additional information can be derived from ICP waveform after head injury? *Acta Neurochir (Wien)* 146:131–141
3. Czosnyka M, Guazzo E, Whitehouse M, Smielewski P, Czosnyka Z, Kirkpatrick P, Piechnik S, Pickard JD (1996) Significance of intracranial pressure waveform analysis after head injury. *Acta Neurochir (Wien)* 138:531–541, discussion 541–532
4. Czosnyka M, Smielewski P, Kirkpatrick P, Laing RJ, Menon D, Pickard JD (1997) Continuous assessment of the cerebral vasomotor reactivity in head injury. *Neurosurgery* 41:11–17, discussion 17–19
5. Czosnyka M, Smielewski P, Timofeev I, Lavinio A, Guazzo E, Hutchinson P, Pickard JD (2007) Intracranial pressure: more than a number. *Neurosurg Focus* 22:E10
6. Geeraerts T, Duranteau J, Benhamou D (2008) Ocular sonography in patients with raised intracranial pressure: the papilloedema revisited. *Crit Care* 12:150
7. Jonas JB, Pfeil K, Chatzikonstantinou A, Rensch F (2008) Ophthalmodynamometric measurement of central retinal vein pressure as surrogate of intracranial pressure in idiopathic intracranial hypertension. *Graefes Arch Clin Exp Ophthalmol* 246:1059–1060
8. Kim DJ, Czosnyka Z, Keong N, Radolovich DK, Smielewski P, Sutcliffe MP, Pickard JD, Czosnyka M (2009) Index of cerebrospinal compensatory reserve in hydrocephalus. *Neurosurgery* 64:494–501, discussion 501–492
9. Lundberg N (1960) Continuous recording and control of ventricular fluid pressure in neurosurgical practice. *Acta Psychiatr Scand Suppl* 36:1–193
10. Ragauskas A, Daubaris G, Dziugys A, Azelis V, Gedrimas V (2005) Innovative non-invasive method for absolute intracranial pressure measurement without calibration. *Acta Neurochir Suppl* 95:357–361
11. Reid A, Marchbanks RJ, Bateman DE, Martin AM, Brightwell AP, Pickard JD (1989) Mean intracranial pressure monitoring by a non-invasive audiological technique: a pilot study. *J Neurol Neurosurg Psychiatry* 52:610–612
12. Schmidt B, Klingelhofer J, Schwarze JJ, Sander D, Wittich I (1997) Noninvasive prediction of intracranial pressure curves using transcranial Doppler ultrasonography and blood pressure curves. *Stroke* 28:2465–2472
13. Schmidt B, Czosnyka M, Raabe A, Yahya H, Schwarze JJ, Sackeler D, Sander D, Klingelhofer J (2003) Adaptive noninvasive assessment of intracranial pressure and cerebral autoregulation. *Stroke* 34:84–89
14. Shimbles S, Dodd C, Banister K, Mendelow AD, Chambers IR (2005) Clinical comparison of tympanic membrane displacement with invasive intracranial pressure measurements. *Physiol Meas* 26:1085–1092
15. Voulgaris SG, Partheni M, Kaliora H, Haftouras N, Pessach IS, Polyzoidis KS (2005) Early cerebral monitoring using the transcranial Doppler pulsatility index in patients with severe brain trauma. *Med Sci Monit* 11:CR49–CR52
16. Xu P, Kaspricz M, Bergsneider M, Hu X (2010) Improved non-invasive intracranial pressure assessment with nonlinear kernel regression. *IEEE Trans Inf Technol Biomed* 14:971–978

Realization of a Comprehensive Non-invasive Detection of Intracranial Pressure Analyzer Based upon FVEP and TCD

J.I. Zhong, Yang Li, Xu Minhui, and Zhang Yihua

Abstract Up to now, several methods, such as flash visual evoked potential (FVEP) and transcranial Doppler (TCD), have been studied with regard to assessing intracranial pressure (ICP) non-invasively. However, there are still no instruments that are readily available for non-invasive measurement of ICP in clinical practice. Based on the advantages of FVEP and TCD for ICP assessment, the two methods are synthesized to develop a specific instrument to non-invasively measure ICP more reliably and applicably, as the integration of FVEP and TCD overcomes the shortcomings of a single method of ICP measurement.

Keywords Intracranial pressure (ICP) • Flash visual evoked potential (FVEP) • Transcranial Doppler (TCD) • Instrument • Non-invasive detection

Background

Non-invasive methods of intracranial pressure (ICP) measurement, such as flash visual evoked potential (FVEP) and transcranial Doppler (TCD), have been studied a great deal in the literature [2, 6, 7]. However, owing to the limitations of these methods in the non-invasive detection of ICP, they have not been routinely used in clinical practice. In this paper, FVEP and TCD are synthetically applied in a same-instrument platform using virtual instrument technology. In this way, the applicability and precision of the non-invasive detection of ICP will be improved.

J.I. Zhong (✉) and Y. Li
College of Bioengineering, Chongqing University,
Chongqing 400030, China
e-mail: jizhong@cqu.edu.cn

X. Minhui and Z. Yihua
Department of Neurosurgery, Daping Hospital, the Third Military
Medical University, Chongqing 400042, China

Materials and Methods

FVEP

The basis of the FVEP being used to detect ICP non-invasively is the positive correlation between the latency of the N2 wave and ICP. Currently, the correlation relation is generally believed to be linearity [5, 9]. However, there is a comparatively large error in the high intracranial pressure segment in our clinical experiments. Further study shows that the correlation relation in the high pressure segment could be revised to be a power relation, which reflects the change in ICP more accurately. It can be expressed as $nICP = a \times t^b + c$, where t is the latency of the N2 wave, a is an adjustment coefficient, b is the exponentiation, and c is a constant.

TCD Method

The literature shows that the hemodynamic parameters, such as the pulsatility index (PI), resistance index (RI), systolic peak flow velocity (Vs), end-diastolic flow velocity (Vd), and mean flow velocity (Vm) are related to intracranial hypertension [1, 8]. Nevertheless, the real-time dynamic variation of ICP cannot yet be monitored by TCD. Some scholars have achieved the continuous monitoring of ICP changes by using arterial blood pressure (ABP), cerebral blood flow velocity (CBFV), and ICP in the nonlinear mapping function [3, 4]. In this paper, the hemodynamic parameters were obtained by recording and analyzing the audio signal from the TCD instrument, and computing the ICP value with the nonlinear model between hemodynamic parameters and ICP.

Instrument Realization

Virtual instrument technology, weak signal extraction technology, and biomedical technology are applied to research

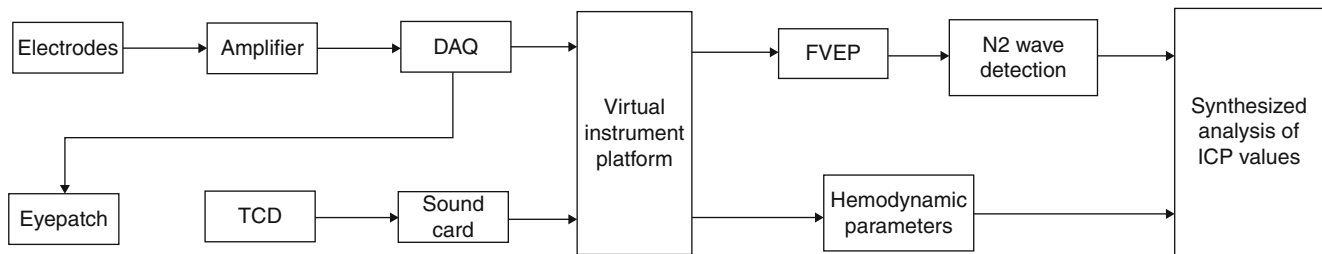
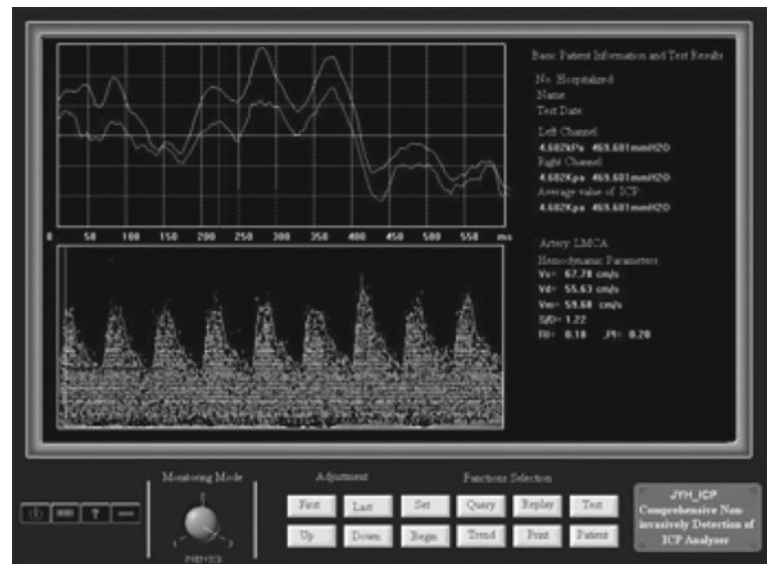


Fig. 1 The instrument diagram

Fig. 2 The instrument interface



and the comprehensive analyzer for non-invasive detection of ICP successfully developed.

The system's hardware consists of flash eye-patches, electrodes, amplifier, data acquisition card (DAQ PCI6221), PC, audio cable, and optional printer, as shown in Fig. 1. The instrument interface is shown in Fig. 2.

Key Results

We applied the instrument in the neurosurgery departments of Xinan and Daping hospitals; the experimental cases consist of 100 patients who did not have the symptoms of visual neural illness, cataract, loss of sight, and eye-ground bleeding. The average age of the patients is 41, ranging from 18 to 80, and the kinds of diseases include cerebral hemorrhage, post-surgery on tumors in the brain stem, after operating on tumors in the cerebellum, brain trauma, and hydrocephalus. The clinical applications show that the instrument can be an effective substitute for invasive ICP measurement, which can reflect the change trend of ICP correctly. The correlation coefficients

r can be larger than 0.912 between the latency of the N2 wave in the FVEP wave and the invasive ICP value. Furthermore, the TCD method is employed at the same time, and these two methods are integrated into a virtual instrument platform; therefore, the instrument can show the results of FVEP and the hemodynamic parameters of TCD in the same window. In this case, doctors can synthesize the information mentioned above and determine the change in ICP more accurately in clinical practice.

Conclusion

This instrument can non-invasively measure ICP with more reliable and applicable values, as the integration of the FVEP and TCD methods overcomes the shortcomings of a single method used for ICP measurement. However, the ICP seamless integration of a unified model for non-invasive detection should be studied based on more adequate clinical cases in order to achieve a wider range of applications for the non-invasive measurement of ICP.

Acknowledgement The present work is supported by the Scientific Research Foundation for the Returned Researchers of the Ministry of Education (Foreign Secretary Education, No.1341), and the Natural Science Foundation of Chongqing (CSTC2009BB5035).

Conflict of interest statement We declare that we have no conflict of interest.

References

1. Bellner J, Romner B, Reinstrup P (2004) Transcranial Doppler sonography pulsatility index (PI) reflects intracranial pressure (ICP). *Surg Neurol* 62:45–51
2. Desch LW (2001) Longitudinal stability of visual evoked potentials in children and adolescents with hydrocephalus. *Dev Med Child Neurol* 43(2):113–117
3. Fard PJM, Tajvidi MR, Gharibzadeh S (2007) High-pressure hydrocephalus: a novel analytical modeling approach. *J Theor Biol* 248:401–410
4. Hu X, Nenov V, Bergsneider M, Martin N (2006) A data mining framework of noninvasive intracranial pressure assessment. *Biomed Sig Process Control* 1:64–77
5. Kesler A, Vakhapova V, Korczyn A, Drory V (2009) Visual evoked potentials in idiopathic intracranial hypertension. *Clin Neurol Neurosurg* 111:433–436
6. Luerksen T (1997) Intracranial pressure: current status in monitoring and management. *Semin Pediatr Neurol* 4(3):146–155
7. Ross N, Eynon C (2005) Intracranial pressure monitoring. *Curr Anaesth Crit Care* 16:255–261
8. Schmidt B, Klingelhofer J (2002) Clinical applications of a non-invasive ICP monitoring method. *Eur J Ultrasound* 16:37–45
9. Zhang YB, Dong WW (2002) The research development of the monitoring and measuring technology of intracranial pressure. *China J Crit Care Med* 22(2):122–123

Electrophysiological Monitoring of Cochlear Function as a Non-invasive Method to Assess Intracranial Pressure Variations

Laurent Sakka, Aurélie Thalamy, Fabrice Giraudet, Thierry Hassoun, Paul Avan, and Jean Chazal

Abstract The “cochlear” aqueduct is a narrow channel connecting the subarachnoid and intralabyrinthine spaces. Through this communication, cerebrospinal fluid (CSF) pressure variations are transmitted to the intralabyrinthine space and modify the impedance of the ear. Distortion-product otoacoustic emissions (DPOAE) are sounds emitted by cochlear sensory cells in response to sonic stimulation. Cochlear microphonic potentials (CMP) express the electrophysiological activity of cochlear sensory cells. At 1 kHz, the phase of DPOAE and CMP varies according to the impedance of the ear and thus to intracranial pressure (ICP) variations. DPOAE and CMP have been shown to strictly follow ICP variations produced during infusion tests performed in the diagnosis of chronic hydrocephalus. DPOAE and CMP recordings appear to be valuable tools for monitoring ICP non-invasively.

Keywords Distortion product otoacoustic emission (DPOAE) • Cochlear microphonic potentials (CMP) • Non-invasive monitoring of intracranial pressure

Introduction

At present, the reference measurement of ICP is an intraventricular catheter connected to an external transducer. The main complications of invasive ICP monitoring are: ventricular

catheter misplacement – leading to brain lesions – and infection. Catheter misplacement mainly occurs in the case of brain edema. The probability of infection increases when the duration of monitoring increases [5]. Increased ICP has been reported to alter the results of audiological tests [8]. In addition, ICP variations induced by postural changes lead to acoustic impedance modifications and changes in cochlear responses to sound [1]. The cochlear aqueduct is a narrow channel connecting subarachnoid to intralabyrinthine spaces. Through this communication, ICP and intralabyrinthine pressure (ILP) equalize in static conditions [3]. An ICP increase induces an ILP increase, which, by pushing the stapes footplate outward, increases the stiffness of the ossicular chain and cochlea [2, 3]. The phase of two signals – namely, distortion-product otoacoustic emissions (DPOAE) and cochlear microphonic potentials (CMP) – produced by cochlear sensory cells in response to sonic stimulation vary according to the ear’s impedance. DPOAE and CMP are routinely collected in audiological clinical practice. DPOAE and CMP phase shift have been reported to be proportional to ICP variations at frequencies near 1 kHz. The goal of this work is to evaluate a non-invasive method of ICP monitoring relying on the electrophysiological monitoring of cochlear sensory cells.

Materials and Methods

Distortion-product otoacoustic emissions are tiny sounds emitted backward into the external auditory meatus by one category of cochlear sensory cells, the outer hair cells, in response to stimulation by a pair of pure tones at neighboring frequencies f_1 and f_2 . The DPOAE at $2f_1 - f_2$ is characteristic of outer hair cell activity around the cochlear place coding for f_2 . For this activity to exist, hearing sensitivity has to be near normal around f_2 , which may not be the case if a subject suffers from advanced presbycusis or from impaired middle ear function. The detection of DPOAEs suitable for monitoring ICP requires the emission of two tones for a few seconds at $f_1 = 1$ kHz and $f_2 = 1.2$ kHz, both of them at 70 dB SPL to ensure a comfortable signal-to-noise ratio. The phase of the DPOAE at 0.8 kHz is extracted

L. Sakka (✉) and J. Chazal
Department of Neurosurgery and IGCNC (Image-Guided Clinical Neuroscience and Connectomics), Clermont University,
UFR Médecine, 63001, Cedex 1, Clermont-Ferrand, France
e-mail: lsakka@chu-clermontferrand.fr

A. Thalamy, F. Giraudet, and P. Avan
Department of Sensory Biophysics, University School of Medicine,
63001, Cedex 1, Clermont-Ferrand, France

T. Hassoun
Department of Sensory Biophysics, University School of Medicine,
63001, Cedex 1, Clermont-Ferrand, France

Echodia, Biopole Clermont-Limagne, 63360
Saint-Beauzire, France

and it has been shown that its shifts relative to a reference recording are proportional to the change in ICP that has occurred since the reference was collected [10].

Cochlear microphonic potentials are electric signals radiated by cochlear outer hair cells reflecting their mechanotransduction currents when excited by a sound stimulus. CMP can be collected between a golden-coated electrode placed inside the external auditory meatus and a skin electrode placed on the forehead, another skin electrode being the ground reference. The technique is similar to auditory evoked potentials recording (that is, synchronous averaging of electroencephalographic signals elicited by repeated sound stimuli and pre-amplified 100,000 times). The detection of a CMP suitable for monitoring ICP requires the emission of one tone for a few seconds at $f = 1$ kHz around 80 dB SPL to ensure a comfortable signal-to-noise ratio. The phase of the CMP at 1 kHz is extracted and it has been shown that, similar to DPOAEs, its shifts relative to a reference recording are proportional to the change in ICP that has occurred since the reference was collected [10]. It has also been shown that when ICP changes, the resulting DPOAE shift is twice the CMP shift in the same ear [3].

Sonic stimulation and DPOAE-CMP recordings were performed by a device (Echodia™) designed to be put in place and sealed into the external auditory meatus on the side that induced the largest DPOAE or CMP signals at around 1 kHz. The sonic stimulation was generated by a miniature loudspeaker at 1 kHz and 80 dB SPL for CMP, and 1 and 1.2 kHz, 70 dB SPL – see above – for DPOAEs. DPOAEs were recorded with the miniature microphone contained in the acoustic probe and CMP with a golden-coated electrode applied against the external auditory meatus wall.

Two experiments were carried out to study DPOAEs and CMPs phase shift according to ICP variation:

1. DPOAEs were recorded along ICP variation produced by postural changes (upright, supine and head-down postures) in eight healthy volunteers with normal hearing. DPOAEs are recorded, amplified, digitalized, and sent to a processor computing the phase at a rate of about one measure every 4 s.
2. DPOAEs and CMPs were recorded along infusion tests performed for the diagnosis of chronic hydrocephalus in adults. The protocol used in our institution consists in injecting a saline solution into the CSF space through an external lumbar catheter at a constant rate of 80 mL/h. Patients undergo neuroleptanalgesia with midazolam–sufentanyl administered intravenously. CSF pressure is continuously monitored by an external transducer connected to the lumbar catheter.

Results

In healthy volunteers, DPOAE phase recordings show a shift in accordance with ICP modulations obtained by postural changes: the postural phase shift (Fig. 1). The average phase

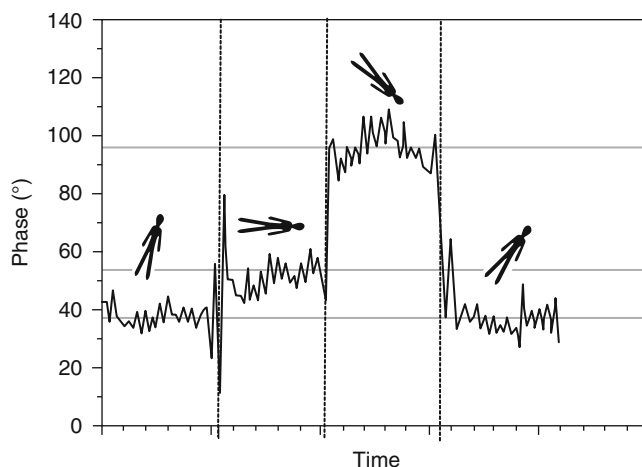


Fig. 1 Distortion-product otoacoustic emissions (DPOAE) postural phase shift. Variations of the phase shift according to intracranial pressure (ICP) modifications induced by postural changes

shift between upright and supine horizontal positions was 9.4° (standard error: 3.4°), and the average shift between the upright and head-down (-20°) body positions was 34.1° (standard error: 8.5°).

The influence of ICP on the DPOAE phase was confirmed by recordings during infusion tests in six patients, showing a phase shift proportional to ICP variations (Fig. 2)

There was a linear correlation between the DPOAE phase shift and ICP variation such that a phase shift of 10° was related to a pressure variation of about 5 cm of water. When CMP were recorded according to the same protocol, we observe a similar linear correlation between the CMP phase shift and the ICP variation, but the CMP phase shift is about the half of the DPOAE phase shift for the same ICP variation (Fig. 3).

Discussion

The cochlear aqueduct is a narrow channel in the petrous portion of the temporal bone connecting the subarachnoid space of the posterior cranial fossa to the *scala tympani* of the cochlea. In static conditions, this communication allows CSF and intralabyrinthine pressures to equalize. This is the reason why ICP variations have been reported to induce auditory symptoms such as tinnitus and hearing losses in different conditions: after lumbar puncture or ventriculo-peritoneal shunts, and at high altitude. Although there are some discrepancies among the publications dealing with the patency of the aqueduct [9, 11, 12], the most thorough anatomical study performed on 101 temporal bones demonstrated that the aqueduct was patent in 97% of the specimens. The cochlear aqueduct patency did not correlate with age [6]. Through this communication the ICP increase is transmitted to the intralabyrinthine space. Therefore, a consecutive ILP

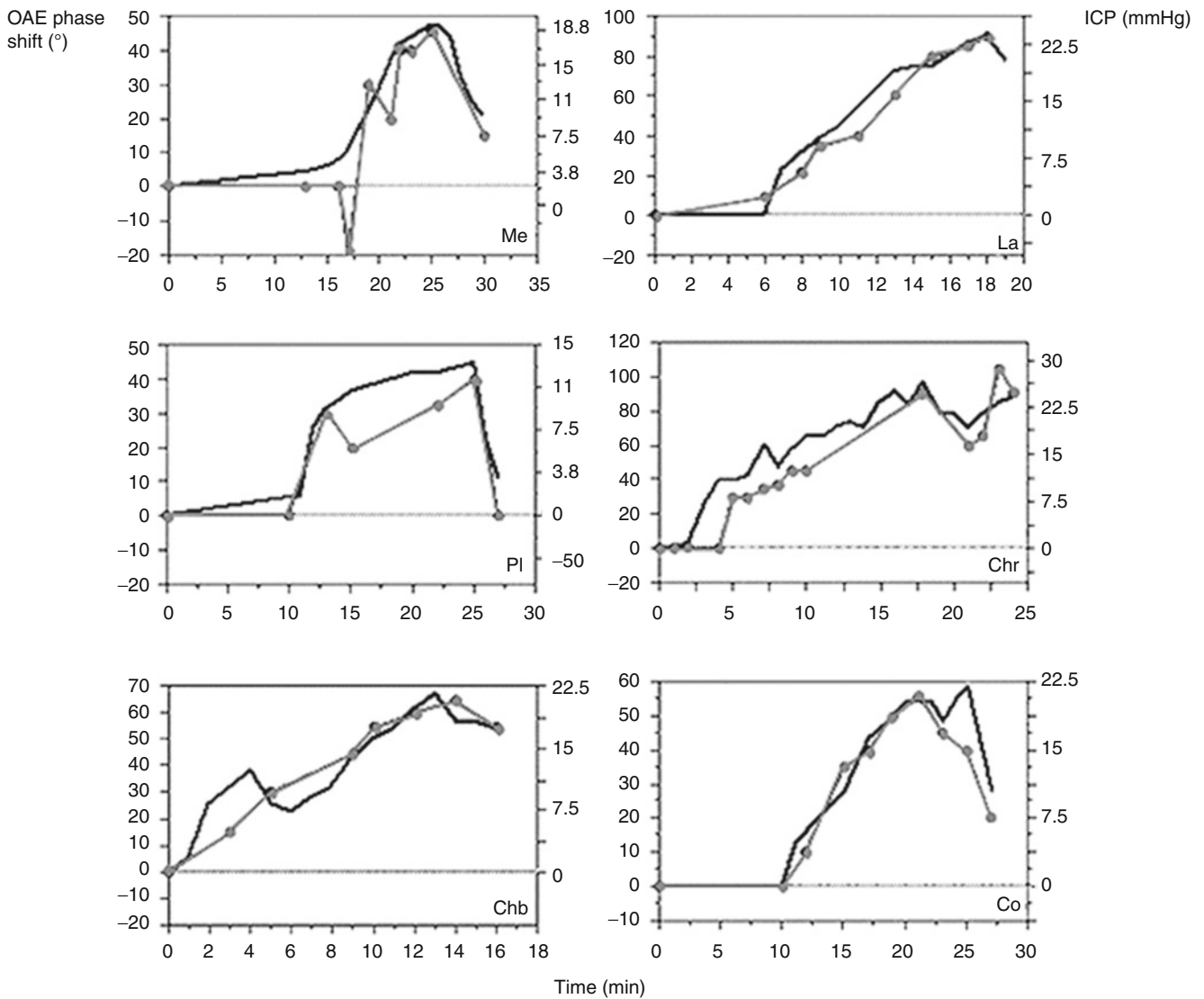


Fig. 2 DPOAE recordings along infusion tests. DPOAE phase variations follow ICP increase. Constant infusion rate of 80 mL/h

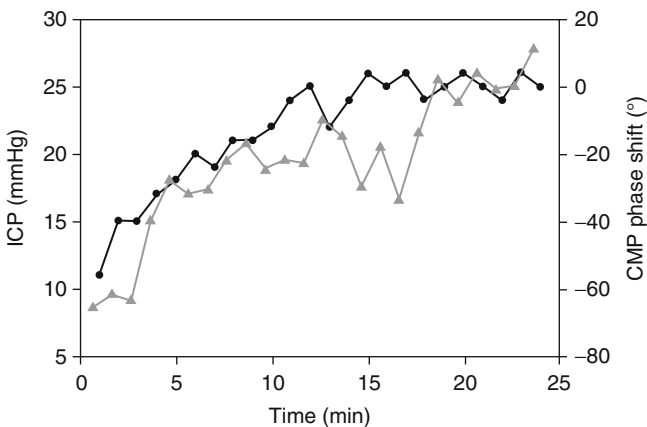


Fig. 3 Cochlear microphonic potentials (CMP) recording along infusion test. CMP phase variations follow ICP increase. Constant infusion rate of 80 mL/h

increase displaces the stapes footplate outward, which in turn increases the stiffness of the ossicular chain and cochlea [3, 7]. The modification of the ear's impedance following ICP variations determines DPOAE and CMP phase shifts. When the sonic stimulus is transmitted to the inner ear through the ossicular chain, the phase undergoes a first shift proportional to the stiffness of the ossicular chain, and when the otoacoustic emissions generated by the outer hair cells come back toward the acoustic probe, they undergo a second phase shift. In experimental studies performed by Büki in which DPOAE were recorded during invasive ICP measurements, a linear regression was reported between ICP variations and the DPOAE phase shift, the relation being: $\Delta\text{ICP} = .20 \times \text{DPOAE Phase Shift}$ [3]. This proportional relationship remains true at intervals of ICP change of more than 30 cm of water [2]. The sensitivity of the DPOAE phase shift

to ICP changes is maximal at around 1 kHz. The drawbacks of DPOAE recordings are their sensitivity to sonic surroundings, making it difficult to have a suitable signal-to-noise ratio and their vulnerability to sensorineural hearing loss, which excludes about 30% of ageing patients from this type of monitoring [4]. CMP generated by cochlear sensory cells reflect the mechanotransduction currents of the outer hair cells when excited by a sonic stimulus. This electric signal, collected between two skin electrodes, is stronger than DPOAE with a better signal-to-noise ratio, and is less influenced by the sonic environment. Moreover, CMP are less affected than DPOAEs by impaired hearing, and pathological conditions such as presbycusis, and the consequences of Menière's disease hardly affect CMP recordings [4]. Recently, CMP have been studied according to ICP variations in infusion tests. CMP phase shift, proportional to ICP variations, is about half that of DPOAEs for a given pressure change because the signal generated by the cochlear outer hair cells, is directly transmitted to the skin electrodes, without modification by the ossicular chain. DPOAE and CMP recordings for the monitoring of ICP still require initial calibration from which the phase shift can be related to ICP variation. DPOAE and CMP phase shifts are related to ICP variations and not to absolute values of ICP. Therefore, at the present time, non-invasive ICP measurements relying on cochlear function monitoring must begin with an initial invasive assessment of ICP. Some data still remain to be defined such as the influence of environmental factors, physiological factors, and medicines on CMP production in relation to ICP variations.

Conclusion

The electrophysiological recordings of the cochlear sensory cells provide promising methods for non-invasive ICP monitoring, even though the drawback of those techniques is that calibration in order to relate initial cochlear responses to an initial ICP value is mandatory. The influence of environmental factors, ageing, biological factors, and drugs on cochlear sensory

cell functioning needs to be studied before their application in clinical practice; yet, the fact that patients serve as their own controls reduces the variability of ICP estimations.

Acknowledgements Echodia has provided the device for DPOAE and CMP recordings. The study has been entirely funded by grant ANR-08-ETEC-001-01.

Conflict of interest statement We declare that we have no conflict of interest.

References

1. Allen GW, Habibi M (1962) The effect of increasing cerebrospinal fluid pressure upon cochlear microphonics. *Laryngoscope* 72:423
2. Avan P, Büki B, Maat B, Dordain M, Wit HP (2000) Middle ear influence on otoacoustic emissions. I: non-invasive investigation of the human transmission apparatus and comparison with model results. *Hear Res* 140:189–201
3. Büki B, Avan P, Dordain M, Lemaire JJ, Chazal J, Ribari O (1996) Otoacoustic emissions: a new tool for monitoring intracranial pressure changes through stapes displacements. *Hear Res* 94:125–139
4. Büki B, Giraudet F, Avan P (2009) Non-invasive measurements of intralabyrinthine pressure changes by electrocochleography and otoacoustic emissions. *Hear Res* 251:51–59
5. Ghajar J (1995) Intracranial monitoring techniques. *New Horiz* 3:395–399
6. Gopen Q, Rosowski JJ, Merchant SN (1997) Anatomy of the normal human aqueduct with functional implications. *Hear Res* 107:9–22
7. Klockhoff I, Anggard G, Anggard L (1964) The acoustic impedance of the ear and cranio-labyrinthine pressure transmission. *Int J Audiol* 4:45
8. Philips AJ, Farrell GB (1992) The effect of posture on three objective audiological measurements. *Br J Audiol* 26:339–345
9. Ritter FN, Lawrence M (1965) A histological and experimental study of cochlear aqueduct patency in the adult human. *Laryngoscope* 65:1224–1233
10. Traboulsi R, Avan P (2007) Transmission of infrasonic pressure waves from cerebrospinal to intralabyrinthine fluids through the human cochlear aqueduct: non-invasive measurements with otoacoustic emissions. *Hear Res* 233:30–39
11. Waltner JG (1948) Barrier membrane of the cochlear aqueduct. *Arch Otolaryngol* 47:656–669
12. Wlodyka J (1978) Studies on cochlear aqueduct patency. *Ann Otol Rhinol Laryngol* 87:22–28

Autoregulatory Model Comparison and Optimisation Methodology

Martin Shaw, Ian Piper, and Michael Daley

Abstract Cerebral pressure autoregulation (AR) is a process by which blood flow is kept constant over a specific cerebral perfusion pressure (CPP) range. There have been a number of advances in recent years in the monitoring and modelling of this physiological variable; however, there has been very little work done on the comparison or optimisation of some of the existing models in clinical use today: pressure reactivity index, highest modal frequency techniques and compartmental modelling. Presented here is a methodology for the comparison and optimisation results for these main AR models. By simple mathematical manipulation of the original modelling end points each model can be converted into a form that is directly comparable to the others. Using a standardised data set with known gold standard AR status indications, the models can then be readily assessed. As a consequence each of the models can then be optimised to maximise specificity and sensitivity.

Keywords CBF autoregulation • Intracranial pressure • Mathematical modelling • Head trauma

Introduction

The application of mathematical modelling to the detection of specific events, such as loss of cerebral blood flow autoregulation, or to the prediction of clinical outcome have been investigated in a number of specific patient populations.

Although some success has been achieved with time-series modelling in specific disease areas, there has not been a systematic study comparing different modelling approaches within a given population of patients.

Cerebral autoregulation is the process by which cerebral blood flow is constantly maintained over varying cerebral perfusion pressure. It is important to the treatment and outcome of TBI patients as the treatment planning might vary depending upon whether or not autoregulation is intact. The non-surgical management of patients with traumatic brain injury (TBI) focuses upon the prevention of secondary insults such as drops in blood pressure (BP) or increased intracranial pressure (ICP). The latter (raised ICP) is of particular concern as increases in ICP will decrease cerebral perfusion pressure ($CPP = BP - ICP$) and can lead to decreases in cerebral blood flow (CBF). Cerebral autoregulation is a physiological mechanism that maintains CBF constant in the face of changing CPP although it can become impaired following brain injury. Currently, there is considerable clinical interest in using an index of autoregulation (AR) in the management of raised ICP and reduced CPP and to this end a number of mathematical models to predict the state of the AR process have been proposed.

Model Comparison

Literature on approaches to comparing these types of models, in terms of their relative accuracy, is sparse. This could be attributed to the difficulty in comparing physiological models that include known autoregulatory parameters with other models that focus primarily on generating an indexed autoregulatory status using a “black box” approach regardless of the underlying physiology. Another difficulty concerns the lack of high quality data upon which to compare models. Without high-frequency “gold standard” data on autoregulatory status, any model could be placed at a disadvantage during such a comparison; furthermore, a major problem in model comparison concerns the range of tests that can be used for comparison with test choice key to the

M. Shaw (✉) and I. Piper
Department of Clinical Physics,
Institute of Neurological Sciences, Sothorn General Hospital,
1345 Govan Road,
Glasgow, Scotland, G514TF, UK
e-mail: martin.shaw@nhs.net

M. Daley
Department of Electrical and Computer Engineering,
University of Memphis,
Memphis, TN, USA

meaningful comparison of the models. One approach we propose would be to perform model comparison on a related statistic, but not necessarily one that is originally generated by any of the models. For example, by taking two models, one of which outputs a direct measure of autoregulation via an index and a second model that outputs a time series trend for intracranial pressure, both of these could generate a third statistic to a known value for autoregulation. This could then be used as the basis for a direct comparison of the models.

Study Aims

This paper reports on the results of our application of this approach to autoregulation model comparison focused upon three models. First, the pressure reactivity index (PRx) [2], second, the highest modal frequency (HMF) [3] analysis, and third, a reworked Ursino model [6].

For each model a normalised autoregulatory parameter will be generated to ease comparison and a high-resolution data set will be used to ensure that all model comparisons are not biased by data sampling rate. We also report on analyses leading to the best choice for model comparison statistics and finally a method of optimising the data window size to yield the best performance of a given model for estimating the status of autoregulation. Models will be compared in terms of performance at detecting baseline autoregulation status from a data set generated from an experimental model of autoregulation disruption based upon pial vessel imaging before and after fluid percussion injury. Models will also be compared against each other as well as before and after application of our data window size optimisation method.

Methods

Reworked Ursino Model

Ursino's original model is a two-compartment model where autoregulation can be thought of as a combination of three processes affecting arterial-arteriolar compliance for a given percentage change in CBF. The first process is the autoregulatory gain, the next is the static sigmoidal autoregulatory response function and the last component is a low pass transfer function. The gain parameter G is essentially a continuous index for cerebral autoregulation. With this in mind Ursino's original model has been rearranged to predict G .

HMF Autoregulatory Predictor

The HMF method [3] using a technique called modal analysis found that when cerebral arterial flow regulation is intact, changes in the highest modal frequency (HMF) are inversely related to changes in cerebral perfusion pressure (CPP). In contrast, when the arterial-arteriolar vascular bed demonstrates autoregulatory impairment, i.e. when CBF shows a CPP dependency, changes in HMF are directly related to changes in CPP.

PRx

The PRx, or pressure reactivity index, described by Czosnyka et al. [2] is a moving Pearson's correlation between ABP and ICP. This method looks at the amount of correlation between the two variables and the decision on whether there is pressure reactivity or not is based on a pressure-passive model. If the correlation is positive, i.e. the ICP is reacting passively, with ABP, then it can be assumed that the subject is not autoregulating and vice versa.

Model Comparison and Optimisation

We used a high-quality data set for model comparison, which consisted of six piglets with a cranial window preparation and a fluid percussion injury model with ICP, ABP and middle cerebral artery (MCA) flow velocity data collected at 250 Hz. The protocol included a number of ABP challenges both before and after injury. A cranial window preparation using pial artery imaging allowed the pial vessel diameter to be measured before and after BP challenge as well as before and after fluid percussion injury. A pressure-passive increase in pial vessel diameter was used as an indication of autoregulation impairment. Across all six animals there were 57 measures of autoregulation: 25 intact and 32 impaired. This data set was prepared so that there were a similar number of calculated results for each model based on a prediction for the autoregulatory state every 6 s. The points at the start of each BP challenge were selected for comparison, to minimise the system compromise from the challenges themselves. For all of the comparison data we selected only the first hour of data before and after fluid percussion injury with the intention that this should make the testing more comparable to a binary intact verses impaired status.

The choice of comparison methodology was driven by the data set and we have selected the Matthews correlation coefficient (MCC) method as the fairest model comparison test. To compare the models using the MCC, two approaches

Table 1 Model predictive ability using Matthews correlation coefficient (MCC)

Model	Baseline MCC	Optimised MCC	Optimised window (min)
PRx	0.09	0.25	66
HMF	0.09	0.55	72
Ursino	0.3	n.a.	n.a.

PRx pressure reactivity index, *HMF* highest modal frequency

Table 2 Intermodel comparisons using MCC

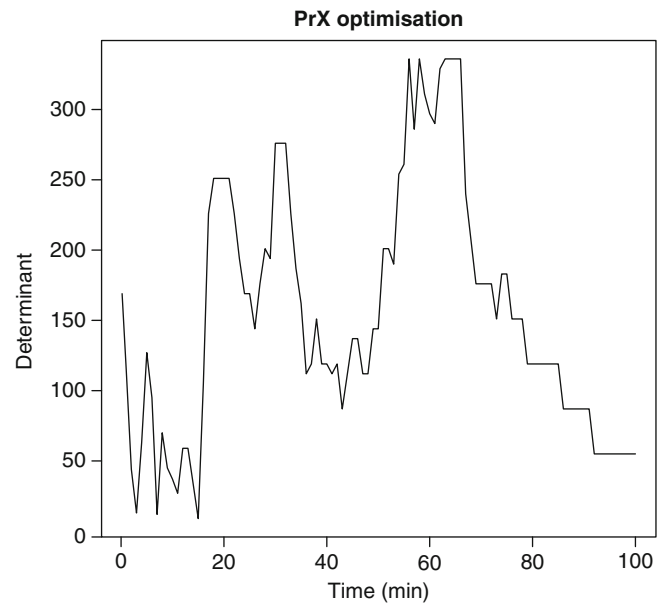
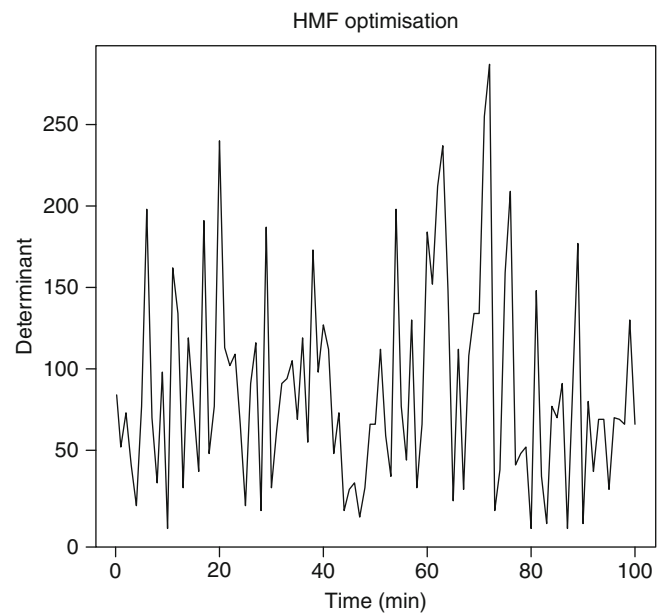
Intermodel comparison	Baseline MCC	Optimised MCC
PRx compared with the HMF	-0.5477226	0.4714045
PRx compared with modified Ursino	-0.75	n.a.
Modified Ursino compared with HMF	0.7302967	n.a.

were used. The first was to base the MCC against the known autoregulatory status derived from the pial artery window of the piglet. This will give an MCC figure both before and after the optimisation. The second was to compare each of the models against each other to produce a relative inter-model comparison.

Each of the models assessed have at their core a window of data over which an analysis or comparison is occurring. For the PRx it is the amount of data used to determine the correlation function, with the HMF it is the collected data over which the slope of the line of the modal frequency changes with time. The modified Ursino model, while it has a window over which data is being processed, does not lend itself well to this method of optimisation so we have focused on optimising only the PRx and HMF models. The optimisation itself is carried out using a quasi-Newton method [4]. This method maximises the determinant of the sensitivity-specificity matrix calculated at a variable window size for each of the models in turn. The use of the determinant is merely for efficiency as there is no need to normalise this to calculate the MCC when optimising to a maximum value. The window sizes involved in the calculations are measured in the number of points used in the calculation.

Analysis and Results

The baseline comparisons are shown in Table 1 and inter-model comparisons in Table 2. From Table 1 the MCC results from the comparison between the model prediction and the known autoregulatory status were for the HMF 0.09 and the PRx 0.09, while the reworked Ursino showed an MCC of 0.3. The inter model comparison results from Table 2 showed

**Fig. 1** Pressure reactivity index (*PRx*) model confusion matrix determinant vs window size**Fig. 2** Highest modal frequency (*HMF*) model confusion matrix determinant vs window size

slight agreement between the HMF and the reworked Ursino model and a general disagreement between the PRx and the other two models. The calculated optimal window size values for both the PRx and HMF were 60 and 71 min for each of the models respectively (Table 1). These optimal points can clearly be seen in the graphs of window size against determinant (Figs. 1 and 2). Post-optimisation the baseline model comparison can be seen in Table 1 and the inter model comparison between the HMF and the PRx in Table 2.

Table 1 shows that post-optimisation the MCC for the PRx compared with the baseline known AR status is 0.25 and for the HMF it is 0.55, which, if compared with the baseline, shows that there is an increase in predictive power of between 200% and 600% after optimisation. From Table 2 it can be seen that the MCC is now equal to 0.47, which is a distinct improvement over the non-optimised result.

Discussion

An important step in any comparative methodology is to standardise the data set on which to compare the models. First, it has to have a known AR state so that one can definitively state whether the status is impaired or intact. Second, it has to be of a high enough temporal resolution to evaluate all of the models so as not to disadvantage the model under comparison. The data set used in the study does meet these key criteria, making it a viable candidate for the analysis; however, the question could be raised whether the end points used are correctly chosen. With this data set [3], as the AR predictions are derived from the pial artery response recorded via the cranial window, there is a small area of observation with a small number of vessels in each case. This could introduce a number of complications, including whether the chosen vessels are representative of the whole pial vasculature and as a consequence may not be a valid global measure of autoregulation. With this data set, the fluid percussion injury model, which has been used in many studies is considered a standard method for impairing AR and has been shown to have a global effect on the physiology [5] even though in the collected data set it is monitored very locally via the pial artery–cranial window methodology. Other considerations with this model, such as the inter-subject variability and vessel variability, have been addressed by Coles et al. [1].

Another key methodological issue is the choice of a comparison test. There are a large number of options available for analysing the prediction data. The first and possibly most crucial piece of information governing the choice of test concerns the output of the models, actual or surrogate, as this influences the basic range of test significantly. If the simple AR prediction, intact or impaired, has been chosen as the surrogate target, then only tests on nominal data will be applicable.

From the results of the model comparisons (Table 1) it is easy to see that with the initial model configurations taken from their respective original papers the predictive accuracy of all of the models is quite poor. This could be attributed in part to the data set used in respect of the variability in the AR assessment with the pial artery–cranial window method, but also the influence of data selection bias in order to reduce BP challenge manipulation interference in the data used for comparison.

As the predictive accuracy is lower than expected for all of these models it leads to the question, could the predictive accuracy of most of these models be increased by the correct choice of window over which the data are sampled and analysed? The results from the optimisation of the HMF and PRx can clearly be seen to have an effect on the predictive ability of the models (Table 1) and the inter-association of the two models (Table 2). With a methodology now in place for both model comparison and optimisation there is a need to validate this approach on an alternative data set, particularly one where there is a longer monitoring period post-injury to allow investigation of optimisation windows beyond that of 2 h. Application of single data set validation techniques like the K-fold cross-validation approach, frequently used in neural network training and testing, would not be appropriate here because of the dependence of autoregulatory status on time post-injury.

Conclusion

This work has provided a methodological approach to optimising data window size for testing models of autoregulation. We have also made a case for the use of MCC as a method of choice for model comparison. In the data set we had available (Piglet data with fluid percussion injury using pial artery visualisation), Ursino's physiological model performed best overall without any form of data window size optimisation. Post-data window size optimisation, only the data-driven models could be compared, of which Daley's HMF model showed better performance than the PRx model as a measure of the status of autoregulation. In view of the large variation observed in the autoregulation status observed with this data set, further model comparison studies with other data sets and methods for testing dynamic autoregulation are warranted.

Conflict of interest statement We declare that we have no conflict of interest.

References

1. Coles JP, Fryer TD, Bradley PG, Nortje J, Smielewski P, Rice K, Clark JC, Pickard JD, Menon DK (2006) Intersubject variability and reproducibility of 150 PET studies. *J Cereb Blood Flow Metab* 26:48–57
2. Czosnyka M, Piechnik S, Richards HK, Kirkpatrick P, Smielewski P, Pickard JD (1997) Contribution of mathematical modelling to the interpretation of bedside tests of cerebrovascular autoregulation. *J Neurol Neurosurg Psychiatry* 63:721–731
3. Daley ML, Pourcyrous M, Timmons SD, Leffler CW (2004) Assessment of cerebrovascular autoregulation: changes of highest

- modal frequency of cerebrovascular pressure transmission with cerebral perfusion pressure. *Stroke* 35:1952–1956
4. Nocedal J, Wright S (2006) *Numerical optimization*, 2nd edn. Springer, Berlin/New York. ISBN 978-0-387-30303-1
 5. Shibata M, Einhaus S, Schweitzer JB, Zuckerman S, Leffler CW (1993) Cerebral blood flow decreased by adrenergic stimulation of cerebral vessels in anesthetized newborn pigs with traumatic brain injury. *J Neurosurg* 79:696–704
 6. Ursino M, Lodi CA (1997) A simple mathematical model of the interaction between intracranial pressure and cerebral hemodynamics. *J Appl Physiol* 82:1256–1269

Assessment of Cerebral Autoregulation from Respiratory Oscillations in Ventilated Patients After Traumatic Brain Injury

Philip M. Lewis, Peter Smielewski, Jeffrey V. Rosenfeld, John D. Pickard, and Marek Czosnyka

Abstract Phase shift (PS) between oscillations in arterial blood pressure (ABP) and transcranial Doppler (TCD) cerebral blood flow velocity (CBFV) is thought to describe cerebral autoregulation. Ventilated patients show high amplitude and regular respiratory oscillations in ABP and CBFV, allowing reliable PS measurement. We analysed recordings of ABP, CBFV and intracranial pressure (ICP) from 187 TBI patients treated at Addenbrooke's Hospital, Cambridge, UK, from 1993 to 1998. Monitored data were recorded and PS, TCD autoregulation (Mx) and pressure reactivity (PRx) were calculated using ICM+. PS was computed by peak detection in the ABP/CBFV cross-spectrum. Recordings with low coherence (<0.5), unstable respiratory rate (RR), or PS wraparound were excluded. Median RR was 14 bpm (range 10–20 bpm). Group median PS was 13° (range -37 – 56°). Average PS (PSa) correlated with RR (Spearman's $R = -0.302$, $p < 0.01$, and cerebral perfusion pressure ($R = -0.373$, $p < 0.01$). Correlations of PS with Mx and PRx were weak but significant ($p < 0.01$). Kruskal–Wallis test for outcome vs. PS was non-significant (PSa: $p = 0.14$, minimum PS (PSm): $p = 0.27$). Mann–Whitney test for mortality vs. PS was significant ($p < 0.05$) for PSm only. Respiratory PS responds to changes in CPP and RR and correlates weakly with CA. Respiratory PS may have some prognostic value for patients with TBI.

Keywords Cerebral perfusion pressure • Traumatic brain Injury • Cerebral autoregulation • Transcranial Doppler

P.M. Lewis (✉) and J.V. Rosenfeld
Department of Neurosurgery, Alfred Hospital,
Prahran, VIC 3181, Australia

Department of Surgery,
Monash University,
Prahran, VIC, Australia
e-mail: p.lewis@alfred.org.au

P. Smielewski, J.D. Pickard, and M. Czosnyka
Department of Neurosurgery, Addenbrooke's Hospital,
Cambridge, UK

Introduction

The calculation of phase shift between slow oscillations in arterial blood pressure (ABP) and cerebral blood flow velocity (CBFV) in the middle cerebral artery (MCA) as a measure of cerebral autoregulatory capacity is well described in the literature [1, 4, 10–12, 17]. The method draws on the hypothesis that cerebral autoregulation behaves principally as a high-pass filter, damping out slow fluctuations in ABP as a mechanism to prevent entirely pressure-dependent cerebral blood flow. Previous studies have examined ABP/CBFV phase shift (PS) at low (<0.07 Hz) and high (0.07–0.3 Hz) frequencies in clinical settings such as carotid stenosis [15], subarachnoid haemorrhage [10] and traumatic brain injury [11, 12]. The general consensus from the bulk of the literature on this topic is that reduced PS indicates impaired autoregulation and correlates with poor outcome.

Given the typically low coherence between ABP and CBFV at frequencies below 0.07 Hz even during forced manoeuvres [6], the PS method is most useful when oscillations in ABP and CBFV are present at higher frequencies. Oscillations in ABP and CBFV can be seen occurring spontaneously at 0.1 Hz, and are thought to be generated independently of those seen in recordings of ABP [9]. These oscillations may be augmented or supplanted by those produced by purposefully breathing at the same rate, producing higher amplitude swings in ABP that provoke autoregulatory adjustments in cerebrovascular resistance [4].

Intubated and ventilated patients show regular, large amplitude swings in ABP that are similar to those elicited by simple deep breathing. Moreover, typical ventilatory rates lie in the region put forward by some authors as a pseudo 'transition band' of the putative high pass filter that is dynamic cerebral autoregulation [5, 17]. Accordingly, we analysed ABP/CBFV PS at the respiratory frequency in a previously studied cohort of ventilated traumatic brain injury patients, to examine patterns of PS change and their relationships to outcome.

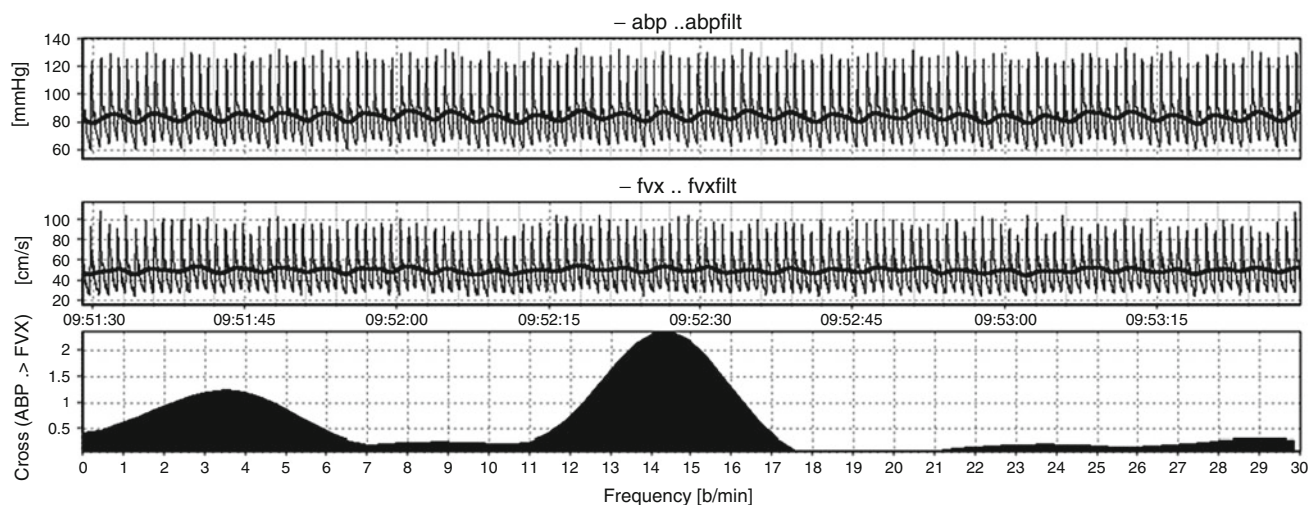


Fig. 1 Arterial blood pressure (ABP) and cerebral blood flow velocity (CBFV) raw and filtered tracings, superimposed to clearly show the respiratory fluctuations. The lower plot is the amplitude cross-spectrum, showing a well-defined peak at 14 breaths/min or 0.23 Hz

Materials and Methods

We retrospectively analysed recordings of ABP, CBFV and intracranial pressure (ICP) from 187 TBI patients treated at Addenbrooke's Hospital, Cambridge, UK, from 1993 to 1998. Monitored data were recorded to a laptop computer using ICM+ (Cambridge Enterprise, Cambridge, UK), from which PS and other indices of CA were derived (Mx, MxA, PRx index). PS was computed at the RR via cross-spectral peak detection in the region 0.167–0.333 Hz (10–20 breaths/min [bpm]) (Fig. 1). Results were excluded from analysis on the basis of low coherence (<0.8), high RR variability (RR interquartile range >1 bpm), or PS wraparound. Significance testing of spectral peaks was not performed. If bilateral TCDs were performed, the average across each hemisphere (PSa), and minimum (PSm) PS of the two hemispheres were analysed. PSm was analysed hypothesising that it should be most predictive of outcome. In order to examine the influence of respiratory rate on outcome statistics, calculations were repeated after selecting a group of patients who were ventilated at 12 bpm. The RAP index [3] was calculated as a measure of cerebrospinal compensatory reserve. Non-parametric statistics were used for correlations and between-group analyses throughout, unless variables demonstrated clearly normal distributions. All statistical calculations were performed using SPSS 15.0 (SPSS Inc, Chicago, IL, USA).

Results

Three hundred and eighty-four files were available for analysis in total (Tables 1 and 2).

Individual Observations

Respiratory PS was seen to consistently respond inversely to changes in CPP, with a variable pattern of return to baseline. Figure 2a, b shows two examples of PS responding to CPP fluctuations, with Fig. 2a showing the response to a sudden and sustained drop in CPP due to an ICP plateau wave. The drop in CPP, lasting approximately 30-min, is quickly followed by an increase in respiratory PS, which normalises midway through the wave. Both indices of autoregulation (Mx, PRx) indicated autoregulatory failure throughout. Figure 1b shows a 20-min recording window demonstrating a rise in CPP of approximately 15 mmHg from a baseline of 85 mmHg, secondary to an episode of systemic arterial hypertension. Both Mx and PRx transiently lowered then returned to baseline levels indicating poor autoregulation, whereas PS was slightly but persistently lowered after the onset of arterial hypertension.

Statistical Evaluation

Mean group PS was 14° (range -22 – 56°). The average respiratory rate was 14 bpm, corresponding to a respiratory frequency of 0.233 Hz. PS was inversely related to respiratory rate (Spearman's $R = -0.302$, $p < 0.000001$) and CPP ($R = -0.373$, $p < 0.000001$). Minimum PS was higher in non-survivors (Mann–Whitney test: $Z = -2.42$, $p = 0.015$). Across all outcome groups individually, no significant differences in PS were found (Kruskal–Wallis test, $\chi^2 = 6.821$, $p = 0.078$, Fig. 3). At 12 bpm only ($n = 61$), average PS remained higher in non-survivors (average PS = 21.5°) compared with

Table 1 Basic statistics for recorded signals

	Average \pm SD	Max	Min	<i>n</i> (# files)
ABP (mmHg)	90 \pm 14	131	51	412
ICP (mmHg)	20 \pm 11	71	0	412
CPP (mmHg)	69 \pm 16	109	8	412
FV (cm/s)	58 \pm 27	166	6	412

Note that heart rate (*HR*) and respiratory rate (*RR*) were both computed from arterial blood pressure (*ABP*) data, and are included in Table 2

ICP intracranial pressure, *CPP* cerebral perfusion pressure, *FV* flow velocity

Table 2 Basic statistics for computed parameters

	Average \pm SD	Max	Min	<i>n</i> (# files)
HR (bpm)	82 \pm 18	136	49	413
RR (bpm)	14 \pm 2	20	10	413
Mx (average)	0.025 \pm 0.37	−0.8	0.95	410
Mx (max)	0.049 \pm 0.38	−0.79	0.94	410
Phase (°, average)	14 \pm 13	56	−22	384
Phase (°, min)	13 \pm 13	56	−22	384
RAP	0.38 \pm 0.23	0.93	−0.35	413
ICPamp (mmHg)	1.9 \pm 1.4	12	0.10	413

Note that not all files were long enough to permit phase shift (*PS*) calculation; hence, fewer files have *PS* data. The identical range of *PS* for both the minimum and average *PS* is because of the file in question having only one transcranial Doppler (*TCD*) signal present

Mx autoregulatory index, *RAP* index of intracranial compliance, *amp* amplitude

survivors (average *PS* = 17.2°); however, the difference was not statistically significant. Both averaged and minimum *PS* correlated weakly, but significantly with the *Mx* and *PRx* index (*PSa*: $r=0.146$, $p=0.004$ [*Mx*]; $r=0.150$, $p=0.003$ [*PRx*]. *PSm*: $r=0.148$, $p=0.004$ [*Mx*]; $r=0.153$, $p=0.003$ [*PRx*]) (Fig. 3).

Discussion

The first notable finding from our study is that respiratory *PS* in ventilated patients exhibits a continuum of non-zero values, which were roughly in agreement with those previously reported [5]. The second and arguably controversial finding is that in patients who did not survive, *PS* between *ABP* and *CBFV* at respiratory frequencies was higher. This contrasts with our current understanding of *ABP/CBFV PS* and its interpretation, which suggests that increased *PS* reflects an actively regulating cerebrovascular bed, which, by extension, should theoretically be predictive of a good outcome. Explanations for our findings may be drawn from several sources. First, in a modelling study Kirkham et al. produced evidence to suggest that low *PS* may not always reflect impaired cerebral autoregulation [8]. These findings would seem to be supported by another modelling study in which it was suggested that *PS* was also a function of intracranial compliance [18]. In our data, the correlation between *PS* and the *RAP* index [3] was very poor

($R=0.007$, $p=0.892$), although the relationship is likely to be non-linear, so this result may not be meaningful. In both previously mentioned papers, the authors also suggested that with the addition of transfer function gain measurements, more inferences may be possible about the current state of autoregulation than by simply measuring *PS* alone. Notably, whilst gain was calculated as part of our physiological data analysis procedure, it was not included in our wider dataset for final statistical analysis. The utility of gain measurement was also highlighted by two studies in which (reduced) gain at respiratory frequencies was found to be the more sensitive parameter with respect to discriminating between degrees of carotid stenosis and by extension the degree of autoregulatory impairment [7, 15]. Interestingly, gain at respiratory frequencies has been proposed as a parameter that more likely reflects the mechanical properties of the cerebrovascular bed than dynamic autoregulation per se [5, 17]. In a recent study examining the influence of phenylephrine-induced arterial hypertension on the *ABP/CBFV* transfer function, *PS* was seen to decrease in a dose-dependent manner, whilst gain decreased in a similar stepwise fashion [18]. The authors combined these findings with their modelling results to suggest that at frequencies >0.07 Hz, both gain and *PS* likely reflect mechanical, or steady-state properties of the vascular bed rather than actively controlled properties. Revisiting our results, we observed a poor correlation between indices of autoregulation, *Mx* and *PRx*, with *PS*, adding further weight to the suggestion that *PS* either measures a mechanistically discrete aspect of autoregulation, or indeed

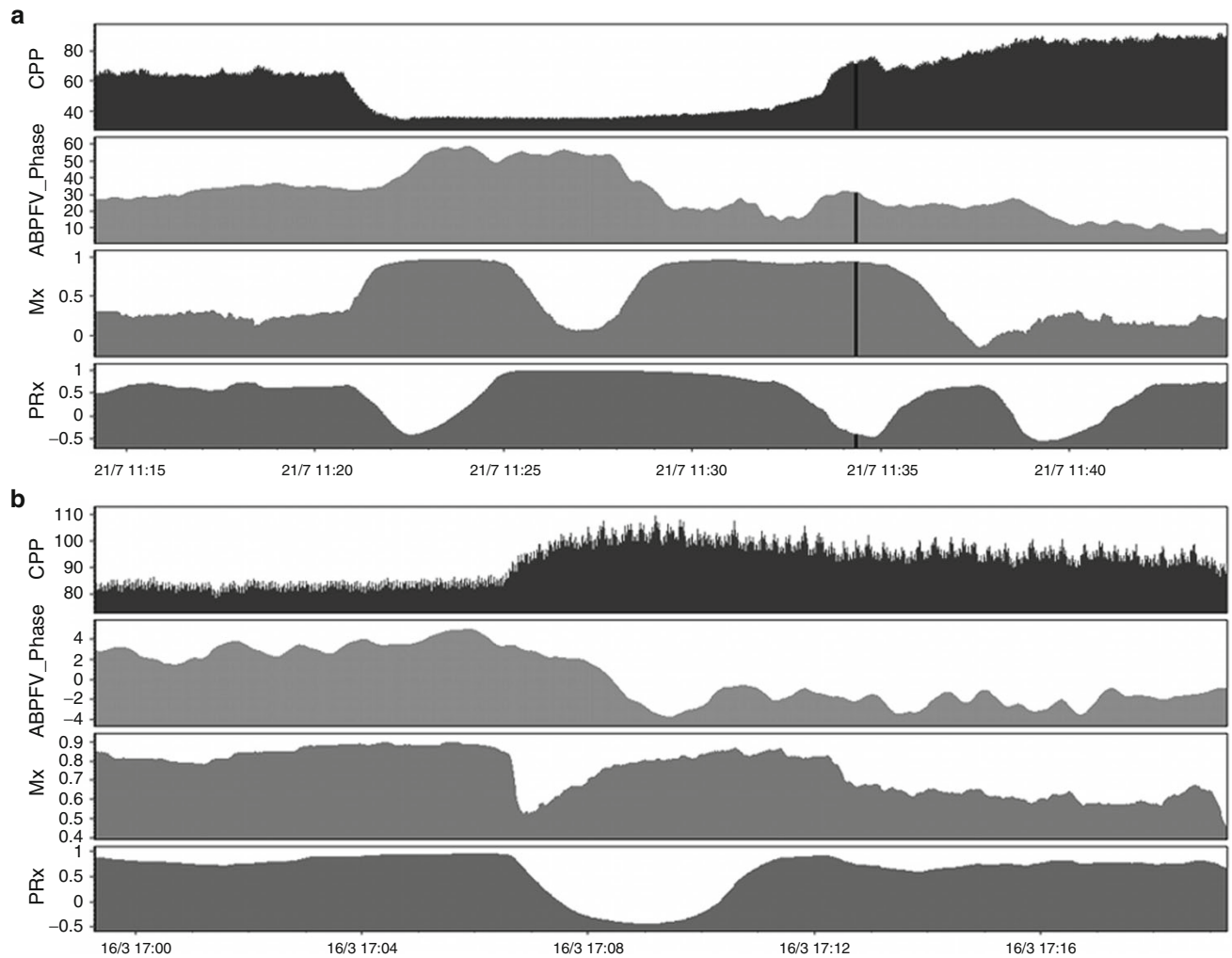


Fig. 2 (a, b): Observations of (in order from *top to bottom*). cerebral perfusion pressure (CPP), respiratory ABP/FV phase shift (PS), autoregulatory index (Mx) and pressure reactivity index (PRx) changes during intracranial hypertension (a, *top*) and arterial hypertension (b, *bottom*)

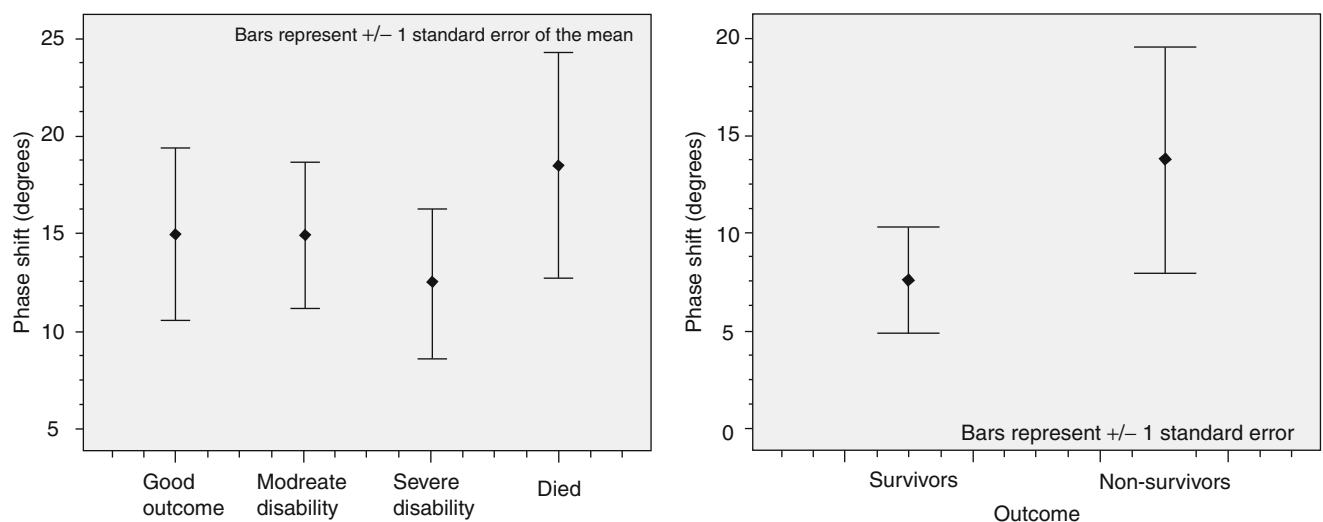


Fig. 3 Error bar plots showing mean PS across individual Glasgow Outcome Score (GOS) groups (*left*) and after grouping into survivors and non-survivors. Vegetative state ($n=4$) patients were removed from the dataset before analysis

another phenomenon altogether. Fitting well with the observations made in Zhang et al.'s study [18] was that in our data, PS was inversely proportional to CPP. What is less clear is the influence of the respiratory rate on our PS measurements, given that patients were all ventilated at different rates. Whilst the high-pass filter model of autoregulation essentially predicts lower PS with higher respiratory frequency, we must consider the influence of carbon dioxide. Further inspection of our results revealed that respiratory rate was significantly higher in those patients who died, as was intracranial pressure (Mann–Whitney test: $Z=-2.1$, $p=0.032$; $Z=-3.7$, $p<0.001$ respectively). Given this finding, it is reasonable to assume that $p\text{CO}_2$ was lower in the non-surviving patients. Unfortunately, we did not have E_tCO_2 or $p\text{CO}_2$ data to include in our analysis; however, in patients with refractory intracranial hypertension, titration of CO_2 as a last-resort measure to reduce ICP is not uncommon; thus, the assumption would seem a relatively safe one. That said, the influence of CO_2 on PS, particularly at respiratory frequencies, is poorly studied and not entirely clear. Carrera and colleagues used 5% CO_2 inhalation in healthy volunteers to demonstrate a reduction in PS at 0.1 Hz during controlled breathing [2]. Comparing healthy volunteers breathing spontaneously with patients with TBI, Muller and coworkers studied PS up to 0.25 Hz during normo- and hypocapnia [13]. Whilst not specifically discussed in the paper, their plots of PS suggest that hypocapnia produced an increase in PS above 0.2 Hz in both the healthy volunteers and TBI patients [13]. Contradicting these observations, however, Ogoh et al. found that exercise-induced hypocapnia actually caused a reduction in PS in the 0.07–0.20 Hz band [14].

Before summing up, our method of PS calculation deserves some comment. Classical methods of RR calculation involve the detection of respiratory sinus arrhythmia [16], or in ventilated patients it may be easily detected as the fundamental frequency of the end-tidal CO_2 tracing. Unfortunately, neither ECG nor E_tCO_2 data were present in our dataset, so we relied on the detection of the fundamental peak in the ABP/CBFV cross-spectrum in what was assumed to be the respiratory frequency band of 8–30 cycles/min (cpm). Having noted a number of situations in which this method failed to accurately identify the respiratory peak, we suggest that inclusion of either ECG or (ideally) end-tidal carbon dioxide recordings would provide more reliable options for estimating RR from the raw data.

Conclusion

We find that the ABP/CBFV phase shift in our patients behaves in a manner consistent with not only the high-pass filter model of autoregulation, but also the relatively scarce data available in the literature on PS behaviour at respiratory

frequencies above 0.1 Hz. The precise interpretation of PS at the frequencies under study is unclear, but accumulating evidence suggests that rather than measuring dynamic autoregulation, it may reflect a combination of steady-state cerebrovascular resistance and intracranial compliance. The poor correlation with autoregulation seen in our results supports this view. Further study is required to not only validate these relationships, but also to examine the confounding influence of carbon dioxide on respiratory phase shift measurement.

Conflict of interest statement Peter Smielewski and Marek Czosnyka have a financial interest in a part of the licensing fee for ICM+. All other authors have no conflicts of interest to disclose.

References

1. Brown CM, Marthol H, Zikeli U, Ziegler D, Hilz MJ (2008) A simple deep breathing test reveals altered cerebral autoregulation in type 2 diabetic patients. *Diabetologia* 51:756–761
2. Carrera E, Lee LK, Giannopoulos S, Marshall RS (2009) Cerebrovascular reactivity and cerebral autoregulation in normal subjects. *J Neurol Sci* 285:191–194
3. Czosnyka M, Guazzo E, Whitehouse M, Smielewski P, Czosnyka Z, Kirkpatrick P, Piechnik S, Pickard JD (1996) Significance of intracranial pressure waveform analysis after head injury. *Acta Neurochir (Wien)* 138:531–541; discussion 541–532
4. Diehl RR, Linden D, Lucke D, Berlitz P (1995) Phase relationship between cerebral blood flow velocity and blood pressure. A clinical test of autoregulation. *Stroke* 26:1801–1804
5. Diehl RR, Linden D, Lucke D, Berlitz P (1998) Spontaneous blood pressure oscillations and cerebral autoregulation. *Clin Auton Res* 8:7–12
6. Hamner JW, Cohen MA, Mukai S, Lipsitz LA, Taylor JA (2004) Spectral indices of human cerebral blood flow control: responses to augmented blood pressure oscillations. *J Physiol* 559:965–973
7. Hu HH, Kuo TB, Wong WJ, Luk YO, Chern CM, Hsu LC, Sheng WY (1999) Transfer function analysis of cerebral hemodynamics in patients with carotid stenosis. *J Cereb Blood Flow Metab* 19:460–465
8. Kirkham SK, Craine RE, Birch AA (2001) A new mathematical model of dynamic cerebral autoregulation based on a flow dependent feedback mechanism. *Physiol Meas* 22:461–473
9. Lang EW, Diehl RR, Timmermann L, Baron R, Deuschl G, Mehdorn HM, Zunker P (1999) Spontaneous oscillations of arterial blood pressure, cerebral and peripheral blood flow in healthy and comatose subjects. *Neurol Res* 21:665–669
10. Lang EW, Diehl RR, Mehdorn HM (2001) Cerebral autoregulation testing after aneurysmal subarachnoid hemorrhage: the phase relationship between arterial blood pressure and cerebral blood flow velocity. *Crit Care Med* 29:158–163
11. Lewis PM, Rosenfeld JV, Diehl RR, Mehdorn HM, Lang EW (2008) Phase shift and correlation coefficient measurement of cerebral autoregulation during deep breathing in traumatic brain injury (TBI). *Acta Neurochir (Wien)* 150:139–146; discussion 146–137
12. Muller M, Bianchi O, Erulku S, Stock C, Schwerdtfeger K (2003) Brain lesion size and phase shift as an index of cerebral autoregulation in patients with severe head injury. *Acta Neurochir (Wien)* 145:643–647; discussion 647–648

13. Muller M, Bianchi O, Erulku S, Stock C, Schwerdtfeger K (2003) Changes in linear dynamics of cerebrovascular system after severe traumatic brain injury. *Stroke* 34:1197–1202
14. Ogoh S, Dalsgaard MK, Yoshiga CC, Dawson EA, Keller DM, Raven PB, Secher NH (2005) Dynamic cerebral autoregulation during exhaustive exercise in humans. *Am J Physiol Heart Circ Physiol* 288:H1461–H1467
15. Reinhard M, Muller T, Guschlbauer B, Timmer J, Hetzel A (2003) Transfer function analysis for clinical evaluation of dynamic cerebral autoregulation – a comparison between spontaneous and respiratory-induced oscillations. *Physiol Meas* 24:27–43
16. Saul JP, Berger RD, Albrecht P, Stein SP, Chen MH, Cohen RJ (1991) Transfer function analysis of the circulation: unique insights into cardiovascular regulation. *Am J Physiol* 261:H1231–H1245
17. Zhang R, Zuckerman JH, Giller CA, Levine BD (1998) Transfer function analysis of dynamic cerebral autoregulation in humans. *Am J Physiol* 274:H233–H241
18. Zhang R, Behbehani K, Levine BD (2009) Dynamic pressure-flow relationship of the cerebral circulation during acute increase in arterial pressure. *J Physiol* 587:2567–2577

Monitoring of the Association Between Cerebral Blood Flow Velocity and Intracranial Pressure

Philip M. Lewis, Peter Smielewski, Jeffrey V. Rosenfeld, John D. Pickard, and Marek Czosnyka

Abstract Slow waves in intracranial pressure (ICP) are believed to originate from changes in cerebral blood volume secondary to adjustments in arteriolar diameter. Blood flow velocity (FV) signals recorded with transcranial Doppler ultrasound show similar oscillations. We investigated a continuous measure of FV/ICP association and its relationship to cerebral perfusion pressure (CPP), ICP, cerebral autoregulation (CA) and outcome after severe traumatic brain injury (TBI). We analysed recordings of arterial blood pressure (ABP), FV and ICP from 187 TBI patients treated at Addenbrooke's Hospital, Cambridge, UK, from 1993 to 1998. Monitored data were recorded and the flow-ICP index (FIx) was derived as a moving correlation between the two signals over 4-min periods using ICM+. FIx was compared with the autoregulatory index (Mx), pressure reactivity index (PRx), ICP, CPP and outcome. FIx correlated with ICP (Spearman's $R = -0.40, p < 0.01$), Mx ($R = -0.54, p < 0.00005$) and CPP ($R = 0.34, p < 0.01$), but not with PRx ($p = 0.84$). FIx was significantly associated with outcome after grouping into Glasgow Outcome Score (GOS) 1–3 or GOS 4–5 (Mann-Whitney $p = 0.009$). FIx may provide unique insights into the behaviour of the cerebral circulation during intracranial hypertension.

Keywords Traumatic brain injury • Transcranial Doppler • Intracranial pressure • Compliance

Introduction

Haemodynamic signals recorded from the brain: intracranial pressure (ICP), cerebral perfusion pressure (CPP), middle cerebral artery blood flow velocity (FV) and cortical blood flow (LDF), are seen to innately fluctuate at low frequencies (20-s to 3-min periods) [12]. The association between slow fluctuations in CPP and FV has been previously exploited to derive a measure of cerebral autoregulation [2], as has the correlation between slow waves in arterial blood pressure (ABP) and ICP [3]. The relationship between ICP and FV is relatively poorly studied, with the majority of work in the area largely concentrating on the behaviour of FV and ICP during plateau and B waves in head injury [4, 9], healthy volunteers [6], normal pressure hydrocephalus [6, 8] and subarachnoid haemorrhage [11]. The relationship between ICP and FV was briefly examined in a study on head injured patients, with the authors finding little of note [5]. A recent study by Haubrich et al. suggested that the amplitude of FV slow waves may be inversely related to mean ICP, however the authors did not correlate FV with ICP slow waves [7]. In a more detailed treatment of the FV/ICP relation, Panerai and co-workers employed transfer function analysis to show that FV oscillations precede those in ICP over a wide range of low frequencies (< 0.5 Hz), supporting the concept that slow ICP fluctuations are principally derived from those in FV [1, 10]. Notably, the authors also suggested that the relationship may be exploited to derive information about intracranial compliance [10]. Despite the existing body of work on this topic, data on the general clinical relevance of the FV/ICP relationship and its dynamic changes with other haemodynamic variables are lacking. To that end, we examined patterns of change and relationships to outcome of a continuous correlation between ICP and FV, for which we have coined the term 'FIx', an abbreviation for 'flow-ICP index'.

P.M. Lewis (✉) and J.V. Rosenfeld
Department of Neurosurgery,
Alfred Hospital,
Prahran, VIC 3181,
Australia

Department of Surgery,
Monash University,
Prahran, VIC,
Australia
e-mail: p.lewis@alfred.org.au

P. Smielewski, J.D. Pickard, and M. Czosnyka
Department of Neurosurgery,
Addenbrooke's Hospital,
Cambridge, UK

Table 1 Basic statistics for recorded and computed parameters

	Average \pm SD	Max	Min	<i>n</i> (# files)
ABP (mmHg)	90 \pm 14	147	51	528
ICP (mmHg)	21 \pm 12	69	0	528
CPP (mmHg)	69 \pm 17	109	8	528
FV (cm/s)	61 \pm 27	169	13	528
Mx	0.01 \pm 0.39	0.94	-0.88	528
PRx	0.07 \pm 0.34	0.99	-0.79	528
Flx	0.41 \pm 0.32	0.96	-0.82	528

ABP arterial blood pressure, FV flow velocity, CPP cerebral perfusion pressure, Mx autoregulatory index, Flx flow-ICP index

Materials and Methods

We retrospectively analysed recordings of ABP, FV and ICP from 187 TBI patients treated at Addenbrooke's Hospital, Cambridge, UK, from 1993 to 1998. Recorded data were processed using ICM+ (Cambridge Enterprise, Cambridge, UK). A measure of FV/ICP association (the Flx index) was derived as a moving continuous correlation coefficient between 30 time-averaged (over 10-s periods) FV and ICP samples over 5-min periods. The autoregulatory index (Mx) was calculated in a similar manner by correlating CPP with FV. Outcome was recorded as the Glasgow Outcome Score (GOS) at 6 months after injury. Patients in a persistent vegetative state ($n=6$ in total) were excluded from analysis. Relationships between haemodynamic variables were assessed using Spearman's correlation coefficient and error bar plots. Clinical relevance was assessed by comparing haemodynamic indices across GOS groups (one-way ANOVA) and after grouping into favourable/unfavourable outcome (GOS 1–3 = unfavourable outcome, GOS 4–5 = favourable outcome). Statistical significance was set at an alpha of 0.05.

Results

A basic summary of the data is provided in Table 1.

Individual Observations

Figure 1 shows the pattern of Flx change during a period of intracranial hypertension (Fig. 1a) and arterial hypotension (Fig. 1b). In each example, Flx has a tendency to remain positive when Mx is negative. During the ICP plateau (Fig. 1a), Mx increases, indicating maximal vasodilatation and loss of

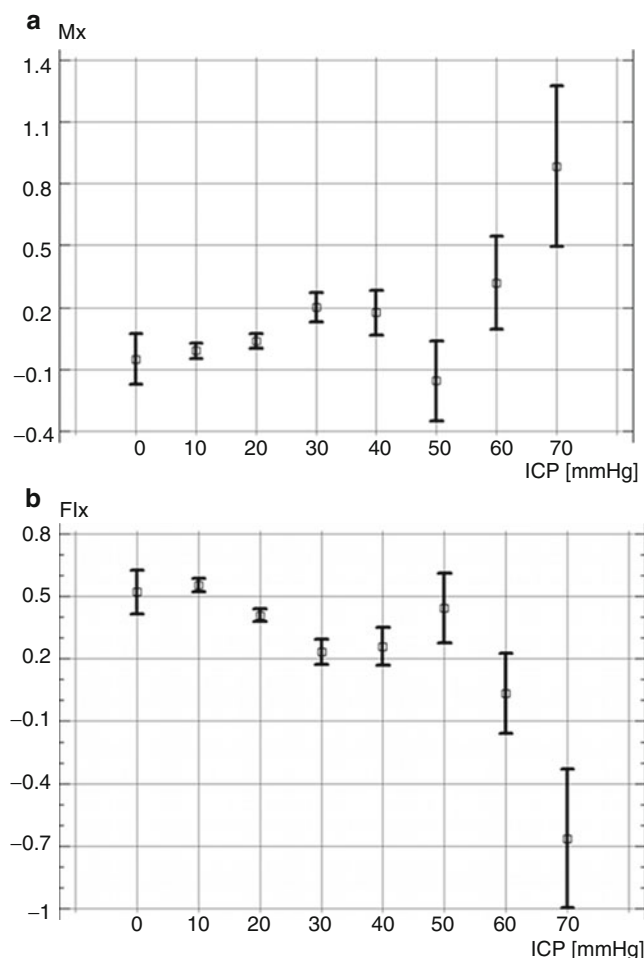
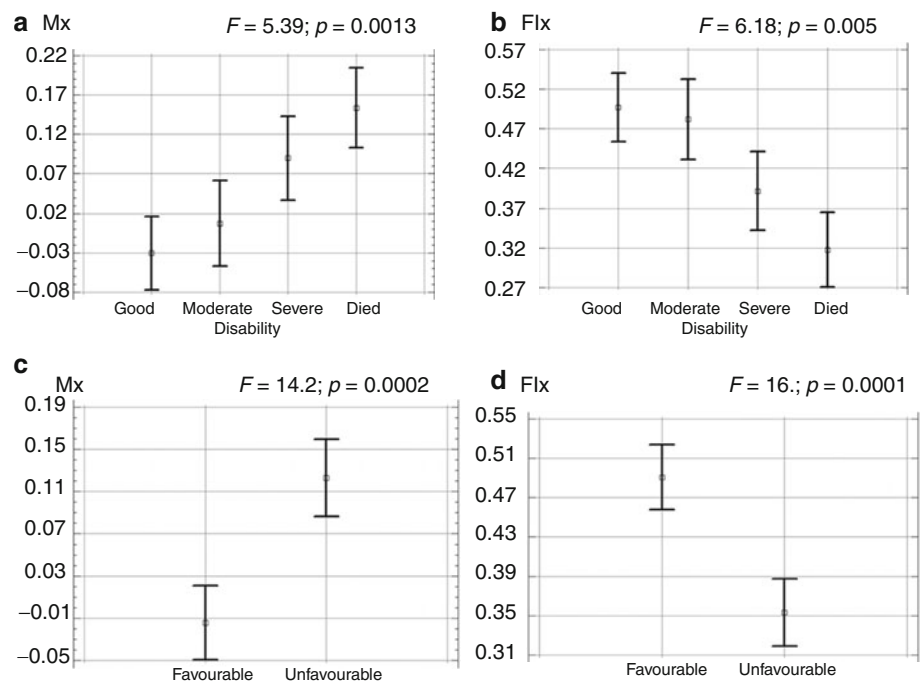


Fig. 1 Error bar plots showing Mx (a) and Flx (b) vs. ICP. Note the breakpoint at approximately 50 mmHg, beyond which average Flx appears to decrease sharply

autoregulation. A similar transient loss of autoregulation can be seen during the period of arterial hypotension (Fig. 1b). Mx, previously showing effective autoregulation, deteriorates and becomes positive, with Flx closely mirroring the changes.

Fig. 2 Plots of mean Mx and Flx against outcome groups. (a) Mx vs. Glasgow Outcome Score (GOS). (b) Flx vs. GOS. (c) Mx vs. outcome after grouping into favourable (GOS 4–5) and unfavourable (GOS 1–3). (d) Flx vs. outcome after grouping into favourable (GOS 4–5) and unfavourable (GOS 1–3)



Statistical Analysis

Flx was significantly negatively associated with ICP ($R = -0.40$, $p < 0.01$) and autoregulation (Mx index: $R = -0.54$, $p < 0.00005$) but not with pressure reactivity (PRx index: $R = -0.01$, $p = 0.98$). Flx was positively correlated with CPP ($R = 0.326$, $p < 0.0001$), the plot of which showed a monotonically increasing character (graph not shown). This contrasts with Mx, which showed the characteristic U-shaped curve when plotted against CPP. The distribution of Mx versus ICP shows a largely monotonically increasing character (Fig. 1a: $R = 0.271$, $p < 0.0001$). The distribution of Flx versus ICP was fairly flat up to a visually apparent upper breakpoint of 50 mmHg, beyond which Flx abruptly decreases (Fig. 1b). Comparing the results of one-way ANOVA for GOS vs. Mx (Fig. 2a) and Flx (Fig. 2b) respectively, we see that differences in Flx across groups are marginally more significant ($F = 5.39$ [Mx] vs. $F = 6.18$ [Flx], $p < 0.005$ in both cases). After collapsing outcome into good and poor groups (good outcome = GOS 4–5, poor outcome = GOS 1–3), Flx again discriminated slightly more significantly between the groups compared with Mx (Fig. 2c, d: $F = 14.2$ [Mx] vs. $F = 16.2$ [Flx], $p < 0.0005$ in both cases).

Discussion

Given that this report is to our knowledge the first describing the relation between FV and ICP in terms of the correlation between the two, it is useful to briefly explain the

interpretation of Flx with respect to the existing literature. Most of the studies examining the relationship between FV and ICP thus far have described the synchrony of slow waves in terms of ‘phase’, or a time lag between the two signals. For example, in a group of head injured patients Newell et al. described B-waves in FV and ICP as being ‘completely synchronous’ and ‘always in phase’ [9]. Their findings fit well with previously reported measurements of pial vessel diameters oscillating in synchrony with ICP in cats [1]. Droste et al. on the other hand described ‘no significant delay’ between B waves (described as B-wave equivalents [BWEs] for FV) in FV and ICP whilst also stating that ‘BWEs occurred simultaneously with directly measured ICP B-waves’ [6]. In a more formal analysis of the FV/ICP relation, Panerai et al. showed that there was a negative phase shift with FV leading ICP, however the authors did not describe its magnitude or dynamic properties [10]. Notably, the coherence between FV and ICP was < 0.8 across the entire frequency spectrum (up to 0.5 Hz) [10]. Over the course of a genuine vasogenic plateau wave, FV will typically suddenly drop as CPP is reduced to critically low levels [4]. This contrasts with a rise in ICP caused by rapid fluctuations in ABP, or a change in ABP in the setting of impaired autoregulation, which will produce parallel changes in FV and ICP [4]. Drawing the link between Flx and phase, it is useful to highlight that a plot of the Pearson’s correlation between two incrementally phase-shifted sine waves takes a cosine form. Therefore, when ICP and FV are in phase, their correlation will be 1. When ICP and FV are out of phase, their correlation will trend towards -1 , with a continuum in between.

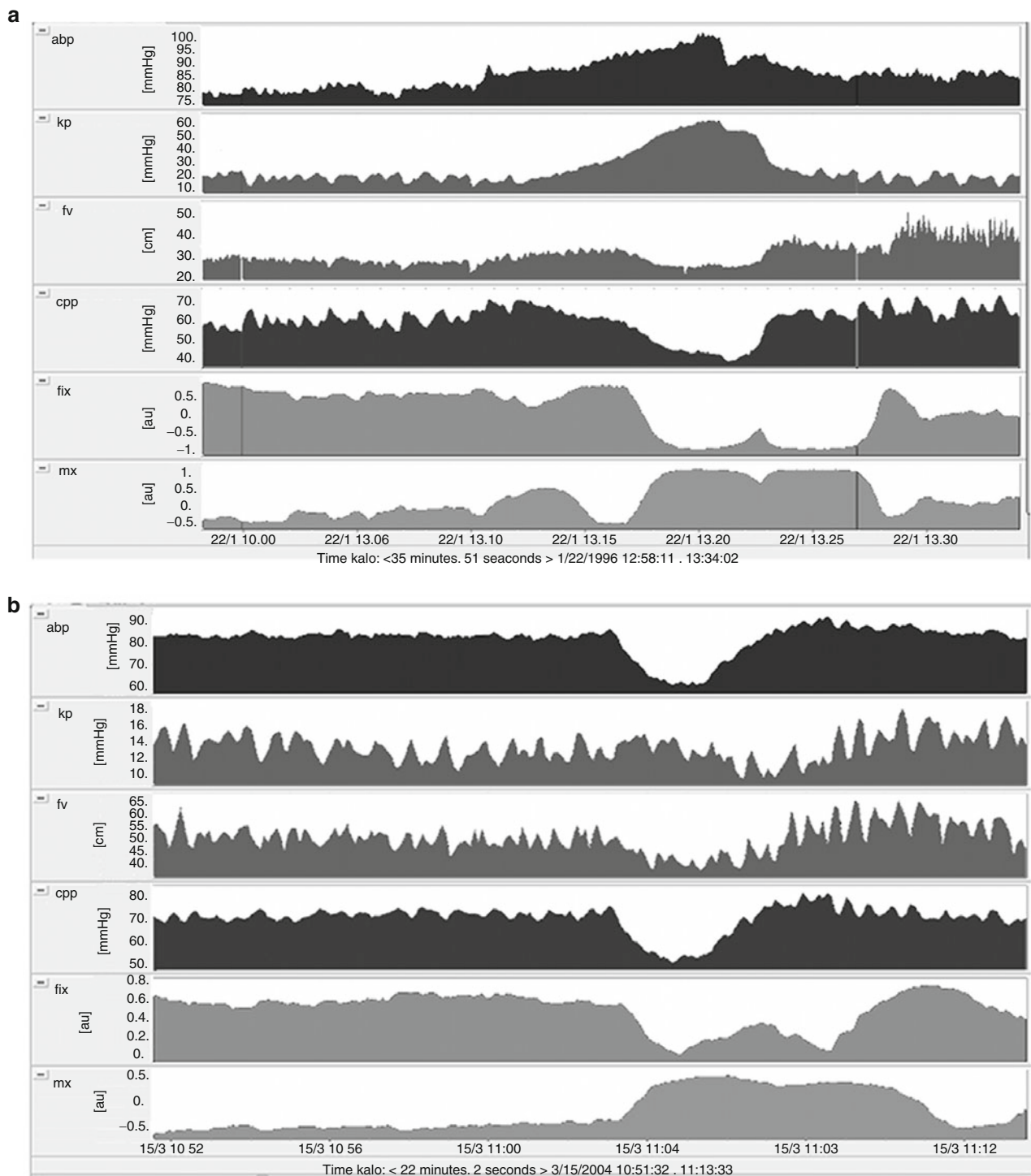


Fig. 3 (a) (From top to bottom) arterial blood pressure (ABP), intracranial blood pressure (ICP), flow velocity (FV), cerebral perfusion pressure (CPP), autoregulatory index (Mx) and flow-ICP index (Flx) during

an ICP plateau wave. (b) (From top to bottom) ABP, ICP, FV, CPP, Mx and Flx during a short period of arterial hypotension

The individual examples presented in this report confirm that Flx is typically positive, as expected. Some interesting patterns can be seen during large swings in CPP or ABP. During an ICP plateau wave (Fig. 3a), Flx is seen to become strongly negative, indicating that FV and ICP are out of phase by the peak of the plateau. Similarly, a drop in CPP

due to a period of arterial hypotension (Fig. 3b) produces a drop in Flx, although in this case the index drops to zero rather than becoming negative. In this case, the response of ICP to the hypotension was minimal despite preserved autoregulation, suggesting good cerebrospinal compensatory reserve.

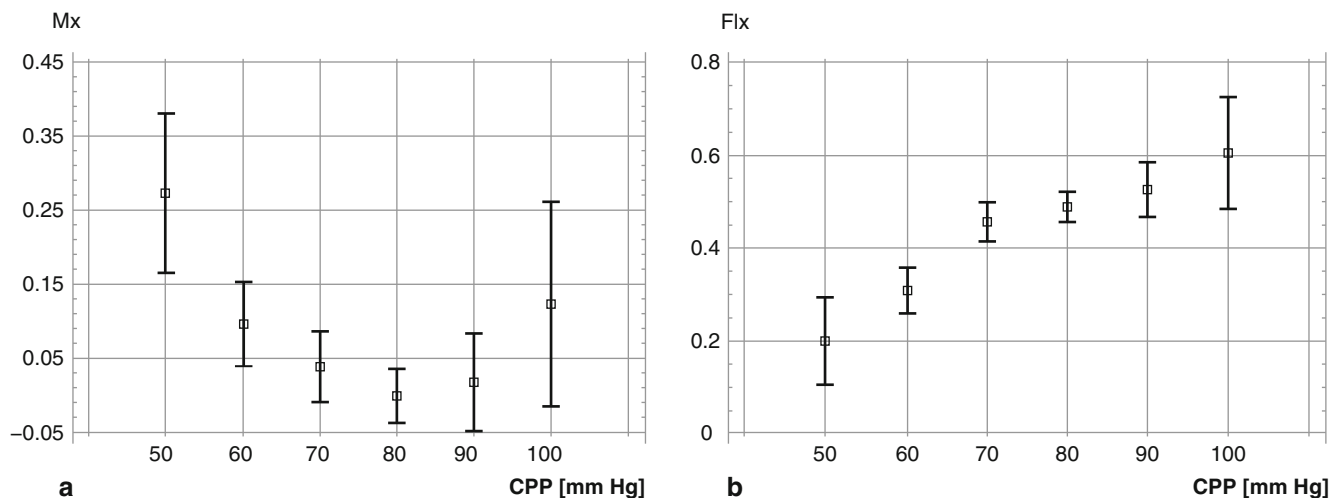


Fig. 4 Comparison of distribution of Mx versus mean CPP (a) and Flx versus CPP (b). While Mx suggests U-shape relationship on CPP, Flx uniformly increases with raising CPP

The correlation between Mx and Flx was moderate ($r = -0.54$, $p < 0.00005$), which begs the question: is Flx simply measuring autoregulation? Examining the distribution of Mx versus CPP, we see the typical U shape (Fig. 4a). The plot of Flx versus CPP (Fig. 4b), however, has a monotonically increasing character. One implication of this finding is that unlike Mx, Flx is unlikely to be of any value in the optimisation of CPP. The plot of Flx vs. ICP provides some interesting insights into its potential utility. An upper breakpoint is noted at around 50 mmHg, above which Flx appears to drop sharply to negative levels. Given our observations of changes in Flx during a plateau wave, this may be a reflection of the behaviour of Flx during vasogenic intracranial hypertension. Further work comparing Flx in patients with persistent (i.e. cytotoxic) intracranial hypertension and impaired autoregulation with those demonstrating plateau waves would provide some interesting insights into the utility of Flx. Its precise interpretation aside, the slightly more significant relationship of Flx with outcome in combination with the moderate correlation between Flx and Mx further underscores the suggestion that the Flx index is capturing some unique pathophysiological relationships that have clinical relevance in head injury.

Conclusion

While often high, the correlation between FV and ICP is clearly variable, and sensitive to disturbances in both arterial blood and intracranial pressures. The precise patterns of Flx variation remain to be fully investigated, however our initial observations reveal that the relationship between ICP and FV has obvious clinical significance and warrants further investigation.

Conflict of interest statement Peter Smielewski and Marek Czosnyka have a financial interest in a part of the licensing fee for ICM+. All other authors have no conflicts of interest to disclose.

References

1. Auer LM, Sayama I (1983) Intracranial pressure oscillations (B-waves) caused by oscillations in cerebrovascular volume. *Acta Neurochir (Wien)* 68:93–100
2. Czosnyka M, Smielewski P, Kirkpatrick P, Menon DK, Pickard JD (1996) Monitoring of cerebral autoregulation in head-injured patients. *Stroke* 27:1829–1834
3. Czosnyka M, Smielewski P, Kirkpatrick P, Piechnik S, Laing R, Pickard JD (1998) Continuous monitoring of cerebrovascular pressure-reactivity in head injury. *Acta Neurochir Suppl* 71:74–77
4. Czosnyka M, Smielewski P, Piechnik S, Schmidt EA, Al-Rawi PG, Kirkpatrick PJ, Pickard JD (1999) Hemodynamic characterization of intracranial pressure plateau waves in head-injury patients. *J Neurosurg* 91:11–19
5. Czosnyka M, Smielewski P, Piechnik S, Steiner LA, Pickard JD (2001) Cerebral autoregulation following head injury. *J Neurosurg* 95:756–763
6. Droste DW, Krauss JK, Berger W, Schuler E, Brown MM (1994) Rhythmic oscillations with a wavelength of 0.5–2 min in transcranial Doppler recordings. *Acta Neurol Scand* 90:99–104
7. Haubrich C, Czosnyka Z, Lavinio A, Smielewski P, Diehl RR, Pickard JD, Czosnyka M (2007) Is there a direct link between cerebrovascular activity and cerebrospinal fluid pressure-volume compensation? *Stroke* 38:2677–2680
8. Krauss JK, Droste DW (1994) Predictability of intracranial pressure oscillations in patients with suspected normal pressure hydrocephalus by transcranial Doppler ultrasound. *Neurol Res* 16:398–402
9. Newell DW, Aaslid R, Stooss R, Reulen HJ (1992) The relationship of blood flow velocity fluctuations to intracranial pressure B waves. *J Neurosurg* 76:415–421
10. Panerai RB, Hudson V, Fan L, Mahony P, Yeoman PM, Hope T, Evans DH (2002) Assessment of dynamic cerebral autoregulation based on spontaneous fluctuations in arterial blood pressure and intracranial pressure. *Physiol Meas* 23:59–72
11. Steinmeier R, Bauhof C, Hubner U, Bauer RD, Fahlbusch R, Laumer R, Bondar I (1996) Slow rhythmic oscillations of blood pressure, intracranial pressure, microcirculation, and cerebral oxygenation. Dynamic interrelation and time course in humans. *Stroke* 27:2236–2243
12. Zweifel C, Czosnyka M, Lavinio A, Castellani G, Kim DJ, Carrera E, Pickard JD, Kirkpatrick PJ, Smielewski P (2010) A comparison study of cerebral autoregulation assessed with transcranial Doppler and cortical laser Doppler flowmetry. *Neurol Res* 32:425–428

How Does Moderate Hypocapnia Affect Cerebral Autoregulation in Response to Changes in Perfusion Pressure in TBI Patients?

Christina Haubrich, Luzius Steiner, D. J. Kim, Magdalena Kasproicz, Piotr Smielewski, Rolf R. Diehl, John D. Pickard, and Marek Czosnyka

Abstract In traumatic brain injury, the hypocapnic effects on blood pressure autoregulation may vary from beneficial to detrimental. The consequences of moderate hypocapnia (HC) on the autoregulation of cerebral perfusion pressure (CPP) have not been monitored so far.

Thirty head injured patients requiring sedation and mechanical ventilation were studied during normocapnia (5.1 ± 0.4 kPa) and moderate HC (4.4 ± 3.0 kPa). Transcranial Doppler flow velocity (Fv) of the middle cerebral arteries (MCA), invasive arterial blood pressure, and intracranial pressure were monitored. CPP was calculated. The responsiveness of Fv to slow oscillations in CPP was assessed by means of the moving correlation coefficient, the Mx autoregulatory index. Hypocapnic effects on Mx were increasing with its deviation from normal baseline (left MCA: $R^2=0.67$; right MCA: $R^2=0.51$; $p<0.05$). Mx indicating normal autoregulation (left: -0.23 ± 0.23 ; right: -0.21 ± 0.24) was not significantly changed by moderate HC. Impaired Mx autoregulation, however, (left: 0.37 ± 0.13 ; right: 0.33 ± 0.26) was

improved (left: 0.12 ± 0.25 ; right: -0.0003 ± 0.19 ; $p<0.01$) during moderate HC. Mx was adjusted to normal despite no significant change in CPP levels. Our study showed that short-term moderate HC may optimize the autoregulatory response to spontaneous CPP fluctuations with only a small CPP increase. Patients with impaired autoregulation seemed to benefit the most.

Keywords Intracranial pressure • Cerebral autoregulation • Traumatic brain injury • Moderate hypocapnia • Transcranial Doppler

Introduction

Intact cerebral autoregulation is important in preventing secondary insults to the injured brain [1]. Disturbed *autoregulation* may result in an imbalance among cerebral blood flow, blood volume, and the metabolic requirements of the cerebral tissues [2]. Transient episodes of cerebral ischemia, hyperemia, and/or uncontrollable increases in cerebral blood volume are particularly detrimental to a favorable outcome after traumatic brain injury (TBI) [3]. Hence, *neurointensive care of head-injured patients is aimed at a sufficient cerebral autoregulation*.

However, uncertainty remains about effects of ventilatory treatment on cerebral blood flow regulation in patients with TBI. Moderate HC seems to be less harmful when applied for the short-term [4]. What we do not know though is whether mild HC does improve cerebral blood flow regulation without altering the CPP. In healthy volunteers hypocapnia has been shown to improve autoregulation [5]. In TBI patients, however, the autoregulatory capacity to preserve sufficient cerebral blood flow despite continuous fluctuations in CPP. The impact of mild HC on perfusion pressure autoregulation, however, has not been investigated so far. This study for a first time focuses on how moderate hypocapnia affects the autoregulatory response to spontaneous fluctuations in cerebral perfusion pressure.

C. Haubrich (✉)

Department of Academic Neurosurgery, Addenbrooke's Hospital, Cambridge, UK

Department of Neurology, University Hospital Aachen, Pauwelsstrasse 30, 52074 Aachen, Germany
e-mail: chaubrich@ukaachen.de

L. Steiner

Department of Anaesthesia, University Hospital Lausanne, Lausanne, Switzerland

D.J. Kim, P. Smielewski, J.D. Pickard, and M. Czosnyka

Department of Academic Neurosurgery, Addenbrooke's Hospital, Cambridge, UK

M. Kasproicz

Department of Academic Neurosurgery, Addenbrooke's Hospital, Cambridge, UK

Institute of Biomedical Engineering and Instrumentation, Wrocław University of Technology, Wrocław, Poland

R.R. Diehl

Department of Neurology, Alfried-Krupp-Krankenhaus, Essen, Germany

Table 1 Physiological parameters at baseline and during mild HC given as mean \pm standard deviation

	Impaired baseline autoregulation	Moderate hypocapnia	Normal baseline autoregulation	Moderate hypocapnia
ICP	14.27 \pm 5.94	11.97 \pm 5.45*	17.31 \pm 7.03	12.84 \pm 6.66*
ABP	98.31 \pm 7.40	101.87 \pm 11.63	95.61 \pm 10.91	97.76 \pm 13.65
CPP	84.03 \pm 10.24	89.90 \pm 12.81	78.31 \pm 7.73	84.83 \pm 12.41*
FVr	78.74 \pm 22.43	64.17 \pm 17.45*	73.42 \pm 27.69	56.24 \pm 16.13*
FVI	80.07 \pm 48.42	69.69 \pm 39.88*	72.03 \pm 23.98	57.26 \pm 15.52*
Mxl	0.37 \pm 0.13	0.12 \pm 0.25*	-0.23 \pm 0.23	-0.14 \pm 0.20
Mxr	0.33 \pm 0.26	0.0003 \pm 0.19*	-0.21 \pm 0.24	-0.14 \pm 0.19

Significant differences are indicated with * $p < 0.01$

ICP intracranial pressure, ABP arterial blood pressure, CPP cerebral perfusion pressure, Fv flow velocity

Materials and Methods

The analysis was performed on data collected from 29 head-injured patients (39.0 \pm 14.1 years) with Glasgow Coma Scale score < 12 , sedated (propofol and fentanyl) and mechanically ventilated. Approval for monitoring and analysis was given by our local ethics committee. Inclusion criterion was a normocapnic baseline with CPP > 70 mmHg and endtidal CO₂ (ETCO₂) of more than 35 mmHg (4.7 kPa). Exclusion criteria were respiratory failure and the early phase of TBI (first 48 h).

The monitoring included

- Radial artery blood pressure (ABP; Edwards Lifesciences, Irvine, CA, USA).
- Intraparenchymal ICP (Codman MicroSensors ICP Transducer, Codman & Shurtle, Raynham, MA, USA).
- Mainstream ETCO₂ (Marquette Solar 8,000 M, GE Medical Systems, UK).
- Arterial CO₂ partial pressure (PaCO₂) using an AVL Omni blood gas analyzer (AVL Omni, Graz, Austria).
- Fv assessed using a head band with transcranial Doppler probes insonating the middle cerebral arteries (MCA) bilaterally at a depth of 51–53 mm.

Following a 20-min recording of baseline data at constant ETCO₂, the minute volume of the ventilator was increased by 15–20% and was kept stable for another 30 min of moderate HC. If this intervention resulted in the violation of standard treatment guidelines the protocol was abandoned. Care was taken not to exceed limits of PaCO₂ < 3.5 kPa and/or jugular bulb oxygen saturation (SJO₂) $< 55\%$.

Analog signals were sampled at 30 Hz and digitized using waveform time integration. Averaged 6-s values for ICP, ABP, CPP, Fv, and respiratory rate were calculated and stored continuously on a computer. Data analysis was performed using ICM+software (Cambridge University, UK). Autoregulation was assessed continuously using the Mx autoregulatory index (Mx), which was calculated as the moving correlation coefficient between consecutive 24 samples of 10-s averages of Fv and CPP waveforms. Mx may principally vary between -1 and +1. Previous studies, based on analysis of outcome

from a large cohort of TBI patients have shown $Mx \leq 0.25$ if autoregulation is intact, whereas disturbed autoregulation is reflected by values larger than 0.25 [1]. Hence, increasing Mx signifies worsening autoregulation while decreasing Mx indicates improving autoregulation. This method for autoregulation testing has been validated against others [6].

The relationship between Mx changes and Mx baseline was assessed using a second degree polynomial regression analysis. For the comparison between baseline and moderate HC as well as between patient subgroups we applied the mixed between-within subjects ANOVA of the multiple interdependencies concerning Mx, CPP, ICP, ABP, and Fv using SPSS 17.0 analysis. Statistical significance was set at $p < 0.01$.

Results

Baseline ICP of 30 patients included in this analysis ranged from 5.2 to 27.6 mmHg. All patients were studied at normocapnia (5.1 \pm 0.4 kPa) and moderate hypocapnia (4.4 \pm 3.0 kPa). In response to HC, ICP and MCA-Fv have dropped to levels significantly lower than baseline (Table 1).

Moderate HC did not simply shift the Mx to a similar extent in all patients (Fig. 1a). Hypocapnic effects on Mx were depending on Mx baseline levels (left-MCA: $R^2 = 0.67$; right-MCA: $R^2 = 0.51$; Fig. 1b): Mx indices indicating impaired baseline autoregulation were adjusted to normal levels. Normal baseline Mx autoregulatory indices did not significantly change during moderate HC (Table 1). This optimizing effect on the Mx autoregulatory index was, however, not associated with a significant increase in mean CPP levels.

Discussion

This study attempts to answer the question whether moderate HC alters the CPP responsiveness of cerebral blood flow. Whereas in patients with normal Mx autoregulatory index at

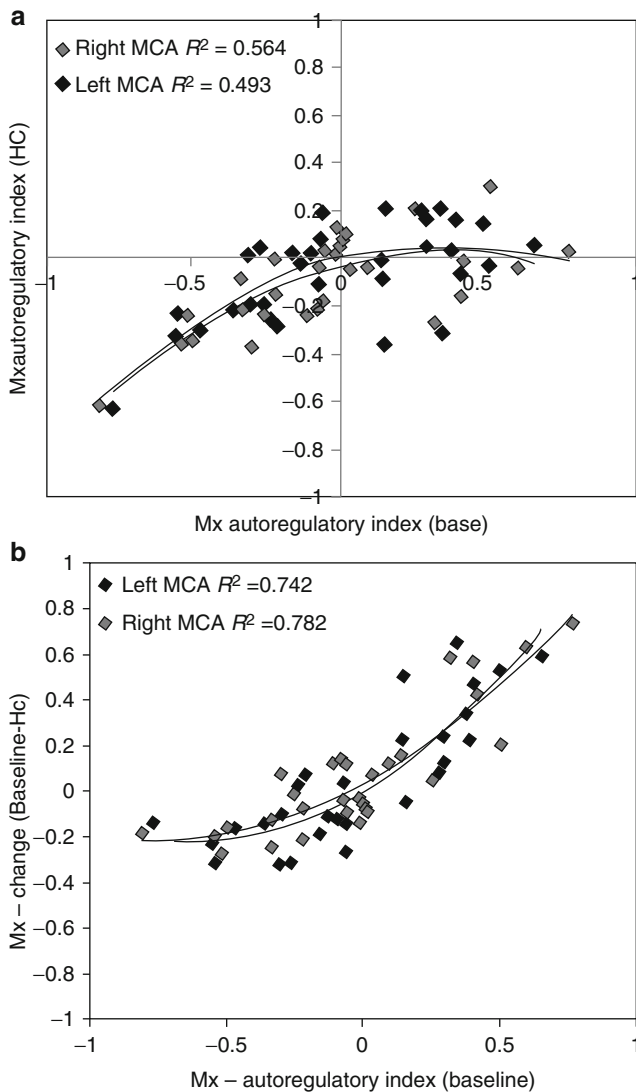


Fig. 1 Mx at baseline plotted against baseline (a) and Mx changes (Baseline-HC) significantly correlated with Mx baseline (b) graph also published in *J. Neurotrauma* 2011;28:1133–1137

baseline moderate HC induced no significant changes, and the CPP responsiveness improved, especially in those with Mx indicating impaired baseline autoregulation.

The effects of hyperventilation reported in TBI seem to vary from beneficial to detrimental [7–11]. Newell et al., for instance, have shown that HC may improve the cerebral blood flow regulation in response to induced changes in blood pressure [9]. Imberti et al. have shown that hyperventilation (27–32 mmHg; 3.5–4.1 kPa) is accompanied by a significant increase in mean CPP [8]. Our study showed that with higher arterial pCO_2 levels (4.4 ± 3.0 kPa) dynamic cerebral autoregulation in TBI can be adjusted to normal with only a small CPP increase. This observation may on the one hand be explained by the fact that the relationship between CPP and Mx is U-shaped. Therefore, an autoregulatory improvement may be achieved with even small increases in CPP if the Mx indicates impaired autoregulation.

On the other hand, does HC expand the autoregulatory capacity toward lower levels of CPP. A regained autoregulatory capacity may protect the brain from fluctuations in CPP. As however, critical $PaCO_2$ levels are not specified, moderate HC has to be limited to a brief time span and normocapnia should be re-instituted as soon as is feasible [4].

Conclusion

This study suggested that short-term moderate HC improves, but does not impair cerebral autoregulation in patients with TBI. Moderate HC may provide temporary protection of the brain from spontaneous changes in CPP. The transient optimization of cerebral autoregulation via moderate HC may help bridging procedures or emergencies in neurointensive care when cerebral perfusion pressure is at risk of leaving its optimal level.

Acknowledgements The authors are in debt to the whole team participating in data collection and all the nursing and research staff at the Department of Neurosurgery.

Funding Disclosure Dr. C. Haubrich is supported by a Feodor-Lynen scholarship of the Alexander-von-Humboldt Foundation; Dr. M. Kasprzowicz is a scholar of the Foundation for Polish Science, Dr. M. Czosnyka and Dr. P. Smielewski are supported by MRC grant No.: G9439390, ID 65883. Dr. M. Czosnyka is on unpaid leave from Warsaw University.

Conflict of interest statement ICM+software (www.neurosurg.cam.ac.uk/icmplustwww.neurosurg.cam.ac.uk/icmplust) is licensed by the University of Cambridge, UK, and P. Smielewski and M. Czosnyka have a financial interest in the licensing fee.

References

1. Czosnyka M, Smielewski P, Kirkpatrick P, Menon DK, Pickard JD (1996) Monitoring of cerebral autoregulation in head-injured patients. *Stroke* 27:1829–1834
2. Miller JD, Becker DP (1982) Secondary insults to the injured brain. *J R Coll Surg Edinb* 27:292–298
3. Muizelaar JP, Ward JD, Marmarou A, Newlon PG, Wachi A (1989) Cerebral blood flow and metabolism in severely head injured children, part 2: autoregulation. *J Neurosurg* 71:72–76
4. Bratton S, Chestnut RM, Ghajar J, McConnell Hammond FF, Harris OA, Hartl R, Manley GT, Nemecek A, Newell DW, Rosenthal G, Schouten J, Shutter L, Timmons SD, Ullman JS, Videtta W, Wilberger JE, Wright DW (2007) Hyperventilation. *J Neurotrauma* 24:S87–S90
5. Piechnik SK, Yang X, Czosnyka M, Smielewski P, Fletcher SH, Jones AL, Pickard JD (1999) The continuous assessment of cerebrovascular reactivity: a validation of the method in healthy volunteers. *Anesth Analg* 89:944–949
6. Reinhard M, Roth M, Müller T, Guschlbauer B, Timmer J, Czosnyka M, Hetzel A (2004) Effect of carotid endarterectomy or stenting on impairment of dynamic cerebral autoregulation. *Stroke* 35:1381–1387

7. Cold GE, Christensen MS, Schmidt K (1981) Effect of two levels of induced hypocapnia on cerebral autoregulation in the acute phase of head injury coma. *Acta Anaesthesiol Scand* 5:397–401
8. Imberti R, Bellinzona G, Langer M (2002) Cerebral tissue PO_2 and $SjvO_2$ changes during moderate hyperventilation in patients with severe traumatic brain injury. *J Neurosurg* 96:97–102
9. Newell DW, Weber JP, Watson R, Aaslid R, Winn HR (1996) Effect of transient moderate hyperventilation on dynamic cerebral autoregulation after severe head injury. *Neurosurgery* 1:35–43; discussion 43–34
10. Møller K, Skinhøj P, Knudsen GM, Larsen FS (2000) Effect of short-term hyperventilation on cerebral blood flow autoregulation in patients with acute bacterial meningitis. *Stroke* 31:1116–1122
11. Steiner LA, Balestreri M, Johnston AJ, Coles JP, Chatfield DA, Pickard JD, Menon DK, Czosnyka M (2005) Effects of moderate hyperventilation on cerebrovascular pressure-reactivity after head injury. *Acta Neurochir Suppl* 95:17–20

Correlation of Clinical Outcome and Angiographic Vasospasm with the Dynamic Autoregulatory Response After Aneurysmal Subarachnoid Hemorrhage

Martin Barth, Barth Moratin, Martin Dostal, Armin Kalenka, Johann Scharf, and Kirsten Schmieder

Abstract Background: A certain correlation between unfavorable clinical outcome, incidence of vasospasm, and impaired pressure autoregulation in patients following aneurysmal subarachnoid hemorrhage (aSAH) has been suggested. However, determination of vasospasm is inaccurate and the measurement technique of cerebral vasoreactivity seems not to have been sufficiently validated. Therefore, a correlation of clinical outcome and the extent of angiographic VS was performed using an established autoregulation test.

Material and Methods: Proximal and global angiographic vasospasm (pVS, gVS) were determined in bilateral M1 segments. Dynamic tests of pressure autoregulation were performed 1 day before and after, and on the day of angiography using Aaslid's thigh leg cuff test. Patient outcome was assessed using the Extended Glasgow Outcome Scale (GOSE).

Key Results: Complete datasets were available for 22 patients. Mean autoregulatory indices (ARI) around the day of angiography were 3.9 ± 2.3 . Proximal mean reduction of vessel diameter was $-23.3\% \pm 9.1\%$. Global vasospasm was not present in 10 hemispheres, mild in 15, moderate in 15, and severe in 4. Hemispheric ARI values and angiographic data showed a significant correlation (pVS -0.382 , $p=0.015$; gVS -0.477 , $p=0.002$). The degree of angiographic vasospasm and

low ARI values correlated significantly with an unfavorable outcome (0.677 , $p=0.001$).

Conclusion: Incidence of angiographic vasospasm and impaired clinical outcome seems to be related to impaired pressure autoregulation following aSAH.

Keywords Dynamic cerebral pressure autoregulation • Angiographic vasospasm • aSAH

Introduction

Preliminary evidence has already been presented to demonstrate a certain association among unfavorable clinical outcome, development of vasospasm (VS), and the reduced ability of pressure autoregulation in patients following aneurysmal subarachnoid hemorrhage (aSAH) [8, 12]. However, some of these studies exhibit conceptual limitations making it difficult to draw reliable conclusions. First of all, there are no studies investigating the relationship between angiographic VS and the status of cerebral pressure autoregulation in aSAH patients. Information on the degree of VS has been drawn from surrogate parameters such as measurement of the flow velocity in bilateral M1 sections [12]. However, it is known that transcranial Doppler is characterized by a relatively low sensitivity in predicting delayed cerebral infarction due to VS [4, 9]. Second, the methods used for estimating the status of cerebral autoregulation do not seem to have been sufficiently validated. In most publications 'quasi steady state' measurements have been used, which are known to be prone to disturbances caused by brain metabolism, functional activation, or intrinsic pacemakers [1].

For investigating cerebral VS we therefore chose a method that describes the degree of angiographic VS in detail, and that has recently been described in a similar form [10]. For determination of dynamic pressure autoregulation, a measurement technique has been selected that was introduced more than 10 years ago and that has been shown in numerous studies to give reliable and reproducible estimates of cerebral autoregulation [2, 6].

M. Barth (✉), B. Moratin, M. Dostal, and K. Schmieder
Department of Neurosurgery, University Medicine Mannheim,
Medical Faculty Mannheim of the Karl-Ruprecht-University
of Heidelberg, Theodor-Kutzer-Ufer 1-3, D-68167
Mannheim, Germany
e-mail: martin.barth@umm.de; kirsten.schmieder@umm.de

A. Kalenka
Institute for Anesthesiology and Intensive Care Medicine,
University Medicine Mannheim, Medical Faculty Mannheim of the
Karl-Ruprecht-University of Heidelberg,
Theodor-Kutzer-Ufer 1-3, D-68167
Mannheim, Germany

J. Scharf
Department of Neuroradiology, University Medicine Mannheim,
Medical Faculty Mannheim of the Karl-Ruprecht-University of
Heidelberg, Theodor-Kutzer-Ufer 1-3, D-68167
Mannheim, Germany

Clinical Materials and Methods

Consecutive patients meeting the inclusion criteria were prospectively included in the study. During a time period of 6 months 58 consecutive patients with any form of subarachnoid hemorrhage were screened for eligibility. From these patients, 33 were eligible for the study. Inclusion criteria consisted of:

1. Age 18–70 years
2. Initial H&H I–IV
3. DSA-confirmed saccular aneurysm
4. Diffuse or localized thick subarachnoid clot on baseline CT
5. Onset of aSAH symptoms within 48 h

Exclusion criteria consisted of:

1. SAH due to other causes
2. No or only a thin clot on baseline CT (<20 mm length)
3. Severe concomitant disease

The study was approved by the local Research Ethics Committee and Institutional Review Board. All patients received a baseline DSA on admission to the hospital. Together with the local neuroradiologists consensus was established regarding the treatment modality (clipping or coiling of the aneurysm). Arterial pressure was measured invasively in all patients using an arterial catheter.

Further patient management was carried out according to recommendations of the German Neurosurgical Association [11]. Patients were kept under normovolemia with a central venous pressure of ≥ 8 mmHg and a urinary output ≥ 1 mL/kg/h. If clinical data suggested the presence of vasospasm, patients received control DSA. If angiographic vasospasm was confirmed, triple H-therapy was initiated with all concomitant standard medical and pharmacological management of critically ill patients. For further analysis, DSAs were reviewed by an experienced neuroradiologist (JS) similar to the recently described method [10].

In short, for determination of proximal VS (pVS), bilateral diameters of the M1 segments were measured digitally pre- and post-treatment in absolute values. No VS was present with reduction of the vessel diameter of 0–10%, mild VS with reduction of 11–30%, moderate VS with 31–70%, severe VS with reduction more than 71%.

For estimation of global VS (gVS) distal vessel segments were incorporated into the analysis. Therefore, the distal segments (M2+) were examined using a qualitative grading system (none/mild/moderate/severe). By definition, the degree of gVS was determined according to the most affected section, e.g., moderate gVS was present with moderate pVS and mild distal vasospasm, but also with mild pVS but moderate distal vasospasm.

For determination of dynamic pressure autoregulation, Aslid's thigh leg cuff test was performed at 3 days around

Table 1 Patient characteristics

Age	56.5 \pm 9.5
Female	15 (68)
Surgical clipping	13 (59)
Initial World Federation of Neurological Surgeons grade	
Grade 1	3 (14)
Grade 2	6 (27)
Grade 3	0 (0)
Grade 4	6 (27)
Grade 5	7 (32)
Proportion of smokers	13 (59)

Given values are *n* (%) or mean \pm SD when appropriate

the day of control DSA using the procedure described in the original report [2]. Extraction of the autoregulatory indices was performed offline using software supplied by the manufacturer (DWL, Sipplingen, Germany)

Clinical outcome was determined 14 days after bleeding using the Extended Glasgow Outcome Scale (GOSE).

Statistical Analysis

Patient characteristics and clinical outcome parameters are given as *n* (%), mean values \pm standard deviation (SD), or as min/median/max, as applicable. Parametric data such as proximal vessel diameters were analyzed using Student's *t* test. Correlation analysis was performed using Pearson's correlation. Differences were considered to be significant when $p < 0.05$.

Results

Fifty-eight patients with the diagnosis of SAH were screened for eligibility, 33 of who met the inclusion criteria. Reasons for exclusion were admission >48 h postbleeding in 6, presence of mesencephalic SAH or failure to detect an aneurysm in 6, presence of a thin clot on initial CT or traumatic SAH in 5, absence of preoperative DSA in 3, age >70 in 1, blister-like aneurysm in 2, and severe concomitant disease in 3 patients.

From these 33 eligible patients, a further 11 had to be excluded from analysis for the following reasons: refusal to participate in the thigh leg cuff tests in 5, failure to cooperate in 2, inadequate signal quality in 2, missing control DSA at day 8 postbleeding in 1. Thus, 22 patients were eligible for analysis, and the detailed baseline characteristics of this cohort are given in Table 1.

For analysis of pVS 44 hemispheric vessel segments were available for analysis. Compared with baseline, there was a

Table 2 Physiological variables

PaO ₂	112.5 ± 26.7
PaCO ₂	38.3 ± 3.2
ARI left	3.8 ± 2.3
ARI right	4.1 ± 2.3
Proximal vasospasm left	2/1/4
Proximal vasospasm right	2/1/4
Global vasospasm left	2.5/1/4
Global vasospasm right	2/1/4
Extended Glasgow Outcome Scale	5/1/7

Given values are mean ± SD or median/min/max when appropriate

Table 3 Index correlations

	ARI	
	Correlation coefficient	<i>p</i> value
Proximal vasospasm	−0.382	0.015
Global vasospasm	−0.477	0.002
Extended Glasgow Outcome Scale	0.677	0.001

mean reduction in the vessel diameter of 23.3% ± 29. According to the definition provided in the “**Materials and methods**” section, no pVS was present in 12, mild in 12, moderate in 14, and severe pVS in 2 hemispheres. For analysis of gVS, distal vessel segments (M2+) were incorporated into the analysis. According to the most affected vessel segment, 10 segments showed no gVS, 15 mild, 15 moderate, and 4 severe gVS (Table 2).

Around the day of control DSA, 112 ARI values were available for analysis. The mean left and right hemispheric ARI was 3.8 ± 2.3 and 4.1 ± 2.4 respectively (Table 2).

Clinical outcome as measured by the GOSE ranged from 1 (death) to 7 (lower good recovery) with a median of 5 (lower moderate disability; Table 2).

The hemispheric ARI values and pVS revealed that low ARI values indicating impaired pressure autoregulation correlated significantly with the incidence of proximal angiographic vasospasm (−0.382, *p* = 0.015). With correlation of hemispheric ARI values with gVS this relationship seems even stronger (−0.477, *p* = 0.002). Correlation of bihemispheric ARI values with GOSE showed a significant relationship between low ARI values and low GOSE values, indicative of unfavorable clinical outcome (0.677, *p* = 0.001; Table 3).

Discussion

The present study demonstrates that there seems to be a significant relationship between unfavorable clinical status, development of angiographic vasospasm and impaired

dynamic pressure autoregulation. These results seem to be in line with other investigations on this topic. However, there are methodological questions that remain to be clarified, e.g., the comparability of different approaches to measuring or estimating the status of cerebral autoregulation. To retain Aaslid’s nomenclature, a multitude of quasi steady state measurement techniques have evolved with advanced processing of online biosignals such as the PRx, ORx, Mx, or the TOx [5, 7, 12, 13]. All of these autoregulatory indices claim to give certain estimates of the status of cerebral autoregulation. However, simultaneous determination of pressure-, oxygen-, and flow-related indices revealed diverging results in patients following aSAH [3]. Thus, quasi steady state measurement techniques seem to be more delicate with regard to factors such as functional activation, respiration, metabolic fluctuations, and interactions among pO₂, pH, pCO₂, and nitric oxide. Therefore, validation of these techniques seems to be of great importance. At the same time, it is crucial to investigate the natural course of cerebral autoregulation with regard to clinical outcome and VS using an already established measurement method, which has been done in the present study. Determination of the autoregulatory index (ARI) using the thigh leg cuff method is safe, reproducible, and relatively independent of the above-mentioned distracting factors.

A limitation of the study is the fact that ARI values were determined only around the day of angiography. Another study suggested that the decline of an oxygen-related index of cerebrovascular reactivity would be indicative of the development of cerebral infarction in patients following aSAH [8]. Based on the present data we cannot verify if at all or at what time point ARI values become lower in clinically unfavorable patients.

Conclusion

Based on the present data, there is a significant correlation among low ARI values indicating impaired pressure autoregulation, the degree of vessel constriction and unfavorable outcome following aSAH. Analysis of ARI values from day 1+ following aSAH will further elicit the timing of impaired pressure autoregulation in aSAH patients.

Conflict of interest statement We declare that we have no conflict of interest.

Financial Disclosure: There was no financial support in regard of planning, realization, analysis, and submission of the present submission. None of the authors listed have any personal or institutional financial interest in drugs, materials, or devices described in the present submission.

References

1. Aaslid R (2006) Cerebral autoregulation and vasomotor reactivity. In: Baumgartner RW (ed) *Handbook on neurovascular ultrasound*, vol 21. Karger, Basel, pp 216–228
2. Aaslid R, Lindegaard KF, Sorteberg W, Nornes H (1989) Cerebral autoregulation dynamics in humans. *Stroke* 20:45–52
3. Barth M, Woitzik J, Weiss C, Muench E, Diepers M, Schmiedek P, Kasuya H, Vajkoczy P (2010) Correlation of clinical outcome with pressure-, oxygen-, and flow-related indices of cerebrovascular reactivity in patients following aneurysmal SAH. *Neurocrit Care* 12:234–243
4. Carrera E, Schmidt JM, Oddo M, Fernandez L, Claassen J, Seder D, Lee K, Badjatia N, Connolly ES Jr, Mayer SA (2009) Transcranial Doppler for predicting delayed cerebral ischemia after subarachnoid hemorrhage. *Neurosurgery* 65:316–323, discussion 323–314
5. Czosnyka M, Smielewski P, Kirkpatrick P, Laing RJ, Menon D, Pickard JD (1997) Continuous assessment of the cerebral vasomotor reactivity in head injury. *Neurosurgery* 41:11–17, discussion 17–19
6. Hlatky R, Furuya Y, Valadka AB, Gonzalez J, Chacko A, Mizutani Y, Contant CF, Robertson CS (2002) Dynamic autoregulatory response after severe head injury. *J Neurosurg* 97:1054–1061
7. Jaeger M, Schuhmann MU, Soehle M, Meixensberger J (2006) Continuous assessment of cerebrovascular autoregulation after traumatic brain injury using brain tissue oxygen pressure reactivity. *Crit Care Med* 34:1783–1788
8. Jaeger M, Schuhmann MU, Soehle M, Nagel C, Meixensberger J (2007) Continuous monitoring of cerebrovascular autoregulation after subarachnoid hemorrhage by brain tissue oxygen pressure reactivity and its relation to delayed cerebral infarction. *Stroke* 38:981–986
9. Lee JY, Lee MS, Whang K, Lee JM, Kim SH, Lee SS (2006) Accuracy of transcranial Doppler sonography for predicting cerebral infarction in aneurysmal subarachnoid hemorrhage. *J Clin Ultrasound* 34:380–384
10. Macdonald RL, Kassell NF, Mayer S, Ruefenacht D, Schmiedek P, Weidauer S, Frey A, Roux S, Pasqualin A (2008) Clazosentan to overcome neurological ischemia and infarction occurring after subarachnoid hemorrhage (CONSCIOUS-1): randomized, double-blind, placebo-controlled phase 2 dose-finding trial. *Stroke* 39:3015–3021
11. Raabe A, Beck J, Berkefeld J, Deinsberger W, Meixensberger J, Schmiedek P, Seifert V, Steinmetz H, Unterberg A, Vajkoczy P, Werner C (2005) Recommendations for the management of patients with aneurysmal subarachnoid hemorrhage. *Zentralbl Neurochir* 66:79–91
12. Soehle M, Czosnyka M, Pickard JD, Kirkpatrick PJ (2004) Continuous assessment of cerebral autoregulation in subarachnoid hemorrhage. *Anesth Analg* 98:1133–1139, table of contents
13. Zweifel C, Castellani G, Czosnyka M, Carrera E, Brady KM, Kirkpatrick PJ, Pickard JD, Smielewski P (2010) Continuous assessment of cerebral autoregulation with near-infrared spectroscopy in adults after subarachnoid hemorrhage. *Stroke* 41:1963–1968

Comparison of a New Brain Tissue Oxygenation Probe with the Established Standard

Stefan Wolf, P. Horn, C. Frenzel, L. Schürer, P. Vajkoczy, and J. Dengler

Abstract Introduction: Continuous bedside brain tissue oxygenation ($p_{br}O_2$) monitoring using the Licox system is an established method for detecting secondary ischemia in comatose patients with acute brain injury. The purpose of the current study was to compare the newly introduced Raumedic $p_{br}O_2$ probe with the established standard.

Methods: Eighteen patients with acute traumatic brain injury or aneurysmal subarachnoid hemorrhage had $p_{br}O_2$ probes of both types implanted side by side in the same vascular territory at risk of ischemia. Data were analyzed by the Bland–Altman method as well as random effect regression models to correct for multiple measurements per individual.

Results: Both types of probes were able to display spontaneous fluctuations of $p_{br}O_2$ as well as reactions to therapy. Mean measurement difference between the Licox and Raumedic probes was -2.3 mmHg, with corresponding 95% limits of agreement of -32.3 to 27.5 mmHg. Regarding an ischemia threshold of 15 mmHg, both probes were in agreement in 78% and showed disparate results in 22%.

Conclusions: Our data suggest that the $p_{br}O_2$ measurements of the two systems cannot be interchanged. Although we were unable to determine which system delivers more valid data, we do think that more rigorous testing is necessary before implementing the new probe in clinical routine.

Keywords Brain tissue oxygenation • Monitoring • Ischemia • Licox • Raumedic

Introduction

Continuous bedside brain tissue oxygenation ($p_{br}O_2$) monitoring with the Licox system (Integra Neuroscience) is an established method of detecting secondary ischemia in comatose patients with acute brain injury. In patients after traumatic brain injury and subarachnoid hemorrhage, a relationship between $p_{br}O_2$ monitoring and outcome has recently been established [1–3]. Owing to its stability and the lack of competition, the Licox $p_{br}O_2$ sensor became the de facto gold standard.

Recently, a new $p_{br}O_2$ probe by a different manufacturer (Neurovent PTO, Raumedic) was introduced. This new probe facilitates concurrent measurement of intracranial pressure (ICP), brain temperature, and $p_{br}O_2$. Therefore, its use would reduce the invasiveness of multimodal neuromonitoring. However, before new technology is introduced, its performance and compatibility with the existing standards need to be established. The ICP component of the new probe has shown favorable performance in bench testing and multicenter evaluation [4, 5]. The purpose of the present study was to investigate the level of agreement of $p_{br}O_2$ values from the Licox and Raumedic probes in routine clinical use.

Materials and Methods

In 23 comatose patients requiring mechanical ventilation after aneurysmal subarachnoid hemorrhage or traumatic brain injury, a Licox CC1.SB $p_{br}O_2$ probe (Integra Neuroscience, Saint Priest, France) and a Neurovent PTO probe (Raumedic, Münchberg, Germany) were implanted side by side in the same vascular territory at risk of ischemia (Fig. 1). Placement target was the frontal white matter, either the side of the more severely injured hemisphere after traumatic brain injury or the tissue supplied by the aneurysm-harboring vessel after subarachnoid hemorrhage. The indication for implementation of advanced neuromonitoring using parenchymal ICP and $p_{br}O_2$ probes was based solely on clinical grounds at the discretion of the neurosurgeon in charge.

S. Wolf (✉)

Department of Neurosurgery, Campus Virchow, Charité University, Augustenburger Platz 1, Berlin 13353, Germany and
Department of Neurosurgery, Klinikum Bogenhausen, Munich, Germany
e-mail: stefan.wolf@charite.de

P. Horn, C. Frenzel, P. Vajkoczy, and J. Dengler
Department of Neurosurgery, Campus Virchow, Charité University, Augustenburger Platz 1, Berlin 13353, Germany

L. Schürer
Department of Neurosurgery, Klinikum Bogenhausen, Munich, Germany

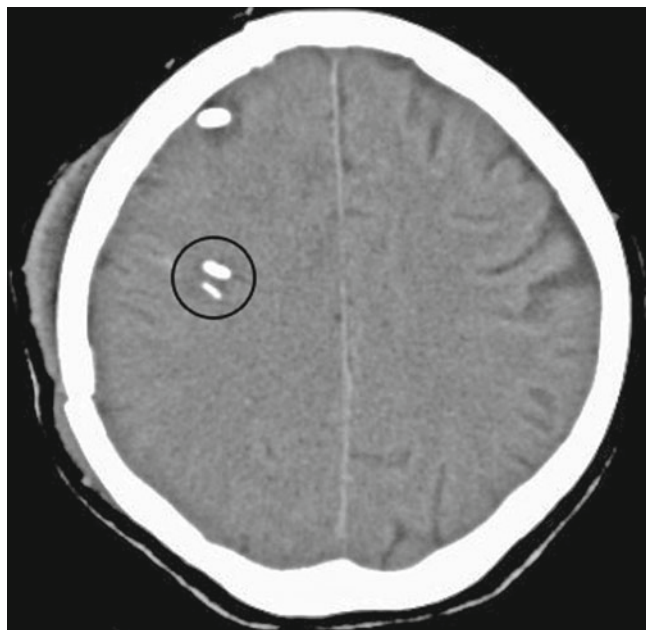


Fig. 1 Sample CT with both brain tissue oxygenation probes (black circle) side by side in the same vascular territory

Patients were treated during 2008 in the Department of Neurosurgery, Klinikum Bogenhausen, Technical University of Munich, Germany and from June 2009 until April 2010 in the Department of Neurosurgery at Campus Virchow, Charité University Berlin, Germany. Thirteen of the patients in Berlin were included in a prospective study investigating the $p_{br}O_2$ reactivity of the two probes. Their next of kin gave informed consent, as required by the local ethics committee. For anonymous review of the data from the other patients, the need for informed consent was waived.

Multimodal neuromonitoring data were stored online with dedicated software (ICUpilot, CMA Microdialysis, Solna, Sweden, in Munich, and ICMplus, University of Cambridge, UK, in Berlin, respectively) and averaged once per minute. Only $p_{br}O_2$ values within the clinical relevant range between 1 and 50 mmHg were investigated. Measurements outside this range were discarded to reduce distortion of the numerical analysis by outlying values.

Data were analyzed graphically by plotting the difference against the corresponding mean of single measurements from both probes, as proposed by Bland and Altman [6]. A second plot was performed with the differences expressed as percentage of the means. In Bland–Altman analysis, the mean of all differences defines the bias of measurements and the borders of the 95% confidence interval of mean differences are traditionally termed as the limits of agreement.

Both plots showed a dependency of the mean differences in magnitude and variance on the mean $p_{br}O_2$. As this and the repeated measurement nature of the data with multiple values per individual are limitations of the classic Bland–Altman analysis [7], random effects modeling was performed for

appropriate statistical analysis [8]. To facilitate comparability with other published work, the classical limits of agreement, without consideration of the aforementioned violations of the Bland–Altman approach, were also calculated.

Results

Data from 18 of the 23 patients were analyzable. In three patients, one of the two probes was located in infarcted tissue on CT following implantation. One patient required craniectomy for refractory ICP due to brain swelling a few hours after probe placement and both probes had to be removed. In another patient, the $p_{br}O_2$ part of the Raumedic probe was malfunctioning after implantation. Consequently, data from these patients were excluded. Additionally, the $p_{br}O_2$ part of five Raumedic probes ceased to function prematurely and data after this time were removed.

Mean analyzed measurement time per patient was 6.7 days. In total, 172,585 min of $p_{br}O_2$ data were evaluated. When all data were pooled, mean $p_{br}O_2$ values were 25.7 (SD 11.5) mmHg using Licox probes and 28.0 (SD 14.9) mmHg with Raumedic probes, giving a mean bias of -2.3 mmHg or -8.8% . Bias was widely scattered between patients (-22.1 to 19.5 mmHg).

Both types of probes were able to display spontaneous fluctuations of $p_{br}O_2$ as well as reactions to therapy. Analysis of single patients revealed no discernible pattern in the relationship between measurement values of the two probes (Fig. 2). Regarding an ischemia threshold of 15 mmHg, as suggested for the Licox system, both probes were in agreement in 78% and showed disparate results in 22% of single measurement points.

The 95% limits of agreement according to a classic Bland–Altman analysis were -32.3 to 27.5 mmHg or -118% to 112% (Fig. 3). Further investigation with a random effects model to consider repeated measurements, non-constant mean difference, and changing variance over the measurement range gave a more appropriate characterization of the data (bold dashed lines in Fig. 3). Bias and 95% limits of agreement were significantly related to the mean $p_{br}O_2$ in each instance of different random effects models with the mean difference expressed either absolute or as a percentage (all: $p < 0.001$). Licox probes showed a tendency toward higher values at low $p_{br}O_2$, while the values from the Raumedic probes were higher at high $p_{br}O_2$.

Discussion

The main finding of our study was that $p_{br}O_2$ measurements of the Licox and the Raumedic systems show a large discrepancy, although both probes were implanted side by side in

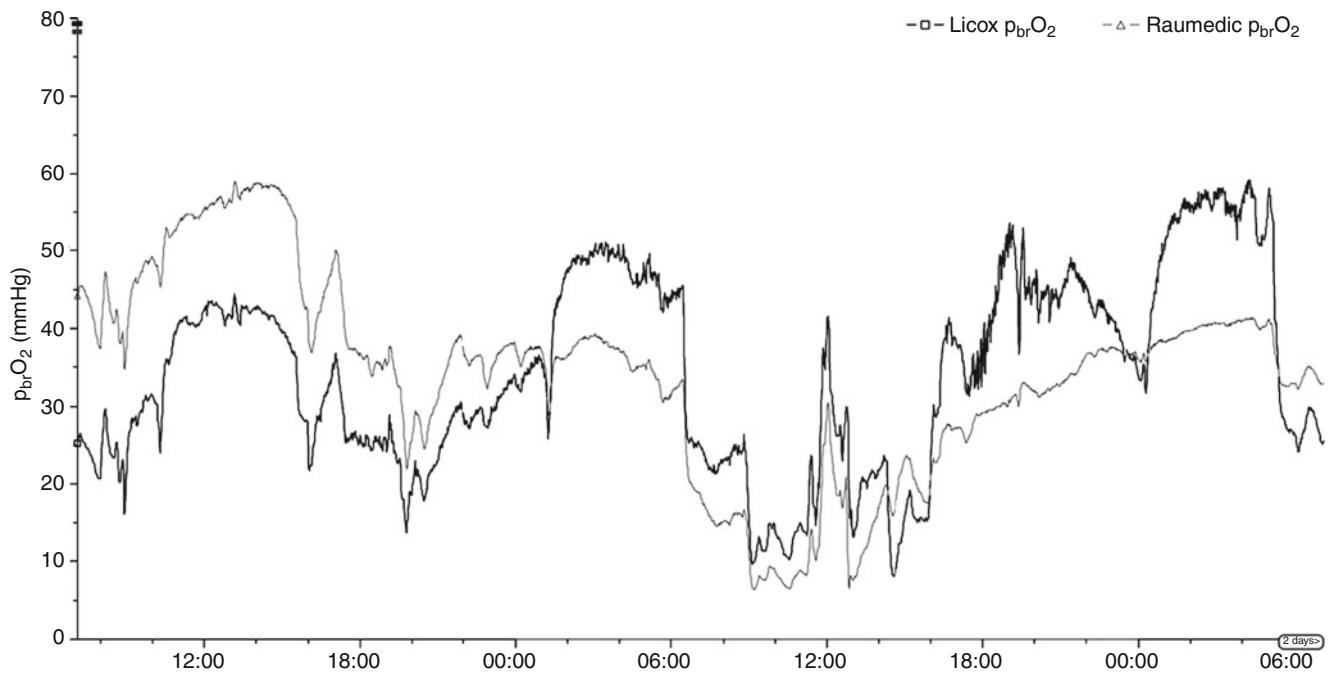


Fig. 2 Measurement time series of the Raumedic and the Licox $p_{br}O_2$ probe (same patient as in Fig. 1). Although both seem to capture short-term trends and fluctuations accurately, there is no constant, recognizable pattern for a transfer function

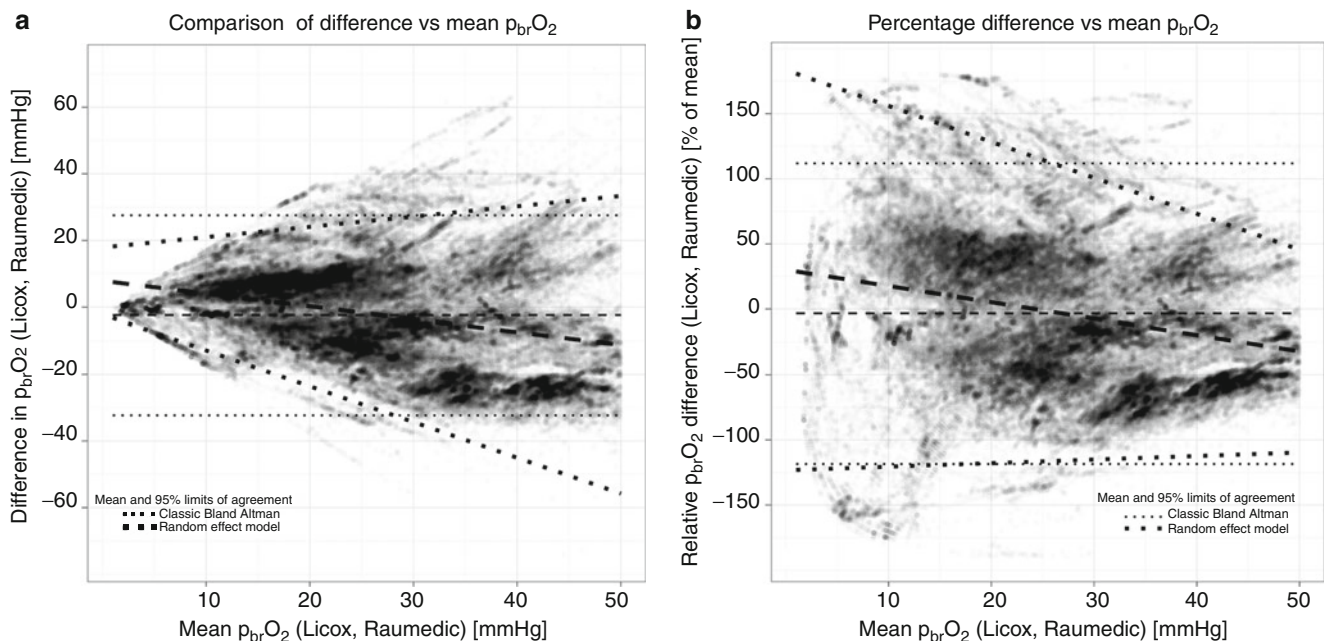


Fig. 3 Bland-Altman plots of (a) mean differences and (b) mean percentage differences of the mean $p_{br}O_2$

the same vascular territory. We were unable to find a reliable transfer algorithm for conversion of measurement data from one system to the other. However, we want to emphasize that our study design did not allow us to determine which system delivers more valid data.

Classic Bland-Altman analysis is known to underestimate the limits of agreement in the case of repeated measurements

in the same individual [7]. Random effects modeling allows a more adequate statistical assessment, but is of course not able to remove the scatter present in the raw data. However, judgment on the exchangeability of measurements from the two devices is a clinical decision that depends on the required accuracy and not on statistical significance. A maximum difference of 30% was proposed to rate two different methods

of measurement as equal [9]. This failed with either type of statistical description.

So far, published data on the comparison of both probes are inconclusive [10–12]. In laboratory bench testing using calibrated oxygenated fluids, both probes were accurate in detecting different oxygen tensions and did not deviate over longer recording times [10]. Differences were found in response time to changes in oxygen tension, favoring the Raumedic system. A swine model showed a similar baseline measurement of the two probes, but revealed significantly different profiles during hyperoxygenation and a faster response time for the Raumedic probe [11]. In their conclusion, the authors questioned whether the existing knowledge on the hypoxic threshold established for the Licox probe might be directly transferred to the new system. A clinical comparison study with a similar design to ours showed limits of agreement of the same magnitude (95% CI: –25.1 to 22.6 mmHg) [12]. Nevertheless, the authors suggested that both probes might be used interchangeably, but cautioned with regard to their interpretation owing to several limitations of their study. Of further concern in this and in our study is a high rate of mechanical failure of the $p_{br}O_2$ part of the Raumedic probe.

The reasons for the wide limits of agreement of $p_{br}O_2$ measurements of the two probes are unknown. A possible explanation may be the heterogeneity of $p_{br}O_2$, especially when it is measured in tissue at risk of ischemia. Furthermore, the Licox probe is based on a Clark-type polarographic electrode, while the Raumedic probe uses luminescence quenching [12]. The level of $p_{br}O_2$ is dependent on the amount of brain edema, cerebral blood flow and metabolism including pH changes induced by hyperventilation. Interactions of biochemical tissue conditions with one or both measurement principles of the $p_{br}O_2$ probes seem at least conceivable. As the clinical implications of ischemia detection using bedside $p_{br}O_2$ measurements are great, both theories warrant further investigation.

Conclusion

Our data suggest that the $p_{br}O_2$ measurements of the two systems cannot be interchanged. We found no reliable transfer algorithm for the conversion of measurement data from one system to the other. Although we want to emphasize that we were unable to determine which system delivers more valid data, we do think that more rigorous testing is necessary

before the new probe is implemented in clinical routine. In our opinion, local $p_{br}O_2$ heterogeneity and the different perception of changes in oxygen tension in biological tissue are possible explanations for the disparate measurements of the two probes and warrant further investigation.

Conflict of interest statement We declare that we have no conflict of interest.

References

1. Ramakrishna R, Stiefel M, Udoetuk J, Udoteuk J, Spiotta A, Levine JM et al (2008) Brain oxygen tension and outcome in patients with aneurysmal subarachnoid hemorrhage. *J Neurosurg* 109(6): 1075–1082
2. Narotam PK, Morrison JF, Nathoo N (2009) Brain tissue oxygen monitoring in traumatic brain injury and major trauma: outcome analysis of a brain tissue oxygen-directed therapy. *J Neurosurg* 111(4):672–682
3. Spiotta AM, Stiefel MF, Gracias VH, Garuffe AM, Kofke WA, Maloney-Wilensky E et al (2010) Brain tissue oxygen-directed management and outcome in patients with severe traumatic brain injury. *J Neurosurg* 113(3):571–580
4. Citerio G, Piper I, Cormio M, Galli D, Cazzaniga S, Enblad P et al (2004) Bench test assessment of the new Raumedic Neurovent-P ICP sensor: a technical report by the BrainIT group. *Acta Neurochir (Wien)* 146(11):1221–1226
5. Citerio G, Piper I, Chambers IR, Galli D, Enblad P, Kiening K et al (2008) Multicenter clinical assessment of the Raumedic Neurovent-P intracranial pressure sensor: a report by the BrainIT group. *Neurosurgery* 63(6):1152–1158; discussion 1158
6. Bland JM, Altman DG (1986) Statistical methods for assessing agreement between two methods of clinical measurement. *Lancet* 1(8476):307–310
7. Bland JM, Altman DG (1999) Measuring agreement in method comparison studies. *Stat Methods Med Res* 8(2):135–160
8. Myles PS, Cui J (2007) Using the Bland-Altman method to measure agreement with repeated measures. *Br J Anaesth* 99(3):309–311
9. Critchley LA, Critchley JA (1999) A meta-analysis of studies using bias and precision statistics to compare cardiac output measurement techniques. *J Clin Monit Comput* 15(2):85–91
10. Purins K, Enblad P, Sandhagen B, Lewén A (2010) Brain tissue oxygen monitoring: a study of in vitro accuracy and stability of Neurovent-PTO and Licox sensors. *Acta Neurochir (Wien)* 152(4):681–688
11. Orakcioglu B, Sakowitz OW, Neumann JO, Kentar MM, Unterberg A (2010) Evaluation of a novel brain tissue oxygenation probe in an experimental swine model. *Neurosurgery* 67(6):1716–1722; discussion 1722–1723
12. Huschak G, Hoell T, Hohaus C, Kern C, Minkus Y, Meisel H (2009) Clinical evaluation of a new multiparameter neuromonitoring device: measurement of brain tissue oxygen, brain temperature, and intracranial pressure. *J Neurosurg Anesthesiol* 21(2):155–160

Comparing Brain Tissue Oxygen Measurements and Derived Autoregulation Parameters from Different Probes (Licox vs. Raumedic)

M. Dengl, M. Jaeger, C. Renner, and J. Meixensberger

Abstract We investigated two commercially available probes for measurement of the partial pressure of brain tissue oxygen (PbrO₂) and calculation of the index of brain tissue oxygen pressure reactivity (OR_x) in 7 patients after aneurysmal subarachnoid hemorrhage (SAH). Simultaneous monitoring of PbrO₂ using the Licox® probe and the multiparameter Raumedic probe (Neurovent PTO®), measuring PbrO₂, intracranial pressure (ICP) and brain temperature (Neurovent PTO) was performed for a median of 9 days (range 7–17 days). Both probes provided stable monitoring throughout the desired period. Mean PbrO₂ from Licox and Neurovent PTO was 16.1 ± 9.0 mmHg and 17.5 ± 11.9 mmHg respectively. Mean OR_x was 0.35 ± 0.44 and 0.31 ± 0.43 respectively. There was a difference in the measurement of PbrO₂ of -2.73 ± 10.1 mmHg (Licox – Raumedic). The difference in the two values for the calculated OR_x was far smaller (0.03 ± 0.31 ; Licox – Raumedic) and the correlation coefficient higher than for both values of PbrO₂ (0.76 for OR_x vs. 0.56 for PbrO₂). The calculation of the autoregulation parameter OR_x seemed more independent of the measurement process than the measurement of PbrO₂ itself and signifies the potential clinical importance of this parameter.

Keywords Aneurysmal subarachnoid hemorrhage • Brain tissue oxygen • Cerebrovascular autoregulation • Neuromonitoring

Introduction

Advanced neuromonitoring of patients suffering from traumatic brain injury (TBI) and aneurysmal subarachnoid hemorrhage (SAH) has significantly improved our understanding of intracranial disease processes and is increasingly used to guide intensive care therapy [5–7]. Apart from measuring intracranial pressure (ICP) and cerebral perfusion pressure (CPP), continuous monitoring of the partial pressure of brain tissue oxygen (PbrO₂) has emerged as a promising clinical tool [7]. PbrO₂, a surrogate marker of cerebral blood flow, also allows calculation of the index of brain tissue oxygen pressure reactivity (OR_x), which provides a bedside assessment of cerebrovascular autoregulation [6], a crucial factor to secondary brain damage in traumatic brain injury and delayed infarction after subarachnoid hemorrhage [4–6].

Probes from different manufacturers are commercially available for monitoring of PbrO₂. They have been extensively tested in vitro by manufacturers and independent investigators [8]. However, only one report compared probes in vivo, mainly in patients after TBI [3]. We aimed to investigate simultaneous in vivo measurements using the Licox and Raumedic system in patients after SAH, and the effects on the OR_x derived. Both probes differ from each other as they use different measurement processes (electro-chemical vs physical) for PbrO₂ [3].

Materials and Methods

Patient demographics are given in Table 1. Patients required artificial ventilation and sedation after occlusion of the aneurysm and were included in our standard neuromonitoring setup with measurement of PbrO₂ via Licox CC1.SB (Integra NeuroSciences Inc.) and ICP and PbrO₂ via Neurovent PTO (Raumedic AG). Because the monitoring of ICP is provided by the multiparameter probe (Neurovent PTO), no additional

M. Dengl (✉), C. Renner, and J. Meixensberger
Department of Neurosurgery, University of Leipzig,
Liebigstrasse 20, 04103 Leipzig, Germany
e-mail: markus.dengl@medizin.uni-leipzig.de

M. Jaeger
Department of Neurosurgery, Liverpool Hospital,
University of New South Wales, Liverpool, NSW, Australia

Table 1 Patient characteristics, clinical course and mean ORx calculated at days 5 and 6 after bleeding from PbrO2 values from either the Licox or the Raumedic device

Patient number	Gender, age (years)	WFNS grade	Aneurysm location	Delayed cerebral infarction	GOS after 6 months	ORx_Licox days 5+6	ORx_Raumedic days 5+6
1	Female, 42	2	Acom	–	3	0.42	0.35
2	Female, 67	4	Acom	+	1	0.56	0.36
3	Female, 44	5	MCA left	–	3	0.38	0.33
4	Female, 63	5	Acom	+	1	0.58	0.51
5	Female, 48	2	MCA left	–	5	0.35	0.26
6	Female, 66	5	Acom	+	1	0.42	0.32
7	Male, 74	5	PICA right	–	2	0.18	0.28

Note: WFNS grade was evaluated at hospital admission, delayed cerebral infarction was confirmed via CAT, GOS was assessed via telephone interview

Acom anterior communicating artery, MCA middle cerebral artery, PICA posterior inferior cerebellar artery

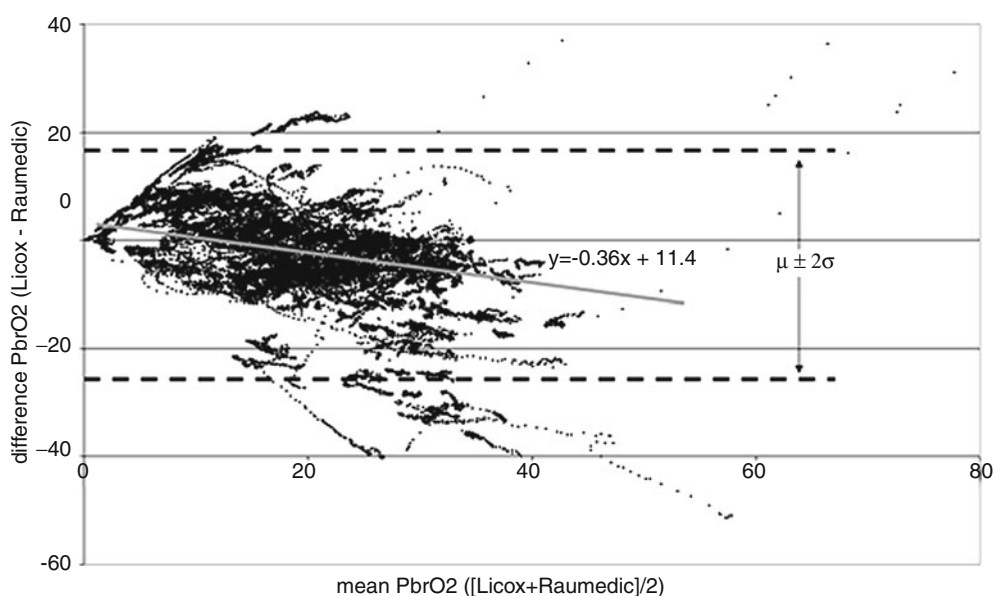


Fig. 1 Bland–Altman plot comparing PbrO2 values obtained via Licox and Raumedic devices. Depicted are the mean PbrO2 on the x-axis and the difference in both PbrO2 values on the y-axis. Depicted in gray is

the linear regression gradient. Note: for clarity only every third data-point is depicted

manipulation or probe insertion was required for this study; the probes were inserted via a standard two-lumen-bolt. Because monitoring of ICP and PbrO2 is part of the routine management in our department, the need for informed consent was waived by the local ethics committee. Data were stored every 30 s and processed using the ICM+ software (University of Cambridge) [2]. ORx was calculated as previously described [6] as the moving correlation coefficient between 120 corresponding CPP and PbrO2 values (i.e., obtained over 1 h). Outcome was assessed after 6 months via telephone interview using the Glasgow Outcome Scale (GOS). Due to small sample size statistical analysis was limited to descriptive statistical methods.

Results

Patients were monitored for a median of 9 days (range 7–17 days). A total of 929 h consisting of 111,474 datapoints of simultaneous PbrO2 data was available for further analysis after removal of artefacts. Both PbrO2 probes measured in the total mean similar values (PbrO2_Licox 16.1 ± 9.0 mmHg vs. PbrO2_Raumedic 17.5 ± 11.9 mmHg) with a mean difference of -2.73 ± 10.1 mmHg (PbrO2_Licox – PbrO2_Raumedic).

Analyzing the Bland–Altman plot in Fig. 1 the following information can be obtained: during high PbrO2, the Raumedic probe appeared to measure higher values and vice versa (Fig. 1). Using the ordinary least squares method for a

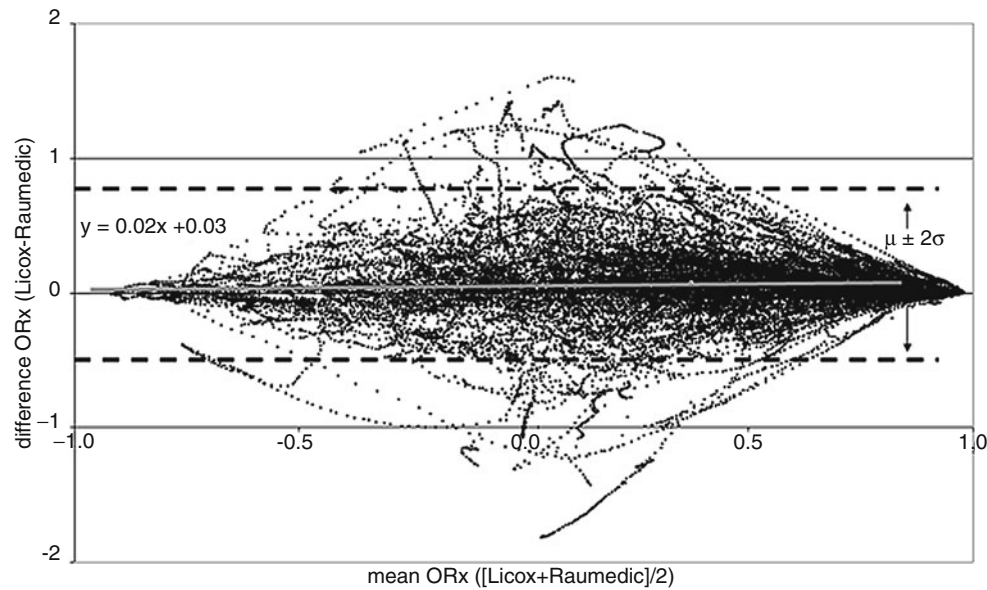


Fig. 2 Bland–Altman plot comparing ORx calculated from PbrO₂ values obtained via the Licox or the Raumedic device. As in Fig. 1 the mean ORx is on the x-axis, the difference in the two values is presented

on the y-axis. Depicted in *gray* is the linear regression gradient. *Note:* for better clarity only every third datapoint is depicted in this figure

linear regression on the plot the gradient was -0.36 and the crossing point with the x-axis was at 11.0 mmHg, supporting the visual impression.

Mean values of ORx were 0.35 ± 0.44 and 0.31 ± 0.43 for Licox and Raumedic. Mean difference in ORx (Licox – Raumedic) was 0.03 ± 0.30 (Fig. 2). Applying the same regression method on this plot the gradient was 0.02 , the crossing point was at -1.67 . The correlation of the ORx values was better than for the PbrO₂ values. Pearson's correlation coefficient for ORx was 0.76 vs. 0.56 for PbrO₂.

ORx from both Licox and Neurovent PTO showed a trend toward an association between impaired autoregulation and poor outcome/occurrence of delayed cerebral infarctions (Table 1).

Discussion

Both probes provided sufficient stability for clinical use throughout the desired monitoring periods. The PbrO₂ values measured by both probes showed debatable difference at most timepoints. No limits of acceptance according to Bland and Altman [1] were defined for this study and direct comparison could therefore not be applied. As absolute critical thresholds concerning PbrO₂ are not clearly defined in the literature this definition would be arbitrary. Would a difference of 10 mmHg be clinically significant, or even 5 mmHg or less? Both probes measured an oxygen partial pressure with a perceivable gradient. Comparing our plot (Fig. 1) and

our data with Huschak et al. [3] the similar results can be acknowledged: at high values the Raumedic probe trends toward higher PbrO₂ values; below about 11.0 mmHg the Raumedic probe returns lower values. Whether this finding harbors clinical importance remains unanswered. Another question is whether the measured differences for PbrO₂ are indeed due to the different measuring devices – for instance both probes have different sizes of sampling area: 13 mm² and 22 mm² for Licox and Raumedic respectively [3] – or are at least in part due to physiological or pathological differences in the brain parenchyma, although both probes are inserted through the same bolt in the frontal white matter.

The assessment of the cerebral autoregulation through PbrO₂ is an important application. We therefore analyzed ORx derived from both probes. As the degree of autoregulation impairment should theoretically be independent of absolute PbrO₂ values a higher level of confidence is expected for the ORx values. This is shown when comparing visually both plots, regarding the mean values and the linear regression parameters. Around the mean value of both ORx of 0.32 the mean difference for both ORx is only 0.03 (estimated with the linear regression model). Of course, it should be admitted that this higher level of confidence is also a result of the nature of the ORx calculation derived from 120 datapoints compared with the single measurements of PbrO₂ values. However, ORx proves to be a stable parameter for evaluation of autoregulation impairment independent of the measuring device applied. The same trend as described by Jaeger et al. [5] could be found when analyzing the impairment of autoregulation and delayed cerebral infarction (Table 1).

To conclude, both probes provide stable PbrO₂ measurements, but we observed a potentially significant difference, in that ORx appears to be less dependent on the type of probe used.

Conflict of interest This study was supported by the RAUMEDIC AG through supplying the monitoring device at no cost. The authors declare that they have no other conflicts of interest.

References

1. Bland JM, Altman DG (1986) Statistical methods for assessing agreement between two methods of clinical measurement. *Lancet* 1(8476):307–310
2. Czosnyka M, Whitehouse H, Smielewski P, Kirkpatrick P, Pickard JD (1994) Computer supported multimodal monitoring in neuro intensive care. *Int J Clin Monit Comput* 11(4):223–232
3. Huschak G, Hoell T, Hohaus C, Kern C, Minkus Y, Meisel HJ (2009) Clinical evaluation of a new multiparameter neuromonitoring device: measurement of brain tissue oxygen, brain temperature, and intracranial pressure. *J Neurosurg Anesthesiol* 2: 155–160
4. Jaeger M, Schuhmann MU, Soehle M, Meixensberger J (2006) Continuous assessment of cerebrovascular autoregulation after traumatic brain injury using brain tissue oxygen pressure reactivity. *Crit Care Med* 34(6):1783–1788
5. Jaeger M, Schuhmann MU, Soehle M, Nagel C, Meixensberger J (2007) Continuous monitoring of cerebrovascular autoregulation after subarachnoid hemorrhage by brain tissue oxygen pressure reactivity and its relation to delayed cerebral infarction. *Stroke* 38(3):981–986
6. Jaeger M, Dengl M, Meixensberger J, Schuhmann MU (2010) Effects of cerebrovascular pressure reactivity-guided optimization of cerebral perfusion pressure on brain tissue oxygenation after traumatic brain injury. *Crit Care Med* 38(5):1343–1347
7. Meixensberger J, Jaeger M, Vöth A, Dings J, Kunze E, Roosen K (2003) Brain tissue oxygen guided treatment supplementing ICP/ CPP therapy after traumatic brain injury. *J Neurol Neurosurg Psychiatry* 74(6):760–764
8. Purins K, Enblad P, Sandhagen B, Lewén A (2010) Brain tissue oxygen monitoring: a study of in vitro accuracy and stability of Neurovent-PTO and Licox sensors. *Acta Neurochir (Wien)* 152(4):681–688

Experimental Comparison of the Measurement Accuracy of the Licox® and Raumedic® Neurovent-PTO Brain Tissue Oxygen Monitors

Matthias H. Morgalla, R. Haas, G. Grözinger, Christian Thiel, Karolin Thiel, Martin U. Schuhmann, and Martin Schenk

Abstract *Background:* Only a few experimental reports are available on the direct comparison of Licox® and Raumedic®-Neurovent-PTO brain tissue oxygen pressure ($P_{br}O_2$) monitors. We compared the two systems regarding their measurement properties under experimental in vitro and in vivo conditions.

Materials and methods: Eight Licox® and Raumedic® Neurovent-PTO® sensors were tested for 10 min at 37°C, atmospheric pressure, at an oxygen content of 0% and 100% before and after the in vivo test. The same probes were implanted in German landrace pigs, which underwent hepatectomy. The mean $P_{br}O_2$ values were recorded every minute. An O_2 challenge with inhalation of 100% O_2 for 10 min was performed 2 h post-abdominal surgery.

Results: At 0% O_2 content values varied from 0.2 to 7 mmHg, at 100% O_2 content from 130 to 165 mmHg. No difference between probes was found. In vivo tests: Raumedic® showed higher $P_{br}O_2$ values (mean +6.3 mmHg, $p < 0.0001$) compared with Licox®. During O_2 challenge, both probes responded similarly; however, Raumedic® had a 10% higher response amplitude ($p < 0.005$). After explantation there was again no difference between the two sensors.

Conclusion: Raumedic® sensors measured higher $P_{br}O_2$ values. There was no significant difference regarding overall measurement of in vitro accuracy between the two probes, which proved to be robust when used consecutively for longer periods and in different environments.

Keywords Brain tissue oxygen partial pressure ($P_{br}O_2$) • Measurement accuracy • Liver failure • In vitro tests • Raumedic®-Neurovent-PTO • Licox® tissue oxygen pressure monitor

M.H. Morgalla (✉), R. Haas, and M.U. Schuhmann
Department of Neurosurgery, Eberhard Karls University Hospital,
Hoppe-Seyler-Str. 3, D-72076 Tübingen, Germany
e-mail: matthias.morgalla@med.uni-tuebingen.de

G. Grözinger, C. Thiel, K. Thiel, and M. Schenk
Department of General and Transplantation Surgery,
Eberhard-Karls-University, Hoppe-Seyler-Str. 3, D-72076
Tübingen, Germany

M.U. Schuhmann and M. Czosnyka (eds.), *Intracranial Pressure and Brain Monitoring XIV*,
Acta Neurochirurgica Supplementum, Vol. 114, DOI: 10.1007/978-3-7091-0956-4_32, © Springer-Verlag/Wien 2012

Introduction

The monitoring of cerebral functions of comatose patients after traumatic brain injury (TBI) remains of paramount importance in order to avoid secondary brain damage and to ensure a satisfactory long-term outcome. Accurate and reliable recording of brain tissue oxygenation ($P_{br}O_2$) may be one of the keys to improving patient outcome after TBI. It has been shown that appropriately guided therapy can improve long-term outcome after severe brain injury [7]. Therefore, $P_{br}O_2$ is increasingly being used to guide clinical therapies in patients with severe TBI. Measurement accuracy remains of vital importance in this setting. While ICP monitors have been analysed in detail under laboratory conditions, O_2 probes still lack similar experimental investigations.

Two types of monitors are currently available. They are based on different technologies: the Clark type of electrochemical sensor (Licox®) and the fluorescent fibre optic probe (Neurovent-PTO®) [3, 5, 6].

Our aim was to examine the measurement properties of both systems under in vitro and in vivo conditions.

Materials and Methods

In Vitro Investigations

All probes were subjected to in vitro bench testing on two occasions: before the in vivo tests and then immediately after the animals had been sacrificed. One Licox® and one Raumedic® sensor were always measured simultaneously in order to ensure a direct comparison.

Two closed bottle systems were prepared. The first bottle contained 100 mL of sterile distilled water with an oxygen content of 0%. This was achieved by adding 1 g of Na_2SO_3 to the solution and stirring it for 1 min. This solution was ready for use after 10 min. The second bottle contained 100 mL of sterile distilled water with an oxygen content of 100%. Both bottles were sealed with a lid and placed in a water basin at

37°C and atmospheric pressure. The two different probes were both positioned in the same bottle via two bolts, which were mounted to the lid. These devices ensured a constant O₂ content within the liquid.

First, the probes were measured at 0% oxygen for 10 min. Then they were positioned in the second bottle with 100% oxygen content and analysed for another 10 min. The reading was recorded at the end of each test.

Subsequently, the probes were implanted in a pig in order to continue with the *in vivo* tests.

In Vivo Investigations

Animal Model

We used German landrace pigs, which offer a head large enough to position our probes well inside the brain parenchyma. This is an important issue because the probes were not positioned in the brain under direct vision via an open craniotomy but via a closed bolt system. The care of the animals, the anaesthetic management and the surgical procedure have been described in detail previously [4].

After fasting the pigs for 12 h before surgery intramuscular premedication was performed by applying atropine sulphate (0.05 mg/kg, Dr. Franz Köhler Chemie GmbH, Alsbach-Hähnlein, Germany), azaperone (4 mg/kg Janssen-Cilag GmbH, Neuss, Germany), ketamine hydrochloride (14 mg/kg Serumwerk Bernburg AG, Bernburg, Germany) and midazolam (0.5 mg/kg Ratiopharm GmbH, Ulm, Germany). Endo-tracheal intubation followed and anaesthesia was continued using ketamine (15 mg/kg/h), fentanyl (0.02 mg/kg/h, Ratiopharm, Ulm, Germany) and midazolam. This medication was infused via a central venous line until death occurred. Additionally, one of the internal carotid arteries and the jugular veins were used for invasive pressure monitoring.

Surgical Procedures

The pigs were turned to a prone position. The hair on the head was shaved and the head fastened. Four small cranial burr holes were performed for continuous intra-parenchymal ICP measurement (Neurovent® P-Temp, Raumedic AG Muenchenberg, Germany), P_{br}O₂ determination (Neurovent®-TO, Raumedic AG Muenchenberg, Germany and Licor® CC1.SB, Integra NeuroSciences, Plainsboro, NJ, USA) and microdialysis. Both oxygen monitors were inserted into the right hemisphere 2 cm posterior to the orbit, 2 cm lateral to the midline and 2 cm apart. All probes were secured using bolt systems that were mounted into the skull. After positioning of the four intracranial probes, the continuous measurement was started.

Subsequently, the pig was turned to a supine position for the abdominal surgery.

A laparotomy was performed and the liver was removed. All animals received infusions of 0.9% sodium chloride, 20% glucose, 6% hydroxyl starch, porcine fresh frozen plasma and porcine erythrocytes as required. The electrolytes and acid base balance were corrected immediately when necessary.

Comparison of the Oxygen Values

The oxygen values were measured simultaneously with both probes and recorded every minute. Afterwards, the values were compared.

Oxygen Provocation Test

Two hours post-abdominal surgery, an oxygen provocation test was performed on each pig. One hundred percent oxygen was inhaled over a period of 10 min and the subsequent response of the P_{br}O₂ was recorded and compared. The amplitude of the increase and the response time were measured.

Statistical Evaluation

The ANOVA test on ranks and the Kruskal–Wallis one-way analysis of variance, as well as the Tukey test, were used for the *in vitro* and *in vivo* tests in order to analyse changes between the two types of sensors. Bland and Altman analysis was also used to compare the P_{br}O₂ values. Differences were regarded as being statistically significant at a probability value of $p < 0.05$.

Results

In Vitro Tests

Eight new Licor® and Raumedic® probes were examined. The *in vitro* bench test, before surgery, revealed values between 0.2 and 7 mmHg at 0% of oxygen content for both sensors without a statistically significant difference (Fig. 1). At the 100% oxygen content values varied between 130 and 165 mmHg. The Raumedic® probes showed slightly higher values, without statistically significant differences between the two types of sensors (Fig. 2). After the animals had been sacrificed the *in vitro* tests were repeated immediately (Figs. 1 and 2). At 0% and 100% oxygen content, both oxygen probes had comparable results without any statistical difference between Licor® and Raumedic®. Also, there was no statistically significant difference between the first and second *in vitro* tests. The measurement accuracy did not seem to be negatively affected by the change in environment of the sensors and the longer period of investigation.

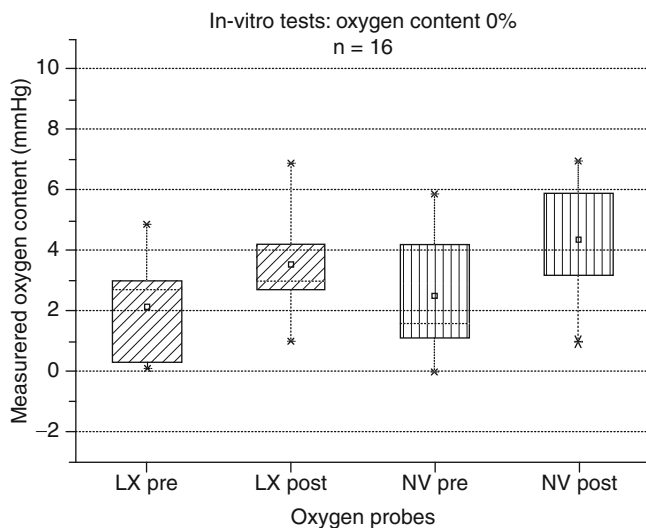


Fig. 1 Box plot diagram of the in vitro tests at an oxygen content of 0%. There are no statistically significant differences between Licox® (LX) and Neurovent® (NV) probes regarding the pre- and post-surgical investigations

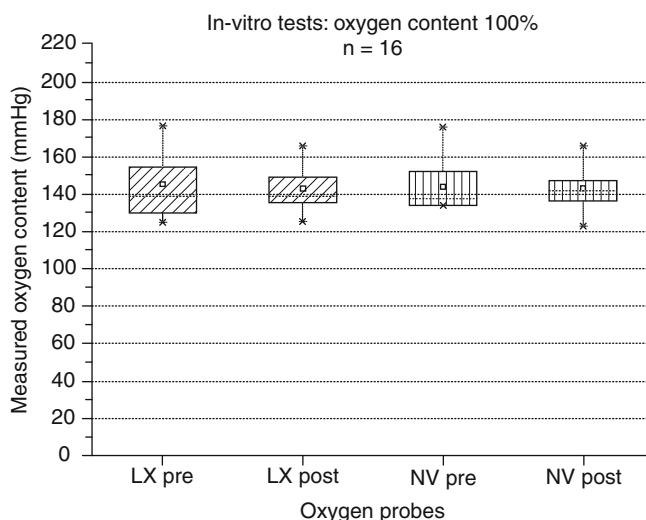


Fig. 2 Box plot diagram of the in vitro pre- and post-surgical examinations at an oxygen content of 100%. The values of both types of probes (LX and NV) varied between 130 and 165 mmHg. The Neurovent® (NV) probes showed a trend towards higher values without statistically significant differences between the two

In Vivo Tests

Comparison of the Oxygen Values

Eight animals were examined. In these eight animals the overall measurement time of both probes was 138.4 h (8,130 data pairs). The trend analysis revealed a parallel course of $P_{br}O_2$ from both probes. However, Raumedic® sensors exhibited constantly higher $P_{br}O_2$ values (Fig. 3). The mean difference between the Neurovent®-TO probe and the Licox probe was +6.3 mmHg with a high statistical significance ($p < 0.0001$).

Oxygen Provocation Test

Eight pigs were examined, but good quality data during oxygen challenge was only available in 7. During the 100% oxygen challenge, both types of sensors responded with comparable speed and time course for both the increase and the decrease. Raumedic® probes, however, showed a 10% higher response (amplitude) compared with Licox®, a difference that was statistically significant ($p < 0.05$).

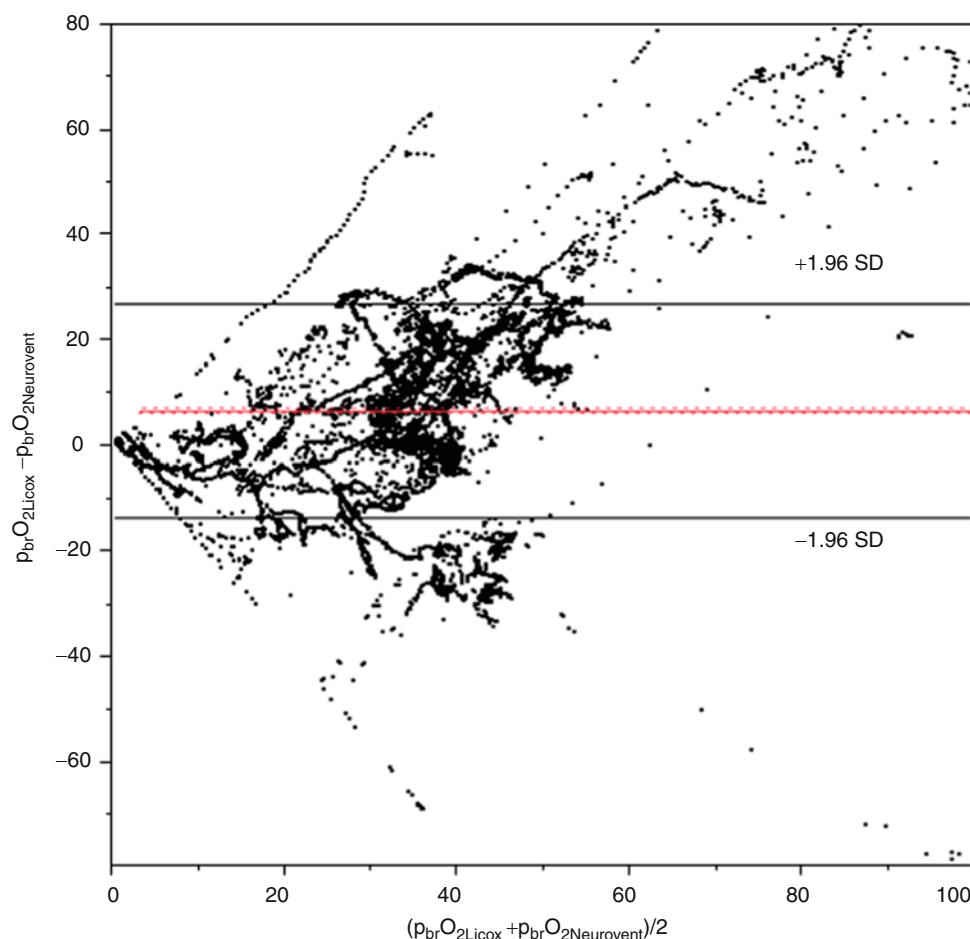
Discussion

Measurement accuracy is of paramount importance during neuromonitoring of comatose patients in the intensive care setting. Oxygen probes are now more commonly used for the monitoring of $P_{br}O_2$ [1]. Autoregulatory processes can also be analysed and allow new monitoring strategies. At present the most commonly used oxygen measurement devices are the Licox® and Raumedic®-Neurovent monitors. Most of the published data have been obtained via the Licox® system so far. However, there are only very few reports on a direct comparison of both systems. To our knowledge, there has been no experimental in vivo comparison of the two systems published. The anhepatic pig model used by us enables the intracerebral autoregulatory processes to be investigated [2]. Both in vitro and in vivo experimental tests are pivotal in order to scrutinise the facilities of the different probes. We did not find any statistically significant differences between the two systems under consideration in our bench tests. Purins and coworkers examined five Licox® and Neurovent® sensors at different gas concentrations and during long-term use. They found stable results with low standard deviations. Both systems were described as accurate in detecting different oxygen tensions and showed no deviation over longer recording times.

The assessment of the measurement properties of the probes under in vivo conditions appears more challenging. The oxygen provocation test serves as a definite stimulus of an exact period and preset oxygen concentration. The simultaneous measurement of the two probes ensures the direct comparison. In this series, we did not find statistically significant differences between the two probes. A response time could be calculated in only three cases in this series. Raumedic® was found to respond faster than Licox® in all three investigations. Purins et al. also compared the response time regarding different oxygen concentrations under in vitro conditions [5]. They reported that Licox® probes responded more slowly than Neurovent®.

The comparison of the in vivo raw data of the two systems found that the Neurovent® measured the $P_{br}O_2$ by about 6 mmHg higher than the Licox® system despite comparable in vitro data.

Fig. 3 Bland and Altman plot of the $P_{br}O_2$ values of total monitoring time (8,130 data points) in eight pigs



One possible explanation is that the higher in vivo $P_{br}O_2$ values of the Neurovent® probe are related to the different measurement technique (e.g. O_2 consumption by the Licox® system). Another possibility is the larger sampling area of the Neurovent® system, which may in this model be covering grey matter, which has a higher perfusion rate and higher $P_{br}O_2$ values.

Conclusion

Both $P_{br}O_2$ monitoring systems showed highly reliable data in all experiments. Raumedic® sensors measured higher in vivo values, but there was no statistically significant difference regarding the overall in vitro measurement accuracy between the two types of transducers. Both sensors proved to be robust even when used for longer periods and in different environments.

Conflict of interest statement Martin U. Schuhmann has received a research grant from Raumedic AG for the implementation of multi-modal monitoring in animal research.

References

1. Barth M, Woitzik J, Muench E, Diepers M, Schmiedek P, Kasuya H, Vajikoczy P (2010) Correlation of clinical outcome with pressure-, oxygen-, and flow-related indices of cerebrovascular reactivity in patients following aneurysmal SAH. *Neurocrit Care* 12(2):234–243
2. Dethloff TJ, Knudsen GM, Larsen FS (2008) Cerebral blood flow autoregulation in experimental liver failure. *J Cereb Blood Flow Metab* 28(5):916–926
3. Jaeger M, Schuhmann MU, Soehle M, Meixensberger J (2006) Continuous assessment of cerebrovascular autoregulation after traumatic brain injury using brain tissue oxygen pressure reactivity. *Crit Care Med* 34(6):1783–1788
4. Knubben K, Thiel C, Schenk M, Etspüler A, Schenk T, Morgalla MH, Königsrainer A (2008) A new surgical model for hepatectomy in pigs. *Eur Surg Res* 40(1):41–46
5. Purins K, Enblad P, Sandhagen B, Lewén A (2010) Brain tissue oxygen monitoring: a study of in-vitro accuracy and stability of Neurovent-PTO and Licox sensors. *Acta Neurochir (Wien)* 152(4):681–688
6. Smielewski P, Lavinio A, Timofeev I, Radolovich D, Perkes JD, Pickard JD, Czosnyka M (2008) ICM+, a flexible platform for investigations of cerebrospinal dynamics in clinical practice. *Acta Neurochir Suppl* 102:145–151
7. Stiefel MF, Spiotta A, Gracias VH, Garuffe AM, Guillaumondegui O, Maloney-Wilensky E, Bloom S, Grady MS, LeRoux PD (2005) Reduced mortality rate in patients with severe traumatic brain injury treated with brain tissue oxygen monitoring. *J Neurosurg* 103:805–811

Is $P_{br}O_2$ Pressure Reactivity Index (ORx) Dependent on the Type of Oxygen Probe? An In Vivo Study

G. Grözinger, Martin Schenk, Christian Thiel, Karolin Thiel, Matthias H. Morgalla, and Martin U. Schuhmann

Abstract Objective: To evaluate if ORx is dependent on the type of brain tissue O_2 ($P_{br}O_2$) probe in an in vivo setting.

Methods: In eight German landrace pigs two types of probes were implanted simultaneously in the same cerebral hemisphere. All pigs underwent hepatectomy and received neuromonitoring until death. A LICOX® probe CCL5, representing a Clarke type electrode, was compared with a Raumedic Neurovent PTO, representing an optode. Data were sampled at 50 Hz. Average values were calculated every 30 s. Cerebral perfusion pressure (CPP) was averaged over 30 s. ORx was calculated for each probe. To increase the signal to noise ratio of the ORx, the ORx values, which had been assessed every minute, were averaged over 1 h.

Results: The overall measurement time was 145.1 h (8,703 data pairs). Despite a mean difference of 6.2 mmHg ($p < 0.0001$) in the measured values of $P_{br}O_2$, the mean ORx_{licox} was 0.139, mean $ORx_{raumedic}$ 0.146 ($p = 0.2098$). Correlation coefficient of ORx values assessed every minute and every hour was 0.52 and 0.58 respectively.

Conclusion: Despite this significant difference in absolute values of $P_{br}O_2$ the derived mean ORx values were not different. Similar to the established Licox system, the Raumedic system seems to enable a valid ORx recording.

Keywords Oxygen reactivity index • Brain tissue oxygen partial pressure ($P_{br}O_2$) • Liver failure • Neuromonitoring

Introduction

In the past few years the topic of autoregulation of cerebral blood flow (cerebrovascular autoregulation) has become an increasing issue in the field of advanced neuromonitoring. This is due to the finding that impairment of autoregulation not only seems to play a role in the pathophysiology of several acute brain diseases (e.g., intracranial hemorrhage [ICH], traumatic brain injury [TBI], and subarachnoid hemorrhage [SAH]), but also seems to be a predictor of outcome of an individual patient. Owing to this knowledge, the development of adequate continuous monitoring of the cerebrovascular autoregulation became an important focus in neuromonitoring efforts [1–5].

The status of cerebrovascular autoregulation can be continuously assessed by several indices that have been developed in the past few years. Among other indices, like the blood pressure-derived Pressure Reactivity Index (PRx), one promising instrument is the concept of an brain tissue oxygen-derived index (ORx), which was introduced by Jaeger et al. in 2006 [5]. A detailed description of the calculation of the index can be studied elsewhere [5]. Briefly, ORx is thought to represent the autoregulation of cerebral blood flow (CBF) derived from the Pearson's correlation index of cerebral perfusion pressure (CPP) and $P_{br}O_2$, using $P_{br}O_2$ as a surrogate marker of CBF. Values from -1 to $+1$ are possible. A positive correlation suggests that $P_{br}O_2$ passively follows CPP, which is indicative of disturbed autoregulation. Values around 0 represent intact autoregulation. Increasingly positive values indicate an increasing impairment of the ability to maintain an adequate CBF.

For the correct calculation of ORx the measurement of the basic parameters (brain tissue oxygen partial pressure $P_{br}O_2$ and cerebral perfusion pressure CPP) is necessary with sufficient temporal resolution. Until now, all published ORx data have been based on $P_{br}O_2$ determination with the Licox CC1. SB.oxygen probe (Integra NeuroSciences, Plainsboro, NJ, USA). Today, the market provides other probes to measure brain tissue oxygenation. As a challenger for the established Licox system we chose the Neurovent-TO probe (Raumedic AG, Münchenberg, Germany). Both types of oxygen probes

G. Grözinger
Department of General and Transplantation Surgery,
Eberhard-Karls-University Hospital, Hoppe-Seyler-Strasse 3,
D-72076 Tübingen, Germany

Department of Neurosurgery, Eberhard-Karls-University Hospital,
Hoppe-Seyler-Strasse 3, D-72076 Tübingen, Germany

M. Schenk, C. Thiel, and K. Thiel
Department of General and Transplantation Surgery,
Eberhard-Karls-University Hospital, Hoppe-Seyler-Strasse 3,
D-72076 Tübingen, Germany

M.H. Morgalla and M.U. Schuhmann (✉)
Department of Neurosurgery, Eberhard-Karls-University Hospital,
Hoppe-Seyler-Strasse 3, D-72076 Tübingen, Germany
e-mail: martin.schuhmann@med.uni-tuebingen.de

are established in clinical routine. The main difference between the two types of probe is the principle that is used to measure the amount of oxygen in the tissue. The Licox device is a so-called Clarke-type electrode (the Clark electrode is an electrode that measures oxygen on a catalytic platinum surface using the net reaction: $O_2 + 4e^- + 2H_2O \rightarrow 4OH^-$). The Neurovent-TO probe, however, is an optode (based on the O_2 quenching of fluorescence light).

Increasing information is provided that in acute liver failure (ALF) impairment of cerebrovascular autoregulation may play a role in the development of brain edema and increased intracranial pressure (ICP) [6, 7].

We investigated the ORx calculations of the two types of oxygen probes in an animal model of experimental ALF.

Materials and Methods

Animal Model

We used eight German landrace pigs, seven of which underwent the surgical procedure described. One animal underwent only a sham operation. The handling of the animals, the anesthetic treatment and the surgical intervention are described elsewhere in detail [8].

The pigs were fasted 12 h before surgery and received atropine sulfate (0.05 mg/kg, Dr. Franz Köhler Chemie GmbH, Alsbach-Hähnlein, Germany), azaperone (4 mg/kg Janssen-Cilag GmbH, Neuss, Germany), ketamine hydrochloride (14 mg/kg Serumwerk Bernburg AG, Bernburg, Germany), and midazolam (0.5 mg/kg Ratiopharm GmbH, Ulm, Germany) intramuscularly for pre-medication. Anesthesia was maintained after oral endotracheal intubation via continuous central venous infusion of ketamine (15 mg/kg/h), fentanyl (0.02 mg/kg/h, Ratiopharm, Ulm, Germany), and midazolam until death.

For measurement of arterial and central venous blood pressure and to collect blood samples, the jugular veins and one internal carotid artery were cannulated. Laparotomy was subsequently performed for hepatectomy. All animals received infusions of 0.9% sodium chloride, 20% glucose, 6% hydroxyl starch, porcine fresh frozen plasma, and porcine erythrocytes as required and the electrolytes and acid base balance were immediately corrected if necessary.

Neuromonitoring

The pigs were turned to a prone position. The hair on the head was shaved and the head fastened. Four small

cranial burr holes were performed for continuous intra-parenchymal ICP measurement (Neurovent® P-Temp, Raumedic AG Muenchenberg, Germany), $P_{br}O_2$ determination (Neurovent® -TO, Raumedic AG Muenchenberg, Germany and Licox® CC1.SB, Integra NeuroSciences, Plainsboro, NJ, USA) and microdialysis. Both oxygen monitors were inserted in the right hemisphere 2 cm posterior to the orbit, 2 cm lateral to the midline, and 2 cm apart from each other. All probes were secured using bolt systems, which were mounted into the skull. After positioning of the four intracranial probes, the continuous measurement was started.

The ICP, oxygen, and arterial blood pressure data were sampled with a frequency of 50 Hz and directly recorded with ICM+software [9].

During off-line analysis artifacts caused by temporary disconnection of catheters or other interventions were eliminated manually from the data sets and PRx and both ORx were recalculated using ICM+software. Time-averaged means for arterial blood pressure, ICP and CPP (CPP = MAP – ICP) were calculated and stored every minute. For calculation of PRx, average values of MAP and ICP were calculated for 10-s intervals using waveform time integration.

Oxygen pressure reactivity (ORx) was calculated as the moving linear (Pearson's) correlation coefficient between values of CPP and $P_{br}O_2$ from the previous 60 min of monitoring. Hence, every 30 s, a new ORx value was calculated from 120 data pairs [5].

Statistics

In stable conditions, the 'running' coefficients (ORx, PRx) are noisy. Moving average with a period of 1 h was used to assess autoregulation at any given time point. Further statistical analysis was performed using JMP statistical software (JMP 8.0.1, SAS Institute Inc., Cary, NC, USA). Results are expressed as mean ± standard deviation and plotted as mean ± standard deviation. Correlation was investigated using Spearman's rho test. Differences between the average values were assessed using the *t* test.

Results

In eight animals the overall measurement time with data of both probes was 145.1 h (8,703 data pairs). The mean difference between the Neurovent TO probe and the Licox probe was +6.3 mmHg ($p < 0.0001$). The mean ORx_{licox} was 0.139, mean $ORx_{neurovent}$ was 0.146 without significant difference ($p = 0.2098$; Fig. 1).

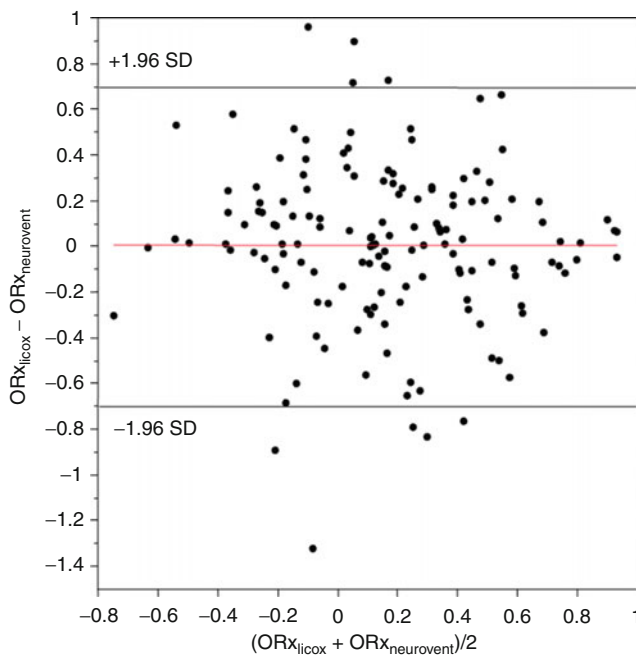


Fig. 1 Bland–Altman plot of hourly averaged ORx values as assessed with the two types of probes. *Horizontal line*: average mean ORx value of both probes. *SD* standard deviation

The Spearman's correlation coefficient of the ORx values assessed every minute was $r=0.52$. The correlation coefficient increased to $r=0.58$ using average values of ORx over an hour (Fig. 2).

Discussion

This investigation could show that it is feasible to calculate ORx with the Licox probe as well as with the Raumedic probe. Both probes were able to detect the status of cerebral oxygenation reliably. However, there is a noticeable difference in the mean values of the underlying $P_{br}O_2$ data.

As changes in $P_{br}O_2$ are of importance for the calculation of ORx, not the absolute values, the ORx results did not differ between the two sensors. Both probes seemed to be able to detect relative changes on their level of measurement in a comparable way, despite the fact that the reaction time to changes in oxygen partial pressure seemed to be lower for the Licox than for the Neurovent device [10]. Despite this problem of different dynamic properties of the two probes, both probes seem to detect trends the same way.

An explanation of the difference between the two probes might be the anatomical conditions in our model. Compared with the human situation, the white matter is thinner. With its smaller sampling area the Licox probe may measure the white matter only, whereas the Neurovent device could be partially measuring the gray matter where blood flow is generally higher.

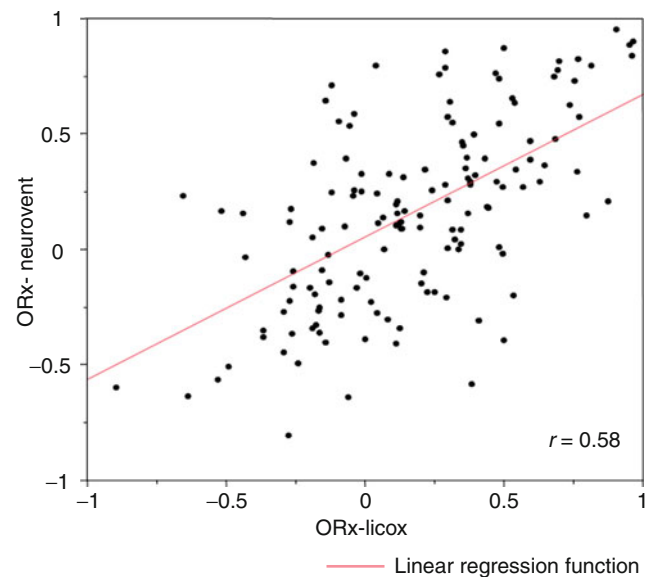


Fig. 2 Correlation graph of the 1-h average values of ORx for both types of probes. *line* represents the linear regression function

Conclusion

This investigation demonstrates that both types of probes can be used to determine ORx. The measured $P_{br}O_2$ levels assessed by the Neurovent probe were significantly higher than those assessed by the Licox probes. However, the derived mean ORx values were not different. Accordingly, the correlation coefficient of ORx indicates adequate agreement, especially if 1-h average values are compared. Similar to the established Licox system the Raumedic system seems to enable a confident ORx recording.

Conflict of interest statement Martin U. Schuhmann has received a research grant by Raumedic AG for the implementation of multimodal monitoring in animal research.

References

1. Jaeger M et al (2007) Continuous monitoring of cerebrovascular autoregulation after subarachnoid hemorrhage by brain tissue oxygen pressure reactivity and its relation to delayed cerebral infarction. *Stroke* 38(3):981–986
2. Barth M et al (2010) Correlation of clinical outcome with pressure-, oxygen-, and flow-related indices of cerebrovascular reactivity in patients following aneurysmal SAH. *Neurocrit Care* 12(2):234–243
3. Diedler J et al (2009) Impaired cerebral vasomotor activity in spontaneous intracerebral hemorrhage. *Stroke* 40(3):815–819
4. Reinhard M et al (2010) Secondary decline of cerebral autoregulation is associated with worse outcome after intracerebral hemorrhage. *Intensive Care Med* 36(2):264–271
5. Jaeger M et al (2006) Continuous assessment of cerebrovascular autoregulation after traumatic brain injury using brain tissue oxygen pressure reactivity. *Crit Care Med* 34(6):1783–1788

6. Vaquero J, Chung C, Blei AT (2004) Cerebral blood flow in acute liver failure: a finding in search of a mechanism. *Metab Brain Dis* 19(3–4):177–194
7. Dethloff TJ, Knudsen GM, Larsen FS (2008) Cerebral blood flow autoregulation in experimental liver failure. *J Cereb Blood Flow Metab* 28(5):916–926
8. Knubben K et al (2008) A new surgical model for hepatectomy in pigs. *Eur Surg Res* 40(1):41–46
9. Smielewski P et al (2008) ICM+, a flexible platform for investigations of cerebrospinal dynamics in clinical practice. *Acta Neurochir Suppl* 102:145–151
10. Purins K et al (2010) Brain tissue oxygen monitoring: a study of in vitro accuracy and stability of Neurovent-PTO and Licox sensors. *Acta Neurochir (Wien)* 152(4):681–688

Continuous Quantitative Monitoring of Cerebral Oxygen Metabolism in Neonates by Ventilator-Gated Analysis of NIRS Recordings

Thomas Heldt, Faisal M. Kashif, Mustafa Sulemanji, Heather M. O'Leary, Adré J. du Plessis, and George C. Verghese

Abstract Oxidative stress during fetal development, delivery, or early postnatal life is a major cause of neuropathology, as both hypoxic and hyperoxic insults can significantly damage the developing brain. Despite the obvious need for reliable cerebral oxygenation monitoring, no technology currently exists to monitor cerebral oxygen metabolism continuously and noninvasively in infants at high risk for developing brain injury. Consequently, a rational approach to titrating oxygen supply to cerebral oxygen demand – and thus avoiding hyperoxic or hypoxic insults – is currently lacking. We present a promising method to close this crucial technology gap in the important case of neonates on conventional ventilators. By using cerebral near-infrared spectroscopy and signals from conventional ventilators, along with arterial oxygen saturation, we derive continuous (breath-by-breath) estimates of cerebral venous oxygen saturation, cerebral oxygen extraction fraction, cerebral blood flow, and cerebral metabolic rate of oxygen. The resultant estimates compare very favorably to previously reported data obtained by non-continuous and invasive means from preterm infants in neonatal critical care.

Keywords Cerebral venous oxygen saturation • Cerebral blood flow • Cerebral metabolic rate of oxygen • Cerebral oxygen metabolism • Preterm infant • Brain injury • Near-infrared spectroscopy • Continuous monitoring

Introduction

Brain injury in the preterm infant comes with tremendous personal hardship and immense societal cost over the lifetime of the affected individual. The primary mode of damage to the developing brain is hypoxic-ischemic injury sustained during antenatal, intrapartum, and early neonatal life [1]. Likewise, hyperoxic insults to the developing brain are also injurious due to a particular susceptibility of developing neural tissue to oxygen free-radicals. Unfortunately, no technology currently exists to monitor cerebral oxygen utilization at the bedside. Clinicians therefore find themselves in the situation of having to titrate oxygen therapy without reliable and sensitive tools for continuous monitoring of cerebral oxygen metabolism.

Cerebral near-infrared spectroscopy (NIRS) has the potential to fill this crucial technology gap, as it provides for continuous and noninvasive assessment of changes in the oxy- and deoxyhemoglobin concentrations in cerebral tissue (comprising arteries, veins, and cerebral microcirculation). In other words, NIRS measures cerebral hemoglobin saturation in the intravascular compartment as a whole, without distinguishing between the arterial or venous compartments. To relate these signals to contributions of individual vascular compartments, and thus to identify important variables of cerebral oxygen metabolism, changes in hemoglobin content need to be induced selectively in one compartment or another. Jugular venous occlusion, for example, induces changes primarily on the venous side of the cerebral vasculature, and therefore provides important insights into cerebral venous oxygen saturation [2]. Nevertheless, repeated temporary occlusion of a preterm infant's cerebral venous outflow is neither a practical nor a safe option. However, positive pressure ventilation commonly required during the early period after premature birth might induce such fluctuations in cerebral venous drainage on a breath-by-breath basis. This forms the basis of the work presented here. Specifically, we examined NIRS signals during the brief interval of impeded venous return imposed by every inspiratory breath by conventional positive pressure ventilation, to estimate important variables of cerebral oxygen metabolism continuously and noninvasively.

T. Heldt (✉), F.M. Kashif, and G.C. Verghese
Computational Physiology and Clinical Inference Group,
Massachusetts Institute of Technology, Room 10-140L,
77 Massachusetts Avenue, Cambridge, MA 02139, USA
e-mail: thomas@mit.edu

M. Sulemanji, H.M. O'Leary, and A.J. du Plessis
Department of Neurology, Children's Hospital Boston,
330 Longwood Avenue, Boston, MA 02115, USA

Materials and Methods

Estimation Algorithm

Our algorithm for estimating cerebral venous oxygen saturation (SvO_2), cerebral oxygen extraction fraction (OEF), cerebral blood flow (CBF), and cerebral metabolic rate of oxygen ($CMRO_2$) is based on the principle that during conventional ventilation, the positive pressure inspiratory phase increases intrathoracic pressure, transiently impeding venous return to the heart. Figure 1 shows an example of the ventilator-associated changes in cerebral oxyhemoglobin and total hemoglobin concentrations in one of our subjects.

Ventilator-induced changes in intrathoracic pressure are usually just a few mmHg. Pressure fluctuations of that magnitude are sufficient to collapse the central veins, and thus to impede venous return. However, they only account for a few percent of arterial transmural pressure and therefore induce negligible changes in arterial blood volume, particularly since the arterial compliance is about 20 times smaller than the venous compliance. It is therefore commonly assumed that cerebral arterial blood volume remains unaffected over the immediate brief inspiratory period, so the changes in cerebral oxyhemoglobin concentration, $\Delta[HbO_2]$, and total hemoglobin concentration, $\Delta[HbT]$ ($=\Delta[HbO_2] + \Delta[Hb]$), imprinted in the NIRS signals reflect changes in the cerebral venous compartment [2, 3]. The ratio $\Delta[HbO_2]/\Delta[HbT]$ gated to the inspiratory phase of each positive pressure breath thus provides an estimate of cerebral SvO_2 on a breath-by-breath basis. By averaging in a least-square-error manner over adjacent breaths, SvO_2 can be estimated on a continuous (i.e., breath-by-breath) basis and in a robust manner.

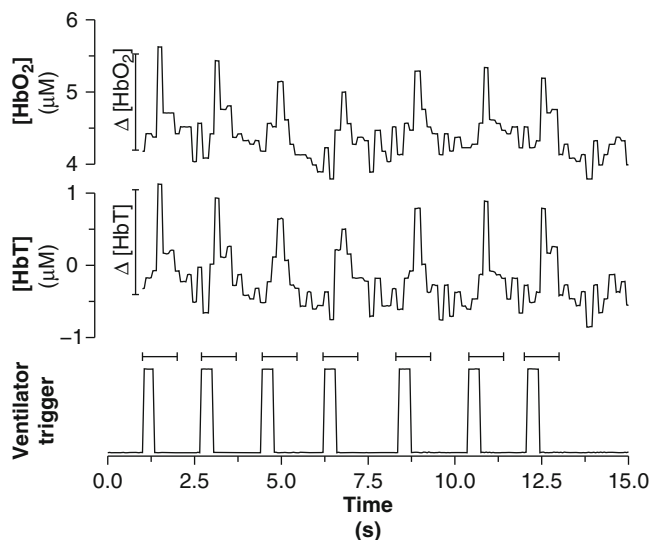


Fig. 1 Oxyhemoglobin concentration (*top*), total hemoglobin concentration (*middle*), and ventilator trigger signal (*bottom*). Also indicated are the windows over which the $[HbO_2]$ and $[HbT]$ signals are analyzed following the start of each inspiratory cycle

From a continuous measurement of systemic arterial oxygen saturation, SaO_2 (gated to arterial pulsations) and estimates of cerebral SvO_2 , we can derive continuous estimates of cerebral oxygen extraction ($OE = SaO_2 - SvO_2$) and cerebral oxygen extraction fraction ($OEF = [SaO_2 - SvO_2]/SaO_2$).

Using a similar approach, we can also estimate tissue-specific CBF (CBF per 100 g of brain tissue), by further analyzing the NIRS-derived $[HbT]$ signal around the inspiratory phase of the respiratory cycle. Assuming that mean arterial blood pressure, systemic oxygen saturation, and cerebral oxygen metabolism remain constant over the brief period of ventilator-induced inspiration, the change in total cerebral hemoglobin concentration, $\Delta[HbT]$, induced by the transient retardation of venous outflow, is directly related to changes in cerebral venous blood volume in the sample volume interrogated by NIRS. The maximum slope of the $\Delta[HbT]$ signal is therefore a measure of regional cerebral blood flow (per 100 g of brain tissue) [2]:

$$CBF = k \cdot \left. \frac{d[HbT]}{dt} \right|_{max}$$

where k is a constant that incorporates the patient's hemoglobin concentration and serves to convert the units of the time derivative of $[HbT]$ to cerebral blood flow (per 100 g tissue). This amounts to a patient-specific calibration of hemoglobin flow. We approximate the derivative above by the ratio of the maximum increase $\Delta[HbT]$ during the analysis window for each breath (as labeled in Fig. 1) to the time required to reach this value after the start of the inspiratory cycle.

Finally, the cerebral metabolic rate of oxygen ($CMRO_2$ per 100 g of tissue) is the product of cerebral oxygen extraction and cerebral blood flow ($CMRO_2 = OE \cdot CBF$).

Study Population

We tested our algorithm on data archived from eight preterm infants born before 32 weeks of gestation and requiring neonatal intensive care with ventilatory support. The research protocol was approved by the institutional review board at Brigham and Women's Hospital, Boston, USA, and we obtained parental written informed consent in all cases.

Instrumentation

To track the systemic cardiorespiratory states of the neonates, we continuously recorded arterial blood pressure (through an umbilical artery catheter), systemic arterial oxygen saturation (by pulse oximetry), the electrocardiogram, and ventilator signals (peak airway pressure, ventilator trigger, and airway flow). We assessed cerebral tissue oxygenation by bihemispheric

NIRS (Hamamatsu NIRO-200) and electrocortical activity through continuous recording of a single-channel EEG. The NIRO-200 provides estimates of *changes* in tissue oxy- and deoxyhemoglobin concentrations from some unknown baseline. The systemic cardiovascular and NIRS signals were streamed to an analog-to-digital converter, sampled at 4 kHz, and archived in a time-locked manner. A trained bedside observer was present continuously to log details of any manipulation or changes in management.

Data Pre-processing

To apply our estimation algorithms, we down-sampled the ventilator trigger, NIRS signals, and systemic oxygen saturation recording to 20 Hz. We used custom-made algorithms to detect the onset of each trigger pulse, which marks the onset of the inspiratory phase of the positive pressure ventilator. We then defined a window of 1 s duration starting with the beginning of the inspiratory period, over which the [HbT] and [HbO₂] signals are analyzed as outlined above.

As shown in Fig. 1, the ventilator-induced changes induced in the NIRS signals can vary from one breath to the next. To mitigate the effect of such fluctuations, and to arrive at robust estimates of SvO₂, CBF, and CMRO₂, we compute these quantities in a least-square-error manner over a rolling window containing 20 breaths.

Results

Figure 2 shows measured mean arterial blood pressure (MAP; black) along with the measured SaO₂ (maroon) and continuous estimates of cerebral SvO₂, cerebral CBF, and CMRO₂ as derived from the right (red tracing) and the left (blue tracing) hemisphere, over the course of 1 h in a preterm neonate with a gestational age of 27 weeks. Although the estimates of SvO₂, CBF, and CMRO₂ were derived independently for the right and left hemisphere, the resultant bilateral estimates bear a notable degree of correspondence at various time-scales, though also some differences and offsets.

Figure 3 summarizes the range and median values of SvO₂ in eight premature infants from our database. (The results shown in Fig. 2 represent a snapshot of the data of Subject 5 in Fig. 3.)

Discussion

Accurate titration of cerebral oxygen therapy to cerebral oxygen demand remains an important and unresolved problem in neonatal care. The importance of this issue relates to the fact that both excessive and insufficient cerebral

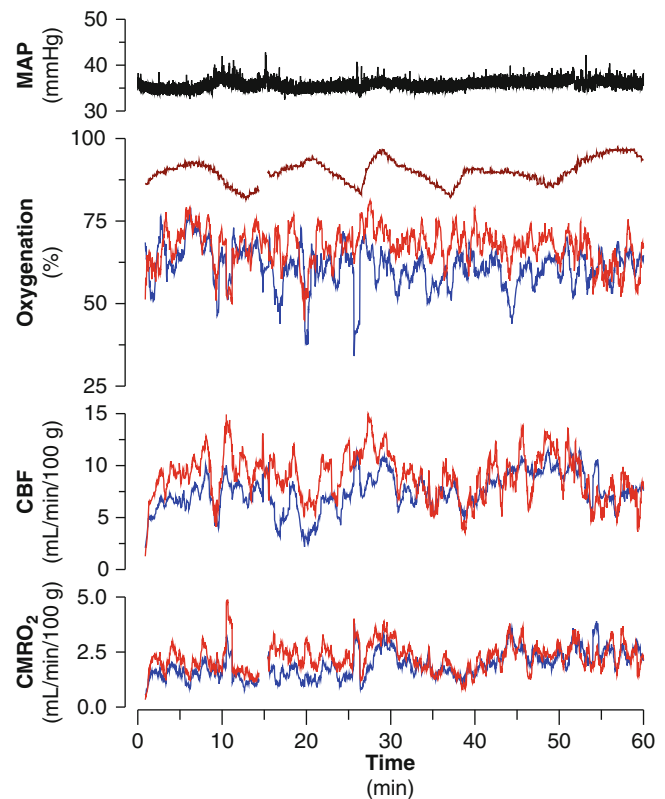


Fig. 2 From top to bottom: Mean arterial blood pressure; systemic arterial and cerebral venous oxygen saturation; cerebral blood flow; and cerebral metabolic rate of oxygen. Red: right hemispheric estimates; blue: left hemispheric estimates

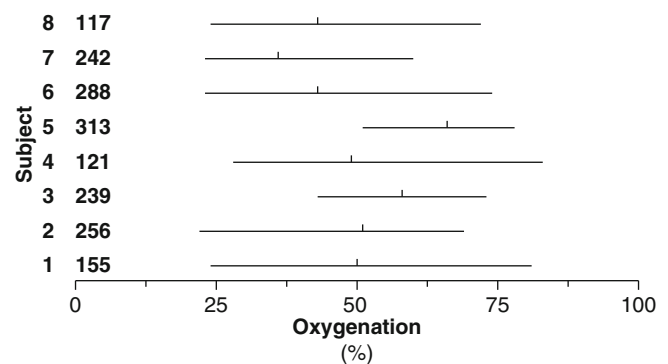


Fig. 3 Range and median (tick mark) of cerebral venous oxygen saturation in eight premature infants. Numbers to the right of the subject identifier signify the duration (in minutes) over which the ranges were computed

oxygenation may be injurious to the immature brain. Furthermore, normal intrinsic autoregulatory systems for regulation of oxygen delivery may be disrupted in these infants. Rational clinical decision making regarding brain tissue oxygenation is currently impaired by our inability to monitor continuously and noninvasively important variables of cerebral oxygen metabolism (such as oxygen extraction and cerebral metabolic rate of oxygen) that reflect oxygen

delivery to, and oxygen demand by, the brain. Here, we present an algorithmic approach to estimating these critical variables of cerebral oxygen metabolism from changes in near-infrared spectroscopy signals imprinted by cyclic variations in intrathoracic pressure associated with positive pressure ventilation. The same strategy has been leveraged by Wolf et al. [3] to estimate cerebral venous oxygen saturation, though they only report intermittent estimates and the details of our respective approaches differ.

Like others [2, 3], we assume that the ventilator-induced changes in the NIRS signal reflect changes in the cerebral venous vascular compartment. Neglecting possible changes in cerebral arterial volume is a common assumption, though it remains to be properly verified.

Our patient-specific estimates of SvO_2 , CBF, and CMRO_2 compare very favorably to what has been reported in the medical literature for these variables in neonates, using other, highly invasive measurements. For example, Volpe [4] summarizes tissue-specific cerebral blood flow measurements for preterm infants from different studies that used intravenous Xenon-133 clearance (see Table 6-28, p. 301 in [4]). For mechanically ventilated infants, CBF measurements pooled from different studies seem to cluster around 10 mL/min/100 g. When averaged over the course of a 4-h period, the specific cerebral blood flow for the patient whose data are shown in Fig. 2 is (6.1 ± 3.4) mL/min/100 g and (7.5 ± 4.1) mL/min/100 g for the left and the right hemisphere, respectively.¹ Our estimates of CBF might underestimate true tissue-specific CBF if the ventilator-induced changes in intrathoracic pressure fail to completely halt cerebral venous outflow temporarily. Furthermore, the computation of the derivative to obtain estimated CBF tends to be susceptible to noise in the data, though computing the slope in a least-squares manner over a window of adjacent breaths mitigates this effect. Finally, we have used a representative value for the hemoglobin concentration in neonates to calculate CBF in this retrospective study. Future application of this method should rely on actual hemoglobin measurements from each patient to convert the time derivative of [HbT] to CBF.

Using positron emission tomography, Altman [5] and coworkers determined CMRO_2 in a group of 16 preterm infants (with mean gestational age of 27 weeks and mean birth weight of 925 g). They report a value of 0.06 mL/min/100 g, which is significantly lower than the blood flow values for the left and right hemisphere in the patient

presented in Fig. 2 [(1.5 ± 1.4) mL/min/100 g and (1.8 ± 1.3) mL/min/100 g]. Inspection of Altman's data suggests that this difference is largely due to the comparatively large oxygen extraction fraction of our subject (0.30 ± 0.09), which resembles that of a term newborn (in the neighborhood of 0.21) rather than the value reported in [4] for preterm neonates (in the neighborhood of 0.06).

Estimates for the right and left hemisphere show a remarkable concordance. The origins of fluctuations seen in the estimated signals remain to be elucidated, but might be reflective of changing regional metabolic demand in response to changing electrocortical activity. This question is currently under investigation with concurrent EEG measures.

Estimates in cerebral SvO_2 can vary substantially over the course of 2–4 h, as indicated by the wide ranges shown in Fig. 3. Some of these variations correlate with variations in SaO_2 (not shown). In other cases, the reasons for the excursions of estimated cerebral SvO_2 are less obvious.

Future work will focus on evaluating these estimates against gold standard measurements in animal studies, as well as investigating the effects of changing peak inspiratory pressure on the robustness and accuracy of our estimates.

Acknowledgment This work was supported in part by the United States National Institutes of Health through grants R01EB001659, K24NS057568, and R21HD056009 by the National Institute of Biomedical Imaging and Bioengineering, the National Institute of Neurological Disorders and Stroke, and the National Institute of Child Health and Human Development, respectively. Further support was provided by the Lifebridge Fund.

Conflict of interest statement The authors declare that they have no conflict of interest.

References

1. Volpe JJ (2009) Brain injury in premature infants: a complex amalgam of destructive and developmental disturbances. *Lancet Neurol* 8:110–124
2. Victor S, Weindling M (2008) Near-infrared spectroscopy and its use for the assessment of tissue perfusion in the neonate, Chapter 6. In: Kleinman CS, Seri I (eds) *Hemodynamics and cardiology – neonatology questions and controversies*. Saunders, Philadelphia
3. Wolf M, Duc G, Keel M, Niederer P, von Siebenthal K, Bucher HU (1997) Continuous noninvasive measurements of cerebral arterial and venous oxygen saturation at the bedside in mechanically ventilated neonates. *Crit Care Med* 25(9):1579–1582
4. Volpe JJ (2008) *Neurology of the newborn*, 5th edn. Saunders/Elsevier, Philadelphia
5. Altman DI, Powers WJ, Perlman JM, Herscovitch P, Volpe SL, Volpe JJ (1988) Cerebral blood flow requirement for brain viability in newborn infants is lower than in adults. *Ann Neurol* 24(2): 218–226

¹Note that over the course of the 4-h period, significant trends in cerebral blood flow exist, which contribute to the relatively large standard deviation.

Near Infrared Spectroscopy as Possible Non-invasive Monitor of Slow Vasogenic ICP Waves

Ruwan Alwis Weerakkody, Marek Czosnyka, Christian Zweifel, Gianluca Castellani, Peter Smielewski, Ken Brady, John D. Pickard, and Zofia Czosnyka

Abstract We aimed to study synchronisation between ICP and near infrared spectroscopy (NIRS) variables induced by vasogenic waves of ICP during an infusion study in hydrocephalic patients and after TBI. Nineteen patients presenting with hydrocephalus underwent a diagnostic intraventricular constant-flow infusion test. The original concept of the methodology, presented in the current paper, was derived from this material. Then the method was applied in 40 TBI patients, with results reported in an observational manner. During monitoring, NIRS deoxygenated and oxygenated haemoglobin (Hb, HbO₂) were recorded simultaneously with ICP. Moving correlation coefficient (6 min) between Hb and HbO₂ was tested as a marker of the slow vasogenic waves of ICP.

During infusion studies ICP increased from 10.7 (5.1) mmHg to a plateau of 18.9 (7.6) mmHg, which was associated with an increase in the power of slow ICP waves

($p=0.000017$). Fluctuations of Hb and HbO₂ at baseline negatively correlated with each other, but switched to high positive values during periods of increased ICP slow-wave activity during infusion ($p<0.001$). Similar behaviour was observed in TBI patients: baseline negative Hb/HbO₂ correlation changed to positive values during peaks of ICP of vasogenic nature.

Correlating changes in Hb and HbO₂ may be of use as a method of non-invasive detection of vasogenic ICP waves.

Keywords Near infrared spectroscopy • Intracranial pressure • Infusion test • Traumatic brain injury

Introduction

Slow waves in intracranial pressure occurring in the low-frequency band (0.3–2.0 cycles per minute) are present across a range of conditions, particularly in the context of intracranial hypertension and reduced pressure volume compensatory reserve (but may also be present in normal individuals) [5].

NIRS allows non-invasive detection of changes in brain tissue oxygenation, cerebral blood volume (CBV) and cerebral blood flow (CBF) by recording relative changes in the concentration of deoxygenated (Hb) and oxygenated (HbO₂) haemoglobin during cyclic haemodynamic changes associated with slow ventilation [6]. We previously studied the relationship between slow waves (slower than respiration waves) of ICP, ABP and indices of cerebral oxygenation derived with NIRS during infusion tests [7], a routine method for assessing CSF dynamics in shunted and non-shunted hydrocephalic patients [3].

Our current aim is to describe changes in ICP and the mutual character of cyclic fluctuations in Hb and HbO₂. This study has been performed in hydrocephalic patients and preliminarily used in a group of patients after traumatic brain injury.

R.A. Weerakkody, M. Czosnyka (✉), P. Smielewski, J.D. Pickard, and Z. Czosnyka
Academic Neurosurgery Unit, Addenbrooke's Hospital,
University of Cambridge, Box 167, Cambridge
CB2 0QQ, UK
e-mail: mc141@medschl.cam.ac.uk

C. Zweifel
Academic Neurosurgery Unit, Addenbrooke's Hospital,
University of Cambridge, Box 167, Cambridge
CB2 0QQ, UK

Department of Neurosurgery, University Hospital, Basel,
Switzerland

G. Castellani
Academic Neurosurgery Unit, Addenbrooke's Hospital,
University of Cambridge, Box 167, Cambridge
CB2 0QQ, UK

Department of Anaesthesia, University Hospital,
Pavia, Italy

K. Brady
Department of Pediatrics, Anesthesia, Critical Care,
Texas Children's Hospital, Baylor College of Medicine,
Houston, TX, USA

Materials and Methods

Patients

After approval by the Local Research Ethics Committee and with informed consent, 19 patients (12 male, 7 female; mean age 43, range 16–76) with a history of CSF circulatory disorder referred by their clinical team for CSF infusion testing were recruited. Patients presented with radiological evidence of ventricular dilatation and/or any combination of symptoms suggesting disturbed CSF dynamics including new or worsened headache, gait disturbance, urinary incontinence, cognitive decline, nausea, visual obscuration and others. CSF infusion testing is a routine clinical method for the accurate analysis of CSF dynamics using constant-rate infusion into the CSF space [3]. The study protocol involved simultaneous monitoring of cerebral oximetry by NIRS and non-invasive arterial blood pressure (ABP) during the infusion test.

To illustrate the wider clinical applicability of a newly derived variable from this study protocol, we additionally used the supplementary data of long-term NIRS, ICP and ABP monitoring from a consenting patient after traumatic brain injury (diffuse axonal injury), ventilated and sedated with initial GCS of 5 (with Ethics Committee approval).

Infusion Test Protocol

The computerised infusion test, a well-established method for assessing CSF dynamics [2], formed the usual clinical protocol in the hydrocephalic patients. Intraventricular infusion of Hartmann's solution (standard compound sodium lactate) at a rate of 1.5 mL/min was initiated after 10 min of baseline measurements, and infusion was continued until a steady-state intracranial pressure plateau (equilibrium between infused and resorbed CSF) was achieved. When the ICP reached the plateau or exceeded 40 mmHg, the infusion was stopped. ICP and NIRS-derived parameters of cerebral oximetry were recorded throughout, including baseline, infusion plateau and after cessation of the infusion until ICP decreased towards steady baseline levels.

Monitoring Cerebral Oxygenation by NIRS

The NIRO 200 (Hamamatsu Photonics K.K.) is a non-invasive bedside monitor that gives simultaneous measurement of the tissue oxygenation index (TOI) – the ratio of oxygenated to total tissue haemoglobin – and changes in the concentration of haemoglobin and other chromophores. Four wavelengths of light (775, 810, 850 and 910 nm) delivered

by four pulsed laser diodes are emitted and the light scattered is detected by three closely-placed photodiodes. The concentrations of the chromophores, namely oxyhaemoglobin (HbO_2), deoxyhaemoglobin (Hb), total haemoglobin (HbT) and cytochrome oxidase are measured by conventional differential spectroscopy (based on the Beer–Lambert principle) whilst TOI is calculated by spatially resolved reflectance spectroscopy [4]. The instrument itself is based on technology used in earlier versions (NIRO 300 and 500) and, along with the underlying theoretical principles, has been described in detail previously [1].

Data Processing and Analysis

Intracranial pressure was continuously monitored via a pressure transducer and saline-filled tube connected to the intraventricular catheter or shunt antechamber.

Values of Hb (deoxygenated haemoglobin concentration), HbO_2 (oxygenated haemoglobin concentration) and waveforms of ICP and NIRS-derived variables were digitalised and captured with a sampling rate of 50 Hz on a personal computer running multimodal data monitoring software (ICM+, www.neurosurg.cam.ac.uk/icmplus).

In the bandwidth $0.3\text{--}2\text{ min}^{-1}$ the value of the transmitted power of the ICP waveform (Slow) was calculated. The moving correlation coefficient between 60 consecutive 6-s averaged values of Hb and HbO_2 was also calculated and presented as time-varying variables.

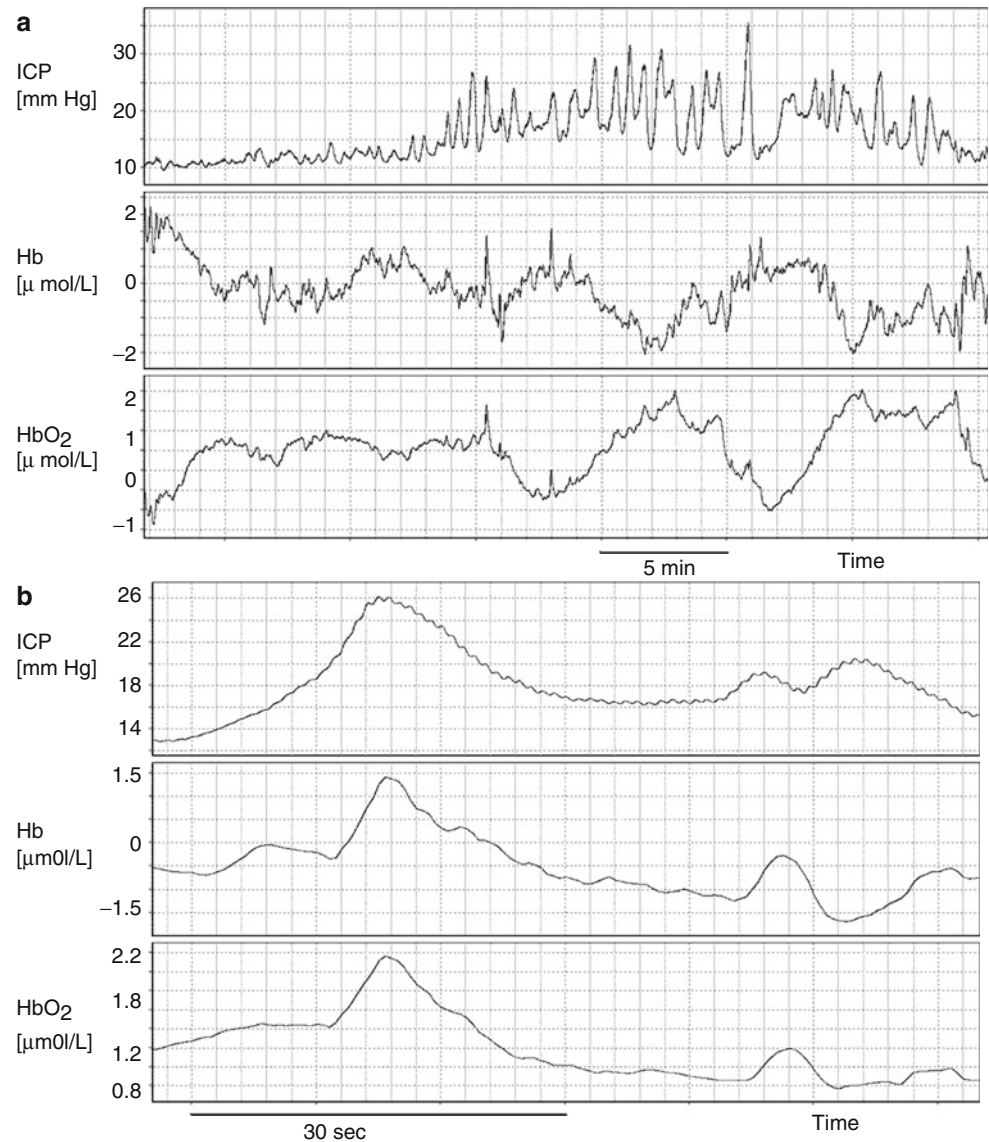
The parametric paired test was used to test differences between analysed variables at baseline and in the plateau phase of the infusion test.

Results

During infusion studies, the true slow waves of ICP were accompanied by synchronous changes in Hb and HbO_2 in phase with each other (Fig. 1a). Where ICP slow waves were not observed (for example, before infusion has started) or were not dominant, “very slow” drift (approximately 0.2 min^{-1}) was recorded in Hb and HbO_2 , occurring independently of ICP. In these cases Hb and HbO_2 were in counter-phase to each other (Fig. 1b). Indeed, correlation analysis between Hb and HbO_2 revealed negative association over longer periods ($<0.2\text{ min}^{-1}$), with positive correlation triggered specifically by the presence of increased slow wave ($0.3\text{--}3\text{ min}^{-1}$) activity in ICP (Fig. 2).

Statistical analysis of our small group of patients confirmed these observations. During infusion study, when mean ICP increased (from 10.7 ± 5.1 to 18.9 ± 7.6 mmHg; $p = 5.1 \times 10^{-10}$); slow waves ICP increased (0.37 ± 0.41 to

Fig. 1 Two distinct patterns of waves in Hb and HbO₂. **(a)** Slow drift (several minutes in duration) of Hb and HbO₂ occurring in opposite directions to each other and seemingly independent of intracranial (ICP) fluctuations. **(b)** Synchronous fluctuations in Hb and HbO₂ coinciding with slow waves of ICP



4.6 ± 4.3 mmHg; $p = 0.000017$). This was accompanied by an increase in correlation coefficient between changes in Hb and HbO₂ from -0.21 ± 0.35 to 0.26 ± 0.29 ($p < 0.001$).

These observations were confirmed, in some cases in spectacular manner, with ICP and NIRS long-term monitoring in patients after TBI. Baseline Hb/HbO₂ correlation coefficient being negative, switched to positive values during sudden (presumed vasogenic) peaks of ICP see Fig. 3.

Discussion

We previously observed high coherence between variables of NIRS and ICP (>0.7) in a frequency range consistent with slow waves of ICP [7].

In the present study, we observed that the relationship between Hb and HbO₂ can be altered. Fluctuations in Hb and

HbO₂ seemed to be normally negatively correlated with each other. Such fluctuations may occur during metabolic changes in brain activation. When cerebral blood flow (CBF) is stable, an increase in Hb (representing deoxygenated blood), would be accompanied by a decrease in HbO₂ (oxygenated blood) and vice versa. However, when changes in CBF occur, as a result of changes in the calibre of the resistance vessels, Hb and HbO₂ would change in the same direction. Such a change would lead to a change in CBV, and the vasogenic waves of ICP.

Although the latter effect will need to be further substantiated, it provides a potential non-invasive marker for strong vasogenic activity in ICP, known to be associated with exhausted compensatory reserve and intracranial hypertension. We investigated the possibility of the non-invasive detection of strong ICP fluctuations by means of a moving correlation coefficient between Hb and HbO₂. During infusion study, when the time of measurement is limited, this

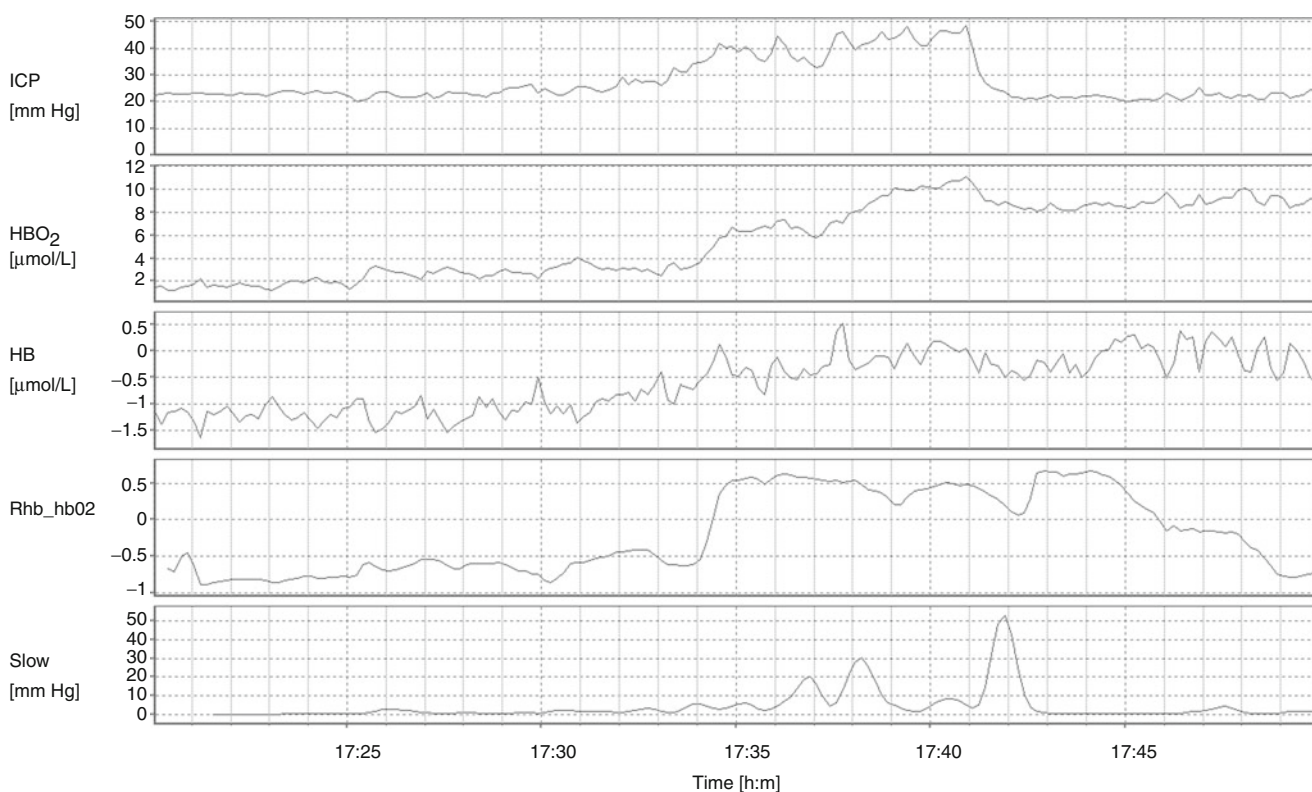


Fig. 2 Correlation coefficient between Hb and HbO₂ (Rhb_hb02): normally negative, switching to positive values during increased slow-wave (20 s to 2 min) fluctuations of ICP on top of infusion plateau. Increased

slow-wave activity, associated with intracranial hypertension, may therefore be detected by monitoring the degree of correlation between Hb and HbO₂

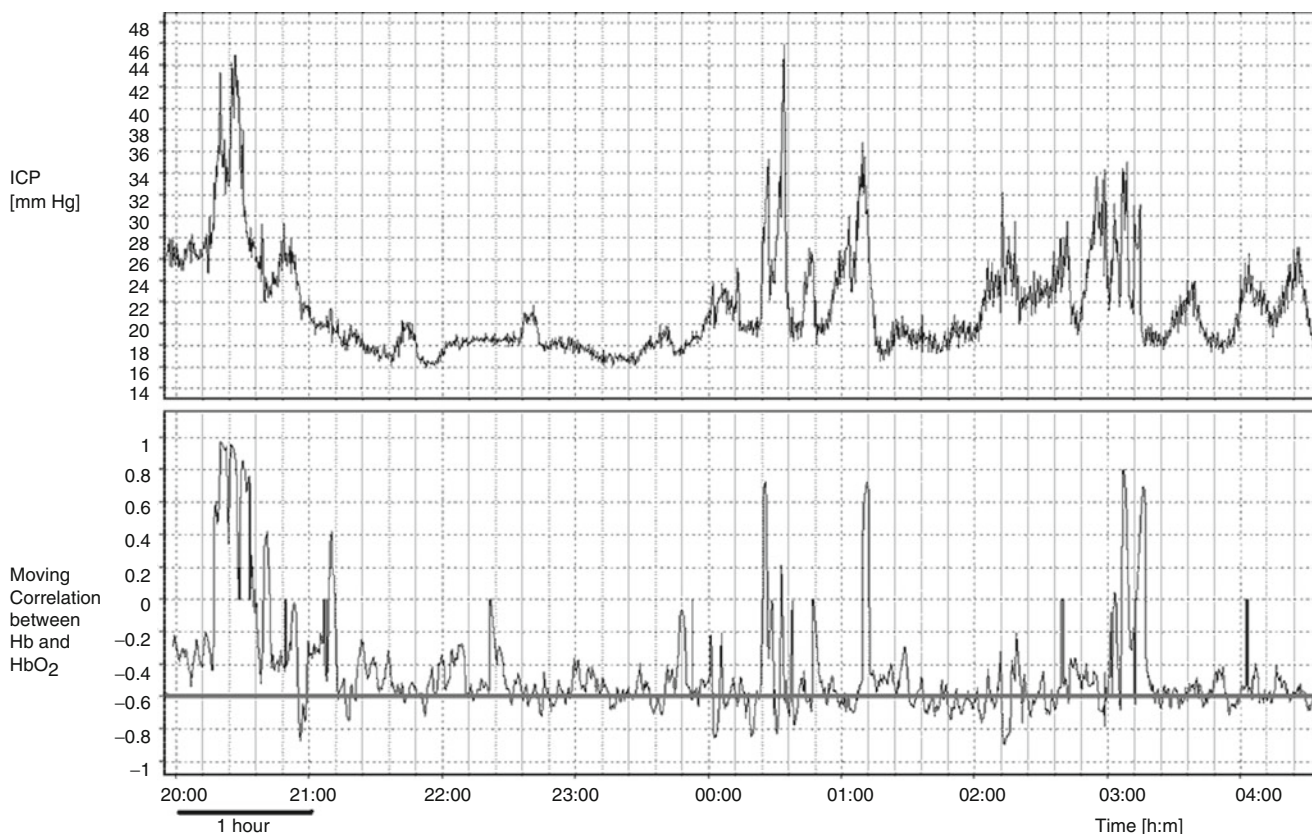


Fig. 3 Illustration of the concept of the moving correlation coefficient between Hb and HbO₂ as a tool for the non-invasive detection of the vasogenic elevations of ICP. Long-term recording was borrowed from a

separate study in head-injured patients. The baseline correlation coefficient is negative (*grey horizontal line*), but whenever vasogenic elevations and waves of ICP occur, it changed to a positive value

potentially useful methodology is seldom as convincingly demonstrated as in Fig. 2. Therefore, to demonstrate the applicability of this variable over a longer period and outside the paradigm of hydrocephalus, we tested it in the context of overnight ICP monitoring in a head-injured patient where this effect was also observed (Fig. 3). Unfortunately, moving correlation coefficient between Hb and HbO₂ is noisy. It almost always increases when ICP rises abruptly (rise of a vasogenic nature), but some fluctuations of correlation can be seen outside these periods (again, Fig. 3). Further basic studies should be performed, aimed at forming an algorithm for automatic detection based on this observation.

In this preliminary observational study, we describe phenomena occurring within the unique paradigm of controlled impairment of the pressure volume compensatory reserve, which undoubtedly occur during the infusion test. We believe that these insights may be generalised to the wider group of pathological conditions involving disturbed pressure volume compensation, with slow wave activity being a generic pathological response. The findings from this observation are of an observational nature – they describe new phenomena that should be confirmed by larger studies – particularly when clinical applications of NIRS are concerned.

Conclusion

Near infrared spectroscopy may be used as a non-invasive marker of increased activity of ICP slow waves. Preliminary analysis suggests that a moving correlation coefficient between Hb and HbO₂ is robust within and outside the context of CSF infusion tests.

Acknowledgement The project was supported by the National Institute of Health Research, Biomedical Research Centre, Cambridge University Hospital Foundation Trust – Neurosciences Theme plus Senior Investigator Award (JDP) and Foundation for Polish Science (MK).

Conflict of interest statement ICM+software (www.neurosurg.cam.ac.uk/icmplplus) is licensed by the University of Cambridge, Cambridge Enterprise Ltd. PS and MC have a financial interest in a part of the licensing fee. CZ received a travel grant from Hamamatsu Photonics, Welwyn Garden City, Hertfordshire, UK.

References

1. Al-Rawi PG, Smielewski P, Kirkpatrick PJ (2001) Evaluation of a near-infrared spectrometer (NIRO 300) for the detection of intracranial oxygenation changes in the adult head. *Stroke* 32:2492–2500
2. Albeck MJ, Gjerris F, Czosnyka M, Laniewski P (1992) Computerized infusion test compared to steady pressure constant infusion test in measurement of resistance to CSF outflow. *Acta Neurochir* 119:12–16
3. Czosnyka M, Whitehouse H, Smielewski P, Simac S, Pickard JD (1996) Testing of cerebrospinal compensatory reserve in shunted and non-shunted patients: a guide to interpretation based on observational study. *J Neurol Neurosurg Psychiatry* 60:549–558
4. Delpy DT, Cope M, van der Zee P, Arridge S, Wray S, Wyatt J (1988) Estimation of optical pathlength through tissue from direct time of flight measurement. *Phys Med Biol* 33:1433–1442
5. Droste DW, Krauss JK, Berger W, Schuler E, Brown MM (1994) Rhythmic oscillations with a wavelength of 0.5–2 min in transcranial Doppler recordings. *Acta Neurol Scand* 90(2):99–104
6. Reinhard M, Wehrle-Wieland E, Grabiak D, Roth M, Guschlbauer B, Timmer J, Weiller C, Hetzel A (2006) Oscillatory cerebral hemodynamics – the macro- vs. microvascular level. *J Neurol Sci* 250(1–2):103–109
7. Weerakkody RA, Czosnyka M, Zweifel C, Castellani G, Smielewski P, Keong N, Haubrich C, Pickard J, Czosnyka Z (2010) Slow vasogenic fluctuations of intracranial pressure and cerebral near infrared spectroscopy – an observational study. *Acta Neurochir (Wien)* 152(10):1763–1769

Drift of the Bowman Hemedex® Cerebral Blood Flow Monitor Between Calibration Cycles

Stefan Wolf, P. Vajkoczy, J. Dengler, L. Schürer, and P. Horn

Abstract Introduction: Since its introduction into clinical practice, the Bowman Hemedex® regional cerebral blood flow (CBF) monitor has provided a valuable tool for the bedside assessment of CBF in neurointensive care. The purpose of our study was to estimate the accuracy of CBF measurements between automatically performed self-calibration cycles at regular intervals.

Methods: We analyzed data from 75 CBF probes, predominantly implanted into patients after severe subarachnoid hemorrhage. Automatic recalibration of the regional CBF device was performed every 30 min. CBF data were averaged once per minute and the measurement cycles pooled. Statistical analysis was performed with generalized additive modeling and bootstrapping methods.

Results: Mean regional CBF was 24 mL/100 g/min after calibration and showed a mean drift of 2.3 mL/100 g/min per measurement cycle ($p < 0.001$). In every patient, the drift over the measurement cycle followed an exponential trend, with large heterogeneity between patients (-3.67 to 12.0 mL/100 g/min). A highly significant difference in drift was found for the internal software versions of the monitoring devices ($p < 0.001$).

Conclusions: Data from the Bowman Hemedex® regional CBF monitor shows an upward measurement drift of clinically relevant magnitude. As the drift follows a stable exponential function over time, recalculation of drift-corrected data is possible after termination of the measurement.

Keywords Regional cerebral blood flow • Monitoring • Thermodiffusion measurement • Drift

Introduction

Accurate assessment of cerebral blood flow (CBF) is a crucial problem in unconscious patients in neurointensive care. The Bowman Hemedex® perfusion monitor facilitates continuous and quantitative measurement of regional brain tissue perfusion with a thermodiffusion microprobe [1]. Since its introduction into clinical practice in 2000, it has provided a valuable tool for bedside assessment of CBF disturbances and monitoring therapeutic effects, predominantly in patients with aneurysmal subarachnoid hemorrhage [2–4].

The technology relies on regular and repeated estimation of the conductive and convective thermal properties of the brain tissue around the probe. This is performed through alternating between calibration phases and monitoring phases at fixed intervals. During calibration, the tip of the probe is heated by about 2°C above the surrounding tissue temperature for a short period. The energy required to maintain the resulting spherical temperature field is proportional to the regional CBF. During monitoring phases, regional CBF is mathematically calculated from a set of differential equations parameterized by the preceding calibration period. As this interpolation accounts inevitably for a distinct amount of error and measurement drift, we wanted to assess the uncertainty of the thermodiffusion CBF measurement between the calibration cycles.

Materials and Methods

We analyzed data from 75 QFlow 500 CBF microprobes (Hemedex, Cambridge, MA, USA) implanted in patients either suffering from severe aneurysmal subarachnoid hemorrhage or being evaluated for complex cerebrovascular bypass surgery. All probes were connected to a Hemedex

S. Wolf (✉)

Department of Neurosurgery, Campus Virchow, Charité University, Augustenburger Platz 1, Berlin 13353, Germany

Department of Neurosurgery, Klinikum Bogenhausen, Munich, Germany
e-mail: stefan.wolf@charite.de

P. Vajkoczy, J. Dengler, and P. Horn
Department of Neurosurgery, Campus Virchow, Charité University, Augustenburger Platz 1, Berlin 13353, Germany

L. Schürer
Department of Neurosurgery, Klinikum Bogenhausen, Munich, Germany

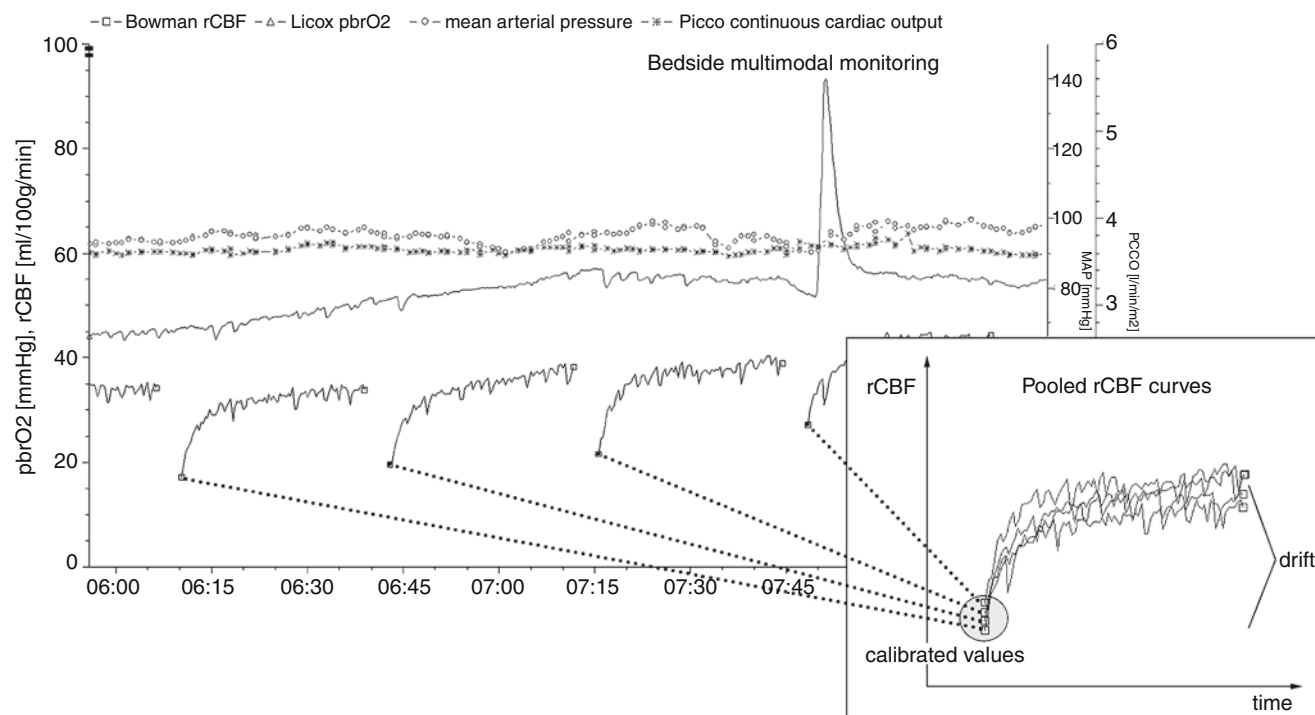


Fig. 1 Principle of drift analysis. The main part shows a typical screen of a bedside multimodal monitoring system. The small figure in the lower right demonstrates the pooling of the multiple measurement cycles

Bowman perfusion monitor. Probe placement was 2–2.5 cm subdural in the white matter of the vascular territory estimated to be at risk of ischemia. Indication for monitoring was based on a clinical decision in every case. Thirty-two patients were treated in the Department of Neurosurgery, Academic Hospital Bogenhausen, Munich, Germany, from March 2005 to July 2008, and 43 from August 2008 to September 2010 in the Department of Neurosurgery at Charité University, Berlin, Germany.

During the time of data gathering, perfusion monitor devices with four different internal software versions were used (versions 3.0.3–3.0.6). Software upgrades were performed during regularly scheduled maintenance carried out by the manufacturer. Reasons for software upgrades included bug fixes and further improvement of the monitoring technology. Regional CBF was recorded at the bedside once per second with dedicated software; however, for the current analysis, the transcribed raw data files from the monitor devices were used.

The recalibration interval of the regional CBF device was mainly set at 30 min, resulting in measurement cycles of approximately 25 min. Only full cycles were used and shorter ones with user-driven premature recalibration or other reasons for interruption were discarded.

For analysis, the continuous measurement data of a patient were averaged with a mean once per minute and afterwards the measurement cycles pooled (Fig. 1). Therefore, the first minute of the pooled measurement cycles equals the mean of

all values immediately after the calibration periods. The difference of the pooled mean of following minutes to this first value after calibration represents the drift over time. Statistical analysis was performed with the statistical environment R 2.11.1 [5]. The statistical significance of drift over time was analyzed with generalized additive modeling to allow for arbitrary relationships without linearity assumptions [6]. Bootstrapping [7] was used for assessment of the necessary number of measurement cycles.

Results

In total, 435,125 min of measurement data, corresponding to 17,405 full measurement cycles, were analyzed. Mean monitoring time per patient was 5.3 days. Raw data volume was 3.02 Gigabyte of continuous regional CBF data.

All patients pooled, regional CBF was 24.0 mL/100 g/min at the beginning and 26.3 mL/100 g/min at the end of the measurement cycles between the two recalibration periods, thus representing a mean drift of 2.3 mL/100 g/min per measurement cycle ($p < 0.001$).

The drift over the measurement cycles of the four software versions used in the Hemedex monitors during the time of data collection varied. Version 3.0.3 showed a mean decay of -0.67 mL/100 g/min, while versions 3.0.4–3.0.6 showed an

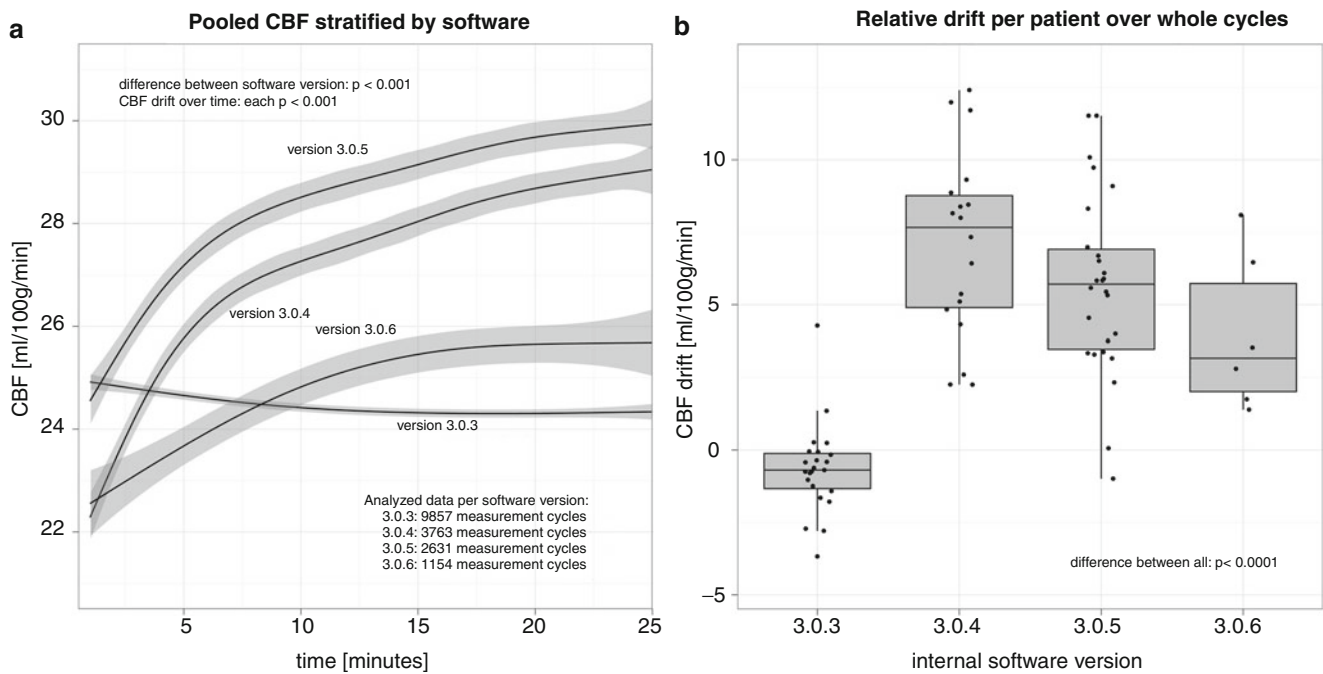


Fig. 2 (a) Regional CBF drift, stratified by the four different versions over time in absolute units (pooled data). The shaded gray areas denote the 95% confidence intervals of the mean. (b) Mean relative drift value at the end of the measurement cycles in different patients

increase during the measurement cycle of 7.3, 5.9, and 3.6 mL/100 g/min respectively (Fig. 2a). In all patients, the drift over the measurement cycle followed an exponential trend, with large heterogeneity between patients (-3.67 to 12.0 mL/100 g/min, Fig. 2b). Drift over time and between software versions were both statistically highly significant ($p < 0.001$).

Figure 3a shows temperature fluctuations during the measurement cycles. Again, the different software versions showed a statistically significant difference ($p < 0.001$). Additionally, the time used for calibration and temperature stabilization differed between the software versions ($p < 0.001$, Fig. 3b).

Discussion

The purpose of the present paper was to investigate the stability of continuous regional cerebral blood flow measurements performed at the bedside in the neurosurgical intensive care unit. The major finding is that the Bowman Hemedex CBF monitor shows drift over the measurement cycles between the automatically performed recalibrations. The magnitude of this drift is rather heterogeneous between different patients and depends on the internal software versions of the monitor. The drift pattern is stable and follows an exponential pattern over time, depending on the software version used. Therefore, in principle, a correction of measured data for drift is feasible.

Prerequisite for the presented stochastic method for drift analysis is a sufficiently large amount of measurement cycles, as otherwise the analysis of drift would be indistinguishable from naturally occurring regional CBF fluctuations. According to our experience with real and simulated data the method is reliable in most patients when more than 20–30 measurement cycles are pooled, depending on naturally occurring real CBF fluctuations and the amount of drift.

A possible explanation for our findings may be instabilities of the temperature field surrounding the tip of the probe after calibration. Each software version shows different subtle imbalances of the measured brain temperature to the magnitude of one hundredth of a centigrade during the monitoring phase. These imbalances are more pronounced immediately after calibration and fade during the measurement cycle. As the estimated cerebral blood flow during the measurement phase is proportional to temperature fluctuations at the proximal thermistor, this may explain the larger regional CBF drift at the beginning of the measurement cycles. The two software versions with the lower magnitude of drift, 3.0.3 and 3.0.6, have longer mean calibration times, thus allowing for better temperature stabilization after heating the tip of the probe necessary for calibration. However, as we are unaware of the intimate details of the algorithm used for regional CBF estimation, this explanation remains speculative and other factors beyond our knowledge may contribute.

We consider our findings relevant for scientific and clinical practice. The median drift shows a magnitude of 35% of the measured value at the end of a 30-min measurement

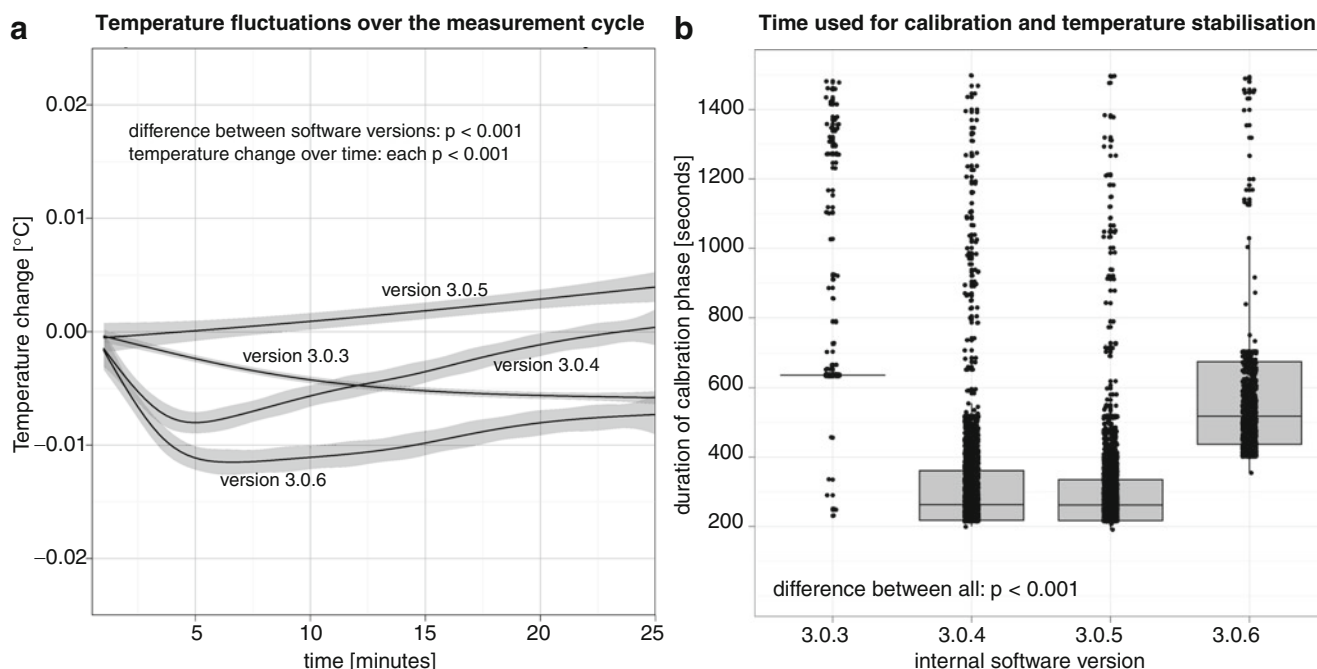


Fig. 3 (a) Relative temperature fluctuations over the measurement cycle in the four different software versions. (b) Comparison of the time needed for single calibration and stabilization episodes, stratified by software

cycle. This may give rise to problems in recognizing the effect of therapeutic interventions aiming for an increase in CBF. In cardiac output monitoring, another flow-measuring technique used in critical care, a 30% difference between a newly introduced device and the reference technique is proposed as an upper threshold to accept exchangeability [8]. Therefore, a comparison of the Hemedex® system with other techniques measuring CBF values in absolute terms poses problems. Furthermore, the drift of the measurement values over time makes the development and validation of threshold-based therapeutic algorithms particularly difficult.

In our opinion, the best solution to ensure valid regional CBF data is to perform frequent recalibrations. The latest software available, version 3.0.6, was introduced in spring 2010 and includes automatic premature recalibration if the estimated regional CBF changes above a predefined threshold during the monitoring phase. Although this reduces the ratio of clinical available measurement time to necessary calibration, we consider this an important and timely improvement.

Conclusions

Data from the Bowman Hemedex® regional CBF monitor show a measurement drift of clinically relevant magnitude. At present, the only solution to ensure valid data is to perform frequent recalibrations. As the drift follows a stable exponential function over time, recalculation of drift-corrected data is possible after termination of the measurement.

Acknowledgement The authors are indebted to Prof. Dr. Friedrich Leisch, Department of Statistics, Ludwig-Maximilians-University, Munich, Germany, for statistical consultation and advice.

Conflict of interest statement We declare that we have no conflict of interest.

References

1. Vajkoczy P, Roth H, Horn P, Lucke T, Thomé C, Hubner U et al (2000) Continuous monitoring of regional cerebral blood flow: experimental and clinical validation of a novel thermal diffusion microprobe. *J Neurosurg* 93(2):265–274
2. Vajkoczy P, Horn P, Thome C, Munch E, Schmiedek P (2003) Regional cerebral blood flow monitoring in the diagnosis of delayed ischemia following aneurysmal subarachnoid hemorrhage. *J Neurosurg* 98(6):1227–1234
3. Muench E, Horn P, Bauhof C, Roth H, Philipps M, Hermann P et al (2007) Effects of hypervolemia and hypertension on regional cerebral blood flow, intracranial pressure, and brain tissue oxygenation after subarachnoid hemorrhage. *Crit Care Med* 35(8):1844–1851
4. Wolf S, Martin H, Landscheidt JF, Rodiek SO, Schürer L, Lumenta CB (2010) Continuous selective intraarterial infusion of nimodipine for therapy of refractory cerebral vasospasm. *Neurocrit Care* 12(3):346–351
5. R Development Core Team (2010) R: A language and environment for statistical computing. R Foundation for Statistical Computing, Vienna, Austria. ISBN 3-900051-07-0, URL: <http://www.R-project.org/>
6. Wood SN (2006) Generalized additive models: an introduction with R. Chapman & Hall, Boca Raton
7. Davison AC, Hinkley D (1997) Bootstrap methods and their application. Cambridge University Press, New York
8. Critchley LA, Critchley JA (1999) A meta-analysis of studies using bias and precision statistics to compare cardiac output measurement techniques. *J Clin Monit Comput* 15(2):85–91

Quantification of Pulsatile Cerebrospinal Fluid Flow within the Prepontine Cistern

Robert Hamilton, Justin Dye, Andrew Frew, Kevin Baldwin, Xiao Hu, and Marvin Bergsneider

Abstract *Background:* Phase-contrast MRI (PC-MRI) has previously been used for the quantification of CSF and blood flow throughout the body. We propose a new method of semi-automated segmentation for the prepontine cistern based on anatomical and pulsatility information.

Methods: Scans were conducted on 48 patients (69.83 ± 14.28 years) ranging in age from 32 to 88 years along with an additional 11 controls (51.91 ± 21.13 years) ranging in age from 22 to 72 years. The segmentation algorithm developed consists of four stages: anatomical, flow quantification for the aqueduct and prepontine cistern, and blood vessel detection.

Results: Complete results are presented in Table 1, the 37 preoperative patients and controls had a prepontine cistern stroke volume of 464.32 ± 202.30 and 447.38 ± 75.49 respectively.

Conclusion: Reliable quantification of volumetric CSF flow in complex cisternal spaces is possible using a methodology combining known anatomical features with the pulsatile nature of CSF flow.

Keywords Phase contrast MRI • Hydrocephalus • Aqueduct of Sylvius • Cerebrospinal fluid (CSF)

Introduction

Although first described nearly half a century ago, the treatment and/or diagnosis of normal pressure hydrocephalus (NPH) remains complicated. The pathophysiological mechanisms underlying NPH include altered hydrodynamics within the cerebrospinal fluid (CSF) system causing changes in CSF flow, reduced absorption, and changes in compliance of the cerebral vasculature. Traditionally, NPH is characterized clinically by the presence of dementia, gait disturbance, and urinary incontinence, along with radiological evidence of ventriculomegaly.

Cine phase contrast MRI (PC-MRI) has become a fundamental component of clinical practice, providing a wide range of clinical applications for characterization of flow dynamics non-invasively. Commonly used for quantification of blood flow throughout the body [1], PC-MRI has been extended to cerebrospinal fluid (CSF) for possible diagnosis and treatment of hydrocephalus and Chiari malformation, along with non-invasive measurements of elastance and intracranial pressure [2–4]. Initially described as a flow void [5], CSF flow was characterized as pulsatile within the aqueduct of Sylvius as early as the late 1980s [6].

The pulsatile movement of cerebrospinal fluid (CSF) in the basal cisterns may play an important role in the pathogenesis of so-called “communicating” hydrocephalus. Contrary to the basal cistern, the flow of CSF within the cerebral aqueduct and its potential impact on the diagnosis and/or treatment of hydrocephalus have been extensively studied [5, 7–9]. We hypothesized that the increase in ventricular displacement of CSF during systole is due to a reduction in cisternal CSF volume buffering. Unfortunately, the quantitative measurement of this parameter presents considerable technical challenges. Imaging the subarachnoid space (prepontine cistern) adds a level of complexity that is not found in the cerebral aqueduct. The prepontine cistern contains a

R. Hamilton, X. Hu (✉) and M. Bergsneider
Neural Systems and Dynamics Laboratory,
Department of Neurosurgery,
David Geffen School of Medicine,
University of California, NPI 18-265,
Los Angeles, CA 90095, USA

Biomedical Engineering Graduate Program,
Henry Samueli School of Engineering and Applied Science,
University of California,
Los Angeles, CA 90095, USA
e-mail: xhu@mednet.ucla.edu

J. Dye and K. Baldwin
Neural Systems and Dynamics Laboratory, Department of
Neurosurgery, David Geffen School of Medicine, University of
California, NPI 18-265, Los Angeles,
CA 90095, USA

A. Frew
Ahmanson-Lovelace Brain Mapping Center,
Department of Neurology,
David Geffen School of Medicine at
the University of California Los Angeles (UCLA),
Los Angeles, CA, USA

complex system of connective tissues (trabeculae), cranial nerves, venous and arterial blood flow, and CSF. Various methods were attempted to define the cisternal region of interest; visual segmentation proved too subjective and previously published pulsatile-based segmentation algorithms generated noisy results [10]. Here, we describe a methodology for quantification of CSF flow in the prepontine cistern using a novel outlier detection algorithm along with our initial results for the prepontine cistern and aqueduct.

Materials and Methods

Algorithm Input

While under evaluation at the UCLA Hydrocephalus clinic, patients were enrolled in our PC-MRI study to quantify CSF flow; all scans and procedures were approved by the local IRB committee. Scans were conducted on 48 patients (69.83 ± 14.28 years) ranging in age from 32 to 88 years along with an additional 11 controls (51.91 ± 21.13 years) ranging in age from 22 to 72 years. The gender distribution is relatively equal, with 27 male and 21 female patients and 5 male and 6 female controls. Of the 48 patients scanned, 37 are reported in the present study with scans performed pre-operatively (VP, VA shunt or ETV). All MRI were performed using a 3T Siemens Trio T-class MRI (Siemens Medical Systems, Erlangen, Germany). The participants in the study were placed in the supine position with their neck and head in the neutral position using a standard head coil. The imaging protocol was divided into four sections: standard anatomical sequences, aqueduct localization and flow quantification, prepontine cistern localization and flow quantification, and blood vessel visualization. The initial anatomical section consists of a 3D axial T1-weighted MPRage, axial T2-weighted BLADE, and a sagittal T2-weighted TSE sequence.

The flow quantification is divided by region (aqueduct and prepontine cistern) and further subdivided into: localization, anatomical, velocity estimation, and phase contrast. The protocol for the aqueduct and prepontine cistern are analogous with the exception of location; therefore, a general description follows. Using a midsagittal slice, an oblique plane is defined perpendicular to the presumed direction of CSF flow in either the aqueduct or the prepontine cistern (Fig. 1). A trueFISP sequence is used to visualize the local anatomy of the oblique slice; this scan will be inputted into the segmentation algorithm. Following the trueFISP, a flow scout sequence is utilized to define the velocity encoding parameter (V_{enc}) for the phase contrast sequence. Within the study cohort, the interpatient velocity parameter varied drastically, ranging from 8 to 30 cm/s for the aqueduct and 3–25 cm/s in the prepontine cistern. The V_{enc} is an essential

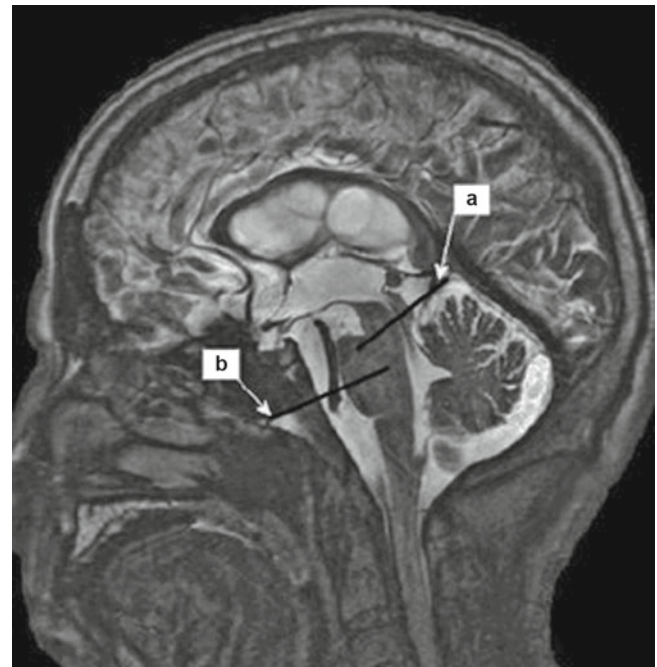


Fig. 1 Midsagittal T2-weighted image, flow acquisition planes for (a) aqueduct of Sylvius and (b) prepontine cistern. Planes defined perpendicular to CSF flow

part of the process as studies have shown the sensitivity of PC-MRI to the V_{enc} . Following the definition of the V_{enc} , the phase contrast sequence is applied; to ensure its accuracy the results are checked for aliasing and further adjustments to the V_{enc} are made if necessary.

Because of the complexity of both the anatomy and the CSF dynamics of the prepontine cistern, additional information was incorporated into the segmentation algorithm. It was found that the pulsatile flow of the basilar artery influenced the results of the PC-MRI for the prepontine cistern. Therefore, a time-of-flight (TOF) sequence was employed to aid in blood vessel identification and removal. The TOF sequence utilizes pre-saturation and unsaturated gradient pulses to image arterial vasculature without contrast medium. The sequence is defined along the identical oblique plane from which the PC-MRI sequence was taken for the prepontine cistern to increase the accuracy of the segmentation. The TOF sequence is not used for the aqueduct as the anatomy does not require it.

Step 1: Reference Waveform

Contrary to current algorithms, where a seed point or manual region of interest is defined, we utilize the information from the local anatomy to define the initial seed point. A standard edge detection algorithm converts the hypertensive CSF to a binary mask. This binary mask ($Region_1$) will be used to define the initial reference waveform (W_1), which is constructed by applying the binary mask to the PC-MRI sequence and averaging the voxel intensity over the 30 time frames

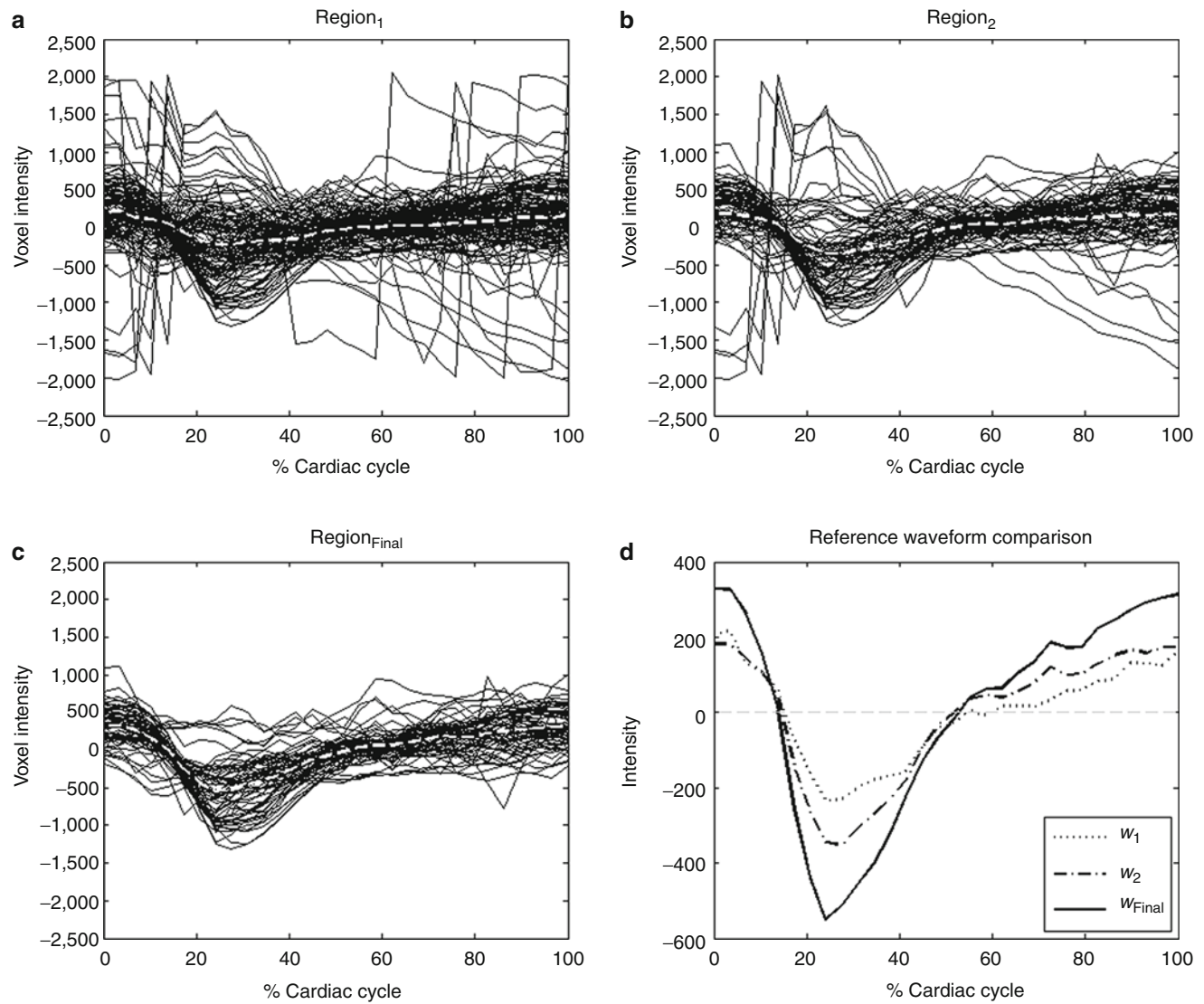


Fig. 2 Step-by-step comparison of the individual voxel waveforms for a given region. (a) Voxel waveform for Region₁. (b) Region₂. (c) Region_{Final}. (d) Comparison of the reference waveforms

that represent the entire cardiac cycle. This method removes the subjectivity in manually selecting seed points that are commonly used in other segmentation algorithms.

Step 2: Correlation Mask and Threshold

In step 1, Region₁ was based solely on anatomical information. It has been shown, however, that manual segmentation produces results that are both inaccurate and difficult to reproduce [10]. Incorporating pulsatility information into the segmentation process adds to the overall accuracy of the segmentation and therefore the results from the quantification. To do this, the reference waveform (W_1) constructed from Region₁ is correlated with each individual voxel of the PC-MRI sequence using Eq. 1:

$$R(i, j) = \frac{C(i, j)}{\sqrt{C(i, i)C(j, j)}} \quad (1)$$

where R is a matrix of correlation coefficients and C represents the covariance matrix between the given elements. In this example i and j represent the voxel waveform (constructed from the 30 time frames) of the reference waveform (W_1) and the waveform of the given voxel respectively. From the correlation values in R a correlation map is created.

Once the correlation map is constructed, a threshold is applied to remove “uncorrelated” voxels. The threshold value of 0.5 was used as it has been validated by phantom experiments in previous studies [10]. The impacts of the threshold value along with the V_{enc} are discussed later in the paper. Unlike other automated segmentation algorithms a boundary is not created, the final ROI comprises the voxels selected through the correlation process; Region₂ is then defined by the selection of the given voxels. The new reference waveform (W_2) is established using the aforementioned method. The new reference waveform provides additional information reducing the influence noise on the ROI (Fig. 2a, b).

Table 1 CSF flow measurements for the cerebral aqueduct and prepontine cistern

Group (N_{aqueduct} , N_{cistern})	Aqueduct			Prepontine cistern		
	Area (mm ²)	Max velocity (cm/s)	Stroke volume (μL)	Area (mm ²)	Max velocity (cm/s)	Stroke volume (μL)
Pre-op (37, 30)	9.4 ± 3.94 (5.47–25.78)	12.26 ± 5.08 (2.87–21.03)	136.04 ± 103.04 (22.01–499.98)	107.46 ± 65.43 (34.79–272.83)	8.78 ± 4.82 (1.45–23.60)	464.32 ± 202.30 (149.1–1093.9)
Control (10, 11)	5.43 ± 1.26 (3.13–7.03)	8.2 ± 3.08 (4.87–14.37)	52.31 ± 14.97 (31.84–84.56)	106.35 ± 35.66 (58.59–169.68)	6.52 ± 2.67 (3.0–11.89)	447.38 ± 75.49 (260.08–539.62)

Reports the values for the aqueduct and the prepontine cistern for the pre-operative group and controls. Metrics included are the ROI area (mm²), maximum velocity (cm/s), and stroke volume (μL); the mean ± standard deviation with the respective range in parentheses

Step 3: Outlier Detection

From Fig. 2b, it can be seen that even though anatomical and pulsatility information has been incorporated within Region₂, poorly selected voxels remain. Due to the complex structure of the prepontine cistern relative to the cerebral aqueduct a method was developed to identify these outlying voxels and remove them from the final segmented region. Using W_2 , defined by the pulsatility-based Region₂, a new correlation map is computed comparing W_2 with each voxel within Region₂. It is important to note the difference between steps 2 and 3; in step 2, the reference waveform (W_1) is compared with each individual time-series waveform within the entire image. In step 3, the new reference waveform (W_2) is only compared with the voxels within Region₂. Once this correlation is computed via Eq. 1, a new intermediate region is created. Due to the sensitivity of this process (Eq. 1) to the reference waveform (input) the process is repeated iteratively until the region is unchanged by the new correlation map and thresholding (thereby producing the same reference waveform as in the previous step); this final region is denoted Region_{FINAL}.

Step 4: Results Calculations

Throughout the literature there are various methods for calculating results from the defined area. In this work we present the basic metrics of: region area (mm²), peak velocity (cm/s), stroke volume (μL), and average flow rate (mL/min).

Phase Offset

The “piston”-like movement of the brain throughout the cardiac cycle caused by the change in intracranial blood volume can have an impact on the aforementioned results. Therefore, a region within the midbrain assumed to have minimal displacement was selected automatically and an offset value was calculated from the average velocity (of the “static tissue”) over the cardiac cycle; this value was used to correct for the periodic brain motion.

Results

Shown in Table 1 are the results for the aqueduct and the cistern for both the pre-operative patients and the control group. Figure 2 shows a step-by-step progression through each stage. Figure 2a shows the initial estimate and the corresponding individual voxel waveforms. Figure 2b, c show the results when the pulsatility information is included. Finally, Fig. 2d compares the reference waveforms generated by each step. In this example an additional iteration was not needed; however, of the cases that were tested 20% required additional iterations before the region became stable. Of those additional iterations, 1.57 ± 0.87 voxels were removed with a range of 1–4 voxels.

Discussion

Phase contrast MRI has been utilized throughout the body as a non-invasive method for flow quantification of blood and CSF. Specifically, within the brain, the flow of CSF within the aqueduct has been studied extensively, though yielding little progress in the diagnosis and/or treatment of NPH. We propose a new semi-automated segmentation algorithm for use in the aqueduct and prepontine cistern.

The foundation of pulsatility-based segmentation is in the definition of the reference waveform. Studies have shown the importance and influence of not only the location of the selection (within the region of interest), but also the number of voxels used to calculate the reference waveform. Alperin and Lee reported a maximum percentage difference of 5.4% with mean values within the internal carotid artery, vertebral artery, and jugular vein lumens of 3.0%, 3.1%, and 3.0% respectively [10] when changing the location of the seed point. The impact of the segmentation area as a function of voxels used to construct the reference waveform was also explored, showing that within the carotid artery 97% of the voxels were identified by only using two voxels to construct the reference waveform. Even though this may suggest that the impact of

the location and number of voxels used to construct the input reference waveform is minimal, when considering the regular lumen structure of the vessels reported, the relatively high velocities compared with the prepontine cistern (3–25 and 80 cm/s respectively), and the absolute size of the regions, the influence of these factors becomes significant. We propose a method that essentially eliminates the subjectivity of reference waveform generation [11].

Limitations

Phase contrast MRI has many applications; however, for CSF flow quantification there are fundamental features that make accurate measurements difficult. For larger regions (usually vessels or other structures with lumens) the area is relatively large compared with the resolution of the scan; however, when looking at the cross-sectional area of the aqueduct (1–3 mm) the impact of the partial volume effect of MRI becomes significant.

Threshold Value

As mentioned previously, the segmentation algorithm is a function of the reference waveform, which in turn is intimately connected to the definition of the threshold value. The threshold value varies drastically between studies. Alperin and Lee reported threshold values of 0.5 and 0.75 depending on the details of the study [10] and Yoshida et al. used a similar correlation-based approach with minimal threshold values ranging from 0.3 to 0.45 [12]. From the drastic difference in methods reported, the use of a static threshold is not ideal for optimal segmentation. Automatically identifying the optimal threshold value on a case by case basis is essential for accurate, reproducible results.

Conclusion

Reliable quantification of volumetric CSF flow in complex cisternal spaces is possible using a methodology combining known anatomical features with the pulsatile nature of CSF flow. Although pulsatility and correlation are not novel methods for segmentation, incorporating automated inputs,

additional anatomical information (arterial blood flow), and increased quantitative restraints on reference waveform selection (iteratively removing voxels) allows effective quantification of pulsatile flow within the cerebral aqueduct and prepontine cistern. The methodology explained here will aid in the exploration of the basal cisterns and their impact on the hydrodynamics of NPH.

Conflict of interest statement We declare that we have no conflict of interest.

References

1. Baledent O et al (2006) Value of phase contrast magnetic resonance imaging for investigation of cerebral hydrodynamics. *J Neuroradiol* 33(5):292–303
2. Alperin NJ et al (2000) MR-intracranial pressure (ICP): a method to measure intracranial elastance and pressure noninvasively by means of MR imaging: baboon and human study. *Radiology* 217(3): 877–885
3. Tain RW, Alperin N (2009) Noninvasive intracranial compliance from MRI-based measurements of transcranial blood and CSF flows: indirect versus direct approach. *IEEE Trans Biomed Eng* 56(3):544–551
4. Menick BJ (2001) Phase-contrast magnetic resonance imaging of cerebrospinal fluid flow in the evaluation of patients with Chiari I malformation. *Neurosurg Focus* 11(1):E5
5. Bradley WG Jr et al (1996) Normal-pressure hydrocephalus: evaluation with cerebrospinal fluid flow measurements at MR imaging. *Radiology* 198(2):523–529
6. Feinberg DA, Mark AS (1987) Human brain motion and cerebrospinal fluid circulation demonstrated with MR velocity imaging. *Radiology* 163(3):793–799
7. Dixon GR et al (2002) Use of cerebrospinal fluid flow rates measured by phase-contrast MR to predict outcome of ventriculoperitoneal shunting for idiopathic normal-pressure hydrocephalus. *Mayo Clin Proc* 77(6):509–514
8. Al-Zain FT et al (2008) The role of cerebrospinal fluid flow study using phase contrast MR imaging in diagnosing idiopathic normal pressure hydrocephalus. *Acta Neurochir Suppl* 102:119–123
9. Abbey P et al (2009) Shunt surgery effects on cerebrospinal fluid flow across the aqueduct of Sylvius in patients with communicating hydrocephalus. *J Clin Neurosci* 16(4):514–518
10. Alperin N, Lee SH (2003) PUBS: pulsatility-based segmentation of lumens conducting non-steady flow. *Magn Reson Med* 49(5): 934–944
11. Luetmer PH et al (2002) Measurement of cerebrospinal fluid flow at the cerebral aqueduct by use of phase-contrast magnetic resonance imaging: technique validation and utility in diagnosing idiopathic normal pressure hydrocephalus. *Neurosurgery* 50(3):534–543; discussion 543–544
12. Yoshida K et al (2009) Phase-contrast MR studies of CSF flow rate in the cerebral aqueduct and cervical subarachnoid space with correlation-based segmentation. *Magn Reson Med Sci* 8(3):91–100

Delta-ADC (Apparent Diffusion Coefficient) Analysis in Patients with Idiopathic Normal Pressure Hydrocephalus

T. Osawa, M. Mase, T. Miyati, H. Kan, K. Demura, H. Kasai, M. Hara, Y. Shibamoto, and K. Yamada

Abstract We have developed the delta-apparent diffusion coefficient (ADC), a new parameter of the water dynamics of brain tissue using MRI. Delta-ADC is the changes in regional ADC values of the brain during the cardiac cycle. The study included 6 idiopathic normal pressure hydrocephalus (iNPH) patients (iNPH group) and 12 healthy volunteers (control group). ECG-triggered single-shot diffusion echo planar imaging ($b=0$ and $1,000 \text{ s/mm}^2$) was used on a 1.5-T MRI. The delta-ADC image was calculated from the maximum minus the minimum ADC value of all cardiac phase images (20 phases) on a pixel-by-pixel basis. Delta-ADC values in the white matter of the frontal, temporal, and occipital lobe were obtained. Delta-ADC values in the iNPH group were significantly higher than those in the control group in all regions. ADC values in the iNPH were also significantly higher than those in the control group, but the differences in the ADC between the groups in each region were much lower than those for the delta-ADC. Although the changes in the delta-ADC and ADC values were similar, there was no significant correlation between the delta-ADC and the ADC. These results suggest that the ADC and the delta-ADC may reflect different kinds of water dynamics. The ADC depends on the water content in brain tissue. On the other hand, delta-ADC depends on not only the water content, but also on the degree of the fluctuation of the water molecules. Delta-ADC analysis makes it possible to obtain non-invasively new and more detailed information on the regional brain condition in iNPH.

Keywords Idiopathic normal pressure hydrocephalus • Apparent diffusion coefficient (ADC) • Diffusion tensor images of MRI

Introduction

There are many unsolved problems in the pathophysiology of idiopathic normal pressure hydrocephalus (iNPH). The diagnosis of iNPH continues to be difficult in some cases and many types of diagnostic examination have been attempted. However, in electing NPH patients for shunt surgery, an unambiguously useful and non-invasive method of examination has not yet been found that can be easily performed, or that is widely accepted in medical centers.

It is reported that the ADC of the periventricular white matter increases in patients with hydrocephalus [2, 5, 7, 10]. It is also reported that the ADC of the periventricular white matter decreases after a tap test or a shunt operation [2, 5, 7, 10]. Diffusion-weighted imaging can detect internal and external cellular fluid volume more accurately than T2-weighted imaging. The diffusion also reflects the subtle movement of the water molecules. Therefore, we suspect it is also affected by brain pulsation, which is caused by heart-beat. Concerning phase dispersion caused by the bulk motion effect of brain pulsation [1, 3, 4, 8], Brockstedt et al. [3], who used single-shot echo planar imaging (EPI), reported that the apparent diffusion coefficient (ADC) was not significantly altered during the cardiac cycle. On the other hand, it has been reported that brain pulsation can give rise to artifactual signal attenuation, leading to over-estimation of the ADC [12–15]. We precisely evaluated dynamic changes in water diffusion during the cardiac cycle by using ECG-triggered single-shot diffusion EPI with high temporal resolution and instantaneous data-sampling to minimize the bulk motion effect [11]. In this study it was suggested that the ADC value changes significantly during the cardiac cycle even if the effect of bulk motion is minimized, i.e., these changes are independent of the bulk motion.

T. Osawa, M. Mase (✉), K. Demura, and K. Yamada
Department of Neurosurgery, Nagoya City University Graduate
School of Medical Sciences, 1-Kawasumi, Mizuho-ku, Mizuho-cho,
Nagoya, 467-8602, Japan
e-mail: mitmase@med.nagoya-cu.ac.jp

T. Miyati and H. Kan
Faculty of Health Sciences, Institute of Medical, Pharmaceutical and
Health Science, Kanazawa University, 5-11-80, Kadotsuno,
Kanazawa, 920-0942, Japan

H. Kasai, M. Hara, and Y. Shibamoto
Department of Radiology, Nagoya City University Hospital,
1-Kawasumi, Mizuho-ku, Mizuho-cho, Nagoya, 467-8602, Japan

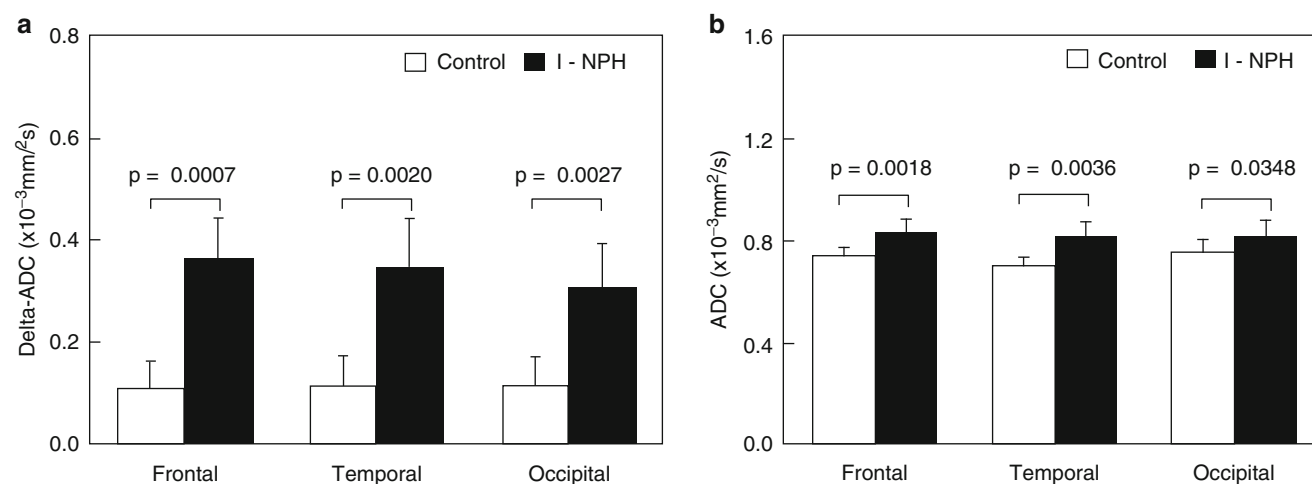


Fig. 1 (a) Delta-apparent diffusion coefficient (*delta-ADC*) values in the control and idiopathic normal pressure hydrocephalus (*iNPH*) groups. In each region, the *delta-ADC* values in *iNPH* were significantly

higher than those in the control group. (b) Result for conventional ADC values. ADC values in the *iNPH* group were significantly higher in each region than in the control group

In this paper, we determined the change in the ADC value during the cardiac cycle (*delta-ADC*) in the white matter of the patients with *iNPH* to clarify the pathophysiology of *iNPH*.

Materials and Methods

Patients

Delta-ADC analysis was performed in patients with *iNPH* ($n=6$) and healthy volunteers (control group, $n=12$). All patients with *iNPH* showed improvement in their symptoms after a CSF tap test and a shunt operation.

MR Imaging Conditions

On a 1.5-T MRI, ECG-triggered single-shot diffusion echo planar imaging ($b=0$ and $1,000 \text{ s/mm}^2$) was used with sensitivity encoding and half-scan techniques to minimize bulk motion, i.e., a data sampling window of approximately 3 ms. The *delta-ADC* image was then calculated from the maximum minus minimum ADC value of all cardiac phase images (20 phases) on a pixel-by-pixel basis. We assessed the *delta-ADC* and the ADC in regions of frontal, temporal and occipital white matter (except the periventricular high-intensity area on T2-weighted imaging) in patients with *iNPH* and in the control group.

The purpose and procedures of all our investigations were fully explained to all patients, and the studies were performed only after obtaining informed consent from each patient.

Results

Delta-ADC values in *iNPH* were significantly higher than those in the control group in the frontal lobe ($p=0.0007$), temporal lobe ($p=0.0020$), and occipital lobe ($p=0.0027$; Fig. 1). The distribution of the *delta-ADC* values is shown in Fig. 2. Delta-ADC values in the brain parenchyma (particularly white matter) were low in healthy volunteers. On the other hand, *delta-ADC* values in the brain parenchyma were high in the *iNPH* group.

Conventional ADC values in *iNPH* were also significantly higher than those in the control group in frontal lobe ($p=0.0018$), temporal lobe ($p=0.0036$), and occipital lobe ($p=0.0348$; Fig. 1). However, differences in the ADC between these groups in each region were much lower than those of the *delta-ADC*. Moreover, there was no significant correlation between the *delta-ADC* and the ADC in the frontal lobe ($R^2=0.214$), temporal lobe ($R^2=0.184$), or occipital lobe ($R^2=0.224$; Fig. 3).

Discussion

The diagnosis of *iNPH* remains difficult in some cases. To address questions regarding pathophysiology, in this study, we tried to evaluate the water dynamics of the cerebral white matter in patients with hydrocephalus non-invasively using MRI.

In the study group, conventional ADC and *delta-ADC* values of the white matter in each region were higher than in the control group. Much water content of the white matter can contribute to the increase in the ADC and *delta-ADC*

Fig. 2 Distribution map of the delta-ADC values. **(a)** Healthy volunteer. **(b)** iNPH patient. The delta-ADC value in brain parenchyma (particularly white matter) was low in healthy volunteers. In contrast, the delta-ADC value in white matter was high in the iNPH group

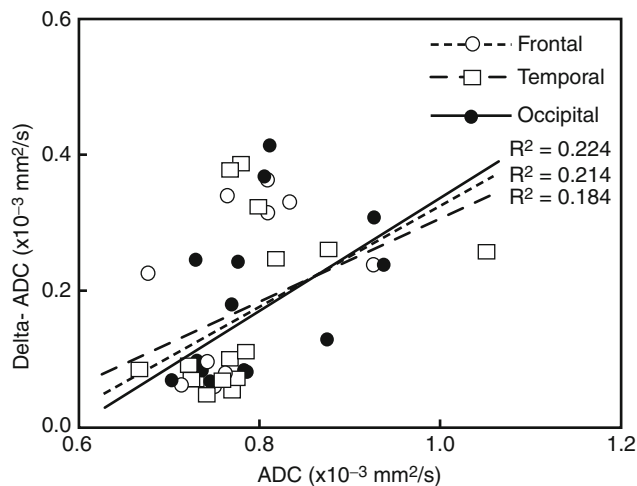
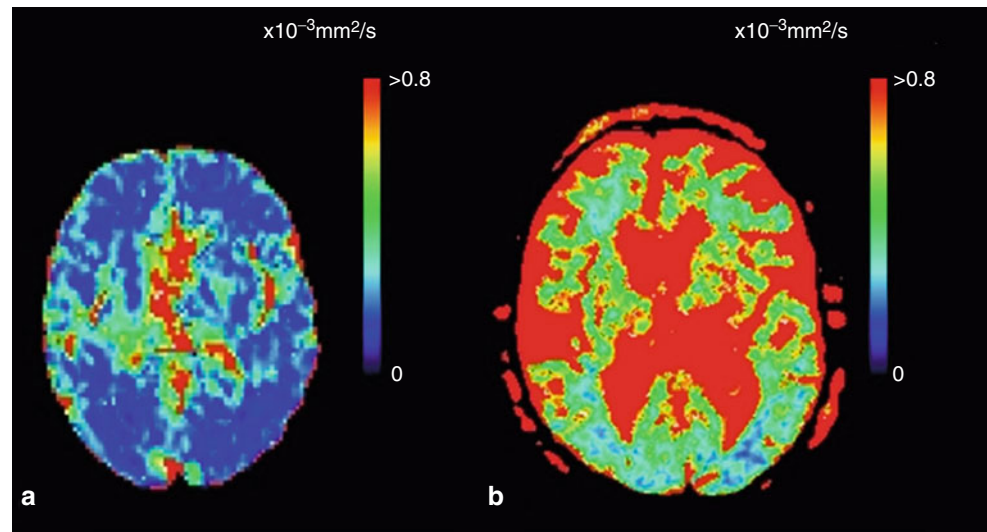


Fig. 3 Relation between the delta-ADC and the ADC. No significant correlation between the delta-ADC and the ADC was found in the frontal lobe, temporal lobe, or occipital lobe

values. However, there was no significant correlation between the delta-ADC and the ADC. These results suggest that the ADC and the delta-ADC may reflect the different kinds of water dynamics. The ADC depends on the water content in brain tissue. On the other hand, the delta-ADC depends not only on water content, but also on the degree of the fluctuation of the water molecules.

The white matter of the patients with hydrocephalus causes axonal dysfunction and the microenvironment of the white matter can change [6, 9]. We suspect that the delta ADC can reflect the special microenvironment of the white matter in the brain with iNPH.

Conclusion

Delta-ADC analysis makes it possible to obtain non-invasively new and more detailed information on the regional brain condition in iNPH and thereby assist in the diagnosis and understanding of the mechanism causing symptoms. Further study will be needed to elucidate the relation between the delta-ADC and the pathophysiology of hydrocephalus.

Conflict of interest statement We declare that we have no conflict of interest.

References

1. Anderson AW, Gore JC (1994) Analysis and correction of motion artifacts in diffusion weighted imaging. *Magn Reson Med* 32(3):379–387
2. Anik Y, Demirci A, Anik I, Etus V, Arslan A (2008) Apparent diffusion coefficient and cerebrospinal fluid flow measurements in patients with hydrocephalus. *J Comput Assist Tomogr* 32(3):392–396
3. Brockstedt S, Borg M, Geijer B et al (1999) Triggering in quantitative diffusion imaging with single-shot EPI. *Acta Radiol* 40(3):263–269
4. Chenevert TL, Pipe JG (1991) Effect of bulk tissue motion on quantitative perfusion and diffusion magnetic resonance imaging. *Magn Reson Med* 19(2):261–265
5. Corkill RG, Garnett MR, Blamire AM, Rajagopalan B, Cadoux-Hudson TA, Styles P (2003) Multi-modal MRI in normal pressure hydrocephalus identifies pre-operative haemodynamic and diffusion coefficient changes in normal appearing white matter correlating with surgical outcome. *Clin Neurol Neurosurg* 105(3):193–202
6. Del Bigio MR (1993) Neuropathological changes caused by hydrocephalus. *Acta Neuropathol* 85(6):573–585

7. Dorenbeck U, Schlaier J, Feuerbach S, Seitz J (2005) Diffusion-weighted imaging in the diagnostic evaluation of the hydrocephalus in patients with acute or chronic increase in cerebral pressure. *Rofo* 177(1):99–104, German
8. Greitz D, Wirestam R, Franck A et al (1992) Pulsatile brain movement and associated hydrodynamics studied by magnetic resonance phase imaging. *Neuroradiology* 34(5):370–380
9. Hattingen E, Jurcoane A, Melber J et al (2010) Diffusion tensor imaging in patients with adult chronic idiopathic hydrocephalus. *Neurosurgery* 66(5):917–924
10. Leliefeld PH, Gooskens RH, Braun KP, Ramos LM, Uiterwaal CS, Regli LP, Tulleken CA, Kappelle LJ, Hanlo PW (2009) Longitudinal diffusion-weighted imaging in infants with hydrocephalus: decrease in tissue water diffusion after cerebrospinal fluid diversion. *J Neurosurg Pediatr* 4(1):56–63
11. Nakamura T, Miyati T, Kasai H et al (2009) Bulk motion-independent analyses of water diffusion changes in the brain during the cardiac cycle. *Radiol Phys Technol* 2(2):133–137
12. Nunes RG, Jezzard P, Clare S (2005) Investigations of the efficiency of cardiac-gated methods for the acquisition of diffusion-weighted images. *J Magn Reson Imaging* 17(1):102–110
13. Robson MD, Porter DA (2005) Reconstruction as a source of artifact in nongated single-shot diffusion-weighted EPI. *Magn Reson Imaging* 23:899–905
14. Skare S, Andersson JL (2001) On the effects of gating in diffusion imaging of the brain using single shot EPI. *Magn Reson Imaging* 19(8):1125–1128
15. Summers P, Staempfli P, Jaermann T et al (2006) A preliminary study of the effects of trigger timing on diffusion tensor imaging of the human spinal cord. *AJNR Am J Neuroradiol* 27(9):1952–1961

Evidence for Altered Spinal Canal Compliance and Cerebral Venous Drainage in Untreated Idiopathic Intracranial Hypertension

Noam Alperin, Byron L. Lam, Rong-Wen Tain, Sudarshan Ranganathan, Michael Letzing, Maria Bloom, Benny Alexander, Potyra R. Aroucha, and Evelyn Sklar

Abstract Idiopathic intracranial hypertension (IIH), or pseudotumor cerebri, is a debilitating neurological disorder characterized by elevated CSF pressure of unknown cause. IIH manifests as severe headaches, and visual impairments. Most typically, IIH prevails in overweight females of childbearing age and its incidence is rising in parallel with the obesity epidemic. The most accepted theory for the cause of IIH is reduced absorption of CSF due to elevated intracranial venous pressure. A comprehensive MRI study, which includes structural and physiological imaging, was applied to characterize morphological and physiological differences between a homogeneous cohort of female IIH patients and an age- and BMI-similar control group to further elucidate the underlying pathophysiology. A novel analysis of MRI measurements of blood and CSF flow to and from the cranial and spinal canal compartments employing lumped parameters modeling of the cranio-spinal biomechanics provided, for the first time, evidence for the involvement of the spinal canal compartment. The CSF space in the spinal canal is less confined by bony structures compared with the cranial CSF, thereby providing most of the craniospinal compliance. This study demonstrates that the contribution of spinal canal compliance in IIH is significantly reduced.

Keywords Intracranial hypertension • Underlying pathophysiology • Cranio-spinal biomechanical properties • Cerebral venous drainage • MRI CSF and blood flow studies

Introduction

Idiopathic intracranial hypertension (IIH), or pseudotumor cerebri, is a debilitating neurological disorder characterized by elevated ICP of unknown cause. IIH manifests as severe headaches, and visual impairment due to increased pressure on the optic nerve. In addition to poor quality of life, IIH is associated with a considerable financial burden. Based on data from the IIH Registry, the total costs of IIH in 2007 in the US alone exceeded \$444 million per year [8]. Most typically, IIH prevails in overweight females of childbearing age, with a high incidence of 22.5 new cases annually per 100,000, and is further rising in parallel with the obesity epidemic.

The origin and evolution of the disorder is not well understood, nor has evidence-based medicine identified an efficient and effective treatment path [7]. Often, individuals are diagnosed with IIH after all other possible identifiable causes have been exhausted. This occurs especially when prominent features such as papilledema and pulsatile tinnitus are not apparent [6], or if a marginally high opening pressure is obtained on lumbar puncture [4]. Currently, there is no established standard treatment for IIH. Treatment is primarily palliative, beginning with medical therapy and progressing to surgical therapy [3, 5]. Prescribed interventions include diet, diuretics, and carbonic anhydrase inhibitors, such as acetazolamide, repeated spinal taps, optic nerve sheath fenestration surgery, and CSF shunting procedures. The efficacy of each treatment varies among patients and the mechanism by which each treatment works is also not clear at present. Treatment often improves symptoms; however, 86% of patients suffer from some degree of permanent visual loss and 10% develop severe irreversible visual loss [15]. Better understanding of the pathophysiology is likely to improve this potentially devastating prognosis.

The most widely accepted theories on the causes of IIH are sinus venous focal narrowing and reduced absorption of CSF due to elevated intracranial venous pressure [10]. However, extra-cranial factors that may be contributing to the increased ICP in IIH and the adaptation of the cranio-spinal system have not been widely investigated.

N. Alperin (✉), R.-W. Tain, S. Ranganathan, M. Letzing, M. Bloom, B. Alexander, and E. Sklar
Department of Radiology, Miller School of Medicine,
University of Miami, 1150 N.W. 14th St., Suite 713, Miami,
FL 33136, USA
e-mail: nalperin@med.miami.edu

B.L. Lam and P.R. Aroucha
Departments of Ophthalmology,
Bascom Palmer Eye Institute, University of Miami,
Miami, FL 33136, USA

The current study aims to investigate the potential involvement of extra-cranial venous drainage and the spinal canal compartment; the latter has not been previously considered as a contributor to the pathophysiology of IIH. As the spinal canal normally contributes to most of craniospinal compliance, it is likely that the elevated ICP is a manifestation of reduced compliance buffering in the spinal canal compartment.

Materials and Methods

Following approval by the Institutional Review Board and informed patient consent, 11 female patients (mean age, 29 ± 9 years; range, 17–44 years) with above-normal BMI (mean BMI, 35.4 ± 6.5 kg/m²; range, 23.9–49.1) and 8 healthy women of comparable age (mean age, 32 ± 11 ; range, 22–50) and BMI (mean BMI, 37.1 ± 6 ; range, 30.9–48.5) were studied by MRI. The aim was to assess potential morphological and physiological differences between newly-diagnosed pretreated IIH patients and healthy subjects. Assessed parameters include gray matter, white matter, and ventricular volumes, total arterial inflow, venous outflow through primary (jugular veins) and secondary channels, estimated supratentorial CSF production rate, and spinal canal compliance contribution, all measured noninvasively by MRI.

Magnetic resonance imaging was obtained at 1.5 T (Siemens Healthcare). The MRI study included high-resolution 3D T1-weighted imaging for segmentation of the ventricular volumes and multiple velocities encoding phase contrast scans for imaging of the blood and CSF flows. High-velocity encoding of 70 cm/s was employed for imaging of blood flow dynamics to and from the cranial vault. Low velocity encoding of 12 and 7 cm/s was employed to image CSF flow through the aqueduct of Sylvius and between the cranium and the spinal canal respectively.

Imaging parameters for the T1-weighted structural brain scan included field of view (FOV) of 25.6×19.2 cm, acquisition matrix of 256×192 , slice thickness of 1.0 mm, which provided 1-mm isotropic resolution. Imaging parameters for the phase contrast series used for imaging of the trans-cranial blood and CSF flows included FOV of 16×15.5 cm, acquisition matrix of 256×174 and slice thickness of 6 mm. A smaller FOV of 11×10 cm with slice thickness of 5.5 mm and acquisition matrix of 320×218 were used for imaging of the aqueductal flow. Minimum effective TR and TE (approximately 13–15 and 9 ms respectively) were always used for maximal temporal resolution.

Cerebral Venous Drainage

Venous drainage occurs through primary (e.g., internal jugular veins) and secondary (e.g., epidural, vertebral, deep cervical) venous channels. Mean volumetric flow rate in each internal jugular vein was calculated and added to obtain total venous drainage through the primary venous drainage channels. As total arterial inflow equals venous outflow, the relative cerebral venous drainage through the jugular veins was obtained by normalizing the total jugular flow with the total arterial inflow. Total arterial inflow, which is also the total cerebral blood flow (tCBF) is obtained by summation of mean volumetric flow rates through the two internal carotid and vertebral arteries. Volumetric flow rates were obtained by summation of the velocities within the blood vessel lumen area. Vessel lumen boundary was identified using the automated pulsatility-based segmentation method [1].

Morphological Assessment

The structural MR images of the brain were automatically segmented to extract the brain tissue for derivation of the intracranial volume using FSL software (Analysis Group, FMRIB, University of Oxford, Oxford, UK). The segmentation process uses a hidden Markov random field model based on image pixel intensity distribution [16]. Ventricular volumes were obtained by manual delineation of the ventricular boundaries by an experienced observer.

Cranio-Spinal Canal Compliance Distribution

A system analysis approach has been applied to estimate the cranio-spinal (CS) compliance distribution. A previously reported subject-specific lumped parameter model was employed to obtain the transfer function of the craniospinal system where the momentary difference between the arterial inflow and the venous outflow to and from the cranial vault is the input and the driving force for the cranio-spinal CSF pulsation, i.e., the output of the system [14]. A schematic representation of the compartmental model of the cranio-spinal system and an example of the MRI-derived waveform of blood and CSF flows demonstrating the input–output relationship between the blood and the CSF flow are shown in Fig. 1. The electrical circuit of the biomechanical analogous model includes the following lumped parameters: cranial and spinal compliance (C_1 and C_2 respectively), cranial and spinal CSF flow resistance (R_1 and R_2 respectively), and an

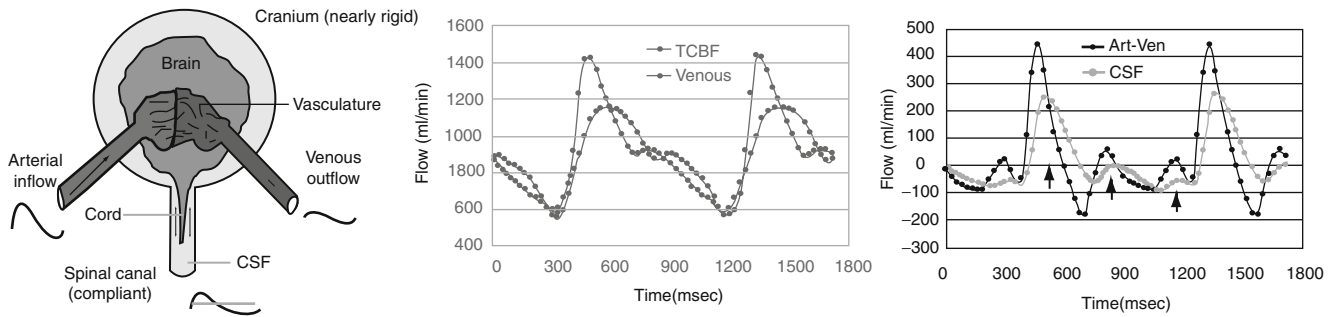


Fig. 1 The cranio-spinal system compartmental model employed to derive the cranio-spinal cerebrospinal fluid (CSF) compliance distribution. The arterial and venous volumetric flow rates are shown. The dif-

ference between these two waveforms (Art-Ven) is the driving force for the cranio-spinal CSF (right)

Table 1 Hemodynamic measures in idiopathic intracranial hemorrhage (IIH) and controls: mean and SD values of main hemodynamic parameters

	IIH (<i>n</i> = 11)	Control (<i>n</i> = 8)	<i>p</i> Value
Age (years)	28.6 ± 8.9	31.8 ± 9.9	0.49
BMI (kg/m ²)	34.2 ± 5.1	36.4 ± 5.8	0.38
Total cerebral blood flow (TCBF) (mL/min)	823 ± 68	804 ± 126	0.68
Total internal jugular flow (TIJF) (mL/min)	539 ± 91 ^a	634 ± 84	0.03
Dominant IJF (mL/min)	385 ± 111	430 ± 104	0.39
Non-dominant IJF (mL/min)	148 ± 68	209 ± 78	0.08
TIJF/TCBF	0.65 ± 0.08 ^a	0.80 ± 0.10	0.004

^aDifference is statistically significant

inertia component (I_2) to model the inertia-dominated CSF flow between the cranium and spinal canal [11]. The biomechanical characteristics of the CS system can be expressed by a transfer function, $H(s)$, shown in Eq. 1, which is the ratio of the Laplace transforms of the output (CSF flow waveform) to the input (arterial minus venous flow waveform).

$$H(s) = \frac{F_{csf}(s)}{F_{a-v}(s)} = \frac{\frac{R1}{I2}s + \frac{1}{I2 \cdot C1}}{s^2 + \frac{1}{I2}(R1 + R2)s + \frac{1}{I2}\left(\frac{1}{C1} + \frac{1}{C2}\right)} \quad (1)$$

The ratio of the cranio and spinal canal compliance is then obtained by dividing the zero order coefficients in the numerator and denominator of the transfer function, as shown in Eq. 2.

$$\frac{C2}{C1 + C2} = \frac{\frac{1}{I2 \cdot C1}}{\frac{1}{I2}\left(\frac{1}{C1} + \frac{1}{C2}\right)} \quad (2)$$

Results

Mean and SD values of total cerebral blood flow (TCBF), total internal jugular flow (TIJF), flows through dominant internal jugular veins (DIJF), nondominant internal jugular veins (NIJF), and total internal jugular flow (TIJF) normalized to total cerebral blood flow are summarized in Table 1. Venous drainage through the primary venous channels is significantly reduced in IIH patient compared with healthy subjects. This difference is further enhanced after normalization with total cerebral blood flow as demonstrated by the smaller *p* value (*p* value < 0.004). Example of a 3D MRV rendering of the extra-cranial venous vasculature from a control subject and from an IIH patient demonstrating the increased drainage through secondary channels in IIH is shown in Fig. 2. Means and SDs of morphological measures, CSF production rates and contribution to spinal canal compliance are summarized in Table 2. A trend toward slightly larger ventricular volumes in the IIH was observed. However, this trend was not statistically significant. No difference was found in CSF production rates between IIH and healthy. However, a larger but not significantly different variability in the CSF production was observed. In contrast to the morphological measures, spinal



Fig. 2 Example of Magnetic resonance venography of cervical venous drainage in a control subject (*left*) and an idiopathic intracranial hypertension (IIH) patient (*right*). In the healthy subjects, the venous drainage

occurs mainly through the jugular veins (*arrows*) while in the IIH patients an increased drainage through the secondary venous channels (e.g., vertebral, deep cervical, epidural veins; *arrowheads*) is observed

Table 2 Intracranial morphology, CSF production rate, and compliance distribution in IIH and controls

	IIH (<i>n</i> = 11)	Control (<i>n</i> = 8)	<i>p</i> Value
Lateral ventricular volume (LVV) (cm ³)	16.5 ± 6.6	14.8 ± 5.5	0.57
Total ventricular volume (TVV) (cm ³)	18.5 ± 6.8	16.8 ± 5.7	0.56
Intracranial volume (ICV) (cm ³)	1374.2 ± 103.2	1335.6 ± 88.9	0.40
TVV/ICV (%)	1.34 ± 0.46	1.27 ± 0.47	0.74
Supratentorial CSF production rate (mL/min)	0.44 ± 0.28	0.44 ± 0.17 ^a	0.99
Spinal canal compliance/total compliance	0.60 ± 0.12 ^b	0.75 ± 0.09	0.026

^aSD of CSF production is not significantly different, *p* = 0.13

^bDifference is statistically significant

canal compliance contribution is significantly different in IIH and controls. A significantly smaller contribution to spinal canal compliance (0.6 vs. 0.75) was found in IIH (*p* = 0.026).

Discussion

An MRI-based comprehensive characterization of the cerebral hemodynamics, venous drainage, cerebral ventricular morphology, and cranio-spinal compliance distribution was applied to homogeneous cohorts of pretreated female IIH subjects and an age- and BMI-similar group of healthy women. Several significant differences that further elucidate the pathophysiology of IIH have been identified. The most significant finding of this study is a contribution to lower spinal canal compliance in IIH.

Mechanical compliance represents the ability of a compartment to accommodate an increase in volume without a large increase in pressure. A subject-specific assessment of the relative contribution of the spinal canal to the overall cranio-spinal compliance based on the relationship of the blood flow and cranio-spinal CSF flow reveals that spinal canal compliance buffering is significantly reduced in IIH.

Conclusion

This finding suggests, for the first time, that the spinal canal plays an important role in the pathophysiology of IIH. It has been documented that ICP fluctuates considerably over a short period of time in IIH. As the spinal canal provides most

of the buffering for increased CSF volume, reduced spinal canal compliance buffering provides a good explanation of the impaired regulation of CSF pressure in IIH. This finding further explains why obesity carries an increased risk of IIH. Hogan et al. reported significantly smaller CSF space cross-sectional areas in obese compared with slim subjects. They attributed the smaller CSF area to inward displacement of the neural foramina contents caused by high abdominal pressure [9]. Therefore, the already compressed spinal canal CSF space in obese subjects is very likely increasing resistance for expansion, thereby reducing the spinal canal compliance buffering. The second important observation of reduced cerebral venous drainage through the primary venous channels is in agreement with an earlier report of increased drainage through secondary venous channels in IIH [2]. As previously suggested, this may reflect increased resistance to venous drainage in IIH.

Conflict of interest statement We declare that we have no conflict of interest.

References

- Alperin N, Lee SH (2003) PUBS: pulsatility-based segmentation of lumens conducting non-steady flow. *Magn Reson Med* 49:934–944
- Alperin N, Lee SH, Mazda M, Hushek SG, Roitberg B, Goodwin J (2005) Evidence of the importance of extracranial venous flow in patients with Idiopathic Intracranial Hypertension (IIH). *Acta Neurochir Suppl* 95:129–132
- Ball AK, Clark CE (2006) Idiopathic intracranial hypertension. *Lancet Neurol* 5:433–442
- Bono F, Cristiano D, Mastrandrea C, Latorre V, D'Asero S, Salvino D, Fera F, Lavano A, Quattrone A (2010) The upper limit of normal CSF opening pressure is related to bilateral transverse sinus stenosis in headache sufferers. *Cephalalgia* 30:145–151
- Digre KB (1999) Idiopathic intracranial hypertension. *Curr Treat Options Neurol* 1:74–81
- Digre KB, Nakamoto BK, Warner JEA, Langeberg J, Baggaley SK, Katz BJ (2009) A comparison of idiopathic intracranial hypertension with and without papilledema. *Headache* 49:185–193
- Friedman DI (2007) Idiopathic intracranial hypertension. *Curr Pain Headache Rep* 11:62–68
- Friesner D, Rosenman R, Lobb BM, Tanne E (2010) Idiopathic intracranial hypertension in the USA: the role of obesity in establishing prevalence and healthcare costs. *Obes Rev* 12(5):1–8
- Hogan QH, Prost R, Kulier A, Taylor ML, Liu S, Leighton M (1996) Magnetic resonance imaging of the cerebrospinal fluid volume and the influence of body habitus and abdominal pressure. *Anesthesiology* 84:1341–1349
- Karahalios DG, Rekeate HL, Khayata MH, Apostolides PJ (1996) Elevated intracranial venous pressure as a universal mechanism in pseudotumor cerebri of varying etiologies. *Neurology* 46:198–202
- Loth F, Yardimci M, Alperin N (2001) Hydrodynamic modeling of cerebrospinal fluid motion within the spinal cavity. *J Biomech Eng* 123:71–79
- Reid AC, Matheson MS, Teasdale G (1980) Volume of the ventricles in benign intracranial hypertension. *Lancet* 316:7–8
- Reid AC, Teasdale GM, Matheson MS, Teasdale EM (1981) Serial ventricular volume measurements: further insights into the aetiology and pathogenesis of benign intracranial hypertension. *J Neurol Neurosurg Psychiatry* 44:636–640
- Tain R, Alperin N (2009) Noninvasive intracranial compliance from MRI-based measurements of transcranial blood and CSF flows: indirect versus direct approach. *IEEE Trans Biomed Eng* 56:544–551
- Wall M, George D (1991) Idiopathic intracranial hypertension: a prospective study of 50 patients. *Brain* 114:155–180
- Zhang Y, Brady M, Smith S (2001) Segmentation of brain MR images through a hidden Markov random field model and the expectation maximization algorithm. *IEEE Trans Med Imaging* 20:45–57

Automated Extraction of Decision Rules for Predicting Lumbar Drain Outcome by Analyzing Overnight Intracranial Pressure

Xiao Hu, Robert Hamilton, Kevin Baldwin, Paul M. Vespa, and Marvin Bergsneider

Abstract *Background:* Extended lumbar drain (ELD) has become a popular pre-shunt workup test to help diagnose normal pressure hydrocephalus (NPH). Unfortunately, this procedure requires a substantial time investment for both the family and hospital. In this study, we investigate how accurate the prediction of ELD outcome can be achieved by using simple decision rules automatically derived from pulse morphological metrics of overnight ICP recordings. Our ultimate goal is to test the hypothesis that overnight ICP monitoring, empowered by subsequent signal analysis, could be an alternative to ELD.

Methods: The present study involved 54 patients with both ELD and overnight ICP recordings; the ICP morphological analysis was performed using the MOCAIP algorithm. Furthermore, the distribution of individual metric from the overnight recording was characterized using five aggregation functions (features). Then an algorithm was developed to automatically discover the most accurate “if-then” decision rule for each of the five feature functions. In addition, the best combination of two decision rules, either using “AND” or “OR” operator, was obtained.

Findings: Rules based on five individual feature functions achieved an accuracy of 70.4%, 72.2%, 74.1%, 72.2%, and 79.6% respectively. However, “OR” combination of two features improved accuracy to 88.9%.

Conclusion: We showed an algorithm to discover decision rules that can potentially predict ELD outcome.

Keywords Intracranial pressure • Pulse morphology • Hydrocephalus • Hierarchical clustering

Introduction

Determining whether a patient with typical normal pressure hydrocephalus (NPH) triad will benefit from shunt implantation is significant because of the complication and malfunction associated with the existing shunt technologies. Extended lumbar cerebrospinal fluid (CSF) drain for 72 h has become a popular pre-shunt workup test in many neurosurgical centers [1–3]. Its popularity stems from the findings of an excellent study that demonstrates the high specificity and sensitivity of predicting shunt response based on lumbar drain [3] test outcome [3, 4]. However, the mechanistic relationship between positive LD outcome and shunt response remains to be elucidated. Therefore, in addition to the LD test, many centers also employ additional tests to assess patients in order to predict their shunt response. Overnight intracranial pressure monitoring is one of such tests. It has been reported in many studies that overnight ICP monitoring is able to reveal many phenomena that a short-term ICP monitoring or lumbar puncture cannot reveal, e.g., large but slow oscillations of ICP that are termed B-waves. The capability of overnight ICP monitoring to predict shunt response has been studied but with controversial results [5, 6]. Some centers have found that large portions of B-wave in an overnight ICP recording is highly predictive of shunt outcome [5], while others have argued that overnight ICP monitoring has a limited amount of predictive information of shunt outcome [7, 8].

Given these existing contradictory results, elucidating the potential prognostic value of overnight ICP monitoring is

X. Hu (✉), R. Hamilton, and M. Bergsneider
Neural Systems and Dynamics Laboratory,
Department of Neurosurgery, David Geffen School of Medicine,
University of California, NPI 18-265, Los Angeles,
CA 90095, USA

Biomedical Engineering Graduate Program, Henry Samueli School
of Engineering and Applied Science, University of California,
Los Angeles, CA, USA
e-mail: xhu@mednet.ucla.edu

K. Baldwin
Neural Systems and Dynamics Laboratory,
Department of Neurosurgery, David Geffen School of Medicine,
University of California, NPI 18-265, Los Angeles,
CA 90095, USA

P.M. Vespa
Neurocritical Care Program, Department of Neurosurgery,
David Geffen School of Medicine, University of California,
Los Angeles, CA, USA

significant. Overnight ICP monitoring could be an important economic alternative to the LD test because it requires a shorter hospital stay for patients if its prognostic value can be fully explored. Unfortunately, many existing analysis methods applied to overnight ICP recordings are very subjective and usually extract a limited amount of information from overnight ICP recordings. On the other hand, a few studies utilizing more advanced ICP signal analysis methods [6, 9] have demonstrated that the amplitude of ICP pulse has excellent predictive value of shunt response. In addition to the lack of complex analysis methods of overnight ICP, a potential limit to the existing studies that use shunt response as an end-point is that such an outcome is also determined by many other post-implantation factors not necessarily associated with overnight ICP characteristics.

Therefore, the present work aims to develop an automated method of feature extraction and decision rule construction from overnight ICP recording. This method is used to assess the predictive accuracy of LD outcome instead of shunt outcome.

Specifically, we used the Morphological Clustering and Analysis of Intracranial Pressure (MOCAIP) algorithm to analyze the overnight ICP recordings. MOCAIP was applied to consecutive short segments of an ICP recording resulting in 128 metrics per each segment. Then, various feature functions were designed to summarize the distribution of the 128 metrics from all the segments per ICP recording. The predictive value of each feature-metric pair was then assessed using the area under curve [3] of the receiver operator characteristic (ROC) curve. Based on the ROC curve, a simple decision rule involving one metric can be derived for predicting LD outcome. To further improve the performance, we proposed an automated way to combine two such simple rules, in either an “AND” or an “OR” manner, to achieve a better performance.

Materials and Methods

Patient Characteristics

The present retrospective study involved 54 patients undergoing pre-shunt workup that included overnight ICP monitoring and 3-day lumbar drain while hospitalized at the UCLA Adult Hydrocephalus Center; all procedures and data collection were approved by the local IRB committee with patient consent. An intraparenchymal ICP microsensor (Codman and Schurtleff, Raynaud, MA, USA) was inserted into the right frontal lobe and monitoring started at least one night before the placement of the LD. Continuous waveform data including ECG and ICP was captured using the BedMaster system with a sampling rate of 240 Hz. Patients were assessed both pre-LD and post-LD before discharge from the hospital by

10-m walking test, and an NPH routine assessment that includes the Mini-Mental State Examination (MMSE). The LD outcome used in the present work was retrospectively collected as indicated from the clinical report of the follow-up visit after the LD procedure and predominantly focused on the improvement in gait. The average age and standard deviation of the 54 patients is 72.05 ± 9.63 years respectively, with a gender distribution of 35 males and 19 females. Among the patient cohort, 12 patients (7 male and 5 female) showed no improvement in gait following the procedure.

Brief Introduction of the MOCAIP Algorithm

The MOCAIP algorithm was reported in our previous publication [10] and has been used in several application studies that include predicting acute ICP elevation, continuously detecting cerebral hypoperfusion and recognizing ICP B-wave [11, 12]. MOCAIP is usually used to process a short segment of ICP and ECG recordings (if ECG is not available, pulse detection can still be done using a modified algorithm [13]). First, each individual pulse is delineated by using a previously published algorithm [10]. Then hierarchical clustering of pulses into different groups takes place based on the Euclidian distance after normalizing each pulse by removing the mean and dividing by the standard deviation. A dominant pulse is then extracted from this segment, which is the average of the largest cluster. This dominant pulse is checked against a reference ICP pulse library to determine the legitimacy of the pulse. Such a check is necessary because a whole segment of ICP recording could be artifacts and the signal is not recoverable. Six landmarks are determined for each dominant pulse, three peaks and three valleys. The determination of these landmarks starts from identifying the peak landmarks following any one of the methods presented in our previous publications [10, 14, 15]. In the present work, we used the original MOCAIP algorithm for this purpose. After identifying the peak landmarks, the corresponding valley points can be readily identified. Based on these six landmarks, we extract 128 MOCAIP metrics for each dominant pulse as illustrated in Table 1, where the labeling convention of each metric is also shown. In the present work, the length of each segment was chosen to be 30 s.

Feature Functions

Once the metrics for each dominant pulse have been computed an additional processing step is used to summarize each of the 128 MOCAIP metrics for one overnight ICP recording via five feature functions. For example, if a patient has 10 h of continuous ICP data there will be approximately

Table 1 One hundred and twenty-eight metrics derived from an ICP pulse based on the six landmarks identified on an ICP pulse

<i>28 basic metrics extracted from individual landmarks or over all characteristics</i>	
$dV_1, dV_2, dV_3, dP_1, dP_2, dP_3$	Amplitude of landmark relative to the minimum point prior to initial rise
$L_{V1P1}, L_{V1P2}, L_{V1P3}, L_{V2P2}, L_{V3P3}$	Time delay among landmarks
$CurV_{v1}, CurV_{v2}, CurV_{v3}, CurV_{p1}, CurV_{p2}, CurV_{p3}$	Absolute curvature of each landmark
$K1, K2, K3, RC1, RC2, RC3$	$K1, K2, K3$ are slope of each rising edge and $RC1, RC2, RC3$ are time constants of each descending edge
mICP, diasICP	Mean ICP and diastolic ICP
L_t	Time delay of V_1 to ECG QRS peak
mCurv	Mean absolute curvature of the pulse
WaveAmp	Maximum among $dP1 \sim dP3$
<i>100 extended metrics calculated as ratios among metrics within each group</i>	
dP_{p1p2}, \dots	Ratio among landmark amplitudes
$L_{V1P1}/L_{t1}, \dots$	Ratio among time delays
$Curv_{v1}/Curv_{v2}, \dots$	Ratio among curvatures
$K/RC_1, \dots$	Ratio among slopes/RCs

1,200 dominant pulses, for each dominant pulse there are 128 MOCAIP metrics, and each of the MOCAIP metrics can be summarized with the five feature functions (below). There is no prior knowledge with regard to the best way of summarizing an overnight ICP recording. Therefore, it is necessary to allow for an automated process to identify the best candidates. We have evaluated the following feature functions:

- *Average feature*: This feature function simply calculates the average of each individual metric across one overnight ICP recording.
- *Standard deviation feature*: This function calculates the standard deviation of each individual metric across one overnight ICP recording.
- *Percentage feature*: This function calculates the percentage of time when a metric is greater than a threshold. This threshold is determined by pooling data from all patients and then determined as the average of the corresponding MOCAIP metric.
- *Percentage of standard deviation feature*: This function calculates the percentage of time of the standard deviation of MOCAIP metrics greater than a threshold calculated from a 5-min ICP. The threshold was determined as the standard deviation of pooled MOCAIP metrics from all patients.
- *Range feature*: This function calculates the difference between the 95 percentile and the 5 percentile of each individual metric of an overnight ICP recording.

Optimal Single-Metric Rule

After applying a feature function, an overnight ICP recording is reduced to a vector of 128 metric-feature pairs. We next seek for a single-metric rule to predict LD outcome in

the following form: “if a metric-feature of an overnight recording is greater (or smaller) than a threshold, then LD outcome will be positive.” Note, rules published in several existing studies [6, 16] can be considered as specific instances of the above form. For each metric-feature, we generate a sequence of threshold values by pooling all the data. This sequence of threshold values can be used to generate two ROC curves for each metric-feature, one of which corresponds to the “greater than” situation and another of which corresponds to the “less than” situation. Then we retain the ROC that has an AUC greater than 0.5 and discard the other one for each metric. Next, for each feature the optimal metric is defined as the one with the greatest AUC. The impact of the optimal metric selection (as a function of the AUC) is explained in the results section.

Automated Combination of Two Rules

After finding the optimal metric feature for each feature function, one natural step further is to determine if one can combine two such rules to obtain a better performance (a combination of two of the five features described above). Considering the combination of two features (A and B) with the corresponding set of false-positive, true-positive, false-negative, and true-negative cases represented (from rule A) as FP_A, TP_A, FN_A , and TN_A respectively, the notation is analogous for rule B. Furthermore, we shall consider two possible combination operations: “AND” and “OR”.

If the “OR” operator is used for combination, then the resultant sets of false-positive, true-positive, false-negative, and true-negative are $FP_A \cup FP_B, TP_A \cup TP_B, FN_A \cap FN_B$, and $TN_A \cap TN_B$. On the other hand, if the “AND” operator is used for combination, then the corresponding sets are

$FP_A \cap FP_B$, $TP_A \cap TP_B$, $FN_A \cup FN_B$, and $TN_A \cup TN_B$. Based on this analysis, the accuracy of the combined predictive rules can be calculated for the OR operator as $\frac{1}{N}(|TP_A \cup TP_B| + |TN_A \cap TN_B|)$ where $|A|$ is used to denote

the number of cases included in the set A, and N represents the total number of patients. Similarly, the accuracy of the “AND” operator can be calculated as $\frac{1}{N}(|TP_A \cap TP_B| + |TN_A \cup TN_B|)$. Therefore, one can choose the combinations with the maximal accuracy.

Data Analysis Protocol

In this section, we summarize the data analysis protocol used in the present work to determine the best rule combination and its accuracy. The following steps were taken to analyze the 54 overnight ICP recordings:

1. Each recording is analyzed using the MOCAIP algorithm on consecutive 30-s segments.
2. Resultant MOCAIP results are then manually checked for any errors in recognizing legitimate dominant pulse and placement of the landmarks. This step is facilitated by using software developed in house.
3. Generate the threshold sequence for each metric that will be used to generate the ROC curve. The i -th value of the sequence of thresholds is calculated for each metric feature by the following equations: $(i-1) \times L$ where L is the mean plus the 10 standard deviation of the metric feature divided by the number of steps, which is 100 in the present work.
4. Each value of the threshold sequence is used to form two simple rules (“greater than” and “less than”), which are then used to assess the 54 cases. The corresponding false-positive rate (FPR) and true-positive rate (TPR) are obtained. After sweeping through the sequence, two ROC curves are obtained but only the one with AUC greater 0.5 is retained.
5. Determine the optimal metric feature. This is achieved by selecting one metric feature that has the largest AUC per each feature function evaluated. In other words, for each feature defined above, the metric (out of the 128 calculated by MOCAIP) with the greatest AUC is defined as the optimal metric feature (five total, one for each feature).
6. Determine the rule. For the optimal metric-feature, the “optimal” point on the ROC curve is selected as the operating point, which gives a false-positive rate less than 0.35.
7. Then the accuracy of 10 (combining two features with a total of five features $2 \times 5 = 10$) pairs of AND combination of the five optimal metric feature rules and those of the OR combination are calculated.
8. The best rule combination is then determined as the one with the greatest accuracy.

Results

Panel f of Fig. 1 displays the ROC curves of each of the 128 metric features (average feature function is used here as an example). The ROC curve shown in bold represents the metric with the greatest AUC; which was selected as the optimal metric-feature for rule construction. The ROC curves of the optimal metric pair corresponding to each of the five feature functions (a: average feature function; b: standard deviation feature function; c: percentage of average feature function; d: Percentage of 5-min standard deviation feature function; e: inter 5–95 percentile feature function) are shown in Panels a–e of Fig. 1 where the selected MOCAIP metric is also spelled out. On each curve, the operating point is circled, which corresponds to the particular threshold value selected for rule construction.

Figure 2 demonstrates the impact of the optimal metric selection; for each of the combination rules (“AND” and “OR”) the accuracy is plotted as a function of the rank of the AUC. The decreasing trend of the accuracy for both “AND” and “OR” combination is clearly present. In summary, the individual metric feature rules found in the present work are:

1. If standard deviation of $RL_{v2p2}L_{p1p2}$ of overnight ICP recording is >0.0547 , then the patient will respond to LD.
2. If the average $RCurv_{p3}Curv_{v2}$ of the overnight ICP recording is >0.9808 , then the patient will respond to LD.
3. If the percentage of RC_1 of the overnight ICP recording greater than 8.76 is $<41.48\%$, then the patient will respond to LD.
4. If the percentage of 5-min segments of ICP with a standard deviation of RRC_3k_2 greater than 57.68 is $>0.49\%$, then the patient will respond to LD.
5. If the inter 95–5 quartile range of $RCurv_{p2}Curv_{p3}$ of the overnight ICP recording is <64.25 , then the patient will respond to LD.

The accuracy for the corresponding features is: 70.4%, 72.2%, 74.1%, 72.2%, and 79.6% respectively. Finally, the OR combination of rules 4 and 5 achieves the best accuracy of 88.9%.

Discussion

We have demonstrated a systemic way of deriving a two-rule combination of simple decision rules from overnight ICP recording to predict the corresponding outcome of a 3-day lumbar drain for patients with the NPH clinical triad undergoing pre-shunt evaluation. Using a cohort of 54 patients, we were able to find an optimal two-rule combination that reaches an accuracy of 88.9%. This rule can be explained in plain English in such a way that it can be readily communicated to

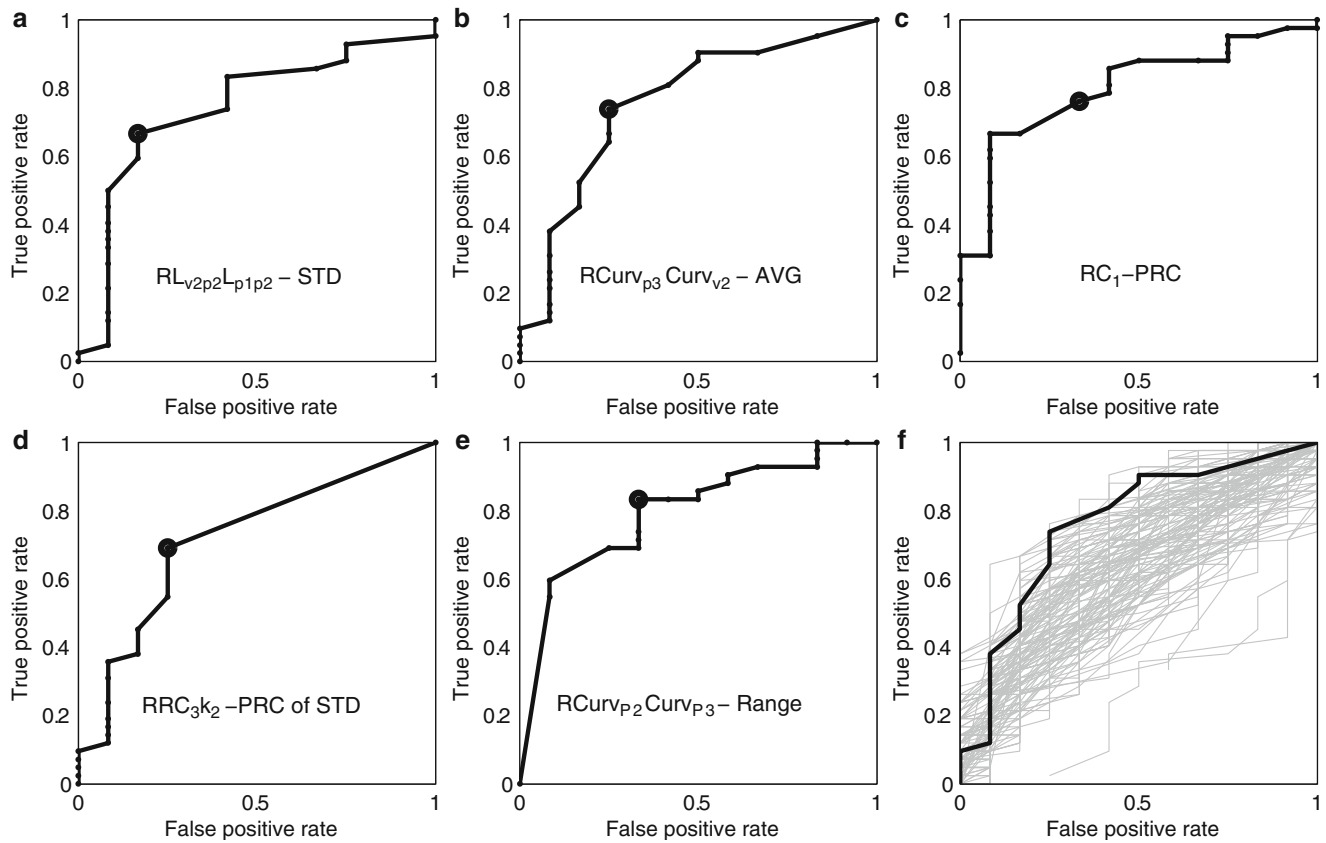


Fig. 1 Receiver operating characteristic (ROC) curves. Panels (a–e) display the ROC of the optimal metric feature for each of the five individual feature functions. (a): Average feature function; (b): Standard deviation feature function; (c): Percentage feature function; (d): Percentage of standard deviation feature function; (e): Range feature function. (f) ROC curves for the 128 metric features using the average feature as an example where the bolder curve corresponds to that of the optimal metric feature

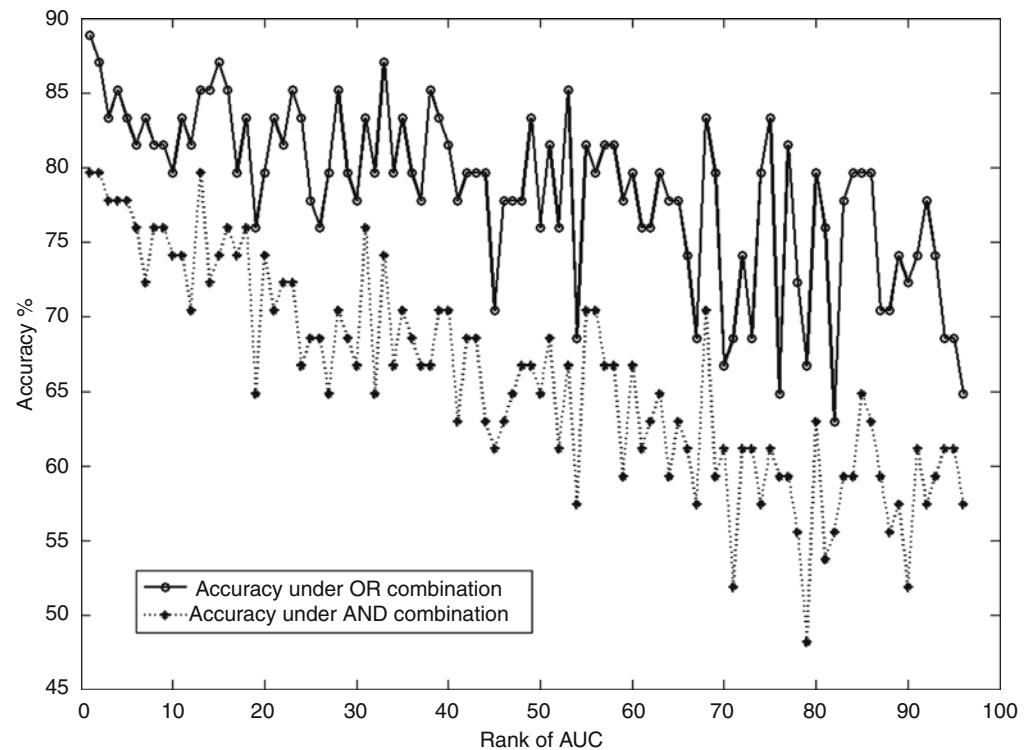


Fig. 2 Accuracy of the combined rules as a function of the rank of area under the curve (*AUC*) of the selected metric feature as the single metric constituents for rule combination. A clear deterioration of the accuracy as metric pairs with smaller *AUC* are selected for rule combination, demonstrating the optimality of choosing the one with the maximal *AUC*

non-technical clinicians and patients. Although further validation with a large patient cohort is needed, technically, the rules found in the present work, in combination with an automated analysis of overnight ICP using the existing MOCAIP algorithm, can readily be built into a decision support system of NPH diagnosis and evaluation that has the potential to reduce the time and cost associated with the existing 3-day lumbar drain procedure.

A systematic way of discovering predictive rules is needed if a large number of ICP pulse morphological metrics are involved to construct rules. Compared with the existing studies that focus on either mean ICP or ICP pulse amplitude, the increased number of ICP metrics demands an objective way of discovering rules to guarantee optimality and avoid bias. Indeed, the five individual optimal metrics found in the present work do not include either mean ICP or ICP wave amplitude, demonstrating the potential power of adopting a more comprehensive ICP pulse morphology characterization.

The proposed rule discovery framework can be easily extended in several aspects. We have proposed five simple feature functions to summarize an overnight ICP recording. More complex feature function can certainly be implemented in future work. In particular, we believe that feature functions characterizing the relationship among MOCAIP metrics could potentially offer better predictive power compared with the single-metric feature functions used here. Furthermore, we have only studied the combination of two rules; we could readily derive the equations to calculate the accuracy of combining multiple rules and check if the predictive accuracy can be further improved.

Conclusion

One fundamental limitation of the present work is the lack of cases to conduct independent evaluation of the rules discovered. It therefore remains to be demonstrated whether the same level of predictive accuracy can be retained when applying the rules discovered using our dataset to process data from other centers and how the data from multi-centers can be utilized to refine the rules. The present work has clearly demonstrated the technical feasibility of such future studies and hopefully more precise and robust predictive rules can be discovered through multi-center collaboration and the adoption of advanced ICP signal analysis and data mining methods.

Conflict of interest statement A PCT application was filed by UCLA for the pulse morphology analysis algorithm used in this work. The present work is partially supported by NINDS grants NS059797, NS054881, and NS066008.

References

1. Governale LS et al (2008) Techniques and complications of external lumbar drainage for normal pressure hydrocephalus. *Neurosurgery* 63(4 Suppl 2):379–384; discussion 384
2. Walchenbach R et al (2002) The value of temporary external lumbar CSF drainage in predicting the outcome of shunting on normal pressure hydrocephalus. *J Neurol Neurosurg Psychiatry* 72(4): 503–506
3. Marmarou A et al (2005) Diagnosis and management of idiopathic normal-pressure hydrocephalus: a prospective study in 151 patients. *J Neurosurg* 102(6):987–997
4. Marmarou A et al (2005) The value of supplemental prognostic tests for the preoperative assessment of idiopathic normal-pressure hydrocephalus. *Neurosurgery* 57(3 Suppl):S17–S28; discussion ii–v
5. Raftopoulos C et al (1992) Morphological quantitative analysis of intracranial pressure waves in normal pressure hydrocephalus. *Neurol Res* 14(5):389–396
6. Eide PK, Sorteberg W (2010) Diagnostic intracranial pressure monitoring and surgical management in idiopathic normal pressure hydrocephalus: a 6-year review of 214 patients. *Neurosurgery* 66(1):80–91
7. Stephensen H et al (2005) Objective B wave analysis in 55 patients with non-communicating and communicating hydrocephalus. *J Neurol Neurosurg Psychiatry* 76(7):965–970
8. Woodworth GF et al (2009) Cerebrospinal fluid drainage and dynamics in the diagnosis of normal pressure hydrocephalus. *Neurosurgery* 64(5):919–925; discussion 925–926
9. Eide PK (2006) A new method for processing of continuous intracranial pressure signals. *Med Eng Phys* 28(6):579–587
10. Hu X et al (2009) Morphological clustering and analysis of continuous intracranial pressure. *IEEE Trans Biomed Eng* 56(3):696–705
11. Hu X et al (2010) Intracranial pressure pulse morphological features improved detection of decreased cerebral blood flow. *Physiol Meas* 31:679–695
12. Kasprócz M et al (2010) Pattern recognition of overnight intracranial pressure slow waves using morphological features of intracranial pressure pulse. *J Neurosci Methods* 190(2):310–318
13. Zong W, Mark R (2003) An open-source algorithm to detect onset of arterial blood pressure pulses. *Comput Cardiol* 30:259–262
14. Scalzo F et al (2009) Regression analysis for peak designation in pulsatile pressure signals. *Med Biol Eng Comput* 47(9):967–977
15. Scalzo F et al (2008) Random subwindows for robust peak recognition in intracranial pressure signals. *Lect Notes Comput Sci* 5358:370–380
16. Eide PK, Brean A (2010) Cerebrospinal fluid pulse pressure amplitude during lumbar infusion in idiopathic normal pressure hydrocephalus can predict response to shunting. *Cerebrospinal Fluid Res* 7:5

Lack of Correlation of Overnight Monitoring Data and Lumbar Infusion Data in iNPH Patients

Andreas Speil, Jordana C. Sosa, Bernd E. Will, and Martin U. Schuhmann

Abstract Objective: Hydrodynamic theories of idiopathic normal pressure hydrocephalus (iNPH) favor a decrease in compliance as an important underlying principle of the disease's immanent pathophysiology. ICP overnight monitoring (ONM) and lumbar infusion study (LIS) are both established methods that aid as supplemental tests in the selection of shunt-responsive patients. Pulse wave amplitude (AMP) and RAP index are measures derived from ONM and are related to intracranial compliance. Elastance (E) and pressure volume index (PVI), parameters derived from LIS, also describe the compliance of the system. We investigated whether the parameters of the two methods correlate with each other.

Methods: Thirty-three patients with probable/possible NPH underwent ICP overnight monitoring and a lumbar infusion study in supine position with ICP recorded from the intracranial compartment.

Results: E and PVI from the lumbar infusion study did not correlate at all with RAP or AMP from ICP monitoring. A qualitative change of the RAP and E pointing towards the same direction of either increased or decreased compliance, however, was found in 60.6% of our patients.

Conclusion: Although data from the infusion test and from overnight monitoring of ICP describe the underlying pathophysiology in at least 60% of patients qualitatively in the same way; there is no direct correlation of parameters. This indicates that the underlying mechanisms of RAP are different from those in principle or in reaction time that are responsible for E .

Objective

Idiopathic normal pressure hydrocephalus (iNPH) is a neurological disorder that can result in severe disability and shows clinical symptoms belonging to Hakim's triad with progressive gait disturbance, memory problems and urinary incontinence [1]. In imaging the patients show ventricular dilatation, but most often normal ICP values are recorded if invasive pressure monitoring is performed [2]. Modern hydrodynamic theories of iNPH favor a decrease in compliance and impairment of cerebrospinal reserve capacity as an important underlying principle of the evolving pathophysiology [3]. For the final establishment of diagnosis and to distinguish iNPH easier from other neurological diseases like Alzheimer's dementia or Binswanger's disease, supplemental investigations are recommended to allow for a better clinical judgement in the identification of possible shunt responders.

Currently, computerized ICP overnight monitoring (ONM), which is a monitoring approach, and constant rate lumbar infusion study (LIS), which is a test, are both established methods of selecting patients with shunt-responsive NPH [4].

The pulse wave amplitude (AMP) and the RAP index, describing the cerebrospinal reserve capacity, are both derived from ONM as mean values of 6–8 h of monitoring and are related in their magnitude to intracranial compliance. RAP is the correlation coefficient between mean ICP and associated changes in pulse wave amplitude of ICP [5]. Elastance E and the pressure volume index PVI are derived from a 30- to 45-min lumbar infusion study, and are as well related to the compliance of the cerebrospinal fluid system [6, 7].

The objective of this article is to investigate whether the parameters RAP and AMP taken from the monitoring of overnight ICP correlate with parameters E and PVI taken from the lumbar infusion test, applied to the lumbar spinal compartment following the day after overnight ICP monitoring.

A. Speil, J.C. Sosa, and B.E. Will
Department of Neurosurgery, Eberhard Karls University Tübingen,
Tübingen, Germany

M.U. Schuhmann (✉)
Department of Neurosurgery, Eberhard Karls University Tübingen,
Tübingen, Germany

Klinik für Neurochirurgie, Universitätsklinik Tübingen,
Hoppe Seyler-Strasse 3, Tübingen D-72076, Germany
e-mail: martin.schuhmann@med.uni-tuebingen.de

Patients and Methods

Computerized overnight monitoring of ICP and lumbar infusion studies are conducted as part of routine clinical practice in our institution. All studies were performed between 2008 and 2010 at the Department of Neurosurgery, University Hospital of Tübingen, Germany.

We identified 33 patients with probable/possible NPH according to the criteria published in the iNPH guidelines [8]. The median age was 76 years (range 59–83 years). The male to female ratio was nearly 1:1. Patients were assessed with a standardized clinical protocol including the modified Kiefer grading scale and the Rankin scale and underwent standardized clinical testing for gait and visio-motor ability (peg board test).

An intra-parenchymal ICP transducer (Neurovent, Raumedic AG, Helmbrechts, Germany) was implanted in the frontal lobe of the non-dominant hemisphere using a strict aseptic technique. ICP data were sampled at 30 Hz using ICM+ software (Cambridge University Enterprise, Cambridge, UK). Data were recorded for the whole night and data from at least 7 h (11 pm to 6 am) when the patient was asleep were analyzed.

The first harmonic from the pulse wave amplitude following Fourier transformation (AMP) is calculated by the software as a robust measure of ICP pulse amplitude, which is expected to be higher the lower compliance is.

The RAP index (correlation coefficient [R] between the pulse amplitude [A] and the mean intracranial pressure [P]) is derived by linear correlation between 40 consecutive, time-averaged data points of AMP and mean ICP, acquired within a 6-s time-window. It describes the degree of correlation between AMP and mean ICP over the last 4 min. An $RAP > 0.6$ indicates a low compensatory reserve or low compliance.

Following overnight ICP monitoring a lumbar infusion test was performed to test CSF dynamics using a lumbar drainage catheter that was connected to an infusion pump containing Ringer's solution with the patient in a supine position. A strict aseptic technique was used to keep the prefilled tubing sterile. After 10 min of baseline measurement of ICP from the intracranial compartment, the lumbar infusion of Ringer's solution was started at a rate of 1.5 mL/min and continued until a steady-state ICP plateau was achieved. E and PVI were calculated from the pressure response in relation to infusion time and infused volume by ICM+ software.

The elastance coefficient E characterizes the ability of the cerebrospinal system to store an extra volume amount [9, 10]. Smaller E indicates that more volume may be stored under the same pressure conditions. We have used a elastance threshold of $>0.15 \text{ mL}^{-1}$ to describe an abnormally low ability to compensate for additional volume. All statistical analyses were performed using PRISM software (GraphPad Software, Inc.).

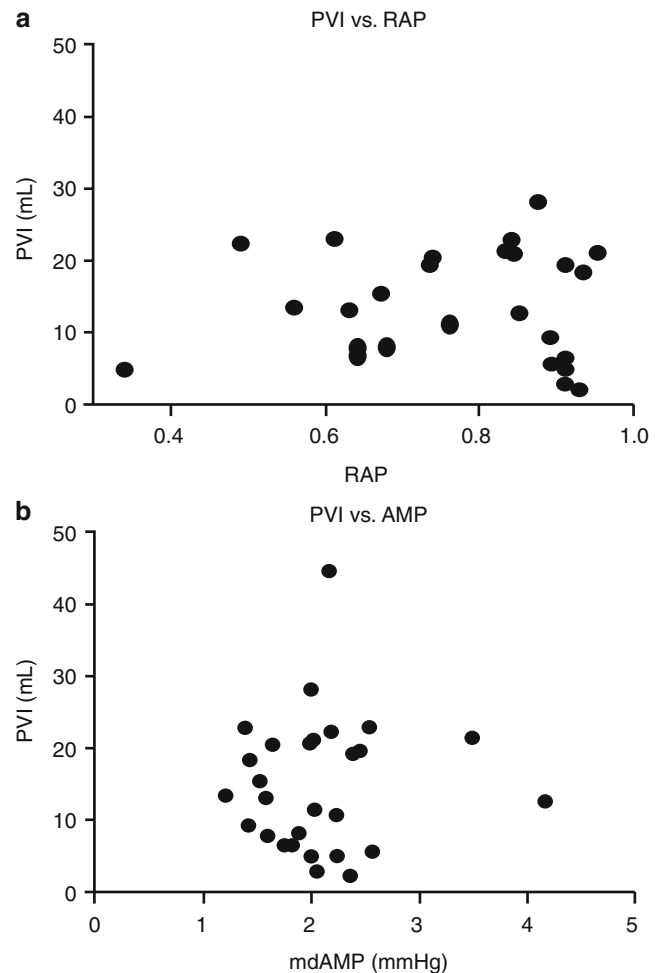


Fig. 1 (a) Scatterplot illustrating the absence of correlation between pressure volume index (PVI; mL) and median correlation coefficient between the pulse amplitude and the mean intracranial pressure (RAP) and (b) PVI (mL) and median amplitude (AMP; mmHg)

Results

Elastance and PVI from the lumbar infusion study did not correlate at all with RAP or AMP from ICP monitoring. PVI showed no correlation with median RAP ($R=0.14$; $P=0.48$) and median AMP ($R=0.037$; $P=0.85$) as shown in Fig. 1. There was also no correlation between E and the median RAP index ($R=-0.72$; $P=0.52$) and median AMP ($R=0.04$; $P=0.84$), as shown in Fig. 2. A qualitative change in the parameters RAP (threshold >0.6) and elastance (threshold $>0.15 \text{ mL}^{-1}$) pointing towards the same direction, was found in 60.6% of our patients (Table 1).

Discussion

The RAP and AMP were derived from a whole night of monitoring as median values. The median RAP from a whole

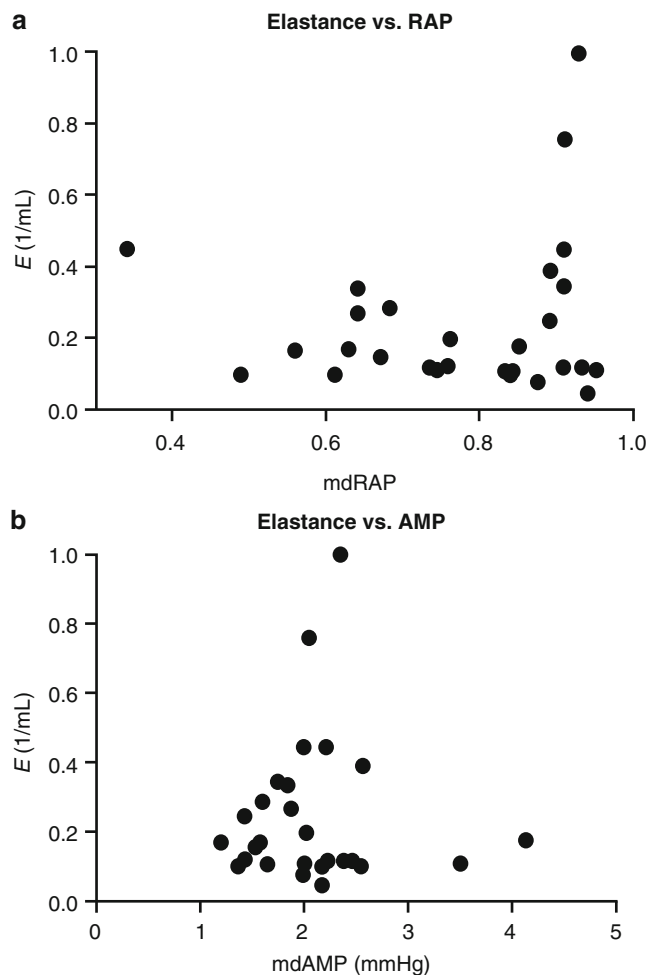


Fig. 2 (a) Scatterplot illustrating the absence of correlation between elastance (1/mL) and median RAP and (b) elastance (1/mL) and median AMP (mmHg)

night is a good measure for assessing the compensatory reserve capacity of the intracranial space during resting conditions at sleep. Derived from ICP as a global measure and depending on the associated ICP amplitude, baseline RAP reflects all components that define the slope of the pressure volume curve of total intracranial compliance at rest. A high baseline RAP despite low or normal ICP values, as it is often found in iNPH patients, therefore indicates, that despite normal ICP levels the total reserve capacity is low and small changes in ICP are directly reflected in synchronous changes in AMP. During vasogenic B-waves associated with the REM phases of sleep, RAP will increase, independently of its baseline level, as an expression of the additional volume load generated by the vasogenic increase in cerebral blood volume.

The infusion study, in contrast to the ONM, is a 45-min test, recording in our case the intracranial pressure response to a lumbar infusion of mock CSF in supine position in an awake patient. Elastance and PVI are dependent on the time necessary to reach a new pressure plateau and are ICP-independent. E is describing the hypothetical compliance

Table 1 Distribution of patients according to RAP and E

	$E > 0.15$ (1/mL)	$E < 0.15$ (1/mL)
RAP index > 0.6	$n = 16$ 48.5%	$n = 12$ 36.4%
RAP index < 0.6	$n = 1$ 3%	$n = 4$ 12.1%

of the intracranial and lumbar CSF space. In this work an elastance threshold of $> 0.15 \text{ mL}^{-1}$ has been used, values above were regarded as elevated. According to the Monroe–Kelly doctrine, the volume of the cerebrospinal system remains constant [11]. An increase in the amount of CSF caused by the infusion study should result in a displacement of blood, primarily from the venous pool. Thus, E might not describe the elasticity of the brain tissue in the first place, but rather the ability to shift blood from the intra- to the extra-cranial compartment. This indicates that the underlying mechanisms of RAP (resulting in a positive correlation of changes in ICP pulse wave amplitude with changes in ICP) are different from those in principle or in reaction time that are responsible for elastance (speed of ICP increase in response to an infused lumbar volume load). RAP might be influenced primarily by the total intracranial pressure/volume relationship, including not only the venous blood pool, but brain tissue properties and the volume of the intra- and extraventricular CSF compartment, whereas elastance might primarily reflect the amount of acutely displaceable venous blood in response to a CSF volume addition.

Conclusion

Lumbar infusion study and long-term ICP overnight monitoring are investigations that describe the underlying pathophysiology qualitatively in the same way in many patients. With the chosen thresholds this was the case in 60% of patients. The second largest group consisted of those with an increase in RAP, but an E value below 0.15. There is no direct correlation of parameters and the overall compliance of the system, reflected by RAP, and the venous reserve volume (amount of acutely displaceable blood), reflected in E /PVI, are two contributing components.

Since the parameters do not correlate, neither investigation is able to replace the other. We therefore recommend combining the two approaches in a complementary fashion to hopefully increase the accuracy of identification of true iNPH, which shows a clinically beneficial response to shunt placement.

Conflict of interest statement We declare that we have no conflict of interest.

References

1. Bekaert O, Grandjaques B, Hodel J, Nseir R, Decq P (2010) Gait disturbance and normal pressure hydrocephalus. *Rev Neurol* 166:229–234
2. Adams RD, Fisher CM, Hakim S, Ojemann RG, Sweet WH (1965) Symptomatic occult hydrocephalus with “normal” cerebrospinal-fluid pressure. A treatable syndrome. *N Engl J Med* 273:117–126
3. Czosnyka M, Whitehouse H, Smielewski P, Simac S, Pickard JD (1996) Testing of cerebrospinal compensatory reserve in shunted and non-shunted patients: a guide to interpretation based on an observational study. *J Neurol Neurosurg Psychiatry* 60:549–558
4. Brean A, Eide PK (2008) Assessment of idiopathic normal pressure patients in neurological practise: the role of lumbar infusion testing for referral of patients to neurosurgery. *Eur J Neurol* 15:605–612
5. Balesteri M, Czosnyka M, Steiner LA, Schmidt E, Smielewski P, Matta B, Pickard JD (2004) Intracranial hypertension: what additional information can be derived from ICP waveform after head injury? *Acta Neurochir (Wien)* 146:131–141
6. Kim DJ, Czosnyka Z, Keong N, Radolovich DK, Smielewski P, Sutcliffe MP, Pickard JD, Czosnyka M (2009) Index of cerebrospinal compensatory reserve in hydrocephalus. *Neurosurgery* 64:494–501
7. Czosnyka M, Czosnyka Z, Momjian S, Pickard JD (2004) Cerebrospinal fluid dynamics. *Physiol Meas* 25:R51–R76
8. Marmarou A, Black P, Bergsneider M, Klinge P, Relkin N (2005) Guidelines for management of idiopathic normal pressure hydrocephalus: progress to data. *Acta Neurochir Suppl* 95:237–240
9. Christensen L, Borgesen SE (1989) Single pulse pressure wave analysis by fast Fourier transformation. *Neurol Res* 11:197–200
10. Czosnyka Z, Czosnyka M, Owler B, Momjian S, Kaspruwicz M, Schmidt EA, Smielewski P, Pickard JD (2005) Clinical testing of CSF circulation in hydrocephalus. *Acta Neurochir Suppl* 95:247–251
11. Czosnyka M, Pickard JD (2004) Monitoring and interpretation of intracranial pressure. *J Neurol Neurosurg Psychiatry* 75:813–821

Shunt-Dependent Hydrocephalus Following Subarachnoid Hemorrhage Correlates with Increased S100B Levels in Cerebrospinal Fluid and Serum

S. Brandner, Y. Xu, C. Schmidt, Irene Emtmann, Michael Buchfelder, and Andrea Kleindienst

Abstract Posthemorrhagic hydrocephalus requiring permanent ventriculoperitoneal shunt placement is a major complication of aneurysmal subarachnoid hemorrhage (SAH). High S100B serum and cerebrospinal fluid (CSF) levels are considered to reflect the severity of brain injury. We prospectively assessed whether S100B levels in serum and CSF were predictive parameters for permanent shunt requirement following aneurysmal SAH. In patients suffering from aneurysmal SAH and treated with an external ventricular drain (EVD), S100B levels in serum and CSF were measured daily as long as the EVD was in place. S100B levels of patients who passed their EVD challenge were compared with those patients who required a permanent ventriculoperitoneal shunt placement. Out of 68 patients included in the study, 43 patients (63.2%) passed the EVD challenge and in 25 patients (36.8%) permanent ventriculoperitoneal shunting was performed. Group comparison revealed that in patients who required shunt placement, S100B was significantly higher in CSF ($p < 0.05$ at days 2, 4, 6, 10; $p < 0.005$ at days 1, 3, 5, 7, 8, 9) and serum ($p < 0.05$ at days 4–7) compared with patients who could be weaned from the EVD. Assessment of S100B levels in CSF and serum may be useful as a predictive parameter for shunt dependency in patients with posthemorrhagic hydrocephalus following aneurysmal SAH.

Keywords Hydrocephalus • Ventriculoperitoneal shunt • Aneurysmal subarachnoid hemorrhage • External ventricular drain

Introduction

Hydrocephalus is a common sequela of aneurysmal subarachnoid hemorrhage (SAH). Development of hydrocephalus may occur due to obstructive adhesions caused by blood products

within the ventricular system or may result from impaired resorption through arachnoid granulations appearing as malresorptive hydrocephalus [4, 7, 10]. The acute treatment of hydrocephalus consists of placement of an external ventricular drain (EVD). However, a considerable percentage of SAH patients develop chronic hydrocephalus resulting in permanent ventriculoperitoneal (VP) shunt requirement. Permanent shunt rate has been reported to range from 8 to 50% [2, 3, 19].

Clinical and radiological factors such as age, Hunt and Hess grade, Fisher score, cerebrospinal fluid (CSF) drainage duration or CSF drainage modality have been analyzed for a potential role as predictive factors for shunt dependency, but their benefit still remains controversial [3, 5, 6, 13, 14, 17, 19]. Usually, patients with posthemorrhagic hydrocephalus undergo a weaning trial from the EVD. This empirical challenge may require a prolonged hospital stay and might subject patients to additional risks. On the other hand, VP shunt placement may contribute to additional morbidity by shunt failure or infection, putting VP shunt placement under dispute [3, 4, 14]. Identifying predictive factors for the risk of shunt-dependent hydrocephalus after SAH is therefore very important in assisting in clinical decision-making with regard to strategies for weaning from the EVD. The neurotrophic S100B protein has been proposed as a biomarker predicting the severity of brain injury. A positive correlation between S100B in serum and CSF and impaired neurological function following traumatic brain injury (TBI), intracerebral hemorrhage and SAH has been reported [1, 9, 11, 12, 15, 16, 18]. The goal of this study was to assess whether S100B levels in serum and CSF are useful as predictive parameters for permanent shunt requirement following aneurysmal SAH.

Materials and Methods

Patient Population

Between January 2008 and December 2009, 68 consecutive patients with aneurysmal SAH were treated at our hospital using an external ventricular drain for posthemorrhagic

S. Brandner (✉), Y. Xu, C. Schmidt, I. Emtmann, M. Buchfelder, and A. Kleindienst
Department of Neurosurgery, Friedrich-Alexander-University
Erlangen-Nuremberg, Schwabachanlage 6, D-91054 Erlangen, Germany
e-mail: sebastian.brandner@uk-erlangen.de

hydrocephalus and survived for at least 6 months afterward. SAH patients without angiographically proven aneurysms, patients who did not receive an EVD, and patients who died within 6 months of admission were excluded. Patient demographic data and Hunt and Hess grade on admission were recorded.

Sample Collection and Processing

Blood and CSF samples were collected daily at 8 AM for up to 10 days after SAH. For all blood draws, 4 mL of venous blood were drawn into serum separator tubes and centrifuged at 3,000 rpm for 10 min at room temperature. The cellular components were discarded and the serum was stored at -80°C until used for assays. CSF was collected at the time of blood draws. For each CSF sample, 5–10 mL were collected into a 15-mL polypropylene tube, immediately placed on ice and centrifuged at 3,000 rpm for 10 min at room temperature.

The cellular components were discarded and the remaining sample was stored at -80°C until used for assays. Serum and CSF S100B concentrations were measured with the Cobas e411[®] electrochemiluminescence assay (Roche Diagnostics, lower detection limit 0.005 $\mu\text{g/L}$).

Protocol for EVD Treatment and VP Shunt Placement

All patients underwent cranial CT upon arrival at our hospital. Patients with evidence of hydrocephalus received immediate placement of an EVD. The EVD was kept open at 15 cm above the external auditory canal. If symptoms of hydrocephalus failed to improve clinically or dilation of the ventricular system persisted in control CT, CSF was drained at a lower pressure level. If there was no clinical evidence of hydrocephalus, CSF was gradually drained at higher levels up to 25 cm above the external auditory canal. The minimal EVD time after SAH was 10 days. A weaning trial from the EVD was initiated when there was no clinical or radiological evidence of hydrocephalus and the CSF cell count was below 10,000/mL. The EVD was clamped after a baseline cranial CT. Intracranial pressure and neurological status were monitored for 72 h. After this clamped EVD challenge, a control CT was performed. Weaning from EVD was considered unsuccessful if patients had any neurological decline that could be relieved by unclamping the EVD, intracranial pressure exceeded 20 cm H_2O for at least 10 min, or if control CT revealed an increased ventricular size. In this case, patients received a VP shunt. In patients who could be successfully weaned from the EVD, the EVD was removed.

Table 1 Clinical classification of SAH patients

	EVD challenge	
	Passed	Failed
Patients	43	25
Mean age (years)	52.5	50.8
Sex		
Male	14 (33%)	8 (32%)
Female	29 (67%)	17 (68%)
H&H grade		
1	12	0
2	15	3
3	10	13
4	6	6
5	0	3
Mean H&H grade	2.23	3.36

Note: 46 SAH patients who received an EVD due to hydrocephalus were classified into two groups. The first group of patients could be successfully weaned from their EVD. The second group of patients received permanent shunt placement because of chronic hydrocephalus. Clinical characteristics of the patients are presented

Statistical Analysis

Patients were stratified according to successful weaning from EVD or VP shunt placement.

Statistical analysis was performed using the Mann–Whitney *U* test for independent samples (SPSS software, version 18.0), and statistical significance was accepted as being $p < 0.05$. All values are given as mean \pm SEM.

Results

Of 68 SAH patients, 46 were female and 22 were male. Forty-three patients (63.2%) passed their EVD challenge and were successfully weaned from the EVD (Table 1). Twenty-five patients (36.8%) could not be weaned from the EVD and received a VP shunt. The mean Hunt and Hess grade in the group that successfully passed the EVD challenge was 2.2, whereas in the group that failed the EVD challenge, the H&H grade was 3.4. The mean age of the patients in the “passed” group was 52.5 years. The mean age of the “failed” group patients was 50.8 years. Mean CSF S100B levels were increased in all patients after SAH (normal CSF S100B level $< 2.5 \mu\text{g/L}$). Maximum S100B levels were found in the “failed” group on the second day after SAH. In the “passed” group, maximum CSF S100B levels were reached on day 6 after SAH. CSF S100B levels were much higher in the shunt-dependent group, especially for the first 5 days after SAH, compared with the group of patients who were successfully

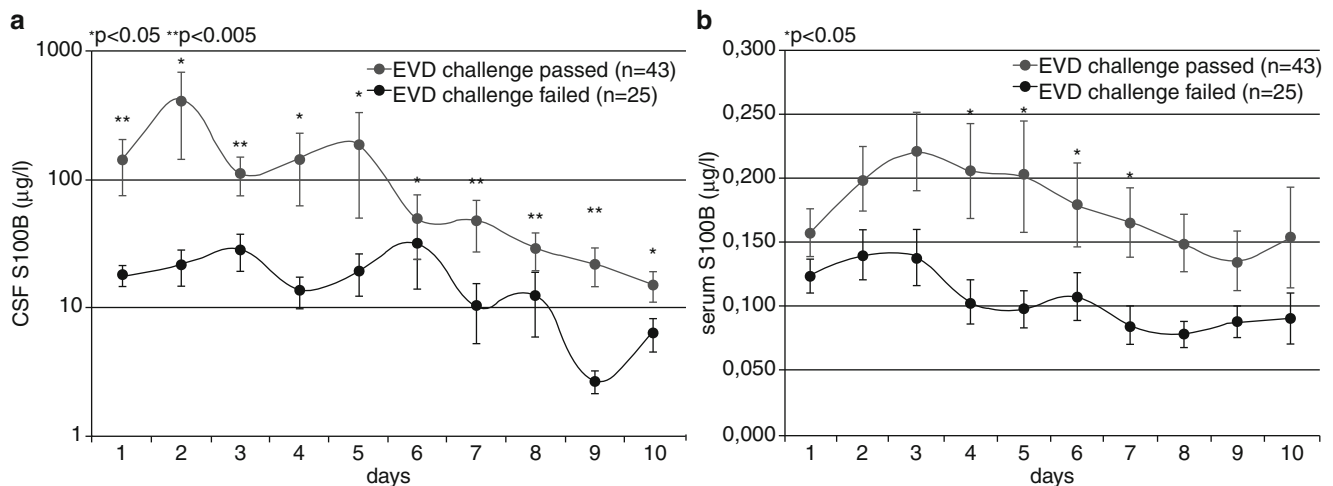


Fig. 1 Course of S100B concentrations in cerebrospinal fluid (CSF) (**a**) and serum (**b**) for 10 days after subarachnoid hemorrhage (SAH). Lower curve: mean S100B levels of patients who were successfully

weaned from their extraventricular drain (EVD). Upper curve: mean S100B levels of patients who did not pass their EVD challenge and received permanent shunt placement

weaned from their EVD (Fig. 1a). However, significantly higher S100B levels persisted in the shunt-dependent patients for the entire period of 10 days after SAH. Similar to the CSF S100B levels, mean serum S100B levels were increased in all patients for the first few days after SAH. We found significantly higher serum S100B concentrations in the “failed” group during days 4–7 after SAH. However, in patients who were successfully weaned from the EVD serum S100B concentrations returned to normal by day 7 after SAH ($<0.11 \mu\text{g/L}$), whereas serum S100B levels of shunt-dependent patients remained elevated for the entire period of 10 days (Fig. 1b).

Discussion

Weaning from an EVD after SAH is a challenging clinical process. Usually, empirical procedures are used for this purpose. As the weaning process implicates additional risks for patients, with a prolonged stay in the intensive care unit, the capability to predict permanent shunt requirement is of high importance [3, 14]. The objective of our study was to investigate if S100B levels in CSF and serum after SAH correlate with permanent shunt requirement due to chronic hydrocephalus. The prevalence of shunt-dependent patients of 36.8% in our study is within the range reported for permanent shunt requirement after SAH [2, 3, 19]. In accordance with others, patients requiring a permanent shunt presented with a higher Hunt and Hess grade [3, 5, 6, 17, 19]. Contrary to previous studies, we could not confirm age or sex to correlate with shunt dependency after SAH [4, 13, 14]. We found significantly increased CSF and serum S100B levels during the first 10 days after SAH in hydrocephalus patients

requiring a permanent shunt placement compared with patients who could be successfully weaned from their EVD.

Possible pathomechanisms underlying these findings remain to be elucidated. Increased CSF and serum S100B levels have been reported to reflect brain damage in many neurological disorders [1, 8, 12, 16]. In SAH patients, CSF S100B concentrations during the first 2 weeks after SAH were reported to be related to the functional outcome and to radiological signs of brain damage [8, 15, 18]. It can be speculated that the more the brain is injured, the more protein breakdown products might interfere with CSF reabsorption at the arachnoid granulations.

Based on our results, we conclude that high CSF and serum S100B levels indicate a high probability of permanent shunt requirement. Hence, measurement of CSF S100B levels after SAH may assist as an additional molecular marker in clinical decision-making with regard to permanent shunt placement.

Conflict of interest statement We declare that we have no conflict of interest.

References

1. Bloomfield SM, McKinney J, Smith L, Brisman J (2007) Reliability of S100B in predicting severity of central nervous system injury. *Neurocrit Care* 6:121–138
2. Bogdahn U, Lau W, Hassel W, Gunreben G, Mertens HG, Brawanski A (1992) Continuous-pressure controlled, external ventricular drainage for treatment of acute hydrocephalus—evaluation of risk factors. *Neurosurgery* 31:898–903, discussion 903–894
3. Chan M, Alaraj A, Calderon M, Herrera SR, Gao W, Ruland S, Roitberg BZ (2009) Prediction of ventriculoperitoneal shunt dependency in patients with aneurysmal subarachnoid hemorrhage. *J Neurosurg* 110:44–49

4. De Oliveira JG, Beck J, Setzer M, Gerlach R, Vatter H, Seifert V, Raabe A (2008) Risk of shunt-dependent hydrocephalus after occlusion of ruptured intracranial aneurysms by surgical clipping or endovascular coiling: a single-institution series and meta-analysis. *Neurosurgery* 15:15
5. Dehdashti AR, Rilliet B, Rufenacht DA, de Tribolet N (2004) Shunt-dependent hydrocephalus after rupture of intracranial aneurysms: a prospective study of the influence of treatment modality. *J Neurosurg* 101:402–407
6. Dorai Z, Hynan LS, Kopitnik TA, Samson D (2003) Factors related to hydrocephalus after aneurysmal subarachnoid hemorrhage. *Neurosurgery* 52:763–769, discussion 769–771
7. Ellington E, Margolis G (1969) Block of arachnoid villus by subarachnoid hemorrhage. *J Neurosurg* 30:651–657
8. Hardemark HG, Almqvist O, Johansson T, Pahlman S, Persson L (1989) S-100 protein in cerebrospinal fluid after aneurysmal subarachnoid haemorrhage: relation to functional outcome, late CT and SPECT changes, and signs of higher cortical dysfunction. *Acta Neurochir (Wien)* 99:135–144
9. Hayakata T, Shiozaki T, Tasaki O, Ikegawa H, Inoue Y, Toshiyuki F, Hosotubo H, Kieko F, Yamashita T, Tanaka H, Shimazu T, Sugimoto H (2004) Changes in CSF S100B and cytokine concentrations in early-phase severe traumatic brain injury. *Shock* 22:102–107
10. Kibler RF, Couch RS, Crompton MR (1961) Hydrocephalus in the adult following spontaneous subarachnoid haemorrhage. *Brain* 84:45–61
11. Kleindienst A, Ross Bullock M (2006) A critical analysis of the role of the neurotrophic protein S100B in acute brain injury. *J Neurotrauma* 23:1185–1200
12. Kleindienst A, Meissner S, Eyupoglu IY, Parsch H, Schmidt C, Buchfelder M (2010) Dynamics of S100B release into serum and cerebrospinal fluid following acute brain injury. *Acta Neurochir Suppl* 106:247–250
13. Kwon JH, Sung SK, Song YJ, Choi HJ, Huh JT, Kim HD (2008) Predisposing factors related to shunt-dependent chronic hydrocephalus after aneurysmal subarachnoid hemorrhage. *J Korean Neurosurg Soc* 43:177–181
14. O'Kelly CJ, Kulkarni AV, Austin PC, Urbach D, Wallace MC (2009) Shunt-dependent hydrocephalus after aneurysmal subarachnoid hemorrhage: incidence, predictors, and revision rates. *Clinical article. J Neurosurg* 111:1029–1035
15. Persson L, Hardemark H, Edner G, Ronne E, Mendel-Hartvig I, Pahlman S (1988) S-100 protein in cerebrospinal fluid of patients with subarachnoid haemorrhage: a potential marker of brain damage. *Acta Neurochir (Wien)* 93:116–122
16. Pleines UE, Morganti-Kossmann MC, Rancan M, Joller H, Trentz O, Kossmann T (2001) S-100 beta reflects the extent of injury and outcome, whereas neuronal specific enolase is a better indicator of neuroinflammation in patients with severe traumatic brain injury. *J Neurotrauma* 18:491–498
17. Salary M, Quigley MR, Wilberger JE Jr (2007) Relation among aneurysm size, amount of subarachnoid blood, and clinical outcome. *J Neurosurg* 107:13–17
18. Takayasu M, Shibuya M, Kanamori M, Suzuki Y, Ogura K, Kageyama N, Umekawa H, Hidaka H (1985) S-100 protein and calmodulin levels in cerebrospinal fluid after subarachnoid hemorrhage. *J Neurosurg* 63:417–420
19. Vale FL, Bradley EL, Fisher WS 3rd (1997) The relationship of subarachnoid hemorrhage and the need for postoperative shunting. *J Neurosurg* 86:462–466

Normal Hypocretin-1 (Orexin A) Levels in Cerebrospinal Fluid in Patients with Idiopathic Intracranial Hypertension

Maria Antonia Poca, Rosa Galard, Elena Serrano, Mari Angels Merino, Patricia Pozo-Rosich, Elisabeth Solana, Olga Mestres, Maria Dolores de la Calzada, and Juan Sahuquillo

Abstract Aim: Low levels of hypocretin-1 (HC-1) have been associated with hypersomnia, obesity, depression, and chronic headaches. These conditions are frequently present in patients with idiopathic intracranial hypertension (IIH) and may be associated with abnormalities of the hypocretin system. The aim of this study was to determine HC-1 concentrations in cerebrospinal fluid (CSF) in a series of patients with IIH and to compare these concentrations with those in a control group with no neurological alterations.

Patients and Methods: This prospective study included a cohort of 26 consecutive patients with IIH who were mostly women (25 vs. 1) with a mean age of 42.5 ± 13.2 . CSF samples were obtained from a lumbar puncture performed between 08:00 and 10:00 a.m. HC-1 was determined by a competitive radioimmunoassay (RIA) using I¹²⁵ as the isotope. Samples of normal CSF were obtained

during spinal anesthesia for urological, general or vascular surgery from 40 patients (10 women and 30 men with a mean age of 63.7 ± 14.8) with no previous neurological or psychiatric history, a normal neurological examination, and MMSE scores of ≥ 24 .

Results: No statistically significant differences were found between HC-1 levels in the CSF of patients with IIH (119.61 ± 21.63 pg/mL) and those of the control group (119.07 ± 20.30 pg/mL; $p = 0.918$).

Conclusions: HC-1 is not associated with the clinical symptoms present in patients with IIH.

Keywords Idiopathic intracranial hypertension • Pseudotumor cerebri • Hypersomnia • Obesity • Headaches • Hypocretin-1 • Orexin A

M.A. Poca (✉) and J. Sahuquillo

Department of Neurosurgery, Vall d'Hebron University Hospital and Vall d'Hebron Research Institute, Universitat Autònoma de Barcelona, Passeig Vall d'Hebron 119–129 08035 Barcelona, Spain and Neurosurgery and Neurotraumatology Research Unit, Vall d'Hebron University Hospital and Vall d'Hebron Research Institute, Universitat Autònoma de Barcelona, Barcelona, Spain
e-mail: pocama@neurotrauma.net

R. Galard

Department of Biochemistry, Vall d'Hebron University Hospital and Vall d'Hebron Research Institute, Universitat Autònoma de Barcelona, Barcelona, Spain

E. Serrano

Department of Anesthesiology, Vall d'Hebron University Hospital and Vall d'Hebron Research Institute, Universitat Autònoma de Barcelona, Barcelona, Spain

M.A. Merino, E. Solana, O. Mestres, and M.D. de la Calzada
Neurosurgery and Neurotraumatology Research Unit, Vall d'Hebron University Hospital and Vall d'Hebron Research Institute, Universitat Autònoma de Barcelona, Barcelona, Spain

P. Pozo-Rosich

Department of Neurology, Vall d'Hebron University Hospital and Vall d'Hebron Research Institute, Universitat Autònoma de Barcelona, Barcelona, Spain

Introduction

Idiopathic intracranial hypertension (IIH), also known as pseudotumor cerebri, consists of raised intracranial pressure with no clinical, laboratory or radiological evidence of intracranial abnormalities. IIH is relatively rare, but its incidence is rapidly increasing owing to the global rise in obesity. The most frequent symptom of IIH is headache, which is almost ubiquitous and extremely disabling. Permanent visual defects are serious and not an infrequent complication. The pathophysiology of IIH is still not fully understood.

Hypocretins (also known as orexins) are excitatory neuropeptides synthesized by neuron groups in the lateral and posterior hypothalamus [5]. Among the functions attributed to hypocretins, and specifically to hypocretin-1 (HC-1), are the activation and maintenance of wakefulness and sleep homeostasis [5]. However, other functions recently associated with these peptides are the modulation of appetite, energy homeostasis, nociceptive processing, and pleasure [1, 7, 21]. HC-1 has also been related to distinct types of headache, including the ones described by IIH patients [3, 8, 9, 19, 20].

Because of the characteristics of IIH (obesity, headaches, tendency towards depression and anxiety, etc.), it can be hypothesized that these patients will have significantly low levels of HC-1 compared with a control group with no history of IIH. The main aim of this study was to determine HC-1 concentrations in spinal CSF in a series of patients with IIH and to compare these concentrations with those in a control group with no neurological alterations. Secondary aims were first, to correlate HC-1 levels in IIH patients with sleepiness, using the Epworth Sleepiness Scale, and with the body mass index (BMI), and second, to analyze changes in HC-1 levels before and after treatment in 13 patients with IIH treated with a CSF shunt.

Materials and Methods

Patients and General Management Protocol of Suspected IIH

Prospective study of a cohort of 26 patients [mean age: 42.5 ± 13.2 ; range: 23–70; 1 man and 25 (96.3%) women] with IIH consecutively admitted to the Department of Neurosurgery of the Vall d'Hebron University Hospital between January 2007 and June 2009. All patients presented chronic headaches, papilledema, normal neurological examination results and normal MRI findings, including normal ventricular size (Evans' Index < 0.30). The diagnosis of IIH was confirmed by continuous intracranial pressure (ICP) monitoring using an epidural sensor and/or CSF dynamics studies (Marmarou's bolus test and Katzman's constant rate infusion test) [17, 18]. CSF samples were obtained in all patients before CSF dynamics studies and also in 13 IIH patients 6 months after shunt implantation. These patients had an improvement in clinical symptoms and a normalization of the ICP values. The study protocol was approved by the Ethics Committee of our center (PI07/0681) and written informed consent was obtained from all patients.

Control Group

Samples of normal CSF were obtained from 40 volunteers (mean age: 63.7 ± 14.8 ; range: 26–89; 30 [75%] men and 10 [25%] women) with no neurological or psychiatric history and with normal neurological examination results and Mini-Mental State Examination (MMSE) scores of ≥ 24 . CSF was obtained during spinal anesthesia for urological, general or vascular surgery after informed consent was obtained from all patients and approval was given by the Ethics Committee

of our center, PRAG-75/2005. All CSF samples were taken from patients who were operated on during the first few hours of the morning (08:00–11:00).

Obesity and Sleepiness Assessment

Body mass index ($BMI = \text{mass (kg)} / [\text{height (m)}]^2$) was calculated in 25 patients. Sleepiness was estimated in 24 patients using the Epworth Sleepiness Scale (ESS) and was considered abnormal when the ESS score was ≥ 10 (a score of 10 or more is considered sleepy and a score of 18 or more is very sleepy) [11].

CSF Sample Management and Determination of Hypocretin-1 Levels

Cerebrospinal fluid samples were obtained from a lumbar puncture performed between 08:00 and 10:00 under natural light and after at least 8 h of bed rest and fasting. The samples were temporarily placed in plastic tubes with Trasylol (1,000 kU/mL) to avoid proteolysis and were then distributed in 0.5-mL Eppendorf tubes and stored at -80°C until analysis.

HC-1 was determined by a competitive radioimmunoassay (RIA) using I^{125} as the isotope (RIA, Peninsula Laboratories, San Carlos, CA, USA). The samples were previously extracted through reverse-phase chromatography using C18 Sep-Pak columns (Water Associates, Milford, MA, USA). The range of the standard curve was 2–128 pg/tube. The HC-1 concentration was calculated according to the volume used and its final concentration after elution and correction by the total protein concentration in CSF. Intra-assay variability was less than 10%.

Statistical Analysis

All descriptive statistics were analyzed using the SigmaPlot package for Windows (Version 11.0, Systat Software Inc., Germany). The assumption that data were normally distributed was tested using the Shapiro–Wilk test. In normally distributed data, the mean ± 1 standard deviation (SD) was used to summarize the variables. In skewed samples, the median and the interquartile range (IQR) were used. Differences between HC-1 levels from the CSF of patients and controls were analyzed using the Student's *t*-test. Due to the small sample, correlations between HC-1 levels of IIH patients and BMI or EES scores, as well as comparisons between HC-1 levels in IIH patients before and after treatment were

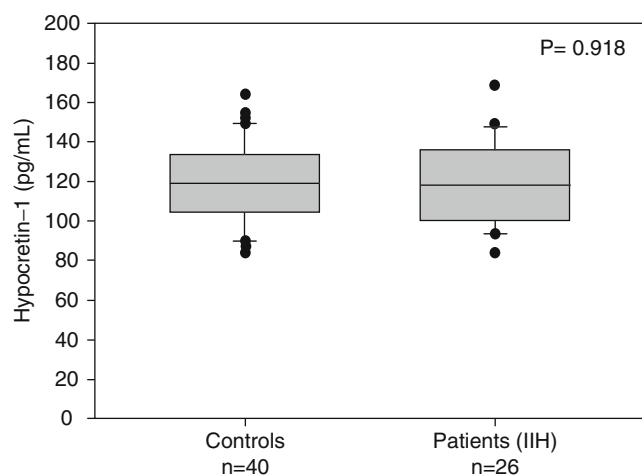


Fig. 1 Box-and-whisker plots showing the hypocretin-1 levels in the CSF of patients with idiopathic intracranial hypertension (IIH) and of controls. No statistically significant differences were found between the two groups ($t = -0.103$, $p = 0.918$)

performed by nonparametric tests. Statistical significance was considered to be indicated when $p \leq 0.05$.

Results

Mean HC-1 levels in the CSF of the 26 patients with idiopathic intracranial hypertension were 119.61 ± 21.63 pg/mL. Mean HC-1 levels in the CSF of the control group ($n = 40$) were 119.07 ± 20.30 pg/mL (Fig. 1). Comparisons of the two groups showed no statistically significant differences between them (t test, $t = -0.103$, $p = 0.918$).

In patients with idiopathic intracranial hypertension, no correlation was found between HC-1 levels and BMI ($n = 25$, $Rho = -0.018$, $p = 0.931$, Fig. 2, top), nor between HC-1 levels and ESS scores ($n = 24$, $Rho = -0.224$, $p = 0.290$). Comparisons between the HC-1 levels of IIH patients with an ESS score of less than 10 ($n = 16$, mean HC-1 levels: 122.27 pg/mL ± 21.4) with the subgroup of patients with an ESS score equal to or higher than 10 ($n = 8$, mean HC-1 levels: 115.32 pg/mL ± 23.6) showed no statistically significant differences (Mann-Whitney Rank Sum Test: $U = 53$, $p = 0.520$, Fig. 2, bottom).

Mean intracranial pressure (ICP) of the 26 IIH patients was 24 ± 12 mmHg. Of these, additional CSF lumbar samples were also obtained in 13 patients 6 months after ventriculo- or lumbo-peritoneal implantation. Although normalization in ICP values occurred after treatment, comparisons between the HC-1 levels of the 13 treated patients before and 6 months after shunting showed no statistically significant differences (Wilcoxon Signed Rank Test, $Z = 0.804$, $p = 0.455$, Fig. 3).

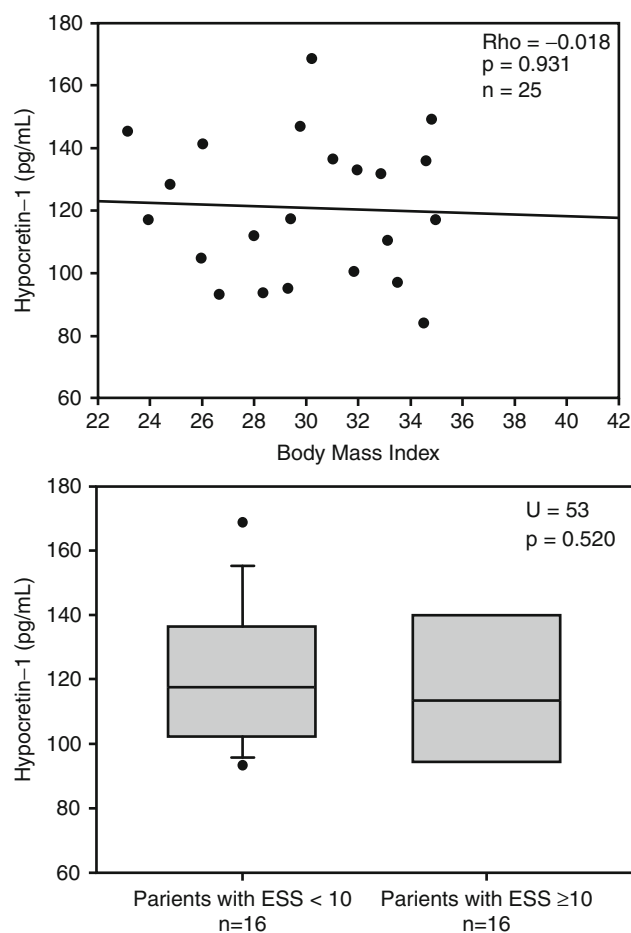


Fig. 2 Top: Correlation of hypocretin-1 levels and body mass index in 25 patients with IIH (Spearman's rank correlation analysis: $Rho = -0.018$, $p = 0.931$). Bottom: Box-and-whisker plots showing the hypocretin-1 levels in the CSF of patients with IIH with an Epworth Sleepiness Scale (ESS) score < 10 and those with an ESS score ≥ 10

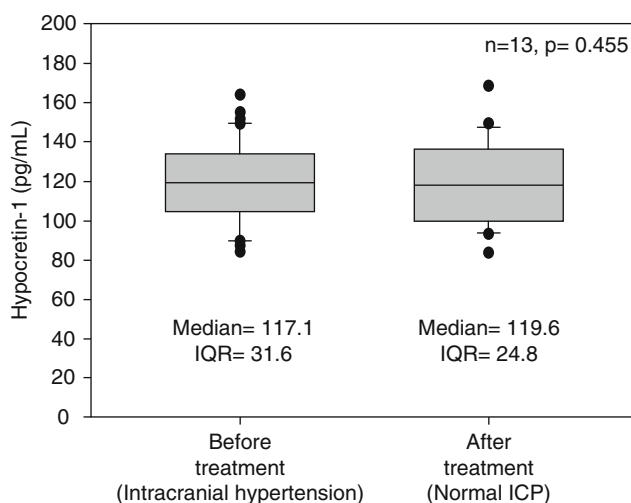


Fig. 3 Box-and-whisker plots showing the hypocretin-1 levels in the CSF of the 13 patients with IIH before and 6 months after shunt implantation, when intracranial pressure (ICP) was normalized (IQR interquartile range)

Discussion

The results of this study demonstrate that there are no statistically significant differences between HC-1 levels in the CSF of patients and controls. HC-1 levels did not change significantly after ICP reduction in patients with IIH in whom a CSF shunt was implanted. We did not find any association between CSF HC-1 levels and weight and sleepiness in the patients studied.

Hypocretin-1 and 2 (also known as orexin A and B) are neuropeptides derived from the same precursor (prepro-orexin, a 130 amino acid precursor peptide) and their expression is restricted to a few thousand neurons of the lateral hypothalamus [5]. Hypocretins bind to 2G-protein coupled receptors (Hcrtr1 and Hcrtr2), elevating the intracellular Ca^{2+} concentrations [5]. From both molecules, HC-1 has equal affinity for both receptors, is fully conserved across species, and it has been suggested to be of greater biological importance than hypocretin-2 [8]. Among other neuropeptides, hypocretins are also reciprocally connected with neuropeptide Y and leptin receptor-positive neurons in the arcuate nucleus [10, 21], an area important in feeding behaviors and endocrine regulation.

Clinical and experimental studies have demonstrated that the level of HC-1 depends on a circadian rhythm. Deboer et al. showed that HC-1 reached the lowest levels in the middle of the resting phase in an experimental study in rats; levels remained low until the start of their active phase and increased progressively to reach the maximum levels within 4 h after onset of animal activity [6]. These authors also demonstrated that HC-1 levels during the end of the activity differed significantly from levels during the end of the resting phase [6]. These findings may help to explain the low levels of HC-1 detected in controls and patients in the present study, compared with other series, as well as the variability of HC-1 levels found in the literature of patients with different neurological conditions in whom CSF samples were obtained in different hours of the day [4, 16].

The hypothalamus contributes to only a small part of the brain, but it is involved in a multitude of brain functions (hormone synthesis, regulation of the autonomic nervous system, thermoregulation, determining biological rhythms, emotional behavior, and arousal, among others). Multiple lines of evidence suggest that hypocretins might play a role in the modulation of these biological functions [5]. Other authors have also attributed a role to the hypothalamus in the pathophysiology of primary headaches through the orexinergic system [8, 9, 19, 20], especially in obese patients [3]. Recently, additional analgesic properties have also been attributed to HC-1 [12]. Sleep deprivation has been associated with high levels of HC-1 in CSF [15], while low levels of HC-1 have been associated with hypersomnia, obesity, depression and chronic headaches [1, 4, 21]. Some of these last symptoms are frequently present in patients with IIH.

Conclusion

Patients with idiopathic intracranial hypertension characteristically present with chronic headaches, obesity, and a tendency toward depression and anxiety [13]. Abnormalities found in serum and CSF leptin levels in IIH may contribute to this symptomatology and suggest a hypothalamic dysfunction in these patients [2, 14], which could also extend to the hypocretin system. However, the results of the present study suggest that HC-1 does not play a role in the pathophysiology of idiopathic intracranial hypertension and that the symptoms present in these patients have no relationship with HC-1 levels. Although to our knowledge this is the only study to analyze HC-1 concentrations in the CSF of IIH patients, a large series will be needed in order to establish definitive conclusions.

Acknowledgements The authors gratefully acknowledge Sabrina Voss for editorial assistance and the collaboration of the neurosurgical nurses in the study of these patients, especially María Angeles Barba (RN) and Lorena Jiménez (RN). This study was supported in part by Grant 07/0681 from the *Fondo de Investigación Sanitaria* (FIS) given to Dr. M.A. Poca.

Conflict of interest statement We declare that we have no conflict of interest.

References

1. Adam JA, Menheere PP, van Dielen FM et al (2002) Decreased plasma orexin-A levels in obese individuals. *Int J Obes Relat Metab Disord* 26:274–276
2. Ball AK, Sinclair AJ, Curnow SJ et al (2009) Elevated cerebrospinal fluid (CSF) leptin in idiopathic intracranial hypertension (IIH): evidence for hypothalamic leptin resistance? *Clin Endocrinol (Oxf)* 70:863–869
3. Bigal ME, Lipton RB, Holland PR et al (2007) Obesity, migraine, and chronic migraine: possible mechanisms of interaction. *Neurology* 68:1851–1861
4. Dauvilliers Y, Baumann CR, Carlander B et al (2003) CSF hypocretin-1 levels in narcolepsy, Kleine-Levin syndrome, and other hypersomnias and neurological conditions. *J Neurol Neurosurg Psychiatry* 74:1667–1673
5. De Lecea L, Sutcliffe JG (2005) The hypocretins and sleep. *FEBS J* 272:5675–5688
6. Deboer T, Overeem S, Visser NA et al (2004) Convergence of circadian and sleep regulatory mechanisms on hypocretin-1. *Neuroscience* 129:727–732
7. Ganjavi H, Shapiro CM (2007) Hypocretin/orexin: a molecular link between sleep, energy regulation, and pleasure. *J Neuropsychiatry Clin Neurosci* 19:413–419
8. Holland P, Goadsby PJ (2007) The hypothalamic orexinergic system: pain and primary headaches. *Headache* 47:951–962
9. Holland PR, Goadsby PJ (2009) Cluster headache, hypothalamus, and orexin. *Curr Pain Headache Rep* 13:147–154
10. Horvath TL, Diano S, van den Pol AN (1999) Synaptic interaction between hypocretin (orexin) and neuropeptide Y cells in the rodent and primate hypothalamus: a novel circuit implicated in metabolic and endocrine regulations. *J Neurosci* 19:1072–1087

11. Johns MW (1991) A new method for measuring daytime sleepiness: the Epworth sleepiness scale. *Sleep* 14:540–545
12. Kajiyama S, Kawamoto M, Shiraishi S et al (2005) Spinal orexin-1 receptors mediate anti-hyperalgesic effects of intrathecally-administered orexins in diabetic neuropathic pain model rats. *Brain Res* 1044:76–86
13. Kleinschmidt JJ, Digre KB, Hanover R (2000) Idiopathic intracranial hypertension: relationship to depression, anxiety, and quality of life. *Neurology* 54:319–324
14. Lampl Y, Eshel Y, Kessler A et al (2002) Serum leptin level in women with idiopathic intracranial hypertension. *J Neurol Neurosurg Psychiatry* 72:642–643
15. Martins PJ, Marques MS, Tufik S et al (2010) Orexin activation precedes increased NPY expression, hyperphagia, and metabolic changes in response to sleep deprivation. *Am J Physiol Endocrinol Metab* 298:E726–E734
16. Mignot E, Lammers GJ, Ripley B et al (2002) The role of cerebrospinal fluid hypocretin measurement in the diagnosis of narcolepsy and other hypersomnias. *Arch Neurol* 59:1553–1562
17. Poca MA, Sahuquillo J, Barba MA et al (2004) Prospective study of methodological issues in intracranial pressure monitoring in patients with hydrocephalus. *J Neurosurg* 100:260–265
18. Poca MA, Sahuquillo J, Topczewski T et al (2007) Is intracranial pressure monitoring in the epidural space reliable? Fact and fiction. *J Neurosurg* 106:548–556
19. Rainero I, De MP, Pinessi L (2008) Hypocretins and primary headaches: neurobiology and clinical implications. *Expert Rev Neurother* 8:409–416
20. Sarchielli P, Rainero I, Coppola F et al (2008) Involvement of corticotrophin-releasing factor and orexin-A in chronic migraine and medication-overuse headache: findings from cerebrospinal fluid. *Cephalalgia* 28:714–722
21. Tsujino N, Sakurai T (2009) Orexin/hypocretin: a neuropeptide at the interface of sleep, energy homeostasis, and reward system. *Pharmacol Rev* 61:162–176

Frontal and Temporal Horn Ratio: A Valid and Reliable Index to Determine Ventricular Size in Paediatric Hydrocephalus Patients?

Sebastian Antes, Michael Kiefer, Melanie Schmitt, Miriam Lechtenfeld, Martina Geipel, and Regina Eymann

Abstract Because there is currently no sufficient and prevalent parameter for estimating ventricular size in paediatric hydrocephalus patients by using cranial ultrasound, a new measurement index, called the “frontal and temporal horn ratio”, is presented in this study. The advantage of the new quotient is that it can be detected in easily obtainable coronal ultrasound planes. A retrospective analysis of 149 MRIs of young hydrocephalus patients proved the new index to be a promising parameter of ventricular size assessment. Statistical comparison between the “frontal and temporal horn ratio” and the already validated “frontal and occipital horn ratio” revealed a strong and linear correlation between the two quotients. Current research is now evaluating the reliability of the new index in the context of an ultrasound study; first results indicate similar positive findings.

Keywords Ultrasound • Hydrocephalus • Ventricular size • Linear measurement • Frontal and occipital horn ratio

developed [1, 8, 11]. Instead, different two-dimensional linear parameters, which had been proven to be valid and reliable indices in determining ventricular size (e.g. Evans index, Huckman number, frontal and occipital horn ratio etc.), have become standard for these purposes [7, 8, 11, 12]. As almost all the parameters described require absolute axial slices of the brain, computed tomography (CT) and magnetic resonance imaging (MRI) are usually performed. However, if the patient belongs to the paediatric population, cranial ultrasound (cUS) is the primary method used to evaluate the brain [3, 6, 9, 10, 13–15]. If standard anterior fontanelle imaging is performed, coronal and sagittal slices of the brain can be detected for neurological investigations [3, 9, 10, 13]. This fact implies that the determination of the abovementioned quotients is hardly feasible. Therefore, a new two-dimensional index, called the “frontal and temporal horn ratio”, which can be measured in easily obtainable coronal slices of the infant brain, is recommended.

Introduction

The assessment of the ventricular system in hydrocephalus patients is of high clinical importance [1, 6, 12], especially for timely detection of typical shunt complications (e.g. overdrainage, underdrainage, subdural haematoma etc.). Volumetric measurements – which can be performed using different imaging methods – provide the most accurate estimate of true ventricular volume [1, 2, 4, 11, 12]. However, appropriate volumetric techniques are not widely used in clinical routine because a simple and user-friendly method has not yet been

Materials and Methods

One hundred and forty-nine MRIs (Siemens Sonata, 1.5 T) of 61 hydrocephalus patients (35 male, 26 female) aged 0–11 years (average: 3.1 ± 3.0 years) were retrospectively analysed. The aetiology of hydrocephalic ventricle configuration had been Chiari II malformation (33%), intraventricular haemorrhage (25%), congenital cerebral malformations such as the Dandy–Walker complex or schizencephaly (20%), congenital aqueductal stenosis (10%), occlusive tumours (7%) and postinflammatory diseases (5%). In every single image, the already validated and well-known frontal and occipital horn ratio (FOHR) was measured in axial slices as usual. The FOHR is the average frontal and occipital horn width divided by the interparietal diameter (Fig. 1). The new frontal and temporal horn ratio (FTHR) was determined in coronal planes of the same imaging series. The FTHR is analogously defined as the average frontal and temporal horn width divided by the broadest skull diameter at the level of the foramen of Monro (Fig. 1). Resulting quotients were

S. Antes (✉), M. Kiefer, M. Schmitt, M. Lechtenfeld, and R. Eymann
Department of Neurosurgery, Saarland University, Medical School,
Kirrberger Straße, Building 90.5, 66421 Homburg, Saar, Germany
e-mail: sebastian.antes@uks.eu

M. Geipel
Department of Paediatric and Juvenile Medicine, Saarland University,
66421 Homburg, Saar, Germany

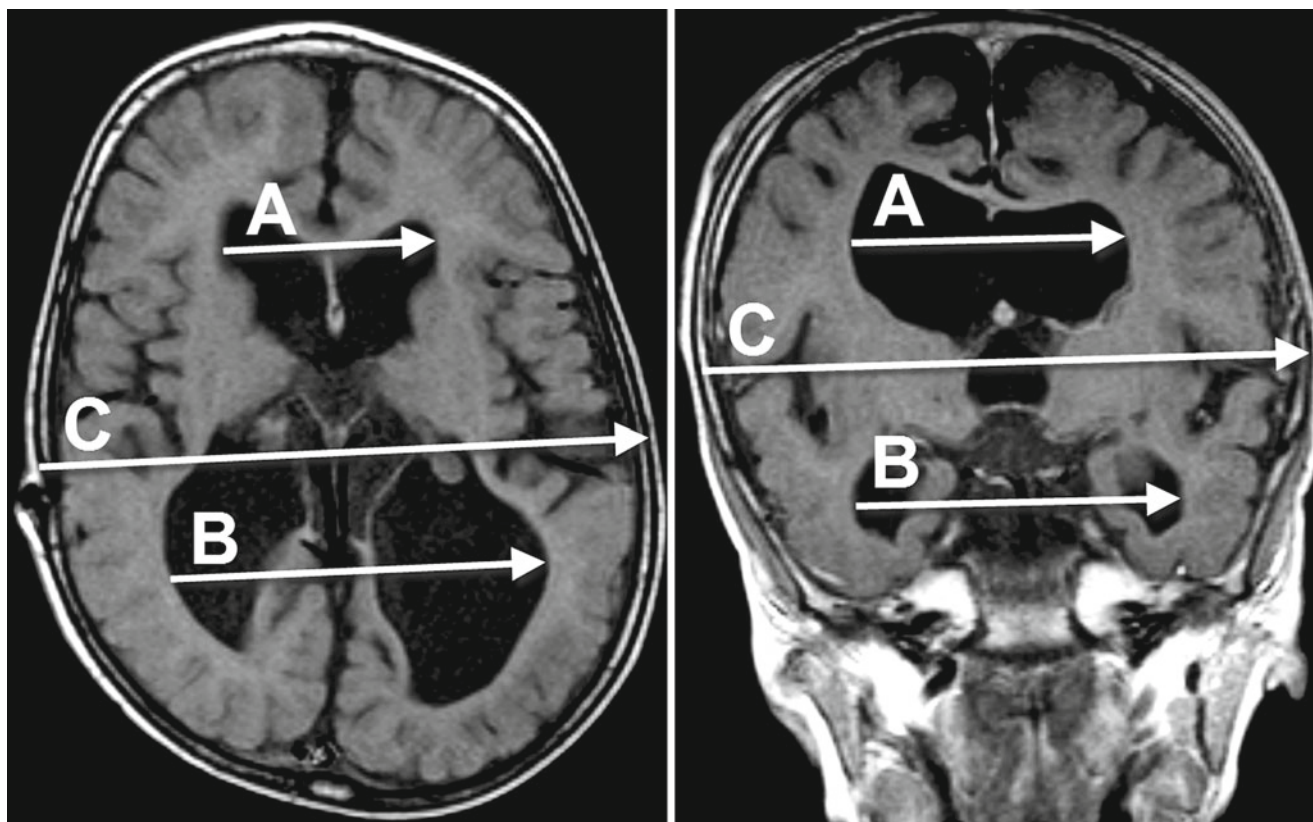


Fig. 1 *Left:* Illustration of frontal and occipital horn ratio (FOHR) measurement on an axial T1-weighted MRI of a 2½-year-old patient suffering from post-haemorrhagic hydrocephalus ($\text{FOHR} = (A + B) /$

$(2 \times C) = 0.48$). *Right:* Analogous determination of the new frontal and temporal horn ratio (FTHR) in a coronal MRI plane of the same imaging series ($\text{FTHR} = (A + B) / (2 \times C) = 0.47$)

finally compared using Spearman's correlation coefficients. In a second series, a correlation analysis of three single patients with multiple brain imaging (Child 1 with 11 MRIs, Child 2 with 8 MRIs, Child 3 with 7 MRIs) was performed to verify the permanence in long-term observations and/or the constant coherence of both ratios. Finally, the same procedure was rendered by using 8 ultrasound images (GE Healthcare, Vivid S5 ultrasound system) of eight different preterm infants suffering from hydrocephalus due to intra-ventricular haemorrhage. Therefore, anterior fontanelle imaging was performed to determine the FOHR in axial slices and the new FTHR in coronal slices, each at the level of the foramen of Monro (Fig. 2).

Results

Referring to all 149 MRIs, the average value of the FOHR was 0.47 ± 0.13 (range: 0.25–0.78), the mean FTHR was 0.50 ± 0.13 (range: 0.22–0.80). Correlation analysis revealed a strong and linear correlation implying the highest level of statistical significance between the two gathered datasets. The Spearman's coefficient was 0.85 ($p = 0.000$), an

associated graph demonstrating the strong coherence is shown in Fig. 3. Similar results could also be obtained in the second series with multiple images of the same infant: Child 1 presented a correlation coefficient between FOHR and FTHR of 0.98 ($p = 0.000$), Child 2 0.83 ($p = 0.010$) and Child 3 0.88 ($p = 0.009$). The recent but not yet completed study with 8 different ultrasound images pointed to similar results. Both ratios showed very similar values; the mean FOHR was 0.49 ± 0.08 (range: 0.42–0.61) and the average FTHR was 0.48 ± 0.09 (range: 0.40–0.63). The appendant correlation coefficient was 0.97 ($p = 0.058$).

Discussion

Knowledge of the ventricular volume in hydrocephalus and its changes resulting from different therapeutic strategies (e.g. because of shunt therapy or endoscopic third ventriculostomy) is of high clinical relevance [1, 6, 12]. In addition to the patient's condition, imaging is frequently requested to characterise the ventricular system [11]. Several studies in the past revealed a significant difference between subjective visual ratings of the ventricular size compared with the

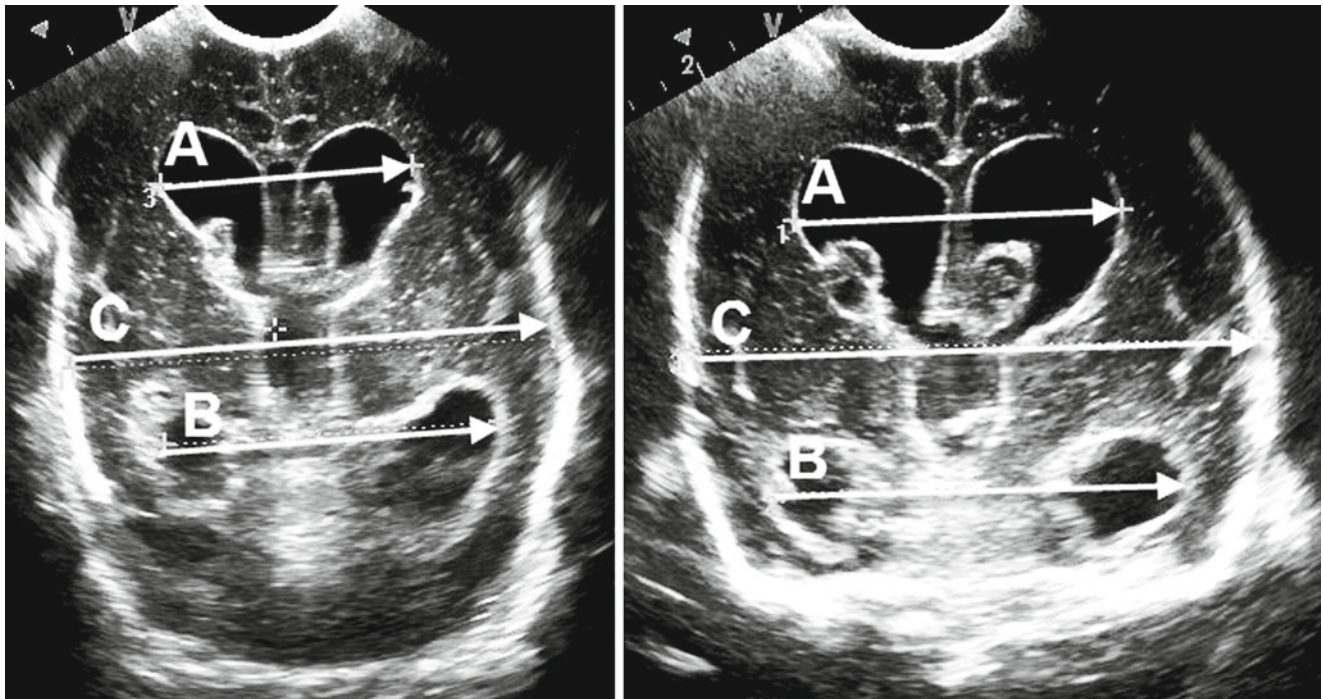


Fig. 2 Cranial ultrasound of a preterm infant born at a gestational age of 30 weeks suffering from hydrocephalus due to intrauterine intraventricular haemorrhage. Both images were obtained through the anterior fontanelle.

On the *left side* the axial ultrasound plane with a FOHR of 0.61, on the *right side* the corresponding coronal plane with an FTHR of 0.63

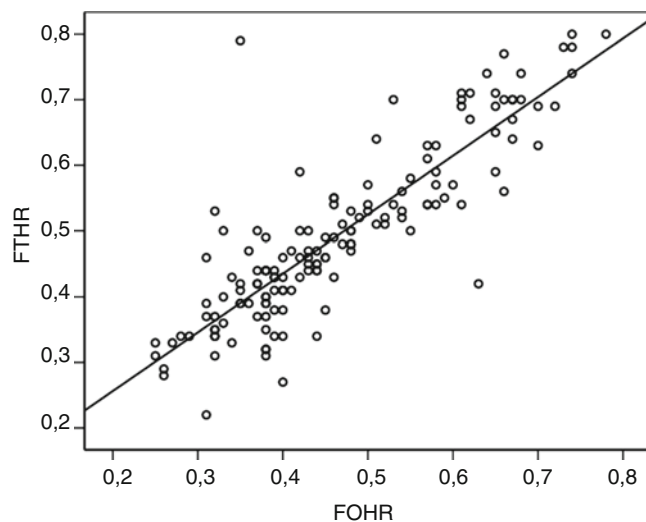


Fig. 3 The FOHR on the abscissa vs. the FTHR on the ordinate. *Straight line* elucidates the strong correlation (Spearman's coefficient=0.85, $p=0.000$) between the two quotients

measured size [8, 11, 16]. There is a general consensus that interpretations of the ventricular system should not be based on subjective ratings, but rather on measurements [8, 11]. Volumetric techniques, which are supposed to be the most accurate method of volume assessment [1, 2, 4, 11, 12], have currently not been introduced commercially and have

not been validated for routine usage [1, 8, 11]. Thus, linear measurements of the ventricular system in standard imaging methods such as CT and MRI are the first choice (e.g. Evan's index, Huckman number, FOHR etc.), at least in adult patients [7, 11, 12].

With reference to the paediatric population, the implementation of (multiple) CTs or MRIs for examination of the ventricular system is completely unsustainable. These imaging methods require time, man-power, enormous effort, and often sedation or anaesthesia to prevent motion artefacts [4]. In cases of CT children are exposed to disproportionate ionising radiation, and it is generally known that young patients are more vulnerable to the increased dose-volume ratio [5, 15]. Repetitive follow-ups with ionising radiation (CT and "shunt series") lead to a cumulative risk of inducing malignancy [15]. For these and many other reasons, cUS has been established as the primary method of investigation of the young brain [3, 6, 9, 10, 13–15]. Usually, coronal and sagittal planes, by using the anterior fontanelle as the acoustic window, belong to the standard evaluation of the ventricular system and its adjacent structures [3, 9, 10, 13]. Yet a linear parameter for comparisons of the ventricular size is currently not available and almost all of the existing quotients have to be determined in axial planes (e.g. FOHR etc.). The crux of the matter is that axial planes are nearly impossible and time consuming to render using cUS, especially when ossification of the anterior fontanelle is well advanced.

Owing to the problems mentioned, we developed a new linear index called the frontal and temporal horn ratio that can be measured in easily obtainable coronal slices of ultrasound images. According to its proven validity and reliability [7, 8, 11, 12], the well-known frontal and occipital horn ratio has been chosen in this study as the comparative parameter for the evaluation of the new FTHR.

The results of the MRI measurements confirmed a strong and linear correlation between the FOHR and the new FTHR (correlation coefficient 0.85, $p=0.000$). Similar findings were also seen in the second series with multiple images of the same children. These points indicate sufficient feasibility and applicability in clinical practice, as a tool for both initial evaluation of the infant brain and for repeated follow-ups.

Although it is generally considered that measurements performed on cUS are consistent with those obtained from MRI [9], it seems advisable to reflect on this. In particular, there may be an inconsistency between MRI and cUS measurements resulting from different perspective projections. On cUS, coronal as well as axial planes are obtained through the anterior fontanelle. To acquire an adequate view including the essential parts of the ventricular system at the level of the foramen of Monro, the ultrasound transducer must be held at an oblique angle. On the contrary, MRI generates images that are obtained in parallel vertical and horizontal planes. Consequently, identical projections are hardly realisable and it cannot be predicted how this difference in angle affects the values of the parameters.

However, the initial results of the latest study with comparative measurements in axial and coronal planes of 8 different ultrasound images indicate that there could be transferability of the observations of the MRI study. As there is an insufficient sample size, the high correlation coefficient of 0.97 ($p=0.058$) is currently of minor significance and cannot entirely answer the question about the reliability of the quotient.

Conclusion

This MRI study proves the coronal FTHR to be a promising estimate of ventricular size in young hydrocephalus patients. The key advantage is the ability to prevent radiation exposure, particularly with respect to often unavoidable control and follow-up examinations. In conclusion, the strong correlation between the FTHR and the FOHR offers the possibility of further encouraging ultrasound investigations.

Conflict of interest statement We declare that we have no commercial interest in the products mentioned in this manuscript and have received no financial support in conjunction with this study. R. Eymann and M. Kiefer have received some financial support during the past for other research by the Raumedic AG, Helmbrechts, Germany. M. Schmitt and

S. Antes have received financial support in the past for purposes of education by Codman (Johnson & Johnson), Raynham, MA, USA and Aesculap AG (Miethke), Tuttlingen, Germany.

References

1. Ambarki K, Israelsson H, Wåhlin A, Birgander R, Eklund A, Malm J (2010) Brain ventricular size in healthy elderly: comparison between Evans index and volume measurement. *Neurosurgery* 67:94–99
2. Csutak R, Unterassinger L, Rohmeister C, Weninger M, Vergesslich KA (2003) Three-dimensional volume measurement of the lateral ventricles in preterm and term infants: evaluation of a standardised computer-assisted method in vivo. *Pediatr Radiol* 33:104–109
3. Di Salvo DN (2001) A new view of the neonatal brain: clinical utility of supplemental neurologic US imaging windows. *Radiographics* 21:943–955
4. Gilmore JH, Gerig G, Specter B, Charles HC, Wilber JS, Hertzberg BS, Kliewer MA (2001) Infant cerebral ventricle volume: a comparison of 3-D ultrasound and magnetic resonance imaging. *Ultrasound Med Biol* 27:1143–1146
5. Hall EJ (2009) Radiation biology for pediatric radiologists. *Pediatr Radiol* 39:57–64
6. Iova A, Garmashov A, Androuchtchenko N, Kehrer M, Berg D, Becker G, Garmashov Y (2004) Evaluation of the ventricular system in children using transcranial ultrasound: reference values for routine diagnostics. *Ultrasound Med Biol* 30:745–751
7. Jamous M, Sood S, Kumar R, Ham S (2003) Frontal and occipital horn width ratio for the evaluation of small and asymmetrical ventricles. *Pediatr Neurosurg* 39:17–21
8. Kulkarni AV, Drake JM, Armstrong DC, Dirks PB (1999) Measurement of ventricular size: reliability of the frontal and occipital horn ratio compared to subjective assessment. *Pediatr Neurosurg* 31:65–70
9. Leijser LM, Srinivasan L, Rutherford MA, Counsell SJ, Allsop JM, Cowan FM (2007) Structural linear measurement in the newborn brain: accuracy of cranial ultrasound compared to MRI. *Pediatr Radiol* 37:640–648
10. Liao MF, Chaou WT, Tsao LY, Nishida H, Sakanoue M (1986) Ultrasound measurement of the ventricular size in newborn infants. *Brain Dev* 8:262–268
11. Mann SA, Wilkinson JS, Fourney DR, Stoneham GW (2009) Comparison of computed tomography 3-dimensional volumetric analysis of ventricular size to visual radiological assessment. *J Comput Assist Tomogr* 33:789–794
12. O'Hayon BB, Drake JM, Ossip MG, Tuli S, Clarke M (1998) Frontal and occipital horn ratio: a linear estimate of ventricular size for multiple imaging modalities in pediatric hydrocephalus. *Pediatr Neurosurg* 29:245–249
13. Poland RL, Slovis TL, Shankaran S (1985) Normal values for ventricular size as determined by real time sonographic techniques. *Pediatr Radiol* 15:12–14
14. Reeder JD, Kaude JV, Setzer ES (1983) The occipital horn of the lateral ventricles in premature infants. An ultrasonographic study. *Eur J Radiol* 3:148–150
15. Smyth MD, Narayan P, Tubbs RS, Leonard JR, Park TS, Loukas M, Grabb PA (2008) Cumulative diagnostic radiation exposure in children with ventriculoperitoneal shunt: a review. *Childs Nerv Syst* 24:493–497
16. Sze RW, Ghioni V, Weinberger E, Seidel KD, Ellenbogen RG (2003) Rapid computed tomography to measure ventricular volumes in the child with suspected ventriculoperitoneal shunt failure II. *J Comput Assist Tomogr* 27:668–673

Intraventricular Cooling During CSF Infusion Studies

Melanie Schmitt, Regina Eymann, Sebastian Antes, and Michael Kiefer

Abstract We implemented ventricular infusion studies on 33 patients suspected of idiopathic normal pressure hydrocephalus (iNPH), benign intracranial hypertension (BIH) or occlusive hydrocephalus (HOC) in order to confirm shunt indications. The initial scope was to study O_2 supply during infusion tests to exclude further violation of already vulnerable brains during ICP elevation. Intraventricular infusion was performed via ventricle catheters with the ICP tip sensor, while brain tissue oxygenation was measured with intraparenchymal Raumedic PTO probes. In 15 out of 23 (65%; 8 NPH, 2BIH, 5 HOC), pO_2 increased constantly (average 140%), while brain temperature decreased (range: 0.2–4.5°C) during the infusion studies. In another six patients, O_2 values remained largely stable during the infusion studies (4NPH, 1BIH, 1HOC). Cerebral deoxygenation during infusion tests occurred only in two patients (1NPH, 1HOC).

Overall cerebral oxygenation and temperature inversely correlated well with some temporary delay regarding oxygenation state as a consequence of cerebral temperature. Probably, this effect is a consequence of reduced cerebral metabolism caused by local cooling. We hypothesise that such cooling is mediated via the large basal arteries and suggest that such a pathophysiology, ICP-controlled local cooling, might offer a new option for brain protection (e.g. in an ICP crisis).

Keywords ICP • ICP treatment • Cerebral metabolism • CSF hydrodynamics • Cerebral oxygen partial pressure • Cerebral temperature

Introduction

We performed ventricular infusion studies in patients with suspected idiopathic normal pressure hydrocephalus (iNPH), benign intracranial hypertension (BIH) or occlusive

hydrocephalus (HOC) to confirm shunt indications. To exclude cerebral O_2 desaturation during such ICP elevation, we monitored brain tissue oxygenation.

Materials and Methods

Ventricular infusion studies were implemented in 33 patients, who were divided into three groups: Idiopathic normal pressure hydrocephalus (iNPH, 16 patients: 11 female, 5 male), benign intracranial hypertension (BIH, 5 patients: 4 female, 1 male) and occlusive hydrocephalus (HOC, 12 patients: 4 female, 8 male). Average age of the iNPH, BIH, and HOC groups were 72.87 ± 7.9 , 32.4 ± 13.1 and 54.75 ± 19.9 years respectively. Evans index served as ventricular size estimation.

To reduce the bias as much as possible, only patients in whom we performed ventricular infusion studies and who obtained general anaesthesia (at the patient's request) were included in the study. As a general in-house policy of our anaesthesiologists concerning patients with increased intracranial pressure (ICP), FiO_2 was kept constant at 100%. Further on, to ensure sufficient cerebral perfusion pressure (>60 mmHg), mean arterial blood pressure (MAP) was kept between 85 and 95 mmHg. Throughout the whole procedure, patients were positioned strictly horizontal (supine).

For mock-CSF infusion, one-lumen ventricular drainages with tip sensor (Spiegelberg®, Hamburg, Germany or Raumedic®, Raumedic AG, Helmbrechts, Germany) were inserted into the left frontal horn via a standard precoronal approach.

Additionally, via the same burr hole, a Neurovent PTO probe (Raumedic®) was implanted into the frontal white matter, allowing parallel measurement of local temperature, oxygenation and ICP.

We performed a constant rate infusion test [8]. As mock-CSF we used 0.9% sodium chloride solution (NaCl) at 20°C, which was infused at a constant infusion rate of 3 mL/min. If ICP reached no plateau pressure at ICP levels below 35 mmHg, the infusion was promptly interrupted and all data were further collected until the resting pressure was reached again.

M. Schmitt (✉), R. Eymann, S. Antes, and M. Kiefer
Department of Neurosurgery, Saarland University, Medical School,
Kirrberger Straße, Building 90.5, 66421 Homburg, Germany
e-mail: m.schmitt@uniklinikum-saarland.de

Table 1 Data of patients with a constant O₂ increase with some temporary delay to decreasing cerebral temperature and increasing intracranial pressure (ICP)

Patient ID	Initial O ₂ (mmHg)	Maximal O ₂ (mmHg)	Final O ₂ (mmHg)	Maximal cT (°C)	Minimal cT (°C)
23	134.4	200	191.4	36.32	34.98
27	32.6	55.3	55.3	36.07	35.81
29	27.5	82.7	82.7	36.34	35.88
30	53.8	62.6	62.6	36.6	36.06
31	16.6	64.3	64.3	36.59	35.6
33	11.9	68.5	68.5	37.25	36.35
3	44.9	58.3	58.3	36.54	35.95
6	31.9	44.9	44.9	36.79	36.31
8	10.1	13.5	13.5	36.25	36.05
10	37.7	67.8	67.8	35.85	34.74
12	33.3	65.5	65.3	36.71	35.48
13	35.8	78.1	78.1	36.45	36.04
14	10.6	19.9	19.9	37.09	35.87
17	13.3	17.6	17.6	35.55	35.21
20	7.1	41.7	40.1	36.76	36.28

During the infusion studies, all data were stored online on PC and Raumedic®'s datalogger. Rigorous data quality control was performed and patients with unreliable data were excluded secondarily: O₂ measurement was assumed to fail if the measured values were below 7 mmHg, since parenchymal O₂ levels <7 mmHg are typically assumed to indicate cerebral ischaemia, which was not given in any of these patients according to imaging and post-interventional clinical course. Consecutively, 10 of the 33 patients who were included initially had to be excluded secondarily and the study is based on the data of 23 patients.

For further data analysis the software Microsoft Excel 2003 (Redmond, USA), WinSTAT for Excel (R. Fitch software, Bad Krozingen, Germany) and PASW Version 18 (SPSS Inc., Chicago, IL, USA) were used. For statistical analysis, Spearman's (if no normal distribution pattern was given) and Pearson's (normal distribution pattern given) correlation tests (significance level $p < 0.05$) as well as the U test were used.

Results

Duration of ventricular infusion tests was averaged 26 ± 0.007 min (range: 15–57 min). During the infusion of mock-CSF, intracranial pressure (ICP) increased and cerebral temperature steadily decreased between 0.2°C and 4.5°C until infusion was stopped. After infusion had been stopped, in parallel with an ICP decrease, cerebral temperature increased again and normally reached the initial level.

pO₂ increased constantly with some temporary delay to rising ICP and decreasing cerebral temperature during infusion studies in 15 out of 23 patients: eight patients with iNPH (8 out of 12; 66.67%), two patients with BIH (2 out of 3; 66.67%) and five patients with occlusive hydrocephalus (5 out of 12; 41.67%). Initial oxygen values were on average exceeded by 140.2% (range: 16.4–487.3%). Raw data are listed in Table 1. Despite ICP and cerebral temperature having recovered to the initial levels, cerebral oxygenation remained at a higher level compared with the resting values for the rest of the monitoring period.

In 6 patients, oxygenation decreased parallel to rising ICP during mock-CSF infusion, while it increased during the effusion period and thereby reached higher levels than initially: 3 patients with NPH (3 out of 16), 1 patient with BIH (1 out of 3) and 2 patients with occlusive hydrocephalus (2 out of 12; raw data are shown in Table 2).

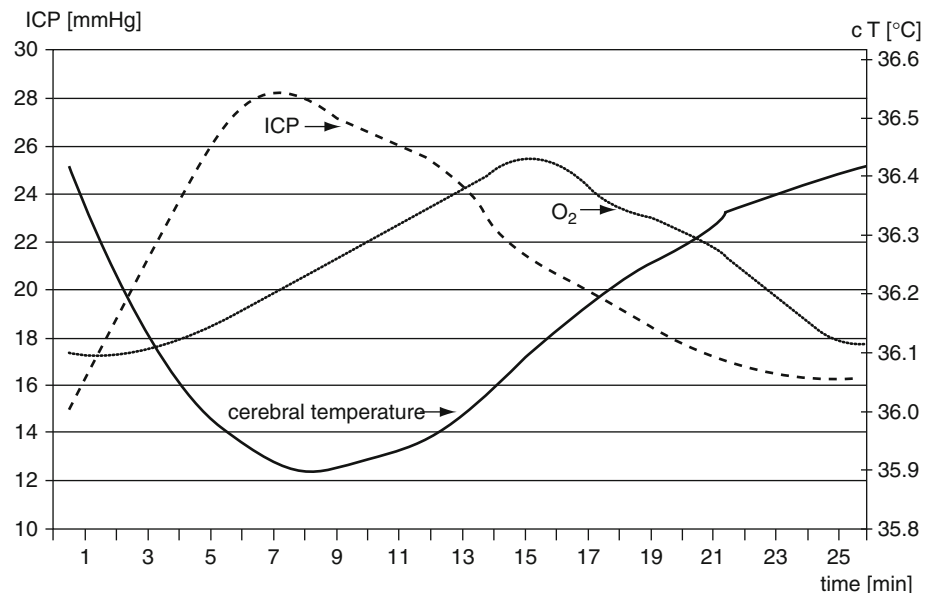
A continuous decrease in oxygen partial pressure during ventricular infusion studies could be detected in 2 out of 23 patients in total (1 out of 16 patients with NPH and 1 out of 12 patients with HOC).

To demonstrate the effect that in the vast majority the temperature slope was inverse to the ICP course and that cerebral oxygenation typically increased with some temporary delay after the decrease of brain temperature, the data of all patients were averaged in Fig. 1.

Oxygen saturation and cerebral temperature correlated well ($p < 0.000$; Pearson $r = 0.13$ in the NPH group; Pearson $r = 0.12$ in the HOC group; Spearman $r = 0.14$ in the BIH group). The same holds true when testing the data of all patients with the Mann–Whitney U test ($p < 0.000$).

Table 2 Data of patients with O_2 decrease during ICP increase, yet O_2 increase during the effusion phase, reaching higher O_2 levels than initially

Patient ID	Initial O_2 (mmHg)	Maximal O_2 (mmHg)	Final O_2 (mmHg)	Maximal cT ($^{\circ}\text{C}$)	Minimal cT ($^{\circ}\text{C}$)
2	9.3	18.2	18.2	35.42	34.92
18	48.3	62.4	62.4	37.1	36.34
25	37.8	43.6	43.6	36.5	36.04
22	19.2	24.4	24.4	36.62	32.12
9	7.2	10.1	8.7	36.7	35.53
21	38.6	42.9	42.9	36.32	33.75

Fig. 1 Averaged mean data of all patients (displayed without standard deviation) showing the time course of ICP, brain temperature and cerebral oxygenation

During all ventricular infusion studies, no harmful local or systemic side effects occurred during or at any time after the procedure.

Evans index of iNPH patients was on average 0.36 ± 0.06 , that of BIH patients 0.27 ± 0.01 and that of HOC patients 0.37 ± 0.1 . No correlation between the decrease in cerebral temperature or the increase in cerebral oxygenation and ventricular size could be detected.

Discussion

The initial objective to study cerebral oxygenation during infusion studies was to exclude ICP elevation from effectuating further brain violation due to O_2 desaturation. To examine this issue with minimal additional burden for patients, only infusion tests that had to be performed on the ventricular root were considered. Our in-house policy for ventricular infusion studies is using this access in cases of questionable free communication of all CSF spaces, which also includes cases with serious spinal canal stenosis. Furthermore, we favor the ventricular root to avoid an underestimating of the resistance to

outflow in cases of an accidental and hidden CSF leakage due to a needle laceration of the spinal meninges.

Contrary to our initial hypothesis that ICP elevation during infusion studies might harm cerebral oxygenation, we found in 65% of the patients rising pO_2 values during these tests, a clear decrease in oxygenation occurred in only less than 10%. This at first glance unexpected finding may result from a lower O_2 consumption due to reduced cerebral metabolism. The latter might be a consequence of a brain cooling. We hypothesise that the mock CSF at 20°C causes local cooling of the large basal arteries. In this way, the cooling effect is transmitted throughout the whole brain.

The assumption that the artificial ventilation effectuates higher cerebral oxygenation can be disproved by looking at Fig. 1, which demonstrates that at constant ventilation parameters ($FiO_2 = 100\%$) cerebral oxygenation decreases again during the late effusion phase of the infusion test, when cerebral temperature increases. Obviously, cerebral oxygenation directly or indirectly depends on cerebral temperature with metabolism as a link between the two.

A decade earlier, systemic cooling was recommended for ICP control in traumatic brain injury (TBI) with the same underlying pathophysiological concept [1–3, 6, 7]. Yet, due

to harmful systemic side effects [1, 4, 10], such as arrhythmia or pneumonia for example, this option is no longer recommended. The idea of local cooling has already been established in animal experiments using inter alia the application of cold pads [5, 9] with moderate beneficial effect. The major disadvantage of this idea, however, is that craniotomy is required for local cooling. In contrast, our concept of local cooling requires only a ventricular catheter with tip sensor ICP measurement.

Ideally, a two-channel ventricular catheter for parallel infusion and effusion of fluids would be qualified to perform such local cooling. Such modulation of cerebral metabolism might be not only restricted to TBI treatment, but could be useful for any situation with critical cerebral oxygen supply (e.g. cerebral ischaemia, stroke). In particular, penumbra tissue might benefit from such measures.

Conclusion

Whether or not this occasional finding might be a starting point for new strategies to modulate cerebral metabolism requires further detailed studies and significantly larger sample sizes as well as the control whether the effect vanishes when infusing mock-CSF at 37°C. Appropriate studies are on the way.

Conflicts of interest statement M. Schmitt and S. Antes have received financial support for the purposes of education by Codman (Johnson and Johnson Company)/Raynham, MA, USA and Aesculap (Miethke)/Tuttlingen, Germany. R. Eymann and M. Kiefer have received some financial support during the past for other research work by the Raumedic AG/Helmbrechts, Germany.

References

1. De Deyne CS (2010) Therapeutic hypothermia and traumatic brain injury. *Curr Opin Anaesthesiol* 23:258–262
2. Feng JF, Zhang KM, Jiang JY, Gao GY, Fu X, Liand YM (2010) Effect of therapeutic mild hypothermia on the genomics of the hippocampus after moderate traumatic brain injury in rats. *Neurosurgery* 67:730–742
3. Fox JL, Vu EN, Doyle-Waters M, Brubacher JR, Abu-Laban R, Hu Z (2010) Prophylactic hypothermia for traumatic brain injury: a quantitative systematic review. *CJEM* 12:355–364
4. Grände PO, Reinstrup P, Romner B (2009) Active cooling in traumatic brain-injured patients: a questionable therapy? *Acta Anaesthesiol Scand* 53:1233–1238
5. King C, Robinson T, Dixon CE, Rao GR, Larnard D, Nemoto CE (2010) Brain temperature profiles during epidural cooling with the ChillerPad in a monkey model of traumatic brain injury. *J Neurotrauma* 27:1895–1903
6. Kollmar R, Staykov D, Dörfler A, Schellinger PD, Schwab S, Bardutzky J (2010) Hypothermia reduces perihemorrhagic edema after intracerebral hemorrhage. *Stroke* 41:1684–1689
7. Lampe JW, Becker LB (2011) State of the art in therapeutic hypothermia. *Annu Rev Med* 62:79–93
8. Meier U, Künzel B (1988) Computer-assisted model trials of cerebrospinal fluid dynamics of the craniospinal system. *Zentralbl Neurochir* 49:233–237
9. Szczygielski J, Mautes AE, Schwerdtfeger K, Steudel WI (2010) The effects of selective brain hypothermia and decompressive craniectomy on brain edema after closed head injury in mice. *Acta Neurochir Suppl* 106:225–229
10. Waibel BH, Schlitzkus LL, Newell MA, Durham CA, Sagraves SG, Rotondo MF (2009) Impact of hypothermia (below 36 degrees C) in the rural trauma patient. *J Am Coll Surg* 209:580–588

An Uncommon Case of Idiopathic Intracranial Hypertension with Diagnostic Pitfalls

Manuel Mrfka, Karin Pistracher, Bernadette Schöckler, Sonja Wissa, and Senta Kurschel-Lackner

Abstract We report on an unusual case of Idiopathic Intracranial Hypertension (IIH) in a woman of normal weight. Papilledema and increased intracranial pressure are symptoms of cerebral venous sinus thrombosis or idiopathic intracranial hypertension. Because of the different treatment strategies, it is important to keep these two diseases separate. We show that the use of different imaging methods is an important tool in obtaining an effective diagnosis.

Keywords Idiopathic intracranial hypertension (IIH) • Sinus venous thrombosis

Introduction

Idiopathic intracranial hypertension (IIH) is a neurological disorder characterized by raised cerebrospinal fluid (CSF) pressure in the absence of any intracranial pathological features or secondary causes of intracranial hypertension. The pathogenesis of raised intracranial pressure in this condition remains unclear. A multiplicity of factors has been suggested to play a role in the pathogenesis. This includes obesity, sex hormones, prothrombotic abnormality, and CSF dynamics. Although the disorder is not limited to these patients, those most commonly affected are overweight women between the ages of 15 and 45 years [1].

The most common presenting symptoms are headache and papilledema (more than 90% of cases), transient visual obscurations (68%), photopsia (54%) and retrobulbar pain (44%) [2]. The diagnosis of IIH requires imaging of the brain (preferably an MRI), raised CSF pressure with normal CSF constituents and exclusion of other causes of raised CSF pressure. Cerebral venous thrombosis (CVST) must be ruled out using MR venography or CT venography [3].

Case Presentation

A 38-year-old woman of normal weight presented with a 6-month history of persistent headaches. Cranial CT showed no abnormalities. Two months later, she developed photophobia, blurred vision, and intermittent diplopia. Cerebral MRI demonstrated bilateral optic nerve swelling (Fig. 1a) and a small temporo-occipital meningioma, suggesting infiltration and compression of the ipsilateral right transverse sinus (Fig. 1b). Neuro-ophthalmological examination showed normal visual fields and pupillary responses, and funduscopy confirmed bilateral papilledema.

Magnetic resonance venography showed complete occlusion of the right transverse sinus (Fig. 2). Further evaluation of sinus patency with CT venography demonstrated normal flow conditions in all venous sinuses (Fig. 3). Consequently, we performed continuous intraparenchymal ICP monitoring for several days. ICP was elevated between 30 and 50 mmHg.

During monitoring acetazolamide was administered but did not reduce the intracranial pressure levels or stop the headaches, whereas CSF tapping resulted in reduced ICP. Further treatment consisted of the placement of a lumboperitoneal shunt.

Two months later, clinical examination was normal. Follow-up funduscopy revealed bilateral papilledema in regression. One year later no papilledema is detectable.

Discussion

Both conditions – cerebral venous sinus thrombosis and idiopathic intracranial hypertension – may present with identical symptoms, such as papilledema and increased intracranial pressure.

Because of the different treatment strategies, it is important to keep these two diseases separate [4]. The first suspected diagnosis in our case was a sinus venous thrombosis caused by a meningioma, which led to an increased intracranial pressure with papilledema.

M. Mrfka (✉), K. Pistracher, B. Schöckler,
S. Wissa, and S. Kurschel-Lackner
Department of Neurosurgery, Medical University Graz,
Auenbruggerplatz 29, A-8010 Graz, Austria
e-mail: manuel.mrfka@medunigraz.at

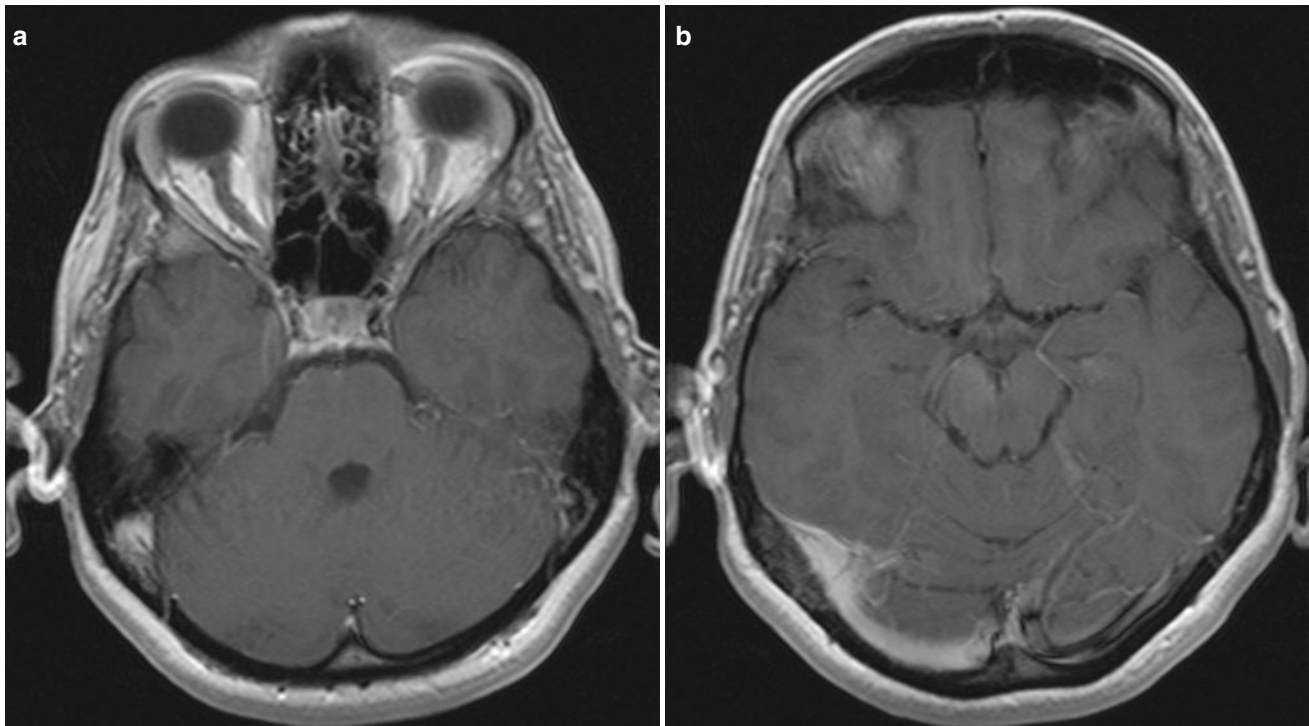


Fig. 1 (a, b): Cerebral MRI demonstrated bilateral optic nerve swelling and a temporo-occipital meningioma

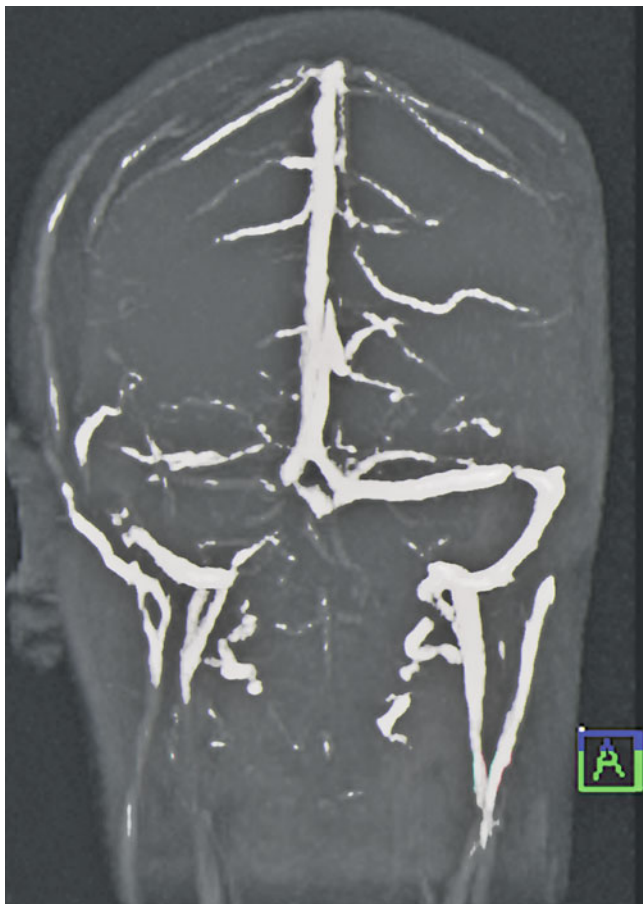


Fig. 2 MR venography showed complete occlusion of the right transverse sinus

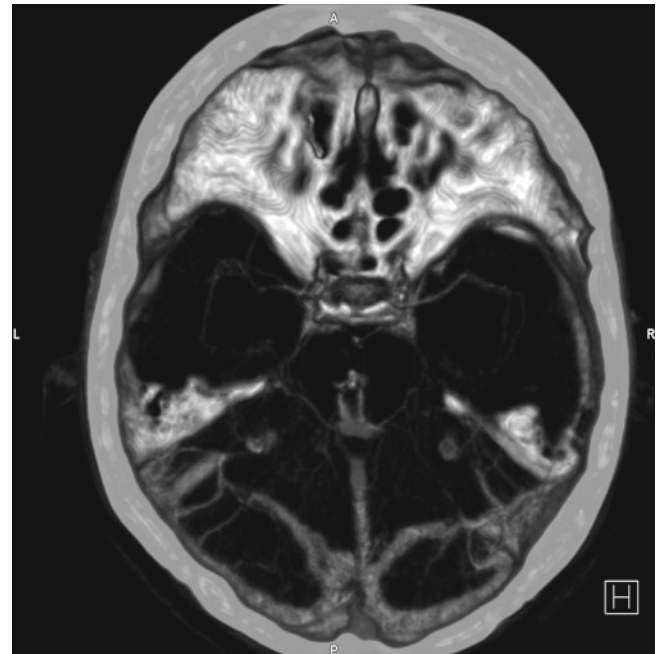


Fig. 3 CT venography demonstrated normal flow conditions in all venous sinuses

The MRV shows the suspected venous sinus thrombosis. However, as seen in the work by Ayanzen et al. [5] transverse sinus flow gaps can be observed in as many as 31% of patients with normal MR imaging findings. This prompted us to carry out further evaluation with CT venography,

which showed, however, normal flow conditions in all sinuses. Therefore, a venous pressure increase is not the cause of the papilledema. The patient was further investigated with ICP measurement. This clearly shows increased intracranial pressure values. Further treatment was carried out as described above.

Conclusion

We present an unusual case of IIH in a woman of normal weight. In addition, we show that the use of different imaging methods is an important tool in obtaining an effective diagnosis.

Conflict of interest statement We declare that we have no conflict of interest.

References

1. Radhakrishnan K, Thacker AK, Bohlega NH, Maloo JC, Gerryo SE (1993) Epidemiology of idiopathic intracranial hypertension: a prospective and case-control study. *J Neurol Sci* 116:18–28
2. Dhungana S, Sharrack B, Woodroffe N (2010) Idiopathic intracranial hypertension. *Acta Neurol Scand* 121:71–82
3. Lin A, Foroozan R, Dansh-Meyer HV, DeSalvo G, Savino PJ, Sergott RC (2006) Occurrence of cerebral venous sinus thrombosis in patients with presumed idiopathic intracranial hypertension. *Ophthalmology* 113:2281–2284
4. Brazis PW (2008) Clinical review: the surgical treatment of idiopathic pseudotumour cerebri (idiopathic intracranial hypertension). *Cephalalgia* 28:1361–1373
5. Ayanzen RH, Bird CR, Keller PJ, McCully FJ, Theobald MR, Heiseman JE (2000) Cerebral MR venography: normal anatomy and potential diagnostic pitfalls. *Am J Neuroradiol* 21:74–78

Micro-fabricated Shunt to Mimic Arachnoid Granulations for the Treatment of Communicating Hydrocephalus

Francis Kralick, Jonghyun Oh, Tim Medina, and Hongseok (Moses) Noh

Abstract Hydrocephalus is the abnormal accumulation of cerebrospinal fluid (CSF) within the confines of the skull that if left untreated results in significant morbidity and mortality. The treatment for hydrocephalus has remained essentially unchanged for over 50 years. It was a technological advance in materials that allowed John Holter, in conjunction with neurosurgeons Spitzer and Nulsen, to devise a valve and shunt system that diverted excess CSF from the ventricular space to the peritoneum. This ventriculo-peritoneal (VP) shunt is far from ideal, with problems associated with under/over shunting, mechanical mismatch, infection, high failure rates, disconnection and erosion. With the advances in the field of micro-fabrication and micro-machines we propose an innovative shunt system that would mimic the function of arachnoid granulations. This micro-fabricated shunting device, or micro-mechanical arachnoid granulation (MAG), consists of a multiplicity of micro-valves each 210 μm in diameter that each adhere to individual micro-needles. This work demonstrates the design and initial test results of the micro-valve with parameters for low cracking pressure, optimal flow rate, and reflux that would mimic the function of the native arachnoid granulations.

Keywords Hydrocephalus • Ventriculo-sino shunts • Micro-fabrication • Micro-valves • Micro-needles • Ventriculo-peritoneal shunt

F. Kralick (✉)
Department of Neurological Surgery, Drexel University
College of Medicine, Hahnemann University Hospital,
231 N. Broad Street, Suite 101 Philadelphia,
PA 19107, USA
e-mail: fkralick@yahoo.com

J. Oh and H.(M.) Noh
Department of Mechanical Engineering and Mechanics,
Drexel University, Philadelphia, PA, USA

T. Medina
College of Medicine, Drexel University, Philadelphia,
PA, USA

Introduction

Current treatment for communicating hydrocephalus involves diversion of CSF from the ventricular spaces to another non-physiological site of absorption, most commonly the peritoneum. This system has remained essentially unchanged for over 50 years as the result of the work of Holter, Spitz, and Nulsen [2]. While this has saved many lives difficulties with imprecise shunting and high failure rates make it a far from perfect system. Imprecise shunting is most likely due to the mechanical mismatch between the proximal (ventricular) and distal (peritoneal) pressure differential especially with postural changes from recumbent to standing. Failure rates of 50% at 2 years and 95% at 5 years have been cited. In addition to imprecise shunting, failure due to infection, clogging, disconnection, and a growing child are encountered. Different valve designs and the introduction of programmable valves have demonstrated no significant advantage [3]. The annual cost of CSF shunts in the United States is approximately a billion dollar per year [11].

We proposed an innovative CSF diversion device consisting of a micro-fabricated array of a plurality of micro-valves in conjunction with micro-needles. This device would be surgically placed with the proximal opening or inlet in the subarachnoid space (SAS; Fig. 1). The distal opening or outlet would be located in the superior sagittal sinus (SSS) [4, 6–10, 13, 14]. The micro-needles would act as the conduit that pierces the dura comprising the wall of the SSS. The micro-valves at the base of the micro-needle function as simple flap valves, opening and closing in response to the pressure differential between the SAS and SSS. In this way we can mimic the physiological location and function of native arachnoid granulations [1, 5, 12]. This work focuses on the design of the micro-valve with parameters for low cracking pressure, optimal flow rate and reflux that would be required to mimic the function of the native arachnoid granulations. Several micro-valve designs were tested for flow utilizing a bench-top pressure rig to test flow rates given different pressures in the forward and reverse directions.

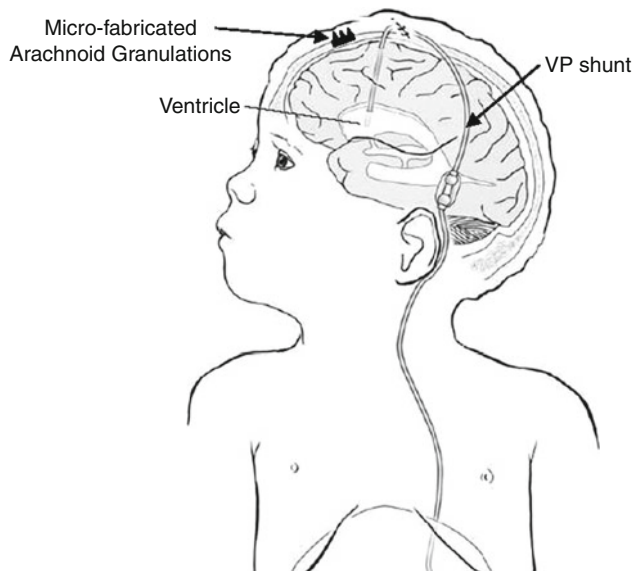


Fig. 1 Diagram of current VP shunt with proposed site of implantation of micro-fabricated arachnoid granulations (micro-valve/micro-needle) in the wall of the superior sagittal sinus (SSS)

Materials and Methods

The micro-fabricated device was designed to adhere a passive valve system to each individual micro-needle (Fig. 2). 7×7 and 10×10 arrays of micro-valves were designed within

an area of $5 \times 5 \text{ mm}^2$. The desired valve performance was $0.3\text{--}0.5 \text{ mL/min}$ at a pressure range of $500\text{--}1,500 \text{ Pa}$. Valve diameter, thickness of membrane, and opening shape were the main parameters that were varied. The micro-valve was made of composite layers of polydimethylsiloxane (PDMS) and polyparaxylylene (Parylene). First, dome-shaped molds were fabricated by the diffuser photolithography process. A negative photoresist, SU-8 2035, was spin coated on a Cr patterned glass plate. This substrate was then placed upside down and exposed to UV light through a diffuser glass plate that has opal on one side. The dome-shaped SU-8 patterns were then obtained through post-exposure bake and developing. Next, PDMS and Parylene were coated onto the mold to the desired thickness via spin coating and vapor phase deposition respectively. It turned out that the thickness ratio between PDMS and Parylene is very important to minimize wrinkle formation in the composite layers. PDMS was thick ($\sim 70 \text{ }\mu\text{m}$) at the bottom of the valve, but very thin (a few microns) at the top. Parylene thickness was uniform ($10 \text{ }\mu\text{m}$). Finally, laser micro-machining was used to cut open the micro-valves. KrF excimer laser (wave length = 248 nm) was used for this purpose and the ablation gap size of the valve was about $6 \text{ }\mu\text{m}$.

Bench flow testing of the cross cut slit and the single slit was investigated. Figure 3 shows the flow test set-up that consists of two flow chambers that simulate SAS and SSS, a pressure transducer (maximum 1 psi, Omega Co., Ltd,

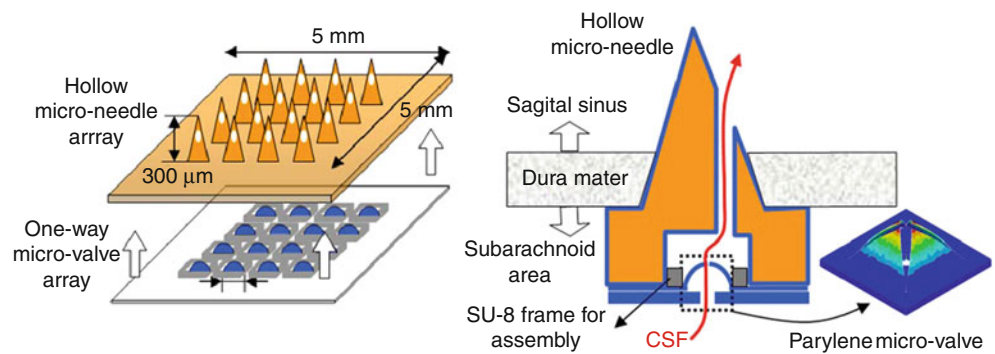


Fig. 2 Close-up of micro-needles and micro-valve: array (left) and single (right) device

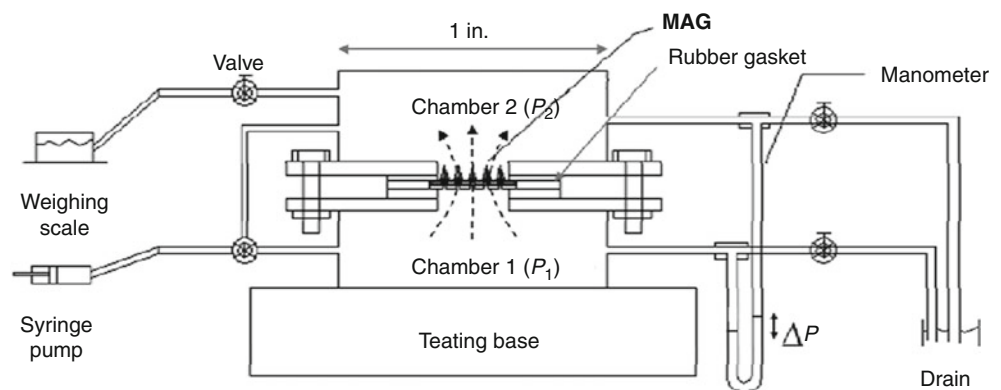


Fig. 3 Diagram of flow testing apparatus

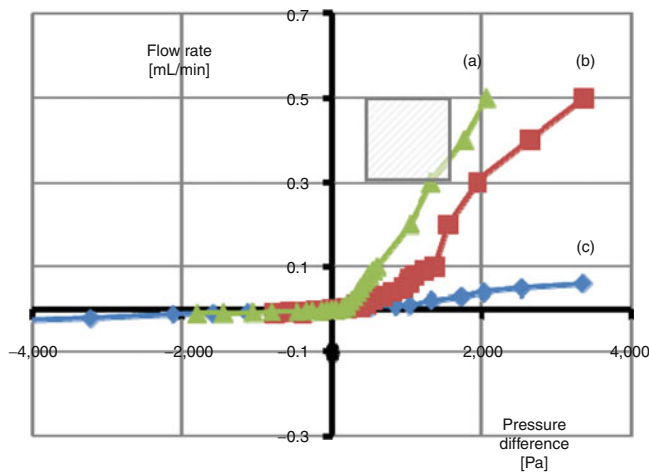


Fig. 4 Graph demonstrating flow characteristics in response to pressure for 10×10 array micro-valves with a $210\text{-}\mu\text{m}$ diameter: (a) cross-cut opening ($210 \times 60\text{ }\mu\text{m}$), (b) cross-cut opening ($210 \times 30\text{ }\mu\text{m}$), and (c) slit-cut opening ($210\text{ }\mu\text{m}$). Hatched area indicates desired working region

Stamford, CT, USA), a read-out, and a syringe pump. The micro-valves to be tested were tightly fixed to the test chamber using a PDMS gasket to ensure sealing. Differential pressures between the top and bottom sides of the micro-valve were measured under various flow rate conditions. The range of pressure difference measured in this test was between 0 and 8 kPa at a flow rate of up to 0.8 mL/min. Pressure difference for forward and backward flows was measured after the flow reached steady-state. To obtain reverse flow data, the valve was simply switched to the opposite direction. The flow test was repeated five times for measuring the characteristics of each valve. None of the valves was deformed after several tests.

Results

The flow test results of 10×10 array micro-valves are shown in Fig. 4. Positive pressure differential indicates forward flow and negative pressure differential backward flow. The slope of the curve is inversely proportional to the flow resistance of the device. Cracking pressure is the pressure at which fluid begins to flow in a forward direction. An ideal micro-valve for the treatment of hydrocephalus needs to have a cracking pressure close to zero, a forward flow rate of $0.3\text{--}0.5\text{ mL/min}$ at pressure differences between 500 and 1,500 Pa, as marked as a hatched area in the Fig. 4.

Three different designs are compared in the graph:

- (a) Cross-cut opening ($210 \times 60\text{ }\mu\text{m}$)
- (b) Cross-cut opening ($210 \times 30\text{ }\mu\text{m}$)
- (c) Slit-cut opening ($210\text{ }\mu\text{m}$)

Initially, we designed only two valves: slit-cut and cross-cut. It was found from the initial experiment that the slit-cut opening provides a better flow rectification (better sealing in backward flows) and the cross-cut opening provides a higher flow rate in forward flows. Based on the initial result we designed intermediate opening shapes. These can be called partially cross-cut openings ($210 \times 60\text{ }\mu\text{m}$ and $210 \times 30\text{ }\mu\text{m}$). It was found that these partially cross-cut designs have better flow rectification performance than slit-cut or fully cross-cut designs. Curve (a) shows a low cracking pressure, significant forward flow (part of the curve passes through the desired working zone of the micro-valve), and a negligible backward flow (the maximum backward flow was not detected within the pressure differential range used in this experiment).

Among the various designs tested in our experiments, curve (a) in Fig. 4 can be selected as the optimal micro-valve design with the valve performance mimicking arachnoid granulations. This valve has quick opening for forward flow (low cracking pressure) and a better sealing effect for backward flow. Also, the flow slope ($0.25\text{ }\mu\text{L/Pa}\cdot\text{min}$) of this micro-valve array passes through the desired working zone of arachnoid villi (forward flow rate of $0.3\text{--}0.5\text{ mL/min}$ at a pressure difference between 500 and 1,500 Pa).

Discussion

The need for a new “smart shunt” to treat hydrocephalus to replace the current system of a single valve/tube system has been recognized. We have proposed an innovative micro-fabricated system consisting of a plurality of the micro-valves in conjunction with micro-needles with the proximal end located in the SAS and the distal end in the SSS. We have successfully designed and fabricated a valve to be used in such a system that meets the flow criteria and prevents backflow by using a simple flap valve design that is $210\text{ }\mu\text{m}$ in diameter. This simple micro-system micro-fabricated device can respond to alterations in the pressure gradient between the SAS and the SSS. This obviates the need for power or complex microprocessors. The value of shunting between these two areas eliminates the imprecise shunting that is seen with current VP shunts that are in common use today. The disparity between the pressure differential while standing and recumbent is eliminated.

Previous shunts have placed the distal end into the SSS with some success; however, current VP shunt tubing is used and can cause problems of sinus damage and sinus thrombosis. We hope to avoid this problem by replacing a single 3- to 4-mm silastic tube with the tip of many micro-needles that would project into the SSS only a few microns. The plurality of the device reflects the presence of many arachnoid granulations and provides redundancy for the system. That is, if

one valve fails or becomes clogged with debris then there will be continued flow. This eliminates the higher clogging rates of a single tube and valve design. Current work is focusing on micro-needle design that is capable of piercing the dura, forming the wall of the SSS without damage. Effects of fibrosis, thrombosis, and toxicity are also under investigation. The proposed site of implantation is along the SSS anterior to the rolandic vein. In the event of damage to the SSS, it can be occluded without neurological deficit.

This micro-system is small enough to function within the confines of the skull for protection, which also avoids current problems with disconnection, fracture, and the need for lengthening a VP shunt in a growing child. A domed petal shape with a diameter of 210 μm with a transverse opening and small center slit demonstrated low cracking pressure, and flow rates between 0.3 and -0.5 at pressures between 0 and $-2,000$ Pa. It also showed no reflux in the reverse direction to $-2,000$ Pa.

The above-described initial flow test result is very promising. We are currently performing a more comprehensive parametric study to optimize the micro-valve design through numerical simulation and experiments. Micro-needle arrays are also under development for integration with the micro-valves.

Conclusion

A novel PDMS/Parylene composite 10 x 10, 5x5 mm array micro-valves with a 3-D dome petal shape has been successfully designed, fabricated, and tested for incorporation into a shunt from the subarachnoid space to the superior sagittal sinus for the treatment of hydrocephalus.

New micro-fabrication techniques such as dome-shaped SU-8 mold fabrication and laser machining for valve opening have been utilized to make the proposed micro-valves. Diverse micro-valve designs were tested to achieve the desired flow characteristics. Partial cross-cut designs showed satisfactory performance, including low cracking pressure, sufficient forward flow, and negligible backward flow. The slit-cut opening provides a better flow rectification capability, while a cross-cut opening provides a lower cracking

pressure and flow resistance. The initial flow test results are encouraging and several important insights regarding micro-valve design have been obtained.

Conflict of interest statement We declare that we have no conflict of interest.

References

1. Aizenberg J et al (2004) Biological and bioinspired materials and devices, vol 823. In: Materials Research Society symposium proceedings, Warrendale, 2004
2. Boockvar JA, Loudon W, Sutton LN (2001) Development of the Spitz-Holter valve in Philadelphia. *J Neurosurg* 95:145–147
3. Drake JM, Destle J, Milner R et al (1998) Randomized trial of cerebrospinal fluid shunt valve design in pediatric hydrocephalus. *Neurosurgery* 43:294–305
4. Gardeniers JGE, Luttge R, Berenschot JW, de Boer MJ, Yeshurun Y, Hefetz M, van't Oever R, van der Berg A (2003) Silicon micro-machined hollow needles for transdermal liquid transport. *J Microelectromech Syst* 6(1):855–862
5. Grzybowski DM, Holman DW, Katz SE, Lubow M (2006) In vitro model of cerebrospinal fluid outflow through human arachnoid granulations. *Invest Ophthalmol Vis Sci* 47(8):3664–3672
6. Henry S, McAllister DV, Allen MG, Prausnitz MR (1998) Microfabricated microneedles: a novel approach to transdermal drug delivery. *J Pharm Sci* 87(8):922–925
7. Lin L, Pisano AP (1999) Silicon-processed microneedles. *J Microelectromech Syst* 8(1):78–84
8. Lizhofer A, Ritter B, Tsakmakis Ch (1995) Development of passive microvalves by the finite element method. *J Microelectromech Microeng* 5:226–230
9. Noh H-S, Huang Y, Hesketh PJ (2004) Parylene micromolding, a rapid and low-cost fabrication method of parylene microchannel. *Sens Actuators B Chem* 102:78–85
10. Noh H-S, Moon K-S, Cannon A, Hesketh PJ, Wong CP (2004) Wafer bonding using microwave heating of parylene intermediate layers. *J Micromech Microeng* 14:625–631
11. Patwardhan RV, Nanda A (2005) Implanted ventricular shunts in the United States: the billion-dollar-a-year cost of hydrocephalus treatment. *Neurosurgery* 56(1):139–145
12. Upton ML, Weller RO (1985) The morphology of cerebrospinal fluid drainage pathways in human arachnoid granulations. *J Neurosurg* 63(6):867–875
13. Wang X-Q, Tai Y-C (2000) A normally closed in-channel micro check valve. In: The thirteenth annual international conference on MEMS, Miyazaki, 2000, pp 68–73
14. Wang X-Q, Lin Q, Tai Y-C (1999) A Parylene micro check valve. In: The twelfth IEEE international conference on MEMS, Orlando, 1999, pp 177–182

On the Method of a Randomised Comparison of Programmable Valves with and Without Gravitational Units: The SVASONA Study

Johannes Lemcke, Ullrich Meier, Cornelia Müller, Michael Fritsch, Michael Kiefer, Regina Eymann, Uwe Kehler, Niels Langer, Martin U. Schuhmann, Andreas Speil, Friedrich Weber, Victor Remenez, Veit Rohde, Hans-Christoph Ludwig, and Dirk Stengel

Abstract Objective: The supremacy of low-pressure valves (LPV) in the therapy of patients with idiopathic normal pressure hydrocephalus (iNPH) has been proven by the Dutch NPH study. The downside of LPVs is the high rate of overdrainage complications. In the meantime gravitational units have been developed with the objective of minimising overdrainage complications. Do these gravitational units allow the same favourable outcomes as in the Dutch NPH study without overdrainage complications? The goal of this prospective randomised controlled multicentre trial is to compare the rate of overdrainage complications after shunt surgery with programmable valves with or without a gravitational unit.

Method: Patients suspected with iNPH with gait ataxia and one or two other symptoms of Hakim's triad and enlarged ventricles on CT or MRI underwent a cerebrospinal fluid (CSF) infusion test, CSF tap test and/or continuous ICP measurement in seven experienced centres. If iNPH was diagnosed the patients were randomised to receive a ventriculoperitoneal shunt with a

programmable valve with or without a gravitational unit. The patients were followed up for 3, 6 and 12 months after surgery. The primary hypothesis of the study was that programmable valves with gravitational units will reduce the rate of overdrainage from 25% to 10%. The outcome measured by iNPH-specific outcome scales (Kiefer score, Black grading scale) and the generic quality of life (short form 12, SF12) was defined as the secondary endpoint. To detect the hypothesised difference in the incidence of overdrainage with a type I error of 5% and a type II error of 20%, correcting for multiple testing and an anticipated drop-out rate of 10%, we planned to enrol 250 patients. To ensure safety and efficacy we performed a planned interim analysis halfway.

Results: The study design has been found to be effective with regard to the primary hypothesis.

Conclusion: The design of the SVASONA study was developed to be able to confirm the primary hypothesis. Thus, the method of the study should solve the dilemma of the Dutch NPH study by the randomised comparison of LPVs with and without gravitational units.

Keywords Idiopathic normal pressure hydrocephalus • Controlled randomised study • Programmable valves • Gravitational units • Overdrainage

J. Lemcke (✉) and U. Meier

Department of Neurosurgery, Unfallkrankenhaus, Berlin, Germany
e-mail: johannes.lemcke@ukb.de

C. Müller and M. Fritsch

Department of Neurosurgery, Ernst-Moritz-Arndt-University of Greifswald, Greifswald, Germany

M. Kiefer and R. Eymann

Department of Neurosurgery, Saarland Medical University, Homburg/Saar, Germany

U. Kehler and N. Langer

Department of Neurosurgery, Asklepios Hospital Altona, Hamburg, Germany

M.U. Schuhmann and A. Speil

Department of Neurosurgery, Eberhard-Karls-University of Tübingen, Tübingen, Germany

F. Weber and V. Remenez

Department of Neurosurgery, Hospital Cologne-Merheim, Cologne-Merheim, Germany

V. Rohde and H.-C. Ludwig

Department of Neurosurgery, Georg-August-University of Göttingen, Göttingen, Germany

D. Stengel

Center for Clinical Research, Unfallkrankenhaus, Berlin, Germany

Background

The idiopathic normal pressure hydrocephalus (iNPH) is a neurodegenerative disorder that has a severe impact on patients' daily lives. A typical gait ataxia, urinary incontinence and mnemonic disturbances as far as dementia are found together with dilated ventricles in the absence of increased intracranial pressure. Recent findings suggest that the entity is a complex disorder of cerebral blood flow and possibly senescent changes in CSF physiology rather than a simple mismatch of CSF production and resorption [1].

Although surgical therapy with ventriculoperitoneal shunts (vp shunts) can provide symptomatic relief, compromises had to be accepted as there is evidence that LPVs lead to a better outcome than medium pressure valves, but also

cause overdrainage complications such as subdural hygromas in a large percentage of patients [2]. The underlying problem is the different hydrostatic pressure in a vp shunt in the upright and the horizontal position. Gravitational units have been constructed to face this effect by switching between a low pressure mode in the horizontal and a high pressure mode in the upright position.

Gravitational units are ball-in-cone valves. The closing force is applied by a weighted sliding ball that works on the valve ball if the device is moved into the upright position [3].

At present there is no proof of the efficiency of gravitational units in direct comparison to differential pressure valves.

This study was designed as a randomised comparison of LPVs without gravitational units with LPVs with gravitational units. The primary end point was to examine whether programmable shunt valves in a low pressure adjustment with or without gravitational units are more effective in avoiding overdrainage complications. The secondary end point was the outcome as measured by specific iNPH scales and the quality of life as measured by the short form 12 (SF 12).

Thus, the study continues the approach of the Dutch NPH study at the same evidence level.

Materials and Methods

Study Design/Sample Size Calculation

In order to compare LPV with or without gravitational units, patients were randomly allocated to two treatment groups. To increase patients' safety, programmable valves were used. The valves were implanted with an opening pressure of 100 mmH₂O. Three months after surgery, the valves were adjusted into the low pressure range (70 mmH₂O). As there is no precisely programmable valve commercially offered with or without a gravitational unit, Group I received proGAV valves (Aesculap/Miethke, Potsdam, Germany) and Group II received Codman Medos programmable valves (CMPV, Codman, Johnson & Johnson) [4, 5].

To achieve significant results, a sample of 250 patients was calculated. An interim analysis was planned after recruitment of 57 patients in each group, if the experimental device were to produce a statistically significant advantage over the control treatment. It was planned that the study would be stopped in this case.

Enrolment Criteria

The inclusion criteria were:

1. A gradually developed gait disturbance in both legs, unexplained by other conditions, and at least one other symptom of Hakim's triad;

Inclusion	Exclusion
<ul style="list-style-type: none"> • Idiopathic NPH • Older than 80 years • legally competent to sign 	<ul style="list-style-type: none"> • Secondary NPH • life expectance <24 months • Severe dementia • Older than 18 years

Fig. 1 Recruitment criteria

2. A CT showing communicating hydrocephalus with an Evans' index of at least 0.3 clinically relevant parenchymal lesions;
3. A positive lumbar infusion test and/or a positive spinal tap test and/or a positive B-wave analysis.

Exclusion criteria included any of the following: a secondary NPH, patient aged 80 years or older, severe comorbidity with a life expectancy restricted to less than 12 months, or contraindications for surgery (Fig. 1) [6].

Results

Surgery

All patients underwent implantation of a vp shunt with either a proGAV or a CMPV. In every centre only three experienced surgeons who were accredited for the study performed the operations.

Randomisation

An independent biostatistician (DS) who was not involved in recruitment randomly allocated the patients to the treatment groups. The randomisation results were in closed envelopes and were opened by the particular surgeons in the operating theatre directly before shunt surgery.

Outcome Measures/Follow-up Examinations

Clinical assessment including the Kiefer score and the SF12 was conducted before and 6 and 12 months after surgery. The NPH recovery rate was calculated from the Kiefer score. CTs were performed preoperatively, at the time of discharge, and after 3, 6 and 12 months (Fig. 2).

The first end point of the study was overdrainage, defined as subdural hygromas or subdural haematomas of at least 3 mm or clinical signs of overdrainage that led to

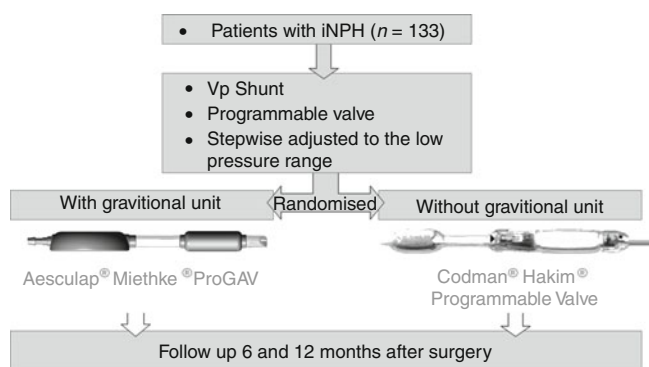


Fig. 2 Study design

readjustment of the valve to 90 mmH₂O or more in both groups, or back-fitting of a gravitational unit in the patients of group II.

Role of the Funding Source

The sponsor had no role in the study design, data collection, data analysis, data interpretation, or writing of this report. UM, JL and DS had full access to all the data in the study and have final responsibility for publication and presentation.

Discussion

The Dutch NPH Study

There are only very few high-level iNPH studies according to the principles of evidence-based medicine. One of these studies is the Dutch NPH study, which was conducted in the early 1990s [2, 7–11]. The Dutch NPH study proved the hypothesis that shunt valves with a low opening pressure lead to better results in the therapy of iNPH patients. As in that era the opening pressure was the only adjustable parameter, this was a very important finding. Beyond that, the study was methodically unassailable.

However, the dilemma of the result was that the excellent results with LPVs were overshadowed by high rates of overdrainage complications.

The aim of the study was to assess whether LPV with gravitational units are able to achieve the same preferable outcome results proven for LPV without gravitational units in the Dutch NPH study, and without overdrainage complications.

SVASONA Study Design

To allow a stepwise adaptation of the brain to the new CSF dynamics after shunting and to have additional security in

the case of complications, we did not use simple LPV, but programmable valves adjusted to a low opening pressure. There are no manufacturers offering programmable valves with and without a gravitational unit. As the programming unit of the proGAV, which represents the low pressure unit, active in the horizontal position, has the same hydrodynamic characteristics as the CMPV, we decided to compare these two devices [12, 13]. This might be seen as a weak point of the study. We think that this comparison is pragmatic and reflects the real opportunities.

It is not an aim of the study to examine other hydrostatic devices such as the anti-siphon device or to compare the two different valves.

Multicentre Conception

The iNPH is a disease with a low incidence of about 5.5 in 100,000 inhabitants [14]. Thus, specialised centres in Germany treat between 20 and 30 new patients per annum. According to the sample size calculation, 250 patients were needed to achieve significant results. Against this background, the only realistic option was a multicentre study. This caused heterogeneity of the diagnostic pathways used in the centres. Nevertheless, all patients enrolled in the study passed through at least one type of invasive liquor dynamic diagnostics. All centres have major experience with diagnostic and treatment of the iNPH. Thus, there is adequate security that one consistent entity has been treated in this study.

Conclusion

The design of the SVASONA study was developed to be able to confirm the primary hypothesis. Thus, the method used in the study should solve the dilemma of the Dutch NPH study by the randomised comparison of LPVs with and without gravitational units.

Conflicts of interest statement The study has been conducted as an investigator-initiated trial and has been monitored by the centre of clinical research ukb, represented by DS. All participants have received grants per enrolled patient from B. Braun Aesculap, Melsungen, Germany.

References

- Greitz D (2007) Paradigm shift in hydrocephalus research in the legacy of Dandy's pioneering work: rationale for third ventriculostomy in communicating hydrocephalus. *Childs Nerv Syst* 23(5):487–489
- Boon AJ, Tans JT, Delwel EJ, Egeler-Peerdeman SM, Hanlo PW, Wurzer HA et al (1998) Dutch normal-pressure hydrocephalus study: randomized comparison of low- and medium-pressure shunts. *J Neurosurg* 88(3):490–495

3. Meier U, Kiefer M, Sprung C (2004) Evaluation of the Miethke dual-switch valve in patients with normal pressure hydrocephalus. *Surg Neurol* 61(2):119–127
4. Lemcke J, Meier U (2010) Improved outcome in shunted iNPH with a combination of a Codman Hakim programmable valve and an Aesculap-Miethke ShuntAssistant. *Cen Eur Neurosurg* 71(3):113–116
5. Meier U, Lemcke J (2006) First clinical experiences in patients with idiopathic normal-pressure hydrocephalus with the adjustable gravity valve manufactured by Aesculap (proGAV(Aesculap)). *Acta Neurochir Suppl* 96:368–372
6. Meier U, Bartels P (2001) The importance of the intrathecal infusion test in the diagnostic of normal-pressure hydrocephalus. *Eur Neurol* 46(4):178–186
7. Tans JT, Boon AJ (2002) How to select patients with normal pressure hydrocephalus for shunting. *Acta Neurochir Suppl* 81:3–5
8. Boon AJ, Tans JT, Delwel EJ, Egeler-Peerdeman SM, Hanlo PW, Wurzer HA et al (2000) The Dutch normal-pressure hydrocephalus study. How to select patients for shunting? An analysis of four diagnostic criteria. *Surg Neurol* 53(3):201–207
9. Boon AJ, Tans JT, Delwel EJ, Egeler-Peerdeman SM, Hanlo PW, Wurzer HA et al (1999) Dutch normal-pressure hydrocephalus study: the role of cerebrovascular disease. *J Neurosurg* 90(2): 221–226
10. Boon AJ, Tans JT, Delwel EJ, Egeler-Peerdeman SM, Hanlo PW, Wurzer JA et al (1998) Does CSF outflow resistance predict the response to shunting in patients with normal pressure hydrocephalus? *Acta Neurochir Suppl* 71:331–333
11. Boon AJ, Tans JT, Delwel EJ, Egeler-Peerdeman SM, Hanlo PW, Wurzer HA et al (1997) Dutch normal-pressure hydrocephalus study: prediction of outcome after shunting by resistance to outflow of cerebrospinal fluid. *J Neurosurg* 87(5):687–693
12. Oikonomou J, Aschoff A, Hashemi B, Kunze S (1999) New valves – new dangers? 22 valves (38 probes) designed in the ‘nineties in ultralong-term tests (365 days)’. *Eur J Pediatr Surg* 9(Suppl 1): 23–26
13. Aschoff A, Kremer P, Benesch C, Fruh K, Klank A, Kunze S (1995) Overdrainage and shunt technology. A critical comparison of programmable, hydrostatic and variable-resistance valves and flow-reducing devices. *Childs Nerv Syst* 11(4):193–202
14. Brean A, Eide PK (2008) Prevalence of probable idiopathic normal pressure hydrocephalus in a Norwegian population. *Acta Neurol Scand* 118(1):48–53

Idiopathic Normal Pressure Hydrocephalus: Results of a Prospective Cohort of 236 Shunted Patients

Maria Antonia Poca, Elisabeth Solana, Francisco Ramón Martínez-Ricarte, Mónica Romero, Dario Gándara, and Juan Sahuquillo

Abstract *Aim:* To describe the outcomes and complication rates in 236 patients with idiopathic normal pressure hydrocephalus (INPH) after treatment.

Patients and Methods: Among a cohort of 257 patients with suspected INPH, 244 were shunted and 236 were followed up at 6 months after shunting (145 men [61.4%] and 91 women [38.6%] with a median age of 75 years). The study protocol of these patients included clinical, radiological, neuropsychological and functional assessment. The decision to shunt patients was based on continuous intracranial pressure monitoring and CSF dynamics studies. A differential low-pressure valve system, always combined with a gravity compensating device, was implanted in 99% of the patients.

Results: After shunting, 89.9% of the patients showed clinical improvement (gait improved in 79.3% of patients, sphincter control in 82.4%, and dementia in 63.7%). Two patients (0.8%) died. Early postsurgical complications were found in 13 of the 244 shunted patients (5.3%). Six months after shunting, the follow-up CT showed asymptomatic hygromas in 8 of the 236 (3.4%). Additional postsurgical complications were found in 7 patients (3%), consisting of 6 subdural hematomas (3 acute and 3 chronic) and 1 distal catheter infection.

Conclusions: Currently, a high percentage of patients with INPH can improve after shunting, with early and late complication rates of less than 12%.

Keywords Normal pressure hydrocephalus syndrome • Idiopathic normal pressure hydrocephalus • Adult chronic hydrocephalus • Outcome • Complication rates

Introduction

Normal pressure hydrocephalus (NPH) is one of the few conditions that can cause reversible cognitive and motor worsening in the elderly and, consequently, it is of great importance to establish an accurate diagnosis and to apply the correct treatment in these patients. Although the pathophysiology of NPH is still not fully understood, the recognized abnormalities in cerebrospinal fluid (CSF) reabsorption associated with age [1] have increased the interest in this pathological condition because of the extended life expectancy. Guidelines for the diagnosis and management of idiopathic normal pressure hydrocephalus (INPH), which have had a large following in the last few years, were published in 2005 [12]. However, INPH is a pathological condition that is not yet free from controversy.

In these guidelines, it is recognized that improvement rates after treatment have been obtained mainly from limited retrospective studies and that the best results were obtained in patients with the complete clinical triad and/or predominating gait disturbance associated with “typical” radiological criteria (obliterated or normal cortical sulci size and periventricular lucencies). In these patients the improvement rates were fairly consistent, ranging from 61% to 75% [9]. However, previous studies from our group have demonstrated that higher percentages of improvement (almost 90%) are also possible in patients with several factors traditionally associated with unfavorable outcome: the idiopathic form, prolonged disease duration, the presence of cerebral atrophy, severe dementia, incomplete clinical triad, and absence of periventricular lucencies [16, 18]. According to the guidelines, some of these

M.A. Poca (✉), J. Sahuquillo, and F.R. Martínez-Ricarte
Department of Neurosurgery, Vall d’Hebron University Hospital and
Vall d’Hebron Research Institute, Universitat Autònoma de Barcelona,
Passeig Vall d’Hebron 119-129, 08035 Barcelona, Spain

Neurosurgery and Neurotraumatology Research Unit, Vall d’Hebron
University Hospital and Vall d’Hebron Research Institute, Universitat
Autònoma de Barcelona, Barcelona, Spain
e-mail: pocama@neurotrauma.net

E. Solana

Neurosurgery and Neurotraumatology Research Unit, Vall d’Hebron
University Hospital and Vall d’Hebron Research Institute, Universitat
Autònoma de Barcelona, Barcelona, Spain

M. Romero and D. Gándara

Department of Neurosurgery, Vall d’Hebron University Hospital and
Vall d’Hebron Research Institute, Universitat Autònoma de Barcelona,
Passeig Vall d’Hebron 119-129, 08035 Barcelona, Spain

patients have been included in the category of “possible INPH” and probably not treated.

The main aim of this study was to determine the outcomes and complication rates in a large prospective series of 236 patients with idiopathic NPH 6 months after treatment, using continuous intracranial pressure (ICP) monitoring as the key diagnostic tool. We also looked at whether the management of these patients would have been different if we had followed the diagnostic algorithms proposed in the guidelines.

Materials and Methods

Patients and General Management Protocol of Suspected INPH

Between March 1998 and June 2007, 257 consecutive patients with suspected INPH syndrome were evaluated in the Department of Neurosurgery at Vall d’Hebron University Hospital by two of the authors (MAP and JS). The protocol for the evaluation and management of NPH patients in our department has been published elsewhere [14, 15, 19]. All patients had an increase in ventricular size (Evans’ Index ≥ 0.30) on CT or magnetic resonance imaging (MRI) and at least two of the following symptoms, unexplained by other neurological or non-neurological conditions: gait dysfunction, sphincter incontinence, cognitive impairment, and/or parkinsonism refractory to medical treatment. Complementary neuropsychological examination and several rating scales to record the patient’s functional behavior and to assess the degree of dependence for activities of daily living were also used. The decision to shunt patients was based on continuous intracranial pressure (ICP) monitoring and/or study of CSF dynamics [16, 18, 19]. Informed consent for all aspects of the study was obtained from each patient or a close relative.

Clinical Assessment: NPH Scale, Length of Step, Walking Speed, and Functional Status

In all patients, the three main symptoms of the disease, gait, sphincter control and cognitive functioning, were evaluated according to the NPH Scale (Table 1) [19]. This scale evaluates the severity of gait, cognitive, and sphincter disturbances. The minimum possible score on this scale is 3 points, which indicates that the patient is bedridden or unable to walk, has no contact with the environment and has urinary and fecal incontinence (vegetative or in a state of minimal consciousness). The maximum score of 15 points indicates that the patient has normal gait, no objective or subjective sphincter dysfunction, and that cognitive disturbances are only found

Table 1 Normal pressure hydrocephalus (NPH) scale used to assess the clinical triad [19]

	Score
1. <i>Gait evaluation (GE)</i>	
Patient is bedridden or unable to ambulate	1
Ambulation is possible with help	2
Independent walking is possible but unstable or the patient falls	3
Abnormal but stable gait	4
Normal gait	5
2. <i>Cognitive functions (CF)</i>	
Patient is vegetative or in a state of minimal consciousness	1
Severe dementia	2
Severe memory problems with behavior disturbances	3
Memory problems reported by patient or family	4
Cognitive disturbances are only found by specific tests	5
3. <i>Sphincter Disturbances (SD)</i>	
Urinary and fecal incontinence	1
Continuous urinary incontinence	2
Sporadic urinary incontinence	3
Urinary urgency	4
No objective or subjective sphincter dysfunction	5

NPH Score = GE + CF + SD. Minimum possible score = 3 points. Maximum score = 15 points

by specific neuropsychological tests. Clinical assessment also included the evaluation of step length and walking speed in the last 202 patients who were included in the study. To calculate the step length and walking speed, the patient was asked to walk 5 m at a normal pace and the number of steps and the time required were calculated. Two attempts were made. The mean speed was calculated by dividing the meters walked by the seconds required (m/s) and the mean step length was calculated by dividing 500 cm walked by the number of steps taken. Normal values for these parameters were previously obtained from a control group of 30 healthy subjects aged 65–90 years: mean step length was 51.9 ± 8.3 cm (range 38.5–71.4 cm), and the mean walking speed was 0.89 ± 0.3 m/s (range 0.48–1.67 m/s) [20].

Each patient and a close relative were also given several rating scales to record the patient’s functional behavior and to assess the degree of dependence for activities of daily living: the Rapid Disability Rating Scale-2 (RDRS-2) [10], a modified Stein and Langfit Scale [3], and the Everyday Activities scale [5].

ICP Monitoring and CSF Dynamics Studies

In 223 of the 236 patients, continuous ICP was monitored using an extradural device [17]. The presence of A-waves and B-waves [11] was evaluated and expressed as the percentage

Table 2 Type of shunt, clinical improvement, and complications ($n=236$)

	Patients	(%)
<i>Type of shunt</i>		
Programmable Hakim Medos valve ^a +low-pressure gravity compensating accessory (GCA) ^b	68	28.8
Delta valve (performance level of 0.5) with antisiphon device ^c	52	22.0
Ventriculo-peritoneal catheter with a low-pressure GCA ^b	43	18.2
Dual Swith Mietke ^d 5/30, 5/40, 5/50 ^e	47	19.9
Hakim Medos valve (closing pressure range 40 ± 10 mmH ₂ O) ^b	15	6.4
Hakim Medos valve (closing pressure range 10 ± 10 mmH ₂ O) ^b	5	2.1
Low-pressure Novus valve with an antisiphon ^f	3	1.3
Medium-pressure Novus valve with an antisiphon ^f	3	1.3
<i>Clinical improvement</i>		
Increase of 1 point in the total NPH scale (<i>moderated improvement</i>)	30	12.7
Increase of >1 point in the total NPH scale (<i>marked improvement</i>)	182	77.1
No improvement	18	7.6
Some worsening	6	2.5
Improvement in every day activities scale ($n=195$)	114	58.5
Reduction in the degree of disability assessed by the RDRS-2 ($n=206$): from a median of 32 (IQR: 16.25, min: 19, max: 60) before surgery to a median of 26 (IQR: 12, min: 18, max: 54) after shunting ($W=-12701.0$, $p<0.001$).		
<i>Mortality and early and late complications</i>		
Mortality	2	0.8
Early complications ($n=244$) (subdural hematoma=4; shunt malfunction=2; systemic complications=4; postural hypoaecusia=1; parenchymal hematoma=1; hemorrhagic complication when the burr hole was performed=1)	13	5.3
Late complications ($n=236$) (asymptomatic hygromas=8; subdural hematomas=6, 3 acute and 3 chronic; distal catheter infection=1)	15	6.4

NPH normal pressure hydrocephalus, RDRS-2 rapid disability rating scale-2, IQR interquartile range

^aMedos S.A., Le Locle, Switzerland

^bNMT Neurosciences Implants S.A., Nice, France

^cMedtronic PS Medical, Goleta, CA, USA

^dBraun-Aesculap, Braun Melsungen AG, Germany

^eThe bipedestation pressure was selected according to the patients' height

^fNovus™ Valve Systems, Integra™

of the total monitoring time. Independent of the mean ICP recorded, patients with more than 10% of B-waves in the total recording time were selected for shunting. When the diagnosis of NPH was based only on the study of CSF dynamics or when B-waves were present for $\leq 10\%$ of the total recording time, patients with a resistance to absorption (Rout) of more than 10 mmHg/mL/min, determined by Katzman and Hussey's constant rate infusion test [6, 8], were also selected for shunting. Ex-vacuo hydrocephalus was considered when mean ICP was below or equal to 12 mmHg, with no pathological waves, and with a Rout ≤ 10 mmHg/mL/min. These patients were not considered to be candidates for shunting.

pressure valve with an antisiphon device was implanted. The types of valve used in the present series are shown in Table 2.

Outcome was independently assessed by the neurosurgeon and neuropsychologist using the NPH scale and changes at 6 months after shunting. Because a small change in the NPH scale score represents a substantial change in the patient's functional status, we defined moderate improvement as a 1-point increase and marked improvement as an increase of 2 or more points. Complications in the early postoperative period (first month after shunting) and at 6 months after shunting were evaluated by the neurosurgeon in charge of the patient.

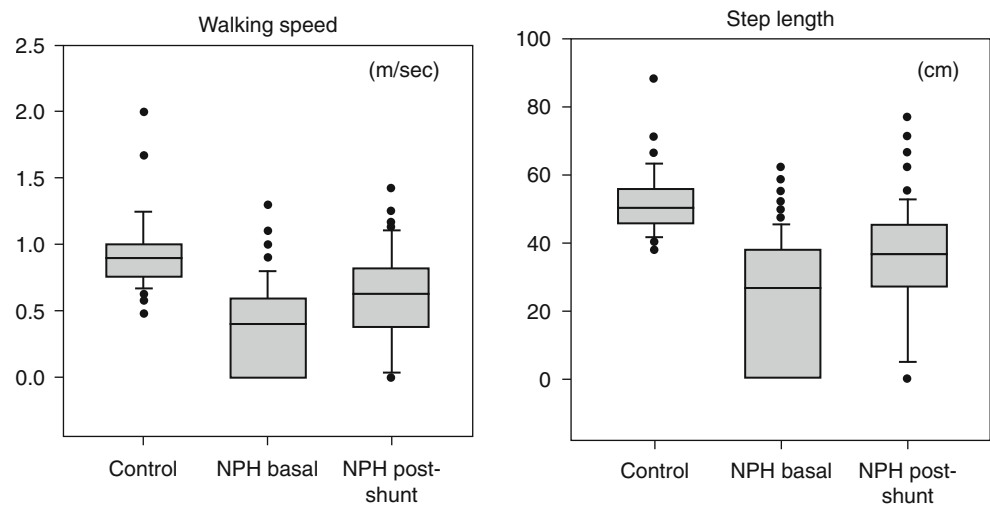
Shunt Selection and Therapeutic Evaluation

A differential low-pressure valve system was implanted and combined with a gravity compensating device in 233 of the 236 patients. In the remaining three patients, a medium-

Statistical Analysis

All descriptive statistics were analyzed using the SigmaPlot package for Windows (Version 11.0, Systat Software Inc., Germany). The assumption that data were normally distributed

Fig. 1 Box-and-whisker plots of walking speed and step length values registered in the control group and in normal pressure hydrocephalus (NPH) patients before shunting, and in the NPH group after shunting



was tested using the Shapiro–Wilk test. In normally distributed data, the mean \pm 1 standard deviation (SD) was used to summarize the variables. In skewed samples, the median and the interquartile range (IQR) were used. Pre- and postoperative step length and walking speed were compared using the non-parametric Wilcoxon matched-pairs signed rank test. Statistical significance was considered to be indicated when $p \leq 0.05$.

Results

Of the 257 patients initially studied, 12 were diagnosed with brain atrophy. In the remaining 245 patients, the diagnosis of idiopathic NPH was confirmed and the patients were considered to be candidates for shunting. One patient refused surgery. One patient died in the postoperative period from a respiratory infection. Three patients died less than 6 months after surgery from causes unrelated to shunting (stroke, chronic respiratory disease, and myocardial infarction). A further 4 patients (1.6%) were lost to follow-up. The final sample consisted of 236 patients (145 men [61.4%] and 91 women [38.6%]) with a median age of 75 years, IQR: 71–78.5). The estimated median duration of symptoms at shunting was 24 months (IQR: 12–36). The median ventricular size before surgery was 0.35 with an IQR of 0.32–0.38.

Continuous ICP monitoring was performed in 223 of the 236 patients (95%). The median ICP of these patients was 7 mmHg (IQR: 4–12). No plateau waves were found in the 223 patients monitored. The percentage of B-waves was highly variable, ranging from 7% to 100% (median=45%, IQR: 30–65%). In the patient with 7% of B-waves, Rout was 11.5 mmHg/mL/min. This patient improved after shunting. CSF dynamics studies were performed in 136 patients. The mean Rout of the 136 patients studied was 16.35 ± 6.49

with a range of 3–41.2 mmHg/mL/min. In 24 of these 136 patients Rout was <10 mmHg/mL/min. All 24 patients had a percentage of B-waves $>10\%$ (median: 39%, IQR: 29.5–52.5). Twenty of these 24 patients (83.3%) improved after shunting.

NPH Scale Scores, Step Length, Walking Speed, and Functional Status Before and After Shunting

Before surgery, 193 patients (81.8%) showed the complete clinical triad (a score of 4 or less in each domain of the NPH scale). After shunting, an increase of 1 or more points in the total NPH scale score was found in 212 patients (89.8%), no improvement was found in 18 patients (7.6%), while some worsening was observed in 6 patients (2.5%). In the 212 patients who showed improvement, this was moderated in 30, and was marked in 182 (a median increase in the NPH scale of 4 points, IQR: 3–6, minimum=2, maximum=11; Table 2). The component that most frequently improved was sphincter dysfunction (82.4%), followed by gait (79.3%), and cognitive symptoms (63.7%). Thirty-six of the 43 patients (84%) with involvement of only two components of the Hakim triad improved after shunting.

Before surgery, the median step length was 27 cm (IQR: 0–63) and the median walking speed was 0.45 ± 0.19 m/s (range 0.14–1). Step length and walking speed were re-evaluated in 183 of the 202 patients initially studied. The median step length after shunting was 37 cm (IQR: 27.4–45.5) and the median walking speed was 0.63 m/s (IQR: 0.39–0.83). Increases in both test results after shunting were statistically significant (step length: $Z = -8.532$, $p < 0.001$; walking speed: $Z = -8.616$, $p < 0.001$; Fig. 1).

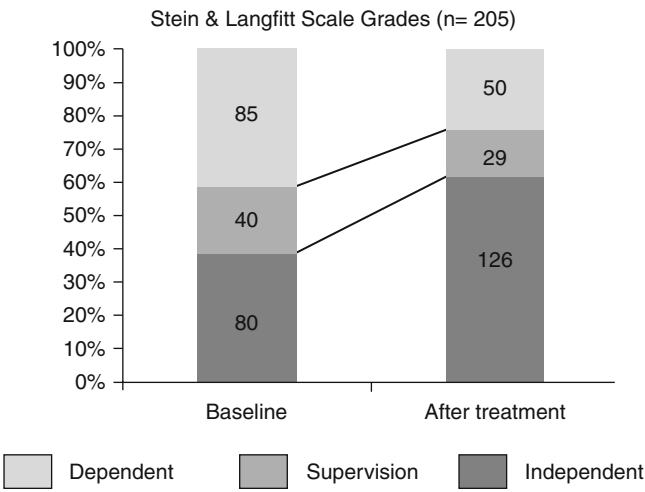


Fig. 2 Patients in each category of the modified Stein and Langfitt Scale in the pre- and postoperative periods

The degree of disability and dependency was significantly reduced after surgery in all the scales evaluated. Table 2 and Fig. 2 show changes in the patients' functional status after shunting.

Mortality and Complications Rate

One of the 244 shunted patients died in the early post-operative period from a respiratory infection (0.4%). Early post-surgical complications were found in 13 of the 243 shunted patients (5.3%; Table 2). Six months after shunting, the follow-up CT showed asymptomatic subdural collections (hygromas) in 8 of the 236 patients who remained under follow-up (3.4%). None of these patients required treatment (Fig. 3). Of the 236 patients, post-surgical complications were found in 7 (3%), consisting of 6 subdural hematomas (3 acute and 3 chronic) and a distal catheter infection. One of

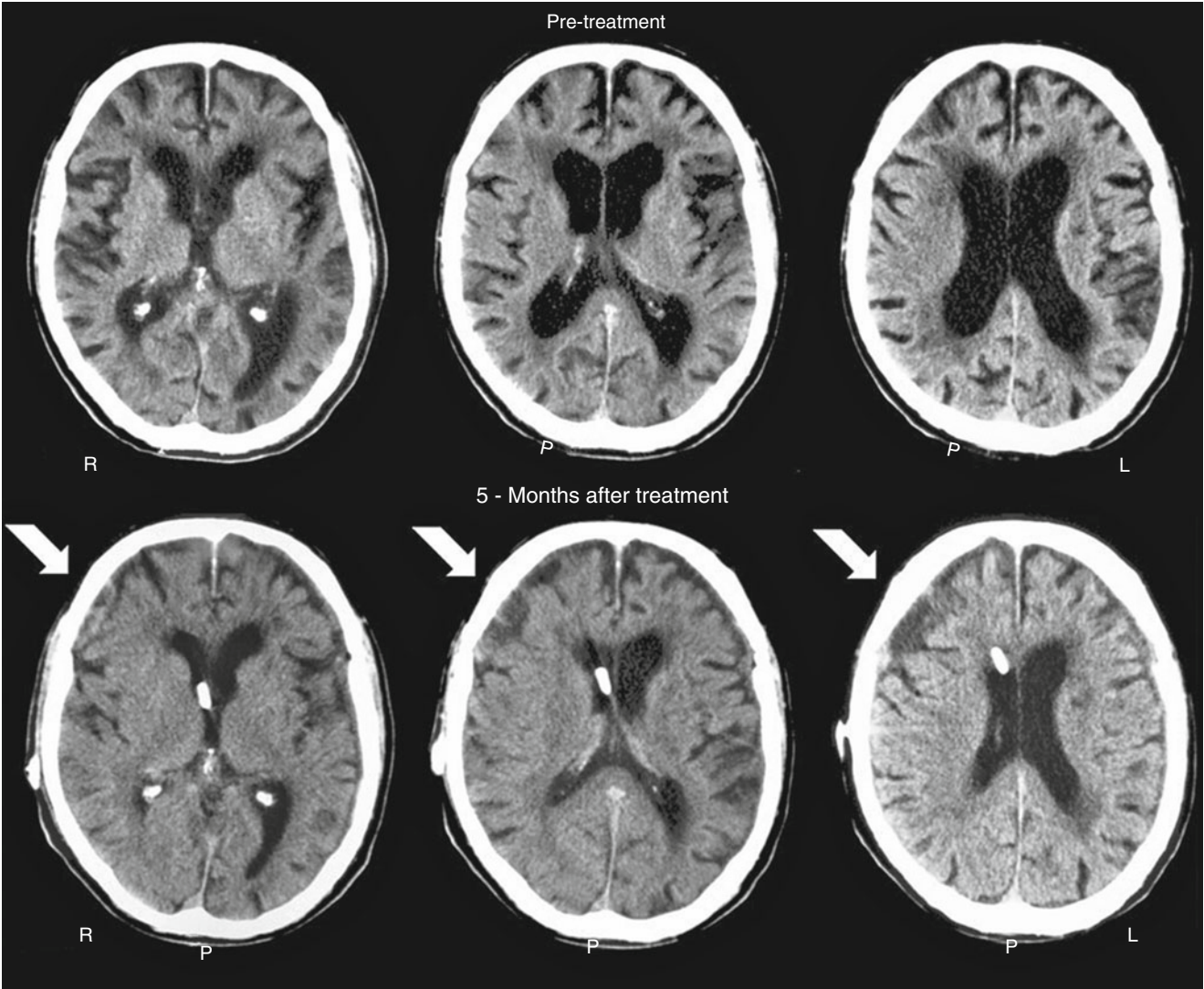


Fig. 3 CT performed before and 5 months after treatment in a patient with idiopathic NPH. Note the small subdural collection in the right frontal lobe (arrows). R right, L left

the patients with an acute subdural hematoma was receiving acenocoumarol and died without further treatment. No shunt malfunctions were observed in this period.

Discussion

Two factors that are critical in the management of patients with INPH are an accurate diagnosis and an appropriate shunt system. The results of the present series show that today almost 90% of these patients can improve after shunting, especially in gait dysfunction and sphincter incontinence.

Although not specifically recommended in the current guidelines, we believe that the use of continuous ICP monitoring is the key diagnostic tool and the selection of a low-pressure opening valve combined with a gravity compensating device have been the most important factors to explain these results. The high risk associated with the use of a low-pressure valve for these fragile patients, which favors very negative ICP while standing and the formation of subdural collections, is greatly reduced by the presence of the gravity compensating device, which may have allowed for the low rates of complication presented. However, additional factors, such as the use of a strict management protocol before and after shunting [16] are also important in explaining the low percentage of complications in this series.

The results observed in our patients have been similar to those published by Eide and Sorteberg in another large series of 131 patients with INPH who went on to have surgery and in whom the authors also used ICP monitoring as part of their diagnostic workup [4]. In this series, 1 patient died shortly after treatment but 103 of the remaining 130 treated patients (79%) improved after shunting. Eide and Sorteberg used the same criteria as our group for clinical evaluation before and after shunting (NPH scale). Both series follow the same criteria used to define improvement after treatment (significant improvement was defined by an increase of 2 points or more on the NPH scale score) [4]. However, in Eide and Sorteberg's series major complications of surgical treatment were seen in 30 of the 130 shunted patients (23%) [4].

Additional important findings of our study were that the presence of an incomplete clinical triad may also be associated with a high rate of improvement after shunting (84%) when the diagnosis of INPH was confirmed by the ICP findings. On the other hand, in 24 of these 136 patients Rout was <10 mmHg/mL/min. All 24 patients had a percentage of B-waves >10% (median: 39%, IQR: 29.5–52.5). Twenty of these 24 patients (83.3%) improved after shunting. If the cut-off for Rout values had been higher, as used by other authors (12, 14, 15 or 18 mmHg/mL/min) [2, 7, 13], the percentage

of false-negatives would have increased from 16.6% to 63.3%. In other words, 63.3% of patients would not have been operated on if our diagnosis had been limited to the use of Rout values. These findings should be considered when following the diagnostic algorithms proposed in the guidelines.

Conclusion

At present we can obtain a high rate of improvement in patients with idiopathic NPH after shunting with low complication rates when using continuous ICP monitoring as the key element in the diagnosis and selection of a low-opening pressure valve in combination with a gravity compensating device for the treatment of this pathological condition.

Acknowledgments The authors gratefully acknowledge Sabrina Voss for editorial assistance and the collaboration of the neurosurgical nurses in the study of these patients, especially María Jesús Peñarrubia (RN) and María Soledad Armengol (RN). This study was supported in part by Grant 07/0681 from the *Fondo de Investigación Sanitaria* (FIS) given to Dr. M.A. Poca.

Conflict of interest statement We declare that we have no conflict of interest.

References

1. Albeck MJ, Skak C, Nielsen PR et al (1998) Age dependency of resistance to cerebrospinal fluid outflow. *J Neurosurg* 89:275–278
2. Boon AJ, Tans JT, Delwel EJ et al (1997) Dutch normal-pressure hydrocephalus study: prediction of outcome after shunting by resistance to outflow of cerebrospinal fluid. *J Neurosurg* 87:687–693
3. Borgesen SE (1984) Conductance to outflow of CSF in normal pressure hydrocephalus. *Acta Neurochir (Wien)* 71:1–45
4. Eide PK, Sorteberg W (2010) Diagnostic intracranial pressure monitoring and surgical management in idiopathic normal pressure hydrocephalus: a 6-year review of 214 patients. *Neurosurgery* 66:80–91
5. Fillenbaum GG (1985) Screening the elderly. A brief instrumental activities of daily living measure. *J Am Geriatr Soc* 33:698–706
6. Hussey F, Schanzer B, Katzman R (1970) A simple constant-infusion manometric test for measurement of CSF absorption. II. Clinical studies. *Neurology* 20:665–680
7. Kahlon B, Sundbarg G, Rehnrcrona S (2002) Comparison between the lumbar infusion and CSF tap tests to predict outcome after shunt surgery in suspected normal pressure hydrocephalus. *J Neurol Neurosurg Psychiatry* 73:721–726
8. Katzman R, Hussey F (1970) A simple constant-infusion manometric test for measurement of CSF absorption. I. Rationale and method. *Neurology* 20:534–544
9. Klinge P, Marmarou A, Bergsneider M et al (2005) Outcome of shunting in idiopathic normal-pressure hydrocephalus and the value of outcome assessment in shunted patients. *Neurosurgery* 57:S40–S52

10. Linn MW, Linn BS (1982) The rapid disability rating scale-2. *J Am Geriatr Soc* 30:378–382
11. Lundberg N (1960) Continuous recording and control of ventricular fluid pressure in neurosurgical practice. *Acta Psychiatr Scand* 36:1–193
12. Marmarou A, Bergsneider M, Relkin N et al (2005) Development of guidelines for idiopathic normal-pressure hydrocephalus: introduction. *Neurosurgery* 57:S1–S3
13. Meier U, Bartels P (2001) The importance of the intrathecal infusion test in the diagnostic of normal-pressure hydrocephalus. *Eur Neurol* 46:178–186
14. Poca MA, Sahuquillo J, Busto M et al (1996) Clinical management of patients with normal pressure hydrocephalus syndrome. *Ann Psychiatry* 6:273–292
15. Poca MA, Sahuquillo J, Ibañez J et al (2001) Study of cerebrospinal fluid dynamics in the diagnosis of adult chronic hydrocephalus. In: Vázquez-Barquero A, Poca MA, Martín R (eds) *Adult chronic hydrocephalus*. Gráficas Calima S.A., Santander, pp 103–122
16. Poca MA, Mataro M, Matarin M et al (2004) Is the placement of shunts in patients with idiopathic normal-pressure hydrocephalus worth the risk? Results of a study based on continuous monitoring of intracranial pressure. *J Neurosurg* 100:855–866
17. Poca MA, Sahuquillo J, Barba MA et al (2004) Prospective study of methodological issues in intracranial pressure monitoring in patients with hydrocephalus. *J Neurosurg* 100:260–265
18. Poca MA, Mataro M, Matarin M et al (2005) Good outcome in patients with normal-pressure hydrocephalus and factors indicating poor prognosis. *J Neurosurg* 103:455–463
19. Sahuquillo J, Rubio E, Codina A et al (1991) Reappraisal of the intracranial pressure and cerebrospinal fluid dynamics in patients with the so-called normal pressure hydrocephalus syndrome. *Acta Neurochir (Wien)* 112:50–61
20. Solana E, Poca MA, Sahuquillo J et al (2010) Cognitive and motor improvement after retesting in normal-pressure hydrocephalus: a real change or merely a learning effect? *J Neurosurg* 112:399–409

Idiopathic Normal Pressure Hydrocephalus (iNPH) and Co-Morbidity: An Outcome Analysis of 134 Patients

Johannes Lemcke and Ullrich Meier

Abstract Objective: The diagnosis and management of idiopathic normal-pressure hydrocephalus (iNPH) remains controversial, particularly in selecting patients for shunt insertion. Diagnostic criteria target the pathological features of the dynamics of the cerebrospinal fluid (CSF); however, the effectiveness in predicting the shunt success has room for improvement. The aim of our study was to systematically assess the influence of the co-morbidity determining the benefit from shunt surgery.

Methods: Between 1997 and 2006 134 patients suffering from iNPH were treated with a ventriculo-peritoneal shunt with a gravity-controlled valve. The coincident disease processes were recorded. Shunt outcome was assessed at 2 years postsurgery in 116 patients (follow up rate 87%). The results of this follow-up examination (Kiefer score, NPH recovery rate) were compared using the preoperative co-morbidity index (CMI).

Results: Of the 134 patients 76 (56.7%) had a CMI of 0–3 and 58 patients (43.3%) had a CMI of 4–8. Two years after surgery 65 out of 70 shunt responders (93%) could be identified in the patients group with a CMI of 0–3 and only 29 of 46 (63%) in group with a CMI of 4–8. This difference was significant ($p < 0.0001$). Remarkably few patients scoring between 6 and 8 on the CMI scale experienced a favourable outcome. The patients in this latter group showed excellent outcomes in only 1% and poor outcomes in 33%.

Conclusion: Data in this report affirm that co-morbidity is a statistically significant predictor of the quality of the clinical outcome for patients with iNPH undergoing shunt therapy. A CMI of more than 3 significantly decreases the chance of a favourable outcome and this should form part of the assessment when the risks and benefits of surgery are considered. According to these data, a successful outcome in patients with a CMI of 6 or more is not to be expected.

J. Lemcke (✉) and U. Meier
Department of Neurosurgery,
Unfallkrankenhaus Berlin,
Warener Strasse 7, D-12683
Berlin, Germany
e-mail: johannes.lemcke@ukb.de

Introduction

In all branches of medicine, a multidisciplinary approach involving the various specialities is necessary for two important reasons. First, for an intervention to be effective, it must be ascertained that the observed symptoms are indeed caused by the disease process targeted by the treatment method and not by some other pathological condition. Second, it is important to recognise situations in which the detrimental influence of co-morbidity on the probable outcome of a given intervention is such that little or no improvement can be expected. Both of these possibilities represent a potential contraindication to operative therapy in general and a contraindication for shunt surgery in the treatment of patients with iNPH. Patients with iNPH are usually elderly and as such often present with multiple co-morbidities. The aim of this study was to evaluate whether the co-morbidity index (CMI) of Kiefer et al. [8] can be used to provide a predictor to help identify those patients who would improve following shunt surgery.

Materials and Methods

In the neurosurgical unit of a major hospital between 1997 and 2006, 134 patients were diagnosed with iNPH and treated surgically.

Diagnosis

Patients who displayed gait ataxia in addition to other symptoms of iNPH and who showed neuroradiological evidence of ventricular enlargement in CT or MR imaging were further assessed with an intrathecal infusion test. All patients properly consented to all surgical procedures according to hospital regulations. To determine the individual CSF flow parameters, a dynamic infusion test, using a computer-assisted constant flow technique with an infusion

rate of 2 mL/min was performed via lumbar puncture. A resistance of 13 mmHg/mL/min or higher was defined as pathological. Immediately following the dynamic infusion test, a diagnostic drainage of at least 60 mL of CSF was carried out using the same puncture site. An improvement in the clinical picture over the ensuing 2 or 3 days served as indication for the implantation of a ventriculo-peritoneal shunt. If the patient's symptoms, particularly the gait ataxia, did not initially improve, then 2–3 days of further, external lumbar drainage (ELD) was commenced. Once more, if

symptoms improved over this period, the shunt operation was indicated [1, 12, 13].

Clinical Grading

The Black Grading Scale for Shunt Assessment and the NPH Recovery Rate (based on the clinical grading for NPH by Kiefer) were used to express the results of the clinical examinations.

$$\text{NPH Recovery Rate} = \frac{\text{NPH Grading preoperative} - \text{NPH Grading postoperative}}{\text{NPH Grading (Kiefer) preoperative}} \times 10$$

Formula 1: NPH Recovery Rate according to Meier [10].

All graded examination results were split into clinical outcome groups (Table 1).

Co-morbidity Index

Kiefer et al. [8] introduced an assessment tool for various pathologies and their clinical effect when present in NPH. By summing the scores for each co-morbid disease process found in Table 2, a co-morbidity index (CMI) score of between 0 and 23 can be calculated.

Operation

All patients underwent surgery in the same hospital. In all cases ventriculo-peritoneal shunts with gravity-assisted valves were implanted. Sixty-five patients received a dual-switch valve (Christoph Miethke GmbH, Potsdam, Germany), 36 patients a proGAV (Christoph Miethke GmbH, Potsdam, Germany) and 33 patients a programmable Medos-Codman valve (Codman, Raynham, MA, USA) in combination with a ShuntAssistant (Christoph Miethke) [9, 11, 17].

Follow-up

The patients were followed up by neurosurgeons in our outpatient department 3, 6 and 12 months after surgery. After the first year annual follow-ups were performed. Of the patients presented in this study at present 116 have been followed up for at least 2 years, 86 patients for at least 3 years,

Table 1 The Black grading scale for shunt assessment relating to the normal-pressure hydrocephalus (NPH) recovery rate

Grading	Description	NPH recovery rate (score)
Excellent	Restoration of pre-morbid activity levels	≥ 7.5
Good	Limited reduction in pre-morbid activity levels	≥ 5
Fair	Gradual improvement	≥ 3
Transient	Transient improvement	≥ 2
Poor	No change or deterioration in symptoms	< 2

Table 2 The co-morbidity index (CMI) introduced by Kiefer

Risk factors	1 point	2 points	3 points
Vascular	Hypertension	Diabetes mellitus	
	Aortofemoral bypass	Peripheral vascular disease	
	Stent	Vascular occlusion	
Cerebrovascular	Posterior circulatory insufficiency	Vascular encephalopathy	Cerebral infarct
	ICA stenosis	TIA / PRIND	
Cardiac	Arrhythmia		
	Valvular disease		
	Heart failure/ stent		
	Aortocoronary bypass		
	Myocardial infarction		
Others		Parkinson's disease	

Table 3 Outcome 2 years after surgery and co-morbidity index

Outcome 2 years after shunt surgery		Poor	Transient	Fair	Good	Excellent	Total
Co-morbidity index	CMI 0–1	1	1	1	6	17	26
	CMI 2–3	4	3	3	17	17	44
	CMI 4–6	12	3	4	7	5	31
	CMI 6–8	5	2	3	4	1	15
	Total	22	9	11	34	40	116

60 patients for at least 4 years, 35 patients for at least 5 years, 23 patients for at least 6 years and 12 patients for at least 7 years. Owing to the number of patients the follow-up data obtained 2 years after shunt surgery achieved statistical significance.

Statistical Analysis

For continuous data, the Mann–Whitney test using the SPSS software was applied. For categorical data, two-sided Chi-squared test was applied. A level of $p=0.05$ was considered significant.

Results

Patient Age and Sex Distribution

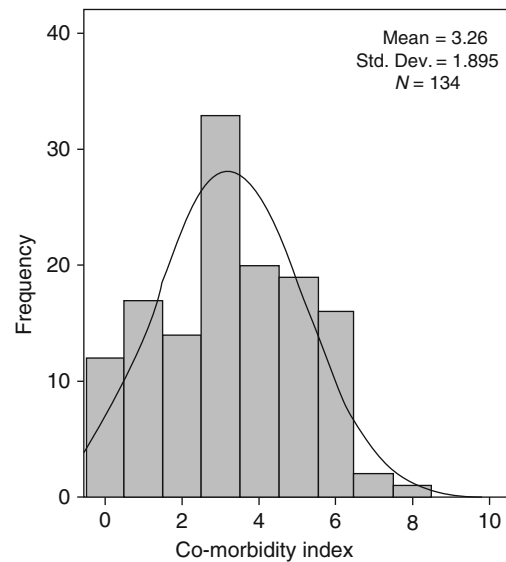
It was possible to follow-up 116 patients (87%) over a 2-year postoperative period. The 80 men and 54 women had an average age of 68 at diagnosis (range 27–85, s.d. 11.3).

Outcome

Seventy-four (64%) of these patients showed an excellent or good outcome, 20 patients (17%) had satisfactory outcome (fair or transient improvement) and 22 (19%) patients did not benefit from shunt surgery. Thus, among the cohort of 116 patients, 94 improved after surgery (responder rate 81%).

Co-morbidity Index

Out of 116 followed up patients 26 (22%) had a CMI of 0 or 1 at the time of surgery, which means they had no or only one marginal co-morbidity. Forty-four patients (38%) had CMI of 2 or 3, 31 patients (27%) a CMI of 4–6 and 15 patients (13%) a CMI of 6 or more (Table 3).

**Fig. 1** Histogram of the co-morbidity index (CMI) in the 116 patients**Table 4** Cross-tabulation of responders and non-responders (Chi-squared test $p<0.0001$)

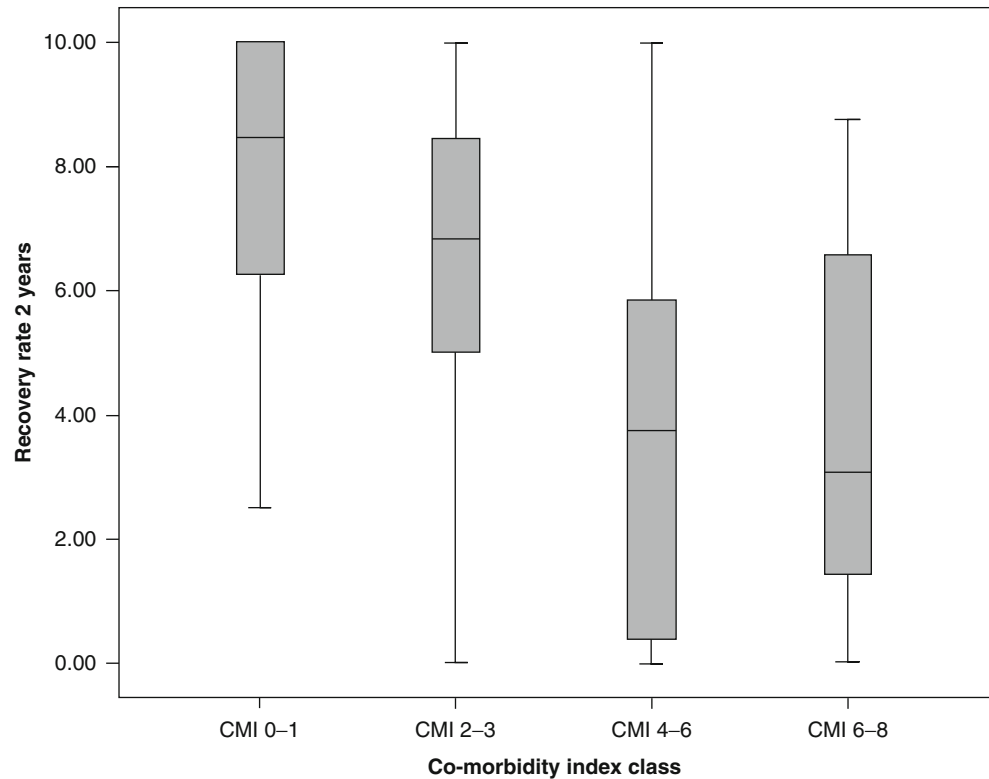
Responder rate 2 years after shunt surgery			
	Non-responder	Responder	Total
CMI 0–3	5	65	70
CMI 4–8	17	29	46
Total	22	94	116

The distribution of the patients with higher or lower CMI was similar to a normal distribution (Fig. 1).

Charting the values into a crosstab after dichotomising the outcome into shunt responder (recovery rate ≥ 2) and non-responders (recovery rate < 2) and dichotomising the CMI into patients with 3 or less and patients with a CMI of 4–8, the Chi-squared test indicated a high significance (Table 4).

If the 116 patients were split according to the CMI in four groups of CMI 0–1, CMI 2–3, CMI 4–6 and CMI 6–8, highly significant differences could be found comparing the group of patients with a CMI of 0–1 with the two groups with CMI values of 4 or more. Comparing the patient group with a CMI of 2–3 with the two groups with more than 4 points, the level of significance was also reached (Fig. 2).

Fig. 2 Significant differences were found comparing the recovery rates of patients with different CMI values. (CMI 0–1/ CMI 4–6 $p < 0.0001$; CMI 0–1/ CMI 6–8 $p < 0.0001$; CMI 2–3/ CMI 4–6 $p = 0.001$; CMI 2–3/ CMI 6–8 $p = 0.009$; Mann–Whitney test)



Discussion

Co-morbidity

A review of the literature gives a mean reported rate of co-morbidity in iNPH of 43%; cerebrovascular insufficiency is described in 45% of these patients. The commonest co-morbidity (78–100%) is vascular encephalopathy [5, 15, 16]. Parkinson's disease were present in 10% of cases, and 10% had histologically unconfirmed, but clinically suspected Alzheimer's disease. In order to distinguish the clinical picture of iNPH from other dementia syndromes, Golomb [4, 5] and Savolainen [15, 16] investigated the coincidence of Alzheimer's disease and iNPH. Centrally limited motor disturbances likewise result in an overlapping entity. In the patient population reported in this study, 8% were found to have Parkinson's disease in addition to iNPH. The exclusion of progressive cerebrovascular disease as a differential diagnosis in iNPH is not an unimportant motivation for the use of invasive diagnostic procedures. Co-morbidities can be clinically quantified in terms of risk factors. Such a system; the co-morbidity index, was introduced in 2006 by Kiefer et al. [8] In it, the most common co-morbid pathological conditions are assigned between 1 and 3 points, which, when totalled as a CMI score, can be referred to as an empirical threshold value after which the likelihood of a good to excellent outcome significantly

decreases. This indirect correlation between outcome and CMI is unequivocally demonstrated in this study. Thus, of those patients with a CMI score of 0 or 1, 65% had an excellent outcome, while 47% of patients with a CMI of between 6 and 8 experienced an unsatisfactory outcome. Kiefer et al. [8], suggest a CMI of 3 as a dividing line between patient groups with a statistically favourable prognosis and those with a tendency towards a poor outcome. The data from this study serve to confirm the value of this cut-off point; 81% of the patients with a CMI of 3 or less experienced a good or excellent outcome. Only 37% of the patients with a CMI > 3 experienced a comparable improvement in symptoms.

Outcome

The general improvement rates reported in the literature for patients with iNPH undergoing a shunt operation vary around a mean of 53% (range 31–96%) [2, 3]. In an analysis by Kahlon et al. [7] 64% of the patients younger than 75 years improved over 5 years' follow-up. Pujari et al. [14] found an improvement of the gait ataxia in 83% of his patients at 3 years' follow-up and in 87% of his patients 7 years after surgery. Long-term experiences with fixed gravitational valves have been published by Hertel et al. [6]. Even if the results represent different types of hydrocephalus a rate of

shunt responders of 93% was reported. The results of our study show an overall improvement rate at 2 years post-shunt of 81%, in keeping with the international literature.

Conclusion

Co-morbidity is a statistically significant predictor of the clinical outcome for patients with iNPH undergoing shunt therapy. A CMI score of 3 points or less allows a good prognosis of the postoperative outcome. A CMI of more than 3 significantly decreases the chance of a good outcome and this should form part of the assessment when the risks and benefits of surgery are considered. Owing to factors arising from co-morbidity, a successful outcome in patients with a CMI of 6 or more is unlikely.

Conflict of interest statement We declare that we have no conflict of interest.

References

1. Al-Zain F, Meier U, Lemcke J (2010) Early shunting using the parallel shunt system in hemorrhagic hydrocephalus: in vitro testing of handling, technical complications and clogging rate. *Acta Neurochir Suppl* 106:117–119
2. Bech RA, Waldemar G, Gjerris F, Klinken L, Juhler M (1999) Shunting effects in patients with idiopathic normal pressure hydrocephalus; correlation with cerebral and leptomeningeal biopsy findings. *Acta Neurochir (Wien)* 141:633–639
3. Borgesen SE (1984) Conductance to outflow of CSF in normal pressure hydrocephalus. *Acta Neurochir (Wien)* 71:1–45
4. Golomb J, de Leon MJ, George AE, Kluger A, Convit A, Rusinek H, de Santi S, Litt A, Foo SH, Ferris SH (1994) Hippocampal atrophy correlates with severe cognitive impairment in elderly patients with suspected normal pressure hydrocephalus. *J Neurol Neurosurg Psychiatry* 57:590–593
5. Golomb J, Wisoff J, Miller DC, Boksay I, Kluger A, Weiner H, Salton J, Graves W (2000) Alzheimer's disease comorbidity in normal pressure hydrocephalus: prevalence and shunt response. *J Neurol Neurosurg Psychiatry* 68:778–781
6. Hertel F, Zuchner M, Decker C, Schill S, Bosniak I, Bettag M (2008) The Miethke dual switch valve: experience in 169 adult patients with different kinds of hydrocephalus: an open field study. *Minim Invasive Neurosurg* 51:147–153
7. Kahlon B, Sjunnesson J, Rehncrona S (2007) Long-term outcome in patients with suspected normal pressure hydrocephalus. *Neurosurgery* 60:327–332
8. Kiefer M, Eymann R, Steudel WI (2006) Outcome predictors for normal-pressure hydrocephalus. *Acta Neurochir Suppl* 96:364–367
9. Lemcke J, Meier U (2010) Improved outcome in shunted iNPH with a combination of a Codman Hakim programmable valve and an Aesculap-Miethke ShuntAssistant. *Cen Eur Neurosurg* 71:113–116
10. Meier U (2002) The grading of normal pressure hydrocephalus. *Biomed Tech(Berl)* 47:54–58
11. Meier U, Lemcke J (2006) First clinical experiences in patients with idiopathic normal-pressure hydrocephalus with the adjustable gravity valve manufactured by Aesculap (proGAV(Aesculap)). *Acta Neurochir Suppl* 96:368–372
12. Meier U, Lemcke J (2007) Diagnostic methods of normal pressure hydrocephalus. *Schweiz Arch Neurol Psychiatr* 158:139–149
13. Meier U, Lemcke J, Neumann U (2006) Predictors of outcome in patients with normal-pressure hydrocephalus. *Acta Neurochir Suppl* 96:352–357
14. Pujari S, Kharkar S, Metellus P, Shuck J, Williams MA, Rigamonti D (2008) Normal pressure hydrocephalus: long-term outcome after shunt surgery. *J Neurol Neurosurg Psychiatry* 79:1282–1286
15. Savolainen S, Paljarvi L, Vapalahti M (1999) Prevalence of Alzheimer's disease in patients investigated for presumed normal pressure hydrocephalus: a clinical and neuropathological study. *Acta Neurochir (Wien)* 141:849–853
16. Savolainen S, Laakso MP, Paljarvi L, Alafuzoff I, Hurskainen H, Partanen K, Soininen H, Vapalahti M (2000) MR imaging of the hippocampus in normal pressure hydrocephalus: correlations with cortical Alzheimer's disease confirmed by pathologic analysis. *AJNR Am J Neuroradiol* 21:409–414
17. Sprung C, Schlosser HG, Lemcke J, Meier U, Messing-Junger M, Trost HA, Weber F, Schul C, Rohde V, Ludwig HC, Hopfner J, Sepehrnia A, Mirzayan MJ, Krauss JK (2010) The adjustable proGAV shunt: a prospective safety and reliability multicenter study. *Neurosurgery* 66:465–474

Intracranial Pressure Measurement in Infants Presenting with Progressive Macrocephaly and Enlarged Subarachnoid Spaces

M. Schulz, S.A. Ahmadi, B. Spors, and Ulrich-W. Thomale

Abstract Introduction: For subarachnomegaly in infants with enlarged external and internal CSF spaces clear treatment decisions, such as observation or ventriculo-peritoneal (VP) shunting, are still lacking. The aim of this study is to measure intracranial pressure (ICP) in these patients to elucidate treatment necessity.

Materials and Methods: Seven children presenting with macrocephaly, moderately enlarged ventricles, and subarachnoid spaces on magnetic resonance imaging (MRI) without neurological deficits or other CSF-associated pathological conditions were enrolled. Continuous ICP recording was conducted using an external ventricular drain. Data recordings during overnight measurements were analyzed offline to calculate baseline, mean ICP values, and a histogram distribution.

Results: Mean age at enrollment was 9.4 months (2–22 months). ICP monitoring was conducted for 2.7 ± 1.1 nights (range 2–5 nights) and revealed baseline values above 10 mmHg in three patients, who went on to receive a VP shunt. One patient with average values over 10 mmHg also underwent VP shunting. Three patients displayed both baseline and average ICP values of less than 10 mmHg. Observational management was chosen for this subgroup. Comparing shunted versus the non-shunted group in a histogram analysis the percentages of recorded ICP values above 8, 10, and 15 mmHg were significantly different ($p < 0.05$).

Conclusion: Subarachnomegaly in infants remains a dilemma to the treating neurosurgeon. Risks and benefits of observational management options need to be weighed against those of VP shunting. Continuous ICP monitoring may help to identify patients who may potentially benefit from the surgical treatment option.

Keywords ICP measurement • Subarachnomegaly • Pediatric Hydrocephalus • infants • macrocephaly

Introduction

A group of infants presents with progressively increasing head circumference, but without obvious neurological and developmental delay. Imaging of these infants usually shows mild ventricular enlargement and dilated external cerebro-spinal fluid (CSF) spaces. Anatomically, the widened external spaces consist of enlarged subarachnoid spaces that can be recognized by a multiplicity of traversing vessels within that space [1]. This clinical picture is treated conservatively in most cases. However, uncertainty exists in those cases if macrocephaly combined with widened internal and external CSF spaces presents with some clinical signs of elevated intracranial pressure (ICP). This uncertainty is reflected in the various proposed treatment options, which range from observation to CSF diversion with shunting [3, 9, 11, 21]. The risk of treatment needs to be carefully weighed against the possible benefit of reducing intracranial pressure by diversion of CSF.

The present study shows our experience with invasive and continuous measurement of the intracranial pressure prior to shunt insertion in children with macrocephaly.

Materials and Methods

Patients and Operative Procedure

From November 2007 to April 2009 all referred infants who presented with macrocephaly and enlarged subarachnoid were identified. Only patients with progressive macrocephaly as characterized by head circumferences within the age-adapted range (10th to 90th percentile) at birth and whose head circumference progressed above the 97th percentile were included. Radiological inclusion criteria were enlarged external and internal CSF spaces as well as a tense fontanel. The enlarged external CSF spaces needed consist of enlarged

M. Schulz, S.A. Ahmadi, and U.-W. Thomale (✉)
Pediatric Neurosurgery, Campus Virchow Klinikum, Charité
Universitätsmedizin Berlin, Augustenburger Platz 1,
13353 Berlin, Germany
e-mail: uthomale@charite.de

B. Spors
Pediatric Radiology, Charité Universitätsmedizin Berlin, Berlin,
Germany

subarachnoid spaces; infants with subdural effusions were not included. The characteristics of enlarged subarachnoid spaces are traversing vessels that are best visualized on T2-weighted images. Absence of other pathological condition – such as arachnoid cysts or evidence of interventricular CSF pathway obstruction – was a prerequisite for inclusion.

Treatment options with a focus on expectant observation or CSF diversion were extensively discussed with the parents. When an operative intervention was agreed upon the possibility of measuring the ICP was discussed. If the parents consented to ICP measurement the child was admitted to the hospital. None of the children who fulfilled the inclusion characteristics of this study was submitted for shunt insertion without preceding ICP measurement.

All children were operated on under general anesthesia with perioperative antibiotics (flucloxacillin 50 mg/kg). The child's position was supine with the head immobilized in a vacuum mattress. After preparation and draping, a right frontal crescent-shaped incision was made and the periosteum was opened. A scalpel or a burr was used to create a trephination of 1 cm in diameter to allow the creation of a tiny dural flap. Because of the relative distance of the cortical surface from the skull, the subarachnoid space was inspected by loupe magnification. The arachnoid trabecula was dissected in order to identify the cortical surface. The frontal horn was then punctured with a standard ventricular drain (Miethke KG & Co., Potsdam, Germany). Intraoperative, transfontanel ultrasound was used to guide the catheter into the ventricular system. The distal end of the drain was tunneled subcutaneously into the parietal region where it was securely sutured to the skin. Transcutaneously placed moderately constricting sutures were placed along the course of the drain in the parietal region to avoid CSF leakage through the skin. The site of the burr hole was closed with approximation of the dural edges and epidural application of gelatin sponge. The periosteum was approximated, which was followed by subcutaneous and skin-surface closure.

The ventricular catheter was connected to the pressure monitor (LiquoGuard®, Möller Medical GmbH, Fulda, Germany) with the sensor taped to the infant's temporal region. The monitoring system was set to record ICP values. Routine analgesics were administered and antibiotics were continued until removal of the external ventricular drain.

After the period of ICP recording a decision was made whether to implant a permanent CSF diverting system on the basis of the data analysis obtained. In the event of a decision in favor of shunting, the infant was taken to the operation theater where the ventricular drain was removed and a ventriculo-peritoneal shunt was implanted using the existing burr hole and the trajectory toward the ventricle. Antibiotic impregnated catheters (Bactiseal, Codman, Raynham, MA, USA) and an adjustable valve with a gravitational unit (proGAV, Miethke, Potsdam, Germany) were used in all cases. After the second procedure the child was discharged

after 3–5 days. If no shunt was to be implanted the ventricular catheter was removed, the puncture site closed with a suture and the child discharged on the same day.

Data Collection and Processing

The ICP values were continuously recorded every 6 s and stored on an internal memory chip of the monitoring device. After discontinuation of ICP recording the data were analyzed offline using standard table calculation software (Microsoft Office Excel, Microsoft Corporation, Redmond, WA, USA). Only nighttime periods from 9 p.m. to 5 a.m., when the infants were assumed to be sleeping, were analyzed and interpreted. Mean values and standard deviation of the recorded ICP values were calculated for all children. Averaging the lowest 60% of all recorded ICP values for each patient approximated the baseline of the recorded ICP values. Frequency distribution of the measured ICP (histograms) and the percentage of individual ICP values above the thresholds of 8, 10, 15, and 20 mmHg were calculated for each patient.

Statistical analysis to compare the fractions of ICP values above the thresholds mentioned in shunted versus non-shunted infants was carried out with the two-tailed *t*-test using Prism 5 software (GraphPad Software, La Jolla, CA, USA).

Results

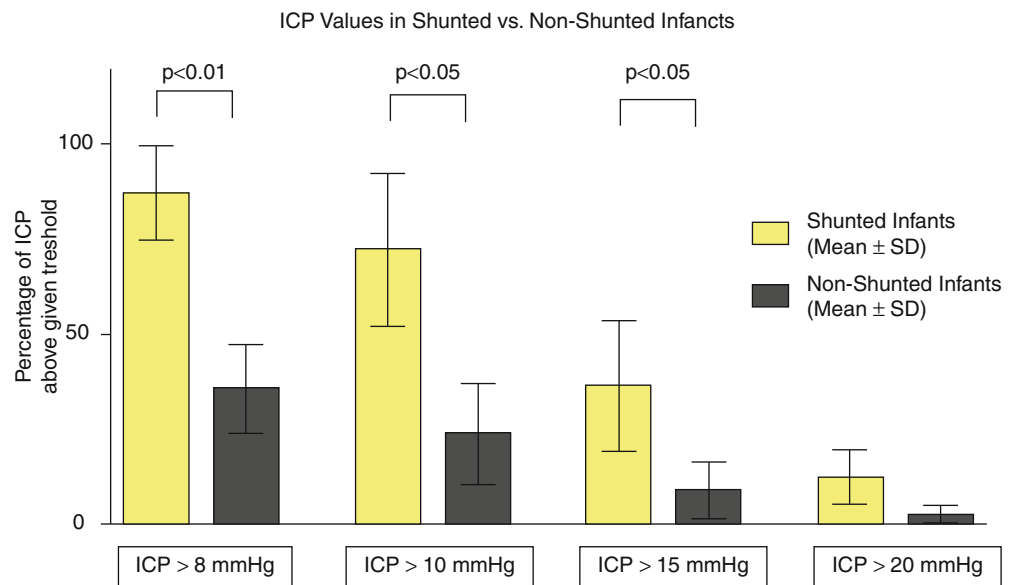
Seven patients (five boys and two girls) were monitored according to the above-mentioned protocol. The mean age at the time of ICP measurement was 9.4 ± 6.4 months (range: 2–22). All patients but one were in their first year of life. The age-adapted head circumference of all children was at a mean of 1.4 ± 0.7 cm above the 97th percentile (range: 0.5–2.5). The clinical examination for all patients revealed no significant abnormality other than macrocephaly and an unspecified developmental delay. No infant had papilledema on fundoscopic examination. All children had tension of the fontanel.

The duration of ICP measurement that was used for data interpretation was 2.7 ± 1.1 nights (range 2–5). The calculation of baseline ICP values, above which periodical elevations occurred, was within the range of 4.6–12.2 mmHg. The mean night-time ICP of all values of the monitored infants was between 7.1 and 15.7 mmHg. For all infants the recorded ICP values were computed and displayed in histograms of ICP distribution (Table 1). The range of ICP values above the threshold of 8 mmHg was 24.2–97.1% for the individual patients. The percentages of ICP values above the threshold of 10 mmHg was within the range of 11.0–89.2%, for a threshold of 15 mmHg from 3.2% to 49.1% and for a threshold of 20 mmHg from 0.7% to 17.5% (Table 1).

On the basis of mean ICP measurements being higher than 10 mmHg, parents of four infants gave consent for VP

Table 1 Patient characteristics (patients who underwent ventriculo-peritoneal (VP) shunting are shaded in gray)

Age (months), sex	Baseline	Mean \pm SD	Percentage of ICP values			
			Above 8 mmHg	Above 10 mmHg	Above 15 mmHg	Above 20 mmHg
10, male	12.2	15.3 \pm 5.0	96.33	83.65	49.13	15.05
12, female	12.2	15.7 \pm 6.9	97.12	89.22	45.32	14.87
6, male	10.1	14.2 \pm 6.0	84.67	72.93	40.08	17.55
22, male	5.7	9.4 \pm 5.5	47.71	37.40	17.42	5.24
7, male	4.0	7.1 \pm 4.7	35.37	23.43	6.17	1.27
7, male	7.9	10.3 \pm 3.8	70.54	44.01	11.58	1.81
2, female	4.6	6.6 \pm 3.3	24.15	11.04	3.19	0.73

Fig. 1 Fractions of measured intracranial pressure (ICP) values above the given thresholds of 8, 10, 15, and 20 mmHg for the subgroup of infants who received a ventriculo-peritoneal (VP) shunt and the subgroup without a shunting procedure and observational management

shunt implantation. This procedure was uneventfully carried out in all cases. No intra- or immediate postoperative complications were encountered after a shunt implantation within the first 6 months. During the long-term follow-up one of the shunted patients required three shunt revisions for proximal catheter obstruction.

In a comparison of the shunted versus the non-shunted group the percentages of recorded ICP values above the threshold of 8, 10, and 15 mmHg were significantly different ($p < 0.01$ and $p < 0.05$ respectively; Fig. 1).

Complications of Invasive ICP Recording

One of the two patients in whom invasive ICP recording did not reveal elevated values developed fever after 2 days. The drain was removed subsequently. A CSF sample obtained prior to removal of the drain grew Gram-positive cocci. Antibiotic treatment was continued after removal of the ventricular catheter for 5 days, after which the patient was discharged in good clinical condition.

Discussion

The combination of progressive macrocephaly in infancy, dilatation of the external CSF spaces and possibly ventriculomegaly is a condition about which there is still debate regarding the appropriate measures to be taken for treatment decision. The diversity of terms to name this condition – such as subarachnomegaly, benign extra-axial fluids of infancy, benign enlargement of the subarachnoid space, benign external hydrocephalus, idiopathic external hydrocephalus, extraventricular obstructive hydrocephalus, and the different proposed treatment strategies – reflects the insecurity with regard to what is the best management. If primary macrocephaly due to pathological growth patterns [17] is ruled out, this condition is thought to be caused by an imbalance between the production of CSF and the absorption capabilities of the presumably immature arachnoid villi and other developing absorption capacities. This leads to an accumulation of CSF predominantly in an expanded frontal subarachnoid space [13, 19].

Uncertainty exists in terms what are considered to be normal ICP values during infancy. A widely cited reference

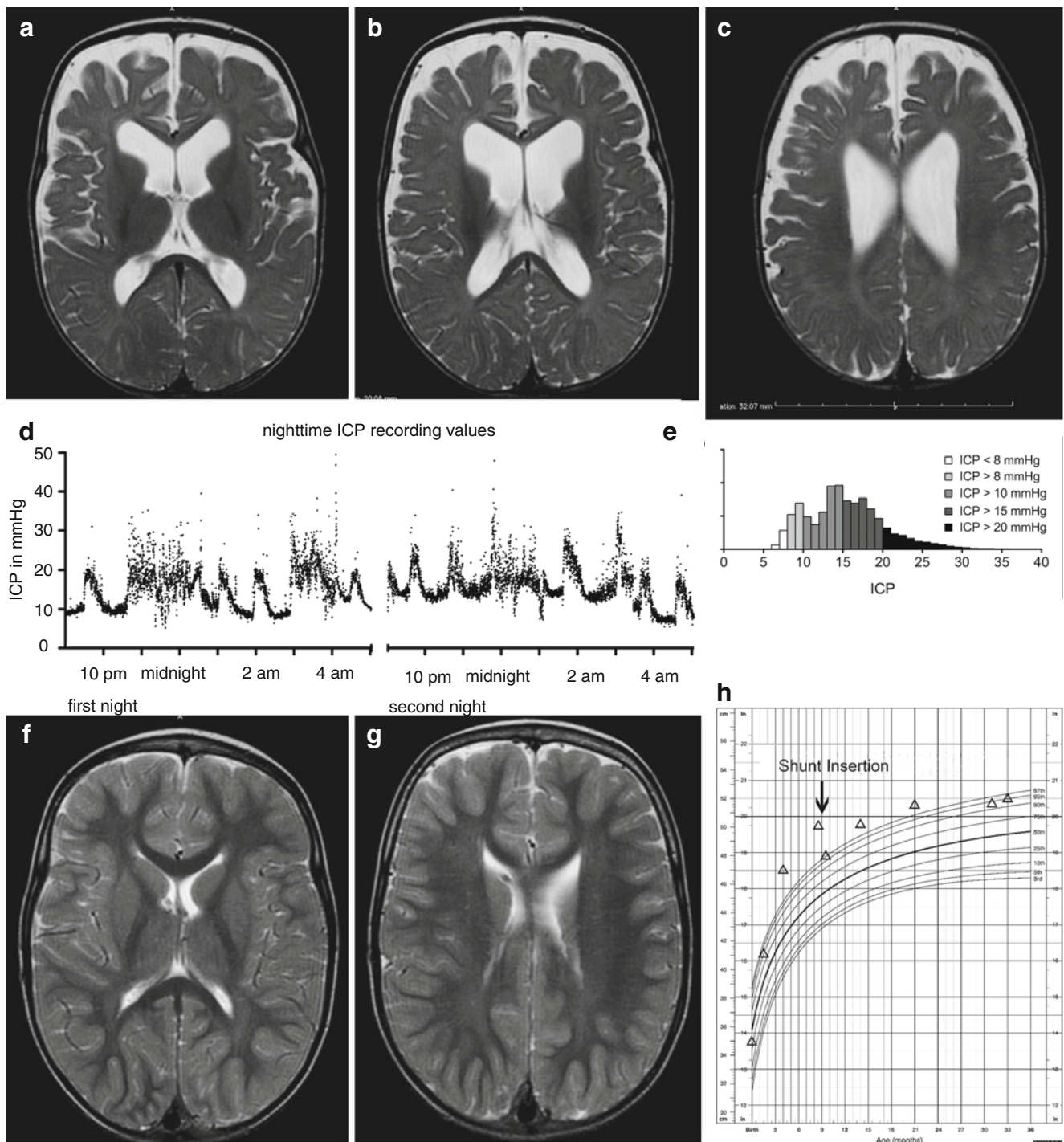


Fig. 2 Case example: A male infant was presented to our service at the age of 10 months. The child was born prematurely at the 31st gestational week. Age-corrected head circumference at birth was between the 50th and 90th percentile [7]. Clinical development was unremarkable except for progressive macrocephaly. By the time of presentation the recorded age-corrected head circumference was 50 cm, which equals 2.5 cm above the 97th percentile [15]. Fundoscopy was without signs of papilledema. MRI showed an enlarged ventricular system as well as widened subarachnoid spaces (a–c). After obtaining consent a

ventricular drain was inserted and ICP was recorded for two consecutive nights (d). The recorded ICP values were significantly elevated – night-time baseline ICP was 12.2 mmHg and average night-time ICP was 15.3 mmHg. (e) Shows the distribution of ICP values. After shunt insertion the MRI showed resolution of the previously dilated internal and external CSF spaces (f and g). The head circumference is normalized and slightly below the 97th percentile (h). Development of the child continues to be normal

defines normal ICP at 3.5 mmHg in neonates, 5.8 mmHg in infants, 6.4 mmHg in children, and 15.3 mmHg in adolescents and adults [16]. In other reports on infants with craniosynostosis, mean ICP values of less than 10 mmHg at rest are cited as being normal [4–6, 20, 25]. After infancy in children with closed sutures normal values are lower than 15 mmHg [8, 12]. However, ICP values may be several -fold higher than the given normal values, can be measured for a short time span, and are well tolerated in an awake, active or crying infant. Also, cyclic night-time elevation of ICP values up to doubling of baseline values associated with REM sleep phases or “active sleep phases” have been documented in infants (Fig 2) [10, 14, 20, 26].

Although subarachnoidomegaly is treated in most cases conservatively, in cases with marked macrocephaly, additionally enlarged ventricles and tense fontanel additional factors may contribute to this pathological condition. Therefore, we decided to offer continuous ICP monitoring to strengthen our recommendation for either a CSF-diverting procedure or expectant observation. The rationale for such a measurement is the fact that elevation of ICP would be appropriately treated by a pressure-regulated CSF diverting system [23]. Possible alternatives are repetitive lumbar punctures or acetazolamide as transient treatment options.

There is evidence that chronically elevated ICP is detrimental to the developing nervous system [22]. The clinical correlation in infancy might be subtle and escape sole clinical assessment. The distribution of ICP values in the subgroup of children who finally received a VP shunt, showed an average of 72.5% of all recorded ICP values above a threshold of 10 mmHg, an average 36.5% above a threshold of 15 mmHg. Therefore, a decision based only on clinical grounds is unreliable for further development. Also, the developmental potential that might be lost due to a state of chronically elevated ICP would be irreversible. This consideration was the background for our treatment decision; however, the well-known risk of VP shunt implantation [2, 18, 24] will need to be weighed against the possible risk of withholding potential beneficial treatment.

Conclusion

Although no clear conclusions about cut-off ICP values can be drawn, according to our study we suggest a mean night-time ICP threshold of 15 mmHg, with a grey zone of 10 to 15 mmHg, for decision-making regarding surgical treatment in these children. However, more experience must be gained to analyze a risk–benefit ratio and to figure out the long-term clinical outcome.

Conflict of interest statement U-W Thomale does cooperate with Miethke Aesculap in terms of lectures and development. We declare that we have no conflict of interest.

References

1. Aoki N (1994) Extracerebral fluid collections in infancy: role of magnetic resonance imaging in differentiation between subdural effusion and subarachnoid space enlargement. *J Neurosurg* 81:20–23
2. Berry JG, Hall MA, Sharma V, Goumnerova L, Slonim AD, Shah SS (2008) A multi-institutional, 5-year analysis of initial and multiple ventricular shunt revisions in children. *Neurosurgery* 62:445–453; discussion 453–444
3. Carolan PL, McLaurin RL, Towbin RB, Towbin JA, Egelhoff JC (1985) Benign extra-axial collections of infancy. *Pediatr Neurosci* 12:140–144
4. Eide PK (2005) Assessment of childhood intracranial pressure recordings using a new method of processing intracranial pressure signals. *Pediatr Neurosurg* 41:122–130
5. Eide PK (2006) Assessment of quality of continuous intracranial pressure recordings in children. *Pediatr Neurosurg* 42:28–34
6. Eide PK, Helseth E, Due-Tønnessen B, Lundar T (2002) Assessment of continuous intracranial pressure recordings in childhood craniosynostosis. *Pediatr Neurosurg* 37:310–320
7. Fenton TR (2003) A new growth chart for preterm babies: Babson and Benda's chart updated with recent data and a new format. *BMC Pediatr* 3:13
8. Gambardella G, Zacccone C, Cardia E, Tomasello F (1993) Intracranial pressure monitoring in children: comparison of external ventricular device with the fiberoptic system. *Childs Nerv Syst* 9:470–473
9. Hamza M, Bodensteiner JB, Noorani PA, Barnes PD (1987) Benign extracerebral fluid collections: a cause of macrocrania in infancy. *Pediatr Neurol* 3:218–221
10. Hayward R, Gonzalez S (2005) How low can you go? Intracranial pressure, cerebral perfusion pressure, and respiratory obstruction in children with complex craniosynostosis. *J Neurosurg* 102:16–22
11. Hellbusch LC (2007) Benign extracerebral fluid collections in infancy: clinical presentation and long-term follow-up. *J Neurosurg* 107:119–125
12. Inagaki T, Kyutoku S, Seno T, Kawaguchi T, Yamahara T, Oshige H, Yamanouchi Y, Kawamoto K (2007) The intracranial pressure of the patients with mild form of craniosynostosis. *Childs Nerv Syst* 23:1455–1459
13. Kendall B, Holland I (1981) Benign communicating hydrocephalus in children. *Neuroradiology* 21:93–96
14. Krauss JK, Droste DW, Bohus M, Regel JP, Scheremet R, Riemann D, Seeger W (1995) The relation of intracranial pressure B-waves to different sleep stages in patients with suspected normal pressure hydrocephalus. *Acta Neurochir (Wien)* 136:195–203
15. Kuczmarski RJ, Ogden CL, Guo SS, Grummer-Strawn LM, Flegal KM, Mei Z, Wei R, Curtin LR, Roche AF, Johnson CL (2002) 2000 CDC Growth Charts for the United States: methods and development. *Vital Health Stat* 11:1–190
16. Minns RA (1984) Intracranial pressure monitoring. *Arch Dis Child* 59:486–488
17. Paciorkowski AR, Greenstein RM (2007) When is enlargement of the subarachnoid spaces not benign? A genetic perspective. *Pediatr Neurol* 37:1–7
18. Parker SL, Attenello FJ, Sciubba DM, Garces-Ambrossi GL, Ahn E, Weingart J, Carson B, Jallo GI (2009) Comparison of shunt infection incidence in high-risk subgroups receiving antibiotic-impregnated versus standard shunts. *Childs Nerv Syst* 25:77–83; discussion 85

19. Prassopoulos P, Cavouras D, Golfinopoulos S, Nezi M (1995) The size of the intra- and extraventricular cerebrospinal fluid compartments in children with idiopathic benign widening of the frontal subarachnoid space. *Neuroradiology* 37:418–421
20. Renier D, Sainte-Rose C, Marchac D, Hirsch JF (1982) Intracranial pressure in craniostenosis. *J Neurosurg* 57:370–377
21. Robertson WC Jr, Chun RW, Orrison WW, Sackett JF (1979) Benign subdural collections of infancy. *J Pediatr* 94:382–386
22. Sasidharan P, Marquez E, Dizon E, Sridhar CV (1986) Developmental outcome of infants with severe intracranial-intraventricular hemorrhage and hydrocephalus with and without ventriculoperitoneal shunt. *Childs Nerv Syst* 2:149–152
23. Schuhmann MU, Sood S, McAllister JP, Jaeger M, Ham SD, Czosnyka Z, Czosnyka M (2008) Value of overnight monitoring of intracranial pressure in hydrocephalic children. *Pediatr Neurosurg* 44:269–279
24. Simon TD, Hall M, Riva-Cambrin J, Albert JE, Jeffries HE, Lafleur B, Dean JM, Kestle JR (2009) Infection rates following initial cerebrospinal fluid shunt placement across pediatric hospitals in the United States. Clinical article. *J Neurosurg Pediatr* 4:156–165
25. Tamburrini G, Di Rocco C, Velardi F, Santini P (2004) Prolonged intracranial pressure (ICP) monitoring in non-traumatic pediatric neurosurgical diseases. *Med Sci Monit* 10:MT53–MT63
26. Wayenberg JL, Hasaerts D, Franco P, Valente F, Massager N (1995) Anterior fontanelle pressure variations during sleep in healthy infants. *Sleep* 18:223–228

Treatment Options for Intracranial Arachnoid Cysts: A Retrospective Study of 69 Patients

Anders Vedel Holst, Patricia L. Danielsen, and Marianne Juhler

Abstract The best surgical treatment of cerebral arachnoid cysts is yet to be established. Treatment options are shunting, endoscopic fenestration or microsurgical fenestration through craniotomy.

Data from 69 patients with cerebral arachnoid cysts treated in our institution between 1997 and 2007 were reviewed.

Cysts were located infratentorially in 20% ($n=14$) and supratentorially in 80% ($n=55$); of these 73% ($n=40$) were in the middle cranial fossa. Mean cyst size was 61 mm (range 15–100 mm). The most common symptoms were headache (51%), dizziness (26%), cranial nerve dysfunction (23%), seizure (22%), nausea and vomiting (18%), and hemiparesis (13%). Surgery was performed in 83% ($n=57$). First-line treatments were microsurgical fenestration ($n=30$), endoscopic fenestration ($n=15$), and cystoperitoneal/ventriculoperitoneal shunting ($n=11$). More than one intervention was needed in 42% ($n=24$). A particularly high rate of relapse (73%) was observed after endoscopic fenestration, following which 11 patients were admitted for reoperation. By comparison, only eight patients (28%) managed with microsurgical fenestration and four (36%) in the shunted group needed a second surgical procedure. Mean follow-up was 30 months. In the surgical series 79% ($n=45$) had a good outcome.

We conclude that the surgical treatment of arachnoid cysts has an overall good outcome. In our institution the best results were obtained with microsurgical decompression through craniotomy.

Keywords Arachnoid cyst • Microsurgical fenestration • Endoscopic fenestration • Shunting

Introduction

Arachnoid cysts are benign, congenital, intra-arachnoid collections of clear, colorless fluid with the same osmolality as cerebrospinal fluid (CSF) though chemically dissimilar [3]. On brain imaging studies, arachnoid cysts are a common incidental finding with a prevalence of 1.1% in adults [28] and 2.6% in children [1]. Cysts are located along the cranio-spinal axis, with a strong predilection for the temporal fossa [18, 22, 23, 29], predominantly on the left side [9].

Although the majority of arachnoid cysts are asymptomatic, a wide range of symptoms can be present depending on the anatomical location and intracystic pressure [8, 11]. Symptoms include headache, nausea and vomiting, seizures, macrocephaly, endocrine dysfunction, cognitive decline, and focal neurological deficits [5, 7, 13, 14, 16, 17, 20, 21].

The treatment of choice is still debated. Shunting procedures have been suggested as first-line treatment by various authors [2, 6, 10]. Obtaining shunt independence by cyst excision [24], fenestration through craniotomy or the key-hole approach [15], or endoscopic fenestration [12, 19, 26] has also been recommended.

The aim of this present study was to characterize the clinical presentation, imaging features, and surgical management with an emphasis on treatment options and their outcome. Current treatment options in our institution are shunting procedures, endoscopic fenestration and microsurgical fenestration through craniotomy.

Materials and Methods

Data from patients with cerebral arachnoid cysts admitted to our institution between 1997 and 2007 were reviewed. The files were identified by searching for the diagnostic codes Q04.6 *cystis cerebri congenita* and G93.0 *cystis cerebri* in the hospital archives. Only patients with radiologically evident arachnoid cysts were included in the study whereas other cystic lesions were excluded. Diagnosis was based on radiological findings on MRI. Epidemiological and

A.V. Holst (✉) and M. Juhler
Department of Neurosurgery 2092, Rigshospitalet, University of Copenhagen, Blegdamsvej 9, 2100 Copenhagen, Denmark
e-mail: vedelpt@gmail.com

P.L. Danielsen
Department of Dermatology, Copenhagen Wound Healing Center, Bispebjerg Hospital, University of Copenhagen, Copenhagen, Denmark

Table 1 Cyst location

Location	No. of cases
<i>Supratentorial</i>	55 (80%)
Sylvian fissure	40
Fronto-parietal convexity	8
Occipital lobe	2
Quadrigeminal plate	2
Parasagittal	1
Clivus	1
Sellar–suprasellar	1
<i>Infratentorial</i>	14 (20%)
Cerebellar hemisphere	6
Fourth ventricle	3
Cerebello-pontine angle	2
Interhemispheric	2
Cerebello-medullary cistern	1

anatomical features were registered. The treatment of choice was based on the individual estimation and experience of the senior surgeon. In some cases this was preceded by conference discussion. Evaluation of outcome was based primarily on clinical examination with the support of post-operative imaging. The relapse rate or lack of improvement after the first line treatment and the need for additional surgical procedures were registered, as was the surgical technique in the second and in a few cases in the third and fourth interventions. Finally, the outcome after the last intervention was also registered, based on clinical and imaging features.

Results

Sixty-nine patients were registered in the period 1997–2007. The mean age at admittance was 37.5 (range 0–84) and the average follow-up period was 30 months (0–130 months). Thirty-nine male and 30 female patients were admitted. In 25% ($n=17$) patients were under 15 years old. Five of these were infants (<12 months). Supratentorial location of cysts was noted in 80% ($n=55$), of these 73% ($n=40$) were located in the middle cerebral fossa in relation to the sylvian fissure, predominantly on the left side ($n=28$; Table 1).

The mean size was 61 mm (range 15–100 mm). Headache with or without other symptoms of increased intracranial pressure was the most common symptom and was present in 51%. Thus, headache together with nausea and vomiting occurred in 18%. Four pediatric patients presented with macrocephaly and five patients presented with bleeding into the cyst or subdural hematoma.

Symptoms of a focal or possibly focal nature were dizziness (26%), cranial nerve dysfunction (23%), seizures (22%),

Table 2 Clinical presentation

Symptoms	Infants < 12 months	Pediatrics < 15 years	Adults > 15 years
Headache	–	5	30
Nausea/vomiting	1	4	7
Dizziness	–	3	15
Cranial nerve dysfunction	–	3	13
Seizure	2	3	10
Hemiparesis	–	2	7
Cognitive decline	–	1	7
SDH/cystic bleeding	–	1	4
Macrocephaly	2	2	–

hemiparesis (13%), and cognitive decline (12%). In some individual cases a wider array of symptoms were described, such as unilateral hearing loss, syncope, dysarthria, ataxia and paresthesia in the extremities (Table 2).

Surgery was performed on 83% ($n=57$) of the patients whereas 17% ($n=12$) were treated conservatively. First-line treatment was microsurgical fenestration in 53% ($n=30$), endoscopic fenestration in 26% ($n=15$), and cystoperitoneal or ventriculoperitoneal shunting in 19% ($n=11$). Total removal of the cyst membrane was performed in one patient (Table 3).

In the endoscopic series two cases failed due to technical problems, in one case an existing communication to arachnoid space was recognized and in yet another case a blood vessel did not allow sufficient fenestration. In the remaining cases no explanation was given.

Two out of four shunt failures were replacement of sinus shunts. Revision of shunts because of shunt dysfunction due to disconnection, infection or extracranial obstruction was not considered to constitute a relapse. Three patients managed with microsurgical fenestration had doubtful clinical improvement, but because of considerable reduction in the cyst size they were not admitted for repeat surgery. Eight patients had no clinical or radiological improvement after microsurgical fenestration; two of these had a cystoperitoneal shunt implanted. Five underwent redo fenestration because the primary fenestration either was insufficient or had closed over. Redo fenestration failed in two patients and both had a cystoperitoneal shunt implanted.

In our institution we found a significantly higher risk of relapse after endoscopic fenestration compared with microsurgical fenestration, OR 8.2 (95% CI [1.5–46.5]).

Of the 57 patients who had their arachnoid cyst managed surgically 42% ($n=24$) needed reoperation. Eleven patients had a shunt implanted as first-line treatment and additionally 13 became shunt-dependent after repeat surgery. Four patients had their shunt removed at a later occasion with no radiological or clinical relapse.

Table 3 First-line treatment and need for reoperation

	Microsurgery	Endoscopy	Shunting	Excision	Total
Total	30	15	11	1	57
Reoperated	8 (28%)	11 (73%)	4 (36%)	0	23

All together 79% of patients ($n=45$) who underwent surgery had symptom improvement and 77% had reduction of cyst size on postoperative imaging.

Discussion

Most authors argue in favor of a surgical approach in symptomatic arachnoid cyst patients presenting with progressive hydrocephalus, raised intracranial pressure or focal neurological symptoms [4, 18]. Surgery is also recommended in asymptomatic cases [25] although some groups suggest a more conservative approach in such cases [27]. In our institution all patients admitted for surgery were symptomatic with a majority presenting with signs of raised intracranial pressure such as headache, in some cases accompanied by nausea and vomiting. Asymptomatic patients or patients in whom no correlation between imaging and symptoms was found were either followed clinically or referred elsewhere, e.g. to a neurologist.

In our study, 72% of the patients managed with microsurgical fenestration improved and had no need for repeat surgery. Accordingly, Levy et al. [15] reported a cyst reduction in 82% and a clinical improvement in as many as 95% in a series of 50 children with middle fossa arachnoid cysts using microsurgical fenestration.

Failure occurred in 11 patients treated endoscopically necessitating repeat surgical treatment. In all cases a shunt was implanted on a later occasion. Surprisingly, only four patients had a successful endoscopic fenestration as first-line treatment. We found a significantly higher risk of relapse and need for reoperation in the endoscopic series compared with the cases managed with microsurgical fenestration.

In a few cases failure of treatment was due to insufficient fenestration or technical problems, but in most cases the reason remained unclear.

Other groups report far better results using the endoscopic fenestration approach, with clinical improvements in 80–100% [19]. We speculate that thorough preoperative evaluation and selection of patients for either an endoscopic or microsurgical approach might have an impact on the outcome. Additionally, a higher success rate, when managed with microsurgical decompression in our institution, might be explained by the familiarity of traditional micro-neurosurgical techniques that are more accessible to surgeons. An open surgical approach provides certain advantages over endoscopic procedures; control of bleeding can be difficult

in endoscopic procedures, stereoscopic observation through a microscope gives superior depth perception and open procedures permit bimanual manipulation.

The surgical approach in the treatment of arachnoid cysts remains debatable and should be based on the individual surgeon's experience.

Conclusion

In this retrospective study the best clinical outcome was obtained after microsurgical fenestration through craniotomy whereas a significantly higher relapse rate was observed in arachnoid cyst patients managed endoscopically. The reason for this is partially unclear and we intend to conduct a large scale prospective study to investigate this further.

Conflict of interest statement We declare that we have no conflict of interest.

References

1. Al-Holou WN, Yew AY, Boomsaad ZE, Garton HJ, Muraszko KM, Maher CO (2010) Prevalence and natural history of arachnoid cysts in children. *J Neurosurg Pediatr* 5(6):578–585
2. Arai H, Sato K, Wachi A, Okuda O, Takeda N (1996) Arachnoid cysts of the middle cranial fossa: experience with 77 patients who were treated with cystoperitoneal shunting. *Neurosurgery* 39(6):1108–1112
3. Berle M, Wester KG, Ulvik RJ, Kroksveen AC, Haaland OA, Amiry-Moghaddam M, Berven FS, Helland CA (2010) Arachnoid cysts do not contain cerebrospinal fluid: a comparative chemical analysis of arachnoid cyst fluid and cerebrospinal fluid in adults. *Cerebrospinal Fluid Res* 7:8
4. Boutarouch M, El Ouahabi A, Rifi L, Arkha Y, Derraz S, El Khamlichi A (2008) Management of intracranial arachnoid cysts: institutional experience with initial 32 cases and review of the literature. *Clin Neurol Neurosurg* 110(1):1–7
5. Cartwright MJ, Eisenberg MB, Page LK (1991) Posterior fossa arachnoid cyst presenting with an isolated twelfth nerve paresis. Case report and review of the literature. *Clin Neurol Neurosurg* 93(1):69–72
6. Ciricillo SF, Cogen PH, Harsh GR, Edwards MS (1991) Intracranial arachnoid cysts in children. A comparison of the effects of fenestration and shunting. *J Neurosurg* 74(2):230–235
7. Clavel M, Tabora FG, Onzain I (1985) Arachnoid cysts as a cause of dementia in the elderly. *Acta Neurochir (Wien)* 78:28–32
8. Di Rocco C, Tamburrini G, Caldarelli M, Velardi F, Santini P (2003) Prolonged ICP monitoring in Sylvian arachnoid cysts. *Surg Neurol* 60(3):211–218

9. Galassi E, Gaist G, Giuliani G, Pozzati E (1988) Arachnoid cysts of the middle cranial fossa: experience with 77 cases treated surgically. *Acta Neurochir Suppl (Wien)* 42:201–204
10. Germanò A, Caruso G, Caffo M, Baldari S, Calisto A, Meli F, Tomasello F (2003) The treatment of large supratentorial arachnoid cysts in infants with cyst-peritoneal shunting and Hakim programmable valve. *Childs Nerv Syst* 19(3):166–173
11. Helland CA, Wester K (2007) Intracystic pressure in patients with temporal arachnoid cysts: a prospective study of preoperative complaints and postoperative outcome. *J Neurol Neurosurg Psychiatry* 78(6):620–623
12. Hopf N, Perneczky A (1998) Endoscopic neurosurgery and endoscope-assisted microneurosurgery for the treatment of intracranial cysts. *Neurosurgery* 43:1330–1337
13. Kang JK, Lee KS, Lee IW, Jeun SS, Son BC, Jung CK, Park YS, Lee SW (2000) Shunt-independent surgical treatment of middle cranial fossa arachnoid cysts in children. *Childs Nerv Syst* 16(2):111–116
14. Lang W, Lang M, Kornhuber A, Gallwitz A, Kriebel J (1985) Neuropsychological and neuroendocrinological disturbances associated with extracerebral cysts of the anterior and middle cranial fossa. *Eur Arch Psychiatry Neurol Sci* 235:38–41
15. Levy ML, Wang M, Aryan HE, Yoo K, Meltzer H (2003) Microsurgical keyhole approach for middle fossa arachnoid cyst fenestration. *Neurosurgery* 53(5):1138–1144
16. Millichap JG (2003) Temporal lobe arachnoid cyst-attention deficit disorder syndrome: role of the electroencephalogram in diagnosis. *Neurology* 48(5):1435–1439
17. Mohn A, Schoof E, Fahlbusch R, Wenzel D, Dörr HG (1999) The endocrine spectrum of arachnoid cysts in childhood. *Pediatr Neurosurg* 31(6):316–321
18. Oberbauer RW, Haase J, Pucher R (1992) Arachnoid cysts in children: a European co-operative study. *Childs Nerv Syst* 8(5):281–286
19. Oertel JM, Wagner W, Mondorf Y, Baldauf J, Schroeder HW, Gaab MR (2010) Endoscopic treatment of arachnoid cysts: a detailed account of surgical techniques and results. *Neurosurgery* 67(3):824–836
20. Pascual-Castroviejo I, Pascual-Pascual SI (1994) Bilateral arachnoid cysts, seizures and severe encephalopathy: case report. *Neuropediatrics* 25(1):42–43
21. Pascual-Castroviejo I, Roche MC, Martínez Bermejo A, Arcas J, García Blázquez M (1991) Primary intracranial arachnoidal cysts. A study of 67 childhood cases. *Childs Nerv Syst* 7(5):257–263
22. Passero S, Filosomi G, Cioni R, Venturi C, Volpini B (1990) Arachnoid cysts of the middle cranial fossa: a clinical, radiological and follow-up study. *Acta Neurol Scand* 82(2):94–100
23. Rengachary SS, Watanabe I (1981) Ultrastructure and pathogenesis of intracranial arachnoid cysts. *J Neuropathol Exp Neurol* 40(1):61–83
24. Sato H, Sato N, Katayama S, Tamaki N, Matsumoto S (1991) Effective shunt-independent treatment for primary middle fossa arachnoid cyst. *Childs Nerv Syst* 7(7):375–381
25. Sato K, Shimoji T, Yaguchi K, Sumie H, Kuru Y, Ishii S (1983) Middle fossa arachnoid cyst: clinical, neuroradiological, and surgical features. *Childs Brain* 10(5):301–316
26. Schroeder HWS, Gaab MR, Niendorf WR (1996) Neuroendoscopic approach to arachnoid cysts. *J Neurosurg* 85:293–298
27. Sommer IE, Smit LM (1997) Congenital supratentorial arachnoidal and giant cysts in children: a clinical study with arguments for a conservative approach. *Childs Nerv Syst* 13(1):8–12
28. Vernooij MW, Ikram MA, Tanghe HL, Vincent AJ, Hofman A, Krestin GP, Niessen WJ, Breteler MM, van der Lugt A (2007) Incidental findings on brain MRI in the general population. *N Engl J Med* 357(18):1821–1828
29. Wester K (1999) Peculiarities of intracranial arachnoid cysts: location, sidedness, and sex distribution in 126 consecutive patients. *Neurosurgery* 45(4):775–779

A Microdialysis Study of Oral Vigabatrin Administration in Head Injury Patients: Preliminary Evaluation of Multimodality Monitoring

Keri L.H. Carpenter, Ivan Timofeev, Jürgens Nortje, Marek Czosnyka, John D. Pickard, and Peter J. Hutchinson

Abstract Background: We assessed the feasibility of administering a neuroprotective drug, vigabatrin (VGB; gamma-vinyl-gamma-aminobutyric acid) with multimodality monitoring, including cerebral microdialysis, in severe head injury patients, to measure surrogate endpoints and blood–brain barrier (BBB) penetration.

Methods: Patients ($n=20$) were randomised to VGB (0.5 g twice-daily, enteric) or control. ICP, ABP, CPP and cerebrovascular pressure reactivity index (PRx) were monitored. Microdialysate glucose, lactate, pyruvate, glutamate, glycerol, amino acids, VGB and GABA were analysed.

Results: Preliminary evaluation of results (five VGB-treated patients) showed that VGB levels rose in brain microdialysates, followed by a modest increase in GABA. VGB and GABA increased more in abnormal brain than in sites further from lesions, and were higher after multiple VGB doses. Highest VGB and GABA microdialysate levels were 75 and 4 $\mu\text{mol/L}$ respectively. Microdialysate glucose and glycerol sometimes decreased, and glutamate and tyrosine sometimes increased, following VGB administration; causation unproven. VGB did not overtly affect ICP, ABP, CPP, PRx, or microdialysate lactate, pyruvate and lactate/pyruvate ratio.

Conclusion: Multimodality monitoring, including cerebral microdialysis, is feasible for studying surrogate endpoints following drug administration. VGB crosses the BBB, leading to modest increases in extracellular GABA. Further analyses are ongoing. Microdialysis may assist the development of neuroprotective agents by determining penetration into extracellular fluid of the brain.

Keywords Head injury (human) • Multimodality monitoring • Microdialysis • Vigabatrin • GABA

Introduction

Clinical trials of drugs for treating traumatic brain injury (TBI) have produced negative results, and there is still a lack of suitable agents. TBI is the largest single cause of death in the under-45s in developed countries. Survivors of the initial impact experience, in the hours and days that follow, a complex interactive set of changes, which vary with time, involving many processes, for example, energy disturbances, excitotoxicity, spreading depolarisations, inflammation and elevations in intracranial pressure (ICP), with a range of clinical outcomes, varying from good recovery to varying degrees of disability or even death. Drugs that have seemed promising in vitro and in animal studies have failed in clinical trials. This failure is partly due a lack of information on whether the drug in question is able to cross the human blood–brain barrier (BBB) in sufficient amounts at an appropriate dosage, and the pharmacokinetics in the human brain relative to plasma. We assessed the feasibility of administering a neuroprotective drug, vigabatrin (VGB; gamma-vinyl-gamma-aminobutyric acid) with multimodality monitoring, including cerebral microdialysis, in severe head injury patients, to measure surrogate endpoints and BBB penetration. The anticonvulsant VGB is an irreversible inhibitor of gamma-aminobutyric acid transaminase (GABA-transaminase), an enzyme that degrades the neurotransmitter gamma-aminobutyric acid (GABA). VGB and GABA are small water-soluble molecules with molecular weights of

K.L.H. Carpenter (✉), I. Timofeev, J.D. Pickard, and P.J. Hutchinson
Division of Neurosurgery, Department of Clinical Neurosciences,
University of Cambridge, Box 167, Addenbrooke's Hospital,
Hills Road, Cambridge, CB2 0QQ, UK

Wolfson Brain Imaging Centre, Department of Clinical Neurosciences,
University of Cambridge, Box 65, Addenbrooke's Hospital, Hills
Road, Cambridge, CB2 0QQ, UK
e-mail: klc1000@wbic.cam.ac.uk

J. Nortje
Wolfson Brain Imaging Centre, Department of Clinical Neurosciences,
University of Cambridge, Box 65, Addenbrooke's Hospital, Hills
Road, Cambridge, CB2 0QQ, UK

Division of Anaesthesia, Department of Medicine, University of
Cambridge, Box 93, Addenbrooke's Hospital, Hills Road,
Cambridge, CB2 0QQ, UK

M. Czosnyka
Division of Neurosurgery, Department of Clinical Neurosciences,
University of Cambridge, Box 167, Addenbrooke's Hospital, Hills
Road, Cambridge, CB2 0QQ, UK

129.16 Da and 103.12 Da respectively. To our knowledge, this is the first study to measure VGB in TBI patients' brain microdialysates as part of multimodality monitoring.

Materials and Methods

Patient Selection

The study was approved by the Cambridge Local Research Ethics Committee and assent obtained from the next of kin. Patients were over 16 years of age with TBI, requiring ventilation and ICP monitoring. The major exclusion criterion was deranged clotting and/or low platelets. None of the patients had any significant previous neurological conditions or family history of neuro-degenerative disease. Patients (total $n=20$) were randomised to VGB (0.5 g every 12 h, enterically) or control (no VGB). The present report is a preliminary evaluation of results for five of the VGB-treated patients.

Microdialysis Technique

Microdialysis monitoring was started as soon as possible following admission to the Neuro-critical care unit. Microdialysis catheters (CMA71 or CMA70, 100 or 20 kDa molecular weight cut-off respectively, 10-mm membrane; CMA Microdialysis AB, Solna, Sweden) were inserted into the cerebral frontal parenchyma of patients, in conjunction with an ICP transducer (Codman, Raynham, MA, USA) using a triple lumen cranial access device (Technicam, Newton Abbot, UK). Pressure data – arterial blood pressure (ABP), ICP, cerebral perfusion pressure (CPP) and pressure reactivity index (PRx, which is a moving correlation coefficient for ICP vs. ABP [1]) – were read using ICM+ software (University of Cambridge) [9]. The catheters were perfused with CNS perfusion fluid (NaCl 147 mM, KCl 2.7 mM, CaCl₂ 1.2 mM, MgCl₂ 0.85 mM, purchased from CMA Microdialysis AB) at 0.3 μ L/min using a CMA106 pump. Collection vials were changed hourly and analysed for glucose, lactate, pyruvate, glutamate and/or glycerol, using a CMA600 microdialysis analyser utilising automated enzymatic colorimetric assays.

HPLC Analysis

Samples were diluted using the ratio of 5 μ L of microdialysate with 10 μ L of water. Amino acid analysis was performed on an Agilent 1100 series HPLC (Agilent Technologies, Waldbronn, Germany), using methodology based on technical information from Agilent [3] and work by Hutchinson et al. [4]. The HPLC

system comprised a binary pump, refrigerated auto-sampler (at 10°C), and fluorescence detector (at 340 nm excitation, 450 nm emission), with a ChemStation data system. The column was a Phenomenex Luna ODS2 (100 \times 2 mm, particle size 3 μ m, pore size 100 Å; Phenomenex, Torrance, CA, USA), fitted with a Phenomenex SecurityGuard ODS guard cartridge. The mobile phase (flow rate 0.45 mL/min) was continuously vacuum-degassed and the column maintained at 40°C. Using the auto-sampler, each pre-diluted microdialysate sample (1 μ L) was automatically mixed in-needle with 5 μ L of borate buffer (Agilent Technologies; 0.4 M, pH 10.2), 1 μ L of OPA reagent (Agilent Technologies; 10 mg/mL ortho-phthalaldehyde in 0.4 M borate buffer plus mercaptopropionic acid) and 1 μ L of internal standard (25 μ M norvaline) and injected onto the HPLC column. Separation was achieved using binary (A/B) gradient elution. Mobile phase A was composed of 20 mM sodium acetate in water, 107 μ M EDTA, plus 180 μ L of triethylamine and 3 mL of tetrahydrofuran per litre, pH 7.2. Mobile phase B consisted of a 1:2:2 (v/v/v) mixture of 20 mM sodium acetate in water (pH 7.2), methanol and acetonitrile. Initial conditions (at time of injection) were 100% A, 0% B, changing linearly over a period of 17 min to 40% A, 60% B, which was maintained isocratically until 25 min after injection, then returned to initial conditions by 30 min after injection, with a 5-min post-run equilibration period before the next injection. Quantitation was by peak areas relative to the norvaline internal standard, with reference to an external standard mixture of amino acids plus norvaline, GABA and VGB. Plasma samples were available from a subset of patients. Proteins were removed by ultrafiltration (Sigma M0911, 10 kDa molecular weight cut-off; Sigma-Aldrich, Poole, Dorset, UK) and the clear, colourless ultrafiltrates were analysed for VGB by HPLC as described above.

The sequence of microdialysate vials analysed by HPLC commenced several hours before VGB administration, and continued through repeat doses given every 12 h. Not all vials had sufficient microdialysate volume remaining for HPLC analysis, and, in some cases (e.g. when long sequences were being evaluated) microdialysates from two vials were pooled for HPLC analysis.

Results

VGB in Plasma

Plasma levels of VGB were measured by HPLC, before and after the first VGB dose. Figure 1a illustrates the average results for five VGB-treated patients. There was demonstrable uptake of VGB into plasma by 2 h post-dose, rising further (on average) by 4 h, and declining somewhat by 11.5 h. The highest individual plasma VGB level was 29.9 μ M (at 4 h), while the mean (\pm SD) plasma VGB level at 4 h was 22.7 ± 5.5 μ M.

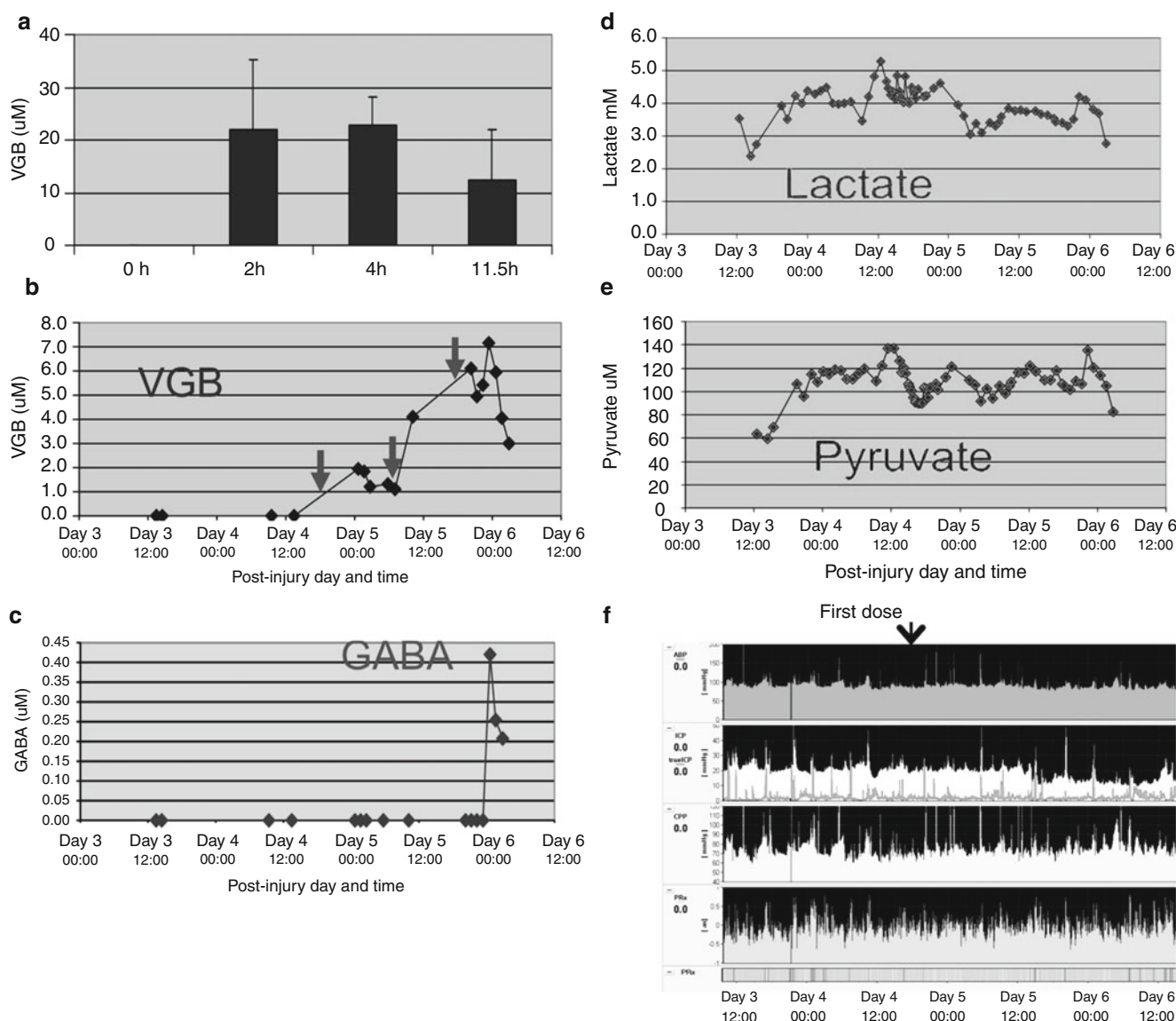


Fig. 1 (a) Levels of vigabatrin (VGB; $\mu\text{mol/L}$) in plasma for the first half-day following the initial dose of VGB (0.5 g, given enterically). VGB was undetectable in plasma collected just before the initial dose (0 h time-point). VGB was measurable in plasma samples at 2, 4 and 11.5 h after the initial dose. Each histogram bar represents mean \pm SD for five patients. (b) Levels of VGB ($\mu\text{mol/L}$) in brain microdialysates from patient W (male, aged 17 years, GCS 3 on admission). The day of injury is designated as Day 0. Microdialysis started on Day 3 post-injury, and VGB treatment commenced on Day 4 post-injury at 18:00. Data are for the first 1.5 days of

VGB administration. VGB (0.5 g) was given enterically every 12 h. Arrows indicate the times of the first three doses. (c) Levels of GABA ($\mu\text{mol/L}$), (d) levels of lactate (mmol/L) and (e) levels of pyruvate ($\mu\text{mol/L}$), all measured in brain microdialysates from patient W. (f) ICM+ traces from patient W. First (top) trace=ABP (mmHg); second trace=ICP (mmHg) shown in white, and "true ICP" (as defined by Czosnyka et al. [2]) shown in grey; third trace=CPP (mmHg) and fourth (bottom) trace=PRx. Ranges plotted on y-axes are: ABP 0–200 mmHg, ICP (and "true ICP") 0–50 mmHg, CPP 40–120 mmHg, and PRx –1.0 to +1.0

Brain Microdialysates and Pressure Monitoring

Case examples (Figs. 1, 2, and 3) illustrate the changes in composition of brain microdialysates, in relation to VGB administration, in three patients. Figure 1 charts patient W through three VGB doses, each separated by 12 h. The first VGB dose was on Day 4 post-injury. VGB was, as expected, undetectable in microdialysates before VGB administration.

VGB showed a progressive increase in concentration with the three VGB doses, peaking at 7.2 μM followed by a partial decline (Fig. 1b). GABA was undetectable until after the administration of the third VGB dose, whereupon it rose to 0.4 μM (Fig. 1c). Previous work without VGB has shown that GABA levels are typically very low or undetectable in non-ischaemic human brain microdialysates [4]. In patient W, there were no marked changes in lactate (Fig. 1d), pyruvate (Fig. 1e) or the lactate/pyruvate (L/P) ratio, or tyrosine. Glucose and glycerol both showed an overall decrease across

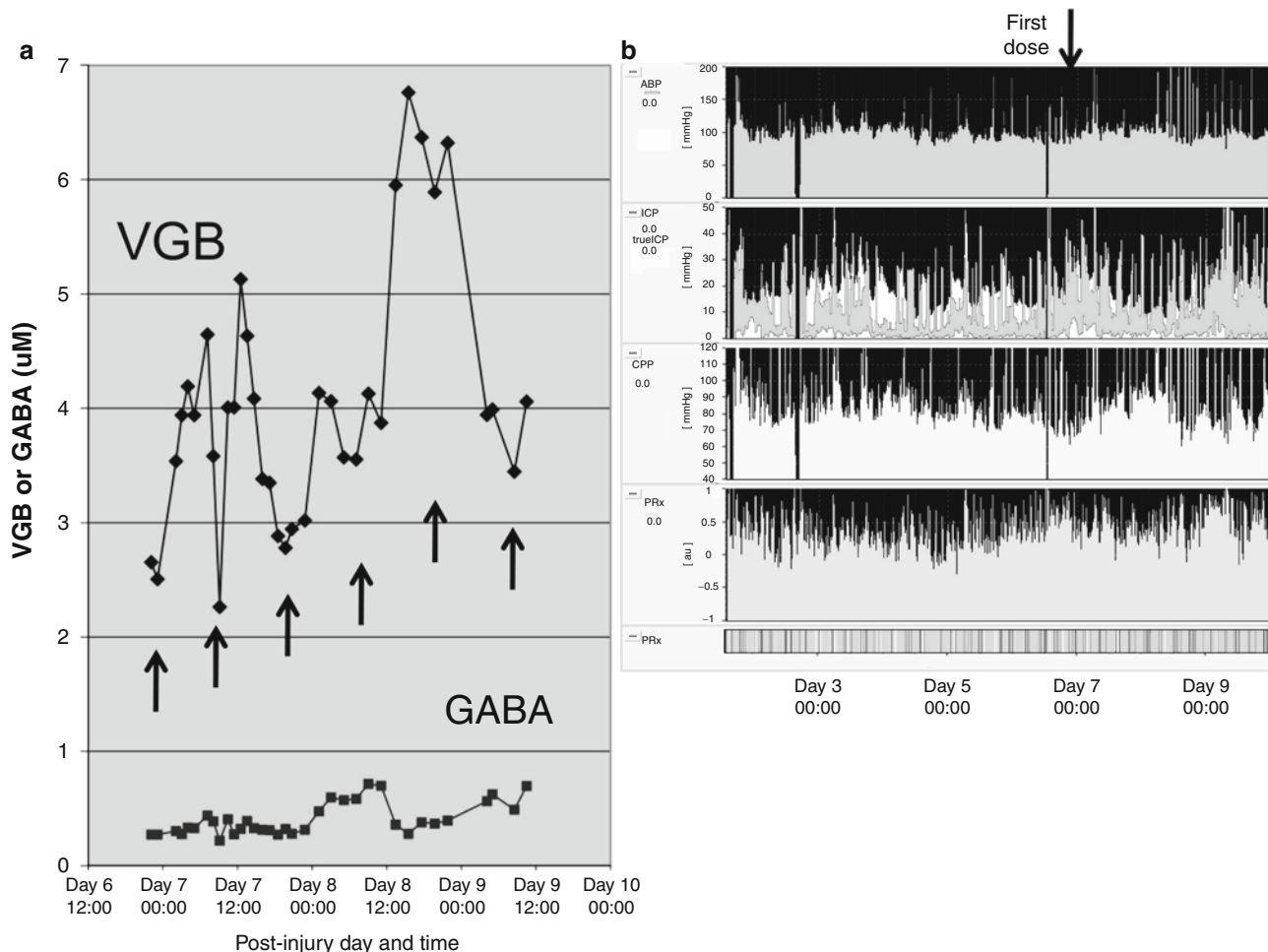


Fig. 2 (a) *Upper plot*: levels of VGB ($\mu\text{mol/L}$) in brain microdialysates from patient R (male, aged 33 years, GCS 14 on admission) plotted vs. time, for the first 2.5 days of VGB administration. *Arrows* indicate the times of the first six doses. Microdialysis commenced on Day 1 post-injury. VGB (0.5 g) was given enterically, commencing on Day 6 post-

injury at 23:05, and subsequently at 08:00 and 20:00 each day. *Lower plot*: levels of GABA ($\mu\text{mol/L}$) in brain microdialysates from patient R, plotted vs. time. (b) ICM+ traces from patient R. Parameters are displayed in the same order, and with the same y-axis ranges, as in Fig. 1f

the first three VGB doses, although their decline appeared to have already started before the first VGB dose. There were no overt changes in ABP, CPP or PRx during the period analysed (Fig. 1f). During the afternoon of Day 5 post-injury, between the second and third VGB doses, hypertonic saline was administered intravenously (at 12:20 and 14:40), and ICP consequently fell (from approximately 20 mmHg down to 15 mmHg; Fig. 1f).

Figure 2 follows patient R through six doses of VGB, the first of which was given on Day 6 post-injury. Microdialysate VGB levels rose following each VGB dose, followed by a degree of decline, though with an overall pattern of ascendancy (Fig. 2a, upper plot). During the period observed, the highest VGB level was 6.8 $\mu\text{mol/L}$ after the fourth VGB dose. GABA levels were approximately 0.3 $\mu\text{mol/L}$ before VGB administration and up to the point of the third VGB dose, after which an increase was seen (Fig. 2a, lower plot). Highest GABA levels were 0.7 $\mu\text{mol/L}$. Lactate levels increased during

VGB administration, but the rise appeared to have already begun before the first VGB dose. Pyruvate levels also rose in parallel, and the L/P ratio consequently showed little change. Glutamate showed a modest overall decrease (albeit with fluctuations) and tyrosine showed a modest increase. Glucose levels showed no clear pattern in relation to VGB administration. There were no obvious changes in ABP, ICP, CPP or PRx (Fig. 2b).

The above two cases (patients W and R) illustrated results in sites not close to focal lesions. In contrast, Fig. 3 focused on an abnormal region of the brain, in patient C, through 16 VGB doses, corresponding to Days 3–12 post-injury. VGB was undetectable in microdialysates before the first dose. VGB started to rise after the first dose, and continued to build following subsequent doses, maximising at 75 $\mu\text{mol/L}$ after the eighth dose (Fig. 3a). GABA levels pre-VGB and up to the second VGB dose were within the range 0.2–0.5 $\mu\text{mol/L}$, then briefly rose to 1.6 $\mu\text{mol/L}$, followed by a more sustained build

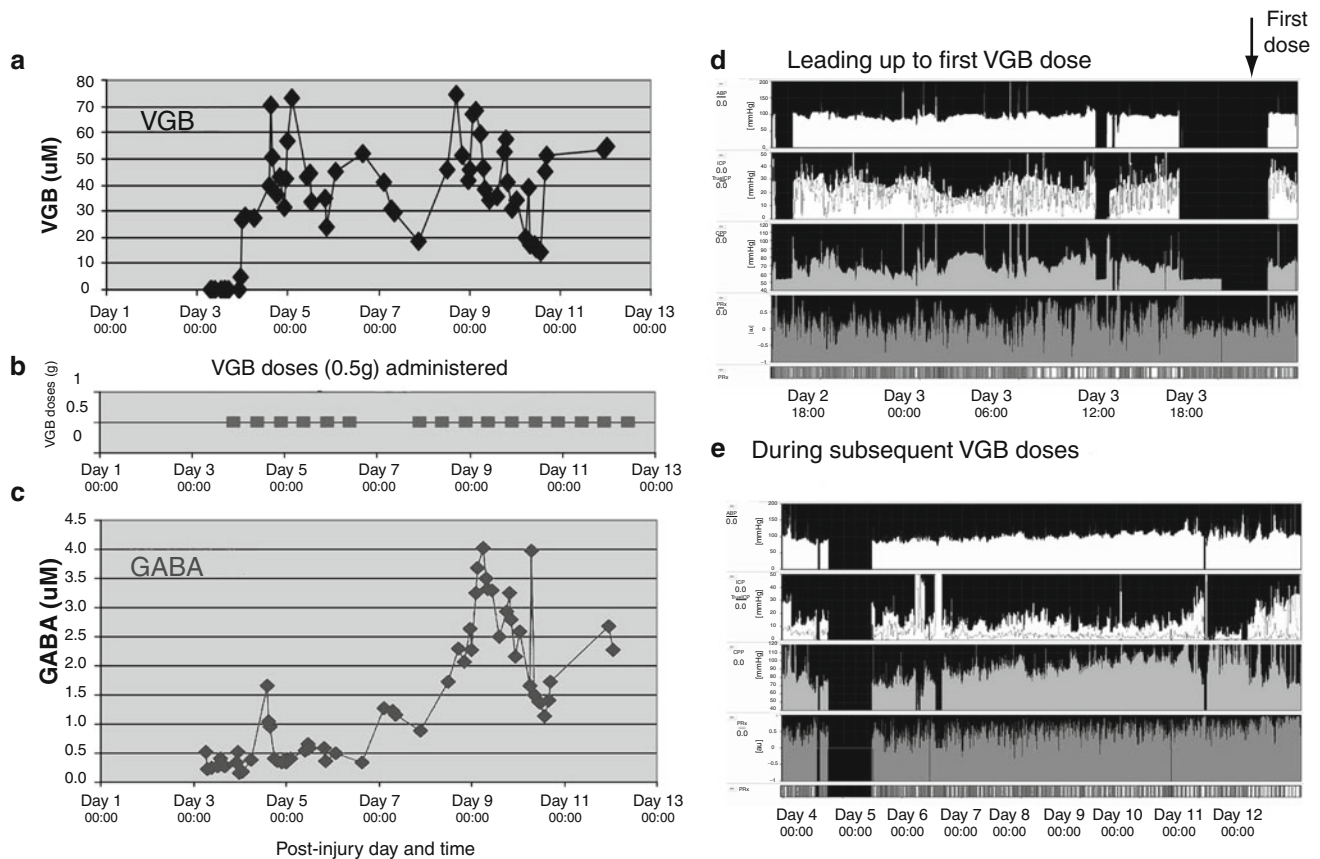


Fig. 3 (a) Levels of VGB ($\mu\text{mol/L}$) in brain microdialysates from patient C (male, aged 66 years, GCS 7 on admission) plotted vs. time, for the first 8.5 days of VGB administration. Microdialysis commenced on Day 2 post-injury. (b) Time-course of VGB administration for patient C. VGB treatment commenced on Day 3 post-injury, at 22:00. VGB (0.5 g) was given enterically every 12 h (at 10:00 and 22:00 each day), except for a gap of 36 h between the sixth and seventh doses. (c) Levels of GABA

($\mu\text{mol/L}$) in brain microdialysates from patient C, plotted vs. time. (d) ICM+traces from patient C, leading up to administration of the first VGB dose, and (e) ICM+traces from patient C, during subsequent doses of VGB. Parameters are displayed in the same order, and with the same y-axis ranges, as in Fig. 1f. Gaps in pressure monitoring in (d) and (e) occurred when leads were disconnected when moving the patient (e.g. for imaging); in these intervals, PRx readings should be disregarded

after the sixth dose, maximising at 4 μM after the ninth dose (Fig. 3c). Glucose levels fluctuated, with no obvious pattern in relation to VGB administration. Lactate and pyruvate began to rise before the first VGB dose. During VGB administration, lactate and pyruvate continued to rise gradually and then declined somewhat by Day 9 post-injury. The L/P ratio showed little overall pattern over the course of VGB administration, rising to around 50, falling to around 30, and then rising again to around 50. Glutamate was already rising before VGB administration started, and continued to rise, reaching a plateau at Days 5–8 post-injury, then partially declined by Day 9 post-injury. Glycerol showed a similar pattern to glutamate, albeit at lower levels. Tyrosine rose following VGB administration. ICP fell somewhat after the commencement of VGB administration, and stayed mostly down throughout several days of VGB treatment, albeit with some high fluctuations, and then began to rise again by Day 12 post-injury while VGB was still being given (the last dose was on Day 12 post-injury at 12:00) (Fig. 3d, e). ABP, CPP, and PRx increased slowly during the course of VGB administration,

though by Day 12 CPP had begun to fall (Fig. 3d, e). Thus, in the absence of an obvious pattern, it is unclear whether any of these variations in pressure were related to VGB or whether they were a consequence of other treatments received by the patient as part of his standard care.

Brain microdialysates from two more VGB-treated patients, from sites not close to focal lesions, showed increases in VGB and GABA, consistent with the findings above.

Discussion

Here we have shown that VGB given enterically to TBI patients can be detected in their brain microdialysates, indicating passage across the BBB. Moreover, VGB's appearance in brain microdialysates was followed by an increase in a target molecule, GABA, consistent with biochemical activity of VGB, as its known function is as an inhibitor of GABA-transaminase, an enzyme responsible for degrading GABA.

A previous study (without VGB) showed that GABA levels were typically very low or undetectable in brain microdialysates from TBI or subarachnoid haemorrhage (SAH) patients, though GABA rose during ischaemia [4].

Previous work on VGB in brain microdialysates has been done in rats, with comparatively large doses (given intraperitoneally) in relation to body weight, and elicited elevation in GABA in brain microdialysates [10]. These GABA increases in rats were more rapid than those in the TBI patients in the present study.

Much of the literature on VGB in humans has focussed on epilepsy. In epilepsy patients, serum VGB concentrations did not correlate well with biological response to the drug [5]. In vivo ^1H magnetic resonance spectroscopy has shown that VGB administration produced elevation in GABA in relevant regions of the brain in epilepsy patients, though brain GABA levels did not fully predict the subjects' responses (full vs. partial responder) to VGB in terms of seizure control [6, 7]. In vivo ^1H magnetic resonance spectroscopy measures combined intracellular and extracellular GABA, and it is recognised that most GABA is intracellular. While extracellular GABA is known to be comparatively very low (as we have also seen in the present study), it is likely to be more significant than total GABA in the context of neurotransmission. It is also noteworthy that GABA concentrations in cerebrospinal fluid (CSF) did not necessarily predict seizure control in epilepsy patients, in response to VGB [8]. We postulate that the brain extracellular space (which can be accessed by microdialysis) is a more relevant compartment than CSF, in the context of biological activity. A potentially important observation to emerge from this preliminary evaluation in TBI patients is that VGB passage across the BBB, and ensuing extracellular levels of GABA, seem to be greater in abnormal than in normal regions of the brain, thus suggesting that VGB is most concentrated and effective in locations where it is likely to be most useful. Moreover, it seems that multiple dosing is required in TBI patients in order to deliver VGB effectively into the brain, further evidenced by the rise in GABA lagging considerably behind VGB.

Conclusion

Multimodality monitoring, including cerebral microdialysis, is feasible for studying surrogate endpoints following drug administration. VGB crosses the BBB, leading to modest increases in extracellular GABA. Further analyses are ongoing. The present study provides proof of principle that microdialysis is able to assist development of neuroprotective agents by determining penetration into extracellular fluid of the brain, in conjunction with simultaneous multimodality monitoring.

Acknowledgements We gratefully acknowledge the following. Study support: the Medical Research Council (Grant Nos. G9439390 ID 65883 and G0600986 ID 79068) and the Academy of Medical Sciences/Health Foundation. Authors' support: KLHC – the Medical Research Council (Acute Brain Injury programme grant) and the National Institute for Health Research Biomedical Research Centre, Cambridge; IT – Codman Inc grant, The Evelyn Trust grant, MRC RESCUEicp trial grant and BP-TNK Kapitza Scholarship; JN – British Journal of Anaesthesia/Royal College of Anaesthetists Fellowship; PJH – Academy of Medical Sciences/Health Foundation Senior Surgical Scientist Fellowship. We thank L Maskell for technical assistance with microdialysis and demography.

Conflict of interest: ICM+ software for brain monitoring (www.neurosurg.cam.ac.uk/icmplplus) is licensed by the University of Cambridge (Cambridge Enterprise Ltd). Dr M Czosnyka has a financial interest in a part of the licensing fee. The other authors have no conflicts of interest concerning this study.

References

1. Czosnyka M, Smielewski P, Kirkpatrick P, Laing RJ, Menon D, Pickard JD (1997) Continuous assessment of the cerebral vasomotor reactivity in head injury. *Neurosurgery* 41:11–17, discussion 17–19
2. Czosnyka M, Steiner L, Balestreri M, Schmidt E, Smielewski P, Hutchinson PJ, Pickard JD (2005) Concept of “true ICP” in monitoring and prognostication in head trauma. *Acta Neurochir Suppl* 95:341–344
3. Gratzfeld-Huesgen A (1999) Sensitive and reliable amino acid analysis in protein hydrolysates using the Agilent 1100 Series HPLC. Technical note. Agilent Technologies publication number 5968-5658E
4. Hutchinson PJ, O'Connell MT, Al-Rawi PG, Kett-White CR, Gupta AK, Maskell LB, Pickard JD, Kirkpatrick PJ (2002) Increases in GABA concentrations during cerebral ischaemia: a microdialysis study of extracellular amino acids. *J Neurol Neurosurg Psychiatry* 72:99–105
5. Lindberger M, Luhr O, Johannessen SI, Larsson S, Tomson T (2003) Serum concentrations and effects of gabapentin and vigabatrin: observations from a dose titration study. *Ther Drug Monit* 25:457–462
6. Mueller SG, Weber OM, Duc CO, Weber B, Meier D, Russ W, Boesiger P, Wieser HG (2001) Effects of vigabatrin on brain GABA+/CR signals in patients with epilepsy monitored by ^1H -NMR-spectroscopy: responder characteristics. *Epilepsia* 42:29–40
7. Petroff OA, Rothman DL, Behar KL, Collins TL, Mattson RH (1996) Human brain GABA levels rise rapidly after initiation of vigabatrin therapy. *Neurology* 47:1567–1571
8. Pitkanen A, Matilainen R, Ruutinen T, Riekkinen P (1988) Levels of total gamma-aminobutyric acid (GABA), free GABA and homocarnosine in cerebrospinal fluid of epileptic patients before and during gamma-vinyl-GABA (vigabatrin) treatment. *J Neurol Sci* 88:83–93
9. Smielewski P, Czosnyka M, Steiner L, Balestreri M, Piechnik S, Pickard JD (2005) ICM+: software for on-line analysis of bedside monitoring data after severe head trauma. *Acta Neurochir Suppl* 95:43–49
10. Tong X, Ratnaraj N, Patsalos PN (2009) Vigabatrin extracellular pharmacokinetics and concurrent gamma-aminobutyric acid neurotransmitter effects in rat frontal cortex and hippocampus using microdialysis. *Epilepsia* 50:174–183

The Atrial Natriuretic Peptide Does Not Serve Osmoregulation but Predicts Outcome Following Brain Injury

Andrea Kleindienst, Georg Brabant, Nils G. Morgenthaler, Irene Emtmann, Nadine Scheufler, and Michael Buchfelder

Abstract Atrial natriuretic peptide (ANP) plays an important role in body fluid homeostasis. ANP has been established as a marker of cardiac dysfunction and may play a role in brain edema development after traumatic brain injury (TBI). In order to identify its specific assignment following TBI, we related clinical data and treatment variables in 63 patients to longitudinal midregional (MR) proatrial natriuretic peptide (ANP) measurements. ANP correlated significantly to age ($p < 0.0001$) and vasopressin release ($p < 0.001$). Following TBI, ANP was increased initially and on day 3 (cut-off 100 pg/L) in 22% of the patients, in 31% on day 7, and was normalized at follow-up examination. The group comparison revealed that ANP levels did not significantly differ with regard to injury severity, but that high ANP levels predicted a worse Glasgow Outcome Score at 6 months ($p < 0.05$). While the initially intact osmoregulation – a correlation of urine volume and high serum sodium ($r = 0.536$, $p = 0.003$) or low urine osmolality ($r = -0.556$, $p = 0.009$) – got lost post-injury, the ANP release was triggered by volume load ($p < 0.005$). High ANP levels correlated with the neuroendocrine stress response, i.e., high cortisol ($p = 0.05$) and prolactin ($p < 0.001$) levels. We conclude that MR-proANP measurements reveal a significant predictive function for the prognosis of TBI.

Keywords Neuroendocrine function • Osmoregulation • Outcome • Natriuretic peptides • Traumatic brain injury

A. Kleindienst (✉), I. Emtmann, N. Scheufler, and M. Buchfelder
Department of Neurosurgery, University of Erlangen-Nuremberg,
Schwabachanlage 6, D-91054 Erlangen, Germany
e-mail: andrea.kleindienst@uk-erlangen.de,
irene.emtmann@uk-erlangen.de,
nadine.scheufler@uk-erlangen.de,
michael.buchfelder@uk-erlangen.de

G. Brabant
Department of Endocrinology, Christie Hospital, Manchester, UK
e-mail: georg.brabant@manchester.ac.uk

N.G. Morgenthaler
Department for Exp. Endocrinology,
Charité EnForCé, Berlin, Germany
e-mail: nils.morgenthaler@charite.de

Introduction

Of all types of injury, those to the brain are among the most likely to result in death or permanent disability. In the United States more than 1 million people experience a traumatic brain injury (TBI) each year, and approximately 5.3 million Americans with TBI have life-long needs for assistance in performing their activities of daily living postinjury (Centers for Disease Control and Prevention CDC, 2006). Such estimates of brain injury incidence, severity, and cost reflect the enormous losses to individuals, their families, and society. The major challenge to physicians to improve acute care of TBI victims and to minimize persistent TBI-related sequelae is evident.

In recent years, biomarkers have been recognized as tools for diagnosis, risk stratification, and therapeutic decision-making. A variety of proteins, small molecules, and lipid products have been proposed to predict brain damage from TBI. Natriuretic peptides and their receptors, which are widely distributed within the central nervous system and play an important role in body fluid homeostasis have not been systematically studied in TBI [6]. They are, however, well established as nonspecific biomarkers of cardiac dysfunction [3, 5], and have been suggested to predict outcome in sepsis [2]. Recently, it has been claimed that they predict outcome of intracerebral hemorrhage [7]. Atrial natriuretic peptide (ANP) appears to prevent ischemic glial swelling [9] and hemorrhagic brain edema [17], but to promote post-traumatic brain edema [4].

Traumatic brain injury has been shown to be associated with a broad spectrum of systemic post-traumatic neuroendocrine dysfunction [11, 18]. Beside these effects on local water movement an impaired osmoregulation with a high incidence of water and electrolyte disturbances has been described [1], contributing to early morbidity [10]. Antidiuretic hormone (syn. arginine-vasopressin, AVP) released from the posterior pituitary as an integral component of the body water homeostasis, appears to be disconnected from its osmoregulatory properties within the first week following TBI. Assessing simultaneously different parameters of water and electrolyte balance and AVP activity – by measurements of copeptin, the stable C-terminal part of

the AVP prohormone – we found a loss of hypothalamic osmoregulation coupled to a significant predictive function for the severity of TBI [12].

Here we investigated the relevance of the atrial natriuretic peptide (ANP) in osmoregulation following TBI, and correlated the measurements with repetitive examinations of different parameters of injury severity.

Materials and Methods

Sixty-three consecutive patients (51 male, 12 female, mean age 53 years, range 18–87 year, mean body mass index (BMI) 25.81, range 19.53–42.45) admitted to our neurosurgical unit were included in the study. As classified by the Glasgow Coma Score (GCS [19]), 15 patients suffered mild (GCS 13–15), 23 moderate (GCS 9–12), and 19 severe (GCS 3–8) TBI. All patients underwent a routine initial computed tomography (CT), which demonstrated open TBI in 19, a skull fracture in 36, a cranio-facial fracture in 7, a skull base fracture in 17, a subdural hematoma in 14, an epidural hematoma in 9, an intracerebral hemorrhagic contusion in 20, a subarachnoid hemorrhage in 17, a midline shift in 2, and findings suggestive of a diffuse axonal injury in 2 patients.

The study protocol was approved by the local Ethics Committee. Informed written consent was given by the patient or the next-of-kin, in each case. Exclusion criteria were age below 18 years, pregnancy, an extremely poor prognosis, a pre-existing endocrine dysfunction, and whenever the patients or their relatives consent could not be obtained.

All patients were assessed neurologically on a daily basis for the first week, and the GCS was documented. On admission to the intensive care unit (ICU), the GCS was 11 (median, range 3–15), and improved to 15 (median, range 3–15). The daily fluid balance was recorded, an output above 3.5 L was considered suggestive of diabetes insipidus. The simplified acute physiology (SAPS) II score (estimation of hospital mortality ~21% at 32 [14]) was 35 (median, range 6–90), and the acute physiology and chronic health evaluation (APACHE) II score (estimation of death rate ~4% at 0–4, ~8% at 5–9, ~15% at 10–14 [13]) was 12 (median, range 2–28).

Blood samples for serum sodium, osmolality and mid-regional (MR)-proANP were obtained on day 0 ($n=63$), on day 3 ($n=63$), on day 7 ($n=41$) and more than 2 years post-injury ($n=23$). Venous blood samples were drawn in the morning between 7:00 a.m. and 9:00 a.m. into pre-cooled tubes. Clotted samples were promptly centrifuged at 3000Xg for 15 min at 40°C, and then the plasma was frozen at –80°C until analysis. Sodium (mmol/L) was measured by indirect potentiometry (predilution 1:20) with an ion-sensitive electrode on an AU2700 analyzer (Olympus diagnostics Coop., Japan) with an inter- and intra-assay CV <1.3%. Osmolality (mosmol/kg)

measurements (CV<±1.0%) were done by freezing-point depression with an autosampler (Osmomat Auto, Gonotec). Arginine-vasopressin (AVP, synthetic antidiuretic hormone) activity was estimated by copeptin (CT-proAVP) measurements that were performed in a blinded fashion in a single batch with a commercial sandwich immunoluminometric assay (B.R.A.H.M.S LUMitest CT-proAVP, B.R.A.H.M.S AG, Hennigsdorf/Berlin, Germany), as described in detail elsewhere [16]. Measurements of pituitary function are performed as described previously [11].

Atrial natriuretic peptide measurements were performed in a blinded fashion in a single batch by a sandwich immunoassay (B.R.A.H.M.S AG, Hennigsdorf/Berlin, Germany). The Glasgow Outcome Score (GOS) assessed outcome at 6 months (1=death, 2=vegetative, 3=severely disabled, 4=moderately disabled, 5=good recovery [8]). Twenty-three patients consented to undergo a follow-up examination 24–36 months after the injury. Continuous variables are summarized as median and interquartile range (IQR; range 25–75th quartile). MR-proANP values are log₁₀-transformed before analysis. Correlations given are Spearman correlation coefficients with corresponding p values. A multivariate regression analysis as well as group comparisons using the Kruskal–Wallis test were performed using R version 2.5.1.

Results

ANP and Injury Severity

Atrial natriuretic peptide in serum was high on admission (median 62.5, range 46.3–88.3 pmol/L), with a steady increment through days 3 and 7 (median 64.2, range 39.6–91.3 and median 79.9, range 49.6–136.0 pmol/L, respectively). 22% of patients were above a cut-off 100 pmol/L, both on admission and on day 3 and this percentage rose to 31% on day 7. In all patients ANP normalized during follow-up (median 21.7 pmol/L, Fig. 1). There was a significant correlation between ANP levels and age ($r=0.67$, $p<0.0001$). The multivariate regression analysis of log $10_{\text{MR-proANP}}$ on age ($F_{1,63}=56.92$, $p<0.001$), sex ($F_{1,63}=0.16$, $p=0.69$), BMI ($F_{1,63}=27.47$, $p<0.001$), the physiology scores SAPS II ($F_{1,63}=0.11$, $p=0.73$), and APACHE II ($F_{1,63}=2.73$, $p=0.10$) as well as the initial GCS ($F_{1,63}=14.16$, $p<0.001$) explains 62.69% of the total variance. The group comparison revealed that ANP levels were not significantly different with regard to injury severity as assessed by the post-resuscitation GCS ($p=0.0929$, Fig. 2) although there was a trend toward elevated ANP levels following moderate TBI. However, ANP levels were significantly different with regard to outcome as assessed by the GOS ($p=0.0491$, Fig. 3). Logistic regression analysis revealed that ANP levels were significantly

Fig. 1 Serum atrial natriuretic peptide (ANP) and sodium concentrations are displayed at different time points following TBI

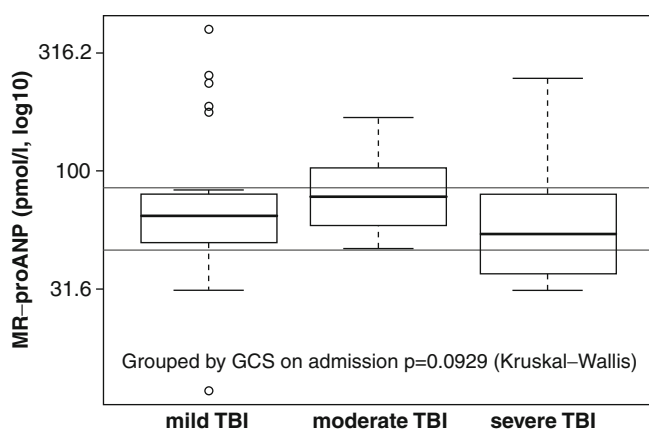
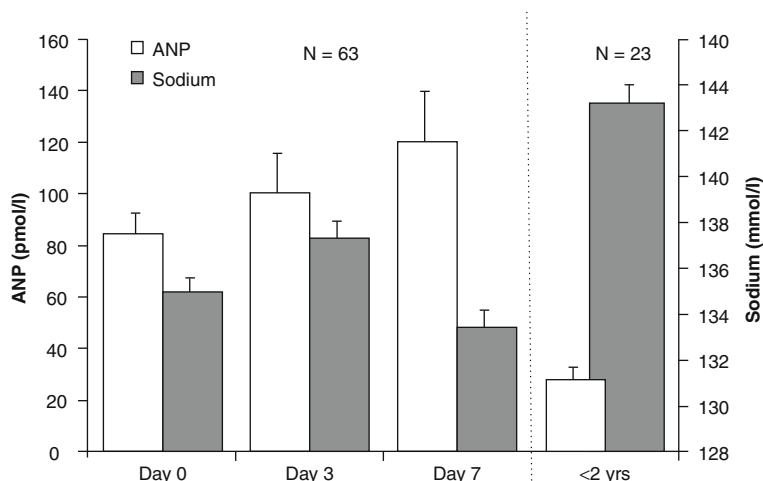


Fig. 2 Serum ANP concentrations are displayed with respect to injury severity as assessed by the Glasgow Coma Score on admission

higher in patients who did not survive (GOS 1; $AUC=0.877$, $p=0.0010$) or remained in a vegetative state (GOS 2; $AUC=0.814$, $p=0.0015$) at 6 months post-injury.

ANP and the Endocrine System

The ANP release following TBI correlated with an activation of the hypothalamic–pituitary–adrenal system, i.e., increased prolactin ($r=0.517$, $p<0.001$) and cortisol levels ($r=0.379$, $p=0.016$). The multivariate regression analysis of \log_{10} MR-proANP revealed a significant association of total triiodothyronine and ANP levels ($F_{1,52}=19.77$, $p=0.011$). As natriuretic peptides like ANP are as important in the body's water and electrolyte balance as the antidiuretic hormone AVP, we analyzed the specific interaction. High ANP levels correlated with high AVP levels, both in the acute period post-injury ($r=0.567$, $p<0.001$ on admission, $r=0.463$, $p<0.001$ on day 3, and $r=0.644$, $p<0.001$ on day 7) and under basal conditions as assessed at the follow-up

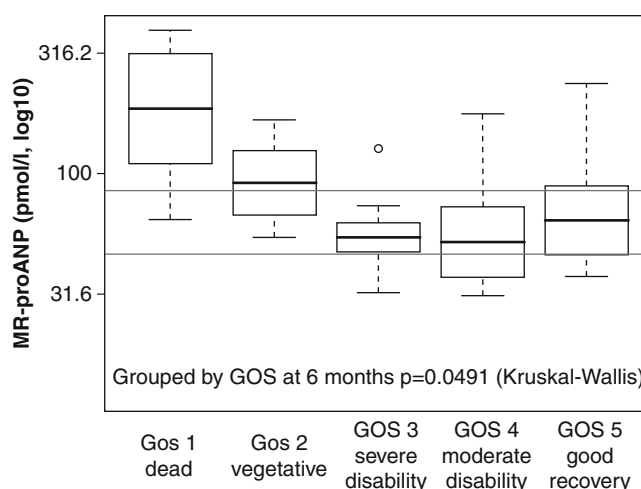


Fig. 3 Serum ANP concentrations are displayed with respect to outcome as assessed by the Glasgow Outcome Score at 6 months

examination ($r=0.690$, $p<0.001$). While on admission, the osmoregulation was intact, i.e., a correlation of urine volume with high serum sodium ($r=0.536$, $p=0.003$) and low urine osmolality ($r=-0.556$, $p=0.009$), this positive correlation got lost during the next few days post-injury and was re-established at the follow-up examination. ANP is released due to atrial distension. Therefore, we examined the correlation of ANP release and the daily fluid balance. A reduced diuresis suggestive for volume load on days 1 and 2 resulted in an increased ANP release on day 3 post-injury ($r=-0.32$, $p=0.0033$ and $r=-0.35$, $p=0.0028$).

Discussion

Traumatic brain injury is still one of the leading causes of death and disability, especially among young adults. Preventive education, increased usage of safety devices,

and TBI management have dramatically increased the potential for surviving a brain injury. However, there is still a need to develop reliable methods for early prediction of the long-term outcome, which may allow us to develop more efficient treatment strategies for treating secondary pathological conditions associated with TBI and improve the overall success rate. As in other fields like cancer, heart failure, or infection biomarkers have shown the potential to fulfill such a role.

ANP as a Biomarker

In the present study, the severity of the TBI-associated injury as assessed by the Glasgow Coma Score or computed tomography did not correlate with serum ANP concentrations. ANP release, however, paralleled the hypothalamic–pituitary–adrenal stress response and high ANP levels predicted an unfavorable outcome assessed by the Glasgow Outcome Score at 6 months.

Traumatic brain injury may alter the endocrine response directly through the traumatic impact to the pituitary–hypothalamic system but also via an adaptive endocrine response to the consecutive critical illness [20]. Due to this double role, the neuroendocrine system may serve as a good candidate for a biomarker not simply for surveillance of an ongoing homeostatic process, but also for outcome prediction. A variety of peptides and proteins have been proposed as potential biomarkers of brain damage from TBI. Natriuretic peptides have been established as non-specific biomarkers of cardiac dysfunction [3, 5], and to predict an unfavorable outcome in sepsis [2] or following intracerebral hemorrhage [7]. Accordingly, here we show that MR-pro ANP measurements facilitate the estimation of TBI prognosis.

Osmoregulation

We further demonstrated that the hypothalamic osmoregulation is still operative immediately after brain injury, but is lost during the further course of illness [12]. As all three systems involved in body fluid homeostasis – e.g., the vasopressinergic system, the natriuretic peptide system, and the renin-angiotensin system – embrace central cardiovascular control [6], the catastrophic event of serious brain injury may engage a shift from osmoregulatory responsibilities toward vasopressor effects [15]. The ANP release during the early post-injury period in the present study is triggered to some extent by volume load, as suggested by the negative correlation with diuresis.

Conclusion

We present a prospective study on TBI patients admitted to our Neurosurgical Department, collecting clinical and neuroendocrinological data longitudinally during the acute phase, and re-evaluating the patients more than 2 years post-injury. We demonstrate:

1. the ANP release to parallel volume load in the absence of osmoregulation following TBI and subsequent intensive care treatment,
2. the ANP release to correspond with the hypothalamic–pituitary stress response, and even more importantly,
3. ANP not to reflect the initial injury severity but serve outcome prediction, i.e., the body's ability to cope with the catastrophic event of TBI.

Acknowledgement The statistical help of Dr. Marx, B.R.A.H.M.S. AG., is gratefully acknowledged.

Conflict of interest Dr. Morgenthaler was an employee at B.R.A.H.M.S. AG, a biotech company that developed the midregional pro-atrial natriuretic peptide (MR-proANP) assay. Dr. Marx has assisted in the statistical analysis on the account of B.R.A.H.M.S. AG.

References

1. Agha A, Thornton E, O'Kelly P, Tormey W, Phillips J, Thompson CJ (2004) Posterior pituitary dysfunction after traumatic brain injury. *J Clin Endocrinol Metab* 89:5987–5992
2. Chen Y, Li C (2009) Prognostic significance of brain natriuretic peptide obtained in the ED in patients with SIRS or sepsis. *Am J Emerg Med* 27:701–706
3. Fuat A, Murphy JJ, Hungin AP, Curry J, Mehrzad AA, Hetherington A, Johnston JJ, Smellie WS, Duffy V, Cawley P (2006) The diagnostic accuracy and utility of a B-type natriuretic peptide test in a community population of patients with suspected heart failure. *Br J Gen Pract* 56:327–333
4. Fukui S, Fazzina G, Amorini AM, Dunbar JG, Marmarou A (2003) Differential effects of atrial natriuretic peptide on the brain water and sodium after experimental cortical contusion in the rat. *J Cereb Blood Flow Metab* 23:1212–1218
5. Giannakoulas G, Dimopoulos K, Bolger AP, Tay EL, Inuzuka R, Bedard E, Davos C, Swan L, Gatzoulis MA (2010) Usefulness of natriuretic peptide levels to predict mortality in adults with congenital heart disease. *Am J Cardiol* 105:869–873
6. Imura H, Nakao K, Itoh H (1992) The natriuretic peptide system in the brain: implications in the central control of cardiovascular and neuroendocrine functions. *Front Neuroendocrinol* 13:217–249
7. James ML, Blessing R, Phillips-Bute BG, Bennett E, Laskowitz DT (2009) S100B and brain natriuretic peptide predict functional neurological outcome after intracerebral haemorrhage. *Biomarkers* 14:388–394
8. Jennett B (1975) Outcome of severe damage to the central nervous system. Scale, scope and philosophy of the clinical problem. *Ciba Found Symp*:3–21
9. Kalisch F, Wurm A, Iandiev I, Uckermann O, Dilsiz N, Reichenbach A, Wiedemann P, Bringmann A (2006) Atrial natriuretic peptide

- inhibits osmotic glial cell swelling in the ischemic rat retina: dependence on glutamatergic-purinergic signaling. *Exp Eye Res* 83:962–971
10. Kaufman HH, Timberlake G, Voelker J, Pait TG (1993) Medical complications of head injury. *Med Clin North Am* 77:43–60
 11. Kleindienst A, Brabant G, Bock C, Maser-Gluth C, Buchfelder M (2009) Neuroendocrine function following traumatic brain injury and subsequent intensive care treatment: a prospective longitudinal evaluation. *J Neurotrauma* 26:1435–1446
 12. Kleindienst A, Brabant G, Morgenthaler NG, Dixit KC, Parsch H, Buchfelder M (2010) Following brain trauma, copeptin, a stable peptide derived from the AVP precursor, does not reflect osmoregulation but correlates with injury severity. *Acta Neurochir Suppl* 106:221–224
 13. Knaus WA, Draper EA, Wagner DP, Zimmerman JE (1985) APACHE II: a severity of disease classification system. *Crit Care Med* 13:818–829
 14. Le Gall JR, Lemeshow S, Saulnier F (1993) A new Simplified Acute Physiology Score (SAPS II) based on a European/North American multicenter study. *JAMA* 270:2957–2963
 15. Lindner KH, Pregel AW, Pfenninger EG, Lindner IM, Strohmer HU, Georgieff M, Lurie KG (1995) Vasopressin improves vital organ blood flow during closed-chest cardiopulmonary resuscitation in pigs. *Circulation* 91:215–221
 16. Morgenthaler NG, Struck J, Alonso C, Bergmann A (2006) Assay for the measurement of copeptin, a stable peptide derived from the precursor of vasopressin. *Clin Chem* 52:112–119
 17. Rosenberg GA, Estrada EY (1995) Atrial natriuretic peptide blocks hemorrhagic brain edema after 4-hour delay in rats. *Stroke* 26:874–877
 18. Schneider M, Schneider HJ, Yassouridis A, Saller B, von Rosen F, Stalla GK (2008) Predictors of anterior pituitary insufficiency after traumatic brain injury. *Clin Endocrinol (Oxf)* 68:206–212
 19. Teasdale G, Jennett B (1974) Assessment of coma and impaired consciousness. A practical scale. *Lancet* 2:81–84
 20. Vanhorebeek I, Van den Berghe G (2006) The neuroendocrine response to critical illness is a dynamic process. *Crit Care Clin* 22:1–15, v

Bedside Study of Cerebral Critical Closing Pressure in Patients with Severe Traumatic Brain Injury: A Transcranial Doppler Study

Corina Puppo, J. Camacho, B. Yelichich, L. Moraes, A. Biestro, and H. Gomez

Abstract Objective: Cerebral critical closing pressure (CrCP) is the arterial pressure (AP) below which small arterial cerebral vessels collapse. Our objective was to estimate cerebral CrCP in 12 severe TBI patients, relating transcranial Doppler flow velocity (FV) and AP data. **Methods:** FV, intracranial pressure (ICP) and invasive AP were prospectively acquired at 50 Hz. CrCP was estimated using three methods (M): M₁: amplitude ratio of FV/AP first harmonics; M₂: AP axis intersection of the regression line between systolic and diastolic values of FV and AP; M₃: AP axis intersection of the regression line between decreasing AP and FV simultaneous values.

Results: There were 12 patients. Frequent negative CrCP values were found. Average M₁: -12 mmHg; M₂: -33 mmHg; M₃: -43 mmHg. Correlation between the three methods was significant ($P < 0.01$). M₁ showed the lowest range and more positive values. The better limits of agreement (Bland and Altman test) were between M₂ and M₃.

Conclusions: The frequently found negative values do not allow us for the moment, to use any of these three methods for clinical guidance.

Keywords Critical closing pressure • Transcranial Doppler • Neuromonitoring • Cerebral perfusion pressure • Intracranial pressure.

Introduction

When the pressure inside a cerebral brain artery decreases, the pressure outside the vessel, represented by the intracranial pressure (ICP), becomes increasingly important in the classic formula of cerebral perfusion pressure (CPP):

$$CPP = \text{Mean arterial pressure (MAP)} - \text{ICP}$$

If arterial pressure decreases more, there is a certain value of arterial pressure at which the small vessels close. This value is called the cerebral perfusion pressure [1]. Thus, the cerebral critical closing pressure (CrCP) is the arterial pressure (AP) at which small arterial cerebral vessels collapse and cerebral blood flow ceases or there is zero flow pressure [2, 3]. Flow ceases before intra-arterial pressure equals ICP, at a greater arterial pressure. The theoretical explanation of this difference is due to another factor that has to be taken into account in the formula of CPP: the small resistance vessels tone, which itself adds to ICP as an extra force that closes the vessel and stops circulation. The concept of CrCP was introduced by Burton [4], based on the observation that cerebral blood flow stops at perfusion pressures significantly higher than zero. However, it cannot be directly measured, at least in humans, in the cerebral circulation.

It was hypothesised that the force that opposes the arterial pressure in the brain has two components: arteriolar wall tension and intracranial pressure [5].

The actual formula of CPP, or effective CPP [6] (CPPe), would therefore be:

$$CPPe = MAP - CrCP$$

From a theoretical point of view, two main arguments favour the measurement of CrCP in neurocritical patients. If ICP is

C. Puppo (✉)
Emergency Department, Hospital de Clínicas, Universidad de la República School of Medicine, Av. Gral. Paz 1208 Apto 601, Montevideo PC 11400, Uruguay
e-mail: coripuppo@gmail.com

J. Camacho
Consejo Superior de Investigaciones Científicas, Ciencia e Investigación, Instituto de Automática Industrial, Madrid, Spain

B. Yelichich
Facultad de Ciencias, Universidad de la República, Laboratorio de Acústica Ultrasonora, Instituto de Física, Montevideo, Uruguay

L. Moraes and A. Biestro
Intensive Care Unit, Hospital de Clínicas, Universidad de la República School of Medicine, Montevideo, Uruguay

H. Gomez
Facultad de Ciencias, Laboratorio de Acústica Ultrasonora, Instituto de Física, Universidad de la República, Montevideo, Uruguay

being monitored and its values are low, there can be a false sensation of low risk, but there can be, however, increased tone at the small vasculature, which diminishes the real perfusion pressure. On the other hand, in patients without ICP monitoring, a high CrCP can guide the physician to either increase arterial pressure or install an ICP monitoring device. As some investigators have underscored [6], effective CPP can be calculated in a non-invasive way, as MAP-CrCP. In both cases, whether ICP is being monitored or not, if a high CrCP is found, a factor of increment of vessels tone or another factor of resistance to flow has to be sought.

Several methods have been proposed to estimate CrCP, using the relation between arterial pressure at a peripheral artery and transcranial Doppler CBFV as an on-line evaluation of changes in CBF.

Objective

The objective was to estimate cerebral CrCP in 12 severe TBI patients, using three different methods that relate transcranial Doppler flow velocity (CBFV) and AP.

Materials and Methods

Twelve patients who had sustained severe traumatic brain injury (TBI), GCS ≤ 8 , admitted to our ICU, were included. Four of the patients had undergone decompressive craniectomies. All patients received controlled mechanical ventilation, sedation and analgesia with midazolam and fentanyl. Their upper body was elevated 30–45°. ICP and invasive arterial pressure were continuously monitored. ICP was monitored by means of parenchymal probes (Codman®) or intraventricular catheters. Invasive MAP was registered by means of an intra-arterial catheter, at the radial, femoral or dorsalis pedis artery. ICP and MAP were zeroed at the same height (foramen of Monro). The protocol for intracranial hypertension treatment included osmotherapy, maintaining CPP greater than 60 mmHg, $\text{CO}_2 \approx 35$ mmHg and muscle paralysis. As an intermediate step indomethacin was administered if ICP was ≥ 25 mmHg [7], and CO_2 was decreased to ≈ 30 . If these measures were not enough, thiopental was added as a final step. Decompressive craniectomy (DC) was also performed in four patients.

Cerebral blood flow velocity (CBFV) at the middle cerebral artery was monitored by means of transcranial Doppler during the trial. An EME-TCD2 64b device was used, with the 2-MHz pulsed Doppler probe fixed to the scalp by means of a headband, in order to maintain the position and angle unchanged. Transcranial Doppler adjustments were kept

constant during the trial. In the four patients with DC, care was taken not to compress the boneless region. AP, ICP and CBFV data were acquired at the bedside, over 30 min, at a sample rate of 50 Hz, with our data acquisition system, made by engineers of our group, which uses an analogue–digital converter card (DAQCard, 6024E, National Instruments) and stores the data on a laptop computer.

Data were acquired for a minimum of 30 min in each patient. Digital signals were processed offline using software developed in house (JC). CrCP was calculated with three methods:

Method 1 (M_1)

The first harmonic method used by Aaslid [8] to calculate CrCP and CPP was used. This method has the advantage of removing the higher harmonics that distort the arterial wave [9], which is registered far from the brain, which would be the ideal site. Fourier analysis was used to determine the amplitudes of the first harmonics (AP and CBFV) of pressure and velocity data. With this method, the regression analysis is done on near perfect linear data. The formula to estimate the CrCP with this method [3] is:

$$\text{CrCP} = \text{AP (t mean)} - \text{CBFV (t mean)} \cdot \text{AP (first h)} / \text{CBFV (first h)}$$

Method 2 (M_2)

Corresponding values of CBFV and AP for single waves were correlated, and the extrapolation to the zero flow velocity was done [10–12].

Method 3 (M_3)

Corresponding systolic and diastolic values of flow and arterial pressure were correlated, and the extrapolation to zero flow velocity was performed.

CrCP average (CrCP_a) was calculated with the formula: $\text{CrCP}_a = (M_1 + M_2 + M_3) / 3$.

Results

Twelve patients were studied. The characteristics of the patients are seen in Table 1.

The values of CrCP_a in the 12 patients can be seen in Fig. 1, upper panel. There was no correlation between values

Table 1 Characteristics of the patients

Patient_N	Age	Gender	Pupils	Lesion	TCDB	Decompressive craniectomy	ICP	CrCP_average
1	16	Male	Unilat. dilat	SDH, C	V	Yes	9	-196
2	54	Male	Bilat. react.	EDH, F	II	No	12	-46
3	61	Male	Unilat. dilat	SDH, F, SAH, F	V	Yes	67	41
5	39	Male	Bilat. react.	EDH, F, Neu	V	No	14	-31
6	22	Male	Bilat. react.	HSD, C, F, Ne	III	No	22	45
7	17	Male	Bilat. react.	C, SAH	II	No	9	-153
8	31	Male	Bilat. react.	SDH, EDH, F, SAH	V	No	19	-59
10	48	Male	Bilat. react.	DBS	III	Yes	17	21
11	19	Female	Bilat. react.	small c	II	No	0	-13
12	29	Male	Bilat. react.	SDH	V	No	22	-45
13	32	Male	Bilat. react.	small c	II	No	19	12
15	18	Female	Unilat. dilat	SDH	V	Yes	19	-29

SDH subdural haematoma, C contusions, EDH extradural haematoma, F skull fracture, SAH subdural haematoma, Neu, and Ne pneumocephalus, DBS diffuse brain swelling, small C small contusions, TCDB traumatic coma data bank, ICP intracranial pressure, CrCP cerebral critical closing pressure

of CrCP and having or not having a decompressive craniectomy. These values are compared in Fig. 1, lower panel. No significant correlation was found between CrCP and ICP. The only parameter that showed a good positive correlation ($R^2=0.841$) with CrCP was PI (Fig. 2, right).

The results of the three methods showed a significant correlation. The correlation coefficients were: between M_1 and M_2 ; $R^2=0.972$; between M_1 and M_3 ; $R^2=0.966$, and between M_2 and M_3 ; $R^2=0.992$. Figure 2 shows the correlation plots.

The values of CrCP with M_2 and M_3 showed a tendency to be more negative than the values found with M_1 . In 4 of the patients the CrCP was higher than the ICP.

The better limits of agreement (Bland and Altman plot) were found between M_2 and M_3 . This plot can be seen in Fig. 3.

Discussion

The CrCP is conceptually greater than zero; we therefore did not expect to find negative values as we did, in half of our patients. Although negative values have been already described by some authors (Panerai, personal communication, Gazzoli et al. [13]), it is extremely difficult to find a plausible explanation for this finding.

We can approach this issue from four different views:

1. (a) An error of measurement. The pressures were zeroed at the same height (foramen of Monroe), to minimise the possible discrepancies between the radial pressure and the pressure at the cerebral arteries and ICP. If they had not been zeroed at the same height, that is, if the arterial pressure had been zeroed at the heart level and the ICP at the foramen of Monroe level, the pressure used to calculate CrCP – the arterial pressure at the radial level – would have been higher than the real cerebral arterial pressure; therefore, the pressure at which vessels collapse would have actually been lower than the measured one (that is, even lower). The error would aggregate in the same direction. There could be another type of discrepancy between real regional pressure at the middle cerebral artery and pressure at the radial artery; however, these values can only be underestimated. If there were a stenosis between the common carotid artery and the middle cerebral artery, the pressure measured at the radial artery would not represent the true arterial pressure that the small cerebral vessels receive. The real pressure that the vessels receive would be lower than the measured radial pressure. This problem was discussed by Panerai et al. [14], referring to patients with carotid stenosis, which is not the case with our patients. The problem with carotid artery stenosis is that the pressure drop not only shifts the pressure scale, but also reduces the slope of the curve. If measured at the real site, the resulting CrCP would be much higher than the value estimated with the pre-stenosis BP (peripheral arteries).
- (b) The calibration difficulties of our acquisition system (re-checked and discarded).
2. The limitations of the formulas (techniques) that extrapolate the quasi-linear relationship between CBFV and

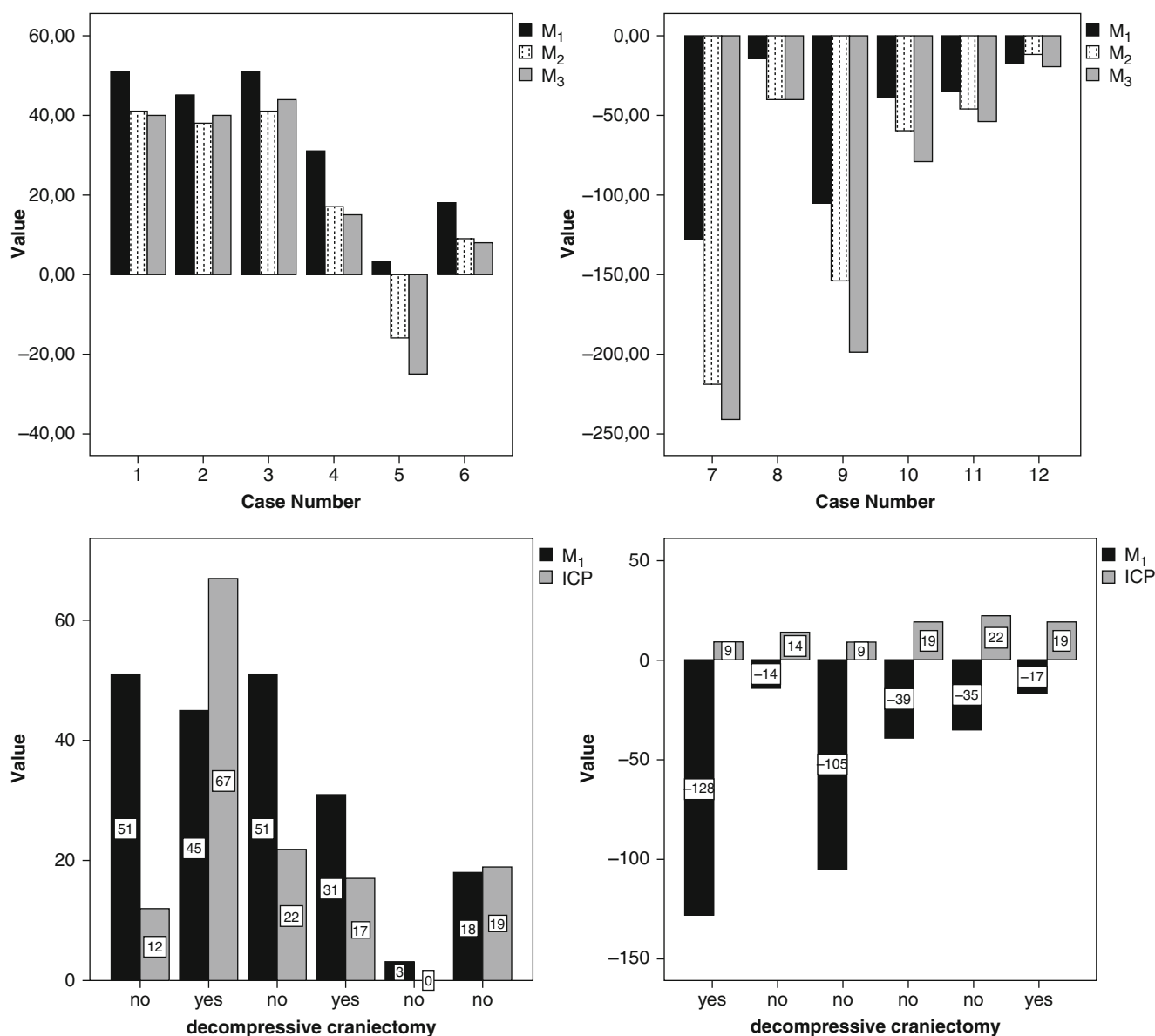


Fig. 1 Upper panel: bar of values of CrCP in mm Hg for each patient, with the three methods. Note that M_1 (first harmonic method), which is the most robust method for several authors, rendered the less negative values. At the right are seen the positive values (with M_1) and at the left

the negative values (with M_1). Lower panel: bar of values of CrCP (M_1) separated for positive and negative values of CrCP, compared with ICP values in the same patient. The patients with decompressive craniectomies are identified (yes/no) in the x axis

BP to the BP axis, which should probably be considered an oversimplification of the phenomenon. On the other hand, CrCP can also be negative because it represents the extrapolation from a much shorter curve. The 95% limits of a regression line become wider and wider when the data are extrapolated away from where the data points are. On the other hand, to the best of our knowledge the methods used that estimate CrCP have not been validated by experimental studies that directly measure CrCP.

3. We searched for certain clinical or therapeutic characteristics (e.g. decompressive craniectomy, CO_2 changes, indomethacin use) in the patients with negative CrCP that could account for the finding, but we could not find any.
4. The finding of negative CrCP was authentic. In this case the phenomenon would be perplexing and would merit reviewing the concept of CrCP.

Our study has some limitations: The number of patients is small; thus, more cases would be needed to confirm our results.

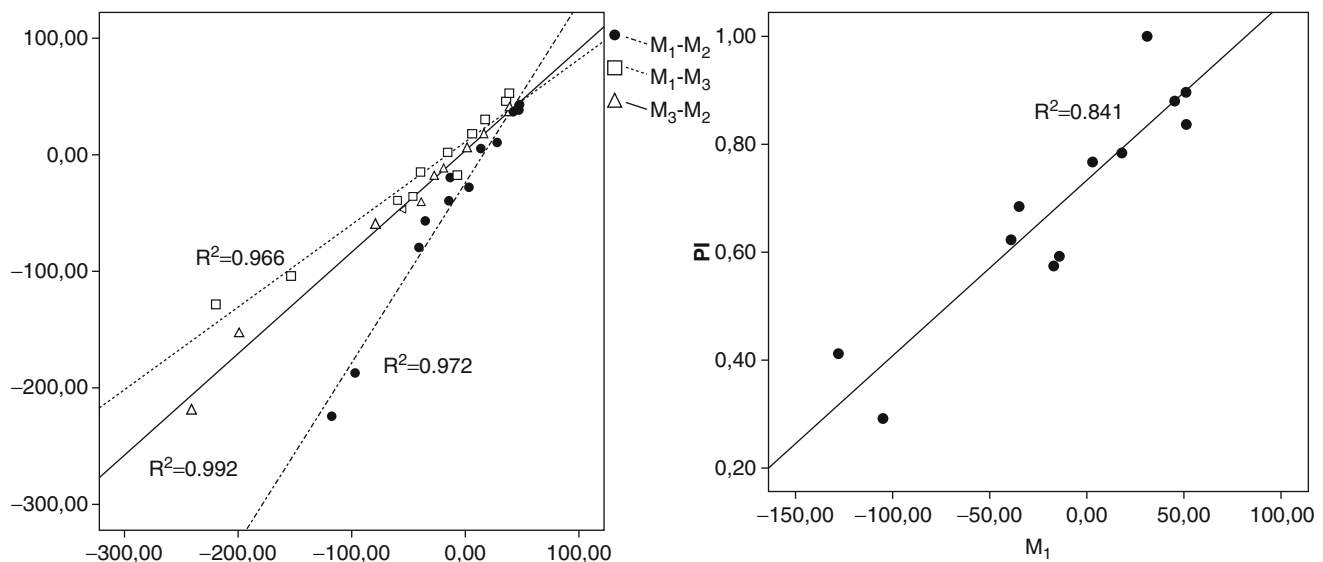


Fig. 2 Left panel: bivariate correlation of CrCP values (in mmHg) for each patient with the three methods. Black circles: correlation between M_1 and M_2 . Open squares: correlation between M_1 and M_3 . Open triangles: correlation between M_3 and M_2 . Correlation coefficient R^2 is

shown for each bivariate comparison. Right panel: bivariate correlation between the pulsatility index (PI) and critical closing pressure in mmHg for M_1 (first harmonic). Correlation coefficient R^2 is shown

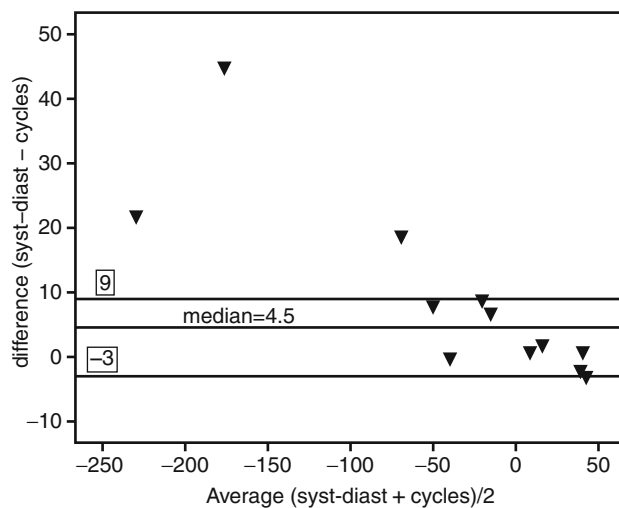


Fig. 3 Bland-Altman plot of the agreement between the best correlated methods: M_2 and M_3 . The values in the x axis correspond to the average of the two methods, and the values on the y axis to the difference between the two methods. Three quarters of the differences between values are contained within a 12-mmHg range

Conclusions

In our experience, for the time being, these methods cannot be used to estimate the critical closing pressure in a non-invasive way.

Conflict of interest statement We declare that we have no conflict of interest.

References

1. López-Magaña JA, Richards HK, Radolovich DK, Kim DJ, Smielewski P, Kirkpatrick PJ, Pickard JD, Czosnyka M (2009) Critical closing pressure: comparison of three methods. *J Cereb Blood Flow Metab* 29:987–993
2. Panerai RB (2003) The critical closing pressure of the cerebral circulation. *Med Eng Phys* 25:621–632
3. Edouard AR, Vanhille E, Le Moigno S, Benhamou D, Mazoit JX (2005) Non-invasive assessment of cerebral perfusion pressure in brain injured patients with moderate intracranial hypertension. *Br J Anaesth* 94:216–221
4. Burton AC (1951) On the physical equilibrium of small brain vessels. *Am J Physiol* 164:319–329
5. Dewey RC, Pieper HP, Hunt WE (1974) Experimental cerebral hemodynamics. Vasomotor tone, critical closing pressure, and vascular bed resistance. *J Neurosurg* 41:597–606
6. Thees C, Scholz M, Schaller MDC, Gass A, Pavlidis C, Weyland A, Hoeft A (2002) Relationship between intracranial pressure and critical closing pressure in patients with neurotrauma. *Anesthesiology* 96:595–599
7. Biestro AA, Alberti RA, Soca A, Cancela M, Puppo CB, Borovich B (1995) Use of indomethacin in brain-injured patients with cerebral perfusion pressure impairment: preliminary report. *J Neurosurg* 83: 627–630
8. Aaslid R, Lash SR, Bardy GH, Gild WH, Newell DW (2003) Dynamic pressure-flow relationships in the human cerebral circulation. *Stroke* 34:1645–1649
9. O'Rourke MF, Nichols WW (1988) McDonald's Blood flow in arteries: theoretical, experimental and clinical principles. Arnold, London, pp 187–190
10. Dawson SL, Panerai RB, Potter JF (1999) Critical closing pressure explains cerebral hemodynamics during the Valsalva maneuver. *J Appl Physiol* 86:675–680
11. Aaslid R (1992) Cerebral hemodynamics. In: Newell DW, Aaslid R (eds) *Transcranial Doppler*. Raven, New York, pp 49–55

12. Czosnyka M, Smielewski P, Piechnik S, Al-Rawi PG, Kirkpatrick PJ, Matta BF, Pickard JD (1999) Critical closing pressure in cerebrovascular circulation. *J Neurol Neurosurg Psychiatry* 66: 606–611
13. Gazzoli P, Frigerio M, De Peri E, Rasulo F, Gasparotti R, Lavinio A, Latronico N (2006) A case of negative critical closing pressure. Abstracts of the 8th International Conference on Xenon CT and related Cerebral Blood Flow Techniques: cerebral blood flow and brain metabolic imaging in clinical practice. *British Journal of Neurosurgery* 20:348
14. Panerai RB, White RP, Markus HS, Evans DH (1998) Grading of cerebral dynamic autoregulation from spontaneous fluctuations in arterial blood pressure. *Stroke* 29:2341–2346

Traumatic Brain Injury in the Elderly: A Significant Phenomenon

B. Depreitere, G. Meyfroidt, G. Roosen, J. Ceuppens, and F. Guiza Grandas*

Abstract Introduction: Traumatic brain injury (TBI) in the elderly is becoming an increasingly frequent phenomenon. Studies have mainly analyzed the influence of age as a continuous variable and have not specifically looked at geriatric patients as a group. The aim of this study is to map the magnitude and characteristics of geriatric TBI and to identify factors contributing to their poorer outcome.

Material and Methods: Based on the ICD-9 register of the University Hospitals Leuven demographic and clinical variables of TBI were analyzed (2002–2008). The influence of older age on physiological variables was assessed using the Brain-IT database.

Results: The elderly (aged ≥ 65 years) accounted for 38.2% of non-concussion TBI and 32.6% of ICU admissions, representing the largest age group. The elderly had a significantly lower ICP (median 10.06 mmHg versus median 14.52 mmHg; $p=0.048$), but no difference in their measure of autoregulation (daily mABP/ICP correlation coefficient) compared with 20–35 year-olds. TBI was caused by a fall in 78.9% of elderly patients and 42.3% suffered a mass lesion. 72.1% had cardiovascular comorbidity. Complications did not differ from their younger counterparts.

Discussion: Geriatric TBI is a significant phenomenon. Poorer outcomes are not yet sufficiently explained by physiological monitoring data, but reduced vascular versatility is likely to contribute. More research is needed in order to develop specific management protocols.

Keywords Traumatic brain injury • Age • Geriatric • Outcome • Intracranial pressure • Autoregulation

Introduction

While it is well known that outcome after traumatic brain injury (TBI) negatively correlates with age, studies on geriatric TBI – i.e. TBI in patients of 65 years of age or older – are scarce. Czosnyka et al. investigated the influence of age on monitoring data in a group of 258 patients with head injury and found a tendency for intracranial pressure (ICP) to decrease and for cerebral perfusion pressure (CPP) to increase with age. Indices of autoregulation indicated worsening of cerebrovascular control with age [1]. In 2005 it was reported by Kiening et al. that intracranial compliance at high ICP, as monitored by using the Spiegelberg probe, decreased with advancing age [4]. A limitation of these studies is that they analyzed the influence of age in groups of patients in which the number of geriatric patients was relatively low.

The aim of the present study is to explore the magnitude of geriatric TBI and investigate factors contributing to its poorer outcome by analyzing accident, injury, physiological and clinical characteristics dichotomizing between geriatric patients and younger counterparts.

Materials and Methods

The University Hospitals Leuven ICD-9-based registry was queried for all TBI-relevant codes in the period 2002–2008. Resultant patient codes were then screened for all concomitant diagnoses in the same registry. These concomitant diagnoses were subsequently categorized into pre-injury morbidity, simultaneous other injuries and complications for the age groups 20–35 years and ≥ 65 years. The patient charts of these two age groups could be retrospectively reviewed for the period 2002–2005 for demographics, comorbidity, accident circumstances, Glasgow Coma Score (GCS) on admission, interventions and Glasgow Outcome Score (GOS). The admission head CT was reviewed for each case in order to be scored

B. Depreitere (✉), G. Roosen, and J. Ceuppens
Division of Neurosurgery, University Hospitals Leuven,
Herestraat 49, Leuven B-3000, Belgium
e-mail: bart.depreitere@uzleuven.be

G. Meyfroidt and F.G. Grandas
Division of Intensive Care Medicine, University Hospitals Leuven,
Herestraat 49, Leuven B-3000, Belgium

* In collaboration with the Brain IT Group

according to the Marshall classification [5] and for identifying all relevant lesion types. An electronic registry of treatment withdrawal codes has been available since 2007 and was consulted for all admitted TBI patients in the period 2007–2008.

Road traffic accident data from the database of “Statistics Belgium” was explored for age relations. This information was available for the period 1995–2008 [7].

The Brain-IT database, which is a multicenter standardized prospective database containing a core dataset including minute-by-minute monitoring data on 200 monitored TBI patients, was explored for the effect of age on intracranial pressure (ICP), mean arterial blood pressure (mABP), cerebral perfusion pressure (CPP), cerebrovascular pressure reactivity and outcome. For that purpose the following variables were assessed: daily mean ICP, number of ICP events, daily mean mABP, daily mean CPP, daily correlation coefficient of ICP and mABP and extended Glasgow Outcome Score (GOS_e). In order to obtain some degree of validation of the daily correlation coefficient of ICP and mABP as a surrogate measure of pressure reactivity, this variable was correlated with outcome, expressed as GOS_e. In addition, a linear multiple regression analysis was done with the first five listed variables as independent and GOS_e as dependent variables. The effect of age was then analyzed by calculating the Pearson correlation coefficient between age and the listed variables. Finally, the listed variables were compared for the age groups 20–35 years and ≥65 years using Mann–Whitney U tests.

Results

Epidemiological Data

A total of 422 patients aged ≥65 years with nonconcussion TBI (i.e., presence of CT abnormalities) were admitted to the University Hospitals Leuven between 2002 and 2008. This geriatric group represented 38.2% of all (nonconcussion) TBI admissions and peaked above other age groups (Fig. 1). The elderly accounted for 32.6% of TBI patients admitted to the ICU.

Physiological Data

The Brain-IT database consists of 200 patients with a mean age of 36.1 years (range 4–83 years). The daily correlation coefficient ICP/mABP negatively correlated with GOS_e (Spearman $r = -0.12$, $p < 0.05$). In the multivariate analysis age ($p < 0.001$), daily mean ICP ($p = 0.047$) and daily ICP/mABP correlation coefficient ($p = 0.025$) came out as independent predictors of outcome ($R^2 = 0.119$). The significant negative relation between the daily correlation coefficient ICP/mABP and outcome supported its further use in the analysis as a

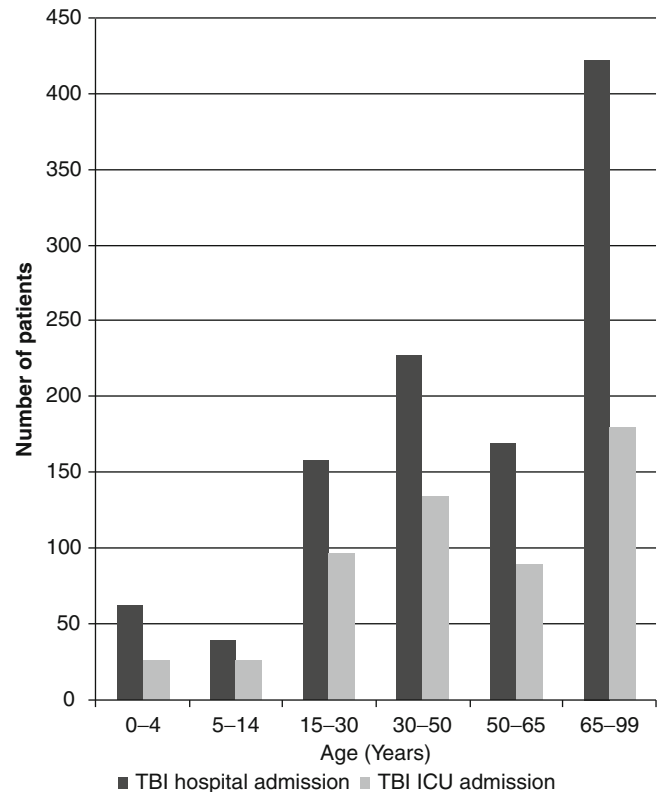


Fig. 1 Traumatic brain injury-related admissions to the University Hospitals Leuven in the period 2002–2008: numbers of patients categorized into age groups

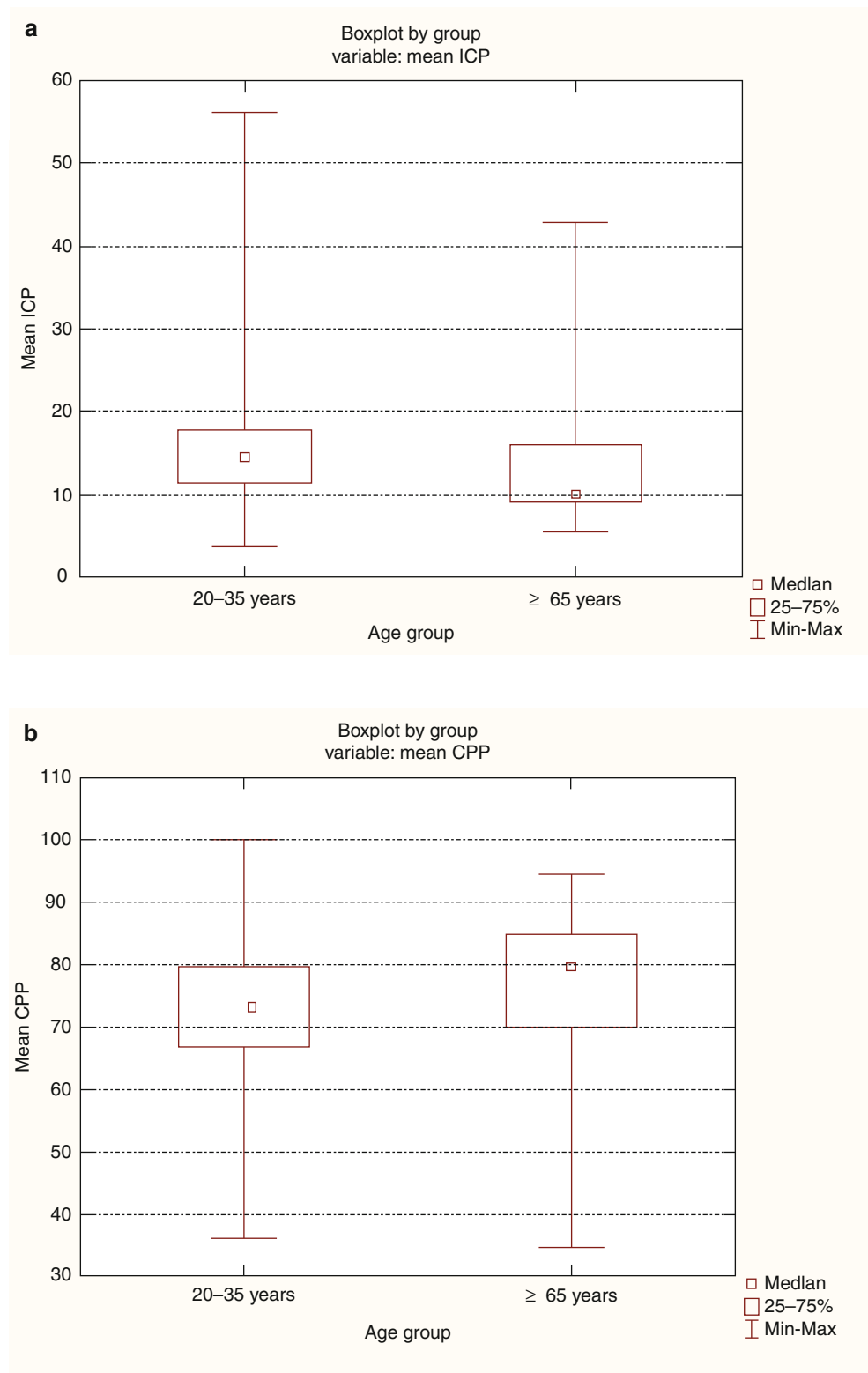
potential surrogate measure of pressure reactivity. As for age correlations, the number of ICP events decreased slightly with increasing age ($r = -0.09$, $p = 0.003$). The daily mean mABP and daily mean CPP tended to increase with increasing age ($r = 0.09$ and $p = 0.002$ for both). The daily mean ICP and the daily ICP/mABP correlation coefficient did not significantly correlate with age. The comparison of the 20–35-year age group ($n = 69$) and ≥65-year age group ($n = 18$) demonstrated lower average ICPs in the elderly (median 10.06 mmHg [9.12–16.03 mmHg] versus median 14.52 mmHg [11.43–17.89 mmHg]; $p = 0.048$). The other variables did not significantly differ between the two age groups (Fig. 2).

Accident and Clinical Data

The analysis of road traffic casualty data in Belgium between 1995 and 2008 showed that on average 7.9% of the casualties in that period were older than 65 years.

Charts were available for review in 175 elderly and in 76 patients from the 20 to 35 age group who sustained TBI with CT abnormalities in the period 2002–2005. Mean ages are 78.0 (range 65–95) for the elderly and 27.6 (range 20–35) for the younger group. The results of the analysis are shown in Table 1.

Fig. 2 Boxplot of average intracranial pressure (ICP) (a) and average cerebral perfusion pressure (CPP) (b) for the age groups of 20–35 years and ≥ 65 years



Concomitant diagnoses were analyzed in the hospital registry for all TBI patients in the 20–35 and ≥ 65 age groups admitted to the intensive care unit. There were 111 patients in the younger age group and 179 patients in the older age group. Pre-injury comorbidity and complications are shown in Fig. 3.

Simultaneous extracranial injuries were present in 33.5% of the elderly (chest trauma in 8.4%, blunt abdominal injury in 0.5% and fractures in 29.6%), as opposed to 58.6% of the younger age group (chest trauma in 32.4%, blunt abdominal injury in 15.3%, urinary tract injuries in 5.4% and fractures in 53.2%).

Table 1 Injury and outcome characteristics of the chart-reviewed traumatic brain injury (TBI) patients

		20–35 years	≥65 years
		<i>n</i> = 76 (%)	<i>n</i> = 175 (%)
Gender	Female	20 (26.3)	89 (50.9)
	Male	56 (73.7)	86 (49.1)
Accident mechanism	Pedestrian	3 (3.9)	10 (5.7)
	Pedal cyclist	17 (22.4)	19 (10.9)
	Motor vehicle	29 (38.2)	2 (1.1)
	Fall	24 (31.6)	138 (78.9)
	Unknown	3 (3.9)	6 (3.4)
GCS on admission	13–15	36 (47.4)	108 (61.7)
	9–12	7 (9.2)	20 (11.4)
	3–8	28 (36.8)	26 (14.9)
	Unknown	5 (6.6)	21 (12.0)
Admission head CT Marshall classification	Diffuse 1	8 (10.5)	1 (0.6)
	Diffuse 2	38 (50.0)	88 (50.3)
	Diffuse 3	17 (22.4)	6 (3.4)
	Diffuse 4	4 (5.3)	3 (1.7)
	Mass lesion	9 (11.8)	74 (42.3)
	Unknown	0 (0)	3 (1.7)
Lesion type	Subarachnoid	23 (30.3)	61 (34.9)
	Extradural	15 (19.7)	29 (16.6)
	Subdural	25 (32.9)	99 (56.6)
	Contusion/ICH	31 (40.8)	77 (44.0)
	Diffuse axonal injury	17 (22.4)	4 (2.3)
GOS	5	39 (51.3)	46 (26.3)
	4	17 (22.4)	26 (14.9)
	3	2 (2.6)	18 (10.3)
	2	3 (3.9)	2 (1.1)
	1	9 (11.8)	58 (33.1)
	Unknown	6 (7.9)	25 (14.3)

GCS Glasgow Coma Score, GOS Glasgow Outcome Score, ICH intracerebral hematoma

In the 2007–2008 period a decision to withdraw treatment or not to expand treatment was taken in 30.0% of the older TBI patients (*n*=120) and in 2.0% of the younger group (*n*=50).

Discussion

According to prognostics from the National Institute of Statistics in Belgium, the proportion of the Belgian population that is 65 years of age or older will grow from 17.2% at present to 26.3% in 2060 [3]. We found that the elderly already account for more than one-third of hospitalizations for TBI in our hospital. It is not just likely, but certain that

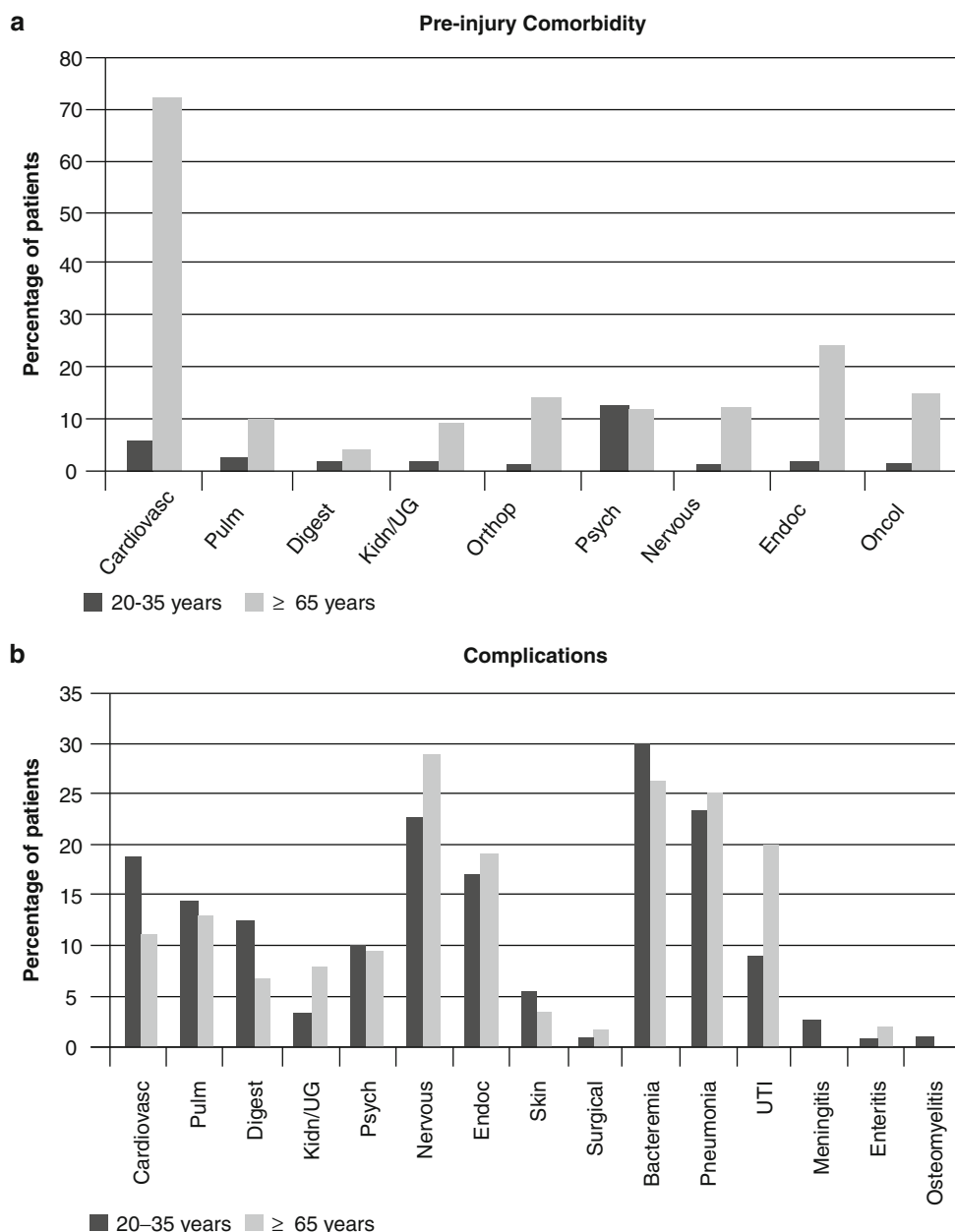
numbers of geriatric TBI will increase in western societies in the future. Hence, there is a strong incentive to look into the phenomenon of geriatric TBI, given that literature on TBI in this specific age group is limited. It is a well established fact that outcome after TBI negatively correlates with age. Figures of mortality after severe head injury in the elderly exceed 70% [6]. And while this feels plausible, a satisfying explanation is still lacking.

The present study demonstrates that geriatric TBI is mostly due to falls and that the vast majority of these falls occur at home. Admission GCS is usually high, meaning that many of these patients arrive in the hospital well and deteriorate subsequently. More mass lesions are seen in the elderly. More than half of the elderly patients suffered a subdural hematoma and over 40% had a contusion or intracerebral hematoma. We showed in a previous study that contusions evolve to larger volumes in the elderly compared with their younger counterparts [2]. The higher incidence of subdural hematomas and (larger) contusions most likely contributes to poorer outcomes, possibly in combination with the reported decrease in intracranial volume challenge compensation with advancing age [4]. In-hospital complications did not really differ between age groups, although the physiological effect of these complications may well have been more severe in the elderly. As expected, pre-injury comorbidity was more frequent in the elderly, most compelling being the high incidence of cardiovascular morbidity. Finally, the outcome in numbers is inevitably affected by the higher incidence of treatment withdrawal decisions in the elderly.

As for the physiological part of the present study, in which 18 elderly patients were compared with a younger age group, it was found that ICP was lower in the elderly and that the surrogate measure of pressure reactivity did not differ. Our assessment of autoregulation may have been limited by the lack of high frequency data. Czosnyka et al. reported a reduction in autoregulation capacity after TBI with increasing age [1]. A limitation of the latter study was the actual low number of elderly patients in the analysis. Nevertheless, it may well be that impaired autoregulation capacity goes hand in hand with cardiovascular morbidity, as an indicator of reduced vascular resilience.

Outcome inevitably results from many factors and decisions taken during the course of treatment. The paucity of data on the subject of geriatric TBI in the literature probably illustrates a pessimistic view. As considerations of the quality of life and subsequent treatment withdrawal decisions are obviously justified in this specific age group, there is a need for better outcome prediction instruments in order to help clinicians in decision-making. On the other hand, there is a strong need for more basic physiological research on geriatric TBI in order to fine tune management strategies and thresholds in those elderly patients who are judged to have a chance of a favorable outcome.

Fig. 3 Pre-injury comorbidity (a) and complications (b) in traumatic brain injury patients of both age groups admitted to the intensive care unit in the period 2002–2008. $N=111$ for the 20–35 age group and $N=179$ for the ≥ 65 age group. *UTI* urinary tract infection



Acknowledgements We wish to thank the Brain-IT Group contributing centers and Steering Group members.

Participating centers and investigators: Barcelona (Spain): Prof. J Sahuquillo, Cambridge (UK): Prof. JD Pickard, Edinburgh (UK): Prof. R. Minns, Glasgow (UK): Mr. L. Dunn, Göteborg (Sweden): Dr. B. Rydenhag, Heidelberg (Germany): Dr. K. Kiening, Iasi (Romania): Dr. S. Iencean, Kaunas (Lithuania): Prof. D. Kavalkis, Leipzig (Germany): Prof. J. Meixensberger, Leuven (Belgium): Prof. J. Goffin, Mannheim (Germany): Prof. J. Vajkoczy, Milano (Italy): Prof. N Stocchetti, Monza (Italy): Dr. G. Citerio, Newcastle upon Tyne (UK): Dr. I. Chambers, Novara (Italy): Prof. F. Della Corte, Southampton (UK): Dr. J. Hell, Uppsala (Sweden): Prof. P. Enblad, Torino (Italy): Dr. L. Mascia, Vilnius (Lithuania): Prof. E. Jarzemaskas, Zurich (Switzerland): Prof. R. Stocker.

Steering Group members: I Chambers (Middlesbrough), G Citerio (Monza), P Enblad (Uppsala), B Gregson (Newcastle upon Tyne), T Howells (Uppsala), K Kiening (Heidelberg), P Nilsson (Uppsala), I Piper (Glasgow), A Ragauskas (Kaunas) and J Sahuquillo (Barcelona).

Conflict of interest statement We declare that we have no conflict of interest.

References

1. Czosnyka M, Balestreri M, Steiner L, Smielewski P, Hutchinson P, Matta B, Pickard JD (2005) Age, intracranial pressure, autoregulation, and outcome after brain trauma. *J Neurosurg* 102:450–454
2. Depreitere B, Van Lierde C, Maene S, Plets C, Vander Sloten J, Van Audekercke R, Van der Perre G, Goffin J (2004) Bicycle-related head injury: a study of 86 cases. *Accid Anal Prev* 36:561–567
3. Federal Planning Bureau Belgium (2008) Population perspectives 2007–2061. www.plan.be/publications
4. Kiening KL, Schoening W, Unterberg AW, Stover JF, Citerio G, Enblad P, Nilsson P, Brain-IT Group (2005) Assessment of the

- relationship between age and continuous intracranial compliance. *Acta Neurochir Suppl (Wien)* 95:293–297
5. Marshall LF, Marshall SB, Klauber MR, Van Berkum CM, Eisenberg H, Jane JA, Luerssen TG, Marmarou A, Foulkes MA (1992) The diagnoses of head injury requires a classification based on computed axial tomography. *J Neurotrauma* 9(Suppl):S287–S292
 6. Patel HC, Bouamra O, Woodford M, Yates DW, Lecky FE (2010) Clinical article: mortality associated with severe head injury in the elderly. *Acta Neurochir (Wien)* 152:1353–1357
 7. Statistics Belgium (2009) Road traffic casualties in Belgium, 1995–2008. www.statbel.fgov.be

Fixed, Dilated Pupils Following Traumatic Brain Injury: Historical Perspectives, Causes and Ophthalmological Sequelae

Adel Helmy, Peter J. Kirkpatrick, Helen M. Seeley, Elizabeth Corteen, David K. Menon, and Peter J. Hutchinson

Abstract Pupillary abnormalities are commonly seen in patients presenting with severe traumatic brain injury (TBI). The objectives of this study were to determine the underlying condition responsible, the natural history of recovery of third nerve palsy and the ultimate clinical outcome in 60 patients admitted to a regional neurosurgical centre with a diagnosis of TBI and unilateral or bilateral fixed, dilated pupils (FDP). In approximately three-quarters of cases, some form of road traffic incident was the mechanism of injury. In patients presenting with a unilateral FDP, the CT-defined condition was most commonly diffuse brain injury (49%) with no obvious lateralising condition. In 34% of cases CT demonstrated a lateralising condition ipsilateral to the side of the FDP and in 9% cases the FDP was contralateral to the side of the CT abnormality. Of those patients who survived an FDP, 72% were left with some form of ophthalmological deficit. Most patients with bilateral FDP did not survive (88%); however, of those who did survive, none was left in a persistent vegetative state or with any ophthalmological sequelae. A FDP is a grave prognostic sign following TBI commonly resulting in long term ophthalmological sequelae; however, a favourable outcome is still attainable.

Keywords Fixed dilated pupil • Ophthalmology • Outcome • Traumatic brain injury

Introduction

Traumatic brain injury (TBI) is a common and often devastating condition with a wide spectrum of severity. At the most severe end of the spectrum a fixed and dilated pupil

(FDP) in a comatose patient has long been recognised as both a neurosurgical emergency and a grave prognostic sign. In 1904, James Collier (1870–1935) was the first to describe herniation of the cerebellar tonsils as a pre-terminal event [4]. Adolf Meyer (1866–1950) later described sub-falcine and transtentorial herniation in 1920 [8]. James Kernohan (1897–1981), an eminent Northern Irish pathologist who later emigrated to the United States, was the first, together with Henry Woltman (1889–1964), to describe a supratentorial mass lesion that compressed the cerebral peduncles at the level of the midbrain against the contralateral free edge of the tentorial hiatus resulting in ipsilateral hemiparesis and contralateral pupillary dilation [6] (Kernohan-Woltman syndrome). Kernohan was also the first to note the importance of the position of the parasympathetic pupillary constrictor fibres on the outer superior aspect of the oculomotor nerve as it traverses the interpeduncular cistern [11]. This description of the pathophysiology of pupillary dilatation in the context of an expanding mass lesion underlies a fundamental physical sign (sometimes referred to as Hutchinson's pupil (Sir Jonathan Hutchinson 1828–1913) [5]) indicating the need for urgent investigation and treatment. The purpose of this study was to systematically assess the causes and consequences of an FDP following head injury in a prospectively collated cohort of head-injured patients admitted to a single neurosurgical unit with a diagnosis of TBI and at least one FDP.

Methods

As part of an ongoing audit of patient outcomes following TBI we prospectively collect data on patients admitted to the Regional Neurosurgical Unit with a diagnosis of TBI. For the purposes of this study we interrogated the database for the period 2004–2008 identifying 428 consecutive patients that required ventilation and admission to the Neurosciences Critical Care Unit (NCCU). Sixty patients (14%) were identified from the database as having one or more FDPs at the

A. Helmy (✉), P.J. Kirkpatrick, H.M. Seeley, E. Corteen, and P.J. Hutchinson
Division of Neurosurgery, Department of Clinical Neurosciences,
University of Cambridge, Box 167, Addenbrooke's Hospital, Hills
Road, Cambridge CB2 0QQ, UK
e-mail: adelhelmy@cantab.net

D.K. Menon
Department of Anaesthesia, University of Cambridge, Cambridge, UK

time of admission to the NCCU. Case records for each of these patients were scrutinised to confirm the diagnosis as well as to collect data regarding patient demographics (age and sex), mechanism of injury, presenting Glasgow Coma Score (GCS), pupillary function and outcome at the 6-month follow-up review (recovery of pupillary function, ophthalmological sequelae, Glasgow Outcome Score [GOS]). A FDP was defined as a pupil unresponsive to light and 5 mm in diameter or greater. Each patient's admission computed tomography (CT) was examined to identify the predominant pathological lesion as well as the side of the lesion. If one or more lesions were present on the CT over or within both hemispheres, the predominant lesion was defined as that causing most midline shift.

Results

Patient Demographics

Sixty patients were identified with one or two FDPs: 43 male and 17 female with a mean age of 41.3 years (range 16–82 years) and 35.2 years (range 17–72 years) respectively with an overall mean age of 39.7 years. Thirty-six patients had a unilateral FDP and 24 patients had bilateral FDPs.

Mechanisms of Injury

Motor vehicle incidents (taking together both motor vehicle occupants and pedestrians hit by vehicles) account for the majority of injuries in this patient cohort responsible for 71% of patients presenting with a unilateral FDP and 54% of patients presenting with bilateral FDPs (Table 1).

CT Findings

The pathological findings on CT for each of the patients with an FDP are in shown in Table 1. One patient with a unilateral FDP did not have any structural abnormalities on CT. It was later found that this patient had only suffered a mild head injury, but had suffered previous trauma to the eye with a long-standing traumatic mydriasis. The pupillary abnormality had prompted the pre-hospital team to intubate and ventilate him as per prescribed guidelines for transfer of TBI patients. This patient was excluded from subsequent analysis.

Table 1 Mechanisms of injury, CT diagnoses and outcome in patients presenting with unilateral and bilateral fixed dilated pupils (FDP)

		Unilateral FDP (%)	Bilateral FDP (%)
Mechanism of injury	Vehicle occupant	54	46
	Fall	23	29
	Pedestrian vs car	17	8
	Assault	6	8
	Work-related	0	4
	Unknown	0	4
CT diagnosis	Diffuse brain injury	49	50
	Acute subdural haematoma	17	38
	Contusions	14	13
	Chronic subdural haematoma	9	0
	Extradural haematoma	6	0
	Intracerebral haematoma	3	0
	No abnormality detected	3	0
	Glasgow Outcome Score (GOS) at 6 months		
	Good recovery [5]	26	4
	Moderate disability [4]	17	4
Glasgow Outcome Score (GOS) at 6 months	Severe disability [3]	3	4
	Persistent vegetative state [2]	6	0
	Death [1]	49	88

Predictive Value of the Side of Pupillary Dilatation

For those patients presenting with a unilateral FDP the side of the CT abnormality was compared with the side of pupillary dilatation (Fig. 1). The majority of these patients had a diffuse brain injury (DBI; 57%), i.e. midline shift <5 mm on CT. In 34% of patients the side of the unilateral FDP predicted the side of a mass lesion on CT. In 9% of cases the side of the mass lesion was on the contralateral side to the FDP.

Sequelae of Fixed, Dilated Pupils

In patients with a unilateral FDP, 17 out of 35 patients died (49%). As expected, the majority of patients with bilateral FDPs died (21 out of 24 patients, 88%); however, in 6 out of 24 cases with bilateral FDPs (25%) the pupils responded at least transiently (Fig. 2). None of the patients with bilateral FDP that survived were left with any residual ophthalmological problems. However, in the unilateral FDP cohort,

8 out of 35 (23%) were left with a long-lasting third nerve palsy and 1 patient (3%) was left with a contralateral (to the fixed pupil) homonymous hemianopia. Of particular interest, in this group of patients it was found that 4 out of 35 patients (11%) did not have a fixed pupil owing to an abnormality of the third nerve. Three patients (9%) had direct trauma to the eyeball, causing traumatic mydriasis: in one case the trauma was so severe that the globe was later exenterated. In one patient (3%), it later transpired that the cause of the enlarged, poorly reactive pupil was an afferent defect in that eye due to a fracture at the optic canal, injuring the optic nerve.

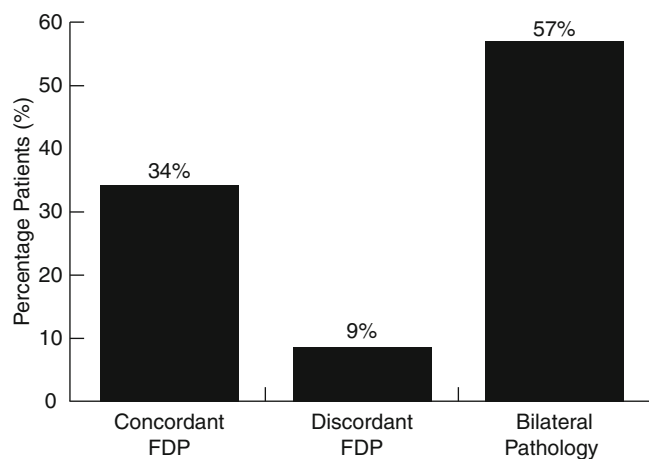


Fig. 1 Predictive power of unilateral fixed dilated pupils (FDP). A concordant FDP is one which is ipsilateral to a supratentorial mass lesion. Bilateral abnormality indicates that there is no focal mass lesion or midline shift

The consensual light reflex in this patient was not documented in the initial assessment (Fig. 2).

Discussion

From the neurosurgical viewpoint an FDP following trauma is the most significant focal finding in the neurological examination. The grave prognosis associated with this finding has been established in many case series, for example, the IMPACT database demonstrated an odds ratio for death of 2.49 for a single FDP and 5.50 for bilateral FDPs [7]. In this study we have addressed specific questions regarding the causes of injury, CT findings (both site and type of pathological lesion), as well as the consequences in terms of clinical outcome and ophthalmological sequelae.

Patient Demographics

As in other case series of patients with TBI there is a large preponderance of male patients (2.5:1 male:female). This is often ascribed to the increased risk-taking behaviour, especially with regard to road traffic incidents and drug/alcohol misuse [9]. The mean age in our patient cohort was 39.7 years. As this cohort is specifically taken from patients admitted to an intensive care unit, there is an intrinsic admission bias against those patients presenting with an FDP, trauma and age above 65 years.

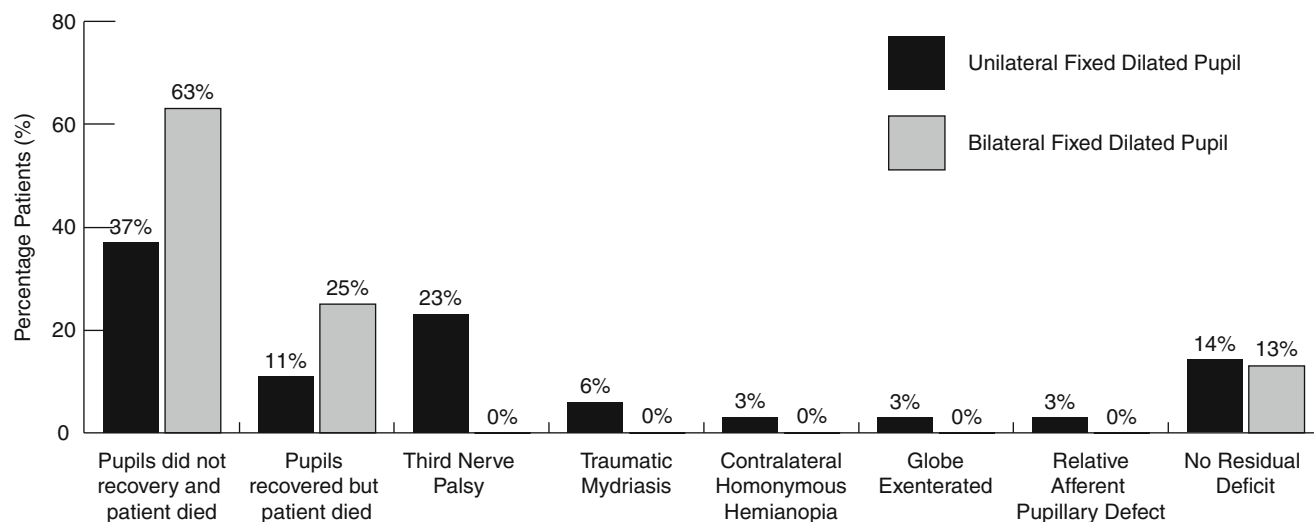


Fig. 2 Ophthalmological sequelae following an FDP. Of those patients who survive following an episode of a single FDP, 72% will have some form of ophthalmological deficit and nearly half will have a third nerve

palsy. Patients who survived bilateral FDP did not have any ophthalmological sequelae suggesting that the pupils were only fixed briefly

CT Findings

The commonest finding on CT was DBI, accounting for half of the conditions. Acute subdural haematomas (ASDH) were approximately twice as common in the bilateral FDP group with a similar number of contusions. As the group of patients with an FDP is at the most severe end of the spectrum of TBI it is not surprising that the injury patterns that are predominantly parenchymal and associated with severe force, i.e. DBI and ASDH, are the most common. In cases where the CT diagnosis was DBI, if there was >5 mm of midline shift assessed at the level of the third ventricle on axial cross-section the patient was considered to have a lateralised lesion for the purposes of gauging whether a unilateral FDP was ipsilateral or contralateral to the predominant condition. In line with previous estimates, we found that in 9% cases the side of the FDP was contralateral to the side of the predominant condition on CT implying midbrain compression against the contralateral free edge of the tentorial hiatus, consistent with Kernohan's initial description [6]. In the majority of cases (57%), the abnormality was bilateral (midline shift <5 mm) calling into question the clinical utility of relying on the side of the FDP in predicting the presence of a unilateral lesion.

Ophthalmological Sequelae

A number of previous studies have attempted to quantify how commonly trauma results in ophthalmological sequelae. Akagi et al. identified 221 isolated oculomotor palsies with 63 acquired third nerve palsies [1]. In this series, third nerve palsies were most commonly a consequence of vascular abnormalities (22 out of 63, 35%), followed by aneurysm (10 out of 63, 16%) and trauma (10 out of 63, 16%). In those aged under 50, trauma was the commonest cause of third nerve palsy. Park et al. have reported a series of 206 patients with an acquired oculomotor palsy, 48 of which were third nerve palsies [10]. Trauma was the second most common cause following vascular lesions and all the third nerve palsies secondary to trauma resolved within 6 months. As our follow-up period was at 6 months, this might suggest that transient third nerve palsies may be even more common but subsequently resolve before assessment in the clinic.

In this study of the patients who survived an episode of a unilateral FDP the majority (72%, 13 out of 18) were left with long-term ophthalmological sequelae. None of the patients with bilateral FDPs who survived were left with any ophthalmological sequelae. We would speculate that this is because those with bilateral FDPs would not have survived unless the time period over which the pupils were fixed was brief. In contrast, patients with unilateral FDPs may have tolerated the causative insult better, resulting in survival, despite a more

prolonged period over which the midbrain and/or third nerve were compressed. In addition, causes of a fixed pupil that are related to the globe rather than transtentorial herniation, such as traumatic mydriasis, would present as a unilateral FDP in the first instance rather than bilateral FDPs. One patient developed a posterior circulation infarct resulting in a homonymous hemianopia contralateral to the side of initial pupillary dilatation, despite the third nerve palsy having resolved.

Outcome

Chaudhuri et al. identified 93 TBI patients with bilateral FDPs and GCS 3 on presentation, of whom only 6 survived; however, 4 of these had a favourable outcome (GOS 4 or 5), mirroring our findings. The factors that affected the likelihood of survival were rapid response of the pupils to hyperosmolar agents and the presence of an evacuable mass lesion [2]. Clusman et al. studied 99 patients with unilateral or bilateral FDPs as a result of a variety of causes (46 trauma, 41 stroke defined as subarachnoid haemorrhage or intracerebral haemorrhage, 12 post-elective surgery), of whom 75% died, 15% had an unfavourable outcome and 10% had a favourable outcome. A short time between pupillary dilatation and intervention improved the likelihood of recovery [3]. In a smaller series Skoglund and Nellgard identified 27 patients with unilateral or bilateral FDPs following trauma [12]. Fifty-nine percent had a favourable outcome (GOS 4, 5), 15% were left severely disabled (GOS 3) and 26% died, with no patients left in a persistent vegetative state. Although the majority of patients in our series died (49% with a unilateral FDP, 88% with bilateral FDPs), of those who did survive, a significant proportion went on to achieve a favourable outcome (GOS 4 or 5). Furthermore, only a few patients were left in a persistent vegetative state. On the basis of both this series and the previous literature in the field we would suggest that even in the presence of an FDP, it is worth persevering with initial management strategies, as in the small proportion of patients who do survive, a favourable outcome is attainable.

The major limitation of this study is that the patients admitted were accepted by the on-call neurosurgeon: the patients with the most severe injuries may therefore already have been excluded.

Conclusion

This study has identified a number of implications of presenting with a FDP following TBI. First, the commonest conditions to cause an FDP (unilateral or bilateral) are diffuse rain

injury, acute subdural haematoma and contusions. Second, in patients with a unilateral FDP, the side of pupillary dilatation is ipsilateral to a lateralised condition in only 34% of cases. In 9% of cases the side of pupillary dilatation is contralateral to the lateralised condition. Third, patients presenting with a unilateral FDP who survive to 6 months have a high incidence (72%) of ophthalmological sequelae most commonly third nerve palsy. Thus, while most patients will recover third nerve function following an episode of an FDP, the majority will be left with some form of ophthalmological deficit. Overall, in patients who survived a favourable outcome was still attainable.

Acknowledgements AH is supported by a Royal College of Surgeons of England Research Fellowship.

PJH is supported by the Academy of Medical Sciences/Health Foundation Fellowship.

DKM is supported by a Senior Investigator Award from the UK National Institute for Health Research.

Conflict of interest statement We declare that we have no conflict of interest.

References

1. Akagi T, Miyamoto K, Kashii S, Yoshimura N (2008) Cause and prognosis of neurologically isolated third, fourth, or sixth cranial nerve dysfunction in cases of oculomotor palsy. *Jpn J Ophthalmol* 52:32–35
2. Chaudhuri K, Malham GM, Rosenfeld JV (2009) Survival of trauma patients with coma and bilateral fixed dilated pupils. *Injury* 40:28–32
3. Clusmann H, Schaller C, Schramm J (2001) Fixed and dilated pupils after trauma, stroke, and previous intracranial surgery: management and outcome. *J Neurol Neurosurg Psychiatry* 71: 175–181
4. Collier J (1904) The false localizing signs of intracranial tumour. *Brain* 27:490–508
5. Greaves D (1978) Sir Jonathan Hutchinson. *Trans Ophthalmol Soc U K* 98:176–177
6. Kernohan JW, Woltman HW (1929) Incisura of the crus due to contralateral brain tumour. *Arch Neurol Psychiatry* 21:274–287
7. Marmarou A, Lu J, Butcher I, McHugh GS, Murray GD, Steyerberg EW, Mushkudiani NA, Choi S, Maas AI (2007) Prognostic value of the Glasgow Coma Scale and pupil reactivity in traumatic brain injury assessed pre-hospital and on enrollment: an IMPACT analysis. *J Neurotrauma* 24:270–280
8. Meyer A (1920) Herniation of the brain. *Arch Neurol Psychiatry* 4:387–400
9. Mushkudiani NA, Engel DC, Steyerberg EW, Butcher I, Lu J, Marmarou A, Slieker F, McHugh GS, Murray GD, Maas AI (2007) Prognostic value of demographic characteristics in traumatic brain injury: results from the IMPACT study. *J Neurotrauma* 24: 259–269
10. Park UC, Kim SJ, Hwang JM, Yu YS (2008) Clinical features and natural history of acquired third, fourth, and sixth cranial nerve palsy. *Eye* 22:691–696
11. Rucker CW, Keefe WP, Kernohan JW (1959) Pathogenesis of paralysis of the third cranial nerve. *Trans Am Ophthalmol Soc* 57:87–98
12. Skoglund TS, Nellgard B (2005) Long-time outcome after transient transtentorial herniation in patients with traumatic brain injury. *Acta Anaesthesiol Scand* 49:337–340

Why Mortality Is Still High with Modern Care of 613 Evacuated Mass Lesions Presented as Severe Head Injuries 1999–2009

Leon Levi, Joseph Guilburd, Jean Soustiel, Gill Sviri, Marius Constantinescu, and Menashe Zaaroor

Abstract Of 1,949 successive acute severe head injuries (SHI) over a period of 11 years 1999–2009, 613 (31.5%) underwent evacuation of mass lesions. Mortality at 3 months of evacuated mass (EM) lesions was higher over 10 years compared with that of non-EM lesions (it was overall 22%). The reduction of mortality was significantly less in EM compared with that for non-surgical cases (14.4–9.4% recently) and for the cases that were operated but not for mass evacuation (18.1–12.1%). A few explanations are: first, more SDH (60.5% of the EM recently compared with 45.9% in the first few years); second, more severe cases and older patients with co-morbidities were treated surgically; third, advances in prehospital care brought more severe patients to operative care – the rate of referrals decreased from 61.5% to 52.8% recently; fourth, part of the significant shortening of the injury to NT admission time (163–141 min) vanished owing to the parallel elongation of admission to operation time (95–100 min), thus, the threshold recommendation of 4 h to mass evacuation was achieved in only 52%; fifth, introducing decompressive craniectomy was not associated with outcome improvement.

Keywords Neurotrauma • Severe head injury, outcome • Regional trauma care • Evacuated mass lesion

Objective

The breakdown of the cohort of SHI according to management pattern is not common. Some hints to that and the observation that the mortality associated with evacuated mass lesions is higher than in nonsurgical patients was raised by a European survey Compagnone C. et al. [2]. In their report of 729 radiologically defined intradural mass lesions (only 55% were presented as SHI) the hospital discharge mortality was 28% in the evacuated mass group versus 22% in the group where the mass was not evacuated. This false impression that the therapy itself is a risk factor was strengthened by the report of 31% mortality when the evacuation was done on the first day of injury versus 21% in the delayed mode of mass evacuation. We report similar findings on longer periods and propose a few explanations.

Methods

Successive 1949 acute SHI cases were admitted to Neurotrauma (NT) during a period of 11 years (1999–2009) and the data were divided into 613 (31.5%) who had evacuated mass lesions (EM). Six hundred and ninety-nine cases had neurosurgery but not for EM (35.9%), and 636 were not operated on, mainly because of overestimation of the neurological injury, which led to intubation and false assessment of coma. Timings of management and mortality at 3 months were taken as outcome indicators.

Results

In ten of the survey years the 3-month mortality of EM was significantly higher than that of non-EM SHI. The improvement in care was significantly less in EM (the non-EM mortality was also below the expected during the successive last 6 years, Table 1).

L. Levi (✉)

Department of Neurosurgery, Rambam Medical Center,
Bat Galim, Haifa, Israel and

Department of Trauma, Rambam Medical Center, Haifa, Israel
e-mail: llevi@rambam.health.gov.il

J. Guilburd, J. Soustiel, G. Sviri, M. Constantinescu,
and M. Zaaroor

Department of Neurosurgery, Rambam Medical Center,
Bat Galim, Haifa, Israel

Table 1 Series characteristics, neurotrauma management, and period

	N SHI	N No Op	N Op	N EM	% Referral No Op	% Referral Op No Mass	% Referral EM	3M Mortality-No Op	3M Mortality-Op No Mass	3M Mortality-EM
Total	1,949	636	699	613	64.80%	47.90%	58.70%	13.20%	16.50%	24.00%
CI	–	–	–	–	61.1–68.5%	44.1–51.5%	55.1–62.9%	10.6–15.8%	13.6–19.1%	20.6–27.4%
1999–2006	1,415	487	509	418	65.50%	51.10%	61.50%	14.40%	18.10%	22.00%
2007–2009	534	149	190	195	62.40%	39.50%	52.80%	9.40%	12.10%	28.20%
07-09 vs 99-06	–0.30%	–0.30%	0.00%	0.40%	–5%	–23%	–14%	–35%	–33%	28%
	Inj-NT No Op	Inj-NT Op No Mass	Inj-NT EM	AD-OR No Mass	AD-OR EM	DTR AD-OR	Referral AD-OR	Inj-OR EM Referral	Inj-OR EM DTR	Inj-OR EM
Total	02:40	02:09	02:37	02:00	01:36	01:56	01:24	04:36	03:18	04:13
CI	$P=0.003$	$P<0.0001$	$P<0.0007$	$P=0.01$	96±9	116±11	124±8	$P=0.03$	198±11	255±34
1999–2006	02:39	02:13	02:43	01:53	01:35	01:54	01:23	04:41	03:17	04:18
2007–2009	02:15	01:48	02:21	02:11	01:40	02:00	01:24	04:26	03:20	04:01
07-09 vs 99-06	–15%	–19%	–14%	16%	5%	5%	1%	–7%	2%	–7%

Abbreviations: AD admission, CI confidence interval, DTR directly evacuated, EM evacuated mass, Inj injury, M month, N number, NT neurotrauma, Op operation, OR operating room, SHI severe head injury

Table 2 Comparison of the main parameters of 110 deceased patient with evacuated subdural hematoma (SDH) versus 201 survivors throughout the two periods

Period		Age	GCS	Abnormal pupil	ISS
1999–2006	Died <i>N</i> =63	53.9±6.7	4.4±0.41	70%	32.8±2.7
	Survivors <i>N</i> =130	41.5±4.6	5.9±0.27	42%	30.5±.6
	Significance	<i>P</i> <0.001	<i>P</i> <0.0001	<i>P</i> <0.0005	<i>P</i> =0.07
2007–2009	Died <i>N</i> =47	59±6.8	4.5±0.55	72%	30±1.9
	Survivors <i>N</i> =71	43.6±5.5	5.9±0.33	42%	30.2±2.4
	Significance	<i>P</i> <0.0003	<i>P</i> <0.0001	<i>P</i> <0.001	<i>P</i> =0.4
All	Died <i>N</i> =110	56.1±4.8	4.4±0.33	71%	31.7±1.8
	Survivors <i>N</i> =201	42.2±3.5	5.9±0.21	42%	30.3±1.2
	Significance	<i>P</i> <0.0001	<i>P</i> <0.0001	<i>P</i> <0.0001	<i>P</i> =0.1

A few explanations are:

1. More SDH (60.5% of the EM recently compared with 45.9% in the first years). Those were the difficult cases with higher mortality – 42.6% vs 33.2% previously (Table 2).
2. More severe cases as well as older patients with co-morbidities were treated surgically. The surviving patients were significantly younger and had less severe injury. The age difference between the surviving and deceased patients rose from 12.7 to 15.1 years recently.
3. Advances in prehospital care brought more severely injured patients to operative care – the rate of referrals decreased from 61.5% to 52.8% recently.
4. Part of the significant shortening of the injury–NT admission time (163–141 min) vanished with the parallel elongation of the admission to operation time (95–100 min). The directly evacuated patients needed longer work-up before neurosurgical operation and the average time from admission to OR rose significantly from 102 to 120 min recently in directly accepted patients. The threshold recommendation of 4 h to mass evacuation was achieved in only 52%. Fifty-seven percent of the 267 patients who received the operation more than 4 h after injury had the main cause of delay in the referring facility. In an additional 40% there was an NT decision to wait with the evacuation while correcting coagulopathy and most of them while monitoring ICP.
5. A double rate of secondary evacuated SDH was noted recently (11.9% compared with 6.2% in the first few years) for whom the outcome was better, yet not sufficient to lower the overall mortality rate for recently evacuated SDH of 39.8%. Introducing decompressive craniectomy was not associated with outcome improvement. Of the 311 evacuated SDH, 94 had their bone flap removed, two-thirds in the first operation, and the mortality was the same as in patients without craniectomy (42.6% vs 32.3%).

Table 3 Age group and type of decompression in 311 evacuated SDH

Age/DC	Died	Survived	Total	Mortality (%)
<50+DC	24	38	62	38.7
>50+DC	16	16	32	50.0
No DC	70	147	217	32.3
Total	110	201	311	35.4

Abbreviations: DC craniectomy for decompression

Discussion

Our figures are similar to those of the European survey, but they serve as proof that the management decision was based on clinical grounds and yet there was significant mortality [2]. The additional factors relating to this lack of improvement were:

1. Change in pattern of referral and primary evacuation brings patients with more severe injury that would be otherwise unsurvivable. This finding is common to series reporting EM timing in the UK [1, 4].
2. A trend toward more severe injury as well as more secondary operations after stabilization of coagulation status [3, 6].
3. Multimodality intensive care even with secondary decompressive craniectomy was not associated with meaningful outcome improvement. The use of decompression in the management of SDH reached a proportion of 47% recently, more than that of the survey of 2001 of 32% [2]. We did not find any support to not consider this operation when clinically appropriate even at ages above 50 years (the mortality rate was similar in elderly and young patients, both higher than in the patients who were not offered craniectomy, Table 3).

We covered the issue in a different way than Leach et al. [5] as we compared all the acute severe head injuries, regardless of their primary department – general intensive care,

pediatric intensive care or neurological intensive care. Additionally, the mortality at 3 months is of less bias than assessment of favorable outcome.

Conclusion

The message that surgical lesions still result in considerable morbidity is strongly supported by the data.

Conflict of interest statement We declare that we have no conflict of interest.

References

1. Butlers D, Belli A (2009) A prospective study of the time to evacuate acute subdural and extradural haematomas. *Anaesthesia* 64:277–281
2. Compagnone C, Murray GD, Teasdale GM, Maas AI, Esposito D, Princi P, D'Avella D, Servadei F (2005) The management of patients with intradural post-traumatic mass lesions: a multicenter survey of current approaches to surgical management in 729 patients coordinated by the European Brain Injury Consortium. *Neurosurgery* 57:1183–1192
3. Härtl R, Gerber LM, Iacono L, Ni Q, Lyons K, Ghajar J (2006) Direct transport within an organized state trauma system reduces mortality in patients with severe traumatic brain injury. *J Trauma* 60:1250–1256
4. Leach P, Childs C, Evans J, Johnston N, Protheroe R, King A (2007) Transfer times for patients with extradural and subdural haematomas to neurosurgery in Greater Manchester. *Br J Neurosurg* 21:11–15
5. Leach P, Pathmanaban ON, Patel HC, Evans J, Sacho R, Protheroe R, King A (2009) Outcome after severe head injury: focal surgical lesions do not imply a better Glasgow Outcome Score than diffuse injuries at 3 months. *J Trauma Manag Outcomes* 3:5
6. Sergides IG, Whiting G, Howarth S, Hutchinson PJ (2006) Is the recommended target of 4 hours from head injury to emergency craniotomy achievable? *Br J Neurosurg* 20:301–305

Late Decompressive Craniectomy as Rescue Treatment for Refractory High Intracranial Pressure in Children and Adults

Catrien van der Meer, Erik van Lindert, and Ronald Petru

Abstract The purpose of this study was to determine the prognosis of children and adults in whom decompressive craniectomy (DC) was used as a rescue treatment to lower refractory high intracranial pressures if maximal conservative therapies failed.

Data of DC patients were retrospectively reviewed. Three-month and 1-year outcomes were evaluated (modified Rankin Score). Twenty-one patients were studied, 8 children and 13 adults. Eleven suffered from traumatic brain swelling, in 10 the primary pathological condition was intracranial hemorrhage, arteriovenous malformation bleeding or subarachnoid hemorrhage. All 13 survivors (62%) had a favorable outcome after 1 year ($mRS \leq 3$), 8 (38%) lacked any disabilities at all. Therefore, decompressive craniectomy offers a chance for a favorable outcome in uncontrollable ICP.

Keywords Refractory • Intracranial hypertension • Modified Rankin Score • Decompressive craniectomy • Children • Rescue

Introduction

High intracranial pressure (ICP) is a major cause of death and disability after severe traumatic brain injury or non-traumatic brain swelling due to intracranial hemorrhage (ICH) or subarachnoid hemorrhage (SAH) in children and adults. A poor prognosis is especially associated with an increase in

ICP within the first 24 h after injury and secondary (3–10 days post-trauma) increases in ICP [15]. Better ICP control has been demonstrated to correlate with improved functional independence and a lower level of disability [2, 10, 11], although optimal thresholds of cerebral perfusion pressure (CPP) and ICP continue to be uncertain, especially in the pediatric population [4]. The optimal management of patients suffering from high ICP remains controversial, with little consensus on second-tier therapies. Despite various conservative therapies, ICP and CPP do not always respond sufficiently; therefore, decompressive craniectomy (DC) is considered to be the ultimate therapeutic approach [3].

Recently, several studies have indicated the potential benefit of decompressive craniectomy on outcome [5, 6, 17]. The majority of patients in most studies suffered from traumatic brain injury and decompressive craniectomy was usually performed shortly after hospital admission.

Functional outcome is crucial in the assessment of the clinical value of DC besides reaching ICP control and decreased mortality. A major argument against the use of DC for ICP control is that by decreasing mortality it might concomitantly increase the percentage of survivors remaining in a persistent vegetative state or being highly dependent in daily living.

This paper describes the evaluation of the clinical course and outcome in children and adults in whom decompressive craniectomy was used as a rescue treatment to lower refractory high intracranial pressures because maximal conservative therapies had failed.

Materials and Methods

In order to report a retrospective case series in our tertiary trauma centre with neurosurgical and intensive care facilities for children and adults, we retrieved files from all patients who underwent a decompressive craniectomy between 2003 and 2009. Only patients who underwent DC as a rescue therapy after optimizing medical treatment were included, excluding all patients in whom DC was performed for mass

C. van der Meer (✉)

Department of Anesthesiology, Radboud University Nijmegen Medical Centre, Postbus 9101, 6500 HB Nijmegen, The Netherlands
e-mail: c.vandermeer@anes.umcn.nl

E. van Lindert

Department of Neurosurgery, Radboud University Nijmegen Medical Centre, Nijmegen, The Netherlands

R. Petru

Department of Intensive Care, Radboud University Nijmegen Medical Centre, Nijmegen, The Netherlands

Table 1 Summary of clinical data, treatment, and outcome in surviving children – the two children who died despite optimal medical treatment and rescue decompressive craniectomy were an 11-month-old baby with severe brain swelling after trauma and a 13-year-old boy suffering from high ICPs up to 80 mmHg after arteriovenous malformation (AVM) bleeding

	Age range (years)	ICP range (mmHg)	Treatment	DC days after hospital admission range	mRS 1 year median (range)
3 post-trauma	12–14	40–68	Sedatives/inotropics/mannitol/hypertonic saline and hypothermia in 1	1.2–6.2	0 (0–1)
3 post-bleeding	9–11	32–60	Sedatives/inotropics/mannitol/barbiturates and hypertonic saline in 1	1.0–13.0	1 (1–3)

ICP intracranial pressure, DC time days after hospital admission, mRS modified Rankin scale

lesions, depressing skull fractures or in which bone flaps were not placed back after evacuation of the mass lesion or hematoma.

Demographic and clinical data, CT characteristics, ICP measurements, treatment, and modified Rankin scores (mRS) [16] were used for the study.

Decision to Operate

All patients were admitted to a dedicated (adult or pediatric) ICU after initial presentation at our emergency room, where a primary survey, resuscitation and neurosurgical evaluation, CT and full routine laboratory examination took place. All patients received intraparenchymal ICP monitoring at some point before DC, because a reliable clinical examination turned out to be impossible because of the low Glasgow Coma Scores initially or a decline during admission. Initial treatment consisted of adequate sedation, till 30° head elevation, normoventilation (PaCO_2 4.5–5 kPa), hemodynamically aiming at a MAP >80 mmHg in adults and above the 5th percentile range in children, using inotropes if necessary. Hyperosmolar therapy consisted of mannitol (20%) or hypertonic saline (NaCl 10%) and was administered in boluses, or as a continuous hypertonic saline infusion in children (0.03–0.3 mL/kg/h), dosed according to efficacy. Patients were kept normothermic using acetaminophen and cooling blankets if necessary. Mild controlled hypothermia to 33°C was used as a second-tier therapy. This was also the case for the use of barbiturates in children. Surgery was indicated in patients in whom high ICP remained refractory (>20 mmHg) despite aggressive medical treatment.

Craniectomy

The operation was performed by the neurosurgeon on call. The objective was to perform as wide a decompression as possible. When mass lesions caused midline shift, decompression

was performed on the side of the injury visible on neuroimages. In patients in whom no predominant lesion with mass effect was present or in whom there was diffuse cerebral edema, a bifrontal craniectomy was performed. The dura mater was always opened. The craniectomy bone flaps were preserved in an abdominal subcutaneous pocket. The bone flap was replaced at an elective date once the brain swelling had subsided and the patient's long-term survival was apparent.

Postoperative Clinical Course

Postoperative management and treatment took place at a dedicated ICU by an interdisciplinary medical and paramedical team including physical therapists and occupational therapists. Further therapy in surviving patients took place in rehabilitation centers. A 1-year follow-up interview and examination were conducted by the neurosurgeon or rehabilitation specialist. Neurological outcomes were evaluated using modified Rankin scores, calculated at 3 and 12 months after decompressive craniectomy. Outcome categories for the modified RS were defined as normal; functionally normal (both intellectually and physically) despite some symptoms; slight disability, able to look after own affairs without assistance, but unable to carry out all previous activities; moderate disability, requiring some help; moderately severe disability, unable to attend to own bodily needs without assistance; severely disabled and totally dependent on care; and death [16]. An mRS of three or less was considered a favorable outcome.

Key Results

Forty-nine patients underwent a decompressive craniectomy. Twenty-one patients fulfilled the mentioned rescue criteria: 8 children (median age 12.3 years, range 0.9–14.3 years; Table 1) and 13 adults (median age 37.4,

range 24.6–57.4 years). Eleven patients suffered from traumatic brain injury (TBI). According to the Marshall CT score [9] the injury could be classified as diffuse injury II (cisterns present with midline shift 0–5 mm and/or small lesions) in three patients, diffuse injury III (cisterns compressed or absent with midline shift 0–5 mm) in two and diffuse injury IV (midline shift >5 mm) in six patients on initial CT; traumatic subarachnoid hemorrhage was present in two patients. Ten patients had sustained high ICP of non-traumatic origin: two patients suffered from intracranial hemorrhage (ICH), four of high intracranial pressure after an arteriovenous malformation (AVM) bleeding, and another four patients with a subarachnoid hemorrhage (SAH; Table 2).

Best median Glasgow Coma Score prior to surgery was 9 (range 3–14). On hospital admission pupils were both reactive in 16 and fixed and dilated in 3, where scores of two patients could not reliably be retrieved from the files.

Patients received conservative treatment initially, according to the guidelines [1, 3] as shown in Fig. 1. A variety of second-tier therapies was applied (Table 2).

Indication for surgery was refractory high ICP. Uni- or bilateral decompressive craniectomy was performed if conservative medical treatments failed and was effective in reducing pressures: preoperative median 40 mmHg (range 30–80 mmHg), vs 1 h postoperative median 8 mmHg (range 0–31). The median time span till craniectomy was 2 days (range 0.3–13.1 days).

The outcome status of the surviving patients was evaluated at 3 and 12 months after decompression.

An mRS of 3 or less was considered as favorable. At follow-up after 3 months, 12 patients had a favorable outcome. All 13 survivors (62%) had a favorable outcome 1 year after surgery; 8 (38%) lacked any disabilities at all (mRs 0–1; Table 2).

Neither the ICP (pre- or postoperative) nor the decrease in ICP correlated with functional outcome. No significant correlations were found between outcome and the time to operation, age, or initial diagnosis, initial GCS or pupillary abnormalities.

Discussion

It is clear that decompressive craniectomy may be effective in the reduction of raised ICP that is refractory to medical therapy [8, 14]. There is, however, uncertainty regarding the

timing of the procedure and there are concerns regarding its potential morbidity. Recent studies suggest early decompressive surgery less than 30 h after trauma to be favorable [5, 13]. An interval of more than 48 h between trauma and decompressive craniectomy has been associated with poor outcome [12]. Others state that patient survival is not affected by craniectomy timing [6]. The timing of surgery in our hospital is an individual decision, based on acute neurological deterioration secondary to raised ICP and its course over time.

Our retrospective study shows that decompressive craniectomy as a rescue treatment causes an effective and persistent reduction in ICP, not only in children or adults with post-traumatic brain edema, but also in patients with intracerebral or subarachnoid bleedings. This effect is independent of the timing of surgery.

Our study is limited by the small number of patients and their heterogeneity. However, it represents a selected group of patients with raised intracranial pressure due to diffuse (secondary) brain swelling only. The results are therefore not obscured by including decompressive craniectomy carried out because of space-occupying lesions. Unlike Kan et al. [7], we found that decompressive craniectomy in patients who underwent surgery for raised ICP was only contributory to a change to a favorable outcome.

Evaluation of outcome at 3 months and 1 year provided a global picture of outcome status. We used a chart review of the treating physician/rehabilitation centre to evaluate outcome; patients were not assessed in person for study purposes. The majority of patients who underwent decompressive craniectomy survived and had a surprisingly good outcome, despite the fact that initial GCSs were low, maximum conservative therapy failed to control the ICP and the preoperative values were very high. All surviving patients had a favorable outcome after 1 year. Apart from one patient with a moderate disability after 1 year, all patients are independent in their daily living.

Conclusion

From our perspective, surgical decompression in secondary brain swelling might be beneficial, not resulting in a higher percentage of patients with a disability, but offering a chance of a favorable outcome.

Conflict of interest statement We declare that we have no conflict of interest.

Table 2 Summary of clinical data, CT findings, treatment, and neurological outcome in all patients

Pre-operative CT Description of pathological condition	Number of patients	Age (years) median (range)	Best preopera- tive GCS median (range)	ICP maximum (mmHg) median (range)	DC days after hospital admission median (range)	ICP postop- eratively median (range)	mRS 3 months median (range)	mRS 1 year median (range)
Survivors								
Diffuse injury II–IV	6	21.6 (12.0–35.8)	7 (6–14)	48 (30–68)	1.7 (0.3–6.2)	6 (1–31)	1.5 (0–3)	0.5 (0–2)
ICH–AVM bleeding	4	11 (9.5–37.5)	7.5 (5–14)	38.5 (32–60)	4.7 (1.0–13.1)	4.5 (4–16)	2 (2–4)	1.5 (1–3)
SAH	3	53.1 (24.6–53.1)	9 (3–11)	33 (30–48)	3.3 (1.7–3.5)	7 (6–16)	2	2 (1–2)
Non-survivors	8	37.7 (0.9–53.4)	9.5 (5–12)	37 (30–80)	2.0 (0.3–10.5)	18 (0–30)	6 (5–6)	6

CT computed tomography, GCS Glasgow Coma Score, ICP intracranial pressure, mRS modified Rankin Scale, diffuse injury II–IV according to the Marshall CT score, ICH intracranial hemorrhage, AVM arteriovenous malformation, SAH subarachnoid hemorrhage

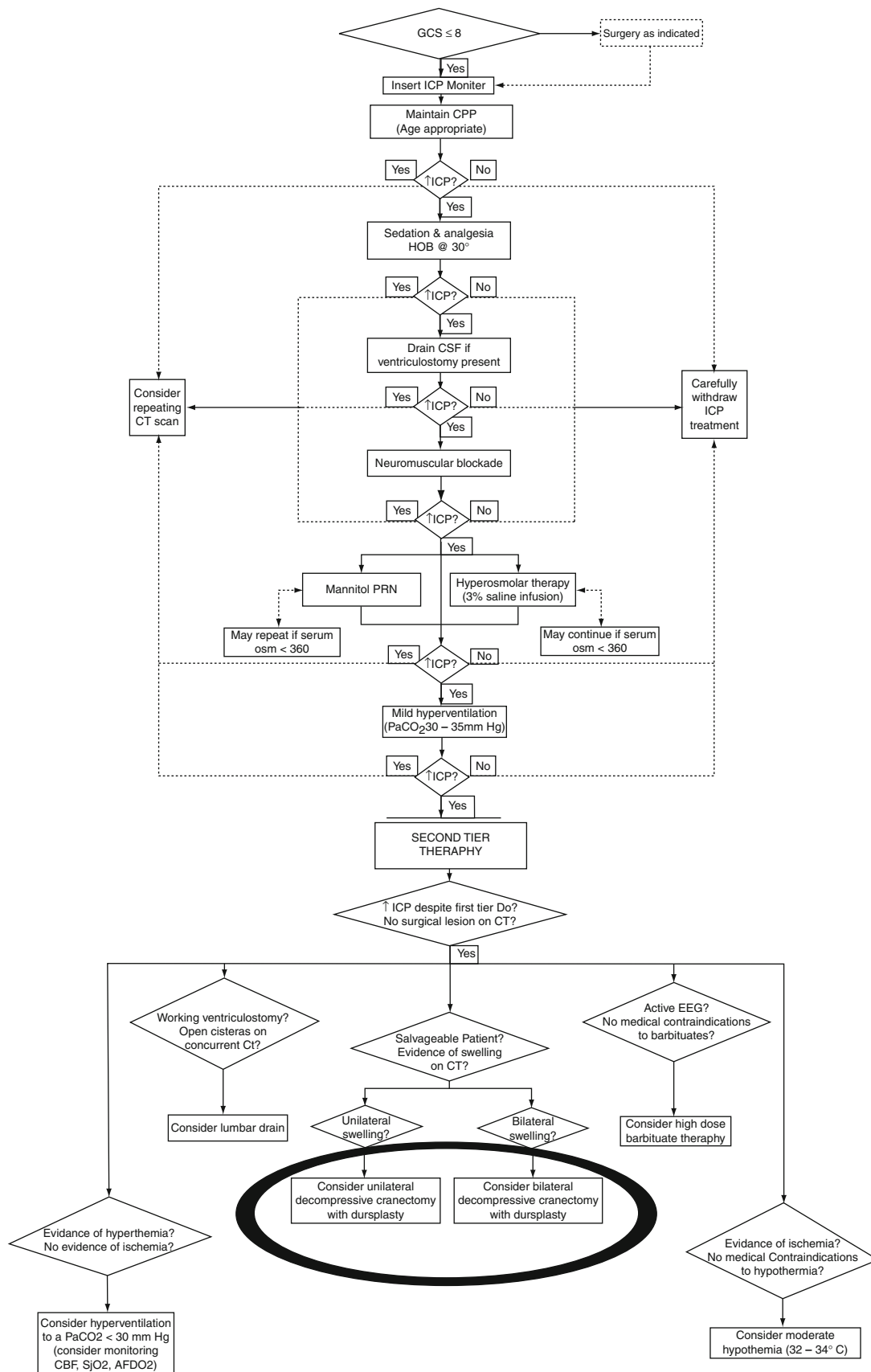


Fig. 1 Intracranial pressure (ICP) treatment algorithm (Adapted from Adelson et al. [1]) GCS Glasgow Coma Score, CPP cerebral perfusion pressure, HOB head of bed, CSF cerebrospinal fluid, CT computed tomography, EEG electroencephalogram

References

- Adelson PD, Bratton SL, Carney NA, Chesnut RM, du Coudray HE, Goldstein B, Kochanek PM, Miller HC, Partington MD, Selden NR, Warden CW, Wright DW, American Association for Surgery of Trauma, Child Neurology Society, International Society for Pediatric Neurosurgery, International Trauma Anesthesia and Critical Care Society, Society of Critical Care Medicine, World Federation of Pediatric Intensive and Critical Care Societies (2003) Guidelines for the acute medical management of severe traumatic brain injury in infants, children, and adolescents. Chapter 17. Critical pathway for the treatment of established intracranial hypertension in pediatric traumatic brain injury. *Pediatr Crit Care Med* 4(3 Suppl):S65–S67
- Bulger EM, Nathens AB, Rivara FP et al (2002) Management of severe head injury: institutional variations in care and effect on outcome. *Crit Care Med* 30:1870–1876
- Carney NA, Ghajar J, Brain Trauma Foundation, American Association of Neurological Surgeons, Congress of Neurological Surgeons, Joint Section on Neurotrauma and Critical Care, AANS/CNS (2007) Guidelines for the management of severe traumatic brain injury. *J Neurotrauma* 24(Suppl 1):S1–S2
- Català-Temprano A, Claret Teruel G, Cambra Lasasa FJ, Pons Odena M, Noguera Julián A, Palomeque Rico A (2007) Intracranial pressure and cerebral perfusion pressure as risk factors in children with traumatic brain injuries. *J Neurosurg* 106(6 Suppl):463–466
- Figaji AA, Fieggan AG, Argent AC, Le Roux PD, Peter JC (2008) Intracranial pressure and cerebral oxygenation changes after decompressive craniectomy in children with severe traumatic brain injury. *Acta Neurochir Suppl* 102:77–80
- Jagannathan J, Okonkwo DO, Dumont AS, Ahmed H, Bahari A, Prevedello DM, Jane JA Sr, Jane JA Jr (2007) Outcome following decompressive craniectomy in children with severe traumatic brain injury: a 10-year single-center experience with long-term follow up. *J Neurosurg* 106(4 Suppl):268–275
- Kan P, Amini A, Hansen K, White GL Jr, Brockmeyer DL, Walker ML, Kestle JR (2006) Outcomes after decompressive craniectomy for severe traumatic brain injury in children. *Neurosurgery* 105(5 Suppl):337–342
- Li LM, Timofeev I, Czosnyka M, Hutchinson PJ (2010) Review article: the surgical approach to the management of increased intracranial pressure after traumatic brain injury. *Anesth Analg* 111(3):736–748
- Maas AI, Hukkelhoven CW, Marshall LF, Steyerberg EW (2005) Prediction of outcome in traumatic brain injury with computed tomographic characteristics: a comparison between the computed tomographic classification and combinations of computed tomographic predictors. *Neurosurgery* 57(6):1173–1182
- Murray LS, Teasdale GM, Murray GD, Miller DJ, Pickard JD, Shaw MD (1999) Head injuries in four British neurosurgical centres. *Br J Neurosurg* 13(6):564–569
- Patel HC, Menon DK, Tebbs S et al (2002) Specialist neurocritical care and outcome from head injury. *Intensive Care Med* 28:547–553
- Polin RS, Shaffrey ME, Bogaev CA, Tisdale N, Germanson T, Bocchicchio B, Jane JA (1997) Decompressive bifrontal craniectomy in the treatment of severe refractory posttraumatic cerebral edema. *Neurosurgery* 41(1):84–92
- Ruf B, Heckmann M, Schroth I, Hügens-Penzel M, Reiss I, Borkhardt A, Gortner L, Jödicke A (2003) Early decompressive craniectomy and duraplasty for refractory intracranial hypertension in children: results of a pilot study. *Crit Care* 7(6):R133–R138
- Sahuquillo J, Arikan F (2006) Decompressive craniectomy for the treatment of refractory high intracranial pressure in traumatic brain injury. *Cochrane Database Syst Rev* (1):CD003983
- Stocchetti N, Colombo A, Ortolano F, Videtta W, Marchesi R, Longhi L, Zanier ER (2007) Time course of intracranial hypertension after traumatic brain injury. *J Neurotrauma* 24(8):1339–1346
- van Swieten JC, Koudstaal PJ, Visser MC, Schouten HJ, van Gijn J (1988) Interobserver agreement for the assessment of handicap in stroke patients. *Stroke* 19(5):604–607
- Taylor A, Butt W, Rosenfeld J, Shann F, Ditchfield M, Lewis E, Klug G, Wallace D, Henning R, Tibballs J (2001) A randomized trial of very early decompressive craniectomy in children with traumatic brain injury and sustained intracranial hypertension. *Childs Nerv Syst* 17(3):154–162

CT Angiography as a Confirmatory Test in Brain Death

Stefan Welschehold, Stephan Boor, Katharina Reuland, Christian Beyer, Thomas Kerz, Andre Reuland, and Wibke Müller-Forell

Abstract *Objective:* From recent studies, it remains unclear whether CT angiography could be an alternative to other established ancillary tests for the diagnosis of brain death. We examined intracranial contrast enhancement in CT angiography after clinically established brain death and compared the results with EEG and TCD findings.

Materials and Methods: Prospective study between April 2008 and January 2010. EEG, TCD and CT angiography were performed in 40 patients aged between 18 and 88 years (mean 56 years) who fulfilled the clinical criteria of brain death.

Results: In all cases, the common carotid artery, cervical internal carotid artery, cervical vertebral artery and superficial temporal artery opacified in an arterial CT angiography series. 37 out of 40 cases demonstrated no opacification of both MCA-M4, ACA-A3, PCA-P2 segments, and BA.

Conclusion: CT angiography is a promising method of evaluating intracranial circulatory arrest in brain death with a high spatial and temporal resolution, superior to all other established technical procedures. The examination is easily accessible in most hospitals, operator independent, minimally invasive and inexpensive. Therefore, CT angiography has the potential to enlarge the existing armamentarium of confirmatory brain death tests.

Keywords Computed tomography • CT angiography • Brain death • Cerebral perfusion • Intracranial circulatory arrest

Introduction

When brain death cannot be declared on clinical grounds or a longer observational period is not feasible, confirmatory tests for brain death (BD) diagnosis such as electroencephalography (EEG), transcranial Doppler ultrasonography (TCD), or evoked potentials (EP) are compulsory. All established additional confirmatory tests have their specific advantages and disadvantages. Cerebral angiography (CA) traditionally has been thought of as the gold standard for confirming BD because this method has the advantage of direct visualisation of arrested cranial blood flow. However, owing to the potential hazards of transporting, the invasiveness of the procedure and possible side-effects of contrast media application [1–3], cerebral angiography is not recommended as the first choice in brain death in several countries [4]. Computed tomographic angiography (CT-A) has already emerged as an alternative to other confirmatory tests, but available data are scarce. If CT-A could reliably demonstrate the arrest of intracerebral blood flow, this would facilitate timely technical confirmation of BD in almost every hospital [5–7]. In this study, we present our results on intracranial contrast enhancement in arterial and venous imaging series of cranial vascular territories in BD and compared CT-A with the well-established tests like EEG and TCD.

Materials and Methods

Between April 2008 and January 2010, we prospectively studied 40 patients admitted to two intensive care units (Departments of Neurosurgery and Anaesthesiology) of our University Hospital (21 male, 19 female, age 18–88 years, mean 56 ± 19 years). Table 1 shows demographic data. This study was approved by the local ethics committee. Informed consent was given by a legal representative in each case.

S. Welschehold (✉), K. Reuland, C. Beyer, T. Kerz, and A. Reuland
Department of Neurosurgery, University Medicine Mainz,
Johannes-Gutenberg-University, Langenbeckstrasse 1,
Mainz 55131, Germany
e-mail: welsch@uni-mainz.de

S. Boor and W. Müller-Forell
Institute of Neuroradiology, University Medicine Mainz,
Johannes-Gutenberg-University, Langenbeckstrasse 1,
Mainz 55131, Germany

Table 1 Patient demographics

Patient number	Sex	Age (years)	Pathological condition	Time interval admission – BD
1	Female	49	SAH	69 h
2	Male	18	ICH	21 h
3	Male	24	TBI	40 h
4	Female	29	Hypoxia	5 days
5	Female	79	SAH	13 days
6	Male	57	ICH	5 days
7	Male	68	Cerebellar hemorrhage	19 h
8	Female	53	SAH	19 h
9	Female	72	ICH	25 h
10	Male	63	TBI	53 h
11	Female	52	SAH	79 h
12	Female	79	Cerebellar hemorrhage	34 h
13	Male	53	ICH	54 h
14	Female	44	Cerebellar hemorrhage	85 h
15	Male	35	TBI	99 h
16	Female	87	ICH	44 h
17	Female	61	ICH	38 h
18	Female	74	SAH	19 h
19	Female	48	TBI	40 h
20	Male	39	SAH	8 days
21	Female	36	ICH	34 h
22	Male	26	TBI	8 days
23	Female	77	ICH	72 h
24	Male	34	SAH	79 h
25	Male	46	Stroke	81 h
26	Male	80	TBI	18 h
27	Male	54	ICH	36 h
28	Male	87	ICH	12 h
29	Female	55	ICH	93 h
30	Female	77	SAH	9 days
31	Male	72	SAH	12 days
32	Female	27	ICH	42 h
33	Male	59	TBI	46 h
34	Male	65	ICH	40 h
35	Female	73	SAH	8 days
36	Male	71	ICH	25 h
37	Male	32	TBI	8 days
38	Female	88	Cerebellar haemorrhage	34 h
39	Male	55	SAH	7 days
40	Male	32	ICH	5 days

Definition of Brain Death

According to the German regulations, BD was determined when coma, brain stem areflexia and apnoea (no spontaneous ventilation at $p_a\text{CO}_2 > 60$ Torr) were confirmed by two physicians with experience in neurological/neurosurgical intensive care medicine [8].

Computed tomographic angiography was always performed after definitive determination of brain death by clinical examination and additional investigations (TCD, EEG). The interval between determination of brain death and CT-A was a maximum of 6 h. In all patients, the mean arterial blood pressure was held between 60 and 90 mmHg. Patients were not under sedation and did not suffer from metabolic or endocrine alterations, hypothermia or intoxications.

Data Collection

Data recorded for all patients were: age, sex, time interval between admission and BD, mean arterial pressure, and the results of CT-A, EEG and TCD examinations.

Computed Tomographic Angiography

Patients underwent CT-A after completion of the first BD protocol. A 32-slice CT system (Aquilion®, Toshiba, Japan) was used with the following CT protocol:

First scan (native): spiral scan of the entire brain without contrast agent after acquisition of a lateral scout view to locate skull base, vertex and cervical vertebra 6. The gantry was angled to the patient's orbitomeatal line. Voltage was set at 120 kV, and current at 170 mA. Axial images were reconstructed with 5.0-mm increments.

Second scan (arterial phase): a bolus injection of 65 mL of non-ionic contrast medium (Imeron® 400, Bracco Imaging, Konstanz, Germany), followed by 30 mL of isotonic saline solution in an antecubital vein or a central venous catheter with a rate of 3.5 mL/s using a power injector was performed. A spiral scan from cervical vertebra 6 to the vertex without gantry tilt was started 5 s after opacification of the common carotid artery with more than 150 HU. In this protocol, the voltage setting was 120 kV and the current setting 200 mA. Axial images were reconstructed with 2.0-mm increments.

Third scan (venous phase): 55 s after starting the second scan, a third scan was started using the same parameters.

Image Analysis

Evaluation of contrast enhancement in the above-mentioned vessels was performed by a neuroradiologist and a neurointensivist/neurosurgeon together. Opacification of the external carotid artery (ECA) and the superficial temporal artery (STA) and absent opacification of the terminal segments of the middle cerebral artery (MCA-M4), anterior cerebral artery (ACA-A3), posterior cerebral artery (PCA-P3) and the basilar artery (BA) in the arterial scanning series and no contrast enhancement in internal cerebral veins (ICV) were rated as intracranial circulatory arrest.

Electroencephalogram

For EEG, we used a digital system (NicOne vEEG®, Cardinal Health, Hoechberg, Germany) with a recording time of 30 min with various verbal and painful stimulations according to previous published guidelines [8, 9].

Transcranial Doppler/Duplex Ultrasound

For transcranial Doppler or duplex ultrasound, we used either a transcranial Doppler system (Nicolet Companion®, CardinalHealth GmbH, Hoeschberg, Germany) or a transcranial colour-coded duplex system (Vivid S6®, GE Healthcare, Munich, Germany). According to previously published recommendations, BD was confirmed either if oscillating flow or systolic spikes with a maximum of 50 cm/s was observed in transtemporal and suboccipital windows [8, 10].

Results

Brain death was diagnosed clinically in all patients. Confirmation of BD using both TCD and EEG was possible in all but five patients. In two cases, confirmation by EEG failed due to artefacts, making definitive assessment of electrocerebral inactivity impossible, but TCD revealed arrested intracranial blood flow. In one other case, confirmation by TCD failed because of a missing acoustic window. In two cases, TCD revealed a flow pattern with more than early systolic spikes or pendular flow in one vessel and therefore was not compatible with brain death. EEG of all three patients demonstrated electrocerebral inactivity.

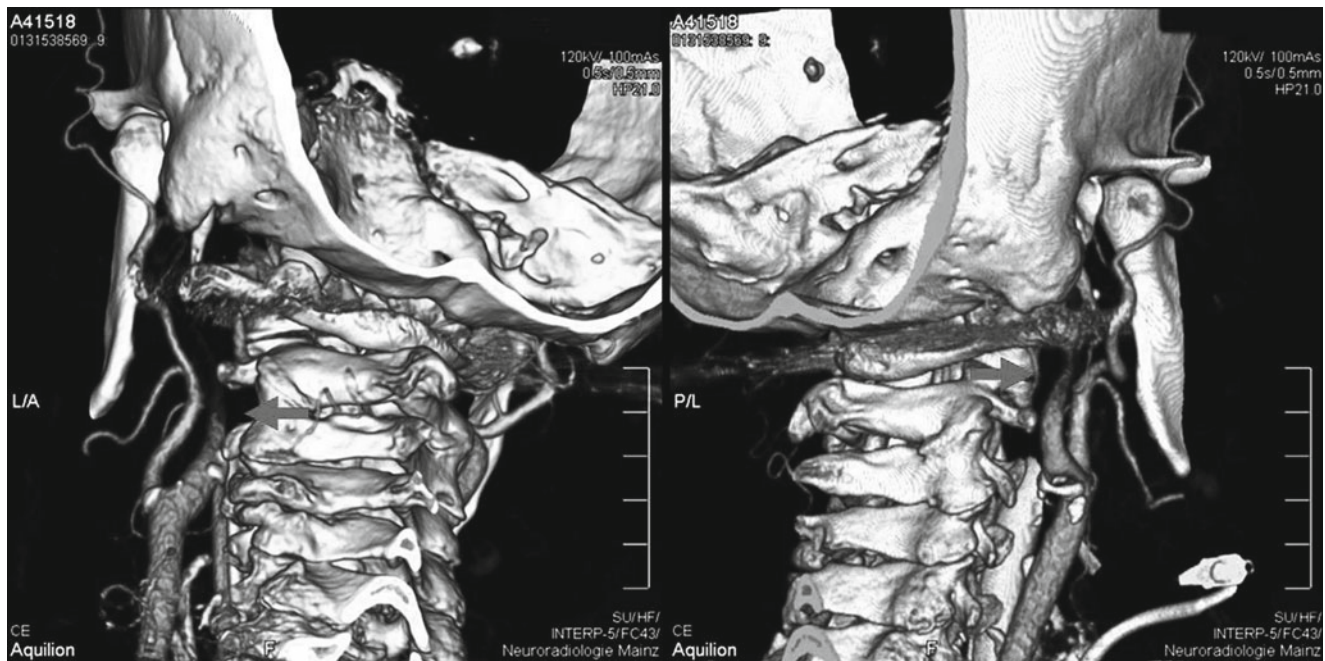


Fig. 1 Arrest of the contrast medium filling of the internal carotid artery (ICA) below the skull base in arterial series (*arrow*). Notice the contrast filling of the external carotid artery (ECA)

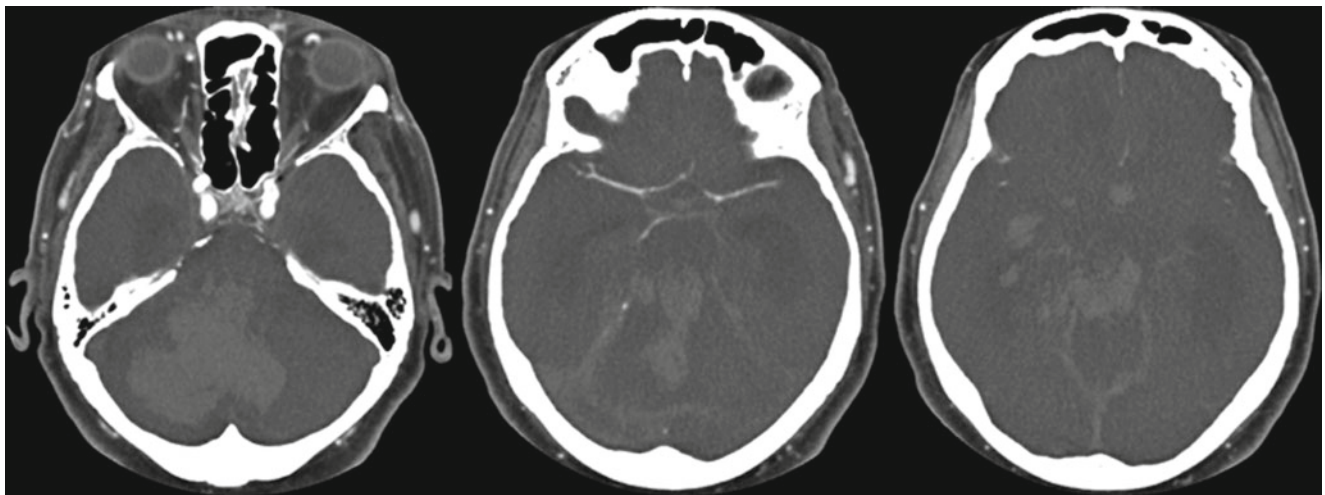


Fig. 2 Residual flow in the middle cerebral artery (MCA), but arrested blood flow in the posterior fossa. Not compatible with intracranial circulatory arrest

In all cases, ECA and STA opacified in arterial as well as in venous series. Contrast filling ceased below or at the level of the skull base in 26 patients (Fig. 1).

No opacification of MCA-A4, ACA-A3, PCA-P3 and BA in the arterial scanning series and concomitant absent opacification of ICA in venous scanning series were demonstrable in 37 patients.

We observed opacification of individual arteries (MCA-A4, ACA-A3, PCA-P3 or BA) in two patients (Fig. 2) and preserved contrast enhancement in all intracranial vascular territories in one patient after decompressive craniotomy.

Discussion

The diagnosis of BD is a clinical diagnosis. There are, however, situations when technical confirmation of BD is helpful or even indispensable. To date, all ancillary tests demand experienced personnel who are not easily available in most hospitals. A simple confirmative test, available in even smaller hospitals, would alleviate the diagnosis of BD and would strengthen the diagnostic safety of BD. CT-A is about to find a place in this setting.

After the first publication by Dupas et al. in 1998, performing CT-A in BD [5] became more popular, but remains

a topic of controversy. Several authors assessed this tool as a reliable and promising new method in BD diagnosis [7, 11–14], whereas others could not confirm these results [6, 15].

In our CT-A series, cerebral blood flow in MCA-M4, ACA-A3, PCA and BA was absent in 37 out of 40 patients in arterial series. Hence, in 37 out of 40 patients the results of CT-A were rated as intracranial circulatory arrest.

The absence of venous blood return into the deep cerebral veins was demonstrable in all 40 patients in the venous series.

Most other CT-A studies evaluated intracranial circulatory arrest by venous CT-A series [6, 11, 12, 16], but literature reports of CT-A criteria in BD are far from being standardised. Several authors are in favour of the arterial phase for perfusion studies [7, 17, 18]. In our study, sensitivity for detecting intracranial circulatory arrest in BD patients was 93% when analysing the intracranial arterial system in early scanning series and venous blood return in late scanning series. The reported sensitivity in detecting intracranial circulatory arrest in CT-A in venous scanning series is up to 63% [6, 12] and therefore inferior to the arterial series, whereas studies could demonstrate a sensitivity of up to 89% [7, 17]. In all of our patients, we found absent contrast enhancement in the deep cerebral veins. Thus, in our study, absent venous blood return in the deep cerebral veins was valid and a 100% sensitive marker for the diagnosis of BD.

In two patients, we demonstrated a residual but severely reduced blood flow in TCD, whereas CT-A indicated intracranial circulatory arrest. In both cases, residual contrast enhancement was demonstrated in one or both MCA-M1. According to all other authors, these findings were not rated as residual flow in CT-A [5–7, 11–13]. In our opinion, these contradictory findings are due to the specific examination techniques, as TCD analyses proximal intracranial vessels, whereas CT-A evaluates distal parts of the intracranial vasculature.

Computed tomographic angiography has a certain rate of false-positive results as individual patients will demonstrate persistent or residual blood flow, e.g. a patient with skull defects, ventricular drainage or due to recanalisation after a certain period of time. This will be the case in every other perfusion study as well as persistent intracranial blood flow can be demonstrated in up to 20% of patients, despite clinical confirmation of brain death [19–24].

Until now, all ancillary brain death tests addressing cerebral perfusion have to demonstrate absent blood flow in the anterior circulation as well as in the posterior circulation [3, 25]. In conventional angiography, the arrest of CBF is defined as no intracranial filling at the level of the carotid bifurcation or circle of Willis, while external carotid circulation is patent [26–30]. In TCD, a typical flow pattern has to be demonstrated in the anterior as well as in the posterior circulation [10] and radionuclide techniques have to demonstrate no intracranial (including structures of posterior fossa) isotope uptake [30–32]. These criteria should also apply with CT-A, and we feel that

the use of CT-A for determination of BD without evaluation of the posterior circulation would be incomplete. In most publications evaluation of blood flow in the posterior fossa was not taken into consideration [6, 12, 13].

On the basis of our data and an analysis of the literature we would like to propose the evaluation of contrast enhancement of the intracranial arterial system in the arterial CT-A phase. Venous blood return should be analysed in the venous CT-A phase.

Conclusion

Computed tomographic angiography is a promising method for evaluating intracranial circulatory arrest and it offers a high spacio-temporal resolution, superior to all other established technical procedures in diagnosing brain death. The examination is easy accessible in most hospitals, operator independent, less invasive and less expensive.

Acknowledgements We thank Mrs. Janice Roberts for editorial help with the manuscript preparation.

Conflict of interest statement We declare that we have no conflict of interest.

Financial support There was no financial support for this study.

References

1. Heran MK, Heran NS, Shemie SD (2008) A review of ancillary tests in evaluating brain death. *Can J Neurol Sci* 35(4):409–419
2. Young GB, Shemie SD, Doig CJ, Teitelbaum J (2006) Brief review: the role of ancillary tests in the neurological determination of death. *Can J Anaesth* 53(6):620–627
3. Wijdicks EF (2001) The diagnosis of brain death. *N Engl J Med* 344(16):1215–1221
4. Haupt WF, Rudolf J (1999) European brain death codes: a comparison of national guidelines. *J Neurol* 246(6):432–437
5. Dupas B, Gayet-Delacroix M, Villers D, Antonioli D, Veccherini MF, Souillou JP (1998) Diagnosis of brain death using two-phase spiral CT. *AJNR Am J Neuroradiol* 19(4):641–647
6. Quesnel C, Fulgencio JP, Adrie C, Marro B, Payen L, Lember N et al (2007) Limitations of computed tomographic angiography in the diagnosis of brain death. *Intensive Care Med* 33(12):2129–2135
7. Escudero D, Otero J, Marques L, Parra D, Gonzalo JA, Albaiceta GM et al (2009) Diagnosing brain death by CT perfusion and multislice CT angiography. *Neurocrit Care* 11(2):261–271
8. Bundesärztekammer WBd (1998) Richtlinien zur Feststellung des Hirntodes. *Dtsch Arztebl* 53(30):A-1861–A-1868
9. American Clinical Neurophysiology Society (2006) Guideline 3: minimum technical standards for EEG recording in suspected cerebral death. *J Clin Neurophysiol* 23(2):97–104
10. Ducrocq X, Hassler W, Moritake K, Newell DW, von Reutern GM, Shiohagi T et al (1998) Consensus opinion on diagnosis of cerebral circulatory arrest using Doppler-sonography: Task Force Group on cerebral death of the Neurosonology Research Group of the World Federation of Neurology. *J Neurol Sci* 159(2):145–150

11. Combes JC, Chomel A, Ricolfi F, d'Athis P, Freysz M (2007) Reliability of computed tomographic angiography in the diagnosis of brain death. *Transplant Proc* 39(1):16–20
12. Frampas E, Videcoq M, de Kerviler E, Ricolfi F, Kuoch V, Mourey F et al (2009) CT angiography for brain death diagnosis. *AJNR Am J Neuroradiol* 30(8):1566–1570
13. Leclerc X, Taschner CA, Vidal A, Strecker G, Savage J, Gauvrit JY et al (2006) The role of spiral CT for the assessment of the intracranial circulation in suspected brain-death. *J Neuroradiol* 33(2):90–95
14. Qureshi AI, Kirmani JF, Xavier AR, Siddiqui AM (2004) Computed tomographic angiography for diagnosis of brain death. *Neurology* 62(4):652–653
15. Greer DM, Strozyk D, Schwamm LH (2009) False positive CT angiography in brain death. *Neurocrit Care* 11(2):272–275
16. Leclerc X (2007) CT angiography for the diagnosis of brain death: recommendations of the French Society of Neuroradiology (SFNR). *J Neuroradiol* 34(4):217–219
17. Berenguer CM, Davis FE, Howington JU (2010) Brain death confirmation: comparison of computed tomographic angiography with nuclear medicine perfusion scan. *J Trauma* 68(3):553–559
18. Shemie SD, Lee D, Sharpe M, Tampieri D, Young B (2008) Brain blood flow in the neurological determination of death: Canadian expert report. *Can J Neurol Sci* 35(2):140–145
19. Cabrer C, Dominguez-Roldan JM, Manyalich M, Trias E, Paredes D, Navarro A et al (2003) Persistence of intracranial diastolic flow in transcranial Doppler sonography exploration of patients in brain death. *Transplant Proc* 35(5):1642–1643
20. Flowers WM Jr, Patel BR (2000) Persistence of cerebral blood flow after brain death. *South Med J* 93(4):364–370
21. Kosteljanetz M, Ohrstrom JK, Skjodt S, Teglbjaerg PS (1988) Clinical brain death with preserved cerebral arterial circulation. *Acta Neurol Scand* 78(5):418–421
22. Alvarez LA, Lipton RB, Hirschfeld A, Salamon O, Lantos G (1988) Brain death determination by angiography in the setting of a skull defect. *Arch Neurol* 45(2):225–227
23. Hansen AV, Lavin PJ, Moody EB, Sandler MP (1993) False-negative cerebral radionuclide flow study, in brain death, caused by a ventricular drain. *Clin Nucl Med* 18(6):502–505
24. Toffol GJ, Lansky LL, Hughes JR, Blend MJ, Pavel DG, Kecskes SA et al (1987) Pitfalls in diagnosing brain death in infancy. *J Child Neurol* 2(2):134–138
25. Young GB, Lee D (2004) A critique of ancillary tests for brain death. *Neurocrit Care* 1(4):499–508
26. Bergquist E, Bergstrom K (1972) Angiography in cerebral death. *Acta Radiol Diagn (Stockh)* 12(3):283–288
27. Bradac GB, Simon RS (1974) Angiography in brain death. *Neuroradiology* 7(1):25–28
28. Heiskanen O (1964) Cerebral circulatory arrest caused by acute increase of intracranial pressure. A clinical and roentgenological study of 25 cases. *Acta Neurol Scand Suppl* 40(suppl 7):1–57
29. Wijdicks EF (1995) Determining brain death in adults. *Neurology* 45(5):1003–1011
30. (1995) Practice parameters for determining brain death in adults (summary statement). The Quality Standards Subcommittee of the American Academy of Neurology. *Neurology* 45(5):1012–1014
31. Facco E, Zucchetto P, Munari M, Baratto F, Behr AU, Gregianin M et al (1998) 99mTc-HMPAO SPECT in the diagnosis of brain death. *Intensive Care Med* 24(9):911–917
32. Wilson K, Gordon L, Selby JB Sr (1993) The diagnosis of brain death with Tc-99m HMPAO. *Clin Nucl Med* 18(5):428–434

The Imaging Diagnosis and Prognosis Assessment of Patients with Midbrain Injury in the Acute Phase of Craniocerebral Injury

Ming-kun Yu and Wei Ye

Abstract We prospectively studied the difference between head CT and MRI in the detection of midbrain injury at the acute stage, the characteristics of MRS in the midbrain, and its relationship to the prognosis. The aim of this study is to propose the imaging diagnosis and outcome assessment indicators for midbrain injury.

According to the clinical diagnosis standard, 22 patients with midbrain injury were chosen as a midbrain injury group, and 20 cases with craniocerebral injury without brain stem injury as the control group, 10 normal adult volunteers as the normal control group. CT was performed on days 1, 3, 5, and 7 respectively, and MRI and MRS within 7 days post-injury. All patients were followed up for 6 months post-injury.

The positive diagnosis rate of 63.64% in MRI for midbrain injury was significantly higher than that of 13.63% found in CT. MRI showed that the location of the midbrain injury was closely associated with prognosis. The reduction of NAA/Cr or NAA/Cho ratio was more obvious and the prognosis of the patients poorer. Midbrain injury can be diagnosed more clearly and its severity or prognosis could also be evaluated by MRI and MRS.

Keywords Midbrain injury • MRI • MRS • Diagnosis • Prognosis

Introduction

With the industrial development, the numbers of traumatic brain injuries caused by traffic accidents, falls and other injuries is increasing. Brain stem injury is a more serious type of

head injury in which midbrain injury is most common. Although the incidence of brain stem injury in head injury accounted for only 3–5%, its death rate was as high as one-third of craniocerebral injury, which is the biggest cause of death and disability.

Currently, diagnosis on brain stem injury is based on clinical manifestations, such as longer duration of unconsciousness, abnormal pupils and eye movements and/or position, positive bilateral pyramidal tract sign and vital sign changes occurred immediately after injury. Brain stem injury lacks the necessary image data in the early stages, making us deviate from the diagnosis, and not be able to more accurately determine the severity and prognosis. According to this view, diagnosis with cranial imaging, especially magnetic resonance imaging (MRI), has not yet formed unified, comprehensive diagnostic criteria. The effect of magnetic resonance spectroscopy (MRS) on the diagnosis of midbrain injury and its relationship to prognosis is unclear.

This article focuses on the difference between head computed tomography (CT) and MRI in the detection rate of the midbrain injury, the relationship of the midbrain injury location shown by MRI to prognosis, and the clinical significance of NAA peak changes in MRS for outcome assessment. Then, we might be able to obtain relatively reliable diagnostic and prognostic indicators for the patients.

Materials and Methods

Three groups were set up in this study. The inclusion criteria of the midbrain injury group are lasting unconsciousness, decorticate or decerebrate rigidity, abnormal pupils, positive pyramidal signs, and change in vital signs. The exclusion criteria include consciousness, and previous cranial nerve injury or brain stem infarct. Twenty-two patients were enrolled in this group, aged 8–59 years old, average 38.4 years, 20 of them had been in car accidents and 2 had a falling injury. Twenty patients with head injury but no brain injury were recruited into the midbrain injury control group, whose inclusion criteria are simple epidural or subdural hematoma,

M.-k. Yu (✉)

Department of Neurosurgery, Changzheng Hospital,
Shanghai, China

Department of Neurosurgery, Changzheng Hospital,
Neurosurgery Institute in Shanghai, 415th Fengyang Road,
Shanghai, China

e-mail: yumingkun01@163.com

W. Ye

Department of Neurosurgery, Changzheng Hospital, Shanghai, China

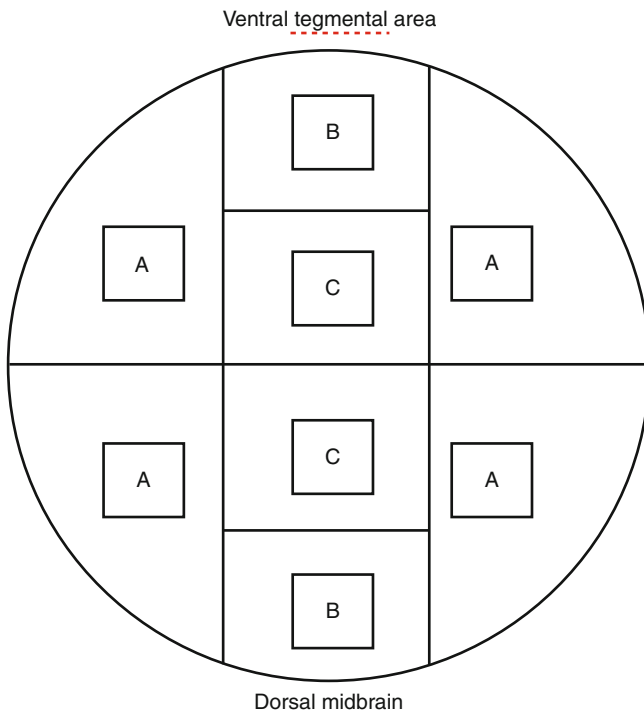


Fig. 1 The specific delineation chart of mesencephalon. A: Lateral mesencephalon; B: Ventral (dorsal) superficial area of the mesencephalon; C: Ventral (dorsal) deep area of the mesencephalon

without unconsciousness and positive signs of brainstem injury. If the volume of the hematoma is too large to compress the brain, the patient would be excluded from this group. The age ranged from 10 to 80 years old, with an average of 47.6 years. Ten normal adult volunteers, whose cranial MRI showed no abnormalities, were chosen as the normal control group.

The head CT was performed on the 1st, 3rd, 5th, and 7th days, and MRI was carried out within 7 days post-injury. The average examination time was 49.2 h. The MRI machine from the General Motor Company was used. The metered volume of the midbrain on MRS was $2 \times 2 \times 2$ cm (8 cm^3). The point-resolved was determined in the collection of spectroscopy. TR/TE was 1500/35. The NAA/Cr, NAA/Cho and Cho/Cr ratios were calculated by the machine. All patients were followed up for 6 months, and their outcome was evaluated using the Glasgow Outcome Scale(GOS) at 6 months post-injury. SPSS 16.0 analysis software was used to analyze the data. Analysis of variance and the Chi-squared test were carried out for analysis. $P < 0.05$ indicates a significant difference and $P < 0.01$ indicates a very significant statistical difference in the results. To compare the relationship of the different regions involved in the midbrain injury with the prognosis, we will divide the midbrain cross-section into three regions (A, B, C) as shown in Fig. 1.

Table 1 Comparison of midbrain magnetic resonance spectroscopy (MRS) results among the three groups

Group	Number of patients	MRS result		
		NAA/Cr	Cho/Cr	NAA/Cho
Midbrain injury group	19	$1.57 \pm 0.22^*$	1.42 ± 0.20	$1.12 \pm 0.18^{**}$
Midbrain injury control group	20	1.83 ± 0.14	1.26 ± 0.10	1.47 ± 0.20
Normal control group	10	1.87 ± 0.12	1.25 ± 0.11	1.51 ± 0.19

* $P < 0.01$, compared with the midbrain injury control group or normal control group respectively

** $P < 0.05$, compared with the midbrain injury control group or normal control group respectively

Results

According to the GOS score 6 months post-injury, 20 patients in the midbrain injury control group have a good prognosis. In 22 patients of the midbrain injury group, 3 patients had a good recovery, 10 had moderate disability, 5 had severe disability, 1 was in a vegetative state, and 3 patients died. The results are as follows:

1. Comparison between the head CT and MRI detection rates for the midbrain injury.
Among 22 patients with midbrain injury within 1 week of the injury, the head CT examination revealed three cases of high density, accounting for 14%; the same MRI examination showed abnormal signals in 14 cases, accounting for 64%.
2. Midbrain MRS results of the three groups (Table 1).
3. Relationship between MRS changes in different regions of the midbrain and prognosis in the midbrain injury group (Table 2).

Discussion

With regard to the head CT examination performed in patients in this group 1, 3, 5, and 7 days after injury, only three cases showed high density on CT of the midbrain regions, and although this seems to be a low detection rate of midbrain injury, cranial CT may be the only image inspection method available in an emergency. If the CT shows high density in the midbrain regions, midbrain injury can be diagnosed. However, because CT is prone to showing artifacts in the skull base of the posterior fossa, a large part of the midbrain injury can produce a negative result.

Table 2 MRS results among sub-groups in different regions of midbrain injury shown by MRI and their outcome

Positive area of midbrain injury shown by MRI	Number of patients	MRS result			Outcome	
		NAA/Cr	Cho/Cr	NAA/Cho	Favorable	Unfavorable
Normal	8	1.73±0.13	1.46±0.13	1.21±0.19	8	0
Unilateral in the lateral midbrain	5	1.63±0.20	1.59±0.23	1.03±0.09	4	1
Bilateral in the lateral midbrain	4	1.51±0.12*	1.25±0.12	1.22±0.14	1	3
Midbrain ventral or dorsal superficial/deep area	2	0.91±0.08**	1.24±0.05	0.72±0.06**	0	2

Outcome: favorable means GOS 4–5 points, unfavorable means GOS 1–3 points

* $P < 0.05$, compared with the normal subgroup

** $P < 0.05$, compared with the other subgroups

According to Hashimoto et al. [1], the rate of detection of brain stem lesions with head CT is about 8.8% (21 out of 239). Our result is 14% (3 out of 22), which is close to the rate in this study.

Fearing et al. [2], studying brain stem imaging of 16 cases with moderate to severe head injury, found that MRI had a higher detection rate of brain stem injury than CT, and the lesion area of the brain stem was also shown more clearly. The study demonstrated that MRI showed better and clearer pathological changes in brainstem damage with no interference from the skull base shadow, by which you can conduct detailed observations of brainstem tissue. In addition, MRI shows high resolution of edematous tissue; therefore, mild edema can be found on T2-weighted images, which show high signal clearly in the early stages of brain stem injury. The brain stem swelling appears as a low signal on T1 and a high signal on T2-weighted images. If this is merged with little hemorrhagic focus in the brain stem, its signal change depends on the injury time. Within 3 days of injury, hemorrhage appears as a low signal on the T2-weighted phase, with high signal in the surrounding edema. Four days later, the T1 and T2 weighting both showed a high signal. MRI was significantly superior to CT regarding the reported detection rate of brain stem injury [3, 4]. This study also confirmed this view. Thus, with the help of MRI, we can detect brain stem lesions earlier and obtain a more accurate diagnosis.

In recent years, the technological development of MRI has allowed us to understand the mechanism of brain stem injury and obtain the most accurate prognostic assessment possible [5, 6]. MRI is considered to be the ideal imaging inspection method [7] for brain stem injury. Gentry et al. [8] studied the mechanism of brainstem injury as early as the early 1990s and described it in general terms. Firsching et al. [9], conducting the MRI examination within 8 days post-injury in 102 patients who had sustained a coma for more than 24 h, found that the mortality rate in patients with bilateral midbrain injury was 24%, while in those with damage to

the bilateral pons it was as high as 100%. It can be concluded that the prognosis of patients with brain stem injury is most closely associated with the location of brain stem injury, and whether or not there is supratentorial brain injury or injury to the middle part of the axon is not the main factor for prognosis. The study by the author showed that if the site of injury in the midbrain is ventral or dorsal, then the mortality rate is very high and the prognosis poor in patients who survived. However, if the site of injury is in the lateral midbrain, whether unilateral or bilateral, the prognosis is good. This conclusion can be also explained by some anatomical evidence as follows. First, periaqueductal midbrain injury in patients with superficial or deep dorsal midbrain damage is serious. Many of the larger neurons in the periaqueductal midbrain form a complex connection with the midbrain reticular ascending activating system, and contact the senior central system to take part in the regulation of respiratory and cardiovascular activity. There are also other regulatory structures such as the dorsal longitudinal fasciculus, medial longitudinal fasciculus, central tegmental tract, and so on, in the deep dorsal midbrain, so that patients with midbrain lesions in the deep dorsal suffer high mortality. Second, patients damaged in the superficial ventral midbrain are most likely harmed in the midbrain ventral tegmental area, which features a very complex range of functions, involving movement, emotion, learning, etc. If patients with the superficial ventral midbrain injury survive, the possibility of them remaining in a vegetative state is considerable. Third, patients suffering from lateral midbrain injury, whether unilateral or bilateral, that does not involve critical nuclei and tracts, are usually only left with a mild or severe disability. Therefore, the relationship between the site of midbrain injury and the prognosis of patients is very close.

Magnetic resonance spectroscopy imaging technology allows us to more easily detect some of the compounds contained within living tissue. MRS is used to measure the material and the state of energy metabolism in the nerve cells, while

it can also provide additional information to enhance the specificity and sensitivity of MRI diagnosis. Three materials can usually be detected by ^1H MRS: N-acetyl aspartate (NAA), choline (Cho), and creatine (Cr). Cr is the most stable metabolite in the brain, and therefore used for internal reference value. The ratio of NAA and Cr could be a marker for the severity of nerve cell damage, which means that the lower the ratio, the more serious the neural cell injury. The ratio of Cho and Cr reflects the proliferation state of nerve cells; the higher the ratio, the stronger the degree of proliferation; thus, the ratio of Cho and Cr after trauma correlates with the condition of nerve tissue repair. The proliferation of nerve tissue in the brain usually starts at a late stage, so the Cho/Cr ratio difference is not obvious among subgroups in the acute phase in this study. In our study, for removal of non-specific changes in the midbrain spectrum caused by head trauma, we determined the normal adult midbrain NAA/Cr and NAA/Cho values, which were compared with those of patients with epidural/subdural hematomas, and found that there were no significant differences between the two groups, indicating that specific spectral change in the midbrain regions is the result of midbrain injury, but not non-specific changes caused by traumatic stress reaction. In the acute period, compared with normal control, the NAA/Cr and NAA/Cho ratio in the midbrain of patients with midbrain injury decreased significantly, indicating the significance of the NAA/Cr and NAA/Cho ratio for judging the severity of patients. We found that the prognosis of patients whose midbrain NAA/Cr and NAA/Cho ratios as examined by MRS in the early phase, were significantly lower (0.91 ± 0.08 and 0.72 ± 0.06 respectively) would be poor. In this regard, we believe that NAA can be more sensitive indicators of neuronal injury. Nerve cell damage in the early stages may accelerate the decomposition of NAA as acetyl coenzyme A and aspartate, so as to meet the lipid synthesis of membrane and myelin repair, and the energy supply at the axonal damage site as well as affording adequate amino acids. Therefore, NAA content was first decreased as long as the nerve cell was damaged. If NAA content decreases in the early phase, indicating the neurons damaged in this region, then a significant decline in NAA content shows more severe neuronal damage condition and poor prognosis in these patients. Hence, NAA is the first choice marker for MRS research into early brain lesions.

We find that if midbrain injury sites shown on MRI were in the superficial ventral or dorsal superficial/deep midbrain, the NAA/Cr and NAA/Cho ratios decreased significantly, and the prognosis of the patients was also poor, whereas if the NAA/Cr and NAA/Cho ratios in injuries to other regions of the midbrain did not decline obviously, the patients' prognosis was relatively good. We think that MRS combined with MRI could help us make a more credible prognostic assessment for patients with midbrain injury in different regions. Firsching et al. [9] summarized the rules on brain stem injury depending on brain stem injury classification and thought

that its prognosis is most closely associated with the site of brain stem injury, but whether it is accompanied by supratentorial brain contusion or diffuse axonal injury of the midline structure is not the main factor for prognosis. Thus, this article did not clearly distinguish the injury site outside the brain stem, such as the scope and site of supratentorial brain injury, in the discussion. Marmarou et al. [10] conducted brain MRS examination in patients with traumatic brain injury and found that the decrease in the NAA/Cr and Cho/Cr ratios was significantly positively correlated with the GCS and GOS. McLean and Cross [11] also considered that in patients who show no abnormal finding on cranial MRI, which is not consistent with clinical symptoms, MRS examination can clarify a diagnosis of brain stem injury. Therefore, MRS can make more accurate judgments regarding prognosis.

Conclusion

Based on the discussion above, it is evident that the detection rate of midbrain injury in cranial MRI was significantly higher than that in head CT. MRI showed that the prognosis of patients with midbrain injury is closely related to the injured area, which are in the order unilateral and bilateral in the lateral region, superficial ventral, and superficial or deep dorsal area of the midbrain on the basis of the outcome from good to poor. As shown by MRS, midbrain NAA/Cr and NAA/Cho ratios decreased significantly after midbrain injury. The more the midbrain NAA/Cr and NAA/Cho ratios decreased, the worse the prognosis will be.

Conflict of interest statement We declare that we have no conflict of interest.

References

1. Hashimoto T, Nakamura N, Richard KE et al (1993) Primary brain stem lesions caused by closed head injuries. *Neurosurg Rev* 16:291–298
2. Fearing MA, Bigler ED, Wilde EA et al (2008) MRI findings in the thalamus and brain stem in children after moderate to severe traumatic brain injury. *J Child Neurol* 23:729–737
3. Kara A, Celik SE, Dalbayrak S et al (2008) Magnetic resonance imaging finding in severe head injury patients with normal computerized tomography. *Turk Neurosurg* 18:1–9
4. Vik A, Kvistad KA, Skandsen T et al (2006) Diffuse axonal injury in traumatic brain injury. *Tidsskr Nor Laegeforen* 126:2940–2944
5. Zheng WB, Liu GR, Li LP et al (2007) Prediction of recovery from a post-traumatic coma state by diffusion-weighted imaging (DWI) in patients with diffuse axonal injury. *Neuroradiology* 49:271–279
6. Mannion RJ, Cross J, Bradley P et al (2007) Mechanism-based MRI classification of traumatic brainstem injury and its relationship to outcome. *J Neurotrauma* 24:128–135

7. Aguas J, Begué R, Díez J (2005) Brainstem injury diagnosed by MRI. An epidemiologic and prognostic reappraisal. *Neurocirugia (Astur)* 16:14–20
8. Gentry LR, Godersky JC, Thompson BH et al (1989) Traumatic brain stem injury: MR imaging. *Radiology* 171:177–187
9. Firsching R, Woischneck D, Klein S et al (2001) Classification of severe head injury based on magnetic resonance imaging. *Acta Neurochir (Wien)* 143:263–271
10. Marmarou A, Signoretti S, Fatouros P et al (2005) Mitochondrial injury measured by proton magnetic resonance spectroscopy in severe head trauma patients. *Acta Neurochir Suppl* 95:149–151
11. McLean MA, Cross JJ (2009) Magnetic resonance spectroscopy: principles and applications in neurosurgery. *Br J Neurosurg* 23: 5–13

The Effect of Intraventricular Thrombolysis in Combination with Low-Frequency Head Motion After Severe Subarachnoid Hemorrhage: Interim Analysis of Safety, Clot Clearance Rate and Delayed Cerebral Ischemia

Sven O. Eicker, Kerim Beseoglu, Nima Etminan, Jason Perrin, Arzu Taskin, Hans-Jakob Steiger, and Daniel Hänggi

Abstract Objective: The current clinical prospective randomized phase II study was initiated in order to analyze the effect of enhanced washout by discontinuous intraventricular thrombolysis in combination with low-frequency head-motion therapy on side effects, clot clearance rate, cerebral vasospasm and clinical outcome after severe subarachnoid hemorrhage (SAH).

Methods: Data from 40 adult patients with aneurysmal SAH were included in this interim analysis. Patients randomized to the study group achieved additional intraventricular application of rt-PA (Actilyse®) bolus 5 mg every 12 h and lateral rotational therapy (RotoRest®). Clot clearance rate was evaluated based on computed tomography (CT). Delayed cerebral ischemia (DCI) and early clinical outcome of patients were determined.

Results: No severe side effects due to the combined therapy were documented. The clot clearance rate was significantly higher in the study group than in the control group regarding the cranial and basal CT slices ($p = 0.003$ cranial slices and $p = 0.037$ basal slices). Delayed ischemic neurological deficits (DIND) were increased in the control group ($p = 0.016$).

Conclusion: The present study demonstrates that a combination of intraventricular thrombolysis and lateral rotational therapy is not associated with a higher complication rate. Furthermore, the therapy leads to a significant acceleration of the clot clearance rate.

Keywords Aneurysm • Cerebral vasospasm • Cisternal lavage • Clot clearance rate • Head motion therapy • Subarachnoid hemorrhage

Introduction

Cerebral arterial vasospasm remains the dominant secondary complication cause of aneurysmal subarachnoid hemorrhage (SAH), and is associated with high rates of morbidity and mortality [6, 7, 11, 13, 20]. Experimental and clinical studies identified clot volume [21, 23] and clearance (CC) rate [14, 21] as independent predictors of vasospasm after aneurysmal SAH. Experimental studies have demonstrated prevention of vasospasm by early clot removal [8], but most clinical studies failed to confirm a similar benefit [24]. Moreover, reduction of cerebral vasospasm has been attempted by intrathecal administration of thrombolytic agents such as urokinase or rt-PA [2, 9, 17–19, 22]. The use of a head-shaking device was introduced in 1990 to accelerate clot removal by a kinetic mechanism. Coupled head-shaking devices [15] and continuous infusion of thrombolytic agents through a ventricular or lumbar (lumboventricular irrigation) catheter and drainage over a second ventricular catheter have been described [10, 11]. The present, prospective study was designed to analyze the combination of kinetic therapy with a minimally invasive and discontinuous application of thrombolytic agents that does not require a second ventricular or lumbar catheter. The intention of the actual trial was to analyze the effectiveness of the discontinuous application of thrombolytic agents and motion therapy on cerebral vasospasm, delayed ischemic neurological deficit (DIND), and clinical outcome. Owing to previous complications [10] an interim analysis of safety and effectiveness after 40 patients was scheduled.

Materials and Methods

This single-centre, randomized, prospective Phase II trial was conducted in the Department of Neurosurgery at Heinrich-Heine-University in Düsseldorf, Germany. Approval of the local Research Ethics Committee and Institutional Review Board was obtained for the study. All patients met the criteria of having an aneurysmal SAH of World Federation of Neurosurgical Societies (WFNS) Grades II–V, corresponding

S.O. Eicker (✉), K. Beseoglu, N. Etminan, J. Perrin, A. Taskin, H.-J. Steiger, and D. Hänggi
Department of Neurosurgery, Heinrich-Heine-University,
Moorenstraße 5, Düsseldorf 40225, Germany
e-mail: eicker.s@mac.com

to Glasgow Coma Scale (GCS) scores of 13–3 and Fisher Grades 3 or 4. Informed consent was obtained from a legal representative for each patient before starting the protocol. Patients younger than 18 years of age, patients with WFNS Grade I SAH or with GCS scores of 14 and 15, patients with Fisher Grades 1 and 2 SAH, patients with traumatic or non-aneurysmal SAH, pregnant women, and patients admitted more than 1 day after SAH were excluded from the study.

For patients included in the study group 5 mg of rt-PA (Actilyse®) bolus were slowly administered intraventricularly every 12 h four times. EVD was closed for 1 h after application and subsequently placed 10 cm above the ear for 48 h. After termination of the thrombolytic procedure the EVD overflow level was placed 18 cm above the ear. In addition to thrombolytic treatment, continuous head and body motion was achieved in a rotational kinetics system as described before (RotoRest bed (KCI™)) [10, 11]. Head motion was continued for 48 h congruent to the thrombolytic treatment. In patients who require additional sedation or comatose patients the kinetic therapy was extended for three additional days.

Assessment of CC Rate

All patients in the control and study group underwent standard follow-up CT 6 h after aneurysm occlusion and on days 1, 2, 4, 5, 9–11 and additionally in the event of neurological deterioration. The scans were saved digitally and evaluated with OsiriX® (v.3.6.1). Integration of entire cranial and basal CT slices was performed, and all pixels between 50 and 90 Hounsfield units indicating acute hemorrhage were counted. The CC rate was defined as the relative amount of subarachnoid blood and reduction in voxel volume (in cubic centimeters) within the time period from day 1 through day 5 (± 1 –2 days).

Assessment of Cerebral Vasospasm and Clinical Outcome

Delayed ischemic neurological deficits were identified during hourly clinical assessments in conscious patients. Moreover, a mean flow velocity of >150 cm/s on TCD in ≥ 1 arterial segments was defined as a Doppler ultrasound arterial spasm. Narrowing of the arterial diameter >30% from baseline was defined as an angiographic vasospasm. Finally, ischemic lesions on CT not related to the initial insult or to surgical manipulation were considered related to the vasospasm. Outcome was measured at the time of discharge.

Table 1 Study population characteristics

Characteristics	Study group (16 patients)	Control group (19 patients)	<i>p</i> value
Mean age in years (\pm SD)	57.5 (\pm 8.53)	56.0 (\pm 14.3)	0.72
Male/female ratio	9:7	8:11	
WFNS grades (%)			0.81
II	1 (6)	0 (0)	
III	2 (13)	4 (21)	
IV	2 (13)	3 (16)	
V	11 (68)	12 (63)	
Fisher grade (%)			0.03
3	6 (40)	2 (10)	
4	9 (60)	17 (90)	
Location of ruptured aneurysm (%)			
ACA	6 (40)	9 (47)	
MCA	8 (53)	4 (21)	
post circulation	1 (7)	6 (32)	
Kinetic therapy in days	3.2 (\pm 0.54)		
Clipping/coiling ratio	12:4	10:9	0.17

ACA anterior cerebral artery, MCA middle cerebral artery, *post* posterior, SD standard deviation

Statistical Analysis

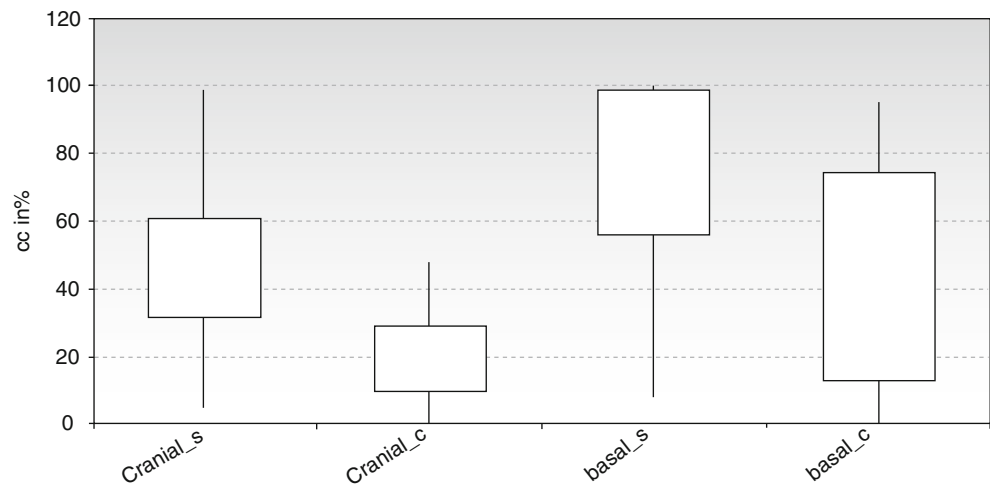
The characteristics of the study population are presented in Table 1. The CC was assessed with a relative change rate between measurements of volume obtained on days 1 and 5 of therapy according to the formula $CC = \frac{C_{1 \text{ day}} - C_{5 \pm 2 \text{ days}}}{C_{1 \text{ day}}} \times 100\%$. All statistical analysis was performed using SPSS software (SPSS 18.0 for Windows: SPSS, Inc., Chicago, IL, USA). Probability values <0.05 were considered significant.

Results

Forty patients with aneurysmal SAHs were included in the study. Median age was 57.5 (\pm 8.53) in the study group and 56.0 (\pm 14.3) in the control group ($p=0.72$, Wilcoxon rank-sum test). Of the 40 patients, 5 were excluded owing to lack of facilities.

The differences in male/female ratio, aneurysm location, Fisher grades, WFNS grades, and the clipping/coiling ratio between the treatment and control groups are listed in Table 1.

Fig. 1 Boxplot demonstrating the clot clearance (CC) rate of the cranial and basal CT slices in the study and control group (_s study group, _c control group)



Clearance and Clot Clearance Rate

The CC as defined above was higher in the study group than in the control group regarding the cranial and basal slices. Cranial a 48.3% (± 29.1) CC rate was achieved in the study group in comparison to 21.3% (± 12.8) in the control group. In the basal slices a CC rate of 74.6% (± 33.6) in comparison to 48.1% (± 33.9) was detected. This difference was statistically significant ($p=0.003$ cranial, $p=0.037$ basal, t -test; Fig. 1).

Cerebral Vasospasm

Clinical observation revealed fewer DINDs in the study group than in the control group. One patient (6%) in the study group, compared with eight patients (42%) in the control group, developed a new neurological deficit during observation. This was statistically significant ($p=0.016$, Chi-squared test).

Angiographic vasospasm was seen in six patients (38%) in the study group, compared with six patients (32%) in the control group ($p=0.713$, Chi-squared test). The blood flow velocities detected on TCD ultrasound showed no statistically significant difference between the two groups (Fig. 2).

Vasospasm-related minor infarctions on CT were less frequent in the study group than in the control group. Ischemic areas related to vasospasm were demonstrated in one patient (6%) in the study group and in six patients (32%) in the control group ($p=0.062$, Chi-squared test).

Clinical Outcome

At discharge, 13% of the patients treated had good mRS scores (0–2), 23% had moderate scores [3, 4], and 64% had poor outcomes (scores 5 and 6). In the control group 21%

had good, 16% had moderate, and 63% of patients had poor outcomes. At the 3-month follow-up there was a marked but not statistically significant improvement in mRS scores in the study group compared with the control group ($p=0.06$, Mann–Whitney Test; Table 2).

Discussion

The present pilot series is to our knowledge the first prospective randomized study in humans investigating the safety and effectiveness of discontinuous intraventricular thrombolysis in combination with low-frequency head motion after severe subarachnoid hemorrhage. Basically, this interim analysis demonstrated that the study treatment proved to be safe and effective regarding the CC and DINDs in awake patients.

A meta-analysis of randomized and nonrandomized trials of intracisternal thrombolysis suggests a clinically relevant and statistically significant beneficial effect for patients after severe SAH [2].

The present, prospective study was designed to analyze the combination of low-frequency head motion with a minimally invasive and discontinuous application of thrombolytic agents that does not require a second ventricular or lumbar catheter. In addition to bolus therapy with a thrombolytic agent, continuous low-frequency head-motion was used in this study to accelerate clot lysis. The head-shaking method was introduced in 1990 using the Neuroshaker (Mizuho), and the effectiveness was documented in a prospective trial investigating the combination of cisternal lavage and head-shaking compared with cisternal lavage alone [15]. In that study a swinging frequency of 1 cycle/s was chosen as the motion pattern. Complications, such as motion sickness, brain swelling, and even hemorrhage, have been reported in patients treated with the Neuroshaker [3]. Because of these complications we decided to apply slow rotation with a

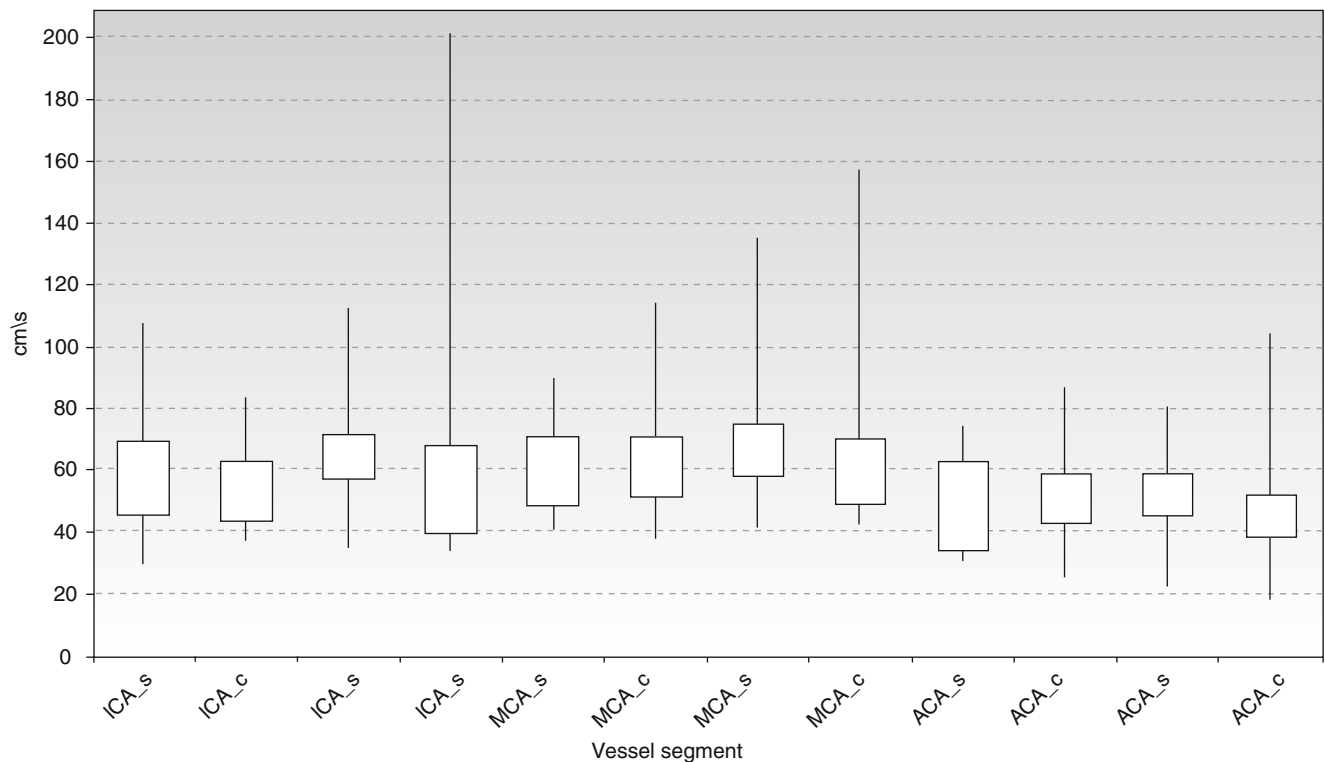


Fig. 2 Boxplot demonstrating blood flow velocity in all segments measured on transcranial Doppler (TCD) ultrasound in the control and study group. ACA anterior cerebral artery, _C control group, ICA internal carotid artery, *l* left, MCA middle cerebral artery, *r* right, _S study group

proven system that has been established for other indications (such as pulmonary problems after traumatic injury).

Clot Clearance Rate

Clot volume and CC rate have been reported to be independent predictors of cerebral vasospasm after aneurysmal SAH [21]. Therefore, attempts to accelerate the CC rate have been made before [5, 12]. The resulting data in the actual study defined the relative amount of blood in the intracranial compartment. The reduction in the measured blood volume over time was defined as the CC rate (in cubic centimeters) from day 1 through day 5 $\pm 1-2$. Overall, our findings demonstrated a significantly increased clearance rate in the study group ($p=0.037$ basal slices and $p=0.003$ cranial slices).

Effectiveness on Cerebral Vasospasm and Clinical Outcome

Our study demonstrated that simultaneous thrombolysis and head motion therapy reduces the incidence of DINDs ($p=0.016$). However, reduction in angiographic vasospasm did not reach statistical significance ($p=0.713$), probably because of the small number of patients. The blood flow

velocities detected on TCD ultrasound showed no statistically significant difference between the two groups. The highest outliers, though, in terms of cerebral blood flow >150 cm/s, were found in the control group associated with clinical and angiographic vasospasm. A correlation between cerebral blood flow velocities after SAH and the number of blood clots noted on CT has been reported [4]. Nevertheless, the role of TCD in the treatment of patients with SAH for detection of cerebral vasospasm remains controversial [1]. The infarction rate related to cerebral vasospasm as seen on CT was higher in the controls than in the study ($p=0.062$). At discharge, 6% of treated patients had good GOS scores [1, 2], 81% had severe disabilities [3], and 13% had poor outcomes [4, 5]. There was no significant contrast to the control group with 21% good, 57% severe, and 22% bad outcomes. Apart from a possible short-term negative impact of the experimental therapy, there is no explanation for these results; in particular the Fisher grades in the control group were significantly higher.

Study Design and Limitations

Only patients who had WFNS Grades II–V (GCS scores 13–3) were studied. The restriction according to the neurological condition was done in the light of our standard management of SAH, which requires EVD placement in patients with GCS scores between 3 and 13 on admission. Therefore,

Table 2 Clinical outcome in the two groups

Outcome	No. of patients (%)		<i>p</i> value
	Study group	Control group	
GOS score at discharge			0.72
1	1 (6)	3 (16)	
2	0 (0)	1 (5)	
3	13 (81)	11 (57)	
4	0 (0)	2 (11)	
5	2 (13)	2 (11)	
mRS score at discharge			0.76
0	0 (0)	0 (0)	
1	2 (13)	2 (11)	
2	0 (0)	2 (11)	
3	1 (6)	0 (0)	
4	3 (19)	3 (16)	
5	9 (56)	9 (46)	
6	1 (6)	3 (16)	
3-month FU mRS score			0.06
0	1 (0)	1 (5)	
1	4 (13)	3 (21)	
2	5 (19)	1 (5)	
3	1 (19)	2 (26)	
4	2 (23)	4 (11)	
5	2 (13)	5 (16)	
6	1 (13)	3 (16)	

FU follow-up, *GOS* Glasgow Outcome Scale, *mRS* Modified Ranking Scale

the experimental protocol did not expose the patients to a substantial additional risk. Moreover, we only included patients who had Fisher Grade 3 or 4 SAH on admission CT. This decision was made because of the well-established association between Fisher grade and cerebral vasospasm [16].

Despite the intention of a homogeneous patient population in the two groups, the control group patients had significantly worse Fisher Grades than the control group ($p=0.03$). There are no publications demonstrating that intraventricular blood is responsible for vasospasm. The distinct detection of intraventricular blood in the control group may therefore be a minor limitation.

Conclusion

The present study demonstrates that a combination of intraventricular thrombolysis and lateral rotational therapy is not associated with a higher complication rate. Furthermore, the therapy leads to a significant acceleration of the clot clearance rate.

Conflict of interest statement We declare that we have no conflict of interest.

References

1. Aaslid R (2002) Transcranial Doppler assessment of cerebral vasospasm. *Eur J Ultrasound* 16:3–10
2. Amin-Hanjani S, Ogilvy CS, Barker FG II (2004) Does intracisternal thrombolysis prevent vasospasm after aneurysmal subarachnoid hemorrhage? A meta-analysis. *Neurosurgery* 54:326–335
3. Aoki N (1995) “Head-shaking syndrome” neurological deterioration during continuous head-shaking as an adjunct to cisternal irrigation for clot removal in patients with acute subarachnoid haemorrhage. *Acta Neurochir (Wien)* 132:20–25
4. Boecker-Schwarz HG, Fries G, Mueller-Forell W, Kessel G, Perneczky A (1998) Cerebral blood flow velocities after subarachnoid haemorrhage in relation to the amount of blood clots in the initial computed tomography. *Acta Neurochir (Wien)* 140:573–578
5. Brouwers PJ, Wijdicks EF, Van Gijn J (1992) Infarction after aneurysm rupture does not depend on distribution or clearance rate of blood. *Stroke* 23:374–379
6. Charpentier C, Audibert G, Guillemin F, Civit T, Ducrocq X, Bracard S, Hepner H, Picard L, Laxenaire MC (1999) Multivariate analysis of predictors of cerebral vasospasm occurrence after aneurysmal subarachnoid hemorrhage. *Stroke* 30:1402–1408
7. Findlay JM, Deagle GM (1998) Causes of morbidity and mortality following intracranial aneurysm rupture. *Can J Neurol Sci* 25:209–215
8. Findlay JM, Weir BK, Steinke D, Tanabe T, Gordon P, Grace M (1988) Effect of intrathecal thrombolytic therapy on subarachnoid clot and chronic vasospasm in a primate model of SAH. *J Neurosurg* 69:723–735
9. Gorski R, Zabek M, Jarmuzek P (2000) Influence of intraoperative using of recombinant tissue plasminogen activator on the development of cerebral angiospasm after subarachnoid haemorrhage in patients with ruptured intracranial aneurysms. *Neurol Neurochir Pol* 34:41–47
10. Hänggi D, Liersch J, Turowski B, Yong M, Steiger HJ (2008) The effect of lumboventricular lavage and simultaneous low-frequency head-motion therapy after severe subarachnoid hemorrhage: results of a single center prospective phase II trial. *J Neurosurg* 108:1192–1199
11. Hänggi D, Eicker S, Beseoglu K, Behr J, Turowski B, Steiger HJ (2009) A multimodal concept in patients after severe aneurysmal subarachnoid hemorrhage: results of a controlled single centre prospective randomized multimodal phase I/II trial on cerebral vasospasm. *Cen Eur Neurosurg* 70:61–67
12. Hirashima Y, Kurimoto M, Takaba M, Endo S, Takaku A (1995) The use of computed tomography in the prediction of delayed cerebral infarction following acute aneurysm surgery for subarachnoid haemorrhage. *Acta Neurochir (Wien)* 132:9–13
13. Kassell NF, Torner JC, Jane JA, Haley EC Jr, Adams HP (1990) The international cooperative study on the timing of aneurysm surgery. Part 2: surgical results. *J Neurosurg* 73:37–47
14. Kasuya H, Shimizu T, Takakura K (1998) Thrombin activity in CSF after SAH is correlated with the degree of SAH the persistence of subarachnoid clot and the development of vasospasm. *Acta Neurochir (Wien)* 140:579–584
15. Kawamoto S, Tsutsumi K, Yoshikawa G, Shinozaki MH, Yako K, Nagata K, Ueki K (2004) Effectiveness of the head-shaking method combined with cisternal irrigation with urokinase in preventing cerebral vasospasm after subarachnoid hemorrhage. *J Neurosurg* 100:236–243
16. Kistler JP, Crowell RM, Davis KR, Heros R, Ojemann RG, Zervas T, Fisher CM (1983) The relation of cerebral vasospasm to the

- extent and location of subarachnoid blood visualized by CT scan: a prospective study. *Neurology* 33:424–436
17. Kodama N, Sasaki T, Kawakami M, Sato M, Asari J (2000) Cisternal irrigation therapy with urokinase and ascorbic acid for prevention of vasospasm after aneurysmal subarachnoid hemorrhage. Outcome in 217 patients. *Surg Neurol* 53:110–118
 18. Mizoi K, Yoshimoto T, Takahashi A, Fujiwara S, Kosu K, Sugawara T (1993) Prospective study on the prevention of cerebral vasospasm by intrathecal fibrinolytic therapy with tissue-type plasminogen activator. *J Neurosurg* 78:430–437
 19. Ohman J, Servo A, Heiskanen O (1991) Effect of intrathecal fibrinolytic therapy on clot lysis and vasospasm in patients with aneurysmal subarachnoid hemorrhage. *J Neurosurg* 75:197–201
 20. Rabinstein AA, Pichelmann MA, Friedman JA, Piepgras DG, Nichols DA, McIver JJ, Toussaint LG 3rd, McClelland RL, Fulgham JR, Meyer FB, Atkinson JL, Wijdicks EF (2003) Symptomatic vasospasm and outcomes following aneurysmal subarachnoid hemorrhage: a comparison between surgical repair and endovascular coil occlusion. *J Neurosurg* 98:319–325
 21. Reilly C, Amidei C, Tolentino J, Jahromi BS, Macdonald RL (2004) Clot volume and clearance rate as independent predictors of vasospasm after aneurysmal subarachnoid hemorrhage. *J Neurosurg* 101:255–261
 22. Seifert V, Stolke D, Zimmermann M, Feldges A (1994) Prevention of delayed ischaemic deficits after aneurysmal subarachnoid haemorrhage by intrathecal bolus injection of tissue plasminogen activator (rTPA). A prospective study. *Acta Neurochir (Wien)* 128:137–143
 23. Suzuki J, Komatsu S, Sato T, Sakurai Y (1980) Correlation between CT findings and subsequent development of cerebral infarction due to vasospasm in subarachnoid haemorrhage. *Acta Neurochir (Wien)* 55:63–70
 24. Taneda M (1982) Effect of early operation for ruptured aneurysms on prevention of delayed ischemic symptoms. *J Neurosurg* 57:622–628

Early CT Perfusion Measurement After Aneurysmal Subarachnoid Hemorrhage: A Screening Method to Predict Outcome?

Marcel A. Kamp, Hi-Jae Heiroth, Kerim Beseoglu, Bernd Turowski, Hans-Jakob Steiger, and Daniel Hänggi

Abstract Objective: The goal of the present study is to analyze the predictive impact of early CT-based perfusion measurement (CTP) on clinical outcome in patients suffering from aneurysmal SAH.

Methods: Fifteen patients with aneurysmal SAH received an early CTP measurement that was performed within the first 6 h after initial bleeding. According to a specific CTP protocol, mean transit time (MTT) and time to peak (TTP) were calculated bihemispherically and correlated with the clinical initial status according to the WFNS grade as well as with the Glasgow Outcome Scale (GOS) at the time of discharge.

Results: The MTT and TTP correlated highly significantly with the initial WFNS grade and the GOS at the time of discharge. Mean bihemispheric MTT was 3.4 s (2.8–4.1 s, SD: 0.5 s) for initially good-grade patients (WFNS° I–III) and 4.5 s (31.2–49.8 s) for poor-grade patients (WFNS° IV–V). ICP monitored in nine patients via EVD was documented within normal intracranial pressure as defined below 18 mmHg.

Conclusion: The determination of MTT and TTP using early CTP measurements in patients suffering from aneurysmal SAH demonstrated a significant correlation with the initial neurological status and the early clinical outcome.

Keywords Subarachnoid hemorrhage • Early perfusion • Early damage • CT perfusion • Clinical outcome

Introduction

Despite the current treatment strategies, aneurysmal subarachnoid hemorrhage (SAH) remains a disease with high morbidity and mortality, causing case fatality rates between 25% and

50% [5]. Potential related causes for bad outcome are initial acute ischemic events and delayed cerebral ischemia (DCI) [8].

The goal of the present pilot study was first to evaluate the feasibility of an early CTP analysis in patients suffering from aneurysmal SAH, and second, to assess the predictive impact of initial CTP measurement on clinical outcome.

Materials and Methods

Patient Population

The single-centre prospective phase I/II trial was approved by the local Research Ethics Committee and institutional review board. All patients integrated in the study protocol met the following inclusion criteria:

1. Aneurysmal SAH grade 1–5 according to WFNS
2. Fisher grade 2–4
3. Informed consent was obtained from a legal representative before starting the protocol

Patients below 18 years, patients with Fisher grade 1, patients with traumatic or non-aneurysmal SAH, pregnant women, and patients admitted later than 6 h after the index hemorrhage were excluded from the study.

General Management

General care followed a standardized protocol including insertion of an external ventricular drainage (EVD) without delay (GCS < 13), angiography and surgical or endovascular obliteration of the aneurysm within 24 h of admission.

Study Design

Within 6 h of the aneurysmal rupture a CTP measurement was performed, with calculation of the mean transit time

M.A. Kamp (✉), H.-J. Heiroth, K. Beseoglu, H.-J. Steiger, and D. Hänggi
Department of Neurosurgery, Heinrich-Heine-University,
Moorenstraße 5, Düsseldorf D-40225, Germany
e-mail: marcelalexander.kamp@uni-duesseldorf.de

B. Turowski
Institute for Radiology, Heinrich-Heine-University, Moorenstraße 5,
Düsseldorf D-40225, Germany

Table 1 Clinical data

No.	Age	Sex	WFNS ^o	Fisher ^o	Aneurysm location	Side	Treatment	GOS	MTT	TTP
1	45	f	I	III	Other	–	–	5	31.5	16.8
2	31	m	I	III	AcomA	–	Clipping	5	28.4	18.7
3	72	m	I	III	AcomA	–	Clipping	5	31.0	12.9
4	42	f	I	III	AcomA	–	Clipping	5	29.8	16.2
5	42	f	I	III	PcomA	ri	Clipping	3	41.1	14.4
6	69	m	II	III	Other	ri	–	4	37.1	29.2
7	63	f	III	IV	AcomA	–	Clipping	3	42.4	26.6
8	56	m	III	III	MCA	ri	Clipping	4	41.5	16.6
9	58	f	IV	IV	BA	–	Coiling	1	47.2	19.9
10	53	f	IV	IV	Pericallosa	ri	Clipping	1	50.7	22.2
11	52	m	IV	IV	Other	ri	Coiling	3	33.4	32.1
12	58	f	IV	III	A2	le	Clipping	4	48.1	16.4
13	70	m	V	IV	AcomA	–	Clipping	2	43.9	25.7
14	41	f	V	III	PcomA	ri	Coiling	4	46.0	18.8
15	68	f	V	IV	BA	–	–	1	40.6	30.9

This table summarizes the clinical data of the 15 patients who underwent early perfusion measurement after subarachnoid hemorrhage *f* female, *m* male, *AcomA* anterior communicating artery, *MCA* middle cerebral artery, *MTT* mean transit time, *PcomA* posterior communicating artery, *BA* basilar artery, *Other* other location of the cerebral aneurysm, *TTP* time to peak, *WFNS* World Federation of Neurological Surgeons, *GOS* Glasgow Outcome Scale, *ri* right, *le* left

(MTT) and selective time to peak of the brain parenchyma (TTP) being determined for each hemisphere, as previously described [16, 17].

Study Parameters and End Points

To correlate the cerebral perfusion as measured by CTP and the clinical status, the WFNS at admission as well as the GOS at the time of discharge were calculated.

Statistical Analysis

All analyses were performed using SAS software (SAS institute, Cary, North Carolina, USA). P values of less than 0.05 were considered significant. Adjustment for multiple testing was not considered.

Results

Study Population

Fifteen consecutive CTP measurements in 15 patients were included in our pilot series. Clinical data, Fisher grade, aneurysm location and treatment are summarized in Table 1. Nine

patients required an EVD according to our routine protocol. ICP of all nine patients at the time of CTP measurement was below 20 mmHg. For the intubated patients, an initial blood gas analysis at the time of administration was documented and revealed a mean pCO₂ of 39.9 mmHg (range 16.7–81.8 mmHg, standard deviation, SD: 17.8 mmHg). At the time of CT perfusion measurement, all patients moderately hyperventilated with a pCO₂ between 30 and 40 mmHg. Systolic arterial blood pressure was adjusted between 100 and 140 mmHg for all patients.

Results of the Early CT Perfusion

Analysis of the mean transit time (MTT) for each hemisphere revealed a mean MTT of 3.4 s for each hemisphere (right hemisphere: range: 2.8–4.1 s, standard deviation, SD: 0.5 s, left hemisphere: range: 2.8–4.3 s, SD: 0.6 s) for patients with an initially good clinical presentation (WFNS^o I–III). For poor initial grades (WFNS^o IV–V) mean transit time was significantly prolonged (right side: 4.5 s, range: 3.1–4.9 s, SD: 0.6 s; left side: 4.7 s, range: 3.5–5.1 s, SD: 0.6 s). The MTT significantly correlated with initial WFNS grade ($P=0.005$; correlation coefficient $r=0.686$; Spearman correlation). Besides MTT, TTP also showed an increase in respect of patient's initial neurological status. Mean TTP was 1.6 s (right hemisphere: range: 1.3–2.6 s, SD: 0.5 s) respectively 1.8 s (left hemisphere: range: 1.2–3.1 s, SD: 0.6 s) for patients with an initial WFNS^o I–III. In contrast,

TTP was increased for WFNS^o IV and V patients (right side: mean: 1.9 s; range: 1.6–2.9 s, SD: 0.6 s; left side: 2.2 s, range: 1.7–3.6 s, SD: 0.7 s). Also, TTP significantly correlated with the initial WFNS grade ($P=0.017$; correlation coefficient $r=0.603$; Spearman correlation). CT perfusion parameter of the particular hemisphere showed no correlation with the location of the vascular pathology on the ipsi- and contralateral sides. No side effects were observed.

Clinical Outcome

At the time of discharge, the clinical examination revealed a good clinical condition (GOS 4–5) in nine patients and an unfavorable outcome (GOS 1–3) in seven patients. Three patients had a fatal outcome (GOS 1). Outcome measured by the GOS correlated highly significant with initial MTT ($P=0.006$; Spearman correlation) and TTP ($P=0.020$; Spearman correlation). Both parameters did not correlate with the development of cerebral vasospasms.

Discussion

Early damage immediately after aneurysmal SAH has been discussed extensively in the literature. Evidence of acute hypoperfusion after SAH gained from animal and from clinical studies using transcranial ultrasound (TCD), conventional and xenon contrast-enhanced perfusion CT, positron emission tomography (PET) or single-photon emission tomography (SPECT) are available [1–4, 9, 10, 12, 13, 15, 18]. Pathophysiologically, subarachnoid blood leads to an acute increase in the intracranial pressure (ICP), a vasoconstriction of the proximal cerebral vessels combined with a decrease in the cerebral metabolic rate of oxygen, the cerebral perfusion pressure (CPP), and the cerebral blood flow (CBF), which tended to be close to zero in some studies [1–4, 9, 10, 12, 13, 15, 18]. This early cerebral vasoconstriction and hypoperfusion are reflected in the early cellular and molecular changes that could be detected after almost 10 min of exposure to blood [6, 14]. In contrast to the bone-breaking evidence, initial cerebral hypoperfusion after SAH plays no role in diagnostic and therapeutic concepts in most neurosurgical departments.

In the present series, measured by CTP, the MTT, and TTP showed significant prolongation in patients with an initially poor clinical performance according to the WFNS grades IV and V, and correlated significantly with clinical outcome. Additionally, the hypoperfusion occurred symmetrically without any correlation with the side of aneurysm location. At last, hydrocephalus as a direct cause of the hypoperfusion, as well as hypocapnia, could basically be excluded in our series because the measured ICP and $p\text{CO}_2$

were within a normal range at the time of CTP measurement for all patients with an EVD.

These results are in line with conception of global initial damage of the brain in response to the subarachnoid blood [1, 7, 12]. Two recent clinical studies assessing acute cerebral hypoperfusion by xenon contrast-enhanced or conventional CT perfusion measurement showed a prolongation of the MTT [11, 12]. Although these studies also described a further correlation between the initial WFNS score and a severe reduction in the CBV, we disclaimed analysis of the impact of the perfusion parameters CBF and CBV, while CT is not suitable for a quantitative measurement of volumes at a single time point [11, 12].

In summary, the results of the present pilot study highly indicate that the MTT and the TTP obtained from early CTP measurements correlate significantly with the initial neurological presentation and the clinical outcome in patients suffering from aneurysmal SAH. Therefore, CTP measurement is a suitable, fast, and safe method estimating early brain hypoperfusion after SAH and providing additional prognostic information. Potentially, CTP measurement in patients suffering from aneurysmal SAH is more accurate than clinical grading and prediction. Therefore, a larger number of patients is needed.

Conclusion

The determination of MTT and TTP using early CTP measurements in patients suffering from aneurysmal SAH demonstrated a significant correlation with the initial neurological status and the early clinical outcome.

Conflict of interest statement We declare that we have no conflict of interest.

References

1. Bederson JB, Levy AL, Ding WH, Kahn R, DiPerna CA, Jenkins AL III, Vallabhajosyula P (1998) Acute vasoconstriction after subarachnoid hemorrhage. *Neurosurgery* 42(2):352–360
2. Brinker T, Seifert V, Dietz H (1992) Cerebral blood flow and intracranial pressure during experimental subarachnoid haemorrhage. *Acta Neurochir (Wien)* 115(1–2):47–52
3. Ebel H, Rust DS, Leschinger A, Ehresmann N, Kranz A, Hoffmann O, Boker DK (1996) Vasomotion, regional cerebral blood flow and intracranial pressure after induced subarachnoid haemorrhage in rats. *Zentralbl Neurochir* 57(3):150–155
4. Frykholm P, Andersson JL, Langstrom B, Persson L, Enblad P (2004) Haemodynamic and metabolic disturbances in the acute stage of subarachnoid haemorrhage demonstrated by PET. *Acta Neurol Scand* 109(1):25–32
5. Hop JW, Rinkel GJ, Algra A, van Gijn J (1997) Case-fatality rates and functional outcome after subarachnoid hemorrhage: a systematic review. *Stroke* 28:660–664

6. Ishiguro M, Murakami K, Link T, Zvarova K, Tranmer BI, Morielli AD, Wellman GC (2008) Acute and chronic effects of oxyhemoglobin on voltage-dependent ion channels in cerebral arteries. *Acta Neurochir Suppl* 104:99–102
7. Koivisto T, Vanninen E, Vanninen R, Kuikka J, Hernesniemi J, Vapalahti M (2002) Cerebral perfusion before and after endovascular or surgical treatment of acutely ruptured cerebral aneurysms: a 1-year prospective follow-up study. *Neurosurgery* 51(2):312–325
8. Lovelock CE, Rinkel GJ, Rothwell PM (2010) Time trends in outcome of subarachnoid hemorrhage: population-based study and systematic review. *Neurology* 74:1494–1501
9. Ostrowski RP, Colohan AR, Zhang JH (2005) Mechanisms of hyperbaric oxygen-induced neuroprotection in a rat model of subarachnoid hemorrhage. *J Cereb Blood Flow Metab* 25(5):554–571
10. Prunell GF, Mathiesen T, Svendgaard NA (2004) Experimental subarachnoid hemorrhage: cerebral blood flow and brain metabolism during the acute phase in three different models in the rat. *Neurosurgery* 54(2):426–436
11. Sanelli PC, Jou A, Gold R, Reichman M, Greenberg E, John M, Cayci Z, Ugorec I, Rosengart A (2011) Using CT perfusion during the early baseline period in aneurysmal subarachnoid hemorrhage to assess for development of vasospasm. *Neuroradiology* 53(6):425–434
12. Schubert GA, Seiz M, Hegewald AA, Manville J, Thome C (2009) Acute hypoperfusion immediately after subarachnoid hemorrhage: a xenon contrast-enhanced CT study. *J Neurotrauma* 26(12):2225–2231
13. Solomon RA, Antunes JL, Chen RY, Bland L, Chien S (1985) Decrease in cerebral blood flow in rats after experimental subarachnoid hemorrhage: a new animal model. *Stroke* 16(1):58–64
14. Takenaka K, Yamada H, Sakai N, Ando T, Okano Y, Nozawa Y (1991) Intracellular Ca^{2+} changes in cultured vascular smooth muscle cells by treatment with various spasmogens. *Neurol Res* 13(3):168–172
15. Tanaka A, Yoshinaga S, Nakayama Y, Tomonaga M (1998) Cerebral blood flow and the response to acetazolamide during the acute, subacute, and chronic stages of aneurysmal subarachnoid hemorrhage. *Neurol Med Chir (Tokyo)* 38(10):623–630
16. Turowski B, Haenggi D, Wittsack HJ, Beck A, Aurich V (2007) Computerized analysis of brain perfusion parameter images. *Rofo* 179(5):525–529
17. Turowski B, Haenggi D, Wittsack J, Beck A, Moedder U (2007) Cerebral perfusion computerized tomography in vasospasm after subarachnoid hemorrhage: diagnostic value of MTT. *Rofo* 179(8):847–854
18. Westermaier T, Jauss A, Eriskat J, Kunze E, Roosen K (2009) Time-course of cerebral perfusion and tissue oxygenation in the first 6 h after experimental subarachnoid hemorrhage in rats. *J Cereb Blood Flow Metab* 29(4):771–779

Cerebrospinal Fluid Lactate Concentration After Withdrawal of Metabolic Suppressive Therapy in Subarachnoid Hemorrhage

Marco Stein, Julia Schomacher, Wolfram Scharbrodt, Matthias Preuss, and Matthias F. Oertel

Abstract Hyperglycolysis is a known phenomenon after severe subarachnoid hemorrhage (SAH) and after brain injury. It is characterized by decreased oxidative metabolism and relatively increased anaerobic glycolysis. Metabolic suppressive therapy reduces the cerebral metabolic rate of oxygen (CMRO₂) and the cerebral metabolic rate of glucose (CMRGluc). If CMRO₂ is suppressed after SAH, withdrawal of metabolic suppressive therapy could lead to the accumulation of lactate. In this project, we assessed the relationship between the withdrawal of metabolic suppressive therapy and cerebrospinal fluid (CSF) lactate concentration. A prospective observational database containing 262 patients with SAH was retrospectively analyzed. CSF lactate levels were compared with the daily dose of metabolic suppressive therapy. Outcome was assessed with the Glasgow Outcome Scale (GOS). In 56% of patients an increase in CSF lactate (mean: 3.2 ± 0.9 mmol/L) after withdrawal of metabolic suppressive therapy was observed. Mean Glasgow Outcome Score (GOS) was lower in patients with an increase in CSF lactate concentration (>0.5 mmol/L) after withdrawal of metabolic suppressive therapy ($p = 0.095$). In 88% of patients who died during the first 30 days after SAH, a CSF lactate elevation of more than 0.5 mmol/L after withdrawal of metabolic suppressive therapy was found ($p = 0.071$).

Keywords Subarachnoid hemorrhage • CSF lactate • Metabolic suppression therapy • Outcome

Introduction

Cerebral hyperglycolysis is a described phenomenon that occurs after subarachnoid hemorrhage (SAH) [9] and traumatic brain injury (TBI) [4]. Hydrocephalus is a common complication after acute SAH. For the treatment of this

complication external ventricular and lumbar drainage of cerebrospinal fluid (CSF) is widely used [2, 5]. In these patients CSF is routinely scanned for pathological germs and the CSF cell count, CSF lactate, and CSF protein. Some authors have demonstrated a correlation between outcome and CSF lactate acidosis after SAH [12]. Several authors showed the prognostic and also the therapeutic importance of CSF acidosis after TBI [3, 10, 11, 13]. A previous report by DeSalles and colleagues demonstrated that persistently high or increasing ventricular CSF lactate is associated with clinical deterioration after TBI [3]. Mori et al. described a variable time course of CSF lactate over the first 12 days after aneurysm rupture [6].

Metabolic suppressive therapy in sedated patients on the intensive care unit (ICU) reduces both the cerebral metabolic rate of oxygen (CMRO₂) and the cerebral metabolic rate of glucose (CMRGluc) [8].

However, the relationship between ventricular CSF lactate, metabolic suppressive therapy and outcome after SAH remains unclear. Previous studies found a decreased CMRO₂ after TBI [8] and after SAH [9]. In cases where CMRO₂ is continuously suppressed, metabolic suppressive therapy may only decrease CMRGluc [8]. Our hypothesis is that after withdrawal of metabolic suppressive therapy CMRGluc will increase more than CMRO₂ [7]. As a consequence, CSF lactate will accumulate.

Materials and Methods

A prospective observational ICU database was retrospectively analyzed. Only patients with the diagnosis of spontaneous SAH and at least eight documented CSF studies during the ICU stay were included. Age was not restricted. Patients were excluded if a CSF infection was documented during the ICU stay.

The hospital charts of all included patients were retrospectively reviewed. We recorded the following clinical and demographic data: CSF lactate, CSF protein, and CSF cell count were recorded every other day. Other parameters included age, gender, aneurysm localization, Glasgow Coma

M. Stein (✉), J. Schomacher, W. Scharbrodt, M. Preuss, and M.F. Oertel
Department of Neurosurgery, University Hospital Giessen-Marburg,
Klinikstrasse 29, Giessen 35385, Germany
e-mail: marco.stein@neuro.med.uni-giessen.de

Score (GCS) on admission, Hunt and Hess grade (H&H), Fisher grade, hydrocephalus, aneurysm clipping, aneurysm coiling, rebleeding, presence of vasospasm, decompressive craniectomy, ventriculoperitoneal shunt implantation. All CSF studies were collected via external ventricular drainage.

The daily doses of midazolam, fentanyl, and propofol were calculated for every patient. The first day with complete metabolic suppressive therapy withdrawal or reduction of metabolic suppressive therapy of at least 50% compared with the day before was defined as day zero (Fig. 1). CSF lactate concentration was compared with the daily dose of metabolic suppressive therapy. Favorable and unfavorable outcome was defined as Glasgow Outcome Scale (GOS) 5–4 and GOS 3–1 respectively.

For univariate analysis, Student's *t* test was used to test differences in continuous variables and the Chi-squared test was used for differences in proportions among patients with and without an increase in CSF lactate after withdrawal of metabolic suppressive therapy.

All statistical analyses were performed using SPSS System 15.0 for Windows (SPSS Inc., Chicago, IL, USA).

Results

Between August 2004 and April 2009, 262 patients with the diagnosis of SAH were admitted to the Department of Neurosurgery at the University Hospital Giessen.

Out of these 262 patients complete CSF diagnostics (≥ 8 studies) were available in 87 patients. A total of 721 CSF studies were identified. In 56% of the patients an increase in CSF lactate concentration (>0.5 mmol/L) after withdrawal of metabolic suppressive therapy was observed.

Table 1 shows the main characteristics of the group with a CSF lactate increase (56%) observed and of the group without a CSF lactate increase (44%) after withdrawal of metabolic suppressive therapy.

Overall, CSF lactate concentration ranged from 0.95 to 6.26 mmol/L. The duration of mean metabolic suppressive therapy before withdrawal was 9 ± 2 days.

The average CSF lactate concentration in the group with and without increase in CSF lactate after withdrawal of metabolic suppressive therapy was 3.2 ± 0.9 and 3.2 ± 1.5 mmol/L ($p=0.812$) respectively. We found no statistical significant differences in CSF cell count and CSF protein between the both groups.

Seven days before and after withdrawal of metabolic suppressive therapy, the average CSF lactate concentration was 2.9 ± 0.9 and 3.6 ± 0.9 mmol/L ($p<0.001$) respectively (Fig. 2).

Overall 30-day mortality was 9.2%. In 7 of the 8 patients who died in the first 30 days an increase in CSF lactate ≥ 0.5 mmol/L after withdrawal of metabolic suppressive therapy

($p=0.071$) was recorded. In the 79 patients who survived the first 30 days after SAH an increase in CSF lactate ≥ 0.5 mmol/L occurred in 54%.

Mean GOS was 3 ± 1.0 and 3.4 ± 1.3 in the group with and without CSF lactate elevation after withdrawal of metabolic suppressive therapy respectively ($p=0.095$).

Discussion

Midazolam and fentanyl are widely used for the sedation of patients who suffer from severe SAH. Previous studies have indicated that midazolam and fentanyl induce cerebrovascular and cerebral metabolic depression [1]. Several authors have demonstrated that $CMRO_2$ is decreased after SAH and TBI. The daily propofol dose was low in the presented study. Propofol was only used to support sedation therapy with fentanyl and midazolam or for short time sedation of the patients on ICU. Several studies have proven the decreasing effects of propofol on $CMRO_2$. If $CMRO_2$ is decreased, metabolic suppressive therapy will only reduce CMR_{Gluc} [7].

After withdrawal of metabolic suppressive therapy we found an increase in CSF lactate concentration in 56% of the patients in our study cohort. This may be explained by an increase in CMR_{Gluc} that leads to an accumulation of lactate in the brain, measured by a CSF lactate elevation as an indirect marker in the present study.

Elevation of CSF lactate >0.5 mmol/L after withdrawal of metabolic suppressive therapy shows a trend to be associated with lower GOS 30 days after ictus. In contrast to previous reports, there were no significant differences in mean CSF lactate between lower (I–II) and higher initial Hunt and Hess grades (III–V) [12]. None of the clinical or demographic parameters was significantly different between the groups with and without CSF lactate increase after withdrawal of metabolic suppressive therapy.

Elevation of CSF lactate >0.5 mmol/L after withdrawal of metabolic suppressive therapy could be a marker for unfavorable outcome after severe SAH. In patients with a significant increase, lactate accumulation could lead to acidosis and to further cell death in the brain.

Conclusion

The increase in lactate is indirect proof of the hypothesis. A prospective cohort study is warranted to further support the concept.

Conflict of interest statement We declare that we have no conflicts of interest.

Fig. 1 Daily dose of (a) metamizol, (b) fentanyl, and (c) propofol outliers are marked with an open circle and extreme cases with an asterisk

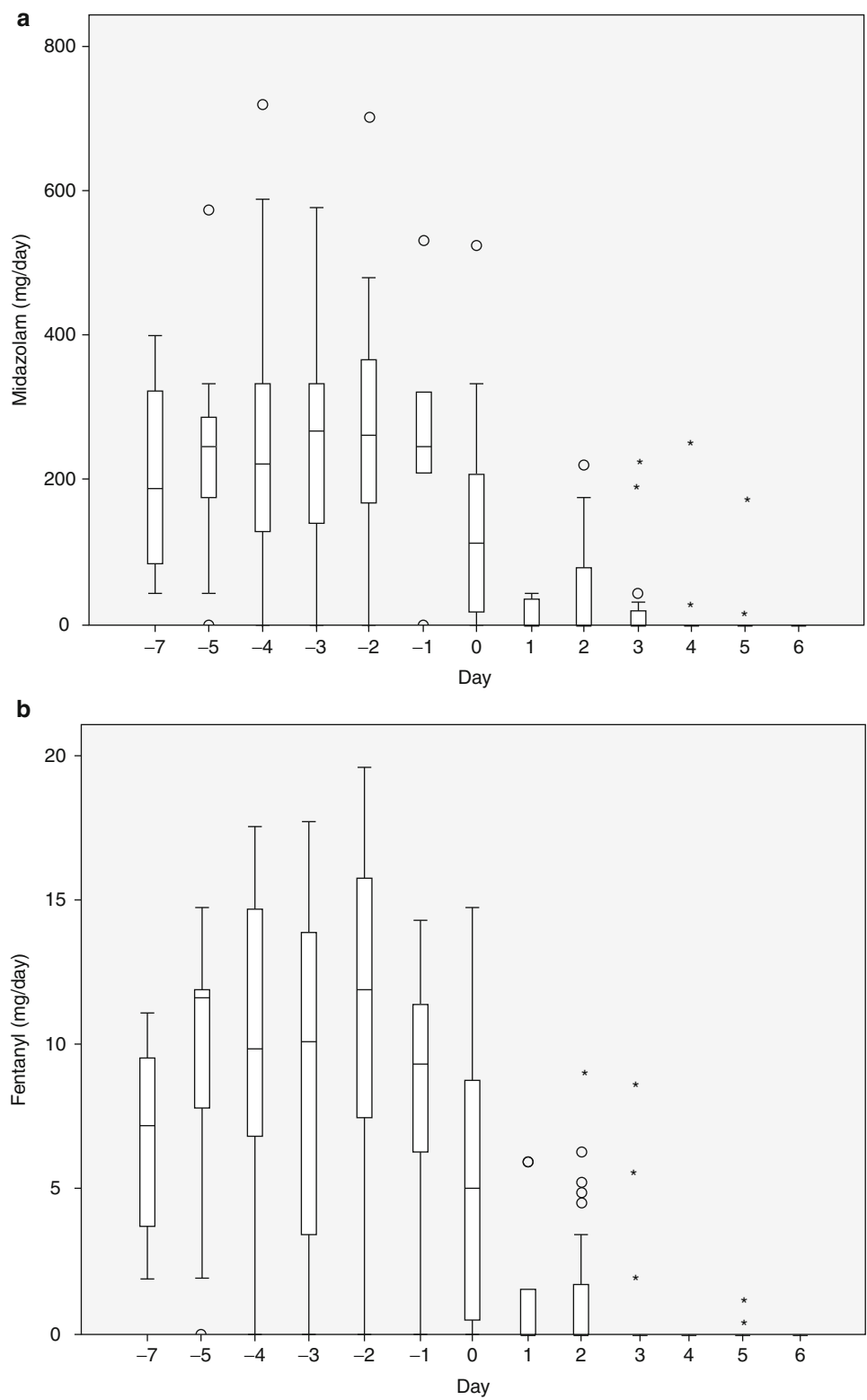


Fig. 1 (continued)

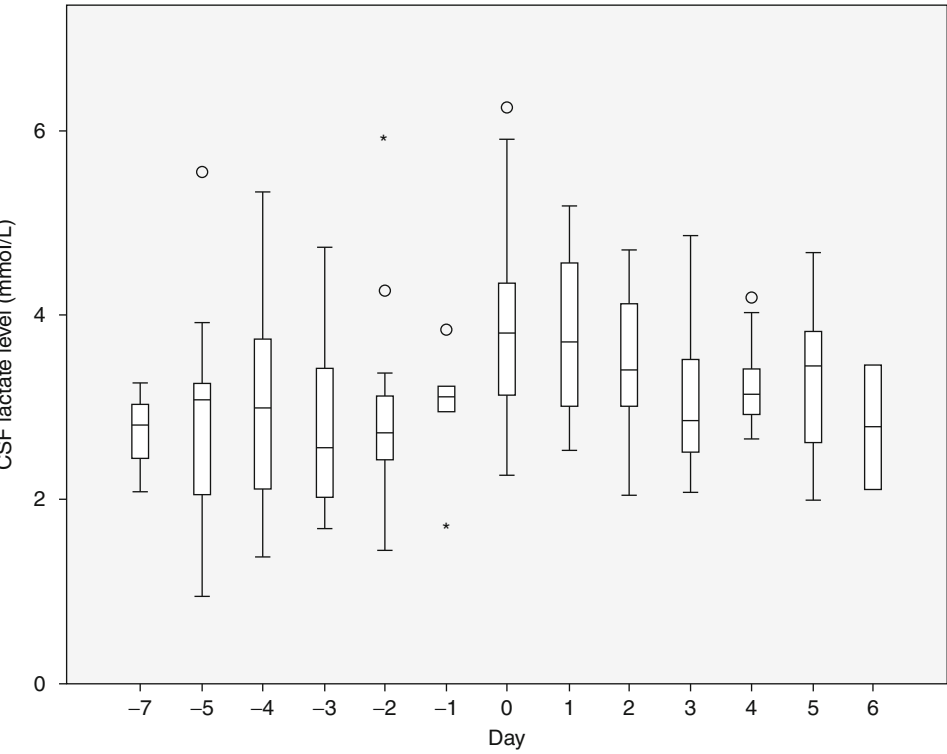
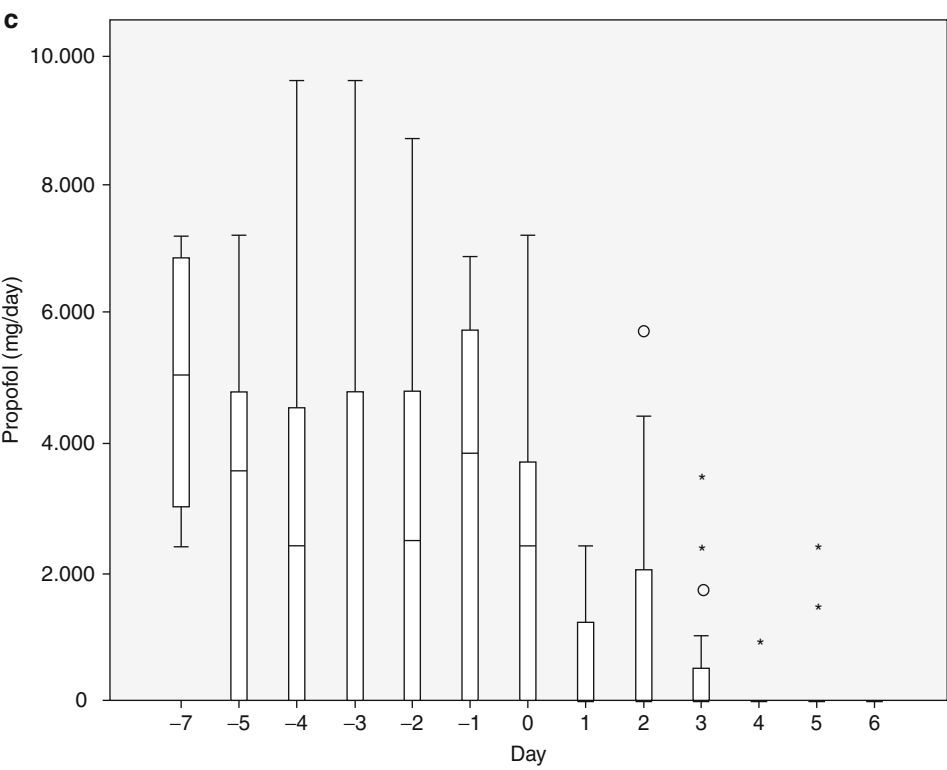


Fig. 2 Time course of CSF lactate before and after withdrawal of metabolic suppressive therapy. Day zero was defined as the first day of metabolic suppressive therapy withdrawal

Table 1 Characteristics of the cohort

Patients	N=49 (56%)	N=38 (44%)	
	Lactate increase n (%)	No lactate increase n (%)	P value
Age	53.5 ± 11.3 ^a	52.1 ± 11.6 ^a	0.819
Gender: n (%)	-	-	-
Male	13 (26.5)	16 (42.1)	0.126
Female	36 (73.5)	22 (57.9)	0.126
Localization of aneurysm: n (%)			
ICA	1 (2.0)	4 (10.5)	0.092
ACoA	11 (22.4)	14 (36.8)	0.141
ACA	6 (12.2)	2 (5.3)	0.264
PCoA	9 (18.4)	6 (15.8)	0.752
MCA	14 (28.6)	9 (23.7)	0.608
BA	4 (8.2)	3 (7.9)	0.964
PICA	1 (2.0)	0 (0.0)	0.376
VA	3 (6.1)	0 (0.0)	0.121
GCS, n (%)	8.9 ± 5.2 ^a	9.7 ± 5.0 ^a	0.500
H&H, n (%)	3.4 ± 1.4 ^a	3.1 ± 1.5 ^a	0.503
Fisher, n (%)	3.4 ± 0.9 ^a	3.5 ± 0.8 ^a	0.397
Hydrocephalus	35 (71.4)	25 (69.4)	0.843
Clipping, n (%)	29 (59.2)	14 (38.9)	0.064
Coiling, n (%)	23 (46.9)	21 (58.3)	0.299
Rebleeding, n (%)	5 (10.2)	4 (11.1)	0.893
Vasospasm, n (%)	23 (47.9)	19 (52.8)	0.659
Craniectomy, n (%)	9 (18.8)	5 (13.9)	0.554
Shunt, n (%)	22 (45.8)	20 (55.6)	0.378
GOS	3.0 ± 1.0 ^a	3.4 ± 1.3 ^a	0.095

^aMean ± SD

References

- Baughman VL, Hoffman WE, Albrecht RF, Miletich DJ (1987) Cerebral vascular and metabolic effects of fentanyl and midazolam in young and aged rats. *Anesthesiology* 67:314–319
- Bederson JB, Connolly ES Jr, Batjer HH, Dacey RG, Dion JE, Diringer MN, Duldner JE Jr, Harbaugh RE, Patel AB, Rosenwasser RH (2009) Guidelines for the management of aneurysmal subarachnoid hemorrhage: a statement for healthcare professionals from a special writing group of the Stroke Council, American Heart Association. *Stroke* 40:994–1025
- DeSalles AA, Kontos HA, Becker DP, Yang MS, Ward JD, Moulton R, Gruemer HD, Lutz H, Maset AL, Jenkins L et al (1986) Prognostic significance of ventricular CSF lactic acidosis in severe head injury. *J Neurosurg* 65:615–624
- Glenn TC, Kelly DF, Boscardin WJ, McArthur DL, Vespa P, Oertel M, Hovda DA, Bergsneider M, Hillered L, Martin NA (2003) Energy dysfunction as a predictor of outcome after moderate or severe head injury: indices of oxygen, glucose, and lactate metabolism. *J Cereb Blood Flow Metab* 23:1239–1250
- Hoekema D, Schmidt RH, Ross I (2007) Lumbar drainage for subarachnoid hemorrhage: technical considerations and safety analysis. *Neurocrit Care* 7:3–9
- Mori K, Nakajima K, Maeda M (1993) Long-term monitoring of CSF lactate levels and lactate/pyruvate ratios following subarachnoid haemorrhage. *Acta Neurochir (Wien)* 125:20–26
- Oertel M, Kelly DF, Lee JH, McArthur DL, Glenn TC, Vespa PM, Martin NA (2002) Metabolic suppressive therapy as a treatment for intracranial hypertension – why it works and when it fails. *Acta Neurochir Suppl* 81:69–70
- Oertel M, Kelly DF, Lee JH, McArthur DL, Glenn TC, Vespa P, Boscardin WJ, Hovda DA, Martin NA (2002) Efficacy of hyperventilation, blood pressure elevation, and metabolic suppression therapy in controlling intracranial pressure after head injury. *J Neurosurg* 97:1045–1053
- Oertel MF, Schwedler M, Stein M, Wachter D, Scharbrodt W, Schmidinger A, Boker DK (2007) Cerebral energy failure after subarachnoid hemorrhage: the role of relative hyperglycolysis. *J Clin Neurosci* 14:948–954
- Seitz HD (1976) Gas levels and biochemical changes in cerebrospinal fluid after experimental brain injury: its effect on cerebral circulation and cerebral metabolism as well as its management. *Z Exp Chir* 9:341–354
- Seitz HD, Ocker K (1977) The prognostic and therapeutic importance of changes in the CSF during the acute stage of brain injury. *Acta Neurochir (Wien)* 38:211–231
- Shimoda M, Yamada S, Yamamoto I, Tsugane R, Sato O (1989) Time course of CSF lactate level in subarachnoid haemorrhage. Correlation with clinical grading and prognosis. *Acta Neurochir (Wien)* 99:127–134
- Shiogai T, Nara I, Saruta K, Hara M, Saito I (1999) Continuous monitoring of cerebrospinal fluid acid-base balance and oxygen metabolism in patients with severe head injury: pathophysiology and treatments for cerebral acidosis and ischemia. *Acta Neurochir Suppl* 75:49–55

Effect of Increased ICP and Decreased CPP on DND and Outcome in ASAH

Krissanee Karnchanapandh

Abstract *Background:* When clipping is done early in aneurysmal SAH (ASAH), postoperative increased ICP and decreased CPP may present and influence development of delayed neurological deficit (DND), irreversible neurological deficit (IRND) and poor outcome.

Methods: A retrospective study was performed in 30 early clipping ASAH with postoperative ICP monitoring, flow velocity measurement, triple H–nimodipine therapy, ICP–CPP orientated strategy and a 3-month follow-up period. Chi-squared test was performed on increased ICP, decreased CPP, combination of increased ICP+ decreased CPP and DND, IRND and poor outcome.

Results: Two (7%), 19 (63%) and 9 (30%) patients were H&H 2, 3 and 4 respectively. Mean ICP and CPP were 34.2 and 71.3 mmHg. Mean ICP in H&H 2, 3 and 4 was 17.6, 34.3 and 50.2 mmHg respectively. 58.3%, 58.8% and 70% of patients with ICP \geq 20, 30 and 40 mmHg had DND. 64.7%, 63.3% and 80% of patients with CPP \leq 80, 70 and 60 mmHg had DND. 37.5%, 41.1% and 40% of patients with ICP \geq 20, 30 and 40 mmHg had poor outcome. 41.1%, 27.2% and 40% of patients with CPP \leq 80, 70 and 60 mmHg had poor outcome. Statistical analysis could not demonstrate a significant relationship among any of the parameters.

Conclusion: Postoperative increased ICP is frequent in early clipping especially in poor-grade ASAH; decreased CPP is less frequent, possibly owing to triple H therapy and ICP–CPP orientated strategy. Increased ICP seems to be more detrimental than decreased CPP. Increased ICP and decreased CPP may affect deterioration of neurological function in terms of DND, IRND and poor outcome as secondary insult.

Keywords ICP • CPP • Delayed neurological deficit • Poor outcome • SAH

K. Karnchanapandh
Department of Neurosurgery, Rajavithi hospital, Ministry of Public Health, College of Medicine, Rangsit University, 2 Payathai Road, Bangkok, 10400, Thailand

Department of Medical Services, Ministry of Public Health
College of Medicine, Rangsit University, 2 Payathai Road, Bangkok 10400, Thailand
e-mail: patarapol@hotmail.com

Introduction

Delayed neurological deficit (DND) in aneurysmal SAH (ASAH) has been associated with delayed cerebral ischemia [14] and presence of cerebral vasospasm [7, 8, 24, 25]. During aneurysmal rupture and the acute period of ASAH, ICP is much elevated resulting in decreased CPP and acute global cerebral ischemia [9, 19, 24]. When surgical clipping is done early after ASAH, increased ICP and associated decreased CPP are probably present. We hypothesised that postoperatively increased ICP and decreased CPP in early clipping of ASAH might influence development of DND, irreversible neurological deficit (IRND) and poor outcome.

Materials and Methods

A retrospective study was performed in 30 anterior circulation ASAH patients at Rajavithi Hospital during 1995–1997. All had triple-H and nimodipine therapy and underwent early clipping within 7 days of the recent SAH, postoperative ICP monitoring, intermittent M1/A1 flow velocity measurement, four-vessel cerebral angiography, CT and a 3-months follow-up period. ICP monitoring was performed using a subdural fibre optic ICP monitor (Camino) inserted during dural closure after clipping. Significant increased ICP and decreased CPP was defined as ICP \geq 20, 30 and 40 mmHg and CPP \leq 80, 70 and 60 mmHg. Increased ICP was managed according to an ICP–CPP-orientated strategy. Measures to reduce ICP depended on level of increased ICP and clinical status and included ventricular drainage and/or continuous spinal drainage against pressure of 15 cm H₂O, glycerosteril, mannitol infusion and hemicraniectomy decompression in case of impending uncal herniation. Measures to promote MAP included colloid and dopamine infusion. TCCD-angiographic vasospasm (TCCD-A VSP) was defined by transcranial Doppler ultrasound M1/A1 flow velocity \geq 120 cm/s [1] and severe narrowing of the involved artery on cerebral angiogram. DND was new neurological deficit occurring after admission. IRND and outcome were determined at the end

of the third month. Outcome was assessed by the National Institutes of Health Stroke Scale [3], good outcome was defined by no neurological deficit or NIHSS=0, fair outcome was defined by minor IRND or NIHSS=1–7 and poor outcome was defined by major IRND or NIHSS > 7 or death. Chi-squared testing was performed to assess the relationship between ICP \geq 20, 30, 40 mmHg, CPP \leq 80, 70, 60 mmHg, combination of increased ICP+ decreased CPP and DND, IRND, poor outcome. Statistical significance was defined as P value \leq 0.05.

Results

Of the 30 patients analysed, the age range was 32–75 years, mean age 49.6 years, the male/female ratio was 1/2. Fourteen (46.6%), 8 (26.6%), 6 (19.9%) and 2 (6.6%) patients had AcoA, MCA, PcoA and ventral ICA aneurysms respectively. Four (13.3%), 18 (60%) and 8 (26.6%) patients were Fisher's group [7] F2, F3 and F4 respectively. Two (7%), 19 (63%) and 9 (30%) patients were Hunt and Hess [15] grade 2, 3 and 4 respectively. Mean time from recent haemorrhage to clipping was 3.8 days. Range of ICP monitoring time was 3–14 days. Mean ICP monitoring time was 8 days. ICP range was 16–100 mmHg. Mean ICP was 34.2 mmHg. CPP range was 31–100 mmHg. Mean CPP was 71.3 mmHg. 33.3%, 30% and 12% of patients had ventricular drainage, continuous spinal drainage and VP shunt respectively. Fifteen patients (50%) had focal and/or diffuse brain oedema on postoperative CT. 66.6% of patients with cerebral oedema had midline shift; in 50% of those the midline shift was \geq 10 mm. None had postoperative intracranial haemorrhage. Seventeen patients (56.6%) had TCCD-A VSP. Nineteen patients (63.3%) achieved good outcome, whereas ten patients (33%) had poor outcome. Two patients (6.7%) died.

ICP, CPP, DND, IRND and Poor Outcome

Twenty-four (80%), 17 (56.6%) and 10 (33.3%) patients had ICP \geq 20, 30 and 40 mmHg respectively. Seventeen (56.6%), 11 (36.6%) and 5 (16.7%) patients had CPP \leq 80, 70 and 60 mmHg respectively. Mean ICP in H&H 2, H&H 3 and H&H 4 was 17.6, 34.3 and 50.2 mmHg respectively. Mean ICP in F2, F3 and F4 was 28, 39.3 and 27.6 mmHg respectively. Mean CPP in H&H 2, H&H 3 and H&H 4 was 69, 95 and 66.3 mmHg respectively. Mean CPP in F2, F3 and F4 was 71, 69.2 and 87 mmHg respectively. Incidence of ICP \geq 30, 40 mmHg and CPP \leq 70, 60 mmHg according to the Hunt & Hess grading is summarised in Table 1. Eighteen (60%), 9 (30%) and 10 (33%) patients had DND, IRND and

Table 1 Intracranial pressure (ICP), cerebral perfusion pressure (CPP), delayed neurological deficit (DND), irreversible neurological deficit (IRND), poor outcome and Hunt and Hess (H&H) classification

H&H	n	ICP \geq 30	ICP \geq 40	CPP \leq 70	CPP \leq 60
		n (%)	n (%)	n (%)	n (%)
2	2	1 (50)	–	1 (50)	1 (50)
3	19	11 (57.8)	6 (31.6)	5 (26.3)	1 (5.3)
4	9	5 (55.5)	4 (44.4)	5 (55.5)	3 (33.3)

Table 2 Combination of ICP+CPP and DND, IRND and poor outcome

ICP and CPP (mmHg)	n	DND	IRND	Poor outcome
		n (%)	n (%)	n (%)
ICP \geq 30 + CPP \leq 70	7	4 (57)	2 (28)	2 (28)
ICP \geq 40 + CPP \leq 70	3	3 (100)	2 (66)	2 (66)
ICP \geq 30 + CPP \leq 60	3	3 (100)	2 (66)	2 (66)
ICP \geq 40 + CPP \leq 60	3	3 (100)	2 (66)	2 (66)

poor outcome respectively. Incidence of DND in H&H 2, H&H 3 and H&H 4 was 0%, 63% and 66% respectively. Incidence of DND in F2, F3 and F4 was 0%, 55.5% and 50% respectively. Incidence of IRND in H&H 2, H&H 3 and H&H 4 was 0%, 26.3% and 44.4% respectively. Incidence of IRND in F2, F3 and F4 was 0%, 38.8% and 12.5% respectively. Incidence of poor outcome in H&H 2, H&H 3 and H&H 4 was 0%, 31.5% and 44.4% respectively. Incidence of poor outcome F2, F3 and F4 was 25%, 44% and 12.5% respectively. Incidence of DND in ICP \geq 20, 30, 40 mmHg, CPP \leq 80, 70 and 60 mmHg was 58.3%, 58.8%, 70%, 64.7%, 63.3% and 80% respectively. Incidence of IRND in ICP \geq 20, 30, 40 mmHg, CPP \leq 80, 70 and 60 mmHg was 33.3%, 35.2%, 40%, 35.2%, 27.2 and 40% respectively. Incidence of poor outcome in ICP \geq 20, 30, 40 mmHg, CPP \leq 80, 70 and 60 mmHg was 37.5%, 41.1%, 40%, 41.1%, 27.2% and 40% respectively. DND, IRND and poor outcome according to combination of ICP+ CPP are summarised in Table 2.

Statistical Analysis Results

Intracranial pressure \geq 20, 30, 40 mmHg, CPP \leq 80, 70, 60 mmHg and combinations of ICP \geq 30 + CPP \leq 70, ICP \geq 40 + CPP \leq 70, ICP \geq 30 + CPP \leq 60, ICP \geq 40 + CPP \leq 60 mmHg were not significantly related to DND with $P=0.545$, 0.590, 0.350, 0.547, 0.533, 0.299, 0.597, 0.545, 0.469 and 0.469 respectively. ICP \geq 20, 30, 40 mmHg, CPP \leq 80, 70, 60 mmHg and combinations of ICP \geq 30 + CPP \leq 70, ICP \geq 40 + CPP \leq 70 mmHg, ICP \geq 30 + CPP \leq 60, ICP \geq 40 + CPP \leq 60 mmHg were not significantly related to IRND with $P=0.400$, 0.377, 0.091, 0.690, 0.571, 0.479,

0.657, 0.600, 0.366 and 0.345 respectively. $ICP \geq 20$, 30, 40 mmHg, $CPP \leq 80$, 70, 60 mmHg and combinations of $ICP \geq 30 + CPP \leq 70$, $ICP \geq 40 + CPP \leq 70$, $ICP \geq 30 + CPP \leq 60$, $ICP \geq 40 + CPP \leq 60$ mmHg were not significantly related to poor outcome with $P=0.326$, 0.259, 0.169, 0.259, 0.431, 0.551, 0.571, 0.694, 0.407 and 0.407 respectively.

Discussion

Increased ICP was frequent after early clipping and most pronounced in H&H 4. Mean ICP was higher with higher H&H grades, the same finding as in many other studies [11, 16, 24]. Decreased CPP was not frequent and association with H&H 4 was less obvious possibly because of triple H therapy and an ICP–CPP orientated strategy by which CPP could be maintained. Increased ICP in ASAH has been reported to be associated with changes in CBF [10, 25], vasospasm [8, 24, 25], neurological deterioration [24] and unfavourable outcome [16, 19, 24, 25]. On the contrary, statistical analysis could not demonstrate a significant relationship among any increased ICP, any decreased CPP, their combinations and DND, IRND, and poor outcome, although it is noted that $ICP \geq 40$ was more closely related to IRND and poor outcome than $ICP \geq 20$ mmHg, $ICP \geq 30$ mmHg, decreased CPP and their combination. The finding that only 16.7% had $CPP \leq 60$ mmHg, whereas up to 33.3% had $ICP \geq 40$ mmHg might explain the lack of relationship among increased ICP and DND, IRND and poor outcome. It is speculated that raising CPP as a result of hypervolaemic, hypertensive haemodilution and ICP–CPP-orientated strategy might ameliorate the increased ICP. As reported in head injury, aggressive CPP management led to good neurological outcome despite high ICP [26], and as reported in SAH, elevated ICP with no response to treatment is predictive of clinical deterioration, whereas high CPP decreases the risk of clinical deterioration [20]. And that optimal CPP increases during vasospasm in SAH [2], further supports the speculation that raising CPP might ameliorate increased ICP for up to 63.3% of patients in the study had TCCD-A VSP which might benefit and had better outcome from such raising CPP. Microdialysis study in injured brain suggested CPP of 50–60 mmHg as the threshold below which cerebral ischemia occurred [18]. Decreased CPP to less than 60 mmHg in traumatic brain injury has been associated with poor outcome [6]. In contrast, $CPP \leq 60$ mmHg seemed to be tolerated by ASAH patients in the study as it was demonstrated that no significant relationship among $CPP \leq 60$ and DND, IRND and poor outcome, although it is noted that $CPP \leq 60$ mmHg was more closely related to DND than $CPP \leq 80$ mmHg and $CPP \leq 70$ mmHg. Much evidence supports the association between increased ICP and poor outcome in

brain injury [17]. Different pathophysiology of increased ICP and decreased CPP in ASAH must exist and may explain why increased ICP and decreased CPP were less closely related to poor outcome compared with that in traumatic brain injury. Instead of increased ICP and decreased CPP, other specific secondary insults such cerebral vasospasm [8, 24, 25], microthrombosis [23] or primary insults at rupture resulting in early brain injury [4] and consequences of primary insults such apoptosis [21] may have a more deleterious effect and thus be a major determinant of poor outcome. In the study outcome seemed to be related to H&H grading on admission; thus, it is speculated that primary insults of SAH might determine outcome. As demonstrated in one study, occurrence of secondary insults in SAH had no significant effect on functional outcome [20]. Increased ICP seemed to be related to clinical grade on admission as well; thus, further speculation conjectures that at least partly postoperative increased ICP might involve primary insults or early events of ASAH. Since increased ICP may represent results of various events [11, 12] such as cerebral oedema [5, 22], which was found in up to 50% of patients in the study, luxury perfusion [25] and increased cerebral blood volume [10–12] could at the same time inevitably exert a deleterious effect on the brain as a cofactor of other insults. As demonstrated by one study, elevated ICP in ASAH is associated with a worse outcome, but not an independent outcome predictor [13]. Thus, treatment of increased ICP should be mandatory, if not the first priority, in the management of ASAH.

Conclusion

Postoperatively increased ICP is frequent in early clipping especially in poor-grade ASAH. Decreased CPP occurred to a lesser extent, possibly owing to triple H therapy and an ICP–CPP orientated strategy. Increased ICP seems to be more detrimental than decreased CPP. Increased ICP and decreased CPP may affect deterioration of neurological function in terms of DND, IRND and poor outcome as a secondary insult, but its effect and role in determining outcome are unlikely to be major in post-early clipping ASAH.

Conflict of interest statement We declare that we have no conflict of interest.

References

1. Aaslid R, Huber P, Nornes H (1984) Evaluation of cerebrovascular spasm with transcranial Doppler ultrasound. *J Neurosurg* 60:37–41
2. Bijlenga P, Czosnyka M, Budohoski KP, Soehle M, Pickard JD, Kirkpatrick PJ, Smielewski P (2010) “Optimal cerebral perfusion pressure” in poor grade patients after subarachnoid hemorrhage. *Neurocrit Care* 13(1):17–23

3. Brott T, Adam HP, Olinger CP et al (1989) Measurements of acute cerebral infarction: a clinical examination scale. *Stroke* 20:864–870
4. Cahill WJ, Calvert JH, Zhang JH (2006) Mechanisms of early brain injury after subarachnoid hemorrhage. *J Cereb Blood Flow Metab* 26:1341–1353
5. Claassen J, Carhuapoma JR, Kreiter KT, Du EY, Connolly ES, Mayer SA (2002) Global cerebral edema after subarachnoid hemorrhage: frequency, predictors and impact on outcome. *Stroke* 33(5):1225–1232
6. Clifton GL, Miller ER, Choi SC et al (2002) Fluid thresholds and outcome from severe brain injury. *Crit Care Med* 30:739–745
7. Fisher M, Kistler JP, Davis JM (1980) Relation of cerebral vasospasm to subarachnoid hemorrhage visualized by computerized tomographic scanning. *Neurosurgery* 6:1–9
8. Fukuhara T, Douville CM, Elliott JP, Newell DW, Winn HR (1998) Relationship between intracranial pressure and the development of vasospasm after aneurysmal subarachnoid hemorrhage. *Neurol Med Chir* 38:710–717
9. Grote E, Hassler W (1988) The critical first minutes after subarachnoid hemorrhage. *Neurosurgery* 22:654–661
10. Grubb RLJR, Raichle ME, Eichling JO, Gado MH (1977) Effects of subarachnoid haemorrhage on cerebral blood volume, blood flow and oxygen utilization in humans. *J Neurosurg* 46:446–453
11. Hayashi M, Marukawa S, Fuji H, Kitano T, Kobayashi H, Yamamoto S (1977) Intracranial hypertension in patients with ruptured intracranial aneurysm. *J Neurosurg* 46:584–590
12. Hayashi M, Marukawa S, Fuji H, Kitano T, Kobayashi H, Munemoto S, Yamamoto S (1978) Intracranial pressure in patients with diffuse cerebral arterial spasm following ruptured intracranial aneurysms. *Acta Neurochir* 44:81–95
13. Heuer GG, Smith MJ, Elliott JP, Winn HR, LeRoux PD (2004) Relationship between intracranial pressure and other clinical variables in patients with aneurysmal subarachnoid hemorrhage. *J Neurosurg* 101:408–416
14. Hijdra A, Van Gijjn J, Stefanko S, Van Dongen KJ, Vermeulen M, Van Crevel H (1986) Delayed cerebral ischemia after aneurysmal subarachnoid hemorrhage: clinicoanatomic correlations. *Neurology* 36:329–333
15. Hunt WE, Hess RM (1968) Surgical risk as related to time of intervention in the repair of intracranial aneurysms. *J Neurosurg* 28:14–20
16. Kassell NF, Peerless SJ, Reilly PL (1976) Intracranial pressure aneurysm and subarachnoid hemorrhage. In: Beck JWF, Bosch DA, Brock M (eds) *Intracranial pressure III*. Springer, Berlin/Heidelberg/New York, pp 147–151
17. Marmarou A, Anderson RL, Ward JD et al (1991) Impact of ICP instability on outcome in patients with severe head trauma. *J Neurosurg* 75:s59–s66
18. Nordstrom CH, Reistrup P, Xu W et al (2003) Assessment of the lower limit for cerebral perfusion pressure in severe head injuries by bedside monitoring of regional energy metabolism. *Anesthesiology* 98:809–814
19. Nornes H, Magnaes B (1973) The role of intracranial pressure in the arrest of hemorrhage in patients with ruptured intracranial aneurysm. *J Neurosurg* 39:226–234
20. Ryttefjors M, Howells T, Nilsson P, Ronne-Engstrom E, Enbal P (2007) Secondary insults in subarachnoid hemorrhage: occurrence and impact on outcome and clinical deterioration. *Neurosurgery* 61:704–715
21. Sabri M, Kawashima A, Ai J, Macdonald RL (2008) Neuronal and astrocytic apoptosis after subarachnoid hemorrhage: a possible cause for poor prognosis. *Brian Res* 1238:163–171
22. Shigeno T, Fritschka E, Brock M, Schramm J, Shigeno S, Cervos-Navarro J (1982) Cerebral edema following experimental subarachnoid hemorrhage. *Stroke* 13(3):368–379
23. Vergouven MDJ, Vermeulen M, Coert BA, Stroes ESG et al (2008) Microthrombosis after aneurysmal subarachnoid hemorrhage: an additional explanation for delayed cerebral ischemia. *J Cereb Blood Flow Metab* 28:1761–1770
24. Voldby B, Enevoldsen E (1982) Intracranial pressure changes following aneurysmal rupture. Part 1: clinical and angiographic correlation. *J Neurosurg* 56:186–196
25. Voldby B, Enevoldsen E, Jensen FT (1985) Regional CBF, intraventricular pressure and cerebral metabolism in patients with ruptured intracranial aneurysms. *J Neurosurg* 62:48–58
26. Young JS, Blow O, Turrentine F, Claridge JA, Shulman A (2003) Is there an upper limit of intracranial pressure in patients with severe head injury if cerebral perfusion pressure is maintained? *Neurosurg Focus* 15:1–7

Prior Statin Use Has No Effect on Survival After Intracerebral Hemorrhage in a Multiethnic Asian Patient Cohort

Nicolas K.K. King, Vincent Khwee-Soon Tay, John Carson Allen, and Beng-Ti Ang

Abstract *Background:* Statins have been shown to reduce mortality and morbidity in ischemic stroke, subarachnoid hemorrhage, and traumatic brain injuries, but their effect on intracerebral hemorrhage (ICH) remains to be determined. This study aimed to investigate the effect of prior statin use on survival following spontaneous primary intracerebral hemorrhage in a multi-ethnic Asian population.

Subjects and Methods: A study cohort of patients admitted with spontaneous primary ICH was obtained from our database. There were 1,381 patients who met the inclusion criteria. Multivariate logistic regression was used to identify independent predictors and computed odds ratios for 30-day mortality. Kaplan–Meier and Cox proportional hazard survival analyses were used to examine the effect of prior statin use on survival after ICH.

Results: Multivariate logistic regression controlling for baseline characteristics and in-hospital interventions, did not demonstrate any effect of prior statin use ($p=0.781$) on mortality. Survival analyses also failed to demonstrate any differences in survival after ICH with prior statin use. Similarly subgroup analyses showed no difference.

Conclusion: No beneficial effect on survival after ICH of prior statin use could be demonstrated in our large multi-ethnic Asian patient cohort.

Keywords Intracerebral hemorrhage • Hemorrhagic stroke • Statin • Mortality

Introduction

Intracerebral hemorrhage (ICH) is a type of stroke that has been associated with high morbidity and mortality. Despite on-going advances, the case fatality from ICH has not improved worldwide since the 1980s. Its incidence in Asia is about twice that of the rest of the world and represents a significant burden on medical resources and on society [13]. The difference in incidence appears to be multifactorial with differences attributed to different risk profiles, genetics, and other undetermined factors governing the outcomes of ICH experienced amongst Asians compared with the western population [4, 13].

The HMG-CoA reductase inhibitors, also known as statins, have been demonstrated to be beneficial in ischemic stroke [1, 8], subarachnoid hemorrhage, and traumatic brain injury [12]. As such, the effect of prior use of statins on survival after ICH has generated much interest. In addition to its known lipid-lowering effects, statins have been purported to have neuroprotective properties [2, 14]. It is these properties that may prove to be effective in improving the sequelae of ICH. However, with different studies showing varying effect on hematoma expansion [3], peri-hematoma edema [10], mortality [3, 5, 9, 11], and functional outcome [3, 5, 6, 9], the overall beneficial effect on statin use in ICH remains to be determined.

This study aims to examine the effect of prior statin use on survival after intracerebral hemorrhage in our multiethnic Asian population, which is representative of Southeast and East Asia.

Subjects and Methods

The Centralized Institutional Review Board of Singhealth (CIRB), Singapore, approved this study.

N.K.K. King and B.-T. Ang (✉)

Department of Neurosurgery, National Neuroscience Institute
Singapore, 11, Jalan Tan Tock Seng, Singapore 308433, Singapore
e-mail: beng_ti_ang@nni.com.sg

V.K.-S. Tay and J.C. Allen

Centre for Quantitative Medicine, Duke-NUS Graduate Medical
School, 8 College Road, 169857 Singapore

Inclusion and Exclusion Criteria

A prospective database of the Department of Neurosurgery, National Neuroscience Institute (NNI), Singapore, containing medical records of patients admitted with ICH between July 2004 and August 2009 was reviewed. Based on clinical and radiological records, all patients admitted for the treatment of spontaneous primary ICH were selected. Patients were excluded if the cause of the ICH was traumatic, secondary to ischemic stroke, tumor, arteriovenous abnormality or coagulopathy. A small group of patients were also excluded if their prior medication usage was not recorded.

Data Collection and Computation

All clinical data on the acute presentation were taken from data obtained at the initial evaluation in the emergency department. The initial head computed tomography (CT) images and reports were used to derive radiological information, including presence of intraventricular hemorrhage (IVH), presence of hydrocephalus (as reported by the duty radiologist), location of ICH and ICH clot volume (using the ABC/2 method, independently calculated by one of the authors [VKT]). Patient demographic data, medical history, and in-hospital interventions were extracted from medical records. Thirty-day mortality was obtained from data held on a centrally updated online electronic patient record.

Statistical Analyses

Univariate analyses were conducted using Chi-squared and Fisher exact tests for categorical variables, and Student's *t* and Wilcoxon rank-sum tests for continuous variables. Multivariate logistic regression analyses were performed using 30-day mortality as the dependent variable. A stepwise selection algorithm was implemented to screen for potential predictors of 30-day mortality meeting the $p \leq 0.15$ level of significance. Variables considered clinically relevant were then introduced into the model and retained if statistically significant at the $p < 0.05$ level. The final model was used to compute the adjusted odds and hazard ratios. Kaplan–Meier analysis, log-rank test, and Cox proportional hazard analysis were used to examine the effect of prior statin use on survival. All analyses were performed using Stata (version 11.0, Stata Corporation, TX, USA) where $p < 0.05$ was considered

statistically significant unless otherwise stated. All tests were two-sided.

Results

Study Cohort

From the clinical database, 1,453 cases of non-traumatic intracerebral hemorrhage were obtained. Medication history indicating presence or absence of prior statin use was not available for 72 cases (5%), and these patients were excluded from further analysis. A final study cohort of 1,381 cases was derived with 292 (21%) pre-morbid statin users and 1,089 (79%) non-users. The characteristics of the cohort are summarized in Table 1.

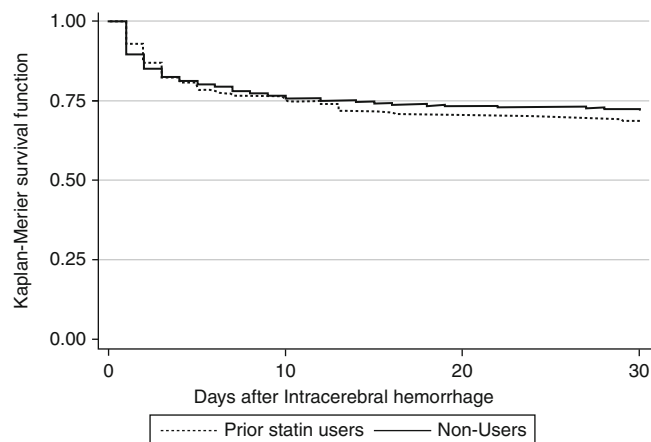
The overall 30-day mortality rate was 28.5%, with no significant difference between the prior statin users (31.5%) and non-users (27.7%; $p = 0.205$). The prior statin user group was significantly older and had more medical co-morbidities (including diabetes mellitus, hypertension, hyperlipidemia, previous stroke, and other conditions requiring warfarin and/or antiplatelet therapy). In the prior statin user group, the proportion of patients presenting with infratentorial ICH was larger ($p = 0.024$) and a smaller proportion underwent a surgical evacuation ($p = 0.013$). There was no significant difference in the volume of ICH or other ICH characteristics between the two groups (Table 1).

Effect of Prior Statin Use on Post-ICH Survival

The log-rank test that compared the Kaplan–Meier curves (Fig. 1) yielded no difference between the prior statin users and non-users ($p = 0.274$). The multivariate logistic regression and Cox proportional hazard models used to calculate the adjusted odds ratio and hazard ratio (Table 2) controlled for baseline characteristics (age, warfarin use, antiplatelet use, known hypertension, previous stroke, diabetes mellitus, hyperlipidemia), presentation of ICH (GCS, infratentorial location, ventricular hemorrhage, hydrocephalus) and in-hospital treatment (external ventricular drain placement, surgical evacuation of ICH). Prior statin use did not demonstrate an effect by reducing 30-day mortality after controlling for other independent predictors of early mortality (adjusted odds ratio = 0.96; 95% confidence interval: 0.51, 1.78). There was also no effect on early survival observed (adjusted hazard ratio = 0.95; 95% confidence interval: 0.64, 1.40).

Table 1 Patient and intracerebral hematoma characteristics

	Overall (n = 1,381)	Prior statin user group (n = 292)	Statin non-user group (n = 1,089)	p
<i>Post-ICH mortality</i>				
Mortality at ≤30 days	394 (28.5%)	92 (31.5%)	302 (27.7%)	0.205
<i>Patient characteristics</i>				
Age (SD)	64.1 (±14)	66.7 (±11)	63.4 (±15)	<0.001
Female gender (%)	564 (41)	118 (40)	446 (41)	0.867
Diabetes mellitus (%)	361 (26)	150 (51)	211 (19)	<0.001
Known hypertension (%)	1,155 (84)	280 (96)	875 (80)	<0.001
Hyperlipidemia (%)	648 (47)	291 (99)	357 (33)	<0.001
Warfarin use (%)	90 (7)	38 (13)	52 (5)	<0.001
Antiplatelet use (%)	261 (19)	145 (50)	116 (11)	<0.001
Previous stroke (%)	347 (25)	148 (51)	199 (18)	<0.001
Mean presenting GCS	11.2	11.2	11.2	0.887
<i>Intracerebral hematoma characteristics</i>				
Mean ICH volume (SD)	27.9 (±40)	27.6 (±41)	28.0 (±39)	0.860
ICH volume ≥30 mL (%)	393 (30)	78 (27)	315 (30)	0.344
<i>Location (%)</i>				
Basal ganglia	616 (45)	115 (39)	501 (46)	0.213
Lobar	231 (17)	49 (17)	182 (17)	
Thalamus	288 (21)	63 (22)	225 (20)	
Cerebellum	118 (8)	33 (11)	85 (8)	
Pons	104 (7)	27 (9)	77 (7)	
Multiple	24 (2)	5 (2)	19 (2)	
Infratentorial ICH (%)	237 (17)	63 (22)	174 (16)	0.024
Presence of IVH (%)	583 (42)	124 (42)	459 (42)	0.922
Hydrocephalus, n (%)	355 (26)	77 (26)	278 (26)	0.770
Surgical evacuation (%)	104 (8)	12 (4)	92 (8)	0.013

**Fig. 1** Kaplan–Meier curves for the prior statin users and non-users groups showing that no difference in survival at 30 days was observed (log-rank test, $p=0.274$)**Table 2** Effect of prior statin use on mortality after intracerebral hemorrhage

<i>Logistic regression modeling</i>	Odds ratio (95% CI)
Odds ratio of 30-day mortality with prior statin use	0.83 (0.63, 1.10)
Adjusted odds ratio of 30-day mortality with prior statin use	0.96 (0.51, 1.78)
<i>Cox-proportional hazard modeling</i>	Hazard ratio (95% CI)
Hazard ratio with prior statin use	1.20 (0.91, 1.59)
Adjusted hazard ratio with prior statin use	0.95 (0.64, 1.40)

Adjusted for baseline characteristics (warfarin, antiplatelet, hypertension, previous stroke, diabetes mellitus, hyperlipidemia, GCS, infratentorial location, ventricular hemorrhage, hydrocephalus) and in-hospital treatment (external ventricular drainage and surgical evacuation of the clot)

Subgroup Analyses

No effect on survival with prior statin use compared with non-statin use was found when stratified by statin type, gender, ethnicity (Chinese, Malay, and Indian) and surgical intervention (evacuation of hematoma and extra-ventricular drain placement) rendered. There was also no difference in mean volume of ICH in patients with intratentorial ICH between the prior statin users and non-users.

Discussion

In this study in our multiethnic Asian patient cohort, no protective effect of prior statin use on survival after ICH could be found with regard to 30-day mortality. There was also no difference in the ICH clot size, with no statistically significant difference in the mean volume of ICH or proportion of patients with larger ICH between the prior statin users and non-users. Our study was limited in that data on functional survival was not available to assess if statins had any effect on functional recovery in those patients who survived. As ours was an observational study, another limitation was that the dose prescribed was for the treatment of hypercholesterolemia [7] and may not have been sufficient for conferring neuroprotection. It was also found that the patients who suffered an ICH and who were also on a statin had significantly more medical comorbidities, which would have been expected to increase mortality. Thus, the protective effect of statins may have been masked.

Conclusion

In this large multiethnic Asian patient group, prior use of statin at doses used for prevention of cardiovascular disease was not found to confer additional protective benefit with regard to mortality. Patients who were taking a statin prior to their ICH can, however, safely continue to do so.

Conflict of interest statement We declare that we have no conflict of interest.

References

1. Amarenco P, Labreuche J (2009) Lipid management in the prevention of stroke: review and updated meta-analysis of statins for stroke prevention. *Lancet Neurol* 8:453–463
2. Amarenco P, Moskowitz MA (2006) The dynamics of statins: from event prevention to neuroprotection. *Stroke* 37:294–296
3. Eichel R, Khoury ST, Ben-Hur T, Keidar M, Paniri R, Leker RR (2010) Prior use of statins and outcome in patients with intracerebral haemorrhage. *Eur J Neurol* 17:78–83
4. Feigin V, Carter K, Hackett M, Barber PA, McNaughton H, Dyal L, Chen MH, Anderson C (2006) Ethnic disparities in incidence of stroke subtypes: Auckland Regional Community Stroke Study, 2002–2003. *Lancet Neurol* 5:130–139
5. FitzMaurice E, Wendell L, Snider R, Schwab K, Chanderraj R, Kinnecom C, Nandigam K, Rost NS, Viswanathan A, Rosand J, Greenberg SM, Smith EE (2008) Effect of statins on intracerebral hemorrhage outcome and recurrence. *Stroke* 39:2151–2154
6. Gomis M, Ois A, Rodriguez-Campello A, Cuadrado-Godia E, Jimenez-Conde J, Subirana I, Davalos A, Roquer J (2010) Outcome of intracerebral haemorrhage patients pre-treated with statins. *Eur J Neurol* 17:443–448
7. Hankey GJ, Wong KS, Chankrachang S, Chen C, Crimmins D, Frayne J, Kim JS, Li Y, Liou CW, Merican JS, Misbach J, Navarro J, Shinohara Y, Wang Y, Yoon BW (2010) Management of cholesterol to reduce the burden of stroke in Asia: consensus statement. *Int J Stroke* 5:209–216
8. Lakhan SE, Bagchi S, Hofer M (2010) Statins and clinical outcome of acute ischemic stroke: a systematic review. *Int Arch Med* 3:22
9. Leker RR, Khoury ST, Rafaeli G, Schwartz R, Eichel R, Tanne D (2009) Prior use of statins improves outcome in patients with intracerebral hemorrhage: prospective data from the National Acute Stroke Israeli Surveys (NASIS). *Stroke* 40:2581–2584
10. Naval NS, Abdelhak TA, Urrunaga N, Zeballos P, Mirski MA, Carhuapoma JR (2008) An association of prior statin use with decreased perihematoma edema. *Neurocrit Care* 8:13–18
11. Naval NS, Abdelhak TA, Zeballos P, Urrunaga N, Mirski MA, Carhuapoma JR (2008) Prior statin use reduces mortality in intracerebral hemorrhage. *Neurocrit Care* 8:6–12
12. Tapia-Perez JH, Sanchez-Aguilar M, Schneider T (2010) The role of statins in neurosurgery. *Neurosurg Rev* 33:259–270; discussion 270
13. Van Asch CJ, Luitse MJ, Rinkel GJ, van der Tweel I, Algra A, Klijn CJ (2010) Incidence, case fatality, and functional outcome of intracerebral haemorrhage over time, according to age, sex, and ethnic origin: a systematic review and meta-analysis. *Lancet Neurol* 9:167–176
14. Van der Most PJ, Dolga AM, Nijholt IM, Luiten PG, Eisel UL (2009) Statins: mechanisms of neuroprotection. *Prog Neurobiol* 88:64–75

The Impact of Silver Nanoparticle-Coated and Antibiotic-Impregnated External Ventricular Drainage Catheters on the Risk of Infections: A Clinical Comparison of 95 Patients

Johannes Lemcke, Felix Depner, and Ullrich Meier

Abstract *Background:* Infection, i.e. meningitis or ventriculitis, is a major complication of external ventricular drainage (EVD). In order to prevent this complication rifampin-impregnated and clindamycin-impregnated silicone catheters and EVDs impregnated with nanoparticles of silver and an insoluble silver salt have been developed. Sparse data are published concerning the efficacy of these catheters in reducing bacterial colonization.

Methods: Between July 2003 and June 2006, 95 patients (age range 12–84 years, mean 53.6 years) underwent implantation of an EVD catheter for CSF diversion for several indications. All surgeries were performed in a standardized way at a single medical center. We used standard polyurethane catheters in 32 patients, Codman Bactiseal silicone catheters in 31 patients, and Spiegelberg Silverline catheters in 32 patients. Samples of the cerebrospinal fluid (CSF) were taken at the time of implantation, every 10 days and at the time of removal. The samples were microbiologically analyzed.

Results: In 32 standard catheters we saw infections in 5 patients (15.6%). By contrast, 2 of the 31 patients with a Bactiseal catheter (6.5%) and 3 with a Silverline catheter (9.4%) developed an infection.

Conclusion: Rifampin-impregnated and clindamycin-impregnated EVDs as well as silver-impregnated EVDs decreased the infection rate. Randomized studies are needed to assess the advantage of these catheters compared with standard polyurethane catheters.

Keywords External ventricular drainage • Infection • Antibiotic impregnation • Silver impregnation

J. Lemcke, F. Depner, and U. Meier (✉)
Department of Neurosurgery, Unfallkrankenhaus Berlin,
Warener Strasse 7, D-12683 Berlin, Germany
e-mail: ullrich.meier@ukb.de

Background

The implantation of external ventricular drainage for different indications is one of the most common procedures in neurosurgery to achieve an ad hoc reduction and control of the intracerebral pressure (ICP). Often, the cerebrospinal fluid (CSF) is initially sterile. As the EVD perforates the three protective coverings of the intracranial space (skin and galea, skull bone and dura mater), it represents a locus minoris resistentiae for infections. In order to decrease the infection rates of EVDs polyurethane catheters containing a combination of metallic silver and an unsoluble silver salt (Silverline®, Spiegelberg, Hamburg) were developed as well as catheters, which were impregnated with rifampicin und clindamycin after maceration with chloroform under increased pressure (Bactiseal®, Codman, Johnson & Johnson, Norderstedt). Sparse data are published concerning the efficiency of these devices. The authors evaluate in a prospective observation study the possibility of a reduction of the infection rate by using coated or impregnated catheters in comparison to standard polyurethane catheters (Spiegelberg, Hamburg).

Materials and Methods

All 95 patients who obtained an EVD between July 2003 and June 2006 in our hospital for the first time and without a previously existing infection were included. Patients with perforating head injuries were excluded. The indications for the implantation of an EVD were closed head injury, subarachnoidal hemorrhage (SAH), intracerebral hemorrhage (ICH) and nonhemorrhagic hydrocephalus internus with an increase in the ICP.

Surgery

The implantation was performed under general anesthesia with a single shot of antibiotics (1,500 mg cefuroxime). After partial hair shaving, skin disinfection und sterile surgical coverage with plastic film a borehole trepanation at Kocher's point was performed. Following the dural incision the ventricular drainage stabilized by a mandarin was introduced 6 cm into the anterior horn of the lateral ventricle. The EVD was tunneled at least 5 cm subcutaneously. All EVDs were Luer-lock-connected with the same collection bag (Spiegelberg External Ventricular Drainage Kit).

Each type of EVD was implanted in our hospital for 1 year. From July 2003 to June 2004 we used the standard polyurethane catheter in 32 patients, from July 2004 to June 2005 the Codman Bactiseal catheter in 31 patients, and from July 2005 to June 2006 the Spiegelberg Silverline catheter in 32 patients. Thus, no selection of the patients due to the indication of EVD implantation or other parameters took place.

Microbiological Examination

We carried out laboratory tests including cell count, lactate and protein and microbiological examinations of the CSF at implantation and removal as well as every 10 days. In the case of clinical suspicion of CSF infection, like opacity of the CSF, an unexplainable increase in inflammation parameters or clinical symptoms of meningitis, we also took CSF probes. The evidence for ventriculomeningitis was the proven germs in the liquor cerebrospinalis.

Statistical Analysis

Explorative statistics were performed using the Wilcoxon test in the Statistical Package for the Social Sciences (SPSS) software version 15.0. $p \leq 0.05$ was defined as the level of significance.

Results

Fifty-one men (54%) and 45 women (46%) with a mean age of 53.6 (12–84) years were included. Neither the sex distribution nor the age in the three groups showed statistically significant differences.

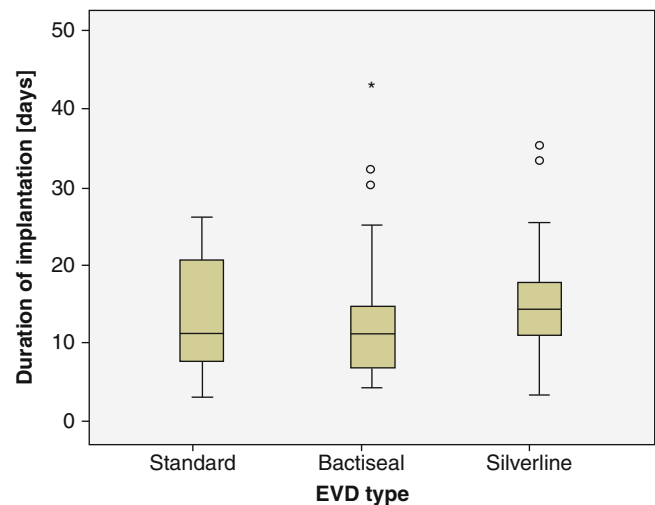


Fig. 1 Duration of implantation in the three patient groups

Indications

Ten patients (11%) had a severe head injury, 36 patients (38%) suffered from SAH, and 43 (45%) from ICH. Six patients (6%) underwent EVD implantation because of expansion lesions. The distribution of the indications to the three groups showed no relevant differences.

The duration of drainage was 13.7 days on average. No statistically relevant differences were recorded for the three patient groups (standard EVD 13.2 days, Bactiseal EVD 13.0 days, Silverline EVD 14.8 days) (Fig. 1).

Infections

We diagnosed infections of the CSF in 10 patients (11%). All infections occurred between the 8th and the 19th day after surgery. Even though we did not find a specific time pattern of the infections in the three groups of patients (standard EVD days 8, 9, 13, 16, 17/Bactiseal EVD days 10, 17/Silverline EVD days 10, 13, 19), the authors observed distinct differences in the number of infections. Whilst 5 out of 32 patients with standard EVDs had an infection (15.6%), only 2 out of 32 patients with Bactiseal catheters (6.5%) and 3 out of 32 patients with Silverline catheters (9.4%) showed infected CSF. Regrettably, the difference was not statistically significant (Fig. 2).

All patients had ventriculitis with typically catheter-associated bacteria (*Staphylococcus* and *Enterococcus*). Mixed infections were only observed in patients with a standard EVD (Table 1).

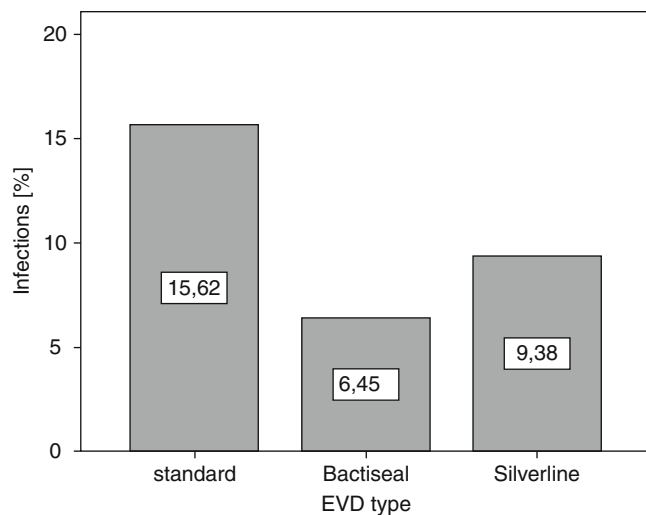


Fig. 2 Infection rates in the three patient groups

Table 1 *Staphylococcus* and *Enterococcus* were observed to be causative agents

Bacteria		Standard EVD	Bactiseal EVD	Silverline EVD
Coagulase-negative <i>Staphylococcus</i>	<i>S. epidermidis</i>	1		1
	<i>S. haemolyticus</i>	1 mixed infection (+ <i>E. faecalis</i>)	1	
	<i>S. simulans</i>	1 mixed infection (+ <i>E. faecalis</i>)		
Coagulase-positive <i>Staphylococcus</i>	<i>S. aureus</i>	2		1
<i>Enterococcus</i>	<i>E. faecium</i>		1	1
	<i>E. faecalis</i>	See above		

Discussion

Owing to the perforation of the physiological barriers by the external ventricular drainage, infections of the cerebrospinal fluid are one of the most common complications of EVDs [1, 7, 8, 11, 14, 18]. Gram-positive coccoids of physiological skin flora dominate the microbiological findings in our patients as well as in the international literature [2, 4, 6, 9, 10, 12, 13, 15–17, 21–26]. The published infection rates range from 0% to 50% [3, 5] because of the different diagnostic methods and patient populations. Against this background the combination of external ventricular drainage with antimicrobial substances is a reasonable approach. The strategy was pursued on the one hand by the impregnation of silicone catheters with antibiotics that are suitable with regard

to their pharmacological stability and their spectrum of activity and on the other hand by the bactericidal effect of the release of cations from a nanosilver coat and a silver salt not specified by the manufacturer.

The patients with standard EVDs in this study clearly exceeded the infection rate of 8.8% which Lozier [9] found in his meta-analysis of 23 publications. With 6.5% the group of patients with Bactiseal catheters were below this threshold. The patients with the Silverline EVD met this value with 9.4% of infections. Comparing the groups in our own patients, both antimicrobially coated catheters showed an advantage over the standard EVD.

The populations in the studies published by Schade et al. [19] and Sloffer et al. [20] showed the best correlation with our patients. Schade et al. [19] compared the infection rates of ventricular and lumbar drainage and found an infection rate of 14.4%. Sloffer (20) published four infections in 100 patients with a Codman Bactiseal EVD.

To the best of our knowledge no studies on patients with Silverline EVDs have been published as yet.

Altogether we found a decrease in the infection rate of 40% for the Silverline EVD (9.4% versus 15.6%) and of 58% for the Bactiseal EVD (6.5% versus 15.6%) compared with the standard EVD. From the view of the clinical neurosurgeon both products can be recommended in order to prevent EVD-associated infections.

Conclusion

Antibiotic impregnated EVDs as well as silver-impregnated EVDs seem to be able to decrease the infection rate of EVDs. Patient safety can be increased by the use of these products.

Conflict of interest statement We declare that we have no conflict of interest.

References

1. Aschoff A, Kremer P, Hashemi B, Kunze S (1999) The scientific history of hydrocephalus and its treatment. *Neurosurg Rev* 22:67–93
2. Aucoin PJ, Cheeseman SH (1984) Late-onset group B streptococcal disease after peripartum ampicillin prophylaxis. *Am J Dis Child* 138:795
3. Chan KH, Mann KS (1988) Prolonged therapeutic external ventricular drainage: a prospective study. *Neurosurgery* 23:436–438
4. Hader WJ, Steinbok P (2000) The value of routine cultures of the cerebrospinal fluid in patients with external ventricular drains. *Neurosurgery* 46:1149–1153

5. Hasan D, Vermeulen M, Wijdicks EF, Hijdra A, van Gijn J (1989) Management problems in acute hydrocephalus after subarachnoid hemorrhage. *Stroke* 20:747–753
6. Khan SH, Kureshi IU, Mulgrew T, Ho SY, Onyiuke HC (1998) Comparison of percutaneous ventriculostomies and intraparenchymal monitor: a retrospective evaluation of 156 patients. *Acta Neurochir Suppl* 71:50–52
7. Khanna RK, Rosenblum ML, Rock JP, Malik GM (1995) Prolonged external ventricular drainage with percutaneous long-tunnel ventriculostomies. *J Neurosurg* 83:791–794
8. Lo CH, Spelman D, Bailey M, Cooper DJ, Rosenfeld JV, Brecknell JE (2007) External ventricular drain infections are independent of drain duration: an argument against elective revision. *J Neurosurg* 106:378–383
9. Lozier AP, Sciacca RR, Romagnoli MF, Connolly ES Jr (2002) Ventriculostomy-related infections: a critical review of the literature. *Neurosurgery* 51:170–181
10. Lyke KE, Obasanjo OO, Williams MA, O'Brien M, Chotani R, Perl TM (2001) Ventriculitis complicating use of intraventricular catheters in adult neurosurgical patients. *Clin Infect Dis* 33:2028–2033
11. Mayhall CG, Archer NH, Lamb VA, Spadora AC, Baggett JW, Ward JD, Narayan RK (1984) Ventriculostomy-related infections. A prospective epidemiologic study. *N Engl J Med* 310:553–559
12. Ohrstrom JK, Skou JK, Ejlersen T, Kosteljanetz M (1989) Infected ventriculostomy: bacteriology and treatment. *Acta Neurochir (Wien)* 100:67–69
13. Paramore CG, Turner DA (1994) Relative risks of ventriculostomy infection and morbidity. *Acta Neurochir (Wien)* 127:79–84
14. Park P, Garton HJ, Kocan MJ, Thompson BG (2004) Risk of infection with prolonged ventricular catheterization. *Neurosurgery* 55:594–599
15. Pfausler B, Beer R, Engelhardt K, Kemmler G, Mohsenipour I, Schmutzhard E (2004) Cell index – a new parameter for the early diagnosis of ventriculostomy (external ventricular drainage)-related ventriculitis in patients with intraventricular hemorrhage? *Acta Neurochir (Wien)* 146:477–481
16. Pfisterer W, Muhlbauer M, Czech T, Reinprecht A (2003) Early diagnosis of external ventricular drainage infection: results of a prospective study. *J Neurol Neurosurg Psychiatry* 74:929–932
17. Poon WS, Ng S, Wai S (1998) CSF antibiotic prophylaxis for neurosurgical patients with ventriculostomy: a randomised study. *Acta Neurochir Suppl* 71:146–148
18. Ratilal B, Costa J, Sampaio C (2008) Antibiotic prophylaxis for surgical introduction of intracranial ventricular shunts: a systematic review. *J Neurosurg Pediatr* 1:48–56
19. Schade RP, Schinkel J, Visser LG, van Dijk JM, Voormolen JH, Kuijper EJ (2005) Bacterial meningitis caused by the use of ventricular or lumbar cerebrospinal fluid catheters. *J Neurosurg* 102:229–234
20. Sloffer CA, Augspurger L, Wagenbach A, Lanzino G (2005) Antimicrobial-impregnated external ventricular catheters: does the very low infection rate observed in clinical trials apply to daily clinical practice? *Neurosurgery* 56:1041–1044
21. Smith RW, Alksne JF (1976) Infections complicating the use of external ventriculostomy. *J Neurosurg* 44:567–570
22. Steinbok P, Cochrane DD, Kestle JR (1996) The significance of bacteriologically positive ventriculoperitoneal shunt components in the absence of other signs of shunt infection. *J Neurosurg* 84:617–623
23. Stenager E, Gerner-Smidt P, Kock-Jensen C (1986) Ventriculostomy-related infections – an epidemiological study. *Acta Neurochir (Wien)* 83:20–23
24. Sundbarg G, Nordstrom CH, Soderstrom S (1988) Complications due to prolonged ventricular fluid pressure recording. *Br J Neurosurg* 2:485–495
25. Winfield JA, Rosenthal P, Kanter RK, Casella G (1993) Duration of intracranial pressure monitoring does not predict daily risk of infectious complications. *Neurosurgery* 33:424–430
26. Zingale A, Ippolito S, Pappalardo P, Chibbaro S, Amoroso R (1999) Infections and re-infections in long-term external ventricular drainage. A variation upon a theme. *J Neurosurg Sci* 43:125–132

Dependence of Cerebrospinal Fluid Pressure and Volume on the Changes in Serum Osmolarity in Cats

Ivana Jurjević, Jurica Maraković, Darko Chudy, Ivona Markelić, Marijan Klarica, Ana Froebe, and Darko Orešković

Abstract Objectives: To study the effect of blood osmolarity on cerebrospinal fluid (CSF) volume and CSF pressure in cats.

Methods: Three types of methods were used on anesthetized cats. The first, ventriculo-cisternal perfusion (12.96 $\mu\text{L}/\text{min}$) before and after i.v. application of 20% mannitol; the second, measuring the outflow of CSF by cisternal free drainage; and the third, measuring CSF pressure in the ventricles of an intact CSF system, with the second and third method being performed before and after the i.p. application of a hypo-osmolar substance (distilled water).

Results: In the first group, the application of 20% mannitol led to a significantly reduced ($p < 0.005$) outflow volume (from 12.60 ± 0.29 to 0.94 ± 0.09 $\mu\text{L}/\text{min}$). In the second group, the outflow CSF volume significantly increased ($p < 0.001$) after the application of distilled water (from 18.8 ± 0.3 to 28.2 ± 0.7 $\mu\text{L}/\text{min}$). In the third group, after the application of distilled water, the CSF pressure also significantly increased ($p < 0.05$; from 8.3 ± 0.8 to 16.1 ± 0.14 cm H_2O).

Conclusion: We conclude that changes in serum osmolarity change the CSF volume because of the osmotic gradient between the blood and all of the CSF compartments, and also that the change in CSF pressure is closely associated with changes in CSF volume.

Keywords Cat • Central nervous system • Cerebrospinal fluid • Cerebrospinal fluid hydrodynamics • Cerebrospinal fluid pressure • Cerebrospinal fluid volume • Blood osmolarity

Introduction

In accordance with the generally accepted hypothesis of cerebrospinal fluid (CSF) hydrodynamics, CSF is produced in the cerebral ventricular system and then circulates to the subarachnoid space to be absorbed into the venous sinuses through the arachnoid villi [1, 5, 8, 14]. It is believed that CSF is formed mainly by the secretory activity of the choroid plexuses inside the brain ventricles, and that most of the remaining CSF is probably produced by the ependyma [2, 6]. Despite the fact that many aspects of CSF hydrodynamics are still insufficiently understood, this hypothesis represents, with minor modifications, a common point of reference in scientific papers, review articles and in numerous textbooks, and is proffered as an unquestionable fact. Also, based on this hypothesis, the entire physiological volume of CSF within the CSF system should be preserved by the balance between the secretion of CSF inside the brain ventricles and the passive absorption of CSF from the cortical subarachnoid space.

In contrast to the classic hypothesis, it was shown that with physiological intracranial pressure in isolated brain ventricles there are no net CSF formation and CSF circulation [9, 12]. Also, there was no increase in CSF pressure over 190 min, and no ventricles were dilated, which obviously confirmed an absence of active net CSF formation [9]. Furthermore, when labeled water is infused into the lateral ventricle in an open CSF system, it is not distributed to the cisterna magna, but rather absorbed into the periventricular

I. Jurjević, I. Markelić, and M. Klarica
Department of Pharmacology,
University of Zagreb School of Medicine
and Croatian Institute for Brain Research,
Šalata 11, 10 000
Zagreb, Croatia

J. Maraković and D. Chudy
Department of Neurosurgery, Dubrava University Hospital,
Avenija G. Šuška 6, 10 000
Zagreb, Croatia

A. Froebe
Department of Oncology and Nuclear Medicine,
University Hospital,
"Sestre Milosrdnice" Vinogradska c. 29, 10 000
Zagreb, Croatia

D. Orešković (✉)
Laboratory of Neurochemistry and Molecular Neurobiology,
Department of Molecular Genetics,
Ruđer Bošković Institute,
Bijenička c. 54, 10 000
Zagreb, Croatia
e-mail: doresk@irb.hr

capillaries, which indicates that the CSF volume (water) is significantly absorbed inside the ventricles [3, 4]. Based on experimental work, we have recently postulated a new hypothesis regarding CSF hydrodynamics [3, 4, 9, 11], which suggests that CSF is not solely formed inside the brain ventricles and is absorbed outside of them in the cortical subarachnoid space, but rather it equally appears and disappears throughout the whole CSF system. This means that the volume of CSF depends on the hydrostatic gradients and osmotic forces present between the blood (capillaries), on one side, and the interstitial fluid of the central nervous system (CNS) and CSF on the other. Based on the above-mentioned reasons, we wanted to investigate if and how hyper- and hypo-osmolar blood would have any influence on CSF volume. Furthermore, we also desired to examine if the change in CSF pressure after osmotic therapy was the consequence of a change in CSF volume. Namely, CSF pressure depends on the volume of the brain, intracranial blood (arterial and venous), CSF, and any other pathological volume (tumor, hematoma, abscess, edema) within the closed intracranial space. Although hyperosmolar mannitol has long been used in clinical practice to reduce intracranial pressure, the mechanism by which this effect occurs is still unclear.

Materials and Methods

The experiments were performed on adult cats, regardless of age and sex, ranging in weight from 1.8 to 3.2 kg. All experimental procedures were performed in accordance with the European Directive 86/609/EEC on the protection of animals used for experimental and other scientific purposes, and the Law on Animal Rights and Protection of the Republic of Croatia, with the approval of the institutional Ethics Committee. The animals were anesthetized with an intraperitoneal injection of chloralose (α -chloralose, Fluka; 100 mg/kg). After the femoral artery had been cannulated, the blood pressure was recorded via a T-connector and samples of blood were taken for the analysis of blood gases. As the cats continued breathing spontaneously under anesthesia, no significant changes either in blood pressure or gases were observed.

Three types of experiments on anesthetized cats were done: ventriculo-cisternal perfusion; the free drainage of CSF from a cannula put into the cisterna magna; and the measuring of CSF pressure by the cannula put into the lateral ventricle of the brain. In each case the cats were positioned in stereotaxy (Cat model, D. Kopf, Tujunga, CA, USA) with their heads elevated and their external auditory meatus 15 cm above the stereotaxic table (sphinx position). The ventriculo-cisternal perfusion using mock CSF was performed as described in detail in our previous publications [10, 13]. The outflow volume was measured before and after the intravein

(i.v.) application of hyperosmolar (20% mannitol; 1 g/kg/3 min) solutions. In the second group of animals (free drainage of CSF), after the cat was fixed on the stereotaxic frame, an incision was made on the neck and a 22-gauge needle was inserted into the cisterna magna. When the free drainage of CSF stabilized, a hypo-osmolar substance was intraperitoneally (i.p.) administered (distilled water, 100 mL/kg/5 min), and the volume of CSF was measured before and after the application. In the third experiment, the cats were positioned on the stereotaxy, a 22-gauge needle was inserted into the lateral ventricle and the CSF pressure was measured in the intact CSF system before and after the i.p. application of the hypo-osmolar substance (distilled water, 100 mL/kg/5 min), following the same procedure as that followed in the ventriculo-cisternal perfusion experiment. The volume of the samples was determined by weighing (Mettler, Toledo AT 20, Switzerland). At the end of each experiment, an overdose of thiopentone was injected via the femoral vein to euthanize the animals.

A statistical analysis of all the results was performed using paired Student's *t* test.

Results

In the first group of experiments (Fig. 1), in three cats with normal CSF pressure, the outflow rate during ventriculo-cisternal perfusion (12.96 μ L/min; Palmer infusion pump) was measured during each 30 minute time intervals 2 h before and 2 h after the i.v. application of the hyperosmolar solution (20% mannitol; 1 g/kg/3 min). Thirty minutes after the hyperosmolar application, a significant decrease ($p < 0.005$) in the outflow rate (0.94 ± 0.09 μ L/min) was observed in comparison with the outflow rate obtained before the application (12.60 ± 0.29 μ L/min; Fig. 1). It suggests that osmotic forces significantly influence the control of CSF volume, and that the increase in blood osmolarity resulted in a decrease in CSF volume.

In the second group of experiments (Fig. 2), the CSF outflow rate during free drainage at negative CSF pressure (-10 cm H₂O) was measured in four cats at different time intervals (30 min) before and after the i.p. application of the hypo-osmolar solution (distilled water, 100 mL/kg/5 min). Thirty minutes after the hypo-osmolar application, a significant increase ($p < 0.001$) in the outflow rate (28.2 ± 0.7 μ L/min) was observed in comparison with the outflow rate obtained before the application (18.8 ± 0.3 μ L/min). This also suggests that osmotic forces significantly influence the control of CSF volume, and that the decrease in blood osmolarity resulted in an increase in CSF volume.

In the third group of experiments (Fig. 3), the CSF pressure was measured at different time intervals (5 min) in four

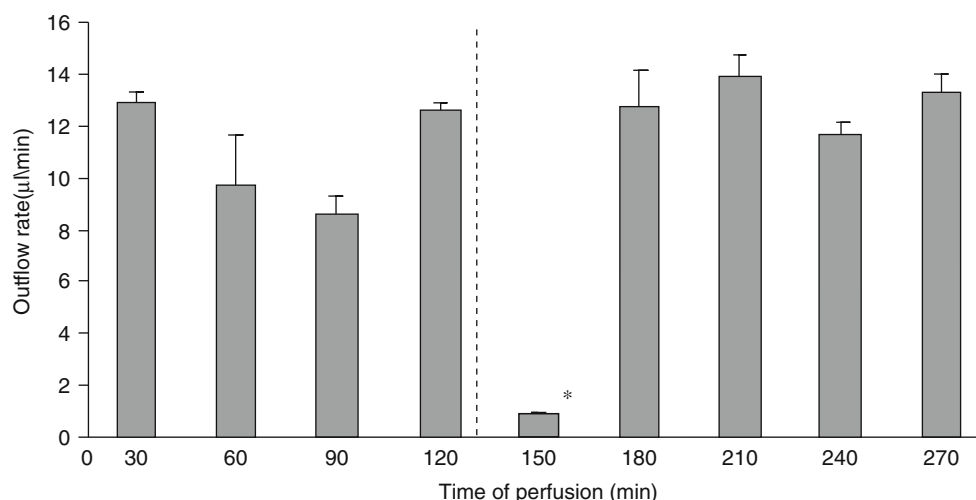
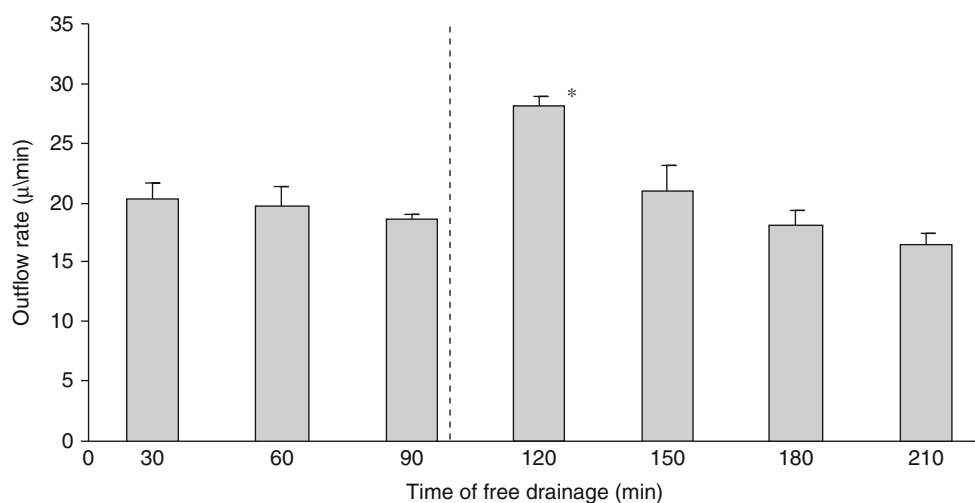


Fig. 1 Effect of hyperosmolar substance (20% mannitol; 1 g/kg/3 min; IV) on the outflow rate of ventriculo-cisternal perfusion with mock CSF (rate of perfusion: 12.96 $\mu\text{L}/\text{min}$) in cats ($n=3$) at +8 cm H_2O . Bars represent perfusion outflow rates and the vertical broken line represents

the time at which the hyperosmolar substance was applied. The results are shown as mean values \pm SEM. Differences between the rate of outflow perfusate before and after treatment are statistically significant (* $p<0.005$)

Fig. 2 Effect of hypo-osmolar substance (distilled water; 100 mL/kg/5 min; i.p.) on the outflow rate during free drainage in cats ($n=4$) at -10 cm H_2O . Bars represent outflow rates and the vertical broken line represents the time at which the hypo-osmolar substance was applied. The results are shown as mean values \pm SEM. Differences between the outflow rates before and after treatment are statistically significant (* $p<0.001$)



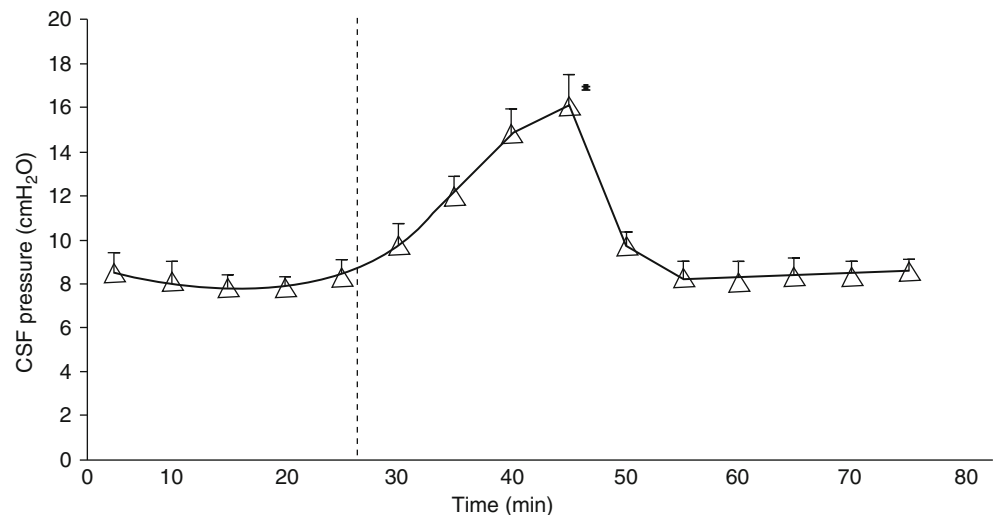
cats before and after the i.p. application of the hypo-osmolar solution (distilled water, 100 mL/kg/5 min). When distilled water was applied, the CSF pressure began to increase from 8.3 ± 0.8 to a significant value of 16.1 ± 0.14 cm H_2O ($p<0.05$) within 20 min. This increase of CSF pressure and CSF volume (Fig. 2) obtained by hypo-osmolar blood indicates that the increase in CSF pressure could be a consequence of the increase in CSF volume.

Discussion

The influence of blood osmolarity on the behavior of CSF volume and CSF pressure was studied in cats. Based on our recent investigation, it is necessary to point out that a change

in CSF osmolarity does not affect CSF formation [12], as was believed during an earlier investigation [7, 15], but rather affects CSF volume all over the CSF system. This was confirmed by a very recent investigation [10] that showed that the volume of CSF depends on both CSF osmolarity and the size of the contact area between the CSF system and the surrounding tissue exposed to hyperosmolar CSF. In other words, this means that if a larger contact area were included, a stronger effect would be obtained, i.e. a greater change in CSF volume. The results we present in this study are also in accordance with the aforementioned investigations. Namely, after a change in blood osmolarity the CSF volume (Figs. 1 and 2), and the CSF pressure (Fig. 3) changed significantly. An increase in blood osmolarity leads to a reduction in CSF volume (Fig. 1), and decreased osmolarity leads to an increase in CSF volume (Fig. 2). It could be concluded that

Fig. 3 Effect of hypo-osmolar substance (distilled water; 100 mL/kg/5 min; i.p.) on CSF pressure in an intact CSF system in cats ($n=4$). The solid line shows CSF pressure and the vertical broken line represents the time at which the hypo-osmolar substance was applied. The results are shown as mean values \pm SEM. Differences between the CSF pressure before and after treatment are statistically significant ($*p<0.05$)



an increase in CSF volume causes an increase in CSF pressure (Fig. 3) because after the same experimental treatment (Figs. 2 and 3) the effect on CSF volume and CSF pressure was similar. Thus, it could be said that if a difference in osmotic pressure exists between the CNS blood and the CSF, it will result in a change in CSF volume. Therefore, total CSF volume within the CSF system should depend on a non-stop (permanent) exchange between the CSF and the interstitial fluid (ISF) of the surrounding tissue throughout the entire CSF system.

Conclusion

Changes in serum osmolarity change CSF volume because of the osmotic gradient between the blood and all of the CSF compartments. Also, a change in CSF pressure is closely related to changes in CSF volume, and CSF pressure increases as a consequence of an increase in CSF volume. Additionally, we expect that CSF volume changes mainly have an influence on intracranial pressure after interventional alteration of serum osmolarity in clinical practice. Furthermore, as the control of CSF volume is not a result of the balance between CSF formation and absorption, as was predicted by the classic hypothesis of CSF formation, circulation and absorption, the results obtained therefore support the recently proposed new hypothesis [3, 4, 9, 11] of CSF hydrodynamics. This means that the CSF exchange between the entire CSF system and the surrounding tissue depends on physiological and pathophysiological processes (trauma, ischemia, inflammation, etc.) that can cause changes in fluid osmolarity in different CNS compartments. In other words, the behavior of fluids in the CNS is very similar to that in other parts of the body.

Acknowledgements We thank Mrs. Katarina Karlo for her skilled technical assistance. This work has been supported by the Ministry of Science, Education and Sport of the Republic of Croatia (Projects: 1. Hydrodynamics of cerebrospinal fluid. No. 098-1080231-2328; and 2. Pathophysiology of cerebrospinal fluid and intracranial pressure. No. 108-1080231-0023).

Conflict of interest statement We declare that we have no conflict of interest.

References

1. Brodlet A, Stoodley M (2007) CSF pathways: a review. *Br J Neurosurg* 21:510–520
2. Brown PD, Davies SL, Speake T, Millar ID (2004) Molecular mechanisms of cerebrospinal fluid production. *Neuroscience* 129:957–970
3. Bulat M, Klarica M (2011) Recent insight into a new hydrodynamics of cerebrospinal fluid. *Brain Res Rev* 65:99–112
4. Bulat M, Lupret V, Orešković D, Klarica M (2008) Transventricular and transpial absorption of cerebrospinal fluid into cerebral microvessels. *Coll Antropol* 31(Suppl 3):43–50
5. Cutler RWP, Page L, Galichich J, Waters GV (1968) Formation and absorption of cerebrospinal fluid in man. *Brain* 91:707–720
6. Davson H, Welch K, Segal MB (1987) *Physiology and pathology of the cerebrospinal fluid*. Churchill Livingstone, Edinburgh
7. Hochwald GM, Wald A, Malhan C (1974) The effect of osmotic gradients on cerebrospinal fluid production and its sodium ion content and on brain water content. *Trans Am Neurol Assoc* 99:219–221
8. Johanson CE, Duncan JAH, Klinge PM, Brinker T, Stopa EG, Silverberg GD (2008) Multiplicity of cerebrospinal fluid functions: new challenges in health and disease. *Cerebrospinal Fluid Res* 5:10
9. Klarica M, Orešković D, Božić B, Vukić M, Butković V, Bulat M (2009) New experimental model of acute aqueductal blockade in cats: effects on cerebrospinal fluid pressure and the size of brain ventricles. *Neuroscience* 158:1397–1405

10. Maraković J, Orešković D, Radoš M, Vukić M, Jurjević I, Chudy D, Klarica M (2010) Effect of osmolarity on CSF volume during ventriculo-aqueductal and ventriculo-cisternal perfusions in cats. *Neurosci Lett* 484:93–97
11. Orešković D, Klarica M (2010) The formation of cerebrospinal fluid: nearly a hundred years of interpretations and misinterpretations. *Brain Res Rev* 64:241–262
12. Orešković D, Klarica M, Vukić M (2002) The formation and circulation of cerebrospinal fluid inside the cat brain ventricles: a fact or an illusion? *Neurosci Lett* 327:103–106
13. Orešković D, Whitton PS, Lupret V (1991) Effect of intracranial pressure on cerebrospinal fluid formation in isolated brain ventricles. *Neuroscience* 41:773–777
14. Pollay M, Stevens A, Roberts PA (1983) Alteration in choroid plexus blood flow and cerebrospinal fluid formation by increased ventricular pressure. In: Wood JH (ed) *Neurobiology of cerebrospinal fluid*, vol 2. Plenum Press, New York, pp 687–695
15. Wald A, Hochwald GM, Malhan C (1976) The effects of ventricular fluid osmolality on bulk flow of nascent fluid into the cerebral ventricles of cats. *Exp Brain Res* 25:157–167

The Effect of Body Position on Intraocular and CSF Pressures in the Lateral Ventricle, and in Cortical and Lumbar Subarachnoid Spaces in Cats

Tomislav Kuzman, Ivana Jurjević, Inga Mandac, Milan Radoš, Darko Orešković, Hrvoje Jednačak, and Marijan Klarica

Abstract Background: Correlation between cerebrospinal fluid (CSF) and intraocular pressure (IOP) is still unclear. We compared CSF pressure from different parts of the CSF system and IOP measured by the same invasive technique in a new experimental model in cats during changes of body position.

Methods: Pressure changes were recorded on anesthetized cats ($n=7$) in the lateral ventricle (LV), in the cortical (CSS) and lumbar (LSS) subarachnoid spaces, and in the anterior ocular chamber. Animals and measuring instruments were both fixed on a board at an adequate hydrostatic level.

Results: In a horizontal position, IOP (18.5 ± 0.6 cm H₂O) and CSF pressures (LV = 17.4 ± 0.9 ; CSS = 17.2 ± 0.7 ; LSS = 17.8 ± 1.2 cm H₂O) were similar. In a vertical position, pressure in the LSS increased (33.5 ± 2.3 cm H₂O), pressures inside the cranial cavity dropped (LV = -4.1 ± 0.9 cm H₂O; CSS = -4.8 ± 0.5 cm H₂O), while IOP slightly decreased (14.3 ± 0.1 cm H₂O).

Conclusion: Change in body position from horizontal to upright causes drastic changes in CSF pressure and relatively small changes in IOP, which indicates that the IOP does not reflect CSF pressure. In an upright position, CSF pressures

were equal at the same hydrostatic level in LV and CSS, which suggests that CSF pressure inside the cranium depends on its anatomical and biophysical features, and not on CSF secretion and absorption.

Keywords Body position • Intraocular pressure • Cerebrospinal fluid pressure • Cerebrospinal fluid hydrodynamics

Introduction

Studies about the correlation between intracranial pressure (ICP) and intraocular pressure (IOP) are contradictory. Some suggest that abnormal IOP is an excellent indicator of abnormal ICP in patients with known intracranial pathological conditions, indicating that IOP and ICP have a good correlation [8, 13]. Others indicate that changes in IOP are a poor predictor of changes in ICP, and that an increase in ICP does not significantly change IOP [4, 14]. However, in patients with intracranial hypertension, CSF pressure is recorded using an invasive method, and IOP is measured using a non-invasive method. Different methods for measuring pressure inside the CSF system and the eye, as well as the fact that the measuring instruments were not set to the same reference point, could be the reasons for the contradictory results that exist in the literature. Thus, in the literature, we found great differences between the control IOP values of animals of the same species, which were measured using different methods. For example, the control IOP values in cat models range from 12.7 ($n=12$) [16], measured using non-invasive methods, to 17.5 ($n=16$), measured using cannulation [10]. As a result, we have developed a new experimental animal model in which CSF pressure and IOP are measured using an identical invasive method, and with the pressure transducers set to the same reference point and positioned at an adequate hydrostatic level. CSF pressure was recorded at three different positions (the lateral ventricle, the cortical and lumbar subarachnoid spaces), and we correlated the changes in CSF pressure and the changes in IOP during alteration of the body position.

I. Jurjević, I. Mandac, M. Radoš, and M. Klarica (✉)
Department of Pharmacology and
the Croatian Institute for Brain Research,
University of Zagreb School of Medicine,
Šalata 11, HR-10 000 Zagreb, Croatia
e-mail: mklarica@mef.hr

T. Kuzman
Department of Ophthalmology,
University of Zagreb School of Medicine,
Zagreb, Croatia

D. Orešković
Laboratory of Neurochemistry and Molecular Neurobiology,
Department of Molecular Genetics, Ruđer Bošković Institute,
Bijenička c. 54, 10 000 Zagreb, Croatia
e-mail: doresk@irb.hr

H. Jednačak
Department of Neurosurgery,
University of Zagreb School of Medicine,
Zagreb, Croatia

Materials and Methods

The study was performed on seven male and female adult cats (2.2–3.4 kg body weight). The animals were kept in cages with natural light–dark cycles and had access to water and food (SP215 Feline, Hill's Pet Nutrition Inc., Topeka, KS, USA). The animals were in quarantine for 30 days and the experiments were performed in accordance with the Croatian Animal Welfare Act. The study was approved by the institutional Ethics Committee (Approval No. 04-76/2006-18).

The cats were anesthetized with α -chloralose (Fluka; 100 mg/kg i.p.) and fixed in a stereotaxic head holder (David Kopf, Tununga, CA, USA) in the sphinx position. The femoral artery was cannulated, the blood pressure was recorded via a T-connector, and samples of blood were taken for the analysis of blood gases. No significant changes, either in blood pressure or blood gases, were observed during these experiments on the cats, which continued breathing spontaneously under the chloralose anesthesia. A stainless steel cannula (i.d. of 0.9 mm) was introduced into the left lateral ventricle at 2 mm lateral and 15 mm anterior to the stereotaxic zero point, and 10–12 mm below the dural surface [15]. A second cannula was placed in the cortical subarachnoid intracranial space on the right side (at 2 mm lateral and 15 mm anterior to the stereotaxic zero point). Cannulas in the LV and CSS were used for the measurement of intracranial CSF pressures. In order to measure the spinal CSF pressure in the lumbar region, a laminectomy (5 × 10 mm) of the L3 vertebra was performed. After the incision of the spinal dura and arachnoidea, a third plastic cannula (0.9 mm i.d.) was introduced into the subarachnoid space.

Leakage of CSF was prevented by applying cyanoacrylate glue to the dura around the cannula. Bone openings in the cranium and vertebra were hermetically closed by the application of a dental acrylic. The fourth cannula (27-gauge) was inserted through the perilimbal side of the cornea into the anterior chamber of the eye for the purpose of measuring IOP. Leakage of humor aqueous was prevented by applying cyanoacrylate around the cannula.

After setting the measuring cannulas, the cat was removed from the stereotaxic device and then fixed in a prone position on a board (Fig. 1). CSF and IOP pressures were recorded by pressure transducers (Gould P23 ID, Gould Instruments, Cleveland, OH, USA), which were connected to a system that transformed the analogous data to digital data (Quand Bridge and PowerLab/800, AD Instruments, Castle Hill, NSW, Australia), and then entered into a computer (IBM, White Plains, NY, USA; Fig. 1).

Pressure transducers were calibrated by use of a water column; the interaural line was taken as zero pressure. Instruments for pressure measurement were fixed on the board in such a way that the membrane of each transducer

was at the same hydrostatic level as the corresponding measuring cannula, so there was no need to additionally adjust the transducers during the body position changes (Fig. 1). CSF and IOP pressure changes were recorded for 10–15 min in the horizontal and vertical (head up) positions.

Data are shown as mean value \pm standard error of the mean (SEM). A statistical analysis of all the results was performed using the paired Student's *t* test. $P < 0.05$ was considered statistically significant.

Results

In a horizontal position, the pressure in the eye (IOP = 18.5 ± 0.6 cm H₂O) and the pressure in different parts of the CSF system (LV = 17.4 ± 0.9 ; CSS = 17.2 ± 0.7 ; LSS = 17.8 ± 1.2 cm H₂O) were similar and did not differ significantly ($P > 0.05$; Fig. 2). In an upright position, the lumbar pressure increased (LSS = 33.5 ± 2.3 cm H₂O), and pressure inside the cranium dropped to a subatmospheric value (LV = -4.1 ± 0.9 cm H₂O; CSS = -4.8 ± 0.5 cm H₂O), while IOP showed a slight decrease (IOP = 14.3 ± 0.1 cm H₂O; Fig. 2).

Discussion

In a horizontal position, all the pressures measured had similar values, so it seemed that IOP could reflect changes in pressure inside the CSF system. However, it is known that IOP values are influenced by body position in different animal species [1, 6]. In these studies, similar to our cat model, there was a slight decrease in IOP during the lifting of the animal's head (Fig. 2). In humans, IOP values are higher in a supine position and lower in a sitting or standing position. Higher IOP values in a supine position could be explained by a higher vein blood pressure, and therefore a slower venous blood flow from the head and eyes, a phenomenon similar to the Valsalva maneuver [9].

Unlike the IOP changes, in our cat model in an upright position we observed drastic changes in CSF pressure in certain parts of the CSF system. Thus, the pressures in the LV and CSS, measured by cannulas that were situated 4 cm from the foramen magnum, and at the same hydrostatic level, were not statistically different and amounted to approximately -4 cm H₂O (subatmospheric or negative pressure; Fig. 2). In addition, at the same time the pressure inside the lumbar space was positive, and the value corresponded to the distance between the measuring point and the cisterna magna (about 33 cm H₂O). These changes were not transient, but the pressures retained the values mentioned for as long as the

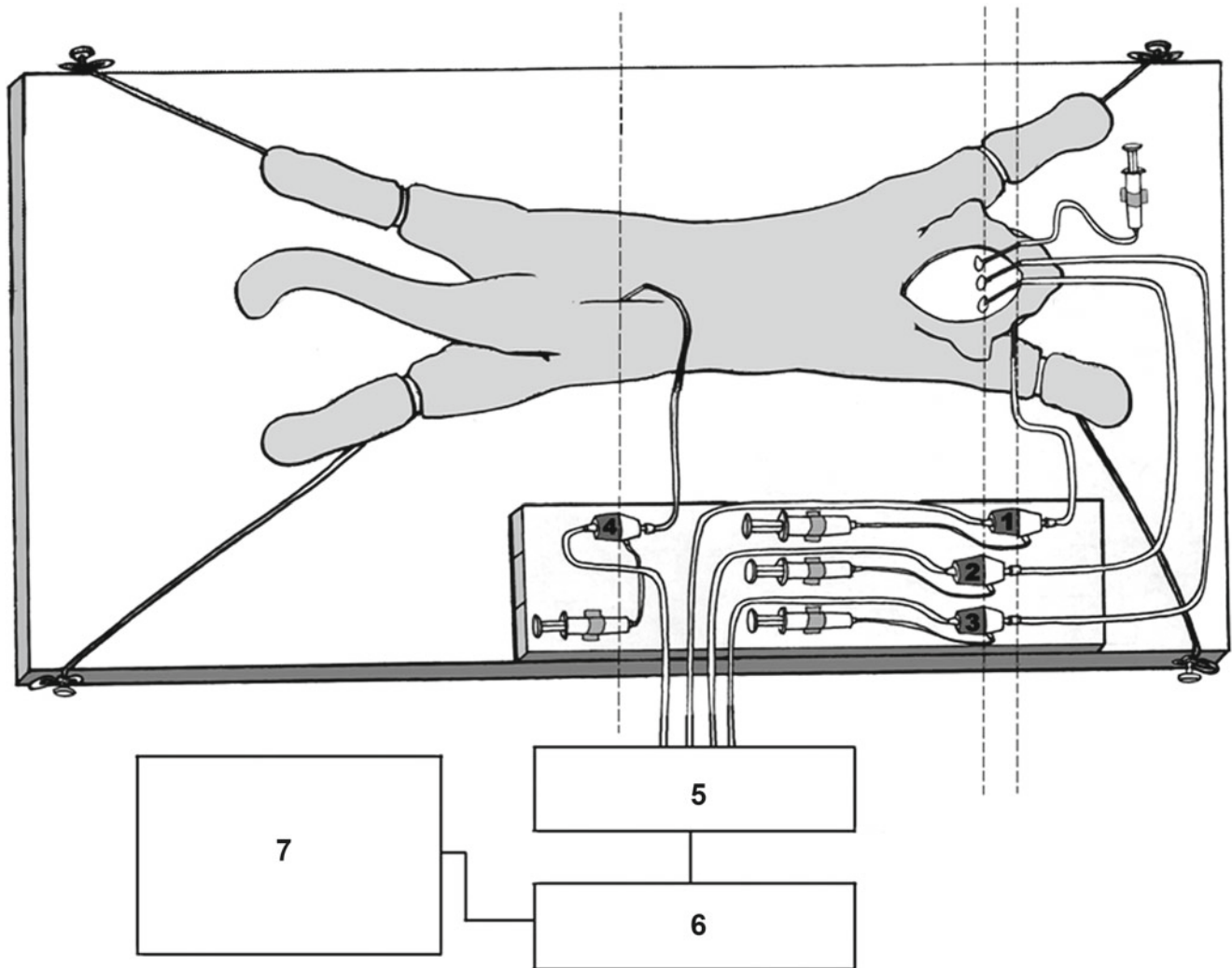


Fig. 1 Scheme of the experimental model: 1 – pressure transducer connected to a cannula in the anterior ocular chamber; 2 – pressure transducer connected to the cannula in the lateral ventricle; 3 – pressure transducer

connected to the cannula in the cortical subarachnoid space; 4 – pressure transducer connected to the cannula in the lumbar subarachnoid space; 5 – Quand Bridge; 6 – PowerLab/800; 7 – personal computer

animal remained in the same position (about 15 min). These results could be explained by the law of fluid mechanics [7], as follows.

In our previous publication [5] we compared the pressure changes inside the CSF system model and inside the cat during lifting of the cat's head and the "cranial" part of the model. The model of the CSF system consists of a distensible "spinal" part and a nondistensible "cranial" part filled with artificial CSF, which were constructed to imitate the anatomical dimensions and biophysical characteristics (distensible/nondistensible) of the CSF system in cats. Pressure changes inside the model have faithfully imitated the changes in CSF pressure in cats. As the "cranial" part of the model is nondistensible, it is evident that it cannot change its total fluid volume. However, in spite of this, pressure change could happen in accordance with the law of fluid mechanics [7]. Namely, the aforementioned law indicates that fluid pressure inside a

nondistensible tube, opened at the bottom, should be negative and of a value that corresponds to the height of the hydrostatic column.

Our results indicate that the decrease in intracranial pressure in an upright position is not due to the displacement of cranial CSF or blood volume to hydrostatically lower body parts, as is usually assumed [2, 11]. This means that the incompressibility of the cranial osseous vault enables constant blood brain perfusion despite sudden changes in head position during normal activity (bipedal walking, dancing, jumping, etc.). In addition, it suggests that in an upright position normal ICP is subatmospheric, and that the cerebral perfusion pressure is higher than we previously believed.

These results are not in accordance with the generally accepted hypothesis about secretion, unidirectional circulation, and absorption of CSF. Namely, CSF cannot flow from the ventricles, where the pressure is about $-4 \text{ cm H}_2\text{O}$, to the

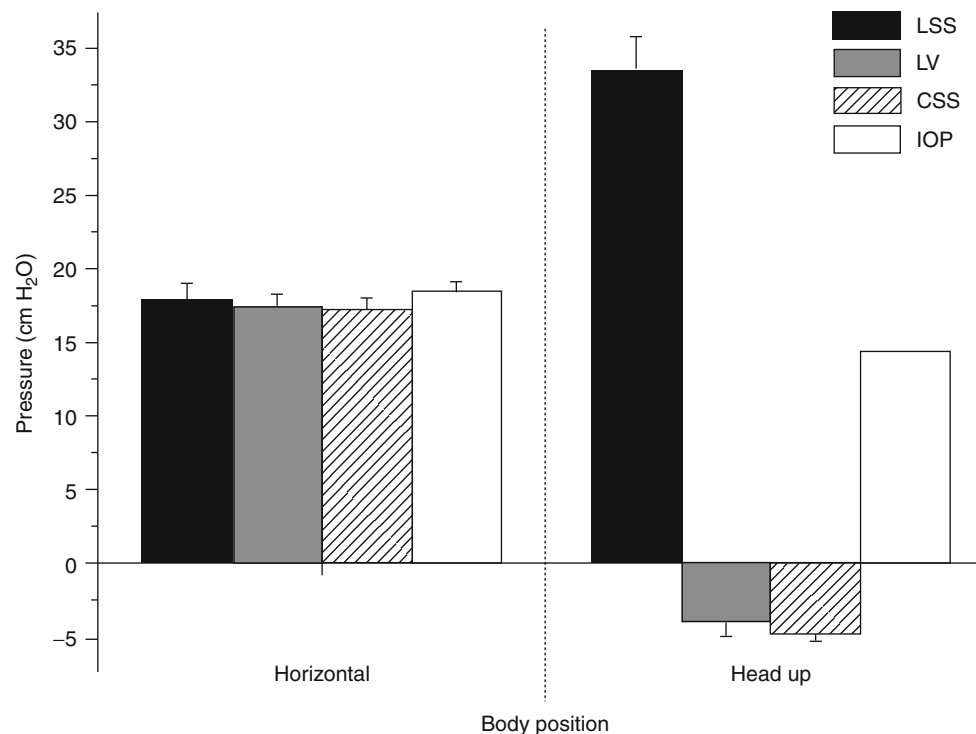


Fig. 2 Effects of change of body position from horizontal to head up on CSF pressures (cm H₂O) in the lateral ventricle (LV), cortical (CSS) and lumbar (LSS) subarachnoid spaces, as well as on intraocular pressure

(IOP) in seven cats. Results are shown as mean value \pm standard error of the mean (SEM)

cisterna magna where the pressure is higher and around zero. Other than that, the pressure inside the ventricles was the same as the pressure in the cortical subarachnoid space at the same hydrostatic level, and in order for CSF to circulate it should be lower (Fig. 2). These results are in accordance with the new hypothesis of CSF physiology [3, 12], which suggests that the volumes of CSF and interstitial fluid are regulated by hydrostatic and osmotic forces among the capillaries, central nervous system tissue, and CSF.

Conclusion

Slight changes in IOP, as well as drastic changes in CSF pressure in certain parts of the CSF system imply that IOP and CSF pressure are not significantly correlated, and that we cannot draw any conclusions regarding the changes in CSF pressure based on IOP.

Acknowledgements We thank Mrs. Ljiljana Krznar for her skilled technical assistance. This work has been supported by the Ministry of Science, Education, and Sport of the Republic of Croatia (Projects: 1. Hydrodynamics of cerebrospinal fluid. No. 098-1080231-2328; and 2. Pathophysiology of cerebrospinal fluid and intracranial pressure. No. 108-1080231-0023).

Conflict of interest statement We declare that we have no conflict of interest.

References

1. Aihara M, Lindsey JD, Weinreb RN (2003) Episcleral venous pressure of mouse eyes and effect of body position. *Curr Eye Res* 27:355–362
2. Alperin N, Hushek SG, Lee SH, Sivaramakrishnan A, Lichtor T (2005) MRI study of cerebral blood flow and CSF flow dynamics in an upright posture: the effect of posture on intracranial compliance and pressure. *Acta Neurochir (Wien)* 95:177–181
3. Bulat M, Klarica M (2010) Recent insight into a new hydrodynamics of cerebrospinal fluid. *Brain Res Rev*. doi: 10.1016/j.brainresrev.2010.08.002
4. Czarnik T, Gawda R, Kolodziej W, Latka D, Sznajd-Weron K, Weron R (2009) Associations between intracranial pressure, intraocular pressure and mean arterial pressure in patients with traumatic and non-traumatic brain injuries. *Injury* 40:33–39
5. Klarica M, Radoš M, Draganić P, Erceg G, Orešković D, Maraković J, Bulat M (2006) Effect of head position on cerebrospinal fluid pressure in cats: comparison with artificial model. *Croat Med J* 47:233–238
6. Komaromy AM, Garg CD, Ying GS, Liu C (2006) Effect of head position on intraocular pressure in horses. *Am J Vet Res* 67:1232–1235
7. Landau LD, Lifshitz EM (2005) Fluid mechanics. In: *Course of theoretical physics*, vol 6, 2nd English edn. Revised. Elsevier, Amsterdam, pp 5–7

8. Lashutka M, Chandra A, Murray H, Phillips G, Hiestand B (2005) The relationship of intraocular pressure to intracranial pressure. *Ann Emerg Med* 45:585–591
9. Longo A, Geiser MH, Riva C (2004) Posture changes and subfoveal choroidal blood flow. *Invest Ophthalmol Vis Sci* 45:546–551
10. Macri FJ, Dixon R, Rall DP (1965) Aqueous humor turnover rates in the cat. I. Effect of acetazolamide. *Invest Ophthalmol* 4:927–934
11. Magnaes B (1978) Movement of cerebrospinal fluid within the cranio-spinal space when sitting up and lying down. *Surg Neurol* 10:45–49
12. Orešković D, Klarica M (2010) The formation of cerebrospinal fluid: nearly a hundred years of interpretations and misinterpretations. *Brain Res Rev* 64:241–262
13. Salman MS (1997) Can intracranial pressure be measured non-invasively? *Lancet* 350:1367
14. Sheeran P, Bland JM, Hall GM (2000) Intraocular pressure changes and alterations in intracranial pressure (letter). *Lancet* 355:899
15. Snider RS, Niemer WT (1964) A stereotaxic atlas of the cat brain, 2nd edn. Meriden Gravure Company, Chicago
16. Wang YL, Toris CB, Zhan G, Yablonski ME (1999) Effects of topical epinephrine on aqueous humor dynamics in the cat. *Exp Eye Res* 68:439–445

Pressure Reactivity Index Correlates with Metabolic Dysfunction in a Porcine Model of Intracerebral Hemorrhage

Edgar Santos, Berk Orakcioglu, Modar M. Kentar, Jennifer Diedler, Yoichi Uozumi, Michael Schöll, Andreas Unterberg, and Oliver W. Sakowitz

Abstract Objective: We correlated oxygen, flow, and pressure indices of cerebrovascular reactivity (CR) with extracellular cerebral metabolite concentrations in a porcine model of intracerebral hemorrhage (ICH).

Methods: Continuous advanced multimodal monitoring including microdialysis, cerebral blood flow and $P_{br}O_2$ probes were placed 1 cm in front of the coronal suture in the grey/white matter junction. Following a period of 1 h of monitoring, an autologous arterial ICH with defined volumes (3 mL) was induced. Pressure-, oxygen-, and flow-related autoregulation indices (PRx, ORx, and FRx) were simultaneously calculated and correlated hourly with extracellular cerebral metabolites, including glucose, lactate, pyruvate, and glutamate.

Results: Seventeen swine were monitored on average 12 continuous hours per animal. FRx correlated highly with ORx (0.96, $P = <0.001$), but values of both FRx and ORx > 0.2 did not correlate with any microdialysis metabolite. Values of PRx > 0.2 correlated highly (0.65, $P < 0.001$) with the lactate/pyruvate ratio, values of PRx > 0.3 correlated with glutamate (0.67, $P < 0.05$), the lactate/pyruvate ratio (0.60, $P < 0.01$), and $P_{br}O_2$ (-0.65 , $P < 0.01$).

Conclusions: We found evidence for impaired CR in a porcine model of ICH. The findings suggest that, among other parameters of CR, positive PRx coefficients have the highest significance and could be associated with microdialysis alterations during hypoxic events.

Keywords Brain metabolism • Cerebrovascular autoregulation • Microdialysis • PRx • Stroke

Introduction

Cerebrovascular autoregulation is an arteriole-mediated mechanism [1] in which changes in mean arterial pressure over a wide range have no significant effect on cerebral blood flow (CBF) [2]. The dynamic change in vascular resistance is called cerebrovascular reactivity (CR). In some patients with traumatic brain injury (TBI), ischemic stroke, subarachnoid hemorrhage, and intracerebral hemorrhage (ICH) there is an impaired autoregulation of cerebral blood flow that contributes to secondary damage. Poor autoregulation measured by different indices is an independent predictor of worse neurological outcome [2–5]. Several investigations on autoregulatory indices have been carried out in TBI patients [6], but some recommendations have been extended to other entities, such as ICH. Czosnyka et al. method [2] is originally a frequency-specific linear correlation between cerebral perfusion pressure (CPP) and CBF- or cerebral blood volume-conferred changes in intracranial pressure (ICP). The method can be used to detect pressure-passive vasculature from spontaneous fluctuations in arterial blood pressure. Different monitoring methods have been applied to this principle [7].

In the case of ICH, blood pressure and blood flow preservation are critical. Excess blood flow could precipitate prolongation of the bleeding, and low perfusion could produce ischemia in the perihemorrhagic area. Additional information given by autoregulation indices could be helpful to maintain optimal perfusion pressure whilst not increasing the risk of hematoma enlargement. It is not clear which index is most suitable to reflect the clinical status and acute deterioration in

E. Santos (✉), B. Orakcioglu, M.M. Kentar,
A. Unterberg, and O.W. Sakowitz
Department of Neurosurgery, University of Heidelberg,
Im Neuenheimer Feld 400, 69120 Heidelberg, Germany
e-mail: edgar.santos@med.uni-heidelberg.de

J. Diedler
Department of Neurology,
University of Heidelberg,
Heidelberg, Germany

Y. Uozumi
Department of Neurosurgery,
National Defense Medical College,
Tokorozawa, Japan

M. Schöll
Department of Medical Informatics,
University of Heidelberg,
Heidelberg, Germany

ICH patients [3], and there are no standardized thresholds of each index to predict secondary damage and outcome with high sensibility and specificity.

Microdialysis (MD) is a continuous bedside neuromonitoring method that can give information about the brain metabolism with relatively good specificity and sensitivity for secondary ischemic damage [8].

In our study we simultaneously calculated pressure (PRx)-, oxygen (ORx)-, and flow (FRx)-related indices of CR, and their correlation with extracellular glucose, lactate, pyruvate, and glutamate concentrations in microdialysates and $P_{br}O_2$ measured close to the perihemorrhagic area in a swine model of ICH.

Materials and Methods

Animal Preparation

Protocols for the experiments were approved by the institutional animal care and use committee (Protocol No.: 35–9185.81/G-60/06).

Male swine ($n=17$) with an average mean weight of 32 kg (range 28–37 kg) were anesthetized with ketamine (10 mg/kg), midazolam (5 mg/kg), and azaperone (40 mg/kg) administered by intramuscular injection. Animals were orally intubated and mechanically ventilated ($FiO_2=0.3$). If brain tissue oxygenation ($P_{br}O_2$) was subthreshold (<15 mmHg), FiO_2 was adjusted. Anesthesia was maintained using 1.5% isoflurane inhalation. Rectal and brain temperature were continuously monitored. Rectal temperature was maintained between 35.5°C and 37°C. After surgical exposure of the right femoral artery a 4-Fr catheter was placed for permanent monitoring of mean arterial blood pressure (MAP). A venous line was placed in the right ear vein and capillary oxygen saturation (SO_2) was monitored from the left ear. CPP was kept >60 mmHg. Seizures were treated with 1–2 mg of a midazolam bolus as needed.

Operative Procedure

All intraparenchymal probes were implanted through burr holes (diameter: 5 mm). An intracranial pressure (ICP) probe (Neurovent-P®, Raumedic AG, Helmbrechts, Germany), a thermal diffusion flowmetry probe (Hemedex td-rCBF, Codman®, USA) to measure regional cerebral blood flow, a $P_{br}O_2$ probe (Neurovent®-TO, Raumedic AG, Helmbrechts, Germany) for determination of tissue oxygenation, and an MD probe (CMA 70, Solna, Sweden). All probes were aimed at the frontal and parietal white matter at the border zone between the vascular territory of the anterior and middle

cerebral artery, 1.5–2.5 cm from the planned site of the blood injection along the coronal suture. An equilibration period of 2 h was allowed for the probes to run in and for the animals to stabilize.

Autologous arterial hematoma was created following the description of Qureshi et al. [9] and Hemphil et al. [10]. Polyvinyl chloride tubing was attached to a stopcock at the distal end of the spinal needle and to the femoral artery. At the initiation of hematoma formation, autologous blood was injected into the brain under arterial pressure via this tubing, targeting the cortico-subcortical area in order to avoid deep seated ICH or intraventricular involvement. The injected hematoma volume was 3 mL. Neither the catheters nor the syringes were flushed with heparin. Monitoring was conducted for 10 h to complete a 12-h monitoring period. At the end of the monitoring period, the cranial vaults were opened and the brain extracted to certify probe locations, ICH size and position.

Monitoring

The MAP, ICP, CPP, brain and rectal temperature, heart rate (HR), oxygen saturation (SO_2), $P_{br}O_2$, and rCBF were simultaneously and continuously recorded.

The MD probes were perfused at a rate of 0.3 μ L/min and samples were taken every 30 min. The microdialysis vials were collected for off-line analysis. All other parameters were recorded on-line. Blood–gas analyses were achieved every 2 h to adjust the ventilator parameters.

Calculation of Autoregulatory Indices

The raw data were cleaned up from noise and clear artifacts resulting from animal manipulation or probe movement. Pearson's correlations were calculated between MAP and ICP, CPP and $P_{br}O_2$, and CPP and TD-rCBF, resulting in indices ranging from -1 to $+1$. Values more than 0.2 represented a positive correlation between the parameters investigated, and values close to $+1$ represented a perfect correlation. Values less than 0.2 represented no correlation or negative correlation, assuming independence between the variables analyzed (a normal CR). A cross-correlation was performed in all cases to search for a long duration response for shorter index positivity.

Pressure, Oxygen and Flow Reactivity Indices

Czosnyka et al. method was used [2]. A Pearson's correlation coefficient was calculated among 30 consecutive 10-s averages of MAP and ICP, resulting in a time-window of 5 min. As the calculation is repeated every 10 s, a “moving” or “running” coefficient is generated.

The oxygen reactivity index was determined according to Jaeger et al. [11]. Pearson's correlations were calculated

Table 1 Summary of indicators of disturbed cerebrovascular reactivity (CR)

	ORx <0.2		ORx >0.2	
	FRx <0.2	FRx >0.2	FRx <0.2	FRx >0.2
PRx <0.2	12	0	0	2
PRx >0.2	2	0	0	1

Average CR indices were calculated over the whole monitoring period. PRx > 0.2, defined as impaired CR, was not in all cases concordant with oxygenation- (ORx) and flow-related (FRx) CR indices. Based on this simple classification absolute numbers of experimental animals are indicated

among 120 consecutive 30-s averages of CPP and $P_{br}O_2$, resulting in a time-window of 1 h.

The flow reactivity index (FRx), as used by Barth et al. [12], was calculated. Values of CPP and rCBF were averaged over consecutive 10-s intervals. Subsequently, Pearson's correlation was calculated among 30 consecutive 10-s averages of CPP and TD-rCBF resulting in a "time window" of 5 min. Then, Pearson's correlations were calculated again after shifting the time frame by 10 s. Thus, every 10 s, a new correlation coefficient was created.

By averaging all coefficients the mean was obtained every hour over the entire monitoring period.

Statistical Analysis

For statistical analysis SPSS v. 17.0 was used. All data were normally distributed. Pearson's correlation was used. The 95% confidence interval was calculated for the mean difference in all parameters. The $P < 0.05$ level was used to assess significance.

Results

Seventeen male swine were monitored on average 11.7 continuous hours per animal (range 9–13). Mean age was 5 months (range 4–7 months). Median PRx of all animals during the entire artifact-free recording time was 0.001 (range −0.791 to 0.977; SD, 0.24). Median FRx of all animals during the entire artifact-free recording time was 0.12 (range, −0.441 to 0.95; SD 0.25). Median ORx of all animals during the entire artifact-free recording time was 0.11 (range, −0.399 to 0.848; SD 0.22).

For all CR studies a threshold of >0.2 was set to indicate impairment. Table 1 summarizes the average results for the animals. In four animals the overall CR results were discordant. In all other animals ($n = 12$) CR indices were concordant.

Mean extracellular concentrations of metabolites (glucose, lactate, pyruvate, glutamate) during the whole monitoring period showed non-significant differences between animals with PRx > 0.2 and those with PRx < 0.2, and no correlation was found between the number of hours/monitored time with metabolite concentrations.

Hourly Correlation of PRx

Cross-correlations between different cohorts of PRx and $P_{br}O_2$ and metabolites were performed. There was no correlation between PRx and both ORx and FRx. PRx correlated with pyruvate (-0.23 , $P = 0.003$) and the lactate/pyruvate ratio (0.271 , $P < 0.001$). In the case of PRx > 0.2 there is a correlation with lactate (0.405 , $P = 0.029$), the lactate/pyruvate ratio (0.65 , $P < 0.001$), and $P_{br}O_2$ (-0.332 , $P = 0.045$). It can be seen that with increasing thresholds for PRx, stronger correlations of lactate/pyruvate, glutamate were found. For PRx > 0.3 and PRx > 0.4, the correlation of lactate/pyruvate was stronger (0.67 and 0.81 respectively, $P < 0.01$), and glutamate correlated highly with PRx > 0.3 (0.677 , $P = 0.01$) and PRx > 0.4 (0.98 , 0.001), and $P_{br}O_2$ correlated significantly with PRx > 0.3 (-0.65 , $P < 0.01$). In Fig. 1 the cross-correlations of the PRx > 0.3 cohort are shown. During PRx > 0.4 increases there is a significant correlation with glucose concentration (-0.697 , $P = 0.037$), and a correlation with $P_{br}O_2$ (-0.599 , $P = 0.052$), which was nevertheless non-significant.

Hourly Correlation of ORx and FRx

ORx and FRx correlated strongly with each other (0.965 , $P < 0.001$), but no significant correlation with any metabolite was found even when coefficients were >0.2, >0.3, and >0.4. A correlation of the ORx and FRx was tried with the extracellular concentration for the previous and following hour of each metabolite, but no significant correlation was found (data not shown).

Distribution of PRx > 0.3 According to ICP

A distribution of the PRx recording according to 2-mmHg ICP groups was performed to see whether the correlations seen when PRx is >0.3 can be explained with increases in ICP of more than 20 mmHg. We found that ICP > 20 has a strong influence on PRx increase, but most of the time when PRx > 0.3 was recorded, ICP was under 20 mmHg (data not shown).

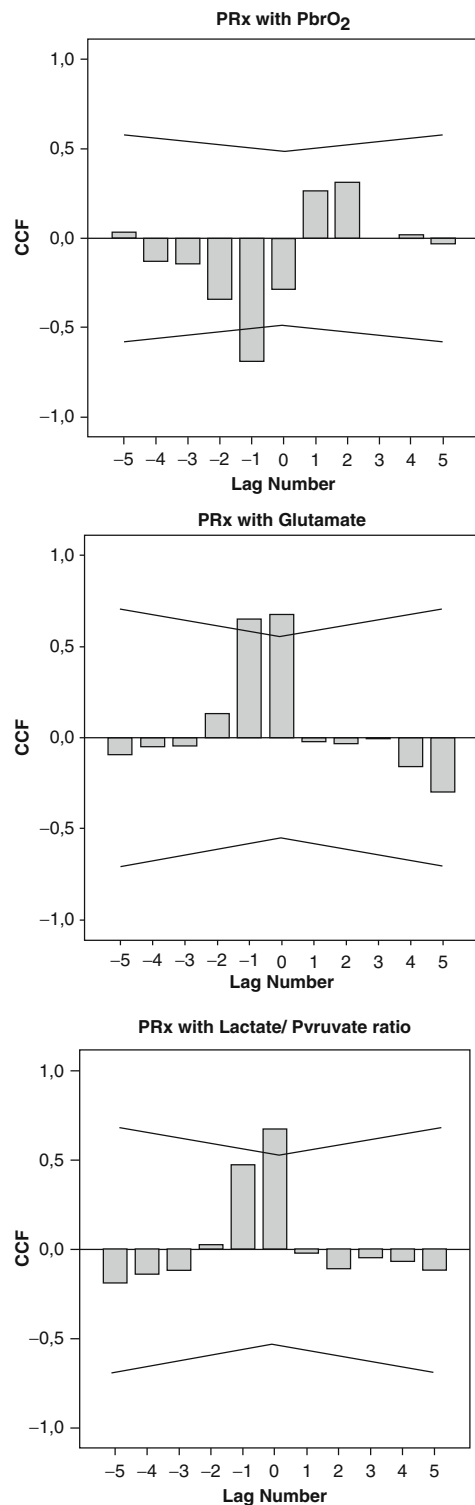


Fig. 1 Cross-correlation between the pressure-related autoregulation index (PRx) and $P_{br}O_2$, glutamate, and the lactate/pyruvate ratio when $PRx > 0.3$. The thin lines represent the upper and lower confidence limits; the bars represent the coefficient of correlation (CCF). The correlation of PRx with $P_{br}O_2$ and glutamate occurs during the time lag of -1 (-1 h). $P_{br}O_2$ is reversed (maybe because of the therapeutic increase in FiO_2) and does not correlate with PRx at the same time point (during lag number=0), but the significant correlation of glutamate persists. Lactate/pyruvate ratios correlate with PRx at the same time point

Discussion

In this study we were able to continuously assess cerebral vasomotor reactivity over a mean of 11.7 h in 17 swine with ICH without inducing changes in MAP. We defined CR by PRx , ORx or $FRx > 0.2$. That threshold was taken, considering the studies from Czosnyka et al. [6] where $PRx > 0.2$ could predict worse outcome in TBI patients. Considering the mean of each index of the whole monitoring period, we found two animals with impaired CR defined by abnormal PRx , two animals where ORx and FRx were elevated (>0.2), and one animal where PRx , ORx and FRx were abnormal. Nevertheless, most animals had periods where some indices were positive, alternating with periods where indices were negative.

In our study, probes were implanted into peri-hemorrhagic tissue, a place where we think more metabolic and vascular changes take place during the first hours post-hemorrhage. We decided to monitor in this location based on the assumption of an especially vulnerable perihemorrhagic boundary zone, where secondary ischemic injuries are more likely to occur. Several studies have found impaired autoregulation in this area of primarily non-ischemic tissue [5, 13]. In stroke models tissue acidosis is considered to be one factor responsible for the loss of autoregulation. In our correlations we found that changes in oxygen, lactate/pyruvate and glutamate correlated with changes in PRx in the next hour.

One advantage of the selected method of autoregulation assessment is that we could not only measure autoregulation as normal or impaired, but with quantification according to the grade of correlation in every index. Using different threshold levels of correlation we found that when PRx is closer to +1, extracellular concentrations of lactate/pyruvate and glutamate are increased.

PRx has been shown to react dynamically to changes in cerebral perfusion pressure [14]. Many studies in head-injured patients validated PRx by additional methodology, such as the PET-CBF static rate of autoregulation [15] and the TCD-based index Mx [2] correlated this index with a state of low CBF and cerebral metabolic rate of oxygen. The PRx is easier to monitor over prolonged periods of time than the TCD-based indices as it does not require fixation of external probes [7].

On the other hand, Dohmen et al. [5] found that the lactate/pyruvate ratio was higher in patients with malignant infarction as early as 24 h after stroke, and it was closely correlated with ORx , supporting the assumption that tissue acidosis might be involved in the impairment of autoregulation in peri-infarct tissue. ICH could share some part of the pathophysiology with those stroke patients, such as reperfusion leading to increased local production of reactive oxygen species [16] damaging arteriolar smooth muscles, vasogenic edema with a space-occupying effect with secondary

ischemia when CPP is outside the physiological range [17]. Similarly, a vicious cycle leads to propagation of the damage to primary healthy tissue. Impaired autoregulation could be an important parameter for identifying secondary damage, especially when microdialysis is not available. CPP adjustment could potentially reverse the damage and the impaired autoregulation [15].

It has been stated that cerebral autoregulation is not disturbed in the first 24 h after ICH [18]. Based on our results, additional monitoring, such as microdialysis might help to distinguish the random periods of positive PRx from those that really represent CR disruption, even when ICP is under 20 mmHg. Therapeutic strategies could be tried using this model, to see whether impaired CR can be reversed, while validating with microdialysis.

Conclusion

We found evidence for impaired cerebral vasomotor activity in a porcine model of ICH. The findings suggest that at least PRx abnormalities could be associated with microdialysis alterations during the first 12 h after ICH.

Conflict of interest statement We declare that we have no conflict of interest.

References

1. Daley ML, Pourcyous M, Willis A, Leffler CW (2002) Variation of proposed correlation indices of cerebrovascular reactivity with change of arteriolar diameter. *Acta Neurochir Suppl* 81:151–153
2. Czosnyka M, Smielewski P, Kirkpatrick P, Laing RJ, Menon D, Pickard JD (1997) Continuous assessment of the cerebral vasomotor reactivity in head injury. *Neurosurgery* 41(1):11–17; discussion 17–19
3. Diedler J, Sykora M, Rupp A, Poli S, Karpel-Massler G, Sakowitz O et al (2009) Impaired cerebral vasomotor activity in spontaneous intracerebral hemorrhage. *Stroke* 40(3):815–819
4. Bijlenga P, Czosnyka M, Budohoski KP, Soehle M, Pickard JD, Kirkpatrick PJ, et al (2010) “Optimal cerebral perfusion pressure” in poor grade patients after subarachnoid hemorrhage. *Neurocrit Care* [Internet]. 2010 Apr 20; available from: <http://www.ncbi.nlm.nih.gov/pubmed/20405341>
5. Dohmen C, Bosche B, Graf R, Reithmeier T, Ernestus R, Brinker G et al (2007) Identification and clinical impact of impaired cerebrovascular autoregulation in patients with malignant middle cerebral artery infarction. *Stroke* 38(1):56–61
6. Czosnyka M, Balestreri M, Steiner L, Smielewski P, Hutchinson PJ, Matta B et al (2005) Age, intracranial pressure, autoregulation, and outcome after brain trauma. *J Neurosurg* 102(3):450–454
7. Czosnyka M, Brady K, Reinhard M, Smielewski P, Steiner LA (2009) Monitoring of cerebrovascular autoregulation: facts, myths, and missing links. *Neurocrit Care* 10(3):373–386
8. Bellander B, Cantais E, Enblad P, Hutchinson P, Nordström C, Robertson C et al (2004) Consensus meeting on microdialysis in neurointensive care. *Intensive Care Med* 30(12):2166–2169
9. Qureshi AI, Ali Z, Suri MFK, Shuaib A, Baker G, Todd K et al (2003) Extracellular glutamate and other amino acids in experimental intracerebral hemorrhage: an in vivo microdialysis study. *Crit Care Med* 31(5):1482–1489
10. Hemphill JC, Morabito D, Farrant M, Manley GT (2005) Brain tissue oxygen monitoring in intracerebral hemorrhage. *Neurocrit Care* 3(3):260–270
11. Jaeger M, Schuhmann MU, Soehle M, Meixensberger J (2006) Continuous assessment of cerebrovascular autoregulation after traumatic brain injury using brain tissue oxygen pressure reactivity. *Crit Care Med* 34(6):1783–1788
12. Barth M, Woitzik J, Weiss C, Muench E, Diepers M, Schmiedek P et al (2010) Correlation of clinical outcome with pressure-, oxygen-, and flow-related indices of cerebrovascular reactivity in patients following aneurysmal SAH. *Neurocrit Care* 12(2):234–243
13. Paulson OB, Strandgaard S, Edvinsson L (1990) Cerebral autoregulation. *Cerebrovasc Brain Metab Rev* 2(2):161–192
14. Czosnyka M, Smielewski P, Kirkpatrick P, Piechnik S, Laing R, Pickard JD (1998) Continuous monitoring of cerebrovascular pressure-reactivity in head injury. *Acta Neurochir Suppl* 71:74–77
15. Steiner LA, Coles JP, Johnston AJ, Chatfield DA, Smielewski P, Fryer TD et al (2003) Assessment of cerebrovascular autoregulation in head-injured patients: a validation study. *Stroke* 34(10):2404–2409
16. Aronowski J, Hall CE (2005) New horizons for primary intracerebral hemorrhage treatment: experience from preclinical studies. *Neurol Res* 27(3):268–279
17. McDonald C, Carter BS (2002) Medical management of increased intracranial pressure after spontaneous intracerebral hemorrhage. *Neurosurg Clin N Am* 13(3):335–338
18. Reinhard M, Neunhoeffer F, Gerds TA, Niesen W, Buttler K, Timmer J et al (2010) Secondary decline of cerebral autoregulation is associated with worse outcome after intracerebral hemorrhage. *Intensive Care Med* 36(2):264–271

Evidence of Spreading Depolarizations in a Porcine Cortical Intracerebral Hemorrhage Model

Berk Orakcioglu, Yoichi Uozumi, Modar M. Kentar, Edgar Santos, Andreas Unterberg, and Oliver W. Sakowitz

Abstract Objectives: To evaluate whether cortical spreading depolarizations (CSD) occur in the early stage after cortical intracerebral hemorrhage (ICH).

Methods: Ten anesthetized male swine were examined over 19 h. Two cerebral probes were inserted around the ICH (microdialysis and thermodiffusion cerebral blood flow), ICP was monitored contralaterally and up to two electrocorticographic grid electrodes were positioned over the hemisphere after hemicraniectomy and dural opening. A right frontal autologous, arterial ICH (3.0 mL) was induced in all the animals studied.

Results: Using a modified injection technique an 80% success rate in ICH formation could be achieved. Eight animals with cortical ICH could be analyzed finally. After induction of ICH, ICP increased non-significantly. Overall, six out of eight animals had CSDs, of either single type or clusters. In one animal a CSD occurred as early as 2 h after ICH; in all other animals the first CSD did not occur before 5 h after onset.

Conclusion: CSD's occur in cortical experimental ICH. As ICP remained stable owing to the hemicraniectomy we cannot argue in favor of ICP-related triggering of CSD. Modifications of the experimental setup avoiding hemicraniectomy may better describe the pathophysiology of CSD related to ICH in future studies.

Keywords ICH • Cortical spreading depolarization • ECoG • Multiparametric monitoring

B. Orakcioglu (✉)

Department of Neurosurgery, Ruprecht-Karls-University,
Im Neuenheimer Feld 400, 69120 Heidelberg, Germany
e-mail: berk.orakcioglu@med.uni-heidelberg.de

Y. Uozumi

National Defense Medical College, Tokorozawa, Japan

M.M. Kentar, E. Santos, A. Unterberg, and O.W. Sakowitz
Department of Neurosurgery,
Ruprecht-Karls-University,
Heidelberg, Germany

Introduction

Many contributing factors to edema growth in the perihemorrhagic zone (PHZ) of spontaneous intracerebral hemorrhage (ICH) have been discussed recently. Cortical spreading depolarization (CSD) is a electrophysiological phenomenon that influences microvascular perfusion and thereby leads to local ischemia, increases in intracranial pressure (ICP) and an increase in secondary neuronal injury, e.g., in patients suffering subarachnoid hemorrhage [1, 2]. Currently, no experimental data are available suggesting such mechanisms in ICH. Intending to describe the existence and propagation of CSD in ICH, we established electrocorticographic (ECoG) monitoring in an established porcine ICH model.

Materials and Methods

Animal Preparation

Animal protocols for the experiments were approved by the institutional animal care and use committee. A standardized operative setup was followed as described elsewhere [3]. Ten male swine were anesthetized with ketamine (10 mg/kg), midazolam (5 mg/kg), and azaperone (40 mg/kg) administered by intramuscular injection. Animals were orally intubated and mechanically ventilated ($F_iO_2=0.3$). Anesthesia was maintained using 1.5% isoflurane inhalation during the operative procedure. During the monitoring episodes the inhaled fraction of isoflurane was reduced to 0.6%. Rectal and brain temperature (T_r , T_{br}) were continuously monitored. Rectal temperature was maintained between 35.5°C and 37°C. After surgical exposure of the right femoral artery a 4-Fr catheter was placed for permanent monitoring of mean arterial blood pressure (MAP). A venous line was placed in the right ear vein and capillary oxygen saturation (SO_2) was monitored from the left ear.

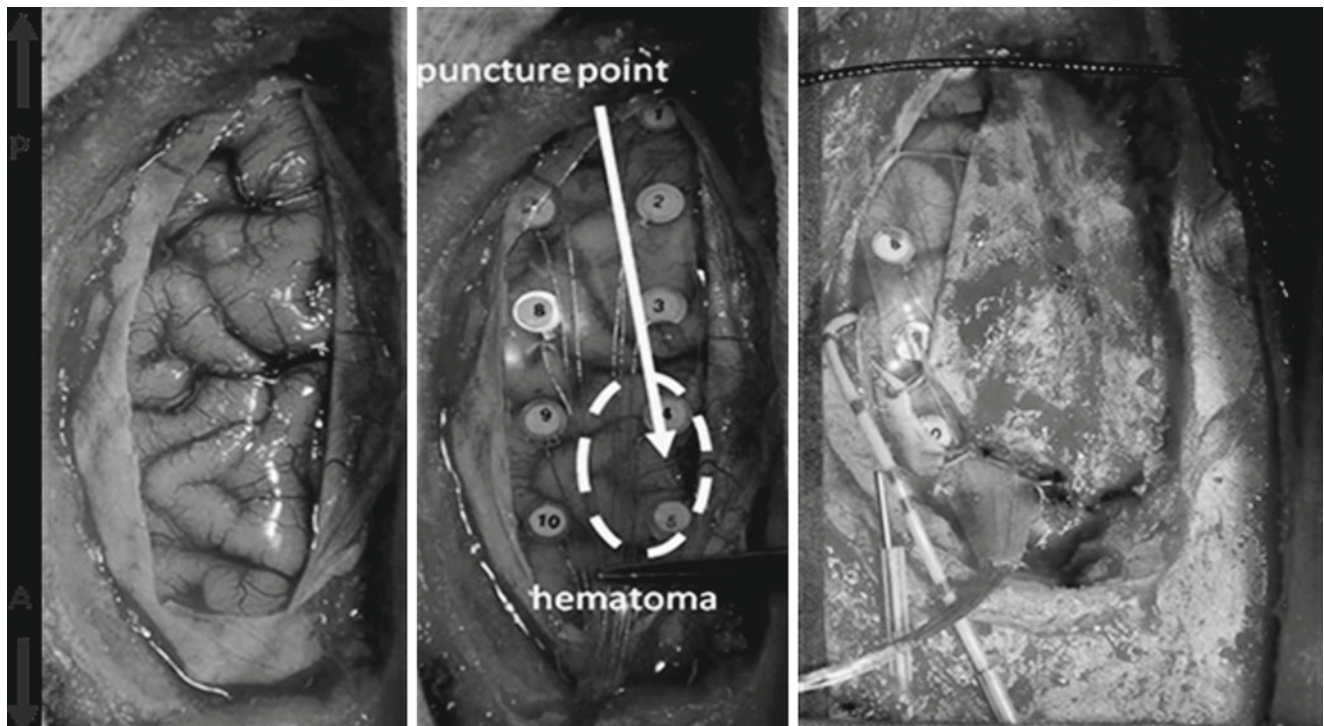


Fig. 1 Arrows indicating anterior (A) and posterior (P). Porcine cortical hemisphere after craniectomy and dural opening (*left*), followed by placement of a grid electrode (10-channel). ECoG electrode positioning and hematoma puncture point and approximate maximum intracranial

hemorrhage (ICH) extent are demonstrated (*center*). Complete monitoring setup with microdialysis, td-CBF probe, and ECoG-grid after dural closure is shown (*right*). Please note that a decompressive effect resulted despite dural re-adaption

Operative Procedure

A hemicraniectomy was performed over the right hemisphere. After dural opening the bridging veins were coagulated and cut. One burr hole was placed contralaterally to allow for placement of an ICP probe (Neurovent-P®, Raumedic AG, Helmbrechts, Germany). Up to two ECoG grid electrodes (each 2×5) were carefully introduced temporally and fronto-parietally. Two monitoring probes were inserted next to each other pre-coronally in close proximity to the ICH site. Medially, the thermodiffusion regional CBF probe (Hemedex td-rCBF, Codman®, Raynham, MA, USA), followed by the microdialysis (MD) probe (CMA 70, Solna, Sweden) more laterally, were positioned (Fig. 1). All intraparenchymal devices were introduced and secured transcutaneously before insertion into the brain. An equilibration period of 2 h was allowed for the probes to run in and the animals to stabilize. Further, a 90° bent 20 G steel cannula for induction of the ICH was introduced frontally, which was located 1.5 cm in front of the coronal suture and 0.8 cm lateral to the sagittal suture. In eight animals an autologous arterial hematoma was successfully created following the description of Qureshi et al. [4] and Hemphill et al. [5]. The injected hematoma volume was 3.0 mL. Following first experiences with the injection method

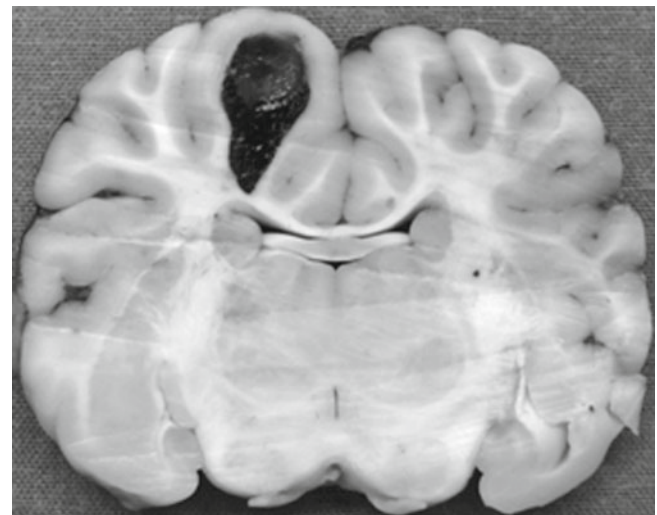


Fig. 2 Typical cortico-subcortical ICH in the right frontal lobe with extension to the fronto-parietal region. Total ICH volume was confirmed after sectioning of the brain post mortem

described we adapted the technique and used a 90° bent steel 20 G cannula. After catheter placements and ICH injection, the dura was carefully readapted, still allowing some decompressive effect. Thereafter, monitoring was conducted for up to 19 h. Post mortem, the cranial vaults

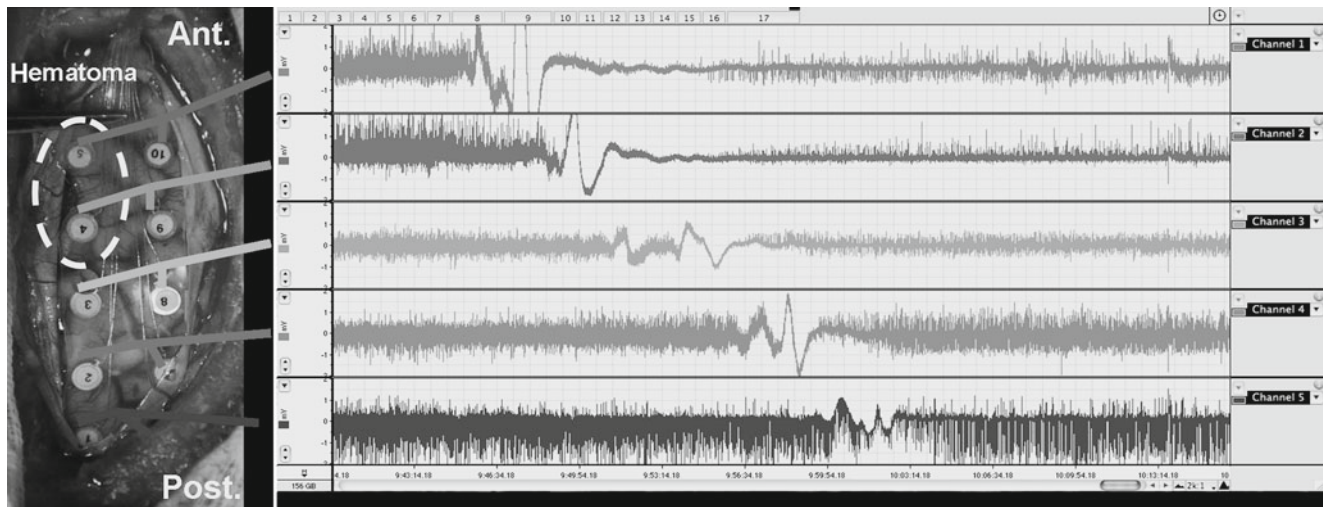


Fig. 3 Original ECoG recording episode (32 min) of an individual animal with a cortical ICH. Interelectrode distance was 4 mm. A cortical spreading depolarization (CSD) with a propagating velocity of 2.7–4.7 mm/min is shown. To facilitate the interpretation of CSD migration

grey-scale bars indicate propagation direction in this bipolar five-channel recording. CSD occurs primarily in the immediate surrounding hematoma, advancing peripherally

were opened completely, brains were removed, and intraparenchymal catheter locations and ICH size and position were macroscopically inspected (Fig. 2).

Monitoring

All relevant physiological parameters, such as mean arterial pressure (MAP), intracranial pressure (ICP), cerebral perfusion pressure (CPP), brain and rectal temperature (T_b , T_r), heart rate (HR), oxygen saturation (SO_2), and rCBF were continuously recorded. Microdialysates were perfused with a rate of 0.3 μ L/min and samples were taken every 30 min. The experiments did not test any therapeutic measure.

Results

We achieved our goal of ICH formation rate using the modified ICH injection technique with the steel cannula in 8 out of 10 animals (80%). During the experiments no ICP increases could be detected. Using bipolar and at a later stage monopolar ECoG recordings early CSD propagation was detected in six out of eight animals (Fig. 3). The spatial resolution could be improved by adding a second ECoG grid electrode, which was placed temporally (not shown). This resulted in a 16-channel recording. CSD occurred after 1.75 h in one animal; in all other animals CSD could not be

detected before 4.5 h after ICH onset. Propagation velocities ranged from 2.7 to 8.2 mm/min. We found single CSD events in two animals, two CSD events in one animal, and clusters of CSDs in the three remaining animals. The ECoG-related findings of these experiments are summarized in Table 1.

Discussion

Our study demonstrated the presence of cortical spreading depressions in an experimental ICH model. CSDs originated from the penumbral hematoma surrounding and migrated along the cortical surface of the cerebral hemisphere examined. The theory that cerebral ischemia contributes to secondary neuronal injury after ICH has been discussed in several publications. There is an ongoing debate about the existence of a “perihemorrhagic ischemic penumbra” [4–7]. CSDs have been proposed to play an important role in the genesis of ischemia in different cerebrovascular diseases [1, 3, 8, 9]. We aimed to identify its impact on the development of the perihemorrhagic edema and/or ischemia. Therefore, this study was performed on the basis of a multimodal monitoring approach with cerebral probes used in the clinical setting (ICP, CBF, and microdialysis). In this study first results of the establishment of the ECoG monitoring and first evidence of the existence of CSD in cortical experimental ICH are presented.

Injection difficulties are common issues in experimental ICH. Once craniotomies and dural opening have been

Table 1 Table summarizing ECoG-related data in all animals.

No.	Monitoring duration (h)	1st CSD after ICH	No. of CSDs	Propagating speed of CSD (mm/min)	Shape of CSDs
1	10	8 h 48 m	1	2.7–4.7	CSD
2	11	No CSD	0		
3	12	8 h 28 m	8	5	CSD
4	14	No CSD	0		
5	16	1 h 43 m	36	4–5	CSD
6	18.5	10 h 48 m	1	8.2	CSD
7	12	4 h 30 m	40	2.5–4	PID-like
8	19	7 h 35 m	2	5–8.2	CSD

CSD cortical spreading depression, *PID* peri-infarct depolarization

performed the tissue resistance will be reduced and the success rate of ICH formation will be significantly reduced. Because of this we adapted the injection method using a modified 90° angled 20 G steel cannula, which reliably led to the formation of consistent ICH of the intended volume. Although ICP remained within normal limits in 6 out of 8 animals (75%), CSD were seen. Improvements in the ECoG monitoring and extension from one-grid to two-grid recording allowed for monopolar recordings with a high spatial resolution.

There are limitations to our study. We do not present histological correlates to our findings. Continuous technical modifications of the experimental setup do not allow accurate analyses of all the monitoring data acquired in relation to the occurrence of CSDs at present.

Conclusion

Further investigations using this model may contribute to the knowledge of CSD pathophysiology, propagation mechanisms and impact on secondary neuronal damage in ICH.

Conflict of interest statement We declare that we have no conflict of interest.

References

1. Bosche B, Graf R, Ernestus R, Dohmen C, Reithmeier T et al (2010) Recurrent spreading depolarizations after subarachnoid hemorrhage decreases oxygen availability in human cerebral cortex. *Ann Neurol* 67:607–617
2. Dreier JP, Major S, Manning A, Woitzik J, Drenckhahn C et al (2009) Cortical spreading ischaemia is a novel process involved in ischaemic damage in patients with aneurysmal subarachnoid haemorrhage. *Brain* 132:1866–1881
3. Dohmen C, Sakowitz OW, Fabricius M, Bosche B, Reithmeier T et al (2008) Spreading depolarizations occur in human ischemic stroke with high incidence. *Ann Neurol* 63:720–728
4. Qureshi A, Ali Z, Suri M, Shuaib A, Baker G et al (2003) Extracellular glutamate and other amino acids in experimental intracerebral hemorrhage: an in vivo microdialysis study. *Crit Care Med* 31:1482–1489
5. Hemphill J, Morabito D, Farrant M, Manley G (2005) Brain tissue oxygen monitoring in intracerebral hemorrhage. *Neurocrit Care* 3:260–270
6. Carhuapoma J, Wang P, Beauchamp N, Keyl P, Hanley D et al (2000) Diffusion-weighted MRI and proton MR spectroscopic imaging in the study of secondary neuronal injury after intracerebral hemorrhage. *Stroke* 31:726–732
7. Orakcioglu B, Becker K, Sakowitz O, Herweh C, Kohrmann M et al (2008) MRI of the perihemorrhagic zone in a rat ICH model: effect of hematoma evacuation. *Neurocrit Care* 8:448–455
8. Fabricius M, Fuhr S, Bhatia R, Boutelle M, Hashemi P et al (2006) Cortical spreading depression and peri-infarct depolarization in acutely injured human cerebral cortex. *Brain* 129:778–790
9. Dreier JP, Woitzik J, Fabricius M, Bhatia R, Major S et al (2006) Delayed ischaemic neurological deficits after subarachnoid haemorrhage are associated with clusters of spreading depolarizations. *Brain* 129:3224–3237

Spontaneous Cortical Spreading Depression and Intracranial Pressure Following Acute Subdural Hematoma in a Rat

B. Alessandri, J. Stephan Tretzel, Axel Heimann, and Oliver Kempfski

Abstract Acute subdural hemorrhage (ASDH) is a frequent and devastating consequence of traumatic brain injury. Tissue damage develops rapidly and makes treatment even more difficult. Management of increased intracranial pressure (ICP) due to extravasated blood volume and brain swelling is often insufficient to control all adverse effects of ASDH. In addition to sheer volume, spontaneously triggered cortical spreading depression (CSD) that leads to cell death following ischemia or trauma may contribute to injury development after ASDH. Therefore, we explored the occurrence of CSD by tissue impedance (IMP) measurement in a rat model subjected to ASDH. IMP and intraventricular and mean arterial pressure were monitored before (baseline), during (blood infusion), and after ASDH for 3 h.

Tissue impedance increased by around 203% of baseline during subdural infusion of 300 µl of autologous, venous blood and dropped back to baseline within 22 min. Fifty-six minutes after the start of ASDH a cluster of four short-lasting (3–3.5 min; 140–160% of baseline) IMP increases started that reflected spontaneous CSDs. This pattern presumes that CSD occurs early after ASDH and therefore may contribute to the rapid lesion development in this disease.

Keywords Cortical spreading depolarization • Acute subdural hematoma • Ischemia • Brain injury • Rat

Introduction

Cortical spreading depression (CSD) is an electrophysiological phenomenon that was first described experimentally by Leão [14]. He found that spontaneous cortical activity is depressed for several minutes following electrical or mechanical stimulation and that this phenomenon spreads from the origin of stimulation. In uninjured tissue CSD is transient. Leão [15] also reported CSD following global ischemia. Since then CSD has been described in various animal models of human diseases [11, 20, 22, 25] and recently also in human patients [5, 7, 9].

Massive disturbance of ionic homeostasis is a basic reaction of CSD. These shifts lead to cell swelling and shrinkage of the extracellular space. Restoration of normal conditions is energy-dependent and the brain copes with vasodilatation [14]. Under pathophysiological conditions (e.g., focal ischemia), however, inverse hemodynamic reactions are observed in regions with pre-existing compromised blood flow. In this case gradients of cerebral blood flow (CBF), oxygen and glucose exist that allow initial persistent, anoxic depolarization in the ischemic core to become a transient depolarization in the surrounding tissue, with reduced CBF and energy supply and a CSD in healthy tissue [12, 16–18, 21].

Consequently, vasoconstriction and increased energy demand lead to cell death in the peri-ischemic area around the core, thereby expanding the injury.

Such a chain of events may also play a crucial role in lesion development in acute subdural hemorrhage. Extravasated blood causes elevated intracranial pressure with ischemia [13, 23]. It seems that factors other than extravasated blood volume alone are important for cell death [3]. Superfusion of cortex with hemolysis products K⁺ and hemoglobin led to focal ischemic damage, which was associated with the occurrence of CSD in rats [6]. Thus, neurotoxicity of a blood-derived product is aggravated by spontaneous, local CSD-induced vasoconstriction. As ASDH pathophysiology includes focal ischemia as well as the effects of blood-derived factors, CSD may play a key role in lesion development in this model. As a first step we tested the

B. Alessandri (✉), J.S. Tretzel,
A. Heimann, and O. Kempfski
Institute for Neurosurgical Pathophysiology,
University Medicine of the Johannes Gutenberg-University Mainz,
D-55131 Mainz, Germany
e-mail: beat.alessandri@unimedizin-mainz.de

feasibility of tissue impedance measurement for assessing CSDs in our model of ASDH in one rat. Here, we report for the first time, to our knowledge, the occurrence of CSD following ASDH, indicating the role played by CSD in lesion development in this particular disease.

Materials and Methods

A male Sprague–Dawley rat (Charles River, Germany) was anesthetized by i.p. injection of chloral hydrate. The initial dose was 36 mg/100 g body weight. To keep the animal under anaesthesia 36 mg was given hourly. The rat was intubated and mechanically ventilated.

Surgical preparation for ASDH is described in detail elsewhere [1, 3]. Briefly, tail artery and jugular vein were cannulated with polyethylene tubing for blood pressure (MAP) monitoring and blood withdrawal, respectively. For ASDH a craniotomy was drilled over the left cortex. An L-shaped, blunted G23-needle was inserted underneath the dura mater. The needle was fixed with Histoacryl® (B-Braun, Germany) and Palavit® 55VS (Heraeus/Kulzer, Germany).

Anterior to the Bregma suture (AP = 2 mm; ML = 2.5–3 mm) small burr holes were drilled to insert impedance electrodes (IMP), made from two stainless steel wires covered in polyvinyl chloride for electrical insulation except for the sharp-pointed tips. Impedance was measured at 1 kHz (10 mV, bias-free). Changes in tissue impedance were accompanied by DC shifts during CSD [20]. Contralateral intraventricular pressure (IVP) was monitored through a G26-needle. IMP electrodes and IVP needle were fixed with Histoacryl®.

Parameters were measured during a 10-min baseline, ASDH induction with 300 µl non-heparinized, autologous venous blood (6 min) and a 180-min post-ASDH period. After the end of monitoring the rat was returned to the home cage for 7 days. Thereafter, it was perfusion-fixed transcardially (0.9% NaCl, 4% paraformaldehyde). Brain was post-fixed for 24 h and embedded in paraffin wax. Sections 3 µm thick were cut throughout the visible lesion at a distance of 250 µm and stained with hematoxylin–eosin. The lesioned area on each section was measured using Optimas 6.1, which received digitized images from a CCD SuperColor CV950 camera (Denmark) mounted on a Zeiss Axiopod 2Plus.

Results

The animal displayed a Cushing reflex during blood infusion that lasted around 20 min. Mean arterial blood pressure rose from 74 mmHg immediately before ASDH to a maximum of 97 mmHg at 9 min after the start of blood infusion. MAP had

normalized at the end of monitoring (73 mmHg). IVP increased from the baseline value of 4.8 mmHg to 32.4 mmHg shortly after the end of blood infusion. Thereafter, IVP dropped to stable levels of around 13 mmHg within 15 min and finally reached 11.7 mmHg. IMP recordings ranged from 2096 to 4988 Ω. All values were normalized to baseline (100%). Subdural blood infusion initiated an elevation of IVP starting within 45 s, whereas IMP remained stable for 90 s (Fig. 1a–c). IVP continued to increase steadily; however, IMP rose quickly to a maximal level of 203% of baseline during the first 5 min of blood infusion (IVP = 23.7 mmHg; Fig. 1c). IMP recovered to baseline within 22 min. A first, short-lasting IMP increase, which reflected spontaneous spreading depression was recorded at 56 min after the start of blood infusion. A total of 4 CSD were observed within the 3-h observation period (Fig. 1a) and each lasted 3–3.5 min (Fig. 1b). Amplitudes reached between 140 and 160% of baseline. Lesion volume at day 7 post-ASDH was 52.9 mm³.

Discussion

Our study demonstrates for the first time the occurrence of spontaneous cortical spreading depolarization following ASDH in a rat. CSDs were recorded using electrodes detecting tissue impedance that reflects CSD assessed by DC potential [19, 20, 24]. CSD is an electrophysiological phenomenon with little impact on healthy tissue. Under pathological conditions like experimental stroke or traumatic brain injury CSD is known to affect cell survival negatively. In an international effort to detect CSD and its impact on injury development in humans CSDs were found following stroke [5], subarachnoid hemorrhage [8], and traumatic brain injury (see also COSBID and [4, 9]). As in most experimental studies, CSDs seem to worsen outcome after injury in patients too.

A main feature of CSD is a disturbance of ionic homeostasis, which results in cell swelling and shrinkage of the extracellular space. ATP production is increased to restore homeostasis. Consequently, dilatation of resistance vessels occurs for increased blood flow, which improves oxygen and glucose delivery. Despite this reaction extracellular glucose remains persistently decreased following KCl-induced CSD [10], imposing a risk to tissue that is already compromised after injury. This is important because an inverse hemodynamic response to CSD is observed in the peri-infarct and peri-contusional microvasculature. Instead of vasodilatation a vasoconstriction is coupled with depolarization in this region. The resulting perfusion deficit aggravates the need for energy substrates. This is seen in prolonged negative shifts of DC potentials and is referred to as cortical spreading ischemia [6, 12, 21, 22]. This pathomechanism in the peri-infarct area leads to cell death and rapid expansion of the lesion [21].

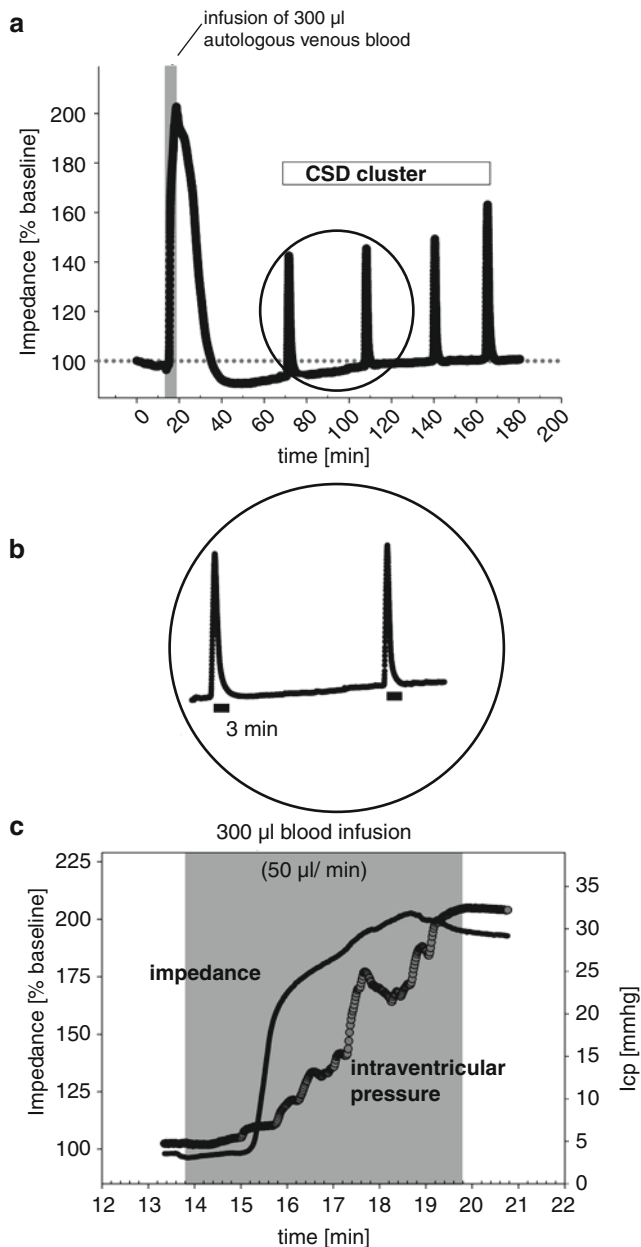


Fig. 1 Increase in tissue impedance after injection of autologous blood and during following episodes of CSD (**a** and **b**). Increase in tissue impedance (**c**) and intraventricular pressure following blood injection

An acute subdural hemorrhage induces focal ischemia underneath the blood clot and brings blood constituents close to brain tissue. Within hours a large ischemic region can be observed by histology and MRI [2, 3, 23]. Generally, it is thought that increased ICP is the main cause of the damage underneath the blood clot. Recently, it became evident that other factors (e.g., thrombin, complement) play an additional role in early lesion development following subdural hemorrhage, see Baechli et al. [3]. Dreier and co-workers demonstrated nicely that products of hemolysis (hemoglobin, K⁺)

on the surface of cortical tissue induce a large ischemic lesion within 48 h. This was due to evoked CSD and a concomitant drop in CBF [6]. Therefore, we speculated that CSD participates in lesion development after ASDH and tried to show CSD in our rodent model of ASDH.

As an equivalent of the measurement of CSD by DC potentials we assessed changes in tissue impedance (IMP). Shrinkage of the extracellular space due to cell swelling leads to increased resistance for AC current between two poles [20, 24]. Electrical stimulation or KCl injection induces immediate but inverse changes in IMP and DC potential. IMP changes also correlated with local CBF increases in healthy tissue and decreases in the peri-infarct area following venous ischemia. The same study reported a significant correlation between spontaneous CSD and the lesion [20]. Thus, IMP is an equivalent measurement to CSD, although it does not record the depolarization of neurons directly.

Monitoring of tissue impedance before, during, and after induction of ASDH showed that during subdural blood infusion a steep increase in IMP occurred. This two-fold elevation was then reversed back to baseline levels within 22 min. During the first 90 s of subdural blood infusion IMP trailed behind the slowly increasing intracranial pressure. Later on IMP did not follow the steady ICP increase, but increased much more quickly to its maximal value (Fig. 1c). These two time courses suggest that cells start to swell within 90 s and that compression of the extracellular space by an extravasated blood volume was not solely responsible for IMP changes. This is supported by the fact the IVP returned to lower and stable values within 9 min of the end of blood infusion, whereas IMP needed almost 16 min. Furthermore, IVP remained elevated by 6–8 mmHg compared with baseline values, but IMP reached baseline values completely.

In addition to this initial time-course of IMP a cluster of four short-lasting IMP increases, i.e., CSDs, occurred thereafter. Fifty-six minutes after the start of blood infusion a first 3-min CSD was observed (Fig. 1a/b). Shape and duration of these peaks are comparable to those found by Otsuka et al. using a model of venous ischemia and KCl injections [20]. CSDs appeared approximately every 35 min. Such clusters seem to be an important factor determining the risk of lesion development [7]. In patients with subarachnoid hemorrhage a cluster consisted of 2.6 events/h. In the present case, 4 CSDs occurred within less than 2 h.

Conclusion

The significance of acute and delayed neuronal cell death has to be elucidated in further studies. Although many experimental and clinical studies support a relationship between the occurrence of CSD in injured tissue and outcome a recent

study by von Baumgarten [25] suggested otherwise. Controlled cortical impact injury in mice elicited 0.38 CSD/h, but contusion volume could not be increased by additional KCl-induced CSDs. We recorded >2 CSD/h in our single experiment. Whether this cluster can be repeated and whether it is harmful for lesion development has to be proven by additional experimentation using this model of ASDH. However, the occurrence of CSD within the first hour of ASDH highlights this phenomenon as a potential factor for rapid lesion development in this disease.

Acknowledgement We thank A. Ehlert, L. Kopacz, F. Kafai, and M. Malzahn for their excellent technical support. Data from this study form part of the doctoral thesis of J.S. Tretzel.

Conflict of interest statement We declare that we have no conflict of interest.

References

- Alessandri B, Nishioka T, Heimann A, Bullock RM, Kempinski O (2006) Caspase-dependent cell death involved in brain damage after acute subdural hematoma in rats. *Brain Res* 1111:196–202
- Alessandri B, Tsuchida E, Bullock RM (1999) The neuroprotective effect of a new serotonin receptor agonist, BAY X3702, upon focal ischemic brain damage caused by acute subdural hematoma in the rat. *Brain Res* 845:232–235
- Baechli H, Behzad M, Schreckenberger M, Buchholz HG, Heimann A, Kempinski O, Alessandri B (2009) Blood-induced brain edema, tissue death and depression of glucose metabolism in rat cortex after acute subdural hematoma is larger than after identical volumes of inert paraffin oil. *J Cereb Blood Flow Metab* 30:576–585
- COSBID (2010) Cooperative study on brain injury depolarisations
- Dohmen C, Sakowitz OW, Fabricius M, Bosche B, Reithmeier T, Ernestus RI, Brinker G, Dreier JP, Woitzik J, Strong AJ, Graf R (2008) Spreading depolarizations occur in human ischemic stroke with high incidence. *Ann Neurol* 63:720–728
- Dreier JP, Ebert N, Priller J, Megow D, Lindauer U, Klee R, Reuter U, Imai Y, Einhaupl KM, Victorov I, Dirnagl U (2000) Products of hemolysis in the subarachnoid space inducing spreading ischemia in the cortex and focal necrosis in rats: A model for delayed ischemic neurological deficits after subarachnoid hemorrhage? *J Neurosurg* 93:658–666
- Dreier JP, Major S, Manning A, Woitzik J, Drenckhahn C, Steinbrink J, Tolias C, Oliveira-Ferreira AI, Fabricius M, Hartings JA, Vajkoczy P, Lauritzen M, Dirnagl U, Bohner G, Strong AJ (2009) Cortical spreading ischaemia is a novel process involved in ischaemic damage in patients with aneurysmal subarachnoid haemorrhage. *Brain* 132:1866–1881
- Dreier JP, Woitzik J, Fabricius M, Bhatia R, Major S, Drenckhahn C, Lehmann TN, Sarrafzadeh A, Willumsen L, Hartings JA, Sakowitz OW, Seemann JH, Thieme A, Lauritzen M, Strong AJ (2006) Delayed ischaemic neurological deficits after subarachnoid haemorrhage are associated with clusters of spreading depolarizations. *Brain* 129:3224–3237
- Hartings JA, Strong AJ, Fabricius M, Manning A, Bhatia R, Dreier JP, Mazzeo AT, Tortella FC, Bullock MR (2009) Spreading depolarizations and late secondary insults after traumatic brain injury. *J Neurotrauma* 26:1857–1866
- Hashemi P, Bhatia R, Nakamura H, Dreier JP, Graf R, Strong AJ, Boutelle MG (2009) Persisting depletion of brain glucose following cortical spreading depression, despite apparent hyperaemia: evidence for risk of an adverse effect of Leao's spreading depression. *J Cereb Blood Flow Metab* 29:166–175
- Katayama Y, Maeda T, Koshinaga M, Kawamata T, Tsubokawa T (1995) Role of excitatory amino acid-mediated ionic fluxes in traumatic brain injury. *Brain Pathol* 5:427–435
- Kumagai T, Walberer M, Nakamura H, Endepols H, Sue M, Vollmar S, Adib S, Mies G, Yoshimine T, Schroeter M, Graf R Distinct spatiotemporal patterns of spreading depolarizations during early infarct evolution: evidence from real-time imaging. *J Cereb Blood Flow Metab* 31:580–592
- Kuroda Y, Bullock R (1992) Local cerebral blood flow mapping before and after removal of acute subdural hematoma in the rat. *Neurosurgery* 30:687–691
- Leão AAP (1944) Pial circulation and spreading depression of activity in the cerebral cortex. *J Neurophysiol* 7:391–396
- Leão AAP (1947) Further observations on the spreading depression of activity in the cerebral cortex. *J Neurophysiol* 10:409–414
- Nallet H, MacKenzie ET, Roussel S (1999) The nature of penumbra depolarizations following focal cerebral ischemia in the rat. *Brain Res* 842:148–158
- Nallet H, MacKenzie ET, Roussel S (2000) Haemodynamic correlates of penumbral depolarization following focal cerebral ischaemia. *Brain Res* 879:122–129
- Nedergaard M, Hansen AJ (1993) Characterization of cortical depolarizations evoked in focal cerebral ischemia. *J Cereb Blood Flow Metab* 13:568–574
- Ochs S, Van Harreveld A (1956) Cerebral impedance changes after circulatory arrest. *Am J Physiol* 187:180–192
- Otsuka H, Ueda K, Heimann A, Kempinski O (2000) Effects of cortical spreading depression on cortical blood flow, impedance, DC potential, and infarct size in a rat venous infarct model. *Exp Neurol* 162:201–214
- Shin HK, Dunn AK, Jones PB, Boas DA, Moskowitz MA, Ayata C (2006) Vasoconstrictive neurovascular coupling during focal ischemic depolarizations. *J Cereb Blood Flow Metab* 26:1018–1030
- Strong AJ, Anderson PJ, Watts HR, Virley DJ, Lloyd A, Irving EA, Nagafuji T, Ninomiya M, Nakamura H, Dunn AK, Graf R (2007) Peri-infarct depolarizations lead to loss of perfusion in ischaemic gyrencephalic cerebral cortex. *Brain* 130:995–1008
- Tsuchida E, Alessandri B, Corwin F, Fatouros P, Bullock R (1999) Detection of ultra-early brain damage after acute subdural hematoma in the rat by magnetic resonance imaging. *J Neurotrauma* 16:595–602
- van Harreveld A (1957) The extracellular space in the vertebrate central nervous system. In: Bourne GH (ed) *The structure and function of nervous tissue*, vol IV. Academic Press, New York and London, pp 447–509
- von Baumgarten L, Trabold R, Thal S, Back T, Plesnila N (2008) Role of cortical spreading depressions for secondary brain damage after traumatic brain injury in mice. *J Cereb Blood Flow Metab* 28:1353–1360

The Peptide AF-16 and the AF Protein Counteract Intracranial Hypertension

Hans-Arne Hansson, Mohamed Al-Olama, Eva Jennische, Kliment Gatzinsky, and Stefan Lange

Abstract Intracranial hypertension develops after, for example, trauma, stroke and brain inflammation, and contributes to increased morbidity, mortality, and persistent neuropsychiatric sequelae. Nonsurgical therapy offers limited relief. We investigated whether the peptide AF-16 and the endogenous protein *Antisecretory Factor* (AF) counteracted abnormal fluid transfer by cells, and lowered raised intracranial pressure (ICP). Adult rats, infected with an encephalitogenic Herpes simplex virus (HSV-1), developed after 5 days' sickness of increasing severity. AF-16 rescued all rats while vehicle treatment only saved 20%. AF-16 from day 4 reduced the ICP in HSV-1-infected rats from 30.7 to 14.6 mmHg and all survived without sequelae. A standardised closed head brain injury in rats raised the ICP. Continuous and intermittent AF-16 kept ICP at an almost normal level. A single dose of AF-16 maintained the raised ICP after a TBI lowered during 3–9 h. The AF protein, enriched in egg yolk, similarly lowered the post-traumatically raised ICP in rats. AF-16 also lowered the ICP in rabbits with diffuse brain injury. We conclude that the peptide AF-16 and the AF protein offer new approaches to treat raised ICP with no side effects.

Keywords Raised intracranial pressure • Herpes simplex virus encephalitis • Neurotrauma • Sagittal rotational acceleration head and neck impulse • Head injury management • Traumatic brain injury • Brain herniation • Antisecretory factor • S5a

H.-A. Hansson (✉), E. Jennische, and S. Lange
Institute of Biomedicine, Sahlgrenska Academy, University of Gothenburg, P.O. Box 440, SE 40530 Göteborg, Sweden
e-mail: hans-arne.hansson@anatcell.gu.se

M. Al-Olama
Institute of Biomedicine, Sahlgrenska Academy, University of Gothenburg, P.O. Box 440, SE 40530 Göteborg, Sweden and Department of Neurosurgery, Sahlgren's University Hospital, SE-41345 Göteborg, Sweden

K. Gatzinsky
Department of Neurosurgery, Sahlgren's University Hospital, SE-41345 Göteborg, Sweden

Introduction

Raised intracranial pressure (ICP) commonly evolves after a head trauma, stroke, blast, intracranial haemorrhage, brain tumour, inflammation or infection [2, 5, 16]. Intracranial hypertension disturbs the blood circulation and hampers the exchange of nutrients, oxygen and metabolites. The turnover of cerebrospinal fluid (CSF) is impaired and the brain parenchyma is concomitantly mechanically distorted and even dislocated by the elevated ICP, especially if pressure gradients develop. The ICP reflects the balance between the close to fixed craniospinal volume and its ability to accommodate additionally added volume to the incompressible content. Swelling of the brain owing to cytotoxic oedema prevails at intracellular fluid accumulation, most evidently in astrocytes [2, 5, 12, 15, 16]. Leakage from blood vessels, i.e. vasogenic or extracellular oedema, and haemorrhage, increases preferentially the extracellular fluid volume. The volumes of brain parenchyma, blood and CSF may vary dynamically. The cytotoxic and the vasogenic mechanisms are concomitantly operative and thereby their relative contributions to elevated ICP may undergo rapid changes. There is presently no medical treatment that safely and persistently counteracts intracranial hypertension [5, 14, 16]. Treatment with osmotic or hypertonic agents relieves mostly only for a few hours and is often associated with side effects. Surgical measures to improve drainage of the cerebrospinal fluid (CSF) or craniotomy may become necessary as does intensive care [5, 16, 17]. Improved non-surgical management is thus demanded to keep the ICP sustained at a sufficiently low level for extended time periods at no or minimal side effects, beneficial for a large number of victims.

The endogenous protein *Antisecretory Factor* (AF) counteracts and normalises disturbed transfer of fluid through cell membranes and cells [8, 9, 11, 18]. AF is in addition anti-inflammatory [3, 11, 18]. A striking observation is that the protein AF and the peptide AF-16 do not affect normal cells and tissues, not even at a high dose [4, 6, 11, 18]. The biomedical effects mentioned are exerted by

an eight amino acid sequence at the amino terminal end of the AF protein [9]. A synthetic peptide, named AF-16, with the amino acid sequence *VCHSKTRSNPENNVGL*, which includes the active antisecretory motive of the AF protein, has been demonstrated to be stable and suitable for experimental work.

The aim of the present study was to evaluate effects of AF-16 on raised ICP evolving after brain inflammation and an experimentally induced traumatic brain injury (TBI). Time windows for the ICP lowering effects by AF-16 and AF will be discussed. Further, differences in effects of AF and AF-16 on injured brains will be elucidated.

Materials and Methods

Animals

Male Sprague–Dawley rats, 190 ± 20 g, (B & W AB, Stockholm, Sweden; $n=90$) and female adult albino New Zealand rabbits (2.3–3 kg b.w.; $n=15$; local breeder) were purchased. Care was taken to keep the number of animals as low as possible and to minimise their suffering. Permission was granted by the Regional Animal Experiments Ethical Committee and the experiments performed in accordance with local and national guidelines (EU 86/609/EEC).

Chemicals

The peptide AF-16 (*VCHSKTRSNPENNVGL*) [9] was synthesised and characterised by Ross Pedersen A/S, Copenhagen, Denmark. The AF protein was supplied as freeze dried egg yolk (B221®; Lantmännen AS-Faktor AB, Stockholm, Sweden) and manufactured from eggs from hens that had received special feed [11]. Isoflurane was purchased from Baxter, and all other chemicals from Sigma-Aldrich.

Treatment with AF-16, AF Protein and SPC

Osmotic minipumps (Alzet® 2001 or 2002), containing AF-16 in phosphate buffered saline (PBS) or just the vehicle, PBS, and prestarted, were implanted subcutaneously in the back of rats for continuous delivery for several days. Further, AF-16 in PBS was either instilled intranasally (i.n.) twice daily or infused intravenously at doses and times indicated. The AF protein, supplied as B221®, was dissolved in the drinking fluid and supplied to rats ad libitum.

Herpes Simplex Virus Type I Encephalitis

Anaesthetised rats were infected by nasal instillation of 25 µL of a diluted solution of an encephalitogenic *Herpes simplex virus type I* (HSV-1) strain, # 2762, originally isolated from a human fatal case of herpes simplex encephalitis (HSE). Matched normal rats received an equal volume of the vehicle, PBS. The animals were sacrificed when distinct symptoms of neurological dysfunction, i.e. HSE, appeared. From either day 1 or day 4 AF-16 in 25 µL PBS was instilled twice daily in the right nostril under deep isoflurane anaesthesia, while additional rats had the vehicle, 25 µL PBS. The ICP was measured with a miniature light optical system (Samba 3200; Samba Sensors AB, V. Frölunda, Sweden) in anaesthetised rats for at least 1 h from day 3–14 [7, 10]. In most experiments two pressure sensors were implanted in parallel, one in each hemisphere. Brains were eventually fixed in 4% formaldehyde in buffered saline and then processed for immunohistochemical investigations to map prevalence and distribution of HSV-1 antigen or for histopathological analysis of stained thin sections [7]. The distribution of viral DNA was investigated and real-time PCR analyses performed to reveal whether AF-16 exerted any effects.

Focal Brain Injury

Rats, anaesthetised by isoflurane inhalation, had the calvarium incised and freed from adherent tissue. A copper rod (144 g) with a tip diameter of 4 mm, immersed in liquid nitrogen, was then applied to the right parietal bone for 30 s, inducing a brain tissue necrosis measuring 3 mm in diameter with a depth of ~1 mm. Great care was taken to keep the exposure conditions reproducible. All animals survived and none showed any obvious signs of impairment. The weight gain was checked and found to be the same as for littermates not subjected to any treatment, except for the day of surgery. The extent of brain damage was visualised with 2,3,5-triphenyl tetrazolium chloride (TTC), which stains living tissue red while non-vital areas were pale and unstained. The ICP was measured as described above.

Diffuse Brain Injury

Rabbits were exposed to a sagittal rotational acceleration trauma to the head and neck, which induced a diffuse brain injury [10]. The ICP increased in a day and the response to AF-16 was then determined.

Results

Normal ICP

The ICP in normal adult rats was 5.3 ± 2.1 mmHg ($n=15$), and varied with the exact position of the head and thorax and with age (Fig. 1a). No rhythmically appearing ICP peaks, either single or in clusters, were demonstrable. Treatment of normal adult rats with 25 μ g AF-16 intranasally neither induced any significant alteration of the ICP, nor any side effects.

HSV-1 Infected and AF-16 Treated Rats

The treatment of HSV-1 infected rats with 1 μ g AF-16 intranasally (i.n.) twice daily for 2 weeks increased the survival rate from 14% for those only having had the vehicle to 40% ($p<0.001$) [7]. AF-16, 25 μ g, i.n., twice daily starting from day 4 rescued all infected rats, i.e. 100% survived. Further, none of the infected rats that had 25 μ g AF-16 developed any signs of sickness, or any late neurological malfunctions. Intermediate survival rate was achieved with 10 μ g AF-16 twice daily. Thus, AF-16 rescued rats with HSE in a dose-dependent manner. We then tried to find out the reason for the beneficial effects of AF-16 regarding the highly significantly improved survival rate. AF-16 changed neither the distribution nor prevalence of HSV-1 antigen, nor the replication of virus DNA. There was no obvious difference in the distribution of reactive cell alterations after the vehicle or AF-16. When measuring the ICP on day 6 we documented that the vehicle-treated HSV-1-infected rats had a mean ICP of 30.7 mmHg ($n=24$), sometimes being as high as 47.9 mmHg. Those animals were sick and suffered obvious neurological malfunctions. Treatment with 25 μ g AF-16 from day 4 to day 14 twice daily i.n. reduced the mean ICP to 14.6 mmHg ($n=14$), and the maximal ICP among HSE rats treated with AF-16 was 21.0 mmHg. A single dose of AF-16 reduced the ICP in rats with distinct signs of HSE within 30 min, and could approach ambient pressure in about 1 h. The lowered ICP persisted for several hours while the rats appeared improved.

Freeze Damage to the Brain and AF-16

Freezing on the exposed parietal bone with a copper probe, chilled by prior immersion in liquid nitrogen, generated a shallow cone-shaped necrosis in the underlying parietal brain

parenchyma. The ICP increased in 24 h to 22.9 mmHg ($n=21$) and remained at an elevated level the next day (Figs. 1b and 2). Two sensors were used in parallel in most of the experiments, enabling demonstration of the ICP in the contralateral brain hemisphere exceeding that in the primarily injured, ipsilateral brain hemisphere by several mmHg. Pressure waves, commonly ranging from 6 to 17 mmHg, and lasting about a minute, occasionally with an amplitude as high as 52 mmHg, were recorded in the injured brains. AF-16, 1 mg/day and kg b.w., infused with the aid of subcutaneously implanted Alzet osmotic minipumps to normal rats for up to 7 days did not alter the ICP. In contrast, the same infusion of AF-16 to rats from 6 h after a freezing injury reduced the mean ICP to about half, i.e. 11.3 ± 2.9 mmHg ($n=9$), and there were no longer any recognisable pressure peaks. There were no side effects by AF-16 or any gross changes in behaviour and weight. Nasal instillation of AF-16 to rats after a freezing injury to the brain kept the ICP from day 2 to day 7 at a significantly lowered level, 10.7 ± 3.4 mmHg ($n=14$; Figs. 1c and 2). After AF-16 administration, the ICP in the cryogenically injured right hemisphere was slightly higher than that in the contralateral brain half, while the opposite was true prior to treatment with AF-16 (Fig. 2). A single nasal instillation of 1 mg/kg b.w. of AF-16 to rats on day 2 after a brain injury resulted in the ICP starting to decrease after a delay of about 30 min, and in 1 h reduced ICP levels were recorded. The ICP lowering effect lasted at least 3 h.

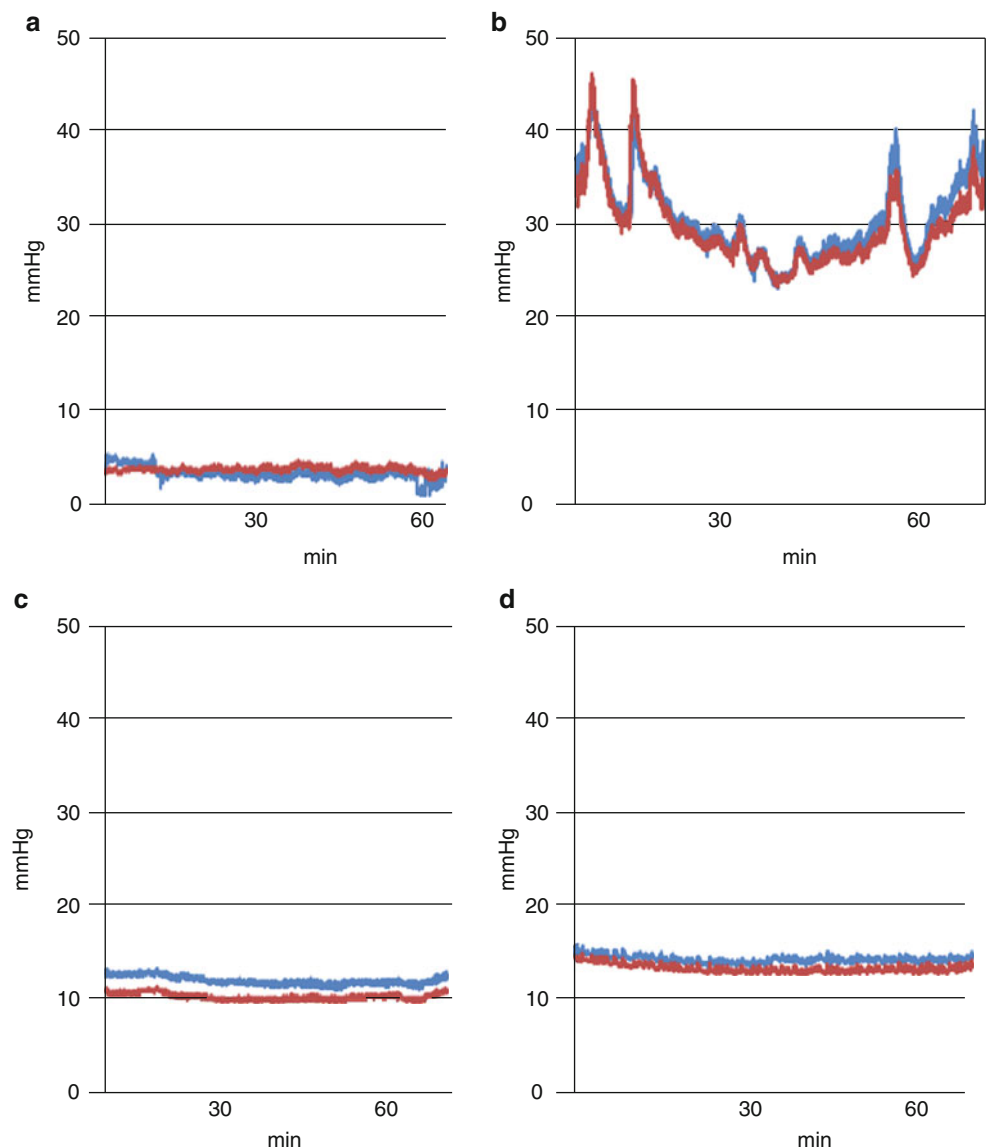
Freeze Damage to Rat Brain and the Protein AF

Rats with freeze-injured brains had the protein AF (B221®; Salovum™) added to their drinking water for the next 7 days from 3 h after the trauma. The mean ICP on days 2–3 and day 5 were 13.8 and 11.9 mmHg respectively (Fig. 1d). Thus, the protein AF (B221®) was efficient at lowering post-traumatically raised ICP.

Diffuse Brain Injury in Rabbit Brains and AF-16

Rabbits were exposed to a sagittal rotational acceleration trauma, which induced a diffuse brain injury [10]. The ICP, measured by a Samba pressure sensor inserted into the brain parenchyma, increased and after 2 days reached 17.7 mmHg. Intravenous infusion of 0.5 mg/kg b.w. AF-16 twice daily transiently reduced in 1 h the ICP to 5.3 mmHg and it remained at about that level for at least another 2 h. No side effects were demonstrable.

Fig. 1 Intracranial pressure (ICP) recordings in rats. Two sensors were used in parallel, implanted in the brain parenchyma, the *blue* in the left and the *red* one in the right hemisphere. **(a)** Shows a normal rat with an ICP, 3–4 mmHg, with minor variations in amplitude during a 1-h recording. **(b)** Illustrates the raised ICP, with prominent variations in amplitude, 3 days after a freezing injury to the brain. Note the pressure peaks. **(c)** Demonstrates that intranasal AF-16 twice daily for 3 days after a brain injury keep the ICP at 10–12 mmHg. **(d)** Shows the ICP from a rat with a brain injury that had received the protein AF (B221®) supplied with the drinking water for 3 days, reducing the ICP to about 14–15 mmHg



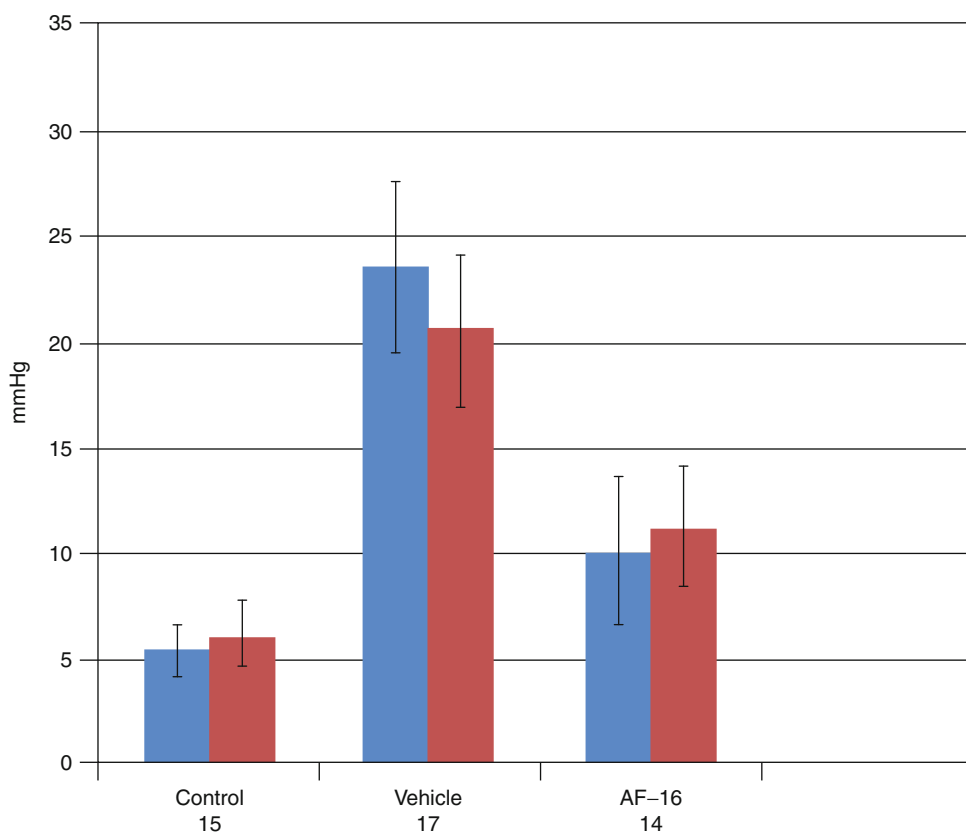
Discussion

A key finding in the present study was that both continuous and intermittent, i.e. twice daily, administration of the peptide AF-16 reproducibly and significantly reduced the raised ICP developing after HSE and after experimentally induced focal and diffuse brain injuries. The pressure lowering effect by AF-16 lasted as long as the treatment was going on, i.e. in the present study in rats, up to 2 weeks. A single dose of AF-16 reduced the elevated ICP after a TBI with a delay of about 30 min and the ICP reduction persisted for at least 3 h. Further, treatment with AF-16 at efficient doses, whether continuous or intermittent long-term delivery or acute administration of a single dose, abolished the evolvement of pressure peaks, prevalent at severe brain injuries. We could further demonstrate that the AF protein (B221®) lowered raised ICP. These results advocate that the peptide AF-16

and the protein AF have in common the ability to transiently reduce and, in some cases even normalise, raised ICP at TBI and HSE. Previous reports have disclosed that an eight amino acid long sequence at the amino terminal end of the AF protein is responsible for the antiseptory activity [9, 11]. The shared chemical structure prevalent is a specific eight amino acid sequence that counteracted oedema irrespective of whether it was caused by a viral infection or a trauma.

The pathogenesis to raised ICP is complex, but a major contributing factor is the rigid cranium and vertebral column, which only allows limited volume expansion [5, 13, 16]. In humans, the brain tissue accounts for about 80% of the intracranial volume while the blood in the vascular system, the extracellular fluid and the cerebrospinal fluid (CSF) contributes the rest. The glial cells constitute a larger fraction of the brain parenchyma than the neurons [1, 2, 16]. An increase

Fig. 2 Intracranial pressure (ICP) from rats on day 2 after a brain injury due to freezing on the right parietal skull bone. The normal, low ICP from control rats contrasts with the increased ICP recorded after treatment twice daily with the vehicle, PBS, intranasally. AF-16 twice daily intranasally reduced the mean ICP to about half. Note that the ICP in the left hemisphere (*blue*) is higher than that in the right (*red*) at vehicle treatment



in any of these intracranial constituents, which is not balanced by a reduction of another, will eventually result in raised ICP. The experimental systems utilised in the present study resulted in mixed cytotoxic and vascular oedema. A histopathologically prominent feature was the swelling of the astrocytes, not only in the penumbra, but throughout the brain parenchyma. A considerable portion of the excess fluid was obviously trapped in astrocytes. We consider that the ICP lowering effects of AF-16 and AF are due to their ability to facilitate the outflow of excessive cell fluid, resulting in reduction of fluid accumulated and immobilised in cells, mainly astrocytes, in the injured and inflamed brain parenchyma. An observation of key importance is that neither AF-16 nor the AF protein seemed to influence the distribution of fluid in normal tissues and organs.

The ICP recordings revealed the prevalence of pressure peaks, often in clusters, demonstrable at both HSE and TBI. Treatment with AF-16 or AF blunted such pressure peaks. We consider such an effect beneficial, as it is likely to reduce the risk of brain damage due to impaired blood circulation, disturbed metabolism and mechanical distortion.

An unexpected result was that nasal instillation of AF-16 lowered the raised ICP whether induced by virus or by a trauma. Studies are in planning to investigate in more detail whether AF-16 is taken up and distributed preferentially by the vascular system or by neuronal mechanisms, e.g. axonal transport.

Conclusion

Both the peptide AF-16 and the protein AF counteracted the raised ICP developing as a consequence of serious brain damage, whether due to viral encephalitis or a TBI. Beneficial effects were demonstrable in both rodents and in rabbits. Both continuous systemic and intermittent delivery of AF-16 and the AF protein kept the ICP at a level low enough not to impair or even injure. A single dose of AF-16 induced a reduction of the abnormally high ICP after a delay of about half an hour and the lowered ICP was maintained for several hours. An important result was that a single dose of AF-16 reduced the IFP even if applied several days after the induction of brain damage. No focal or systemic side effects were observed. It is tempting to advocate the future use of AF-16 and the AF protein to treat human disorders associated with abnormal fluid distribution in the brain and spinal cord as well as intracranial hypertension.

Acknowledgements The authors are grateful to Svante Höjer, Samba Sensors AB, for advice and support, Dr. Hong Zhu and Ms. Iris Gustafsson, Histocenter AB, for performing the immunohistochemistry, and Ms I. Jonson and Ms. M. Rosenkvist for invaluable technical help and support. Supported by grants from the Swedish Government under the LUA/ALF agreement (grant # 71570), Sahlgren's University Hospital (grant # 83030), the Ministry of High Education UAE, JK Jubileumsfond, Magnus Bergvall Foundation, W. and M. Lundgren

Foundation, Frimurare-Barnhus direktionen, Göteborg Medical Society, AB Nectin, and Lantmännen AS-Faktor AB.

Conflict of interest statement E. Jennische, S. Lange and H.-A. Hansson declare potential financial conflict of interest because of patents and patent applications. M. Al-Olama and K. Gatzinsky have no financial conflict of interest.

References

1. Barres BA (2008) The mystery and magic of glia: a perspective on their roles in health and disease. *Neuron* 60:430–440
2. Blumbergs P, Reilly P, Vink R (2008) Trauma. In: Love S, Louis DN, Ellison DW (eds) *Greenfield's neuropathology*, 8th edn. Arnold, London, pp 733–832
3. Davidson TS, Hickey WF (2004) Antisecretory factor expression is regulated by inflammatory mediators and influences the severity of experimental autoimmune encephalomyelitis. *J Leukoc Biol* 74:835–844
4. Eriksson A, Shafazand M, Jennische E, Lange S (2003) Effect of antisecretory factor in ulcerative colitis on histological and laboratory outcome: a short period clinical trial. *Scand J Gastroenterol* 38:1045–1049
5. Greenberg M (2010) *Handbook of neurosurgery*, 7th edn. Thieme, Berlin
6. Hanner P, Rask-Andersen H, Lange S, Jennische E (2010) Antisecretory factor-inducing therapy improves the clinical outcome in patients with Meniere's disease. *Acta Otolaryngol* 130:223–227
7. Jennische E, Bergström T, Johansson M, Nyström K, Tarkowski A, Hansson H-A, Lange S (2008) The peptide AF-16 abolishes sickness and death at experimental encephalitis by reducing increase of intracranial pressure. *Brain Res* 1227:189–197
8. Johansson E, Lönnroth I, Lange S, Jonson I, Jennische E, Lönnroth C (1995) Molecular cloning and expression of a pituitary gland protein modulating intestinal fluid secretion. *J Biol Chem* 270:20615–20620
9. Johansson E, Lange S, Lönnroth I (1997) Identification of an active site in the antisecretory factor protein. *Biochim Biophys Acta* 1362:177–182
10. Krave U, Höjer S, Hansson H-A (2005) Transient, powerful pressures are generated in the brain by a rotational acceleration impulse to the head. *Eur J Neurosci* 21:2876–2882
11. Lange S, Lönnroth I (2001) The antisecretory factor: synthesis, anatomical and cellular distribution and biological action in experimental and clinical studies. *Int Rev Cytol* 210:39–75
12. Leestma JE (2008) *Forensic neuropathology*, 2nd edn. Raven, New York
13. Lundberg N (1960) Continuous recording and control of ventricular fluid pressure in neurosurgical practice. *Acta Psychiatr Scand* 36(149):1–193
14. Marklund N, Bakshi A, Castelbuono DJ, Conte V, McIntosh TK (2006) Evaluation of pharmacological treatment strategies in traumatic brain injury. *Curr Pharm Des* 12:1645–1680
15. Oehmichen M, Auer RN, König HG (2005) *Forensic neuropathology and associated neurology*. Springer, Heidelberg
16. Reilly PL, Bullock R (2005) *Head injury: pathophysiology and management*, 2nd edn. Hodder Arnold, London
17. Sahuquillo J (2009) Decompressive craniectomy for the treatment of refractory high intracranial pressure in traumatic brain injury. *Cochrane Database Syst Rev* 2:1–44
18. Ulgheri C, Paganini B, Rossi F (2010) Antisecretory factor as a potential health promoting molecule in man and animals. *Nutr Res Rev* 23:300–313

Influence of Isoflurane on Neuronal Death and Outcome in a Rat Model of Traumatic Brain Injury

Daniel Hertle, Christopher Beynon, K. Zweckberger, B. Vienenkötter, C.S. Jung, K. Kiening, Andreas Unterberg, and Oliver W. Sakowitz

Abstract In the developing brain agents clinically used for the purpose of analgo-sedation can cause severe neurodegeneration. In patients with TBI analgo-sedation is a first-line treatment for intracranial hypertension. At the same time, damaged neuronal networks undergo conformational changes and use developmental mechanisms to restore brain function. Inhibition of repair mechanisms by sedatives may cause brain dysfunction and neuronal cell death during development and after traumatic brain injury. To test this hypothesis, the influence of sedation was experimentally evaluated in a controlled cortical impact injury model (CCII). One experimental group was preconditioned with regular sedation (isoflurane 1.0 MAC₅₀) and the second group with deep sedation (isoflurane 1.67 MAC₅₀). After controlled cortical impact injury (CCII) we tested the outcome at 4 h and 48 h using histological methods and a neurological test. Increased apoptosis was found in referenced cortical areas as early as 48 h after trauma (TUNEL-positive cells/field of view, mean \pm SEM, 116.6 \pm 9.3 and 45.3 \pm 4.1, both $n = 12$). Along with histological findings neurological outcome was worst as indicated by a higher score in the experimental group with deep sedation (mean \pm SEM 4 h, 13.9 \pm 0.6, $n = 14$ and 20 \pm 0.7, $n = 15$; 48 h, 8.1 \pm 0.6, $n = 14$ and 13.3 \pm 0.6, $n = 15$). Although blood pressure was lower with deep sedation, no frank hypotension occurred. In our experiments deep sedation with high doses of isoflurane caused neurodegeneration and worse outcome compared with regular sedation.

Keywords Traumatic brain injury • TBI • Neuronal death • Isoflurane • Outcome • Sedation

D. Hertle (✉), C. Beynon, K. Zweckberger, B. Vienenkötter, C.S. Jung, K. Kiening, A. Unterberg, and O.W. Sakowitz
Department of Neurosurgery, University Hospital Heidelberg,
INF 400, D-69120 Heidelberg, Germany
e-mail: daniel.hertle@med.uni-heidelberg.de

Introduction

Anesthetic-induced apoptosis is a well-recognized cause of severe neurodegeneration during development. Anesthetics, including all commonly used hypnotics, such as clonazepam, diazepam, isoflurane, ketamine, midazolam, phenobarbital, propofol, sevoflurane and others, affect neuronal survival in a dose-dependent manner [1–4]. In patients with traumatic brain injury (TBI) extensive analgesia and sedation is a first-line treatment for intracranial hypertension. At the same time, damaged neuronal networks undergo conformational changes to restore brain function. Neurite outgrowth and formation of new synapses after brain injury show similarity with developmental alterations and depend on neuronal activity [5, 6]. Although the pathways promoting drug-dependent apoptotic signals during development are not well understood, it seems reasonable to assume similar effects after injury to the brain. The aim of the current study was to investigate the effect of anesthetics on neuroregeneration after TBI. The effect of preconditioning with regular and deep sedation on neuronal survival and neurological outcome after controlled cortical impact injury was studied.

Materials and Methods

Twenty-nine mature Sprague–Dawley rats underwent a left-sided craniotomy and preconditioning with volatile analgo-sedation including N₂O/O₂ (7:3) and isoflurane at a regular sedation (1.0 MAC₅₀) or deep sedation: (1.67 MAC₅₀). Blood pressure, oxygenation and EcoG were continuously monitored during this procedure. After 2 h of sedation a focal brain lesion was created using the controlled cortical impact injury (CCII) model. We then tested neurological outcome after 4 and 48 h, transcardially perfused the animal with fixative, and determined the number of apoptotic (terminal transferase dUTP nick end labeling [TUNEL]-positive) cells after 48 h.

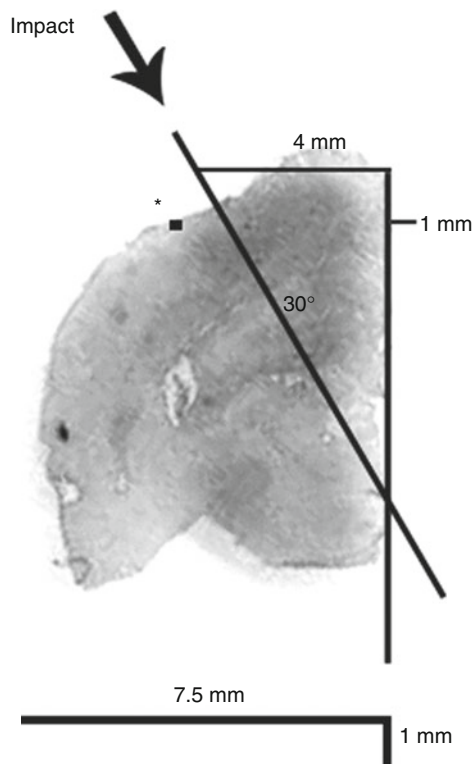


Fig. 1 Controlled cortical impact injury. Site of impact is measured and marked using the stereotactic frame. Pneumatic driven bolt is set at 30° angle and 1.5 mm penetration depth. Sequential coronal cryosections are used for the TUNEL method (imaged slice shown) and referenced to the impact site using Paxinos' *The Rat Brain in Stereotaxic Coordinates*. (*) Region of interest for apoptotic cell count is found 1 mm from the margo superior cerebri at a 90° angle on the cortical surface

Controlled Cortical Impact Injury

We used a pneumatic driven impact device with photoelectric barrier controlled impact velocity at 7 m/s and a bolt tip size of 3–5 mm. For reproducible lesions we used a referenced setup (Fig. 1).

Neurological Outcome

Outcome was assessed 4 and 48 h after brain trauma using a standardized test sequence [7]. For the inclined plane test the rat was placed in the center of an angulated board several times (score 0–30). A higher score indicated worse outcome.

We report here in brief our recent results. Analysis of additional neurological and histological experiments in the animals reported here is currently being conducted.

Result

The main aim of this study was to determine cortical damage and neurological deterioration after preconditioning with two concentrations of isoflurane and traumatic brain injury. To assess cortical damage we counted apoptotic cells, visualized by TUNEL staining, in referenced cortical areas. We found a significant increase in TUNEL-positive cells after deep sedation with isoflurane 1.67 MAC₅₀ compared with regular sedation with isoflurane 1.0 MAC₅₀ (TUNEL+ cells/field of view, mean±SEM, 116.6±9.3 and 45.3±4.1, both $n=12$; Fig. 2). Under deep sedation, arterial oxygenation was unchanged and blood pressure was lower, but within normal range (mean arterial blood pressure range: 108.5, lower/upper 95% CI 104.4/112.7).

We tested both groups using an established test to determine the neurological outcome. To avoid a direct sedative effect of isoflurane on neurological outcome first tests were performed 4 h after discontinuation of analgesedation and re-evaluated 48 h after CCIL. In the inclined plane test we found significantly better outcome in the control group after preconditioning with isoflurane 1.0 MAC₅₀ compared with isoflurane 1.67 MAC₅₀ (mean±SEM 4 h, 13.9±0.6, $n=14$ and 20±0.7, $n=15$; 48 h, 8.1±0.6, $n=14$ and 13.3±0.6, $n=15$; Fig. 3).

In summary, these results suggest that preconditioning with deep sedation worsens apoptotic neurodegeneration and leads to loss of neurological function in rats with TBI.

Discussion

To date mostly beneficial effects of analgesedation after brain injury have been reported [8, 9]. The main objective of these studies was to demonstrate neuroprotection by an “energy saving mechanism”. By reducing brain activity, sedation allows energy consumption, and therefore vulnerability to secondary ischemic–hypoxic injuries, to be reduced. Given that the vast majority of energy is used to maintain normal neuronal homeostasis and only a small portion is used for electrical activity this seems a challenging approach to neuroprotection. Therefore, it is not entirely surprising that the neuroprotective effects of sedation failed to be translated into clinical benefit for the patient [8, 9]. In fact, investigation of isoflurane in models of ischemic brain injury has shown severe neurodegenerative effects in both rats and primates [10, 11]. This has not been demonstrated in experimental models of TBI. We have tested our hypothesis that sedatives might cause brain dysfunction and neuronal cell death in an animal model of contusional brain damage. Although the underlying

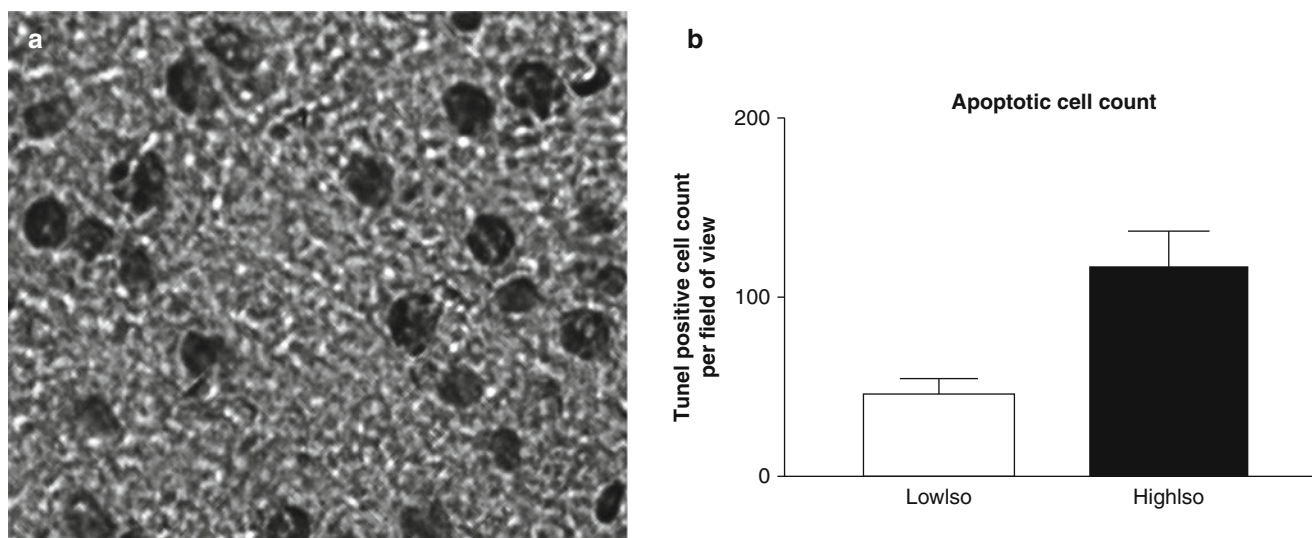


Fig. 2 Increasing isoflurane sedation results in a higher number of apoptotic cells 2 days after traumatic brain injury. (a) Sample tissue of apoptotic cell nuclei labeled with terminal transferase dUTP nick end labeling (TUNEL) method. (b) Comparison of preconditioning seda-

tion with isoflurane at low (*LowIso*) and high (*HighIso*) concentration. Increased alveolar concentration of isoflurane was accompanied by an increased count of TUNEL-positive cells

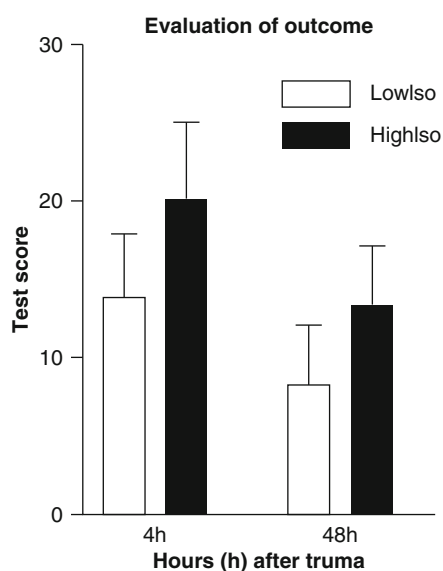


Fig. 3 Examination of neurological outcome 4 and 48 h after trauma. Inclined plane test was used to determine outcome after traumatic brain injury. A higher score indicates worse outcome. Outcome was better after preconditioning with a low (*LowIso*) concentration compared with a high (*HighIso*) concentration of isoflurane

mechanism is unknown, we think that preconditioning the brain with analgosedation might lead to reduced recovery of neuronal function after brain injury. Whether the balance of neuroprotective and neurodegenerative effects conferred by anesthetics is solely dose-dependent depends on application time or there are different cellular mechanisms is still to be investigated.

Although many analgetic and sedative drugs have been proven to cause neurodegeneration, we cannot exclude the possibility that the effect we observe is not caused by the primary neuromodulatory action of isoflurane, but by side-effects from a high dose of isoflurane. Testing other drugs that can be antagonized on their neural receptor may be helpful for a better understanding of the primary cause of neural activity-dependent neurodegeneration.

As the volatile anesthetic isoflurane was administered systemically, systemic reactions may also be relevant in causing neurodegeneration. Indeed, one of the most prominent issues is reduced blood pressure in sedated animals [11]. This might influence cerebrovascular reactivity, cerebral blood flow, microvascular perfusion and therefore cause additional damage. Based on the fact that all animals remained normotensive (no frank hypotension occurred in any of the experiments), we do not believe that this has influenced our results. In any case, further experiments are necessary to rule out this potential confounder.

Conclusion

The findings of this sedative preconditioning CCII study suggest an immediate impact of analgosedation on neurodegenerative processes after traumatic brain injury in the rat model. Apoptotic markers were markedly increased and neurological outcome was worsened after deep analgosedation.

Additional studies are needed to further delineate the longer-term impact of post-traumatic sedation and the pro-apoptotic cascades involved.

Conflict of interest statement We declare that we have no conflict of interest.

References

1. Bittigau P, Sifringer M, Genz K, Reith E, Pospischil D, Govindarajulu S, Dziatko M, Pesditschek S, Mai I, Dikranian K, Olney JW, Ikonomidou C (2002) Antiepileptic drugs and apoptotic neurodegeneration in the developing brain. *Proc Natl Acad Sci USA* 99(23):15089–15094
2. Liang G, Ward C, Peng J, Zhao Y, Huang B, Wei H (2010) Isoflurane causes greater neurodegeneration than an equivalent exposure of sevoflurane in the developing brain of neonatal mice. *Anesthesiology* 112(6):1325–1334
3. Young C, Jevtovic-Todorovic V, Qin YQ et al (2005) Potential of ketamine and midazolam, individually or in combination, to induce apoptotic neurodegeneration in the infant mouse brain. *Br J Pharmacol* 146:189–197
4. Fredriksson A, Pontén E, Gordh T, Eriksson P (2007) Neonatal exposure to a combination of N-methyl-D-aspartate and gamma-aminobutyric acid type A receptor anesthetic agents potentiates apoptotic neurodegeneration and persistent behavioral deficits. *Anesthesiology* 107(3):427–436
5. Jan YN, Jan LY (2010) Branching out: mechanisms of dendritic arborization. *Nat Rev Neurosci* 11(5):316–28, Review
6. Murphy TH, Corbett D (2009) Plasticity during stroke recovery: from synapse to behaviour. *Nat Rev Neurosci* 10(12):861–72
7. Zweckberger K, Simunovic F, Kiening KL, Unterberg AW, Sakowitz OW (2010) Anticonvulsive effects of the dopamine agonist lisuride maleate after experimental traumatic brain injury. *Neurosci Lett* 470(2):150–4, Epub 2010 Jan 5
8. Kawaguchi M, Furuya H, Patel PM (2005) Neuroprotective effects of anesthetic agents. *J Anesth* 19(2):150–6, Review
9. Kitano H, Kirsch JR, Hurn PD, Murphy SJ (2007) Inhalational anesthetics as neuroprotectants or chemical preconditioning agents in ischemic brain. *J Cereb Blood Flow Metab* 27(6):1108–28, Review
10. Drummond JC, Cole DJ, Patel PM, Reynolds LW (1995) Focal cerebral ischemia during anesthesia with etomidate, isoflurane, or thiopental: a comparison of the extent of cerebral injury. *Neurosurgery* 37(4):742–748
11. Nehls DG, Todd MM, Spetzler RF, Drummond JC, Thompson RA, Johnson PC (1987) A comparison of the cerebral protective effects of isoflurane and barbiturates during temporary focal ischemia in primates. *Anesthesiology* 66(4):453–464

Correlation of the Intracranial Pressure to the Central Venous Pressure in the Late Phase of Acute Liver Failure in a Porcine Model

Kathrin Scheuermann, Christian Thiel, Karolin Thiel, Wilfried Klingert, Elmar Hawerkamp, Johannes Scheppach, Alfred Königsrainer, Matthias H. Morgalla, Pamela Leckie, Andrew Proven, Rajiv Jalan, Nathan Davies, Martin U. Schuhmann, and Martin Schenk

Abstract Volume loading is a common method used to ensure adequate circulation. However, in the late phase of acute liver failure complications that often lead to death are cerebral swelling and brainstem edema, which are considered to result from increasing intracranial pressure (ICP). In former studies cerebral venous pressure (CVP) and ICP were reported to be independent entities. Acute liver failure was induced in 25 German land race pigs by acetaminophen intoxication. CVP and ICP were measured continuously. Hydroxyethyl starch solution and noradrenalin were administered to stabilize the circulation at a mean arterial pressure above 60mmHg. There is an increasing correlation in quantity and quality between the CVP and ICP in the last 24 h before exitus. Beginning with a slope of 0.24 (ICP against CVP) and a low correlation coefficient of 0.08. 24h before exitus, this situation remained stable until 16 h to exitus ($m = 0.22$, $r = 0.1$). The correlation increased from 16 to 8 h prior to exitus to a slope of $m = 0.5$ and a correlation of $r = 0.3$ and remained until exitus. In late acute liver failure it seems therefore clinically reasonable to keep circulation within an adequate range by the use of noradrenalin and to avoid fluid overload.

Keywords Intracranial pressure • Central venous pressure • Acute liver failure • Correlation

K. Scheuermann, C. Thiel, K. Thiel, W. Klingert, E. Hawerkamp, J. Scheppach, A. Königsrainer, and M. Schenk (✉)
Department of General, Visceral Transplant Surgery,
Tuebingen University Hospital,
Hoppe-Seyler-Strasse 3, 72076 Tuebingen, Germany
e-mail: martin.schenk@med.uni-tuebingen.de

M.H. Morgalla and M.U. Schuhmann
Department of Neurosurgery, Tuebingen University Hospital,
Tuebingen, Germany

P. Leckie, A. Proven, R. Jalan, and N. Davies
Liver Failure Group, UCL Institute of Hepatology,
Royal Free Campus, London, UK

Introduction

Acute liver failure (ALF) is a rare and life-threatening clinical syndrome following severe hepatic injury [3]. Two distinct complications contribute to high mortality in ALF: rapid development of massive hepatic necrosis and apoptosis give rise to severe hyperammonemia, hepatic encephalopathy, and life-threatening cerebral edema and brainstem edema [1, 3, 4, 12]. This is the consequence of an increase in the intracranial pressure (ICP), which is a major cause of death [4, 11]. The pathogenesis and the molecular mechanisms of cerebral edema in the setting of ALF remain controversial [2, 12] and the metabolic alterations for development of a high ICP are not fully understood [9]. However, there is evidence to suggest that in ALF cerebral hyperammonemia, cerebral hyperemia and pro-inflammatory cytokines may act synergistically to cause brain edema with its complications (intracranial hypertension, brain herniation) by swelling of cerebral glial cells, which may result in high ICP [9–12]. In ALF there is a good correlation between pro-inflammatory cytokines and ICP and this brain pro-inflammatory cytokine production was associated with uncontrolled ICP [13]. ALF induced an increase in extracellular brain ammonia, lactate and glutamate whose effects appear to be potentiated by systemic inflammation (especially the pro-inflammatory cytokine interleukin-1beta) and free radical formation as being the potential mediator of cellular dysfunction [2, 6, 12]. These findings suggest that the worsening of brain edema and its complications in ALF due to pro-inflammatory mechanisms might result from exacerbation of oxidative stress-related mechanisms [2].

All the complications of ALF are accompanied by an increase in ICP. In previous research studies it is described that the central venous pressure (CVP), the intra-abdominal pressure (IAP), and the positive end-expiratory pressure (PEEP) do not have a substantial influence on ICP and that there is no significant correlation between CVP and ICP [5, 10]. In the late phase of ALF volume loading in conjunction with an increase in central venous pressure (CVP) therefore seems to be an appropriate method to guarantee adequate circulation.

Other studies report that the cerebral blood volume increased in proportion to CVP, suggesting simple passive venous distention. Whether this could increase ICP and compromise cerebral perfusion remains unclear [8]. Increased IAP significantly increased CVP above and below the diaphragm, ICP, and mean blood pressure (MBP). There were no changes in cerebral perfusion pressure [7].

Materials and Methods

Study Design

A total of 25 female German domestic pigs weighing 30–50 kg were used in this study. These pigs were intoxicated with acetaminophen through a duodenal catheter until acute liver failure (ALF) was established. ALF was defined as partial thromboplastin time (PTT) <0.3 and designated the Time ALF (T_{ALF}) = 0. The pigs were sedated, ventilated and received full intensive care for the entire period. All pigs continuously underwent cardiac and respiratory monitoring plus hourly blood gas analysis until death. Cerebral microdialysis samples were collected every hour, arterial blood was withdrawn every 4–8 h and tissue samples at $T_{\text{ALF}}=24 \cdot n$ ($n=1, 2, \dots$) and $T=\text{Exitus}$. Twenty-four hours after acetaminophen intoxication different extracorporeal dialysis replacement procedures were used. Death was defined by hemodynamic insufficiency or cardiac arrest in spite of maximal catecholamine treatment.

The study design was approved by the local authorities (C3/09) and the animals were treated according to the National Institutes of Health guidelines.

Animal Model

The pigs were fasted for 12 h before surgery and received atropine sulfate (0.05 mg/kg, Dr. Franz Köhler Chemie, Alsbach-Hähnlein, Germany), azaperone (4 mg/kg, Janssen-Cilag, Neuss, Germany), midazolam (0.5 mg/kg, Ratiopharm, Ulm, Germany), and ketamine hydrochloride (14 mg/kg, Serumwerk Bernburg, Bernburg, Germany) intramuscularly for pre-medication.

Anesthesia was maintained after oral endotracheal intubation via continuous central venous infusions of ketamine (15 mg/kg/h), fentanyl (0.02 mg/kg/h, Ratiopharm GmbH, Ulm, Germany) and midazolam (1 mg/kg/h) until death.

In order to measure the arterial and central venous blood pressure and to collect blood samples, the femoral artery, the right and left femoral vein, one internal and one external jugular vein were cannulated.

Acetaminophen was parenterally substituted through a duodenal catheter with a loading dose of 0.25 g/kg and with a maintenance dose of 2–5 g/h adapted to the serum level, which should be within 300–400 mg/L. Every 4 h the PTT was measured and as soon as the PTT was below 0.3 a confirming laboratory was collected and if its PTT was below 0.3 as well the administration of acetaminophen was stopped. $T_{\text{ALF}}=0$ was defined as the time when the first laboratory reports a PTT <0.3 .

All pigs received infusions of 0.9% sodium chloride, 20% glucose, 8.4% sodium bicarbonate, 6% hydroxyethyl starch solution (HAES), potassium chloride, calcium chloride, noradrenalin and ceftriaxone (Hexal, Holzkirchen, Germany) every 24 h. Porcine erythrocytes were substituted as soon as the hemoglobin was below 7.5 and two porcine fresh frozen plasma were substituted as soon as ALF was established and then fresh frozen plasma was given at a rate of 60 ml per hour until death.

All the pigs were lying on their backs for the whole time. Their position was not changed; thus, increasing ICP cannot be the cause of this changing position.

Intracranial Measurement

Before the surgery started, two holes were drilled into the pig's cranium and a combination probe (Raumedic AG, Muenchberg, Germany) was placed for continuous measurement of the ICP and the oxygen saturation in the brain.

Central Venous Pressure Measurement

The CVP was measured through a catheter, which was inserted into the femoral vein and pushed forward into the abdominal cava inferior vein. Therefore, the measured CVP was independent of the ventilation especially the PEEP.

Calculation

To assess the correlation between ICP and CVP a linear correlation was carried out on a 4-hourly schedule.

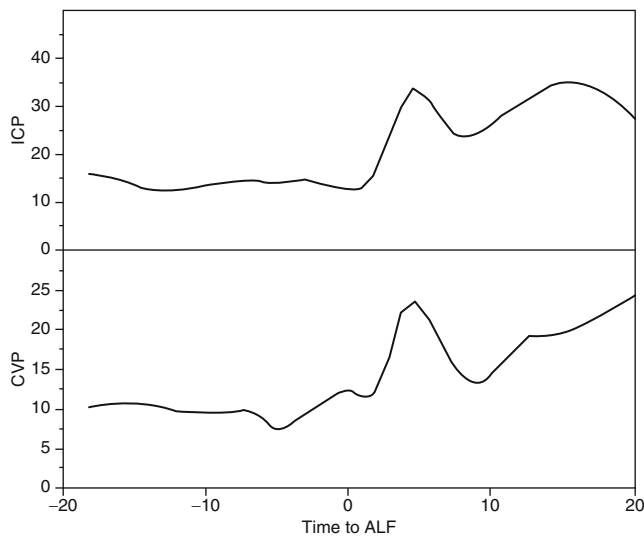


Fig. 1 Trend of intracranial pressure (ICP) and central venous pressure (CVP) in time relative to acute liver failure (ALF) in a single animal

Results

Because of an accidental increase in central venous pressure (CVP) in a single animal it was observed that the intracranial pressure (ICP) followed the CVP increase and later the CVP decrease as soon as the volume infusion was stopped (Fig. 1). The ICP increase (21 mmHg from baseline) exceeded the CVP increase (13 mmHg from baseline) and reached a pathological peak level (33 mmHg).

In this animal the time-independent correlation between CVP and ICP followed a sigmoid pattern: Up to a CVP of 10 mmHg no coherence to ICP was observed (Fig. 2). The ICP closely correlated with the CVP when the CVP was within 10–20 mmHg. At a CVP higher than 20 mmHg no further increase in ICP was recorded.

In all animals an increasing correlation of quantity and quality between the CVP and the ICP, especially in the last 24 h before exitus, which means the late phase of ALF, was seen (Fig. 3). Twenty-four hours before exitus there is a low correlation coefficient ($r=0.08$) and it started out with a slope $m=0.24$. The slope m is the ICP against the CVP. This situation remained stable until 16 h to exitus ($m=0.22$ and $r=0.1$). The correlation increased until 8 h to exitus to a slope $m=0.5$ and a correlation coefficient $r=0.3$. This situation continued until exitus ($m=0.5$ and $r=0.4$).

Discussion

We have seen a definite correlation between the CVP and the ICP in the late phase of ALF. In our porcine model where the ALF was established through acetaminophen intoxication, the CVP is the independent factor and the ICP constitutes the dependent factor. ICP is dependent on the CVP and follows the trend of the CVP. This observation applies for CVP within the range 10–20 mmHg.

Rickels [5] stated that there is no simple correlation between the CVP and the ICP and that increased CVP does not increase the ICP. This was mainly based on the observations of Trevisani et al. [10] in a porcine model of severe brain trauma. However, these observations were made in a mechanical injury model that might not reflect the situation in ALF and were limited to the range below 10 mmHg.

Once the pigs established ALF more volume must be loaded to stabilize circulation. More volume loading increased the CVP. The ICP follows the increase of CVP.

The main cause of this discrepancy may have its background in the deregulation of cerebral blood flow. Wright et al. [13] proposed that ALF patients have a good correlation between arterial pro-inflammatory cytokines and ICP. They observed a positive cerebral cytokine ‘flux’ (production) in ALF patients with uncontrolled ICP and arrived at the conclusion that brain pro-inflammatory cytokine production is associated with uncontrolled ICP, which may indicate a compromised blood–brain barrier. Butterworth [1] argues furthermore that increased brain ammonia may cause brain swelling via the osmotic effects of an increase in astrocytic glutamine concentration or by inhibition of glutamate removal from brain extracellular space.

Butterworth [1] came to the conclusion that brain edema is the consequence of increasing ICP. Brain edema is a major complication of ALF and is therefore a major cause of death in this condition.

For this reason it is advisable to keep the CVP within the normal range to avoid increasing CVP and additionally increasing ICP.

At the end the question remains why other research studies have not seen this correlation between the CVP and the ICP. This may be for the following reasons. First of all they could not have had CVP data over 10 mmHg. We also did not see a correlation between the CVP and the ICP below 10 mmHg. Thus, they just did not have the possibility of making an observation. Second, this correlation is only visible with our special porcine model with acetaminophen intoxication. This must be clarified through

Fig. 2 ICP plotted against CVP in a single animal

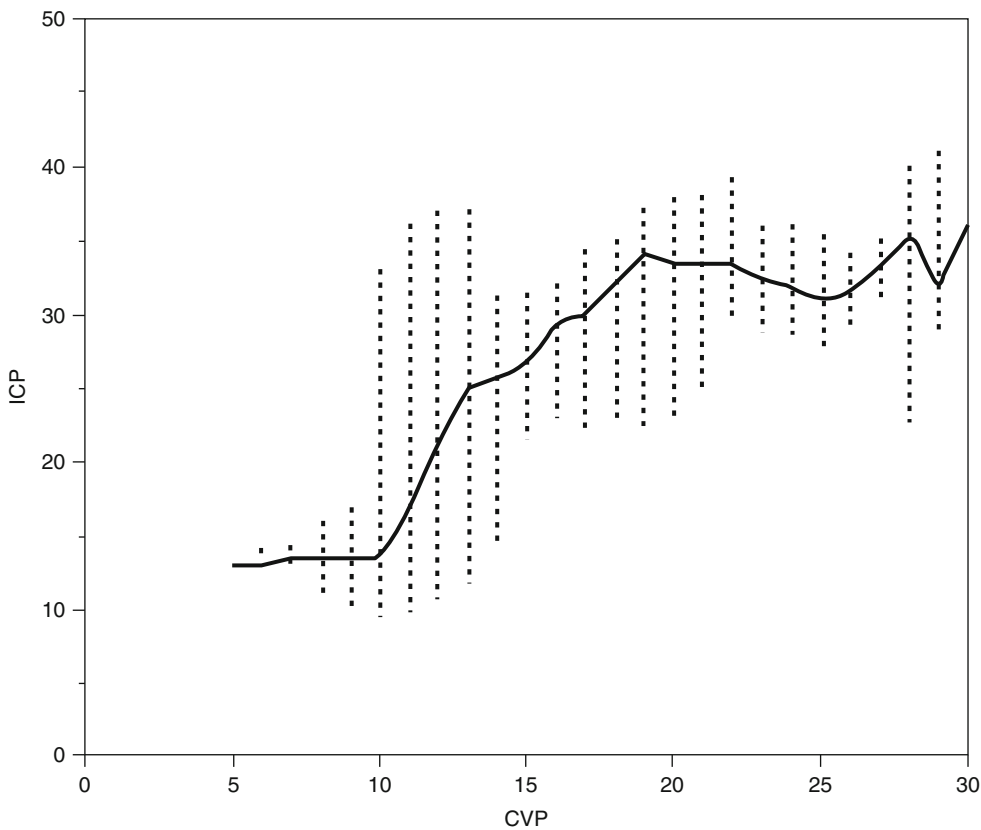
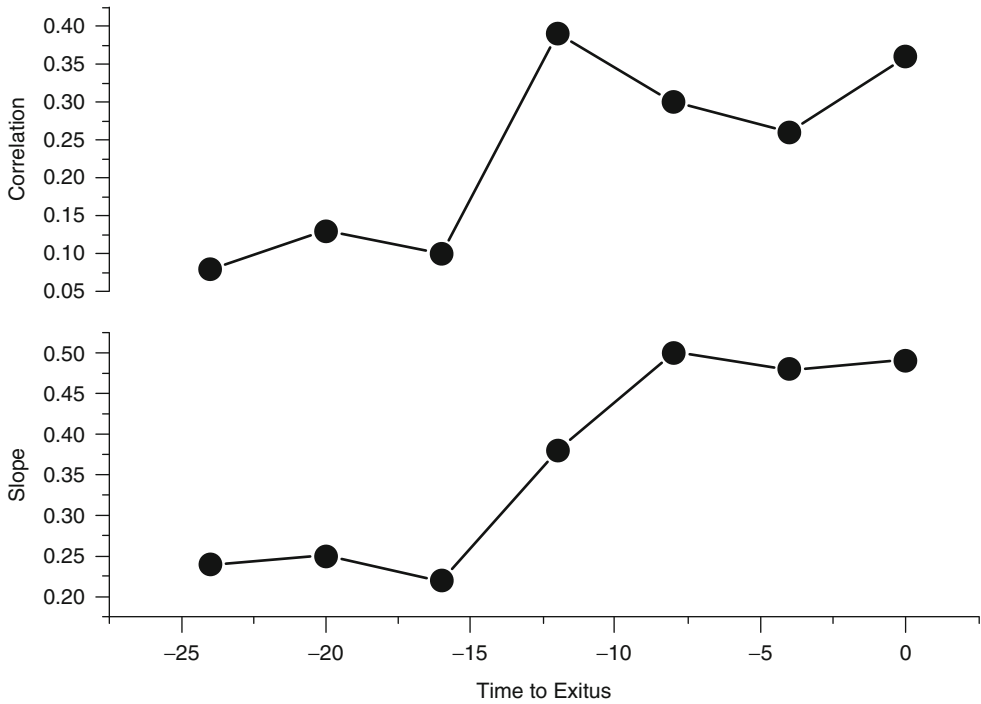


Fig. 3 Slope (m) and correlation coefficient (r) of a 4-hourly linear correlation analysis in time to exitus



further research studies on other animal models and on humans.

Conclusion

To sum up we can say that it seems to be clinically appropriate to keep the arterial blood pressure within an adequate range with the use of vasopressors. Moreover, it is reasonable to avoid fluid overload to hopefully minimize the risk of brain injury.

Conflict of interest statement Martin U. Schuhmann has received a research grant by Raumedic AG for the implementation of multimodal monitoring in animal research. The other authors declare that they have no conflict of interest.

References

1. Butterworth RF (2003) Brain edema in acute liver failure. *Indian J Gastroenterol* 22(Suppl 2):S59–S61
2. Chastre A, Jiang W, Desjardins P, Butterworth RF (2010) Ammonia and proinflammatory cytokines modify expression of genes coding for astrocytic proteins implicated in brain edema in acute liver failure. *Metab Brain Dis* 25:17–21
3. Kramer L (2004) Acute liver failure. *Wien Klin Wochenschr* 116:67–81
4. Patzer JF, Lopez RC, Aggarwal S (2007) Intracranial pressure observations in a canine model of acute liver failure supported by a bioartificial liver support system. *Artif Organs* 31:834–839
5. Rickels E (2009) Monitoring intracranial pressure. Indication, limits, practice. *Anaesthesist* 58:398–404
6. Rose C, Ytrebo LM, Davies NA, Sen S, Nedredal GI, Belanger M, Revhaug A, Jalan R (2007) Association of reduced extracellular brain ammonia, lactate, and intracranial pressure in pigs with acute liver failure. *Hepatology* 46:1883–1892
7. Rosenthal RJ, Friedman RL, Kahn AM, Martz J, Thiagarajah S, Cohen D, Shi Q, Nussbaum M (1998) Reasons for intracranial hypertension and hemodynamic instability during acute elevations of intra-abdominal pressure: observations in a large animal model. *J Gastrointest Surg* 2:415–425
8. Todd MM, Weeks JB, Warner DS (1993) The influence of intravascular volume expansion on cerebral blood flow and blood volume in normal rats. *Anesthesiology* 78:945–953
9. Tofteng F, Larsen FS (2002) Monitoring extracellular concentrations of lactate, glutamate, and glycerol by in vivo microdialysis in the brain during liver transplantation in acute liver failure. *Liver Transpl* 8:302–305
10. Trevisani GT, Shackford SR, Zhuang J, Schmoker JD (1994) Brain edema formation after brain injury, shock, and resuscitation: effects of venous and arterial pressure. *J Trauma* 37:452–458
11. Vaquero J, Chung C, Blei AT (2004) Cerebral blood flow in acute liver failure: a finding in search of a mechanism. *Metab Brain Dis* 19:177–194
12. Wendon J, Lee W (2008) Encephalopathy and cerebral edema in the setting of acute liver failure: pathogenesis and management. *Neurocrit Care* 9:97–102
13. Wright G, Shawcross D, Olde Damink SW, Jalan R (2007) Brain cytokine flux in acute liver failure and its relationship with intracranial hypertension. *Metab Brain Dis* 22:375–388

Visualisation of Cortical pO_2 During an Epidural Mass Lesion in Rodents

Jan Warnat, Gregor Liebsch, Eva-Maria Stoerr, and Alexander Brawanski

Abstract Monitoring $p_{bt}O_2$ is a valuable supplemental procedure for neurocritically ill patients. Here, we utilise an opto-chemical method for measuring cortical pO_2 during a reversibly introduced epidural mass lesion in a rat model. The sensor was placed in a cortical window of 17 ventilated Wistar rats. Inflating the balloon device over the contralateral hemisphere increased ICP. Physiological parameters and cortical pO_2 were recorded. The ICP increased from 6.2 ± 4.6 to 44.6 ± 12.6 mmHg ($p < 0.001$). Cortical pO_2 over arterioles changed from 28.9 ± 2.1 to 19.0 ± 2.1 mmHg ($p < 0.001$), over venules from 14.8 ± 1.2 to 9.9 ± 1.5 mmHg ($p = 0.002$) and over parenchyma from 4.1 ± 0.7 to 2.4 ± 0.8 mmHg respectively ($p < 0.001$), while basic physiological parameters remained constant ($p > 0.05$). During baseline, arterial pO_2 correlated significantly with cortex arteriole and venole pO_2 , but not with cortex parenchyma pO_2 . While ICP was raised, cortical pO_2 did not correlate with arterial pO_2 . In this model, a moderate epidural mass lesion causes a significant decrease in cortical pO_2 . Cortex parenchyma pO_2 appeared to be independent from arterial pO_2 . The correlation of cortex vessel pO_2 with arterial pO_2 disappeared during the epidural mass lesion. These findings show the capability of the device to elucidate the behaviour of functionally different cortex areas at pathophysiological conditions.

Keywords Brain tissue oxygen • $p_{bt}O_2$ • Partial oxygen pressure • Epidural haematoma • Time-resolved luminescence imaging • Neuromonitoring

J. Warnat (✉), E.-M. Stoerr, and A. Brawanski
Department of Neurosurgery, University of Regensburg,
Franz-Josef-Strauß-Allee 11, Regensburg 93053, Germany
e-mail: jan.warnat@klinik.uni-regensburg.de;
alexander.brawanski@klinik.uni-regensburg.de

G. Liebsch
Department of Neurosurgery, University of Regensburg,
Franz-Josef-Strauß-Allee 11, Regensburg 93053, Germany
BIOCAM GmbH, Friedenstraße 30, Regensburg 93053, Germany

Introduction

Current intensive care for SAH and TBI patients relies to a certain degree on neuromonitoring data, including local brain tissue pO_2 measurements. The rationale of the latter is that periods with low $p_{bt}O_2$ seem to increase secondary brain damage and lead to deterioration in outcome [4, 10, 11]. In clinical practice, Clarke-type electrodes or chemo-optical sensors are implanted in the parenchyma usually at a depth of 2–3 cm and allow local $p_{bt}O_2$ to be detected, which is believed to be an estimate for the end-capillary pO_2 [7].

Previously, a new measurement technique had been introduced [8, 9, 14–16] that allows simultaneous pO_2 measurements of distinct areas of the cortex surface including vessels and parenchyma. The method is based on the detection of the oxygen-dependent quenching of the sensor luminescence and allows fast acquisition of both two dimensional pO_2 maps and regular camera views of the cortex under a sensor foil.

Here, we evaluate this experimental approach and measure cortical pO_2 changes under controlled pathophysiological conditions in a rat model with simulation of a reversible epidural hematoma, which is mimicked by the inflation of an epidurally positioned balloon device [2, 3].

Materials and Methods

Animal Preparation

The experimental protocol was approved by the local animal care committee and includes 17 male Wistar rats (303 ± 21 g, Charles River). Narcosis was initiated with a gas mixture of isoflurane (2.5–3.5% vol.), oxygen and nitrous oxide. After endotracheal intubation, the regime was changed to midazolam (2.0 mg/kg), fentanyl (0.01 mg/kg), and medetomidin (0.15 mg/kg). Ventilation was continued with oxygen and

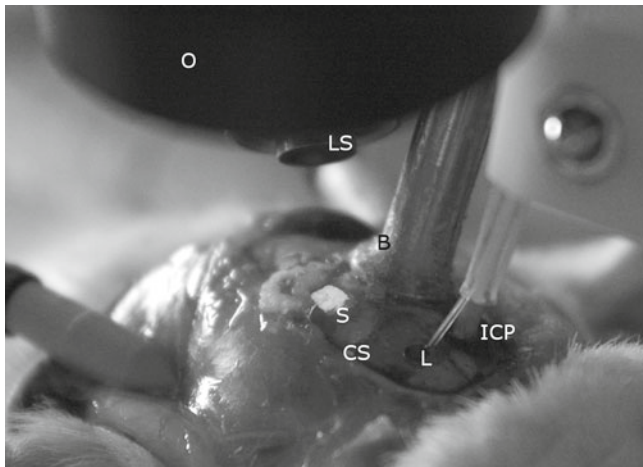


Fig. 1 Experimental set-up. *O* objective, *LS* light source, *B* balloon device, *S* sensor foil (just emitting light), *CS* coronal suture, *L* Licor probe (data not shown), *ICP* intracranial pressure probe

nitrogen. The tail artery was catheterised and the animals were positioned in a stereotactic frame. Rectal body temperature was kept stable between 36.5°C and 37.5°C using a warming lamp. Craniectomies were performed with a drill for the epidural balloon device (left parietal, 5 mm), for the sensor foil (right parietal, 2–3 mm) and for the ICP probe (left frontal, Codman). The dura was carefully opened and removed to gain access for the pO_2 sensor foil and the ICP probe.

Cortical Oxygen Measurement

The oxygen sensor foil (polysulfone containing a platinum [II]–octaethyl–porphyrine) was placed gently on the cortex and was fixed with Cyanoacrylate glue. A colour CCD camera (AVT, Germany; resolution 780×580, 10 bit=1,024 greyscale values) was placed on the axis over the probe. A glass fibre cable connected to the light source was positioned near the objective over the sensor allowing the foil to be illuminated with white light for colour pictures and with blue light ($\lambda=405$ nm) for pO_2 measurement (Fig. 1). Light emissions of the sensor foil were optically filtered by a 455-nm long-pass filter (GG435; Schott, Germany) and detected by the camera. The light source and the camera were precisely controlled by a trigger box (Biocam, Regensburg, Germany). Acquisition software (Biocam) running on a laptop provided an online view of the camera pictures, control of the trigger box and storage of the data. Evaluation software was used for online calculation and display of the resulting oxygen maps (IDL, Creaso; Biocam) as well as for offline analysis with functions to read out the pO_2 -dependent grey-scale values of each pixel of the oxygen maps or of whole regions of interest (ROI).

Measurement Protocol and Data Acquisition

Baseline measurements were recorded for 60 min (“pre” phase). Then the balloon was inflated within 3–5 min up to an ICP of ~45 mmHg for 1 h (“lesion” phase). Afterwards the balloon was deflated within ~1 min and at least one more hour was measured (“post”-phase). FiO_2 was varied in each phase between 15% and 100%.

One measurement cycle consisted of five subsequent images, which were obtained and stored on hard disk. Each image set consisted of a normal colour image, a background luminescence image, an image of the excitation and of the emission phases. The mean arterial blood pressure, ICP, heart rate and rectal body temperature were recorded and a blood gas was drawn for each measurement.

Data Processing and Analysis of pO_2 Maps

Cortical partial oxygen pressure was calculated as previously described via a decay time-dependent parameter R , which was basically calculated by rationing the luminescence images of the excitation and the emission phase of the sensor foil [1, 8, 15]. Regions of interest containing 10×10 pixels were set over an arterial structure, a venule and a parenchymal area without apparent vessels. A 100×100 pixel “overall” ROI was placed in the middle of the measurement area. Vessels were identified in the colour image of each measurement set as well as on the corresponding pO_2 maps. The average pO_2 values for each ROI with its standard deviation were determined for every measurement. Statistical analysis was performed with Sigma Stat (SPSS) using a t test and Pearson’s correlation. Cortical pO_2 values are given as mean with standard error to emphasis the statistical data quality despite high standard deviations, which are due to the intended high variation of FiO_2 /arterial pO_2 according to the protocol. All other values are given as mean with standard deviation.

Results

The ICP increased during balloon inflation from a baseline of 6.2 ± 4.6 to 44.6 ± 12.6 mmHg (lesion) and was reduced to 9.4 ± 7.9 mmHg after balloon deflation (post; Table 1). In all experiments plausible pO_2 measurements of the cortex surface were obtained (Fig. 2). Cortical surface pO_2 over arterioles changed from 28.9 ± 2.1 to 19.0 ± 2.1 mmHg during balloon inflation and increased again to 25.4 ± 2.3 mmHg after balloon deflation. The corresponding values for the cortical venule window were 14.8 ± 1.2 mmHg (pre), 9.9 ± 1.5 mmHg (lesion) and 12.7 ± 1.5 mmHg (post); in the

Table 1 Physiological parameters

	RR (mmHg)	Temp. (°C)	O ₂ art. (mmHg)	CO ₂ art. (mmHg)	pH	FiO ₂ (%)	Pinsp. (mmHg)	ICP (mmHg)
Pre <i>n</i> =66	83.8±19.5	37.0±0.8	178.2±101.6	45.4±10.9	7.35±0.1	58.5±25.5	9.4±1.1	6.2±4.6
Lesion <i>n</i> =55	87.9±28.7	36.9±0.7	194.2±70.3	40.9±9.8	7.36±0.1	64.1±23.8	10.4±1.3	44.6±12.6
Post <i>n</i> =54	79.6±21.5	37.0±0.4	192.3±94.9	42.7±11.1	7.34±0.1	59.1±26.8	10.8±1.6	9.4±7.9

Values are given as mean±standard deviation

FiO₂ inspiratory oxygen fraction, Pinsp inspiratory pressure, *n* number of measurements

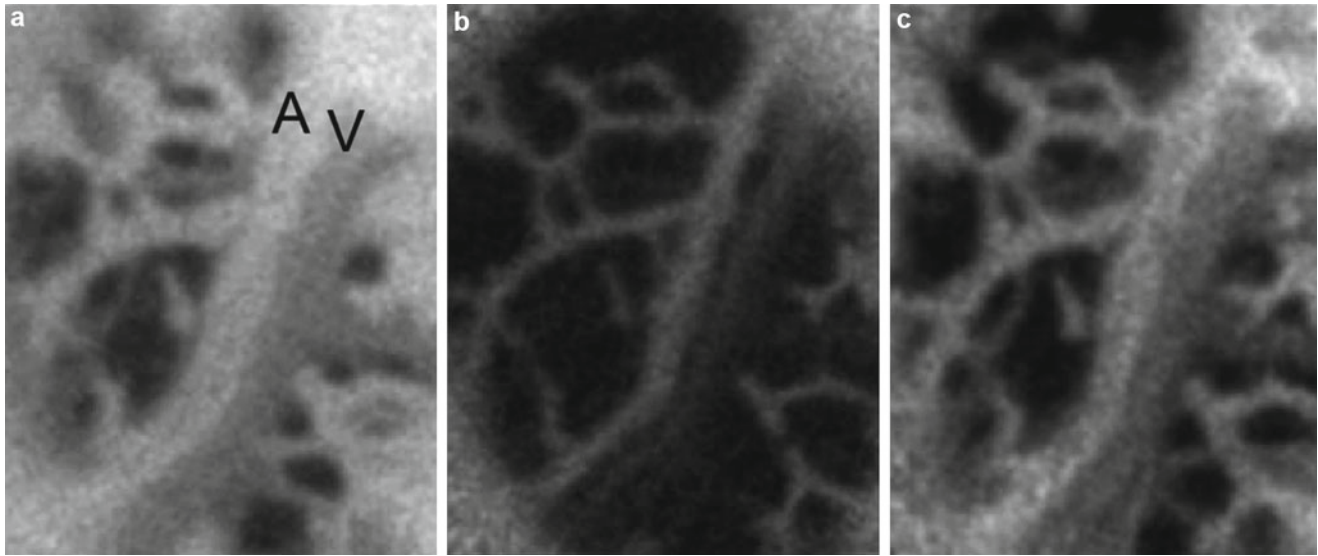


Fig. 2 Exemplary cortical pO₂ maps from baseline measurement (a), after balloon inflation with raised ICP (b) and after balloon deflation (c). Brightness of pixel corresponds to absolute pO₂ values. A arteriole, V venule

parenchyma ROI 4.1 ± 0.7 mmHg (pre), 2.4 ± 0.8 mmHg (lesion) and 3.2 ± 1.2 mmHg (post) was measured (Fig. 3).

The changes in cortical oxygen values due to the lesion were significant in all ROI. After balloon deflation cortical pO₂ again reached levels indistinguishable from the baseline values except for the parenchyma window, which remained at a lower level.

The mean arterial pO₂ and pCO₂ as well as blood pressure, pH, mean FiO₂ and body temperature remained constant ($p > 0.05$); the inspiratory pressure increased slightly during the experiments (Table 1).

During baseline measurement, arterial pO₂ correlated significantly with cortex arteriole and venule pO₂ (correlation coefficient CC=0.269 and 0.273; $p < 0.0002$), but not with cortex parenchyma pO₂ (CC=0.0215, $p = 0.77$). While ICP was raised, arterial pO₂ did not correlate with the cortical pO₂ in all ROI ($0.59 < p < 0.92$).

Discussion

Focusing on cortex surface pO₂ is a unique experimental approach in neuromonitoring. Although the method is still under technical development, simultaneous pO₂ measurements of different cortical structures during an epidural mass lesion

as an exemplary pathophysiological model were obtained for the first time. Changes in cortical pO₂ appeared to be reasonable, although their absolute values were relatively low. This might be due to a certain fluid-filled distance of the sensor foil to the underlying structures. On the other hand, polarographic pO₂ measurements on the rat cortex showed comparable results [5, 6, 12, 13]. However, it must be considered that the sensor foil lies over the structures and measures *on site* and not in some depth, e.g. *in* a vessel.

A rise in ICP due to the epidural lesion resulted in a significant decrease in cortical pO₂ and was restored after balloon deflation except for the parenchymal ROI. Here, the pO₂ remained significantly decreased. It can be assumed that this finding might indicate damage to or alteration of the parenchyma and probably of the capillaries, while the greater cortex vessels and their ability to transport O₂ into their direct surroundings recovered from the lesion.

The response and dependency of the cortical pO₂ to variations of arterial/systemic pO₂ illustrates the capabilities of the measurement method for functional investigations: Systemic pO₂ shows a strong correlation with the cortical arteriole and venule ROI, while there is no correlation with the simultaneously captured parenchymal ROI. One interpretation might be that this discrepancy resembles cortical autoregulation with its effect on the parenchyma.

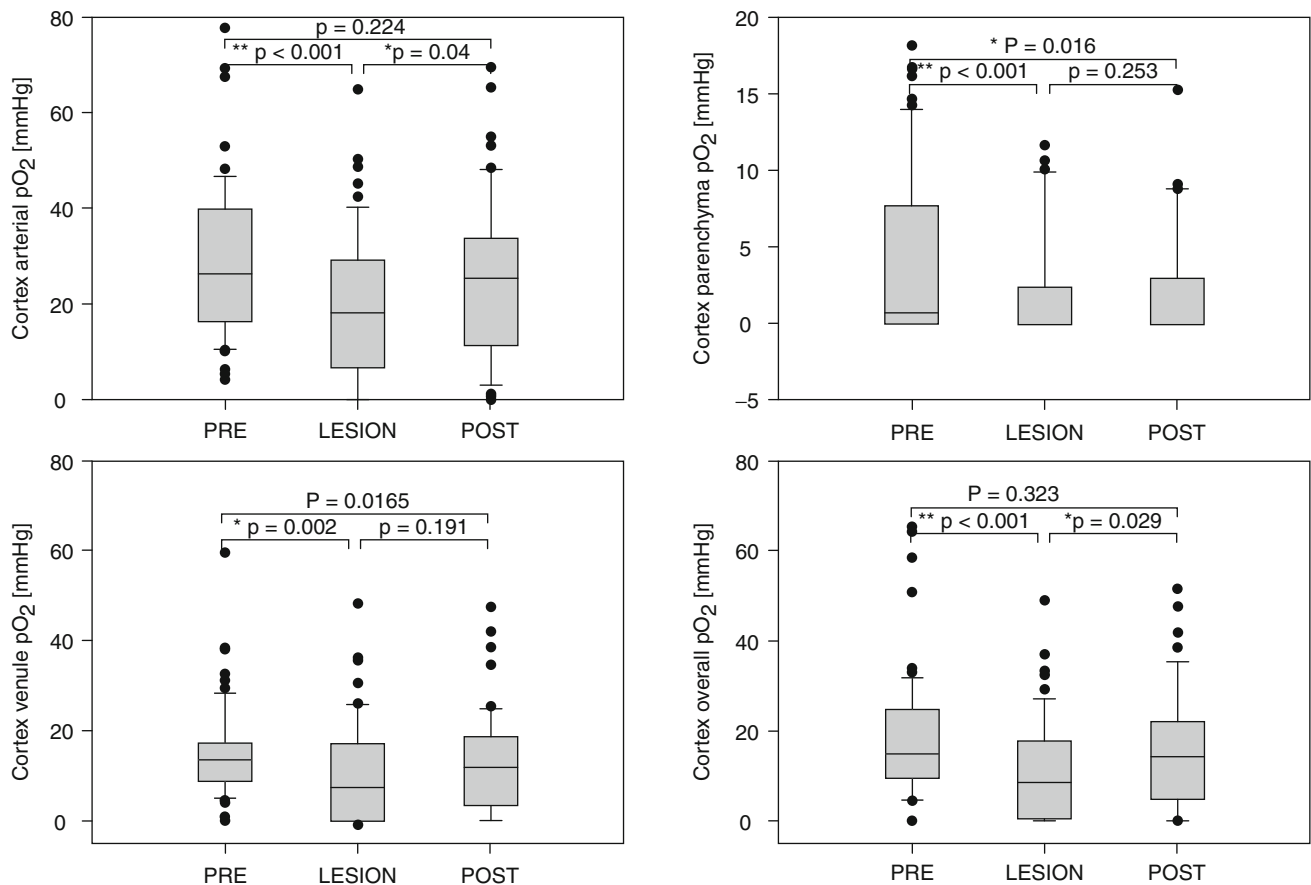


Fig. 3 Course of cortical pO₂ during the phases of the experiment in arteriole, venule, parenchyma and overall region of interest (ROI). High standard deviations are fed back to high variations in arterial pO₂ according to the protocol

In the pathophysiological state with raised ICP cortical pO₂ did not correlate with systemic pO₂. This means that a (therapeutic) rise in arterial pO₂ would affect neither cortical vessel pO₂ nor cortical parenchyma pO₂. In an ICU setting, monitoring the cortical vessels and parenchyma may give additional information on the status of brain oxygenation complementary to the white matter measurements of conventional pO₂ probes.

Conclusion

In this model, a moderate epidural mass lesion caused a significant decrease in cortical pO₂. Cortex parenchyma pO₂ appeared to be independent from arterial pO₂. The correlation of cortex vessel pO₂ with arterial pO₂ disappeared during the epidural mass lesion. These findings show the capability of the device to elucidate the behaviour of functionally different cortex areas at pathophysiological conditions.

Conflict of interest statement We declare that we have no conflict of interest.

References

1. Babilas P, Liebsch G, Schacht V, Klimant I, Wolfbeis OS, Szeimies RM, Abels C (2005) In vivo phosphorescence imaging of pO₂ using planar oxygen sensors. *Microcirculation* 12:477–487
2. Bendszus M, Burger R, Vince GH, Solymosi L (2002) A reproducible model of an epidural mass lesion in rodents. II. Characterization by in vivo magnetic resonance imaging. *J Neurosurg* 97: 1419–1423
3. Burger R, Bendszus M, Vince GH, Roosen K, Marmarou A (2002) A new reproducible model of an epidural mass lesion in rodents. I. Characterization by neurophysiological monitoring, magnetic resonance imaging, and histopathological analysis. *J Neurosurg* 97:1410–1418
4. Dings J, Jager A, Meixensberger J, Roosen K (1998) Brain tissue pO₂ and outcome after severe head injury. *Neurol Res* 20(Suppl 1): S71–S75
5. Ivanov KP, Derry AN, Vovenko EP, Samoilov MO, Semionov DG (1982) Direct measurements of oxygen tension at the surface of arterioles, capillaries and venules of the cerebral cortex. *Pflügers Arch* 393:118–120
6. Ivanov KP, Sokolova IB, Vovenko EP (1999) Oxygen transport in the rat brain cortex at normobaric hyperoxia. *Eur J Appl Physiol Occup Physiol* 80:582–587
7. Kett-White R, Hutchinson PJ, Czosnyka M, Boniface S, Pickard JD, Kirkpatrick PJ (2002) Multi-modal monitoring of acute brain injury. *Adv Tech Stand Neurosurg* 27:87–134

8. Liebsch G, Klimant I, Frank B, Holst G, Wolfbeis OS (2000) Luminescence lifetime imaging of oxygen, pH, and carbon dioxide distribution using optical sensors. *Appl Spectrosc* 54:548–559
9. Liebsch G, Klimant I, Krause C, Wolfbeis OS (2001) Fluorescent imaging of pH with optical sensors using time domain dual lifetime referencing. *Anal Chem* 73:4354–4363
10. Meixensberger J, Vath A, Jaeger M, Kunze E, Dings J, Roosen K (2003) Monitoring of brain tissue oxygenation following severe subarachnoid hemorrhage. *Neurol Res* 25:445–450
11. Nortje J, Gupta AK (2006) The role of tissue oxygen monitoring in patients with acute brain injury. *Br J Anaesth* 97:95–106
12. Vovenko E (1999) Distribution of oxygen tension on the surface of arterioles, capillaries and venules of brain cortex and in tissue in normoxia: an experimental study on rats. *Pflugers Arch* 437:617–623
13. Vovenko EP, Chuikin AE (2010) Tissue oxygen tension profiles close to brain arterioles and venules in the rat cerebral cortex during the development of acute anemia. *Neurosci Behav Physiol* 40:723–731
14. Warnat J, Liebsch G, Stoerr EM, Brawanski A, Woertgen C (2008) A new semi-invasive method for two dimensional pO₂ measurements of cortical structures. *Acta Neurochir Suppl* 102:185–188
15. Warnat J, Liebsch G, Stoerr EM, Brawanski A, Woertgen C (2008) Simultaneous imaging of cortical partial oxygen pressure and anatomic structures using a transparent optical sensor foil. *J Neurosurg Anesthesiol* 20:116–123
16. Woertgen C, Warnat J, Brawanski A, Liebsch G (2009) Non-invasive measurement of the superficial cortical oxygen partial pressure. *Adv Exp Med Biol* 645:167–173

Development of an Experimental Model to Study the Pathophysiology of Cerebral Salt Wasting Following Subarachnoid Hemorrhage

Andrea Kleindienst, Sven M. Schlaffer, Nikhil Sharma, Lisa Linde, Michael Buchfelder, and Joseph G. Verbalis

Abstract Hyponatremia is frequent following cranial neurosurgery or acute brain injury like subarachnoid hemorrhage (SAH), and increases mortality by 30%. The pathophysiology is not understood nor does a causal therapy exist. Since clinical trials are potentially dangerous in this very ill population, we examined whether an established rat model allows studying cerebral salt wasting (CSW) following SAH. The daily urine sodium excretion as well as plasma sodium, osmolality and antidiuretic hormone (ADH) levels were measured for 10 days. Following the injection of 300 μ L of blood into the great cistern (SAH_{severe}), natriuresis peaked twice (days 1 and 3–5, $p < 0.05$) resulting in a plasma sodium nadir (day 1 – 133.9 mmol/L, day 5 – 132.6 mmol/L), while following the injection of 300 μ L saline (ICP_{control}), natriuresis occurred delayed on days 4–5 ($p < 0.05$). Following double SAH (200 μ L twice, 24 h apart), a natriuresis on day 4 resulted in a hyponatremia (131.7 mmol/L, $p = 0.025$). Neither SAH_{mild} (100 μ L), the injection of hemolyzed blood (100 μ L) or hypertonic saline (200 μ L) replicated the effect. The immediate release of ADH (32.23 ± 34.87 pg/mL) following SAH_{severe} normalized over the next few days. We conclude that first, the rat model of SAH is suitable for studying CSW, second the increase in intracranial pressure generates the delayed hyponatremia, and third, the ADH release does not mediate natriuresis.

Keywords Subarachnoid hemorrhage • Hyponatremia • Cerebral salt wasting • Antidiuretic hormone • Natriuresis • Animal model

A. Kleindienst (✉), S.M. Schlaffer, and M. Buchfelder
Department of Neurosurgery, University Erlangen-Nuremberg,
Schwabachanlage 6, D-91054 Erlangen, Germany
e-mail: andrea.kleindienst@uk-erlangen.de;
sven.schlaffer@uk-erlangen.de;
michael.buchfelder@uk-erlangen.de

N. Sharma, L. Linde, and J.G. Verbalis
Department of Medicine, Georgetown University,
Washington, DC, USA
e-mail: ns328@georgetown.edu; inlinde@gmail.com;
verbalis@georgetown.edu

Introduction

Hyponatremia is frequently encountered in patients who suffer from acute brain injury or have undergone neurosurgery for intracranial processes. More than 50% of patients admitted for subarachnoid hemorrhage (SAH) develop hyponatremia [21], and 10–20% of patients admitted to neurosurgical units with intracranial tumors and hematomas and patients undergoing pituitary surgery [20].

The pathophysiology of hyponatremia in acute brain injury is not exactly understood, and may only in part be explained by an increased secretion of the antidiuretic hormone (ADH syn. arginine–vasopressin, AVP) [2, 19]. Furthermore, activation of neither the natriuretic peptide system nor the renin–angiotensin–aldosterone system unequivocally explains the phenomenon of hyponatremia in patients with intracranial disease [9]. Therefore, this condition is referred to as “cerebral salt wasting” (CSW). The critical difference between the “syndrome of inappropriate ADH secretion” (SIADH) and CSW is that CSW involves renal salt loss leading to hyponatremia and volume loss, whereas SIADH is an euvolemic or hypervolemic condition.

The abnormal renal water and/or sodium handling creates an osmotic gradient promoting the shift of water into brain cells [7], thereby worsening cerebral edema and precipitating neurological deterioration. Unless hyponatremia is corrected promptly and effectively, mortality increases up to 30% through seizures, elevations in intracranial pressure, or herniation [3] at plasma sodium <125 mmol/L, and up to 50% at plasma sodium <115 mmol/L [5]. Therefore, awareness is required to provide appropriate management and avoid deleterious outcomes. What is clear from these prevalence data is that hyponatremia is common, and hyponatremia due to all causes increases mortality.

Controlled clinical trials are difficult and potentially dangerous in this very ill population. Therefore, studies using an animal model that mimics the clinical features of hyponatremia offer the best opportunity to understand the underlying pathophysiology and optimize treatment strategies. The experimental rat model of SAH has been demonstrated to

present all common features of human SAH such as blood–brain–barrier changes [4], brain edema [22], vasospasm [6], delayed ischemic brain injury [8], cognitive deficits [10], and to result in a significant natriuresis [11]. The present study was designed to optimize an experimental model of SAH for studying hyponatremia in rats.

Materials and Methods

Adult male Sprague–Dawley rats, weighing 250–350 g, were housed individually in a temperature-controlled room (21–23°C) with lights on from 700 to 1,900 h. All procedures were carried out in accordance with National Institutes of Health (NIH) guidelines on the care and use of animals and an animal study protocol approved by the Georgetown University Animal Use and Care Committee, an American Association for Accreditation of Laboratory Animal Care–approved facility.

Experimental Design

Animals were randomly assigned to six groups in order to examine the effect of SAH on CSW. The rats were subjected to mild or severe SAH by the injection of 100 or 300 μ L of autologous whole blood into the great cistern (SAH_{mild} $n=8$, SAH_{severe} $n=7$), double SAH by injecting 200 μ L of whole blood twice, 24 h apart (SAH_{double} $n=7$), or the injection of 100 μ L of hemolyzed blood (SAH_{hemol} $n=8$). Control rats were subjected to the injection of 300 μ L of isotonic saline (ICP_{control} $n=8$) or 200 μ L of hypertonic saline (HS, $n=8$). The mortality following the injection of hemolyzed blood or hypertonic saline was 25%, resulting in an overall mortality of 15%. At all times, the rats were fed a dry, pelleted AIN-76 formulation diet (BioServe, Frenchtown, NJ, USA) and water *ad libitum*. Rats were housed continuously in metabolic cages (Lab Products, Seaford, DE, USA) to facilitate urine collection. Finally, all rats were killed by decapitation, and both heparinized and K⁺-EDTA blood was collected for serum electrolytes.

Operative Procedures

Anesthesia was induced by isoflurane (5.0 MAC), and the rats were weighed. Thereafter, anesthesia was maintained by isoflurane (1.5 MAC) allowing the animals to breathe spontaneously. The rats were placed on an electric heating pad during surgery to maintain rectal temperature at approximately 37°C. The rats were placed in the prone position, and a skin incision

was made along the midline in the neck. After the occipital bone was cleared of muscular attachment, the occipito-atlantal membrane was exposed for insertion of a 26-gauge needle into the cisterna magna through the arachnoid membrane. After withdrawal of 0.1 mL of cerebrospinal fluid (CSF), autologous blood was removed from the jugular vein catheter placed around a week before by the vendor. The autologous non-heparinized blood was injected over 1 min. Anesthesia was maintained until the wound was closed, and the rats had received an i.m. injection of buprenorphine (0.01 μ g/kg body weight of the rat) for postoperative analgesia. Surgery was concluded with the rats being placed head tilted down by 20° for 30 min. In the double-SAH model, we injected 0.2 mL of autologous non-heparinized blood twice, 24 h apart.

Urine and Plasma Analyses

The body weights (g), food and water intake (mL) were documented daily over the total study period. Blood samples were drawn via the jugular catheter for 10 days following surgery. The rats were housed in metabolic cages, and the daily urine volume (mL) was measured for 10 days.

Urine was analyzed for sodium, potassium (ion-selective electrode system, ELISE electrolyte system; Beckman Instruments, Brea, CA, USA), and osmolality (freezing-point depression, The Advanced Osmometer model 3900; Advanced Instruments, Norwood, MA, USA). Whole blood was centrifuged at 3,000 rpm (Sorvall RT 6000 D; Sorvall, Newtown, CT, USA) at 4°C for 20 min to separate plasma. Plasma was analyzed for sodium, potassium, and osmolality. AVP in plasma was measured by a highly sensitive and selective radioimmunoassay (detection limit: 0.1 pg/mL; cross-reactivity of the antisera with other related peptides was <0.7%; for a detailed description see [12]).

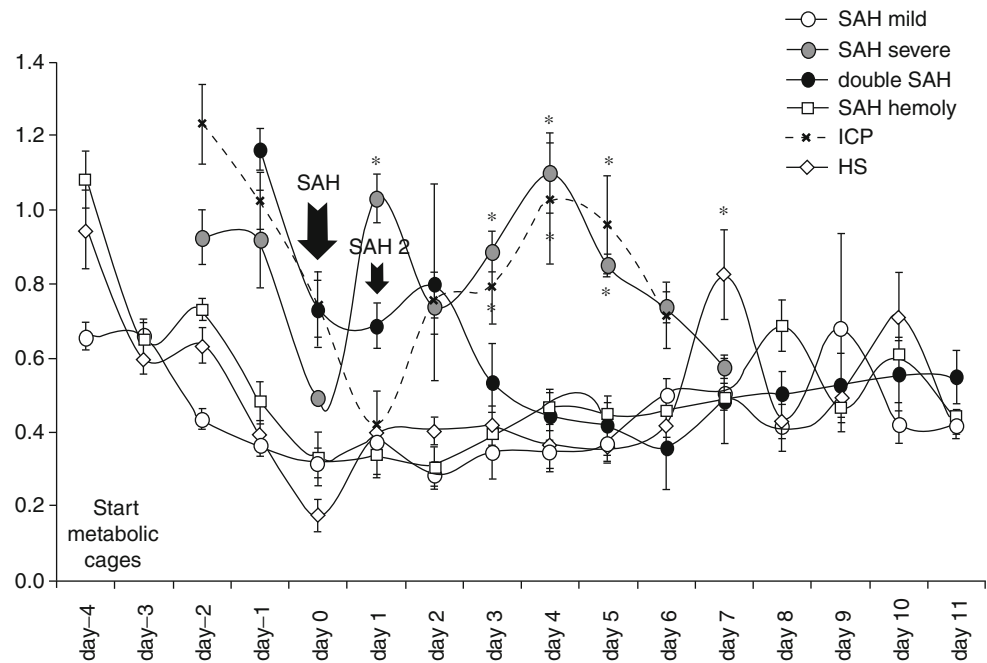
Statistical Analysis

All data were expressed as the mean \pm SEM. Statistical comparison was performed using the ANOVA and Tukey post-hoc analysis (SPSS software). A probability value was significant at $p < 0.05$.

Results

The surgery associated mortality was highest following the injection of hemolyzed blood and hypertonic saline (25%), 14% following severe SAH and double SAH, 12.5% following mild SAH, and 0% following saline injection. At the

Fig. 1 Daily sodium excretion (mmol/day) following subarachnoid hemorrhage. The rats were housed in metabolic cages and the urine was collected over a 24-h period. Subarachnoid hemorrhage (SAH) was induced by the injection of blood into the great cistern ($100\ \mu\text{L} = \text{SAH}_{\text{mild}}$, $300\ \mu\text{L} = \text{SAH}_{\text{severe}}$, two times $200\ \mu\text{L}$ blood 24 h apart = $\text{SAH}_{\text{double}}$, $100\ \mu\text{L}$ hemolyzed blood = $\text{SAH}_{\text{hemoly}}$). The control group was subjected to the injection of $300\ \mu\text{L}$ of isotonic saline (ICP) or $100\ \mu\text{L}$ of hypertonic saline (HS). The values are given as mean \pm SD. The asterisk represents statistical significance compared with mild SAH



ends of the experiments, the correct injection and distribution of blood was confirmed microscopically in all animals.

Verifying Natriuresis

The values of the daily sodium excretion in the different experimental groups are summarized in Fig. 1. After the animals were subjected to the metabolic cages, an initial stress natriuresis normalized within 4 days. Following the injection of $300\ \mu\text{L}$ of autologous blood ($\text{SAH}_{\text{severe}}$), we found a biphasic natriuresis with an early peak at 24 h ($p < 0.001$) and a second peak on days 3–5 (day 3 $p = 0.007$, day 4 $p = 0.003$, and day 5 $p = 0.010$) compared with SAH_{mild} . The injection of $300\ \mu\text{L}$ of saline (ICP_{control}) resulted only in delayed natriuresis with a peak on days 3–5 (day 3 $p = 0.014$, day 4 $p = 0.003$, and day 5 $p < 0.001$) compared with SAH_{mild} . Following double SAH, we found a trend toward increased sodium excretion on day 2, i.e., 24 h following the second blood injection ($p = 0.073$). The injection of $200\ \mu\text{L}$ of hypertonic saline resulted in a trend toward increased sodium excretion on day 7 ($p = 0.087$), and following the injection of $100\ \mu\text{L}$ hemolyzed blood, we found some increased sodium excretion on day 8 ($p = 0.052$).

Plasma Biochemistry

The values of plasma sodium levels following severe SAH and double SAH are summarized in Fig. 2. As expected, plasma sodium demonstrated an early nadir at 24 h

($133.9\ \text{mmol/L}$) and a delayed one on day 5 ($132.6\ \text{mmol/L}$) following severe SAH, and a delayed nadir on day 4 ($131.7\ \text{mmol/L}$, $p = 0.025$) following double SAH. The values of plasma ADH (syn. AVP) levels following severe SAH and double SAH are summarized in Fig. 3. Plasma ADH levels peaked following the injection of $300\ \mu\text{L}$ blood into the great cistern ($\text{SAH}_{\text{severe}}$) at $32.23\ \text{pg/mL}$ and normalized thereafter slowly, while following double SAH, the ADH levels peaked on day 3 at $7.81\ \text{pg/mL}$.

Discussion

This study demonstrated that the experimental model of subarachnoid hemorrhage injecting blood into the cisterna magna in the rat induced increased urinary sodium excretion, resulting in decreased plasma sodium levels, and is thus a suitable model for studying the cerebral salt wasting syndrome, i.e. hyponatremia following acute brain injury.

In accordance with previous studies utilizing the endovascular puncture method to induce the SAH [11], we were able to verify increased urinary sodium excretion following the injection of blood into the great cistern. However, comparing the injection of different volumes of blood, i.e. 100 and $300\ \mu\text{L}$ of blood, we found a significant natriuresis only following severe SAH as induced by the injection of $300\ \mu\text{L}$ blood, but not following mild SAH as induced by $100\ \mu\text{L}$. The time course of the increased sodium excretion was biphasic, presenting an early peak at 24 h and a delayed peak on days 3–5. These findings with two zeniths of an increased renal sodium excretion are in accordance with the literature. Kojima et al. confirmed the early one in an acute study [11],

Fig. 2 Plasma sodium levels (mmol/L) following subarachnoid hemorrhage in the rat. The rats were equipped with jugular catheters, and 200 μ L of blood was collected at different time points following severe SAH or double SAH with subsequent replacement with the same volume of isotonic saline. The values are given as mean \pm SD. The *asterisk* represents statistical significance compared with severe SAH

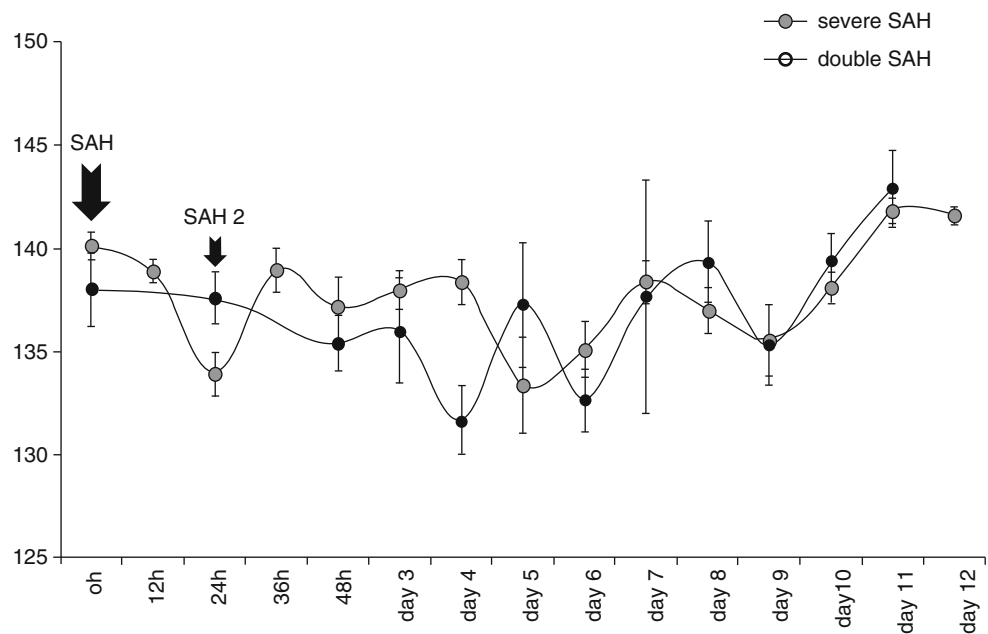
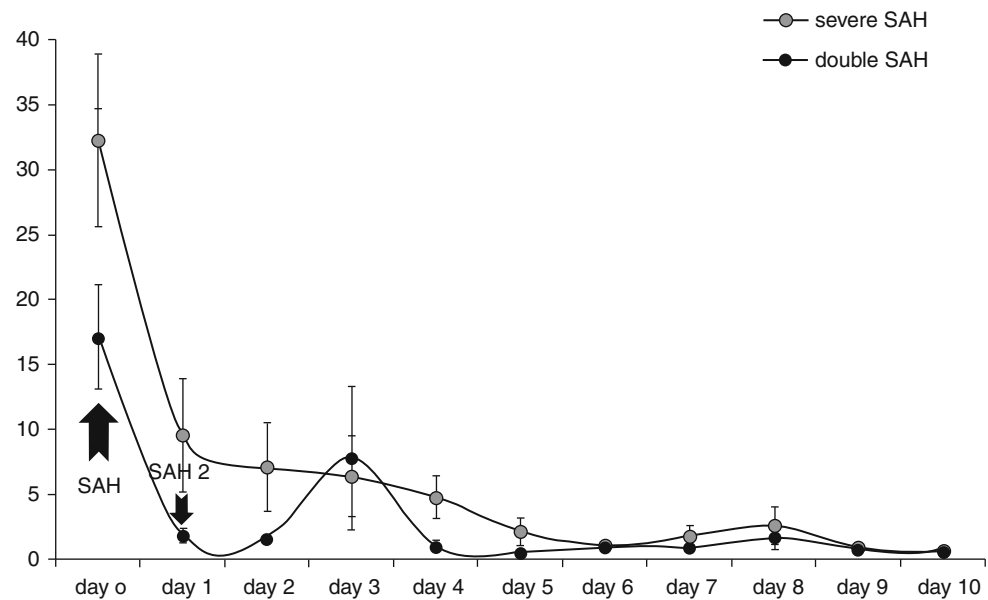


Fig. 3 Plasma levels of antidiuretic hormone (ADH syn. AVP pg/ml) following subarachnoid hemorrhage in the rat. The rats were equipped with jugular catheters, and 200 μ L of blood was collected at different time points following severe SAH or double SAH with subsequent replacement with the same volume of isotonic saline. The values are given as mean \pm SD. The *asterisk* represents statistical significance compared with severe SAH



and Mori et al. the later one on day 4 [17]. Neither the induction of a double SAH known to enhance the effect of cerebral vasospasm [15, 16] nor the injection of hemolyzed blood or hypertonic saline amplified the SAH-induced natriuresis.

The pathophysiology of the two most serious complications of SAH, vasospasm and hyponatremia, has not been precisely clarified. Blood break-down products have been hypothesized to be the initiating agents of the delayed vasospasm and hyponatremia [13]. However, by injecting hemolyzed blood we were not able to enhance the SAH-induced natriuresis, but induced a delayed significant natriuresis on day 7 lasting only for 1 day. In order to analyze the specific contribution of blood-related effects compared with volume-related effects resulting in increased intracranial pressure,

we injected the same volume of 300 μ L of isotonic saline as in SAH_{severe}. We found in the saline control group, the same significantly increased sodium excretion that was present in the SAH_{severe} group, although the very early natriuresis was absent. Therefore, the increase in intracranial pressure may be an integral part of the pathophysiology of CSW.

In our study, we focused on the quantification of urine sodium excretion collected over a 24-h period. We expected the results of these daily urine measurements to more reliably reflect the underlying pathomechanism of natriuresis in CSW [14] than the confirmation of hyponatremia. Especially in a rodent model, blood sodium measurements are prone to be affected by volume loss and saline replacement of the daily blood draws. We found the natriuresis following SAH

to be paralleled by low blood sodium levels although the latter measurements were affected by relevant fluctuations and a considerable standard deviation. The measurements of ADH levels in our study represent the expected course following SAH and double SAH respectively [18], but are not sufficient to elicit the natriuresis. Thus, the natriuresis found in the present study does not result from SIADH, an entity occasionally confused with CSW [1, 9].

Conclusion

In our hands, the measurements of blood sodium or ADH were not reliable parameters of CSW. The natriuresis reflected the severity of SAH, i.e., the injected blood volume, and a substantial part of the effect could be mimicked by saline injection. Double SAH did not enhance natriuresis, but resulted in increased morbidity and weight loss, thereby interfering with the assessment of the electrolyte and fluid balance. We conclude that the rat model of SAH injecting blood into the cisterna magna is suitable for studying CSW.

Conflict of interest statement We declare that we have no conflict of interest.

References

- Costa KN, Nakamura HM, Cruz LR, Miranda LS, Santos-Neto RC, Cosme Sde L, Casulari LA (2009) Hyponatremia and brain injury: absence of alterations of serum brain natriuretic peptide and vasopressin. *Arq Neuropsiquiatr* 67:1037–1044
- Doczi T, Tarjanyi J, Huszka E, Kiss J (1982) Syndrome of inappropriate secretion of antidiuretic hormone (SIADH) after head injury. *Neurosurgery* 10:685–688
- Fraser CL, Arieff AI (1997) Epidemiology, pathophysiology, and management of hyponatremic encephalopathy. *Am J Med* 102:67–77
- Germano A, d'Avella D, Ciciarello R, Hayes RL, Tomasello F (1992) Blood–brain barrier permeability changes after experimental subarachnoid hemorrhage. *Neurosurgery* 30:882–886
- Gill G, Huda B, Boyd A, Skagen K, Wile D, Watson I, van Heyningen C (2006) Characteristics and mortality of severe hyponatraemia – a hospital-based study. *Clin Endocrinol (Oxf)* 65:246–249
- Gul S, Bahadır B, Hanci V, Bektas S, Can M, Kalayci M, Acikgoz S, Acikgoz B (2010) Effect of vardenafil on cerebral vasospasm following experimental subarachnoid hemorrhage in rats. *J Clin Neurosci* 17:1038–1041
- Gullans SR, Verbalis JG (1993) Control of brain volume during hyperosmolar and hypoosmolar conditions. *Annu Rev Med* 44:289–301
- Guresir E, Raabe A, Jaiimsin A, Dias S, Raab P, Seifert V, Vatter H (2010) Histological evidence of delayed ischemic brain tissue damage in the rat double-hemorrhage model. *J Neurol Sci* 293:18–22
- Harrigan MR (2001) Cerebral salt wasting syndrome. *Crit Care Clin* 17:125–138
- Jeon H, Ai J, Sabri M, Tariq A, Macdonald RL (2010) Learning deficits after experimental subarachnoid hemorrhage in rats. *Neuroscience* 169:1805–1814
- Kojima J, Katayama Y, Moro N, Kawai H, Yoneko M, Mori T (2005) Cerebral salt wasting in subarachnoid hemorrhage rats: model, mechanism, and tool. *Life Sci* 76:2361–2370
- Landgraf R, Neumann ID (2004) Vasopressin and oxytocin release within the brain: a dynamic concept of multiple and variable modes of neuropeptide communication. *Front Neuroendocrinol* 25:150–176
- Lee JY, Keep RF, He Y, Sagher O, Hua Y, Xi G (2010) Hemoglobin and iron handling in brain after subarachnoid hemorrhage and the effect of deferoxamine on early brain injury. *J Cereb Blood Flow Metab* 30:1793–1803
- Maesaka JK, Imbriano LJ, Ali NM, Ilamathi E (2009) Is it cerebral or renal salt wasting? *Kidney Int* 76:934–938
- Marbacher S, Fandino J, Kitchen ND (2010) Standard intracranial in vivo animal models of delayed cerebral vasospasm. *Br J Neurosurg* 24:415–434
- Megyesi JF, Vollrath B, Cook DA, Findlay JM (2000) In vivo animal models of cerebral vasospasm: a review. *Neurosurgery* 46:448–460; discussion 460–441
- Mori T, Katayama Y, Kojima J, Moro N, Kawai H, Yoneko M, Kawamata T (2005) Experimental model for investigating hyponatremia after subarachnoid hemorrhage in rats. *Acta Neurochir Suppl* 95:377–380
- Mount DB (2009) The brain in hyponatremia: both culprit and victim. *Semin Nephrol* 29:196–215
- Rabinstein AA, Wijdicks EF (2003) Hyponatremia in critically ill neurological patients. *Neurologist* 9:290–300
- Sherlock M, O'Sullivan E, Agha A, Behan LA, Owens D, Finucane F, Rawluk D, Tormey W, Thompson CJ (2009) Incidence and pathophysiology of severe hyponatraemia in neurosurgical patients. *Postgrad Med J* 85:171–175
- Sherlock M, O'Sullivan E, Agha A, Behan LA, Rawluk D, Brennan P, Tormey W, Thompson CJ (2006) The incidence and pathophysiology of hyponatraemia after subarachnoid haemorrhage. *Clin Endocrinol (Oxf)* 64:250–254
- Thal SC, Sporer S, Klopotoski M, Thal SE, Woitzik J, Schmid-Elsaesser R, Plesnila N, Zausinger S (2009) Brain edema formation and neurological impairment after subarachnoid hemorrhage in rats. Laboratory investigation. *J Neurosurg* 111:988–994

Author Index

A

Abásolo, D., 23
Ahmadi, S.A., 261
Alessandri, B., 373
Alexander, B., 201
Allen, J.C., 343
Al-Olama, M., 377
Alperin, N., 191, 201
Ang, B.-T., 51, 343
Antes, S., 111, 231
Aroucha, P.R., 201
Asgari, S., 5
Avan, P., 131

B

Baldwin, K., 191, 207
Barth, M., 157
Bergsneider, M., 5, 29, 191, 207
Beseoglu, K., 323, 329
Beyer, C., 311
Beynon, C., 105, 383
Biestro, A., 283
Bloom, M., 201
Boor, S., 311
Brabant, G., 277
Brady, K., 181
Brandner, S., 217
Brawanski, A., 35, 393
Britton, J., 61
Buchfelder, M., 217, 277, 399
Budgett, D., 101
Budohoski, K.P., 17, 121

C

Camacho, J., 283
Campbell, P., 61
Carlotti, C., 117
Carpenter, K.L.H., 271
Carrera, E., 157
Castellani, G., 181
Ceuppens, J., 289
Chambers, I., 39, 45
Charbel, F., 81
Chazal, J., 131
Chin, P.L., 51
Chudy, D., 351
Citerio, G., 39
Clarke, M., 227
Clutton, E., 61

Colli, B., 117

Constantinescu, M., 301
Corteen, E., 295
Czosnyka, M., 17, 29, 75, 121, 141, 147, 153, 157, 181, 213, 271
Czosnyka, Z.H., 75, 181

D

Daley, M., 135
Damiano, L.E.G., 117
Danielsen, P.L., 267
Davies, N., 387
de la Calzada, M.D., 221
Demura, K., 197
Dengler, J., 161, 187
Dengl, M., 165
Depner, F., 347
Depreitere, B., 289
Diedler, J., 17, 363
Diehl, R.R., 153
Donald, R., 39, 45
Dostal, M., 157
Drake, J.M., 227
du Plessis, A.J., 177
Dye, J., 191

E

Eicker, S.O., 323
Etmann, I., 217, 277
Enblad, P., 39, 45
Etminan, N., 323
Eymann, R., 105, 111, 227, 231, 243

F

Faltermeier, R., 35
Feng, M., 51
Fernández, J., 23
Fino, J., 81
Fourney, D.R., 227
Frenzel, C., 161
Frew, A., 191
Fritsch, M., 243
Froebe, A., 351
Furreedan, M.S., 11

G

Galard, R., 221
Gándara, D., 247
Gatzinsky, K., 377

Geipel, M., 227
 Giraudet, F., 131
 Glenn, T.C., 11
 Gomez, H., 283
 Gregson, B., 39, 45
 Gregson, R., 61
 Grözing, G., 169, 173
 Guan, C., 51
 Guilburd, J., 301
 Guiza Grandas, F., 289

H

Haas, R., 169
 Hamilton, R., 191, 207
 Hänggi, D., 323, 329
 Hansson, H.-A., 377
 Hanuscin, C.R., 11
 Hara, M., 197
 Hassoun, T., 131
 Haubrich, C., 17, 153
 Hawerkamp, E., 387
 Heimann, A., 373
 Heiroth, H.-J., 329
 Heissler, H.E., 87, 93
 Heldt, T., 177
 Helmy, A., 295
 Heppner, P., 101
 Hertle, D., 383
 Holst, A.V., 267
 Hornero, R., 23
 Horn, P., 161, 187
 Hovda, D.A., 11
 Howells, T., 39, 45
 Hutchinson, P.J., 271, 295
 Hu, X., 5, 11, 191, 207

J

Jaeger, M., 165
 Jalan, R., 387
 Jednacak, H., 357
 Jennische, E., 377
 Juhler, M., 267
 Jung, C.S., 383
 Jurjevic, I., 351, 357

K

Kalenka, A., 157
 Kamp, M.A., 329
 Karnchanapandh, K., 339
 Kasai, H., 197
 Kashif, F.M., 177
 Kasprowicz, M., 17, 29, 75, 121, 153
 Kehler, U., 243
 Kempinski, O., 373
 Kentar, M.M., 105, 363, 369
 Kerz, T., 311
 Kiefer, M., 105, 111, 227, 231, 243
 Kiening, K., 39, 45, 383
 Kim, D.J., 153
 King, N.K.K., 51, 343
 Kirkpatrick, P.J., 17, 157, 295
 Klarica, M., 351, 357
 Kleindienst, A., 217, 277, 399
 Klingelhöfer, J., 121
 Klingert, W., 387
 König, K., 87

Königsrainer, A., 387
 Kralick, F., 239
 Krauss, J.K., 87, 93
 Kurschel-Lackner, S., 235
 Kuzman, T., 357

L

Lam, B.L., 201
 Langer, N., 243
 Lange, S., 377
 Lechtenfeld, M., 227
 Leckie, P., 387
 Lee, K.K., 51
 Lee, S.H., 192
 Lemcke, J., 243, 255, 347
 Leonhardt, S., 111
 Letzing, M., 201
 Levi, L., 301
 Lewandowski, R., 67
 Lewis, P.M., 141, 147
 Liebsch, G., 393
 Lim, M., 101
 Linde, L., 399
 Loy, L.Y., 51
 Ludwig, H.-C., 243

M

Malpas, S., 101
 Mandac, I., 357
 Mann, S.A., 227
 Marakovic, J., 351
 Markelic, I., 351
 Martínez-Ricarte, F.R., 247
 Mascarenhas, S., 117
 Mase, M., 197
 Mattern, J., 39, 45
 McArthur, D.L., 11
 McKeown, C., 61
 Medina, T., 239
 Meier, U., 243, 255, 347
 Meixensberger, J., 157, 165
 Menon, D.K., 153, 295
 Merino, M.A., 221
 Mestres, O., 221
 Meyfroidt, G., 289
 Minhui, X., 127
 Miyati, T., 197
 Moraes, L., 283
 Moratin, B., 157
 Morgalla, M.H., 169, 173, 387
 Morgenthaler, N.G., 277
 Mrfka, M., 235
 Müller, C., 243
 Müller-Forell, W., 311

N

Nilsson, P., 39, 45
 Noh, H.M., 239
 Nonaka, K.O., 117
 Nortje, J., 271

O

Oertel, M.F., 333
 O'Hayon, B.B., 227
 Oh, J., 239

O'Leary, H.M., 177
Oommen, K., 61
Orakcioglu, B., 105, 111, 363, 369
Oreškovc, D., 351, 357
Osawa, T., 197
Ossip, M.G., 227

P

Payoux, P., 97
Perrin, J., 323
Petru, R., 305
Pickard, J.D., 17, 75, 121, 141, 147, 153, 157, 181, 213, 271
Piper, I., 39, 45, 61, 135
Pistracher, K., 235
Plontke, R., 121
Poca, M.A., 221, 247
Pozo-Rosich, P., 221
Preuss, M., 333
Price, D.J., 1
Proescholdt, M.A., 35
Proven, A., 387
Puppo, C., 283

R

Radoš, M., 357
Ragauskas, A., 39, 45
Reinhard, M., 17
Remenez, V., 243
Renner, C., 165
Reuland, A., 311
Reuland, K., 311
Rickels, E., 87, 93
Rohde, V., 243
Romero, M., 247
Roosen, G., 289
Rosenfeld, J.V., 141, 147
Ros, M., 97

S

Sahuquillo, J., 39, 45, 221, 247
Sakka, L., 131
Sakowitz, O.W., 105, 111, 363, 369, 383
Santamarta, D., 23
Santos, E., 363
Scharbrodt, W., 333
Scharf, J., 157
Schenk, M., 169, 173, 387
Schepbach, J., 387
Scheuermann, K., 387
Scheufler, N., 277
Schlaffer, S.M., 399
Schmidt, B., 121
Schmidt, C., 217
Schmidt, E., 97
Schmiedek, P., 157
Schmieder, K., 157
Schmitt, M., 111, 227, 231
Schökler, B., 235
Schomacher, J., 333
Schuhmann, M.U., 169, 173, 213, 243, 387
Schulz, M., 261
Schürer, L., 161, 187
Seeley, H.M., 295
Seluque, W., 117
Serrano, E., 221
Sharma, N., 399

Shaw, M., 61, 135
Shen, L., 51
Sherma, A.K., 11
Shibamoto, Y., 197
Sinnott, R., 39, 45
Sklar, E., 201
Smielewski, P., 17, 75, 121, 141, 147, 153, 181
Soehle, M., 157
Solana, E., 221, 247
Sorrentino, E., 17
Sosa, J.C., 213
Soustiel, J., 301
Speil, A., 213, 243
Spors, B., 261
Stehlin, E., 101
Steiger, H.-J., 323, 329
Steiner, L.A., 153
Stein, M., 333
Stell, A., 39, 45
Stengel, D., 243
Stewart, L., 61
Stoerr, E.-M., 393
Stoneham, G.W., 227
Stone, J.L., 81
Sulemanji, M., 177
Sviri, G., 301
Swider, P., 97

T

Tanaka, K., 117
Taskin, A., 323
Tay, V.K.-S., 343
Thalamy, A., 131
Thiel, C., 169, 173, 387
Thiel, K., 169, 173, 387
Thomale, U.-W., 261
Timofeev, I., 271
Tretzel, J.S., 373
Tuli, S., 227
Turowski, B., 329

U

Unterberg, A., 363, 369, 383
Uozumi, Y., 363, 369

V

Vajkoczy, P., 161, 187
van der Meer, C., 305
van Lindert, E., 305
Vannemreddy, P., 81
Vellaisamy, K., 51
Verbalis, J.G., 399
Verghese, G.C., 177
Vespa, P.M., 5, 11, 207
Vienenkötter, B., 383
Vilela, G.H.F., 117

W

Wainwright, M.S., 67
Wang, C.C., 117
Warnat, J., 393
Weber, F., 243
Weerakkody, R.A., 181
Welschehold, S., 311
Whittle, I., 61

Wilkinson, J.S., 227
Will, B.E., 213
Wissa, S., 235
Wolf, S., 161, 187

X

Xu, Y., 217

Y

Yamada, K., 197
Yameogo, P., 97
Yelicich, B., 283

Ye, W., 317
Yihua, Z., 127
Yu, M.-k., 317

Z

Zaaroor, M., 301
Zhang, F., 51
Zhang, Z., 51
Zhong, J.I., 127
Zweckberger, K., 383
Zweifel, C., 181

Subject Index

A

ACA. *See* Anterior cerebral artery (ACA)
 Acute liver failure (ALF)
 complications, 387
 CVP, 388
 description, 387
 ICP, 387
 materials and methods
 animal model, 388
 calculation, 388
 central venous pressure measurement, 388
 intracranial measurement, 388
 study design, 388
 outcome, 389
 Altered spinal canal compliance and cerebral venous drainage, IIIH
 contribution, 202
 diagnoses, 201
 extra-cranial factors, 201–202
 increased CSF volume, 205
 manifestation, 201
 materials and methods
 assessed parameters, 202
 cerebral venous drainage, 202
 estimation, cranio-spinal (CS) compliance distribution, 202–203
 morphological assessment, 202
 MRI, 202
 structural brain scan, 202
 mechanical compliance, 204
 MRI-based comprehensive characterization, 204
 observations, 205
 outcomes
 contribution, 204
 controls, 204
 hemodynamic measures, 203
 magnetic resonance venography, 204
 papilledema and pulsatile tinnitus, 201
 pathophysiology, 204
 role, 204
 treatment, 201
 Alzheimer's dementia/Binswanger's disease, 213
 Anaesthesia
 as experimental protocol, animal study, 63
 and ICP, 231
 Aneurysmal SAH (ASAH)
 DND, 339
 ICP and CPP, 341
 management, 341
 Aneurysmal subarachnoid hemorrhage, 165, 187, 323. *See also*
 Computed tomography (CT) perfusion measurement

Angiographic vasospasm, 157–159
 ANN. *See* Artificial neural networks (ANN)
 Anterior cerebral artery (ACA), 7
 Arterial blood pressure (ABP). *See also* Cerebral autoregulation
 assessment, respiratory oscillations
 and ICP, 37, 38
 measurement, 18, 20
 and TCD flow velocity, 18
 Artificial neural networks (ANN)
 EUSIG-defined hypotensive events (*see* EUSIG-defined
 hypotensive events)
 warning system, 93
 Artificial ventilation, 233
 ASAH. *See* Aneurysmal SAH (ASAH)
 Atrial natriuretic peptide (ANP), brain injury
 AVP prohormone, 278
 biomarkers, 277, 280
 causes, 279–280
 death/permanent disability, 277
 endocrine system, 279
 injury severity
 ANP levels, 278
 Glasgow Coma Score (GCS), 279
 multivariate regression analysis, 278
 serum ANP and sodium concentrations, 279
 investigation, 278
 long-term outcome, 280
 management, 280
 materials and methods
 blood samples, 278
 exclusion criteria, 278
 Glasgow Coma Score (GCS), 278
 measurements, 277–278
 role, 277
 traumatic, 277
 in US, 277
 Autoregulatory index (ARI), 148, 159

B

BasicWithSlope model, 40
 Bayesian artificial neural network (BANN). *See* EUSIG-defined
 hypotensive events
 BD. *See* Brain death (BD)
 Bilateral carotid disease, 18
 Bioinformatics analysis, mortality
 AUC, 72
 data collection, 68
 descriptive statistics and area calculation, 68
 heat map and dendrograms, data set, 68, 69

- heterogeneous data classes, 67–68
- hierarchical clustering methods, 67–68
- ICP and CPP, 67
- patient demographics and outcome, 68
- pediatric and neurocritical care, 70
- student's *t* test, 68
- survivors and non-survivors, 70, 71
- Body position, intraocular and CSF pressures
 - change, effects, 358, 360
 - CSF system model, 359
 - horizontal position, 358
 - hypothesis, 359, 360
 - ICP, 357
 - materials and methods
 - experimental model, 358, 359
 - leakage, 358
 - male and female adult cats, 358
 - outcome, 358
- Brain death (BD)
 - CT-A (*see* Computed tomographic angiography (CT-A))
 - diagnosis, 311, 314
- Brain edema
 - cytotoxic/vasogenic, 37
 - TBI, 277
- Brain injury
 - monitoring, cerebral oxygen metabolism, 177
 - NIRS, 177
 - preterm infant, 177
- Brain monitoring
 - case approach, data purity, 52
 - feasibility study, 52
 - incomplete data reusability, 55, 57
 - MAP and BTemp, 57–58
 - patients and monitoring, 52
 - patients, TBI, 58
 - predictive method, 58
 - RAE, standard deviation and R2 values, 55, 56
 - reusability
 - imputation error assessment, 53, 55
 - imputation, missing values, 53
 - input data characteristics, 52, 53
 - processes, 53, 54
 - re-usage strategy, 55
 - segmentation, 53
 - simulated missing values, 53
 - TBI, 51–52
- Brainstem auditory evoked response (BAER)
 - defined, 81
 - lesions detection, brainstem, 85
 - and MBAER methodology, 81
- Brain temperature (BTemp)
 - invasive monitoring, 52
 - and MAP, 55, 57, 58
- Brain tissue oxygenation ($p_{br}O_2$)
 - agreement limits, 164
 - analysis, classic Bland–Altman, 163
 - differences, 164
 - effects, 163–164
 - ICP measurement, 161
 - interactions, 164
 - Licox system, 161
 - materials and methods
 - analysis, neuromonitoring data, 162
 - CT, 162
 - differences, magnitude and variance, 162
 - ischemia risk, 161
 - limits, 162
 - mechanical failure, 164
 - monitoring and outcome, 161
 - outcomes
 - bias, 162
 - classic Bland–Altman analysis, 162
 - implantation, 162
 - Licox probes, 162
 - therapy, 162
 - raumedic systems, 162–163
 - time series measurement, 163
- Brain tissue oxygen measurements, Licox vs. Raumedic
 - assessment, cerebral autoregulation, 167
 - Bland–Altman plot and $P_{br}O_2$ values, 167
 - materials and methods
 - calculations, clinical course and mean ORx, 165, 166
 - data storages, 166
 - statistical analysis, sample size, 166
 - neuromonitoring, 165
 - outcomes
 - analyzing, Bland–Altman plot, 166–167
 - autoregulation and poor outcome, cerebral
 - infarctions, 167
 - clinical observations, 166
 - mean values, ORx, 167
 - probe stability, 167
- Brain tissue oxygen partial pressure ($P_{br}O_2$),
 - reactivity index (ORx)
 - acute liver failure (ALF), 174
 - calculation, 173
 - changes, 175
 - description, 173
 - determination, 173
 - human, 175
 - investigation, 175
 - Licox system, 173
 - materials and methods
 - animals, 174
 - neuromonitoring, 174
 - statistics, 174
 - neuromonitoring efforts, 173
 - outcomes
 - Bland–Altman plot, hourly averaged ORx values, 175
 - differences, neurovent TO and Licox probe, 174
 - Spearman's correlation coefficient, 175
 - oxygen probes types, 173–174
- Buffering capacity
 - brain, 3
 - defined, 2
- C**
 - Carotid artery disease, 18
 - CBF. *See* Cerebral blood flow (CBF)
 - CBFV. *See* Cerebral blood flow velocity (CBFV)
 - Centralized Institutional Review Board of Singhealth (CIRB), 343
 - Central nervous system (CNS), 352, 360
 - Cerebral arterial bed
 - ABP measurement, 20
 - materials and methods
 - and CVR, 18
 - data and statistical analysis, 18
 - stenosis, 17, 18
 - waveforms, 18, 19
 - parameters analyzed, 19
 - pulsatile volume modeling, 20
 - time constant, 19, 20
 - transcranial Doppler (TCD), 17

- Cerebral autoregulation assessment, respiratory oscillations
 - ABP and CBFV, raw and filtered tracings, 142
 - analysis, respiratory frequency, 141
 - arterial blood pressure (ABP) mechanism, 141
 - augmentation, 141
 - detection, respiratory sinus arrhythmia, 145
 - ECG, 145
 - gain measurement, 143
 - individual Glasgow Outcome Score (GOS), 144
 - individual observations, 142
 - interpretation, ABP/CBFV PS, 143
 - low coherence, ABP and CBFV, 141
 - materials and methods, 142
 - observations, 144
 - phase shift (PS) calculation, 141
 - phenylephrine-induced arterial hypertension, 143
 - poor correlation, 143
 - PS reduction, 145
 - statistical evaluation
 - average respiratory rate, 142
 - computed parameters, 143
 - Mx and PRx index, 143
 - recoded signals, 143
 - whilst gain calculation, 143
- Cerebral blood flow (CBF)
 - estimation, 178
 - measurements, 180
 - neonates, 180
 - NIRS signals, 179
- Cerebral blood flow velocity (CBFV)
 - corrected CBFV pulse latencies measurement, 7–8
 - cross-spectrum, 145
 - CSF model, 5
 - frequencies, 141
 - vs. ICP, 8
 - interpretation, 143
 - and intracranial pressure monitoring
 - associations, CPP and FV, 147
 - description, B-wave equivalents (BWEs), 149
 - Flx interpretation, 149, 150
 - Flx vs. ICP, 148, 151
 - ICP plateau wave, 150
 - individual observations, 148
 - intracranial compliance, 147
 - materials and methods, 148
 - Mx and Flx vs. outcome groups, 148, 149
 - recorded haemodynamic signals, 147
 - relationships, FV/ICP, 147
 - statistical analysis, 149
 - materials and methods
 - data analysis, 7
 - patient data, 6–7
 - pulse latency, 6
 - phase shift, 145
 - and signals, 7
 - transfer function, 143
- Cerebral critical closing pressure (CrCP), TBI
 - arterial pressure decreases, 283
 - calibration difficulties, 285
 - CPP, 283–284
 - description, 283
 - estimation, CrCP, 284
 - hypothesis, 283
 - limitations, 285–286
 - materials and methods, 284
 - measurement error, 285
 - monitoring, 284
 - negative values, 285
 - objectives, 284
 - outcomes
 - agreements, best correlated methods, 285, 287
 - bivariate correlation, 285, 287
 - characteristics, 284
 - values, 285, 286
 - therapeutic characteristics, 286
- Cerebral oxygen metabolism
 - brain injury, preterm infant, 177
 - clinical observations, 178
 - data pre-processing, 179
 - EEG measures, 180
 - estimation, 180
 - estimation algorithm
 - CBF, 178
 - cerebral venous oxygen saturation (SvO₂), 178
 - inspiratory cycle, 178
 - oxygen extraction, 178
 - gold standard measurements, 180
 - hemoglobin concentration, 180
 - immature brain, 179
 - instrumentation, 178–179
 - invasive measurements, 180
 - mean arterial blood pressure (MAP), 179
 - metabolic oxygen rate, 179
 - near-infrared spectroscopy (NIRS), 177
 - positron emission tomography, 180
 - range and median oxygen saturation, 179
 - rational clinical decision, 179–180
 - regulation, oxygen delivery, 179
 - systemic arterial and cerebral venous oxygen saturation, 179
 - therapy, 179
 - ventilator-induced changes, NIRS, 180
 - Xenon-133 clearance, 180
- Cerebral perfusion pressure (CPP)
 - ASAH, 341
 - fitting, 144
 - fluctuations, 142
 - and ICP, 67, 70, 72
 - ICP and, 339
 - ICP, DND and IRND, 340
 - management, 341
 - observations, 144
 - recorded signals, 143
- Cerebral pressure autoregulation
 - aims, 136
 - data prediction, 138
 - highest modal frequency (HMF) model, 137–138
 - mathematical modelling, 135
 - Matthews correlation coefficient (MCC) method
 - intermodel comparisons, 137
 - model predictive ability, 137
 - methods
 - highest modal frequency (HMF) method, 136
 - model comparison and optimisation, 136–137
 - pressure reactivity index (PRx), 136
 - reworked Ursino model, 136
 - model comparison
 - “black box” approach, 135
 - “gold standard” data, 135
 - perform model, 135–136
 - optimisation, 138
 - physiological mechanism, 135
 - pial artery–cranial window method, 138
 - predictive accuracy, 138
 - pressure reactivity index (PRx) model, 137

- process, 135
- standardise data set, 138
- treatment and outcomes, 135
- validation techniques, 138
- Cerebral salt wasting (CSW)
 - involvement, 399
 - pathophysiology, 402
 - SAH, 400
- Cerebral spinal fluid (CSF)
 - formation rate, 2
 - pulsatility, 5
- Cerebral venous oxygen saturation
 - estimation, 180
 - hemoglobin changes, 177
- Cerebral venous pressure (CVP), 387
- Cerebral venous thrombosis (CVST), 235
- Cerebrospinal fluid (CSF). *See also* CSF dynamics assessment
 - blood osmolarity, 353
 - causing changes, 191
 - characterization, 191
 - description, 351
 - dynamics, 192
 - formation and circulation, 351
 - hydrocephalus and Chiari malformation, 191
 - hyperosmolar application, 352, 353
 - hypertensive, 192
 - materials and methods, 352
 - pressure
 - cannula, 352
 - measurement, 352–353
 - volume, 352
 - pulsatile movement, 191
 - quantification, 192
 - volume
 - behavior, 353
 - blood osmolarity, 353
- Cerebrospinal fluid pressure (CSFP)
 - mean values, 24
 - pulse amplitude, 23
 - signal, 24–26
- Cerebrovascular disease, 17, 78
- Cerebrovascular haemodynamics, 17
- Cerebrovascular reactivity (CR), 365
- Cerebrovascular resistance (CVR)
 - CBFV, 18
 - single resistor and capacitor, 18
- Chronic headaches, 224
- CIRB. *See* Centralized Institutional Review Board of Singhealth (CIRB)
- Cluster analysis
 - hierarchical, data set, 68, 69
 - variations data collection, 70
- CNS. *See* central nervous system (CNS)
- Cochlear microphonic potentials (CMP) recording, 132–134
- Coherence analysis, 36
- Cole–Cole technique, 62
- Co-morbidity index (CMI)
 - description, 256
 - histogram, 257
 - outcome 2 years after surgery, 257
- Comprehensive non-invasive detection, ICP analyses
 - background, 127
 - diseases, 128
 - experiments, 128
 - ICP value, 128
 - integration, 128
 - invasive ICP measurement, 128
 - materials and methods
 - FVEP, 127
 - instrument interface and diagram, 128
 - TCD, 127
 - virtual instrument technology, 127–128
 - reliable and applicable values, 128
 - use virtual instrument technology, 127
- Computed tomographic angiography (CT-A)
 - BD, 313
 - description, 311
 - ECA and STA, 314
 - materials and methods
 - brain death definition, 313
 - data collection, 313
 - EEG, 313
 - image analysis, 313
 - patient demographics, 311–312
 - protocol, 313
 - transcranial Doppler/duplex ultrasound, 313
 - MCA, 314
 - TCD, 315
- Computed tomography (CT) perfusion measurement
 - CBV, 331
 - clinical outcome, 331
 - materials and methods
 - management, 329
 - patient population, 329
 - statistical analysis, 330
 - study design, 329–330
 - study parameters and end points, 330
 - MTT, 330–331
 - SAH, 329, 331
 - study population, 330
- Computerized data analysis, neuromonitoring
 - parameters
 - materials and methods
 - brain, 37–38
 - data analysis, 36–37
 - data phases, 36, 37
 - patient serial CT, 37
 - neurocritical care treatment, 35
 - predicted correlation, ABP and ICP, 35, 36
- Cortical intracerebral hemorrhage (ICH)
 - CSD, 369
 - goal, 371
 - volume, 370
- Cortical pO₂ visualisation
 - description, 393
 - ICP, 396
 - materials and methods
 - animal preparation, 393–394
 - data processing and analysis, 394
 - measurement protocol and data acquisition, 394
 - oxygen measurement, 394
 - outcomes
 - cortical venule window, 394, 396
 - measurements, cortex surface, 394, 395
 - physiological parameters, 394–395
 - ROI, 395
- Cortical spreading depolarization (CSD)
 - description, 369
 - ECOG, 371–372
 - ICH model, 371
 - materials and methods
 - animal preparation, 369
 - monitoring, 371
 - operative procedure, 370–371

- Cortical spreading depression (CSD)
 - ASDH, 373–374
 - DC potential, 374
 - description, 373
 - IMP and IVP, 375
 - materials and methods, 374
 - measurement, 375
 - outcomes, 374
- CPP. *See* Cerebral perfusion pressure (CPP)
- CR. *See* Cerebrovascular reactivity (CR)
- Craniectomy, 14
- Cranio-spinal system, 203
- CSF. *See* Cerebral spinal fluid (CSF)
- CSF dynamics assessment
 - computerised infusion study, 75
 - hardware, 76
 - ICM+ uses, 77–78
 - ICP monitoring, 76–77
 - needles and transducers, 75–76
 - software
 - circulation, 76, 78
 - ICP, 76
 - parameters displayed, infusion study, 76, 77
- CSF lactate concentration
 - cerebral hyperglycolysis, 333
 - elevation, 334
 - materials and methods
 - daily doses, 334–335
 - hospital charts, 333–334
 - metabolic suppressive therapy, 333
 - midazolam and fentanyl, 334
 - outcomes
 - cohort characteristics, 334, 337
 - time course, 334, 336
- CSFP. *See* Cerebrospinal fluid pressure (CSFP)
- CVR. *See* Cerebrovascular resistance (CVR)
- CVST. *See* Cerebral venous thrombosis (CVST)
- D**
- Data analysis, 47
- Data set generator (DSG), 47
- DC. *See* Decompressive craniectomy (DC)
- Decompressive craniectomy (DC)
 - description, 305
 - ICP treatment algorithm, 307, 309
 - materials and methods
 - craniectomy, 306
 - decision, operating, 306
 - postoperative clinical course, 306
 - tertiary trauma centre, 305
 - outcome evaluation, 307
 - second-tier therapies, 307, 308
 - surviving children, 306
- Delayed neurological deficit (DND)
 - ICP and CPP, 339
 - materials and methods, 339–340
 - outcomes
 - Hunt & Hess grading, 340
 - ICP + CPP combination, 340
 - statistical analysis, 340–341
- Delta-apparent diffusion coefficient (ADC) analysis
 - axonal dysfunction, 199
 - cardiac cycle, 197
 - changes, 198
 - conventional ADC, 198
 - and conventional ADC, 198–199
 - CSF tap test, 198
 - diagnosis, iNPH, 197, 198
 - diffusion-weighted imaging, 197
 - echo planar imaging (EPI), 197
 - MRI conditions, 198
 - outcomes, 198
 - pathophysiology, 199
 - performance, 198
 - values and control groups, 198
 - water dynamics, 199
 - white matter
 - axonal dysfunction, 199
 - microenvironment, 199
- Distortion product otoacoustic emission (DPOAE), 131–134
- DND. *See* Delayed neurological deficit (DND)
- DSG. *See* Data set generator (DSG)
- Dynamic cerebral pressure autoregulation
 - analysis, ARI values, 159
 - angiographic vasospasm, 157
 - angiography, 159
 - biosignals, 159
 - determination, autoregulatory index (ARI), 159
 - estimating status, 157
 - investigation and determination, 157
 - limitation, ARI, 159
 - materials and methods
 - determination, proximal VS, 158
 - estimation, global VS (gVS), 158
 - inclusion and exclusion criteria, 158
 - screening, subarachnoid hemorrhage, 158
 - statistical analysis, 158
 - treatment and management, 158
 - measurement techniques, 159
 - outcomes
 - analysis, pVS 44 hemispheric vessel, 158–159
 - autoregulatory indices, 159
 - correlation, hemispheric ARI values, 159
 - diagnosis, SAH, 158
 - patient characteristics, 158
 - physiological variables, 159
- E**
- ECG. *See* Electrocardiogram (ECG)
- ECoG. *See* Electrocorticographic (ECoG)
- Edinburgh University Secondary Insult Grades (EUSIG). *See* EUSIG-defined hypotensive events
- EEG. *See* Electroencephalogram (EEG)
- Electrocardiogram (ECG)
 - QRS detection, 7
 - signals, 6
- Electrocorticographic (ECoG)
 - animals data, 371–372
 - recording episode, 371
- Electroencephalogram (EEG), 313
- Endoscopic fenestration, 269
- EUSIG-defined hypotensive events
 - brain trauma foundation guidelines, 49
 - classification, 48
 - episode prediction, 43
 - false positive suppression, 43
 - Glasgow, 47
 - ICU, 40
 - materials and methods
 - BANN topology and training, 40
 - data analysis, 47
 - data source and preparation, 40
 - event parameters, 46
 - event profiles, 46–47

- Java-based software, 47
 - SQL and PERL scripts, 47
 - test runs, BANN, 40–41
 - model selection, 43
 - phase I model assessment
 - false positive and negative, 43
 - methodology, 42
 - predictions, 43
 - true positive and negative, 43
 - phase I trial, indications, 44
 - physiological measure, 48
 - probability cutoff thresholds, 44
 - secondary insults, 46
 - test set model assessment, 41–42
 - EVD. *See* External ventricular drainage (EVD)
 - Experimental model, 105
 - Experimental swine model, 105
 - Extended lumbar drain (ELD), ICP
 - B-wave, 207
 - development, automated method, 208
 - diagnosis and evaluation, NPH, 212
 - functions
 - automated combination rules, 209–210
 - data analysis, ICP recordings, 210
 - features, 209
 - metrics extraction, 209
 - MOCAIP metrics, 208–209
 - optimal single-metric rule, 209
 - fundamental limitation, 212
 - ICP recordings, 208
 - mechanistic relationship, 207
 - MOCAIP algorithm, 208
 - monitoring, 207–208
 - normal pressure hydrocephalus (NPH), 207
 - optimal two-rule combination, 210–211
 - outcomes
 - accuracy, combined rules, 211
 - corresponding features, 210
 - impact, optimal metrics, 210
 - individual metric feature rules, 210
 - ROC curves, 211
 - patient characteristics, 208
 - receiver operator characteristic (ROC) curve, 208
 - simple decision rules, 210
 - External ventricular drainage (EVD)
 - implantation, 347
 - indications, 348
 - infections
 - rates, patient groups, 348, 349
 - Staphylococcus* and *Enterococcus*, 348, 349
 - materials and methods
 - microbiological examination, 348
 - statistical analysis, 348
 - surgery, 348
 - patients, 349
 - ventricular and lumbar drainage, 349
 - Extracranial vascular diseases, 18
- F**
- FDP. *See* Fixed dilated pupil (FDP)
 - Fiber optic technique, 98
 - Fixed dilated pupil (FDP)
 - bilateral, 296–298
 - defined, 296
 - sequelae, 298–299
 - unilateral, 296–299
 - Flash visual evoked potential (FVEP), ICP, 127
 - Fluid pressure, 98
 - Fluid-saturated model, 97
 - Fourier transform
 - monitoring system, 3
 - replacement, 4
 - Frontal and occipital horn ratio (FOHR), 227, 228
 - Frontal and temporal horn ratio (FTHR),
 - paediatric hydrocephalus
 - abscissa vs. ordinate, 229
 - advantages, 230
 - assessment, ventricular system, 227
 - axial and coronal plane, 230
 - coronal and sagittal planes, 229
 - cranial ultrasound, preterm infant born, 229
 - CT, 227, 229
 - interpretations, 229
 - ionising radiation, 229
 - materials and methods
 - analogy, 227–228
 - anterior fontanelle imaging, 228
 - hydrocephalic ventricle configuration, 227
 - measured FOHR, 227, 228
 - multiple brain imaging, 228
 - ultrasound images, 228
 - measurements, FOHR, 228, 229
 - MRI measurements, 230
 - outcomes, 228
 - requirement, imaging methods, 229
 - shunt therapy, 228
 - size differences, 228–229
 - standard anterior fontanelle imaging, 227
 - ultrasound transducer, 230
 - validity and reliability, 230
 - volumetric measurements and techniques, 227
- G**
- Gamma-aminobutyric acid (GABA)
 - administration, VGB, 273
 - increases, 276
 - levels, 273
 - transaminase, 271
 - GCS. *See* Glasgow Coma Score (GCS)
 - Glasgow Coma Score (GCS), 289, 292
 - Glasgow outcome scale (GOS), 320
- H**
- Haar wavelets, 88
 - Hemedex® cerebral blood flow
 - assessment, 187
 - drift patterns, 189
 - effects, disturbances and monitoring, 187
 - estimation, 187, 189
 - investigation, 189
 - materials and methods
 - diagnosis, 188
 - drift analysis, 188
 - improvement, monitoring technology, 188
 - measurement cycles, 188
 - microprobes, 187–188
 - statistical analysis, environment, 188
 - median drift, 189–190
 - outcomes
 - analysis, measurement data, 188–189
 - regional CBF and mean relative drift value, 189
 - temperature fluctuations, 189, 190
 - scientific and clinical practice, 189
 - software version, 189

- stochastic method, 189
 - techniques, 190
- Herpes simplex virus type I (HSV-1), 378
- Hilbert phase, 36, 37
- HSV-1. *See* Herpes simplex virus type I (HSV-1)
- Hydrocephalus. *See also* Frontal and temporal horn ratio (FTHR), paediatric hydrocephalus
 - acute, 77
 - adult patients, 23, 25
 - CSF dynamics, patients, 75
 - diagnosis, 29
 - monitoring, 29
 - NEUROVENT P-Tel, 114
- Hypersomnia, 224
- Hyponatremia
 - CSW, 402–403
 - description, 399
 - materials and methods
 - experimental design, 400
 - operative procedures, 400
 - statistical analysis, 400
 - urine and plasma analyses, 400
 - outcomes
 - natriuresis verification, 401
 - plasma biochemistry, 401, 402
 - SAH, 402
- Hypotension
 - arterial, 46
 - defined, 40
 - episodes, 42
 - management, 44
 - prevalence, 48
- I**
- ICA. *See* Internal carotid artery (ICA)
- ICH. *See* Intracerebral hemorrhage (ICH)
- ICH porcine model
 - autoregulation assessment, 366
 - blood pressure and flow, 363
 - cerebral autoregulation, 367
 - cerebrovascular autoregulation, 363
 - lactate/pyruvate ratio, 366
 - materials and methods
 - animal preparation, 364
 - autoregulatory indices calculation, 364
 - monitoring, 364
 - operative procedure, 364
 - pressure, oxygen and flow reactivity indices, 364–365
 - statistical analysis, 365
 - microdialysis (MD), 364
 - outcomes
 - CR, 365
 - ORx and FRx hourly correlation, 365
 - PRx distribution, 365
 - PRx hourly correlation, 365–366
- ICM+ software. *See* CSF dynamics assessment
- ICP. *See* Intracranial pressure (ICP)
- ICP B waves. *See* ICP pulse waveform morphology and B waves
- ICP minimally invasive method
 - cerebral ventricles and “vital spirit”, 117
 - clinical implications, 118
 - determination, cranial deformations, 118
 - inextensible skull, 119
 - intracranial contents, 117
 - intracranial pressure variation, 119
 - “in vitro” and “in vivo” experiments, 118
 - measures, bone deformation, 118
 - observations, Monro–Kellie doctrine, 117
 - outcomes
 - “in vitro” tests, 118
 - “in vivo” tests, 119
 - recognition, cerebrospinal fluid, 117–118
 - relationships, cranial deformation and internal pressure, 119
 - skull experiments, 119
 - skull volume, 118, 119
- ICP pulse waveform morphology and B waves
 - amplitudes variation, peaks, 33, 34
 - changes, morphological features, 33
 - description, 29
 - materials and methods
 - oscillations and dominant pulses, 29–31
 - statistical methods, 31
 - wave metrics, 31
 - mean and standard deviations, 31, 32
 - MOCAIP algorithm, 31
 - PW + AS *vs.* SW + NW, 32–33
 - scatter plot, canonical scores, 33
- ICP telemetry
 - Bland–Altman plot, 108, 109
 - methods
 - monitoring, 106, 107
 - operative procedure, 106
 - protocol, 105–106
 - technology, 106, 107
 - ventriculo-peritoneal shunt, 108
- ICP time series analysis
 - Fourier transform, 87
 - Haar wavelets, 88
 - materials and methods
 - discrete wavelet transforms, 89
 - measurement, 88
 - signal acquisition, 88–89
 - properties, 89
 - pseudo 3D wavelet spectrograms, 89, 90
 - scalogram, 88
 - wavelets, 87–88
- Idiopathic intracranial hypertension (IIH)
 - and diagnostic pitfalls
 - cerebral MRI, 236
 - cerebral venous sinus thrombosis, 235
 - Cerebral venous thrombosis (CVST), 235
 - characterization, 235
 - ICP measurement, 237
 - MR and CT venography, 235, 236
 - papilledema, 236, 237
 - persistent headaches, 235
 - role, 235
 - symptoms, 235
 - treatments, 235
- hypocretin-1 (Orexin A) levels
 - abnormalities, 224
 - body mass index, 223
 - characteristics, 222
 - circadian rhythm, 224
 - control, 223
 - description, 221
 - determination, HC-1 concentrations, 222
 - differences, 224
 - functions, 221
 - hypersomnia, 224
 - hypothalamus contributions, 224
 - intracranial pressure, 221
 - materials and methods, 222–223

- neuropeptides, 224
- obesity, 221
- outcomes, 223
- pathophysiology, 221
- restrictions, 224
- shunt implantation, 223
- Idiopathic normal pressure hydrocephalus (iNPH)
 - aim, 248, 255
 - clinical assessment, 248
 - cognitive functions (CF), 248
 - co-morbidity, 258
 - CT, 248, 251
 - description, 247
 - diagnosis, 252
 - evaluation and management, 248
 - gait evaluation, 248
 - guidelines, diagnosis and management, 247–248
 - hydrocephalus types, 258–259
 - ICP monitoring and CSF dynamics, 248–249
 - improvement rates, 258
 - intervention, 255
 - long-term experiences and gravitational valves, 258
 - magnetic resonance imaging (MRI), 248
 - materials and methods
 - Black grading scale, shunt assessment, 257
 - co-morbidity index (CMI), 256
 - diagnosis, 255
 - follow-up by neurosurgeons, 256–257
 - statistical analysis, 257
 - surgery, 256, 257
 - neuropsychological examination, 248
 - NPH scale score, 252
 - operative therapy, 255
 - outcomes
 - age and sex distribution, 257
 - brain atrophy, 250
 - CMI, 257
 - cross-tabulation, responders and non-responders, 257
 - differences, recovery rates and CMI values, 257–258
 - disability and dependency after surgery, 251
 - excellent/good, 257
 - ICP monitoring, 250
 - mortality and complications rate, 251–252
 - recognise situations, 255
 - recognize abnormalities, 247
 - risk and strict management, 252
 - shunt selection and therapeutic evaluation, 249
 - shunt therapy, 259
 - sphincter disturbances (SD), 248
 - statistical analysis, 249–250
- Impedance (IMP)
 - and IVP, 374
 - measurement, 373
- Implantable ICP monitor
 - animal testing, potential ICP sensor, 102–103
 - drift rig, 103
 - ICP monitor design, 102
 - implantable pressure sensor system, 103, 104
 - materials and methods, 102
 - potential configuration options, 102, 103
 - sensor characteristics, ICP, 102
 - treatment, 101
- Increasing intracranial pressure (ICP), 232, 387
- Infusion test
 - computerised, 75
 - Haar wavelets, 88
 - ICP monitoring, 77
- iNPH. *See* Idiopathic normal pressure hydrocephalus (iNPH)
- Internal carotid artery (ICA)
 - patients identification, 20
 - stenosis, 17–19
- Intracerebral hemorrhage (ICH)
 - cohort study, 344, 345
 - description, 343
 - Multiethnic Asian patient cohort, 346
 - prior statin use effect, post-ICH survival
 - Kaplan–Meier curves, 344, 345
 - mortality, 344, 345
 - subgroup analyses, 346
 - subjects and methods
 - CIRB, 343
 - data collection and computation, 344
 - inclusion and exclusion criteria, 344
 - statistical analyses, 344
- Intracranial arachnoid cysts
 - aim, 267
 - asymptomatic patients, 269
 - cerebrospinal fluid (CSF), 267
 - clinical presentation, 268
 - cyst location, 268
 - dizziness, 268
 - explanation, 267
 - failure, 269
 - first-line treatment and reoperation, 269
 - headache, 268
 - hydrocephalus, 269
 - improvement, endoscopic fenestration, 269
 - management, 268
 - materials and methods
 - clinical and imaging features, 268
 - identification, 267
 - lack of improvement, 268
 - MRI, 267
 - review, 267
 - risk, 268
 - shunt failures, 268
 - shunting procedures, 267
 - surgery, 268
 - symptoms, 267, 268
 - techniques, 269
- Intracranial compliance, 35, 37, 38
- Intracranial pressure (ICP)
 - AF-16, 377–378
 - amplitude/mean relationship, 2
 - automated infusion tests, 2
 - bedside intensive care charts, 3
 - Bland–Altman plot, 98, 99
 - brain, 99
 - closed loop control, hypertension, 2–3
 - computer training, 1
 - defined, 97
 - diffuse brain injury, rabbit and AF-16, 379–380
 - first ICP conferences, 1–2
 - Fourier analysis, pulse amplitude, 3, 4
 - Fourier transform, 3
 - freeze damage, brain and AF-16, 379–381
 - HSE and TBI, 381
 - HSV-1 infected and AF-16 treated rats, 379
 - hypertension, 1
 - invasive monitoring, 52
 - and IOP, 357
 - and MAP, 52, 55

- materials and methods
 - animals, 378
 - chemicals, 378
 - diffuse brain injury, 378
 - focal brain injury, 378
 - HSV-1, 378
 - treatment, AF-16, AF protein and SPC, 378
- non-surgical management, 377
- normal adult rats, 379, 380
- on-line monitoring, 2
- pathogenesis, 380
- PbtO₂, 55, 57–58
- RAE, 57
- rat brain and protein AF, 379
- reliance, computer technology, 3
- sensors A and B, 99
- Intracranial pressure (ICP) measurement, infants
 - accumulation, CSF, 263
 - craniosynostosis, 265
 - cyclic night-time elevation, 265
 - data collection and processing, 262
 - developing nervous system, 265
 - imaging, 261
 - macrocephaly, 263
 - management, 263
 - mean ICP values, 265
 - monitoring, 265
 - MRI, subarachnoid spaces, 264
 - operative procedure
 - anesthesia, 262
 - arachnoid trabecula, 262
 - avoid CSF leakage, 262
 - characteristics, 262
 - CSF diversion, 262
 - ICP recording, 262
 - periosteum, 262
 - radiological inclusion, 261–262
 - subarachnoid identification, 261
 - T2-weighted images, 262
 - ventricular catheter connect pressure monitor, 262
 - outcomes
 - clinical examination, 262
 - complications, invasive recording, 263
 - data interpretation, 262
 - fractions, 263
 - histograms, distribution, 262, 263
 - implantation, shunt, 263
 - shunted vs. non-shunted groups, 263
 - treatment, 265
 - uncertainty, 261
- Intraocular pressure (IOP)
 - CSF pressure, 357, 358
 - ICP, 357
- Intraventricular cooling and CSF infusion
 - arrhythmia/pneumonia, 234
 - artificial ventilation, 233
 - cerebral oxygenation, 233
 - confirm shunt indications, 231
 - data, brain temperature and cerebral oxygenation, 233
 - disadvantage, 234
 - ICP elevation, 233
 - materials and methods
 - anaesthesia and ICP, 231
 - data analysis and storage, 232
 - implementation, 231
 - infusion test, mock-CSF, 231
 - mean arterial blood pressure (MAP), 231
 - parallel measurement, 231
 - standard precoronal approach, 231
 - monitor brain tissue oxygenation, 231
 - outcomes
 - Evans index, iNPH, 233
 - Mann–Whitney U test, 232
 - oxygen saturation and cerebral temperature, 232
 - pO₂ increases, 232
 - ventricular infusion tests, 232
 - parallel infusion and fluids effusion, 234
 - TBI treatment, 234
 - traumatic brain injury (TBI) and ICP control, 233–234
- Intraventricular pressure (IVP)
 - elevation, 374
 - IMP, 374
- Intraventricular thrombolysis
 - cerebral arterial vasospasm, 323
 - cerebral vasospasm, 325, 326
 - clearance and clot clearance rate, 325
 - clearance rate, 326
 - clinical outcome, 325, 327
 - head-shaking method, 325
 - materials and methods
 - cerebral vasospasm assessment and clinical outcome, 324
 - clearance rate assessment, 324
 - statistical analysis, 324
 - WFNS, 323–324
 - meta-analysis, 325
 - study design and limitations, 326–327
 - study population characteristics, 324
 - TCD, 326
- IRND. *See* Irreversible neurological deficit (IRND)
- Irreversible neurological deficit (IRND)
 - ICP, CPP and DND, 340
 - incidence, 340
- Isoflurane
 - analgesedation, 384
 - anesthetic-induced apoptosis, 383
 - materials and methods
 - controlled cortical impact injury, 384
 - neurological outcome, 384
 - outcome
 - neurological, 384, 385
 - sedation, 384–385
 - systemic reactions, 385
 - TBI, 383
- K**
- Kernohan–Woltman syndrome, 295
- L**
- Lempel–Ziv complexity. *See* Pulse amplitude and Lempel–Ziv (LZ) complexity
- Licox® and Raumedic®-Neurovent-PTO brain tissue oxygen pressure
 - aim, 169
 - assessment, properties, 171
 - autoregulatory processes, 171
 - explanation, 172
 - in vitro* investigations
 - direct comparison, 169–170
 - ensure constant O₂, 170
 - measures, 170
 - in vivo* investigations
 - animal model, 170
 - oxygen provocation test, 170
 - oxygen values, 170
 - statistical evaluation, 170
 - surgical procedures, 170

measurement accuracy, 171
 monitoring, cerebral functions, 169
 outcomes
 in vitro tests, 170–171
 in vivo tests, 171, 172
 oxygen concentrations, 171
 Licox system, 161
 Liver failure, 169–172, 174, 175
 Locally weighted learning model (LWL), 53, 57
 Lumbar infusion. *See* Overnight monitoring (ONM) and lumbar infusion data, iNPH patients
 LWL. *See* Locally weighted learning model (LWL)

M

Magnetic resonance imaging (MRI)
 credible prognostic assessment, 320
 CT, 317
 diagnosis, 319
 examination, 318
 IIH, 236
 Intracranial arachnoid cysts, 267
 and MRS, 317
 technological development, 319
 Magnetic resonance spectroscopy (MRS)
 MRI and, 317
 NAA, 317, 320
 usage, 319
 Mann–Whitney U test, 232
 MBAER. *See* Modified brainstem auditory evoked response (MBAER)
 MCA. *See* Middle cerebral artery (MCA)
 Mean arterial blood pressure (MAP), 231
 Mean transit time (MTT), 330–331
 Measurement technique, 20
 Micro-fabricated shunt, communicating hydrocephalus treatment
 CSF diversion device, 239
 device reflects, arachnoid granulations, 241–242
 difficulties, imprecise shunting, 239
 materials and methods
 bench flow testing, 240–241
 close-up micro-needles and valve, 240
 cracking pressure, 241
 flow characteristics, 241
 measures, 241
 polydimethylsiloxane and parylene, 240
 micro-needle design, 242
 native arachnoid granulations functions, 239
 outcomes
 cross-cut and slit-cut opening, 241
 flow test, 241
 optimal micro-valve design, 241
 positive and cracking pressure, 241
 power/complex microprocessors, 241
 protection, 242
 shunt placement, 241
 smart shunt, 241
 superior sagittal sinus (SSS), 239
 techniques, 242
 Micro-needles
 comprising wall, SSS, 239
 conjunction, 241
 micro-fabricated shunt, 239
 Microsurgical fenestration, 269
 Micro-valves. *See* Micro-fabricated shunt, communicating hydrocephalus treatment
 Midbrain injury
 CT examination, 318–319

description, 317
 materials and methods
 inclusion and exclusion criteria, 317
 mesencephalon, 318
 MRI and MRS, 317
 MRS results, 318, 319
 NAA and Cr, 320
 NAA/Cr and NAA/Cho ratios, 320
 Middle cerebral artery (MCA)
 blood flow, 315
 CBFV measurement, 7, 8
 opacification, 314
 Modified brainstem auditory evoked response (MBAER)
 description, 81
 materials and methods
 absolute latencies/standard deviations, 83
 normative data, 82
 representative patient preoperative MRI scans, 82
 representative waveforms, 83
 statistical results, latency, 84, 85
 Wave V and Vn, 85
 Moens-Korteweg equation, 6
 Morphological Clustering and Analysis of Intracranial Pressure (MOCAIP), 208
 MRI. *See* Magnetic resonance imaging (MRI)
 MRS. *See* Magnetic resonance spectroscopy (MRS)
 MTT. *See* Mean transit time (MTT)
 Mx autoregulatory index, 154–155

N

NAA. *See* N-acetyl aspartate (NAA)
 N-acetyl aspartate (NAA), 320
 Near infrared spectroscopy (NIRS) and vasogenic ICP waves
 aim, 181
 frequency range, variables, 183
 infusion test, 185
 materials and methods
 clinical observations, 182
 data processing and analysis, 182
 infusion test, assessing CSF dynamics, 182
 monitoring, cerebral oximetry, 182
 measurements, 183, 185
 non-invasive detection, 181, 183
 outcomes
 correlation coefficient, HB and HbO₂, 184
 moving correlation coefficient, 184
 observations, 183
 statistical analysis, 182–183
 waves patterns, Hb and HbO₂, 182, 183
 overnight ICP monitoring, 185
 relationship, HB and HbO₂, 183
 slow waves and intracranial pressure, 181
 Neonatal piglet model, 62
 Neuromonitoring data. *See* Stationarity, neuromonitoring data
 NIRS. *See* Near infrared spectroscopy (NIRS)
 Non-invasive ICP (nICP) estimation
 characteristics, 121
 components, 121–122
 differences, 125
 materials and methods
 characteristics, baseline, 122
 ICM+ software, 122
 ICP waveform, 122
 invasive and non-invasive parameters, 122
 pressure monitoring kit, 122
 RAP and nRAP, 122
 TCD recordings, 122

- monitoring, 121
- outcomes
 - differences, parameters analysis, 122, 124
 - Glasgow Outcome Scale (GOS) score, 122
 - invasive measurements, 122
 - nAmp, 122
 - recordings, ABP, FV and ICP, 123
 - scatter plots, nICP and ICP, 124
- prediction, 125
- pressure–volume compensatory reserve index, 122
- pulse waveform, 121
- signals, 121
- traumatic brain injury (TBI), 121
- waveform, 125
- Non-invasive method assessment, ICP variations
 - brain edema and catheter misplacement, 131
 - CMP phase shifts, 134
 - cochlear aqueduct, 131
 - complications, 131
 - difficulties, 134
 - DPOAE phase shift, 133–134
 - electrophysiological recordings, 134
 - generated cochlear sensory cells, 134
 - infection, 131
 - materials and methods
 - CMP phase shift, 132
 - detection, CMP, 132
 - DPOAE, 131–132
 - electric signals radiations, Cochlear, 132
 - ICP influence, 132
 - Sonic stimulation and DPOAE-CMP recordings, 132
 - Menière's disease, 134
 - modification, ear's impedance, 133
 - patency, cochlear aqueduct, 132
 - signals, 131
 - subarachnoid space, 132
 - symptoms, tinnitus and hearing losses, 132
- Normalisation technique, 64
- Normal pressure hydrocephalus (NPH)
 - iNPH (*see* Idiopathic normal pressure hydrocephalus (iNPH))
 - pathophysiology, 5
- O**
 - Oral vigabatrin administration, head injury
 - anticonvulsant VGB, 271–272
 - blood–brain barrier (BBB), human, 271
 - brain microdialysates and pressure monitoring
 - abnormal region, 274
 - degree of decline, 274
 - dose decreases, 273–274
 - plotted *vs.* time, 275
 - treatment, 275
 - VGB doses and administration, 273, 275
 - clinical observations, 272
 - death, 271
 - description, 271
 - GABA increases, 276
 - HPLC analysis, 272
 - impact, 271
 - lack of information, drug, 271
 - literature, human VGB, 276
 - microdialysis technique, 272
 - plasma levels, VGB, 272, 273
 - rats, 276
 - VGB function, 275–276
- Outflow resistance
 - CSF space compliance, 2
 - and graph, 2
- Overnight monitoring (ONM) and lumbar infusion data, iNPH patients
 - cerebrospinal reserve capacity, 213
 - correlation absence, 214
 - description, iNPH, 213
 - diagnosis, 213
 - elastance and median RAP and AMP, 215
 - elastance threshold, 215
 - intracranial and lumbar CSF space, 215
 - long-term ICP, 215
 - mean values, 213
 - median values, RAP and AMP, 214–215
 - modern hydrodynamic theories, 213
 - objectives, 213
 - outcomes, 214
 - patients and methods, 214
 - RAP increase, 215
 - vasogenic B-waves, 215
- P**
 - Pascal's law, 97, 99
 - Phase contrast MRI (PC-MRI), 191–192
 - Physiological parameters measurement techniques, 12
 - Preterm infant
 - brain injury, 177
 - measurements, cerebral blood flow, 180
 - positron emission tomography, 180
 - Programmable valves and gravitational units
 - cerebral blood flow, 243
 - Dutch NPH, 245
 - hydrostatic pressure, 244
 - iNPH, 243
 - LPVs, 244
 - materials and methods
 - design/sample size calculation, 244, 245
 - inclusion criteria, 244
 - recruitment criteria, 244
 - multicentre conception, 245
 - outcomes
 - measures, 244–245
 - randomisation, 244
 - role, funding source, 245
 - surgery, 244
 - surgical therapy (vp shunts), 243–244
 - SVASONA design, 245
 - Pulsatile and cerebrospinal fluid flow quantification
 - algorithm input
 - correlation mask and threshold, 193
 - CSF dynamics, 192
 - evaluation, 192
 - flow quantification, 192
 - Midsagittal T2-weighted image, 192
 - MRI, 192
 - outcome calculations, 194
 - outlier detection, 194
 - phase offset, 194
 - reference waveform, 192–193
 - time-of-flight (TOF) sequence, 192
 - trueFISP, 192
 - cerebrospinal fluid (CSF) system, 191
 - definition, reference waveform, 194
 - description, 191
 - diagnosis and treatment, 194
 - features, 195
 - impact, hydrodynamics NPH., 195

- limitations, 195
- outcomes
 - CSF flow measurements, 194
 - Voxel waveform, 193
- pathophysiological mechanisms, 191
- phase contrast MRI (PC-MRI), 191
- prepontine cistern, 191–192
- role, 191
- threshold value, 195
- Pulsatile volume modeling, 20
- Pulsatility
 - cortical veins, 5
 - CSF, 5
- Pulsatility index (PI). *See* Transcranial doppler (TCD) pulsatility indices
- Pulse amplitude and Lempel-Ziv (LZ) complexity
 - complex systems analysis, 25
 - correlation, 25, 26
 - CSFP signal, 26
 - description, 23
 - materials and methods
 - data acquisition and complexity analysis, 24
 - infusion studies, neurosurgery, 23
 - lumbar infusion test and derived parameters, 24
 - statistical analysis, 24
 - parameters derived, CSFP signal, 24, 25
 - patients and CSF parameters characteristics, 24
 - physiological systems, 25
- Pulse onset latency
 - hypothesis, 7
 - ICP, 5–6
 - vascular, 6

R

- Radio-frequency identification (RFID) technology, 113
- Rat model, 102, 103
- Raumedic systems, 162–163
- Realistic assessment technique, 39
- Regions of interest (ROI)
 - arteriole and venule, 395
 - pO₂ values, 394
- RFID technology. *See* Radio-frequency identification technology

S

- SAH. *See* Subarachnoid hemorrhage (SAH)
- SDH. *See* Subdural hematoma (SDH)
- Secondary insults
 - classes, 46
 - EUSIG, 47–48
- Sensor
 - animal testing, potential ICP, 102–103
 - ICP characteristics, 102
- Severe head injuries (SHI)
 - methods, 301
 - NT, 303
 - objective, 301
 - parameters comparison, 303
 - SDH, 303
- Shapiro-Wilk test, 250
- SHI. *See* Severe head injuries (SHI)
- Shunt-dependent hydrocephalus and S100B levels
 - acute treatment, 217
 - clinical and radiological factors, 217
 - clinical process, 219
 - description, 217
 - development, 217
 - goal, 217

- materials and methods
 - EVD treatment and VP shunt placement, 218
 - patient population, 217–218
 - sample collection and processing, 218
 - statistical analysis, 218
- measurement, CSF S100B levels, 219
- outcomes
 - clinical classification, SAH patients, 218
 - CSF S100B concentrations, 219
 - pathomechanisms, 219
 - prevalence, 219
- Shunting, intracranial arachnoid cysts
 - failures, 268
 - procedures, 267
- Software
 - circulation, 76, 78
 - ICP, 76
 - parameters displayed, infusion study, 76, 77
- SSS. *See* Superior sagittal sinus (SSS)
- STA. *See* Superficial temporal artery (STA)
- Stationarity, neuromonitoring data
 - entropy, 95
 - materials and methods, 94
 - non-stationarity, 94
 - retrospective monitoring, 95
 - therapeutic control loop, 93, 94
- Statistical modeling techniques, 39
- Statistical technique, 40
- Stenotic disease, 20
- Subarachnoid hemorrhage (SAH)
 - CSW, 400
 - experimental rat model, 399–400
 - neuromonitoring, 165
 - plasma sodium levels, 401
- Subarachnoid megaly, 263, 265
- Subdural hematoma (SDH)
 - EM, 303
 - management, 303
- SubWindow technique, 40, 41
- Superficial temporal artery (STA), 314
- Superior sagittal sinus (SSS), 239
- Suppression techniques, 43, 44

T

- TBH. *See* Transtentorial brain herniation (TBH)
- TBI. *See* Traumatic brain injury (TBI)
- TBW measurement. *See* Total body water measurement
- TCD. *See* Transcranial Doppler (TCD)
- Telemetric ICP measurement
 - animal experiment
 - anesthesia and operative procedure, 112–113
 - design, 112
 - data management and statistics, 113
 - description, 111
 - descriptive statistics, 114, 115
 - intraperitoneal pressures, 113
 - Kaplan-Meier “survival” analysis, 114
 - measurement stability, 114, 115
 - NEUROVENT P-Tel, 114, 116
 - subdural telemetric probes, 116
 - technology, 113
- Telemetric technology, 108
- Telemetry. *See also* ICP telemetry
 - and amplifier circuits, 102
 - and amplifier electronics, 102
 - and inductive power system, 103
- Test Set Model Assessment, 41–42

- Total body water (TBW) measurement, 62
 - Total cerebral blood flow (TCBF), 203
 - Transcranial Doppler (TCD) pulsatility indices
 - gender correlates, 14
 - materials and methods
 - management, patient, 11–12
 - measurement techniques, physiological parameters, 12
 - patient enrollment, 11
 - statistical analysis, 12
 - neurological surgery effects, 14
 - patient demographics, 12–14
 - PI and ICP, 14, 15
 - Transcranial impedance and ICP
 - data-driven approaches, 61
 - goal, research, 62
 - impedance measurements, 62
 - materials and methods
 - experimental protocol, animal study, 63
 - experimental protocol, normative study, 62–63
 - normative study, 63–64
 - patients non-surgical management, TBI, 61
 - practical electrode positions, 65
 - regression plot, 63
 - TBW measurement, 62
 - temporal, mastoid electrode position measurement, 64
 - Transtentorial brain herniation (TBH), 81
 - Traumatic brain injury (TBI)
 - accident and clinical data
 - injury and outcome characteristics, 290, 292
 - pre-injury comorbidity, 291, 293
 - CT determinations, 296, 298
 - description, 51–52, 289
 - epidemiological and physiological data, 290
 - FDP, 298–299
 - fixed sequelae, dilated pupils, 296–297
 - geriatric, 292
 - HSE, 380
 - and ICP control, 233–234
 - injury mechanisms, 296
 - management, 52
 - materials and methods, 289–290
 - and moderate hypocapnia
 - aim, 153
 - effects, hyperventilation, 155
 - effects, ventilatory treatment, 153
 - impacts, 153
 - increases, cerebral blood volume, 153
 - intact cerebral autoregulation, 153
 - materials and methods, 154
 - Mx autoregulatory index, 154–155
 - Mx baseline plotted vs. baseline, 155
 - outcomes, 154
 - temporary protection, 155
 - transient optimization, 155
 - monitoring data, 58
 - ophthalmological sequelae, 298
 - outcome, 298
 - patient demographics, 296, 297
 - patient outcomes, 295
 - patients, ICU, 40
 - pediatric, 70, 72
 - predictive value, pupillary dilatation, 296
 - prognostics, 292
- U**
- Ursino and Lodi model, 62
- V**
- Vasospasm
 - cerebral, 12, 14
 - Pearson and robust correlations, 14
 - Vigabatrin (VGB), 271–275
 - Visco-poro-elastic model, 98
- W**
- Weissler's regression equation, 7
 - WFNS. *See* World federation of neurosurgical societies (WFNS)
 - Wireless
 - ICP monitor, 101
 - power, 102
 - World federation of neurosurgical societies (WFNS), 323–324